ANALYSIS, DESIGN and CONSTRUCTION of BRACED BARREL VAULTS

Edited by

Z.S. MAKOWSKI

Taylor & Francis
Taylor & Francis Group

Also available as a printed book
see title verso for ISBN details
@Seismicisolation

ANALYSIS, DESIGN AND CONSTRUCTION OF BRACED BARREL VAULTS

@Seismicisolation

@Seismicisolation

ANALYSIS, DESIGN AND CONSTRUCTION OF BRACED BARREL VAULTS

Edited by

Z.S.MAKOWSKI

Professor of Civil Engineering,
Space Structures Research Centre,
University of Surrey, Guildford, UK

ELSEVIER APPLIED SCIENCE PUBLISHERS
LONDON and NEW YORK

@Seismicisolation

ELSEVIER APPLIED SCIENCE PUBLISHERS LTD Crown House, Linton Road, Barking, Essex IG11 8JU, England
This edition published in the Taylor & Francis e-Library, 2006.
"To purchase your own copy of this or any of Taylor & Francis or Routledge's collection of thousands of eBooks please go to http://www.ebookstore.tandf.co.uk/. "

Sole Distributor in the USA and Canada ELSEVIER SCIENCE PUBLISHING CO., INC. 52 Vanderbilt Avenue, New York, NY 10017, USA

WITH 14 TABLES AND 395 ILLUSTRATIONS

© ELSEVIER APPLIED SCIENCE PUBLISHERS LTD 1985

British Library Cataloguing in Publication Data Analysis, design and construction of braced barrel vaults. 1. Vaults (Architecture)—Design and construction I. Makowski, Z.S. 624.1′775 TH2160

Library of Congress Cataloging-in-Publication Data Main entry under title: Analysis, design, and construction of braced barrel vaults.
Includes index. 1. Vaults (Architecture)—Design and construction— Addresses, essays, lectures. I. Makowski, Z.S. TH2160.A53 1985 690′.145 85–15902

ISBN 0-203-97594-4 Master e-book ISBN

ISBN 0-85334-377-2 (Print Edition)

The selection and presentation of material and the opinions expressed in this publication are the sole responsibility of the authors concerned.
Special regulations for readers in the USA
This publication has been registered with the Copyright Clearance Center Inc. (CCC), Salem, Massachusetts. Information can be obtained from the CCC about conditions under which photocopies of parts of this publication may be made in the USA. All other copyright questions, including photocopying outside of the USA, should be referred to the publisher.

All rights reserved. No part of this publication may be reproduced, stored in a retrieval system, or transmitted in any form or by any means, electronic, mechanical, photocopying, recording, or otherwise, without the prior written permission of the publisher.

@Seismicisolation

Preface

The industrial and technological developments which have taken place during the last three decades have had a far-reaching effect upon contemporary architecture and modern engineering. New building techniques, new constructional materials and new structural forms have been introduced all over the world.

The architectural search for new structural forms has resulted in the widespread use of three-dimensional structures. The evolution of effective computer techniques of analysis is undoubtedly one of the reasons for the truly phenomenal acceptance of space structures.

Their popularity is growing steadily. The designers realise that with the demand for large unobstructed areas, long-span grids, braced barrel vaults and domes, and triangulated hyperbolic paraboloids frequently provide the right answer for an economic solution. During recent years, architects have re-discovered the advantages of barrel vaults as viable and often highly suitable forms for covering not only low-cost industrial buildings, warehouses, large-span hangars, indoor sports stadia and gymnasia, but also large cultural and leisure centres.

The impact of industrialisation on prefabricated braced barrel vaults has proved to be the most significant factor leading to lower costs for these structures.

The present volume is the outcome of an attempt by the editor to bring together the acknowledged leaders in the design, analysis and construction of braced barrel vaults and to produce an authoritative reference book which, it is hoped, will be of interest and direct help to practising civil and structural engineers, consultants, contractors, architects and research workers.

The 24 chapters have been provided by a carefully selected group of internationally recognised designers and research workers from various universities and government research establishments, as well as leading manufacturing firms responsible for the construction of some of the most important braced barrel vault structures. The collected contributions on various aspects of the analysis, design and construction of braced barrel vaults represent a wealth of experience coming from Canada, Czechoslovakia, France, Italy, Japan, Hong Kong, The Netherlands, The People's Republic of China, Romania, the UK and West Germany.

The designer using this book will find in it a remarkable amount of up-to-date information on the methods of structural analysis applicable to these structures, studies of the behaviour of barrel vaults under loading including the results of recent wind tunnel tests and an extremely valuable review of practical achievements with comprehensive structural details. The book also contains much valuable information on the use of formex algebra, a new and extremely powerful technique developed at the Space Structures Research Centre of the University of Surrey on the practical representation of configurations of various types of braced barrel vault.

Z.S.MAKOWSKI

@Seismicisolation

Contents

Preface v

List of Contributors xi

1. History of Development of Various Types of Braced Barrel Vaults and Review of Recent Achievements all over the World 1
   Z.S.MAKOWSKI
2. Introduction to the Analysis of Braced Barrel Vaults 37
   P.MULLORD
3. Formex Formulation of Barrel Vaults 43
   H.NOOSHIN
4. Double-elliptic Vaults 80
   P.HUYBERS and G.J.ARENDS
5. Analysis of Reticulated Shells by the Equivalent Continuous Method 96
   CAO ZI and ZHANG SHAN-YU
6. Comparison of the Structural Behaviour of Various Types of Braced Barrel Vaults 113
   G.A.R.PARKE
7. Determination of Wind Loads on Barrel Vaults 145
   N.Toy and C.W.WONG
8. Stability Considerations in Barrel Vaults 166
   JAMES F.DICKIE
9. Instability Behaviour of Triangulated Barrel Vaults 180
   VICTOR GIONCU, NICOLAE BĂLUȚ, DORIN PORUMB and NICOLAE RENNON
10. Elastic and Post-buckling Analysis of Braced Barrel Vaults Manufactured from Fibre/Matrix Composite Materials 212
    L.HOLLAWAY and A.RUSTUM
11. Basic Principles in the Design and Construction of Steel Braced Barrel Vault Roofs 232
    H.B.WALKER
12. Some Possibilities Offered by Braced Vault Construction 246
    F.E.S.WEST
13. Analysis, Design and Construction of 'Diamond Truss' Type of Three-way Grid Barrel Vaults 253
    F.MATSUSHITA

@Seismicisolation

14. Architectural Aspects of Braced Barrel Vaults 264

S.DU CHÂTEAU

15. MERO Braced Barrel Vault Structures 281
HERBERT KLIMKE and HELMUT EBERLEIN

16. Triodetic Aluminium and Steel Braced Barrel Vaults 293
H.G.FENTIMAN

17. Design and Construction of Steel Barrel Vaults for Buildings of Medium and Large Spans 308
J.ZEMAN

18. Structural Analysis of Reticulated Vaults 334
M.PAGANO and P.LENZA

19. Theoretical Studies and Experimental Research on Structural Behaviour of Reticulated Vaults 352
M.PAGANO and P.LENZA

20. Probability Analysis of Braced Barrel Vaults Composed of Elements of Random Strength 396
ANTONIO LA TEGOLA

21. Recent Research on Timber Lamella Barrel Vaults 406
CLAUS SCHEER and JEFFREY PURNOMO

22. Recent Examples of Prefabricated Steel Barrel Vaults from Romania: Their Analysis, Design and Construction 422
VICTOR GIONCU, NICOLAE BĂLUȚ, DORIN PORUMB and NICOLAE RENNON

23. Analysis and Design of a Prefabricated Three-way Trussed Grid Vault 436
G.J.ZUNZ, R.HOUGH and M.J.BANFI

24. The Design and Construction of the Liverpool International Garden Festival Exhibition Building 453
T.RAGGETT

Index 466

@Seismicisolation

@Seismicisolation

List of Contributors

G.J.ARENDS
Building Technology Group, Delft University of Technology, Stevin Laboratory, 4 Stevinweg, 2628 CN Delft, The Netherlands. Present address: *J.van Beierenlaan 45, 2613 HZ Delft, The Netherlands*

NICOLAE BĂLUȚ
Building Research Institute, 1900 Timisoara, Str. Traian Lalescu 2, Romania

M.J.BANFI
Ove Arup & Partners, 13 Fitzroy Street, London W1P 6BQ, UK

CAO ZI
Department of Civil Engineering, Beijing Polytechnical University, The People's Republic of China

S.DU CHÂTEAU
Institut le Ricolais, IRASS, 15 rue Hégesippe-Moreau, Paris, 75018, France

JAMES F.DICKIE
Simon Engineering Laboratories, University of Manchester, Oxford Road, Manchester M 13 9PL, UK

H.EBERLEIN
MERO-Raumstruktur GmbH & Co., Steinachstrasse 5, D-8700 Würzburg 1, West Germany

H.G.FENTIMAN
Triodetic Structures Ltd (International), 2753-A Fenton Road, Ottawa, Ontario K1G 3N3, Canada

VICTOR GIONCU
Building Research Institute, 1900 Timisoara, Str. Traian Lalescu 2, Romania

L.HOLLAWAY
Department of Civil Engineering, University of Surrey, Guildford, Surrey GU2 5XH, UK

R.HOUGH
Ove Arup & Partners, 13 Fitzroy Street, London W1P 6BQ, UK

P.HUYBERS

@Seismicisolation

Department of Civil Engineering, Stevin Laboratory, 4 Stevinweg, 2628 CN Delft, The Netherlands

H.KLIMKE
MERO-Raumstruktur GmbH & Co., Steinachstrasse 5, D–8700 Würzburg 1, West Germany

P.LENZA
Cattedra di Complementi di Tecnica delle Costruzioni, Faculty of Engineering, University of Naples, Piazzale Vincenzo Tecchio, Naples, Italy

Z.S.MAKOWSKI
Space Structures Research Centre, University of Surrey, Guildford, Surrey GU2 5XH, UK

F.MATSUSHITA
Tomoegumi Iron Works Ltd, No. 2–20, 6-chome, Ginza, Chuo-ku, Tokyo, Japan

P.MULLORD
Space Structures Research Centre, University of Surrey, Guildford, Surrey GU2 5XH, UK

H.NOOSHIN
Space Structures Research Centre, University of Surrey, Guildford, Surrey GU2 5XH, UK

M.PAGANO
Cattedra di Complementi di Tecnica delle Costruzioni, Faculty of Engineering, University of Naples, Piazzale Vincenzo Tecchio, Naples, Italy

G.A.R.PARKE
Space Structures Research Centre, University of Surrey, Guildford, Surrey GU2 5XH, UK

DORIN PORUMB
Building Research Institute, 1900 Timisoara, Str. Traian Lalescu 2, Romania

JEFFREY PURNOMO
Technical University of Berlin, Strasse des 17 Juni 135, 1 Berlin 12, West Germany

T.RAGGETT
Arup Associates, 7 Soho Square, London W1V 6QB, UK

NICOLAE RENNON
Building Research Institute, 1900 Timisoara, Str. Traian Lalescu 2, Romania

@Seismicisolation

A.RUSTUM
Department of Civil Engineering, University of Surrey, Guildford, Surrey GU2 5XH, UK

CLAUS SCHEER
Technical University of Berlin, Strasse des 17 Juni 135, 1 Berlin 12, West Germany

ANTONIO LA TEGOLA
Department of Civil Engineering, Università degli studi di Calabria, Dipartimento di Strutture, 87030 Arcavacata di Rende, Cosenza, Italy

N.TOY
Department of Civil Engineering, University of Surrey, Guildford, Surrey GU2 5XH, UK

H.B.WALKER
Advisory Services, Constrado, 12 Addiscombe Road, Croydon, Surrey CR9 3JH, UK

F.E.S.WEST
PRC Engineering (UK) Ltd, 200 Great Dover Street, London SE1 4YB, UK. Present address: *2 Hove Court, Raymond Road, London SW19 4AG, UK*

C.W.WONG
Department of Civil and Structural Engineering, Hong Kong Polytechnic, Hung Hom, Kowloon, Hong Kong

J.ZEMAN
11800 Praha, Hradčany, Pohořelec 4, Czechoslovakia

ZHANG SHAN-YU
Department of Civil Engineering, Beijing Polytechnical University, The People's Republic of China

G.J.ZUNZ
Ove Arup & Partners, 13 Fitzroy Street, London W1P 6BQ, UK

@Seismicisolation

1
History of Development of Various Types of Braced Barrel Vaults and Review of Recent Achievements all over the World

Z.S.MAKOWSKI
Space Structures Research Centre, University of Surrey, Guildford, UK

1 INTRODUCTION

Barrel vault is one of the oldest architectural forms, used since antiquity. The brick architecture of the Orient or the masonry construction of the Romans provides numerous examples of the structural use of barrel vaults.

In addition to purely utilitarian forms of roofing, barrel vaults have already been used in Mesopotamia, Persia and especially the Roman Empire in monumental buildings over temples, public baths or audience halls, often achieving quite large spans.

The heavy dead weight of these structures which, as a rule, have been of cylindrical shape produced large horizontal forces that originally had to be resisted by massive and very heavy walls; only gradually did the medieval builders realise the advantage of buttresses.[12]

A logical improvement was the introduction in the nineteenth century of iron bars acting as horizontal tie members resisting the horizontal thrust from the vault and enabling the structure to be supported on slender walls or columns. There is no doubt at all that the introduction of cast iron and wrought iron had a tremendous influence on the construction of roof structures of considerable span.

2 EARLY EXAMPLES

One must mention here the use of this new material for the construction in Paris in 1809–11 of a 40 m clear span ribbed iron dome over the corn market and an iron barrel vault of 19 m clear span over the Diana public baths in Vienna in 1820. This structure consisted of a series of iron arches of semicircular shape.

Probably the best early example of a braced barrel vault is the construction of the famous iron barrel vault designed by Joseph Paxton and erected over the central nave of the Crystal Palace for the Great Exhibition of 1851 in Hyde Park in London.

This extremely well-known structure is regarded by many architects as the best example of early prefabricated single-layer barrel vaults, consisting of a rectangular grid of

@Seismicisolation

Fig. 1.1. Internal view of the iron barrel vault built in 1851 for the Crystal Palace.

prefabricated modular circular ribs and longitudinal members, stiffened by slender diagonal iron rods providing the rigidity against unsymmetrical loads (Fig. 1.1).

The rapid improvements in the manufacturing techniques of iron and in its quality were of fundamental importance in the construction in the nineteenth century of large span roofs over railway stations. As a rule these structures consisted of great soaring iron arches stiffened by diagonal wind bracing members interconnecting the two-dimensional ribs into a truly three-dimensional structure.

The popularity of barrel vaults derived partly from the economy of these structures, as all arches could be constructed as identical members. At the same time, their cylindrical shape provided a great deal of volume under the roof, a distinct advantage for railway stations in the age of steam engines, or for large span warehouses, providing a welcome increase in their storage space.

@Seismicisolation

The realisation of the advantages of prefabricated steel structures which could be built with a small number of identical components has been one of the reasons for the rapid acceptance of the timber lamella roof system, originally developed by a German architect in 1906, Mr Zollinger from Dessau.

This system consists of thin timber lamella units, which are either bolted or nailed together at their points of interconnection, forming a cylindrical single-layer diagonally arranged grid structure. This system proved to be exceptionally popular in Germany before the First World War and its use spread rapidly to Sweden, Norway, Holland,

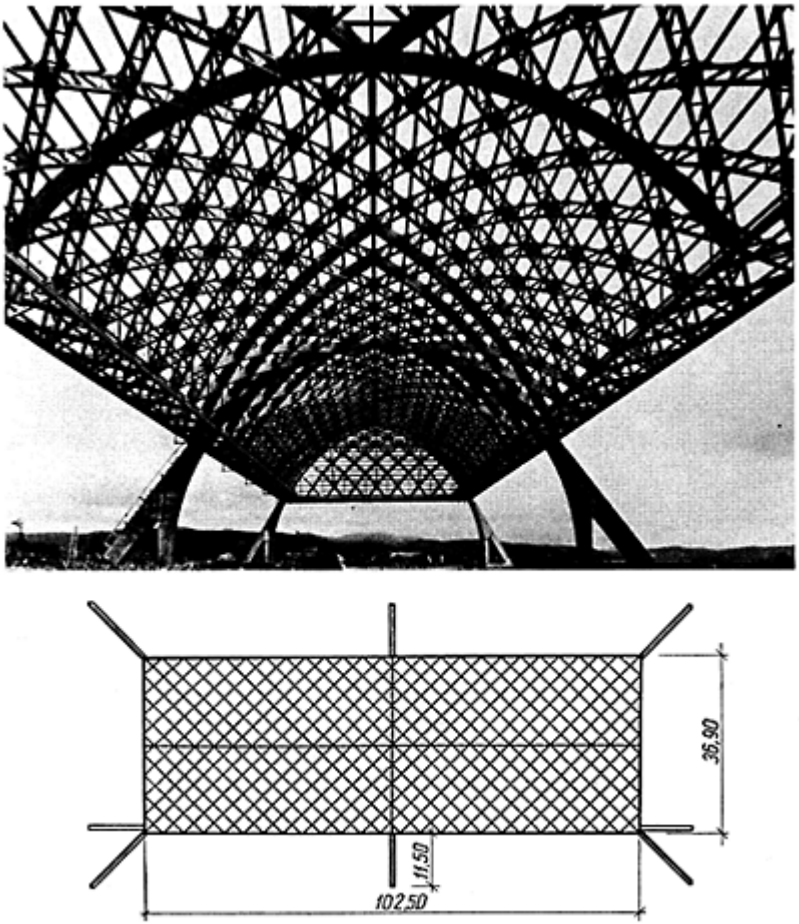

Fig. 1.2. Plan and view of Nervi's hangar.

Switzerland, Poland and Russia. It was introduced by Dr G.R.Kiewitt to the USA in 1925. Since that time numerous timber barrel vaults have been built in the USA.

@Seismicisolation

As the basic geometry of interconnected lamella units forms a diagonal grid which consists of lozenges and is not fully triangulated, as a rule the timber lamella barrel vaults had timber boards forming the top layer covering nailed to the lamella units. This provides the essential rigidity to the structure and also enables it to resist unsymmetrical wind and snow loads.

The architects liked the pleasing pattern of the diagonal grids and appreciated the architectural and decorative appearance of the soffits, and though originally the timber lamella barrel vaults were constructed over warehouses and industrial buildings, their use rapidly extended to roofs over swimming pools, sports centres, churches, etc.

There is no doubt at all that the realisation of the structural advantages of timber lamella barrel vaults induced the famous Italian designer Pier Luigi Nervi to adopt this form of construction for his daring designs of hangars for the Demanio Aeronautico. The hangar, built in 1935 in Cecchignola, near Rome, over an area of 102·5×39·6 m and supported at only six points is already very well known (Fig. 1.2).

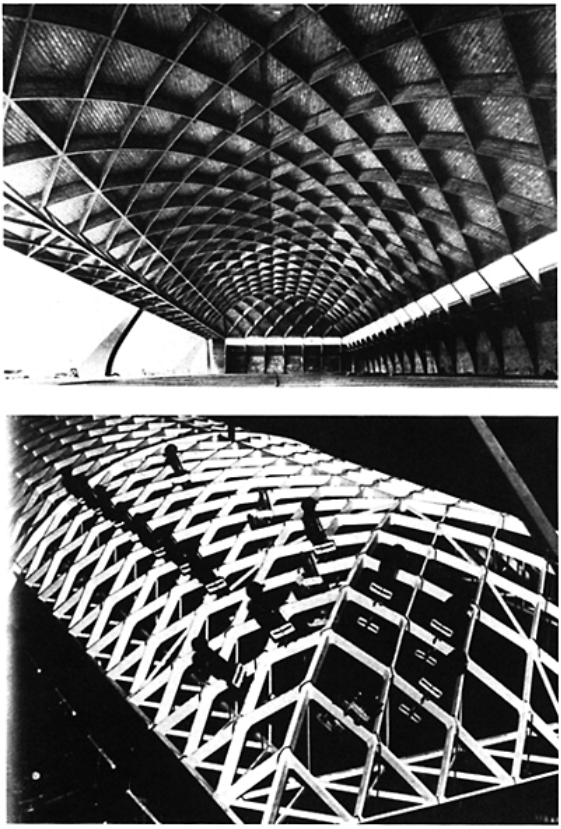

Fig. 1.3. A small scale model of the hangar in Orvieto and the internal view of the finished structure.

@Seismicisolation

Several large span structures have been built by Nervi in this system using precast, prefabricated modular reinforced concrete units which were interconnected on site through welding of the protruding steel reinforcing bars at the nodal points and casting a r.c. slab as the top layer, becoming an integral part of the cylindrical barrel vault structure.

Nervi originally used diagonal grids supported by vertical end diaphragms at both ends of the barrel vault; in some later designs he modified the shape of his structures by using hipped barrel vaults, probably mainly for architectural reasons as the hips were introduced primarily to enhance the final appearance.

The exact stress analysis of such systems by analytical methods was impossible at that time and Nervi is one of the structural designers who used the model analysis of his structures as the basis for the dimensioning of his barrel vaults.Figure 1.3 shows a small scale model of the structure designed by Nervi as a hangar at Orvieto, Italy.

The pioneering work of two German engineers, W.Bauersfeld and F.Dischinger, in 1920 was instrumental in the introduction of thin reinforced concrete shells. The original enthusiastic reception by the architectural profession for this form of construction turned the attention of structural designers to the potential of thin reinforced concrete shells. Often, unfortunately, the advantages of r.c. barrel vaults were over-emphasised.

After the initial wave of enthusiasm around 1955, it became apparent that r.c. barrel vaults, in addition to undoubted architectural advantages, also had several drawbacks. Practical experience showed that, as a rule, r.c. shells require elaborate formwork; they are also slow in construction and their final cost is not as low as predicted by the enthusiasts for their use.

In their search for an economic solution, designers looked back at the earlier work of some English and German engineers. The lessons learned by Joseph Paxton were not forgotten and the results of the studies of August Föppl carried out on latticed barrel vaults in Germany during the second part of the eighteenth century were again re-investigated.

A hundred years ago A.Föppl drew the attention of the structural designers to the potential of certain types of lightweight steel barrel vaults and already in the year 1892 produced the first attempt to determine the stress distribution in these structures.

It is an irony of fate that at that time the German Patent Office refused Föppl’s application on the grounds that braced barrel vaults could not be treated as inventions, since similar types of bracing framework had been used for years as supporting towers for water and gas tanks, although used in vertical and not in a horizontal position.

On the other hand, during the 1950s and 1960s such patent rights were granted in several countries to people claiming to have invented various types of braced barrel vault.

The fact remains that after the publication of Professor Föppl’s famous book on the latticed space truss in 1892 many engineers followed Föppl’s work, having realised the advantages of braced barrel vaults as lightweight self-supporting enclosures over large areas.

The original barrel vault introduced by Föppl consisted of several lattice trusses, spanning the length of the barrel and supported on the gables. After connection of the longitudinal booms of the latticed trusses, they became a part of the braced barrel vault of the single-layer type.

@Seismicisolation

3 TYPES OF BRACING

There are several possible types of bracing which have been used in the construction of single-layer braced barrel vaults in steel, aluminium or timber (Fig. 1.4). The fully triangulated systems can theoretically be analysed as pin-connected structures. The barrel vaults, having the diagonal or hexagonal types of bracing, must have rigid joints to be stable and the influence of bending moments in their stress distribution is much more

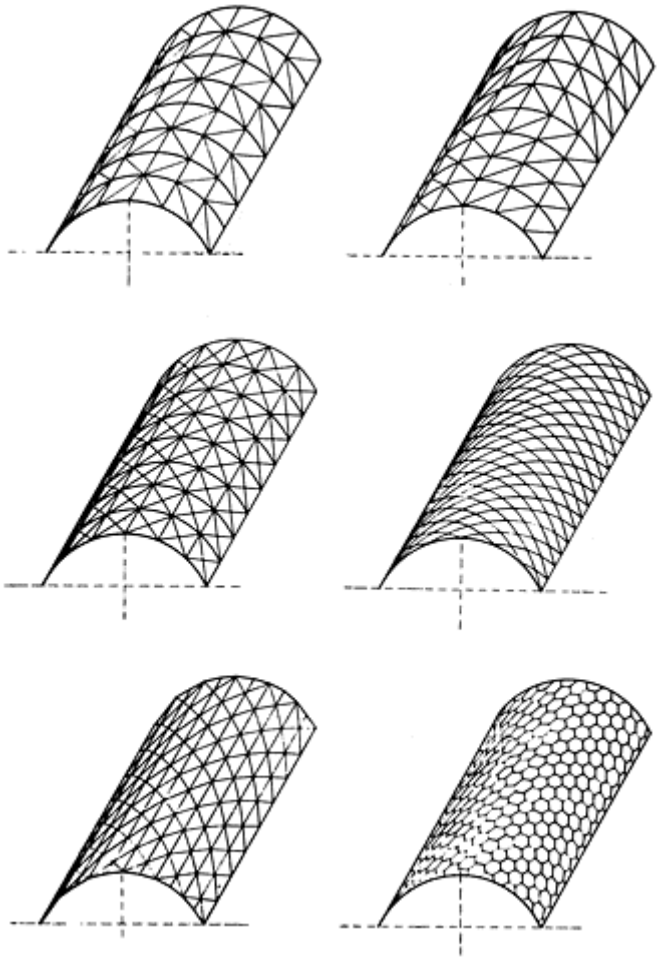

Fig. 1.4. Main types of bracing used for barrel vaults.

pronounced than in the other types. In the original Föppl structures the number of latticed trusses usually varied from six to ten. The analysis will show that the most economical shape in plan is approximately square and in practical design single barrels seldom have a

@Seismicisolation

length/width ratio greater than 2. The rise/width ratio is usually above 0·2; otherwise the lattices after the connection will provide a very flat arched structure and this may introduce the 'toggle' action, resulting in displacements and stresses no longer being proportional to load. This would lead to a substantial reduction in safety factor against instability of the whole barrel vault.

If the area to be roofed is long compared with its width, and internal stanchions are not allowed, continuous braced barrel vaults are used. The recently constructed single-layer barrel vaults in Germany and Romania provide a typical example of such an arrangement, where the long barrel vaults are subdivided into several shorter barrel vaults, supported internally by stiffening space trusses, integrally interwoven into the framework of the structure (Fig. 1.5). The latticed longitudinal trusses, when interconnected, form a braced barrel vault, which may have a circular, elliptical or two-centred arch type cross-section. Usually designers prefer to use trusses of identical dimensions. The lattices can also be arranged to form single or continuous or monitor roofs or even north light roofs. Several roof structures built over factories in the early 1960s and designed by Mr F.J.Samuely are typical examples of such arrangements.

As a rule, the earlier types of braced barrel vaults were constructed as single-layer structures. Nowadays, with clear spans approaching 100 m, double-layer systems are used occasionally. Typical examples are provided by double-layer barrel vaults of a two-way rectangular grid type built in the MERO or TRIODETIC systems.

Large span barrel vaults used in the construction of aeroplane hangars are usually supported directly along their sides on foundation blocks. The sides of the barrel, with low headroom, are generally used for offices or stores. In order to restrict the length of compression members, especially in very wide vaults, a large number of lattices are required. This will produce nearly collinear lattices, with the consequent danger of instability. This can be avoided by the use of double-layer braced barrel vaults. It has also been found that the stiffness of very wide barrels can be further increased by interweaving two sets of lattices or corrugating them. In the latter case every other rib is raised above its neighbours. These 'undulated' barrels are very stiff, and alternate sloping sides can be glazed, thus producing in effect a north light roof.

The interest in braced barrel vaults and the advantages offered by this type of construction led to the introduction of several novel types of bracing. In the original work of Föppl, the basic form of the barrel vault consisted of longitudinal members interconnected to vertical semi-circular ribs and stiffened by diagonals. If the barrel vault is supported on the ground then an improved system can be obtained by interconnecting two groups of arches, joining them together into a space diagonal grid. This has the added advantage of providing a very uniform type of stress distribution, even in long barrel vaults.

This particular arrangement has, of course, already been used in the timber lamella structures originally introduced by Zollinger. In timber structures, the overall stability was obtained through the use of timber boarding nailed to the lamellas and providing a continuous surface for roof covering. In steel structures the stability relied on secondary purlins running in the longitudinal direction. Soon the designers realised that, instead of using a diagonal system of arches stiffened with a secondary system of purlins, the three-way grid bracing provided the easiest solution and also a remarkable degree of rigidity, forming a fully triangulated framework.

@Seismicisolation

Cylindrical barrel vaults are developable surfaces and therefore the three-way grid enables the construction of such systems using equilateral triangles, composed of modular units which are of identical length and which can be interconnected with simple node connectors, the same for the whole structure.

4 EARLY RESEARCH OF STRESS DISTRIBUTION IN BRACED BARREL VAULTS

The author of this chapter has taken a particular interest in braced barrel vaults since 1953 (Fig. 1.6), and since that time numerous dissertations and publications have been produced as a result of research investigations carried out under his guidance, first at Imperial College of Science and Technology, then at Battersea College of Advanced Technology, and now at the University of Surrey. References 2, 6, 8, 19, 20, 21 and 31 give full details of these investigations. One aspect of this research referred to the influence of

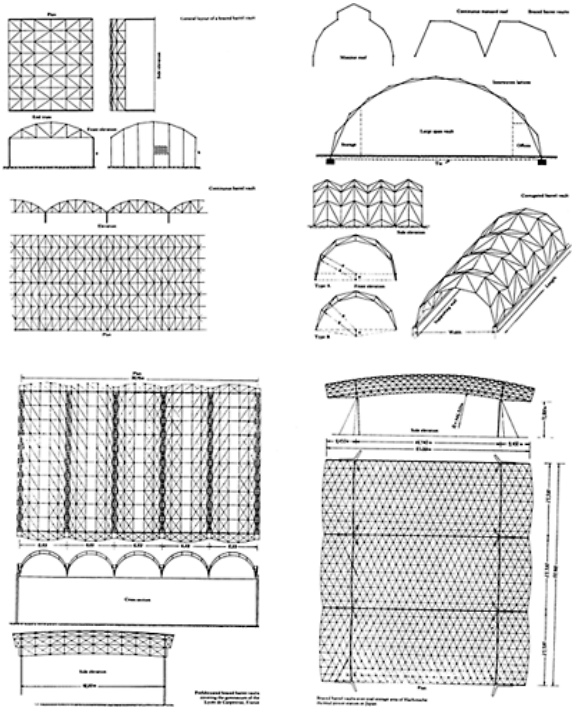

Fig. 1.5. Various arrangements of braced barrel vaults used in practical applications.

@Seismicisolation

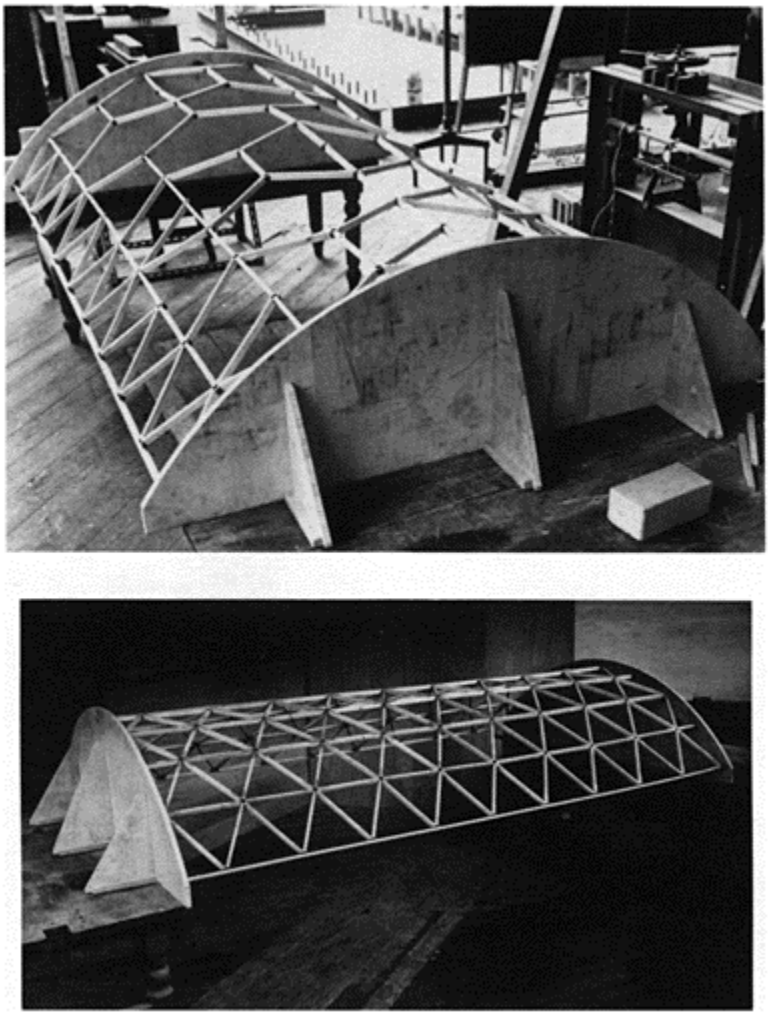

Fig. 1.6. Timber models of three-way grid barrel vaults used by the author in his early experimental work.

different types of bracing on the resulting stress distribution. 20 years ago, the detailed theoretical investigations encountered great computational difficulties. The comparative studies at that time were carried out on small-scale models, some of which are reported by the author in Ref. 13. All the models under investigation had the same length, width and rise. Their bracing members were arranged in such a way that the total weight of the material used to construct the models was almost the same in each case (Fig. 1.7).

The experimental tests on the models proved beyond any doubt that there are significant differences in the behaviour of the structures, and that the type of bracing has

@Seismicisolation

a fundamental influence upon the strength and load-carrying capacity of the braced barrel vaults. The three-way single-layer braced barrel vaults exhibited a very uniform stress distribution under uniformly distributed load covering the whole area (resulting therefore in the design of structures consisting of almost identical component members), and much smaller deflections in the case of unsymmetrical loading than for any of the other types of

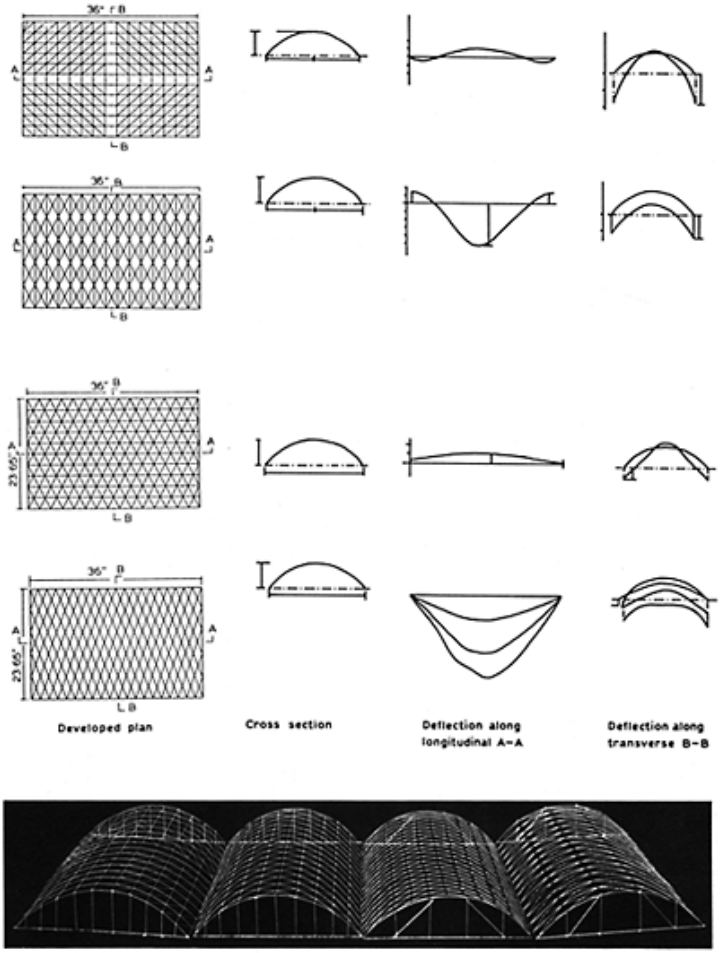

Fig. 1.7. Small scale models of barrel vaults having four different types of bracing used by the author in his research.

@Seismicisolation

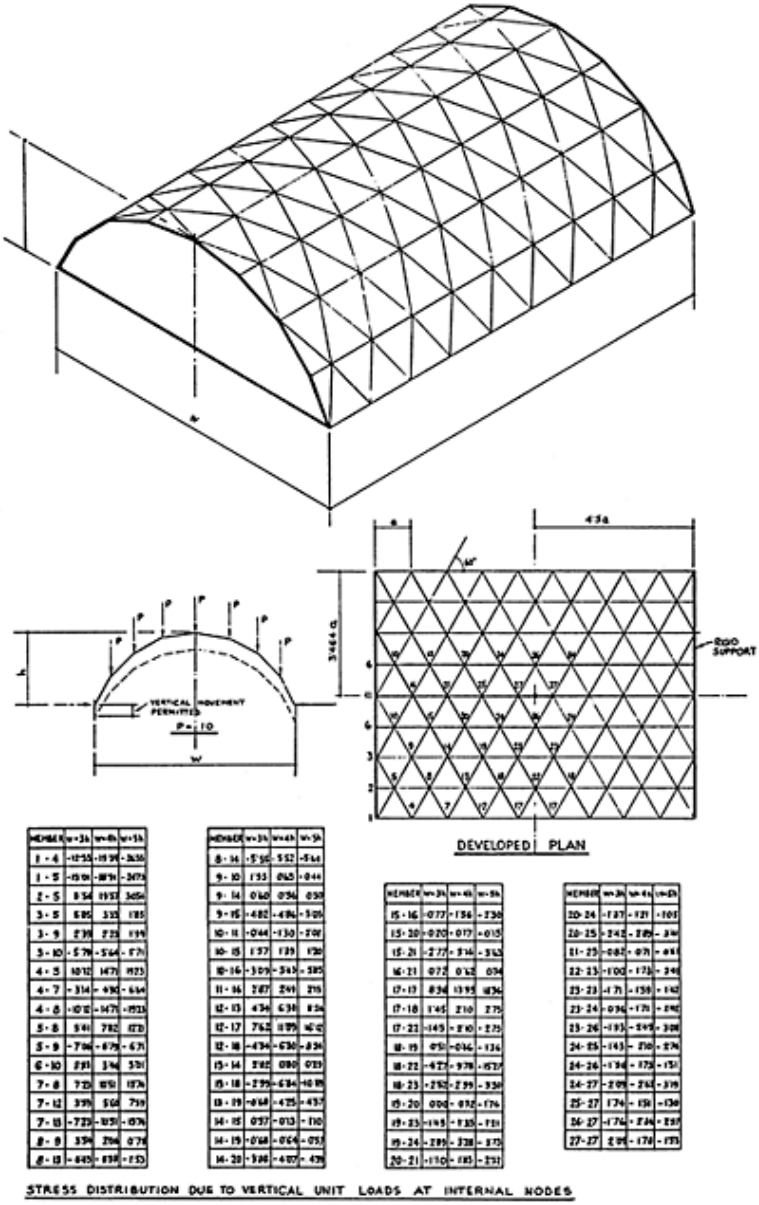

Fig. 1.8. Variation of axial loads in a three-way grid-type barrel vault as a function of the rise-to-span ratio.

@Seismicisolation

bracing. Figure 1.8 shows the variation of axial loads in a three-way grid-type barrel vault as a function of the rise-to-span ratio. An example of a diagonal grid bracing used for a barrel vault covering a tennis court is shown in Fig. 1.9.

5 PRACTICAL APPLICATIONS

5.1 American Examples

Perhaps it should be mentioned that after the introduction of the timber lamella system into the USA around 1925 by Dr Kiewitt the gradual acceptance of this form of construction for numerous large-span gymnasia, ice rinks, etc. eventually led to the formation of an association of twelve American firms specialising in the construction of lamella structural systems (Fig. 1.10).

Thousands of steel structures have been built in the USA using this system within the last 30 years. The remarkably beautiful and highly economical lamella structures

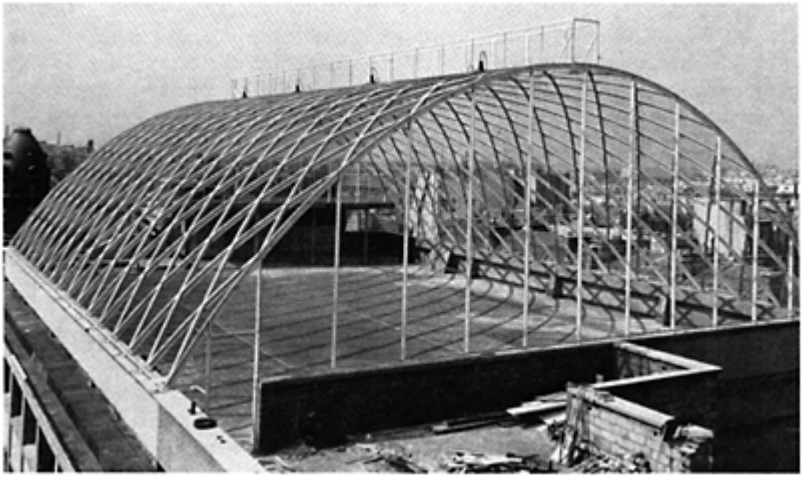

Fig. 1.9. A diagonal grid bracing used for a barrel vault covering a tennis court on top of a building in Paris.

@Seismicisolation

Fig. 1.10. An example of a steel lamella barrel vault designed by Roof Structures, Inc.

produced by Roof Structures, Inc. of St. Louis, Mo., are especially well-known. The detailed methods of analysis of these structures are given in Refs. 6 and 27.

5.2 Japanese Examples

A modified version of this system was introduced to Japan after the Second World War. The Tomoegumi Iron Works Ltd of Tokyo took a special interest in this form of construction, putting on the market the 'diamond' type of barrel vault composed of steel latticed members which, when interconnected by bolting, form a three-way space grid in which all the structural members share the load. This results in a highly economical prefabricated structure without any idle members.

One of the first braced barrel vaults known world-wide was designed by Dr Fujio Matsushita, now the Executive Managing Director of the Tomoegumi Iron Works; this is the structure over the coal storage area of Hachinoche Thermal Power Station in Japan. The structure consists of three braced barrel vaults covering an area of 65 m×66·9 m, supported at only 8 points. It is illustrated at the bottom of Fig. 1.5. The structural designer received a special prize for this beautiful and highly economical structure.

The Japanese experience highlights the remarkable advantages connected with the simplicity of erection of these structures. The usual method of erection relies on forming interconnected unit triangles and producing a rigid and self-supporting structure which itself serves as a scaffold. No separate scaffolding is required for support. For that reason the 'diamond' structures are often referred to as the 'no-scaffolding erection' system. Practical experience shows that large quantities of auxiliary construction material, required conventionally, can be eliminated; the construction period is shortened and large span structures can be built without any hazard at very competitive prices.

Tomoegumi Iron Works Ltd have built numerous steel braced barrel vaults of this type within the last few years, many of them outside Japan in other countries. Some of them have a clear span of almost 100 m. These structures have been found suitable for hangars, car sheds, industrial buildings, warehouses, indoor sports stadia and gymnasia (Fig. 1.11). The interest expressed by many Japanese designers in this form of construction led to a

@Seismicisolation

great deal of original research done within the last few years at various Japanese universities and government research establishments.

More information about the work of Dr Matsushita is contained in the author's article surveying the progress of steel space structures in Japan.[15]

5.3 Czechoslovakian Examples

When discussing steel barrel vaults, one must mention especially the work of Joseph Zeman.[32],[33] This engineer was responsible for the design and construction of many steel barrel vaults built during the last fifteen years in Czechoslovakia and East Germany. His work shows clearly that impressive economies in cost and material consumption can be obtained for large span buildings constructed as steel prefabricated space frames.

Zeman covered numerous sports and public halls in Czechoslovakia with tubular steel segmental barrel vaults. His structures consist of prefabricated units 8 m long, weighing some 200 kg, interconnected into a system of diagonally arranged arches. All the units are of identical dimensions built on a specially prepared rig. This enables minimum tolerances. The main system of segmental arches is supplemented with another system of load-bearing purlins spaced at approximately 2·5 m and arranged in the longitudinal direction of the barrel vault. These purlins stiffen the arch system and convert the whole assembly into a three-way spatial grid. Figure 1.12 gives details of a steel barrel vault designed by Zeman. This structure covers an ice rink and has a clear span of 80 m.

Fig. 1.11. Internal view of Joban Hawaiian Leisure Centre, span 80 m, length 82·7 m, designed by Tomoegumi Iron Works Ltd.

@Seismicisolation

The prefabricated units lend themselves easily to stacking, require little storage area, are light in weight and can be handled manually. There are eight high-tensile bolts at every joint, connecting not only the four main units but also the chords of the purlin members. The recent articles by Professor Lederer would also be of interest, describing in detail many such structures erected recently in Czechoslovakia.[9],[10]

5.4 French Examples

The activities of Monsieur Stéphane du Château in France in the field of steel space structures are already well known. The bottom of Fig. 1.5 shows a layout of five barrel vaults covering the gymnasium of the Lycée in Carpentras in southern France. The detailed analysis of this structure, carried out by the author in 1960 for Monsieur du Château, was one of the first attempts to take into account the rigidity of joints in the determination of stress distribution in a barrel vault of this type. Due to the light weight of the structure, wind loading produced reversal of stress, necessitating the use of double-bracing systems for all diagonals which, being long and very slender, could resist tension only, but would be unable to take compression.

The analysis was based on the assumption of rigid joints between the longitudinal and semicircular rib members, taking into account not only their axial, but also their flexural rigidities.

Another even more interesting example of a barrel vault designed by du Château is the

@Seismicisolation

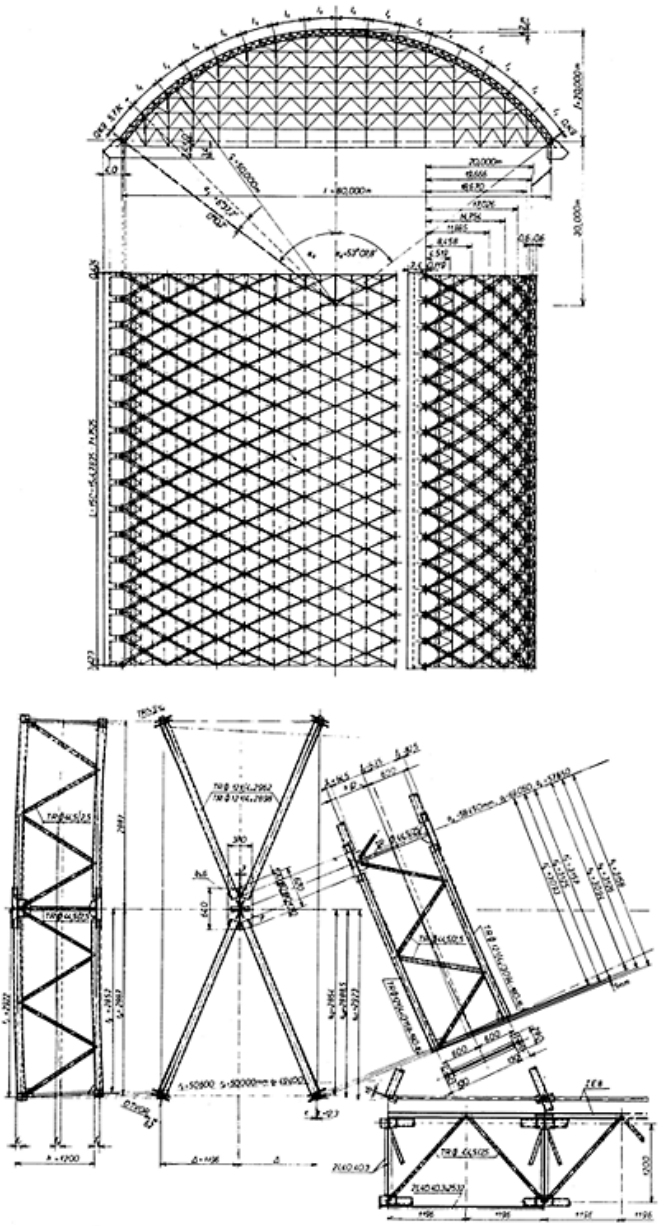

Fig. 1.12. Plan of an ice rink in Czechoslovakia covered with a steel lamella barrel vault having a clear span of 80 m.

@Seismicisolation

covered tennis court for the SNCF at Paris-Vaugirard, giving an almost classical example of the structural simplicity and architectural purity of a three-way grid barrel vault. The covered area of this tennis court is 18 m×36 m, roofed in by a single-layer three-way grid built in tubular members. This structure was prefabricated in longitudinal parts, each having a width of two basic elements. These prefabricated units were erected on the site, supported temporarily by light poles, leaving a gap between the adjacent units of one module. Then, the additional members were inserted between the two parts and welded on site to the nodal points. All the members of this structure have the same length (Fig. 1.13).

A further example of a braced barrel vault designed by Monsieur du Château is the

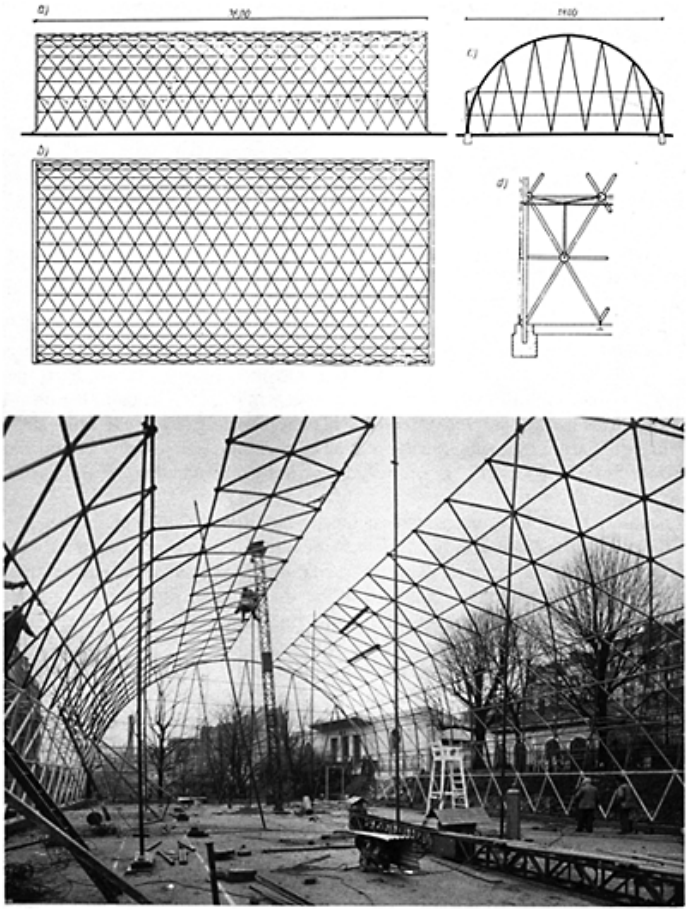

Fig. 1.13. Plan of the Vaugirard barrel vault and a photograph illustrating the method of erection.

@Seismicisolation

structure erected in 1977 in Montpellier and covering a sports hall of the Centre Sportif Universitaire. The structure covers an area of 42 m×23 m and provides an example of an interesting modification of the usual three-way grid. It was constructed in large prefabricated parts which were bolted together using high tensile bolts. The analysis was carried out in the Space Structures Research Centre, taking into account the rigidity of joints. Computer analysis showed that the dead weight stresses are quite small, but the wind loading produced the critical forces. This study provided the opportunity of comparing three different methods of determination of the wind pressure on cylindrical barrel vaults. The simplified methods of the determination of wind forces acting on structures assumed that wind blowing against the structure produces pressure on the windward side and suction of the leeward surface of the roof. There are many empirical formulae giving the numerical values of the coefficients of the pressure and suction. The most commonly used formula is:

$$p = \rho_0 \sin\alpha$$

where ρ_o=intensity of wind pressure on the surface perpendicular to the wind direction and α=the subtended angle of the part of the barrel measured from the vertical line passing through the centre. This formula produces zero wind forces at the top of the barrel.

Unfortunately, wind tunnel tests show a different distribution. The formula given by the British Standards Institution (Chapter V—Loading, part 2—Wind Loads, 1972), provides a more reliable means of determination of the wind distribution. However, the numerical coefficients obtained by this approach differ from those obtained by the formula suggested by the French code of practice. Figure 1.14(a) gives the comparison of the curves illustrating the distribution of external wind pressure according to the three different approaches. In practical design the final wind forces depend also on internal suction or pressure which may develop inside the building. Figure 1.14(b) shows the resultant distribution following the use of the BSI formula. Reference 16 contains details of the distribution of axial forces produced by wind in the members of the barrel vault built at Montpellier.

Monsieur du Château's studies into various possibilities provided by three-way single-layer types of braced barrel vaults also include architectural investigations into cylindrical structures having half semi-spherical domes arranged at the ends of the barrel vaults (Fig. 1.15). The studies carried out by du Château indicate some extremely interesting possibilities provided by the interconnection of several barrel vaults (Fig. 1.16).

The development of the Formex algebra originated by Dr H.Nooshin at the Space Structures Research Centre at the University of Surrey opened new horizons for the analysis and design of complex types of space frames. This new and extremely powerful technique enables the algebraic representation and rapid processing of the configuration of virtually any type of braced barrel vault. Figure 1.17 shows the examples of studies of three-way single-layer barrel vaults carried out by Dr Jaime S.Sanchez Alvarez, a former research student of the Space Structures Research Centre. Using this technique, the designer can easily introduce changes in the geometry of his structure by a modification of the various parameters defining the external shape, e.g. the rise, span, width, boundary conditions, type of bracing, etc.

@Seismicisolation

These are no longer purely academic studies—architects are increasingly interested in more unconventional shapes of barrel vaults.

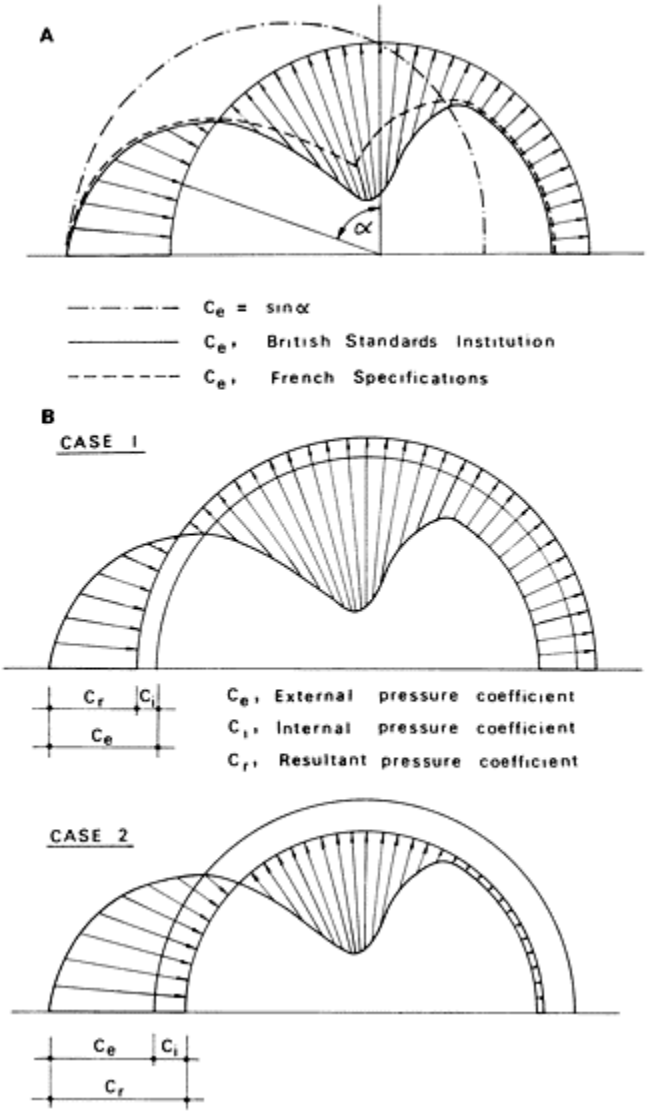

Fig. 1.14. Wind distribution curves for cylindrical barrel vaults.

Figure 1.18 illustrates the perspective drawing of the unusual steel roof structure erected in the USA over the L.Stockwell Jadwin Gymnasium at Princeton University. Located at the southern end of Palmer Stadium, the gymnasium is built on a site which slopes

@Seismicisolation

downward to Lake Carnegie. The roof framing consists of two space frames, the half-dome of elliptical cross-section covering the tennis courts, interconnected with a conical barrel vault which extends over the basketball court. The structure consists of a series of ribs stiffened by a system of diagonally arranged bracing members.

The half-dome is supported at its junction with the barrel vault by a trussed arch spanning over 104 m. As one roof area frames into the top chord of the arch, the adjoining barrel vault frames into the bottom chord, forming a continuous skylight some 6 m high.

This complex structure has been analysed as a space framework using the data generated for the 'Fran' stress analysis program. The perspective of the structure shown in Fig. 1.18 was made automatically by a tape-controlled plotter.

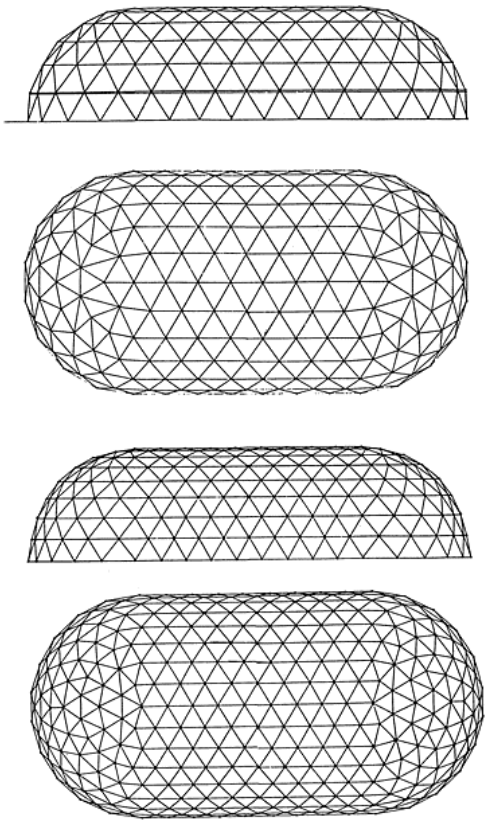

Fig. 1.15. Examples of barrel vaults with semi-spherical domical ends.

This and various other examples show clearly that, with the recently developed computer techniques, designers are able to deal with such structures without undue difficulty.

@Seismicisolation

Figure 1.19 shows a plan of a large span double-layer roof structure over a stadium. In this case the central part constitutes a cylindrical barrel vault interconnected integrally at each end with double-layer half-domes. A very convincing example of such systems is provided by the recently completed two double-layer skeleton huge cantilevers covering the grandstands of the Split Stadium in Yugoslavia, constructed in the MERO system. This structure has unsupported free edges along a distance of 215 m.

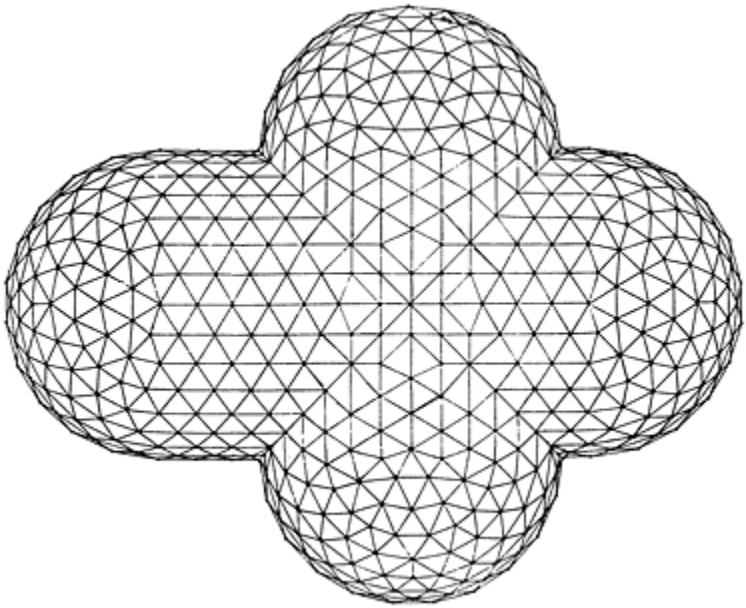

Fig. 1.16. A study of a structure consisting of several interconnecting barrel vaults.

The recent studies in double-layer braced barrel vaults highlight the remarkable rigidity of this form of construction. This has been realised by many designers and, as a result, several highly interesting double-layer braced barrel vaults have been erected very recently.

One should refer especially to the Miami Arch barrel vault completed in 1984 by the Space Structures International Corporation of New York as a large hangar at Miami International Airport for the Pan Aviation Incorporation. This barrel vault has a clear span of 226 ft (68·9 m), height of 65·38 ft (19·92 m) and length of 182·69 ft (55·68 m). The total weight of the aluminium tubular framework is only 90000 lb (40824 kg). This gives a remarkably low dead weight of the structure; only 2·2lb/ft^2 (10·6 kg/m^2). The barrel vault is supported by two edge arches which are 182 ft (55 m) apart. The Miami Arch barrel vault was assembled in three sections requiring only 125 man days. Two other similar structures, designed by the same firm, have been recently shipped in three Boeing 707 aircraft, to Baghdad and erected by the local Iraqi labour force.

@Seismicisolation

Figure 1.20, generated by the computer, shows the perspective and elevation of this remarkable structure, as well as details of the joint developed by the firm. The structural framework is a two-way double-layer grid arranged as a cylindrical barrel vault. The basic module size of the grid is 13·04 ft×13·04 ft (3·97 m×3·97 m).

Another even more recently completed structure is a complex of five interconnected double-layer two-way braced barrel vaults built in 1985 over the Serangoon Country Club in Singapore by a Dutch firm Octatube Space Structures Ltd of Delft, Netherlands, designed by Mr Mick Eekhout. Each barrel vault has a length of 20 m, is 6m wide and supported on four corner points only.

Figure 1.21 shows the overall view of this unusual structure. The five barrel vaults have three different cross-sections; the outer barrel vaults are semi-cylindrical, the central barrel vault consists of a semi-cylindrical upper portion raised on two vertical wall segments, and the two intermediate barrel vaults are unsymmetrical, having only one side extended vertically.

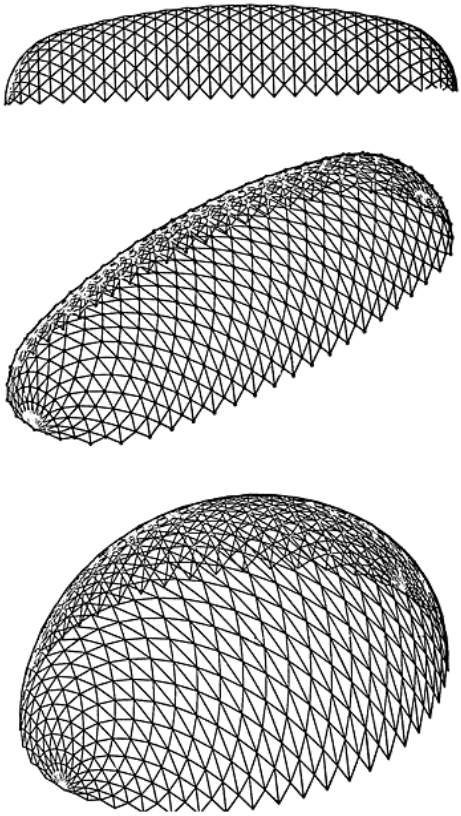

Fig. 1.17. Configurations of barrel vaults produced by computer.

@Seismicisolation

The barrel vaults are interconnected along their edges which form large suspended gutters. The supports are located only along two sides, providing an unobstructed area of 35 m×20 m without any internal supports. The structure is covered with grey tinted laminated glass panels.

One of the most remarkable features of this structure is the technique used by its designer to form the members of the top layer of the barrel vaults. These members are extruded aluminium circular profiles with integral T-profiles on their top used to support the glass panels. The glazing is sealed with silicone sealant, before the covering aluminium sealing strips are screwed to the bars. The aluminium bottom layer members support the

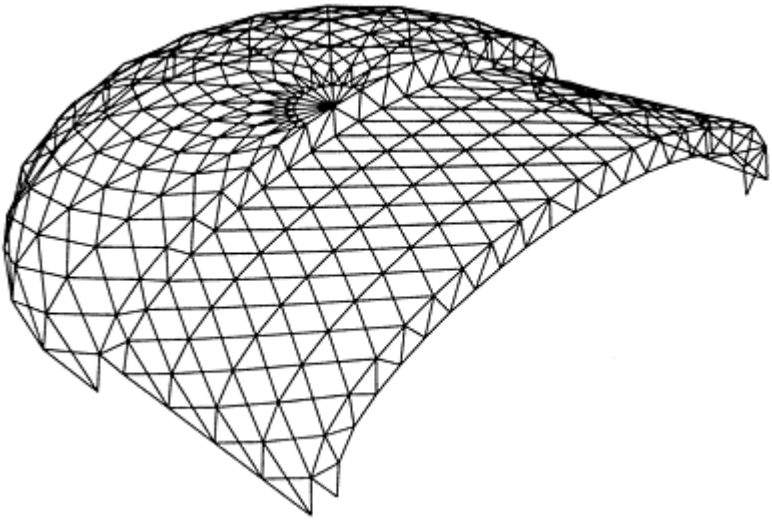

Fig. 1.18. Perspective drawing prepared by a computer of the barrel vaults over the L.Stockwell Jadwin Gymnasium.

movable sun screens which are operated from one central point. Therefore both the outer and bottom layer members have a combined stress function acting not only as structural load-carrying members but also as mullion bars, supporting either the glazing or the sun screens.

The hollow circular aluminium tubes are interconnected with the specially designed spherical nodes in such a way that all electric cables can be located inside the tubes. The

@Seismicisolation

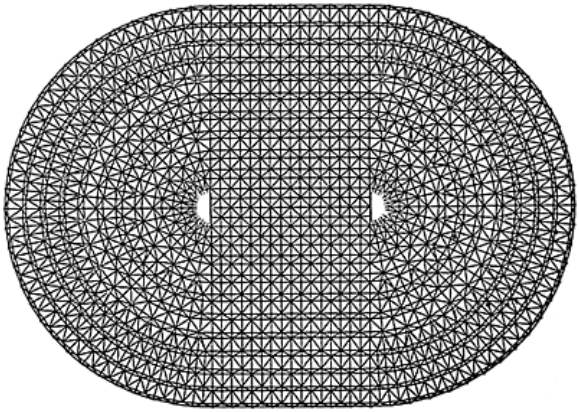

Fig. 1.19. An example of a double-layer barrel vault over a stadium.

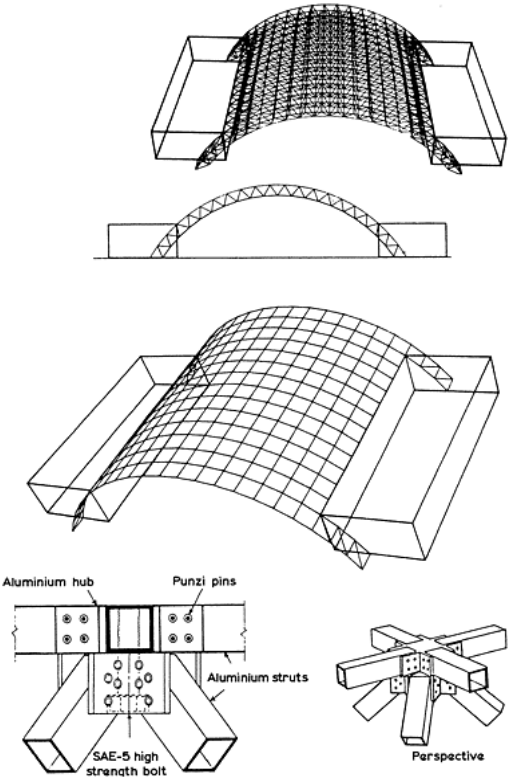

Fig. 1.20. The Miami Arch.

@Seismicisolation

combination of several different functions in one total design is the characteristic of this unusual project, completed in June 1985.

A similar double-layer barrel vault has been recently designed in aluminium by Mr Mick Eekhout as an atrium for a shopping centre in Heerlen, the Netherlands. This barrel vault is 14·4 m wide, 7·2 m high and 28·8 m long. Two different sizes of aluminium tubes have been used for this project, 50 mm×5 mm and 60 mm×5 mm. The spherical aluminium connectors have a diameter of 135 mm.

5.5 English Examples

In Great Britain, several structural engineers started to use various types of braced barrel vaults to cover large span industrial buildings after the Second World War.

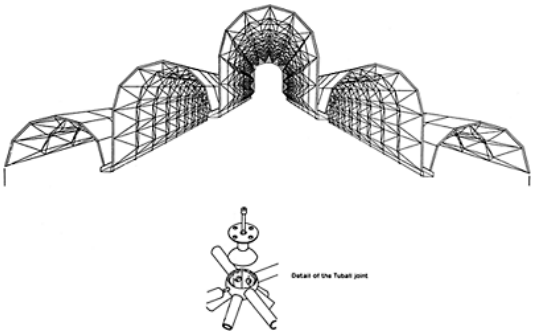

Fig. 1.21. Barrel vault completed June 1985 over the Serangoon Country Club in Singapore.

Fig. 1.22. Erection of a ‘lightweight’ shell structure.

@Seismicisolation

Fig. 1.23. Applying lightweight concrete over a barrel vault.

The ‘lightweight’ shell construction was developed by Mr Cyril Blumfield as a replacement and improvement of the more orthodox types of r.c. shells (Figs 1.22 and 1.23). Another system followed soon, introduced by Messrs Ove Arup and Partners and manufactured by Scaffolding (Great Britain) of Mitcham, Surrey.

This system was known as the lattice shell’ (Figs 1.24 and 1.25). Whereas Mr Blumfield’s type can be described as the rectangular space grid, the ‘lattice shell’ was the precursor of the so-frequently used ‘three-way’ single-layer grid forming a fully triangulated system. Providing a network of support for cladding over large areas, the ‘lightweight shell’ or the ‘lattice shell’ offered the cleanness in design of an r.c. shell with greater flexibility in the choice of position of daylighting. The lattice shell’ used tubular members, whereas the ‘lightweight shell’ used a combination of the various types of more orthodox structural shapes.

Numerous industrial sheds have been covered with these systems. In England many of them were clad with corrugated asbestos cement sheets, hook bolted; some structures were covered with transparent sheet, glass or resin-bonded fibreglass cladding panels. Often expanded metal permanent shuttering was wired under the framework and lightweight concrete spread over the barrel vaults giving good heat insulation and an

@Seismicisolation

adequate foundation for water-proofing. The structures built showed that the form of barrel vaults is not limited to cylindrical shells; indeed many of them were designed as barrels curved in two directions.

One of the most interesting examples of the economical use of tubular three-way type barrel vaults is provided by the roof over the multi-storey 'M' shed in the India and Millwall Docks at the Port of London. This building was designed as a transit shed on ground and first-floor levels, with 'out of time' storage on the second floor. The roof

Fig. 1.24. A 'lattice shell' barrel vault over a shed structure.

@Seismicisolation

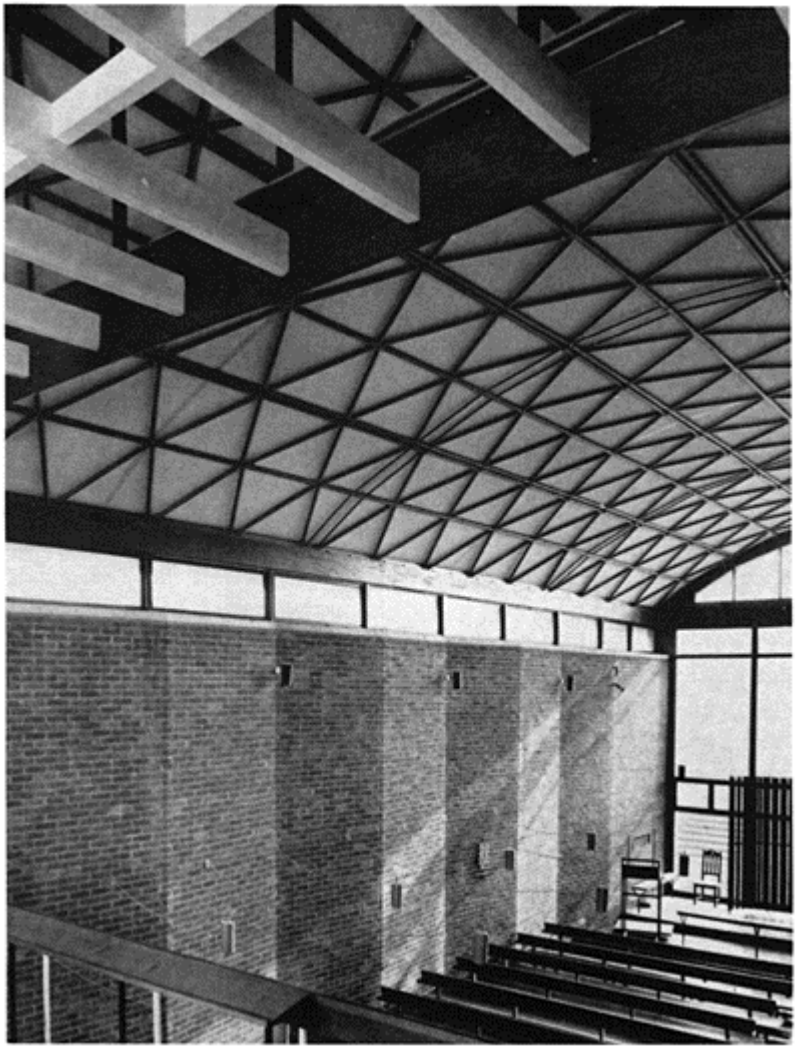

Fig. 1.25. An example of 'lattice shell' barrel vault used for a church.

structure of this building is of particular interest, consisting of seven steel braced barrel vaults, each of 23 m span with a rise of 4·9 m and a radius of 16·1 m. These vaults have been constructed of hollow sections (RHS). The structure was prefabricated in flat fully-triangulated trusses, shop welded in lengths convenient for transportation to site where they were then welded in position to form the barrel vault.

A structural computer analysis and a model test were carried out at the Space Structures Research Centre on behalf of the consulting engineers, Messrs Harris and Sutherland.[25]

@Seismicisolation

6 RECENT DEVELOPMENTS IN TIMBER BARREL VAULTS

A special mention must be made here of several beautiful and economical timber barrel vaults erected in Suffolk, England by the progressive architectural practice of Johns, Slater and Haward of Ipswich.

Fig. 1.26. Internal view of the three-way barrel vault built in timber over a sports hall for the Silver Jubilee Girls Secondary School at Bury St Edmunds.

@Seismicisolation

These architects, who have taken a special interest in timber shell structures, proved that in addition to the architecturally exciting shapes, their structures can be appreciably cheaper per square metre of floor space than the more orthodox forms of sports halls. Indeed in several cases the designers claimed that their structures can be cheaper by more than 25%. This remarkable reduction in the final cost has been achieved not only because of the lightweight shell construction, but also because of significant savings in the surface area of the curved roof forms and reduction or elimination of external walls.

A report on 'Timber domes in the Ipswich area', prepared by Mr Birkin Haward in 1975 for a competition arranged by the Timber Research and Development Association, contains a wealth of interesting details concerning timber domes and barrel vaults designed by the above-mentioned architectural firm.

After experimentation with timber geodesic domes their firm developed a modified dome form suitable for covering gymnasia, tennis courts and sports halls, as a combination of a semi-spherical end section and a central barrel vault.

A tennis court for the Silver Jubilee Girls Secondary School at Bury St Edmunds built in 1968 is probably the best example and is shown in Fig. 1.26. This structure covers an area of 36·6 m×18·3 m (120 ft×60 ft) with a timber barrel vault, having a pointed ridge. The ends were made of the same curvature as the sides producing a segmented barrel vault shell.

The basic timber elements are arranged into a three-way grid pattern; they are 150 mm×50 mm in cross-section and are glued and screwed at the nodal points.

The frame was clad by 150 mm×25 mm tongued and grooved boarding and weather-proofed with 'Evade' built-up bituminous roofing with silver paint finish. The architectural design was prepared in this case in collaboration with the structural engineers, Messrs Stepien and Winiarski, of London.

One must also draw attention to the equally beautiful timber structure for the Halifax Primary School, built in 1971, and covering an area of 16·7 m×30·7 m, as well as the sports halls for the Primary Heath School, 1972, square on plan, 33·8 m, the Handford Hall School, 1972, and the remarkably economical barrel vault for the Thurleston School, 1973, 35 m×25 m. The architects, Johns, Slater and Haward of Ipswich, were responsible for all these structures, showing that structural timber, when used properly, can provide highly efficient solutions.

7 SELF-WEIGHT OF BRACED BARREL VAULTS

The self-weight of steel barrel vaults is relatively small and may be almost negligible in comparison to the snow and wind loads to which these structures will be subjected. Wind tunnel tests carried out within the last five years in the Department of Civil Engineering at the University of Surrey show that the distribution of wind pressure on barrel vaults depends upon the rise-to-span ratio. Unfortunately, only very scarce information exists in the technical literature on the experiments on wind action on barrel vaults.

The studies carried out by Z.S.Makowski and Chi-Wai Wong[17] show that for lightweight barrel vaults (built in steel or aluminium) forces induced in the members of the structural framework can be much larger than the forces induced by self-weight. The design of the components of the barrel vault is therefore often governed by wind forces.

@Seismicisolation

Correct estimation of wind forces and their distribution on the external surface of the barrel vault is therefore of primary importance. On the other hand, the codes of practice provide only a rough indication of the wind pressure distribution on such structures. Application of different codes of practice results in the determination of different forces; the differences can be quite considerable.

A more rational approach than that stipulated by the codes of practice is necessary. This shows clearly that more research is urgently needed and wind tunnel tests are essential to determine with greater accuracy the possible wind forces.

Wind forces can produce a stress reversal in many members and therefore most members have to be designed to resist tension *and* compression. The slenderness ratio of the members is therefore of paramount importance. Configuration in which all members are of the same length is obviously more efficient. This explains one of the reasons for the present popularity of the three-way type of bracing used in many designs of braced barrel vaults.

The comparison of dead weight of steel and aluminium braced barrel vaults designed during recent years in various countries shows that some remarkably light structures can be obtained. This obviously depends on several factors, e.g. the intensity of the superimposed load, clear span, type of bracing and method of supporting. Figure 1.27 gives some useful information on the self-weight Triodetic single-layer tubular braced barrel vaults in steel or aluminium.

The survey of the technical literature shows that some designers have been able to achieve very low steel consumption for their braced barrel vaults. R.Dziewolski claims that for the hangar for Marine Nationale at Brest, having a clear span of 27 m, the dead weight of the structural framework is only 13 kg/m^2.[5]

Zeman, who built numerous barrel vaults in steel in Czechoslovakia, achieved for his winter sports stadium in Kladno roofed with a segmental braced barrel vault over an area of 60 m×60 m a steel consumption of 18·28 kg/m^2, whereas his structure for a winter

@Seismicisolation

Triodetic Barrel Vaults and Toroidal Shells
(Ratio of Height to Width = 1:4)

Bay size	Intensity of External Loading	Aluminium tubes: Max dia of tube	Aluminium tubes: Min dia of tube	Aluminium tubes: Structural Weight	Steel tubes: Max dia of tube	Steel tubes: Min dia of tube	Steel tubes: Structural Weight
20' x 40' (6.1m x 12.2m)	15 psf (73.2kg/sq m)	2" (51mm)	2" (51mm)	1.44 psf (7.0kg/sq m)	1½" (38mm)	1½" (38mm)	2.82 psf (13.8kg/sq m)
	30 psf (146.5kg/sq m)	2" (51mm)	2" (51mm)	1.50 psf (7.3kg/sq m)	1½" (38mm)	1½" (38mm)	2.95 psf (14.4kg/sq m)
	60 psf (292.9kg/sq m)	4" (102mm)	4" (102mm)	3.09 psf (15.1kg/sq m)	3" (76mm)	3" (76mm)	4.85 psf (23.7kg/sq m)
30' x 60' (9.1m x 18.3m)	15 psf (73.2kg/sq m)	2¾" (70mm)	2¾" (70mm)	1.44 psf (7.0kg/sq m)	2" (51mm)	2" (51mm)	2.62 psf (12.8kg/sq m)
	30 psf (146.5kg/sq m)	3" (76mm)	3" (76mm)	1.80 psf (8.8kg/sq m)	2" (51mm)	2" (51mm)	2.62 psf (12.8kg/sq m)
	60 psf (292.9kg/sq m)				3¼" (83mm)	3¼" (83mm)	4.76 psf (23.2kg/sq m)
40' x 80' (12.2m x 24.4m)	15 psf (73.2kg/sq m)	3¼" (83mm)	3¼" (83mm)	2.39 psf (11.7kg/sq m)	2¼" (57mm)	2¼" (57mm)	2.76 psf (13.5kg/sq m)
	30 psf (146.5kg/sq m)				3¼" (83mm)	3¼" (83mm)	3.30 psf (16.1kg/sq m)

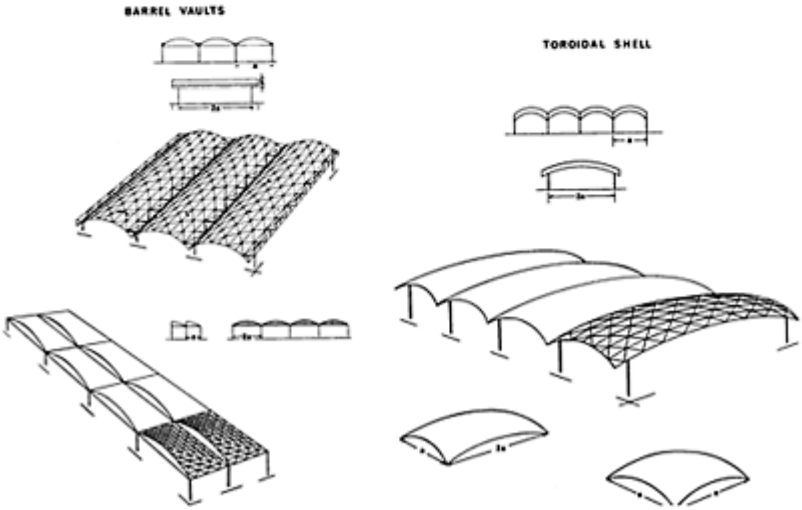

Fig. 1.27. Self-weight of Triodetic barrel vaults and toroidal triangulated shells.

@Seismicisolation

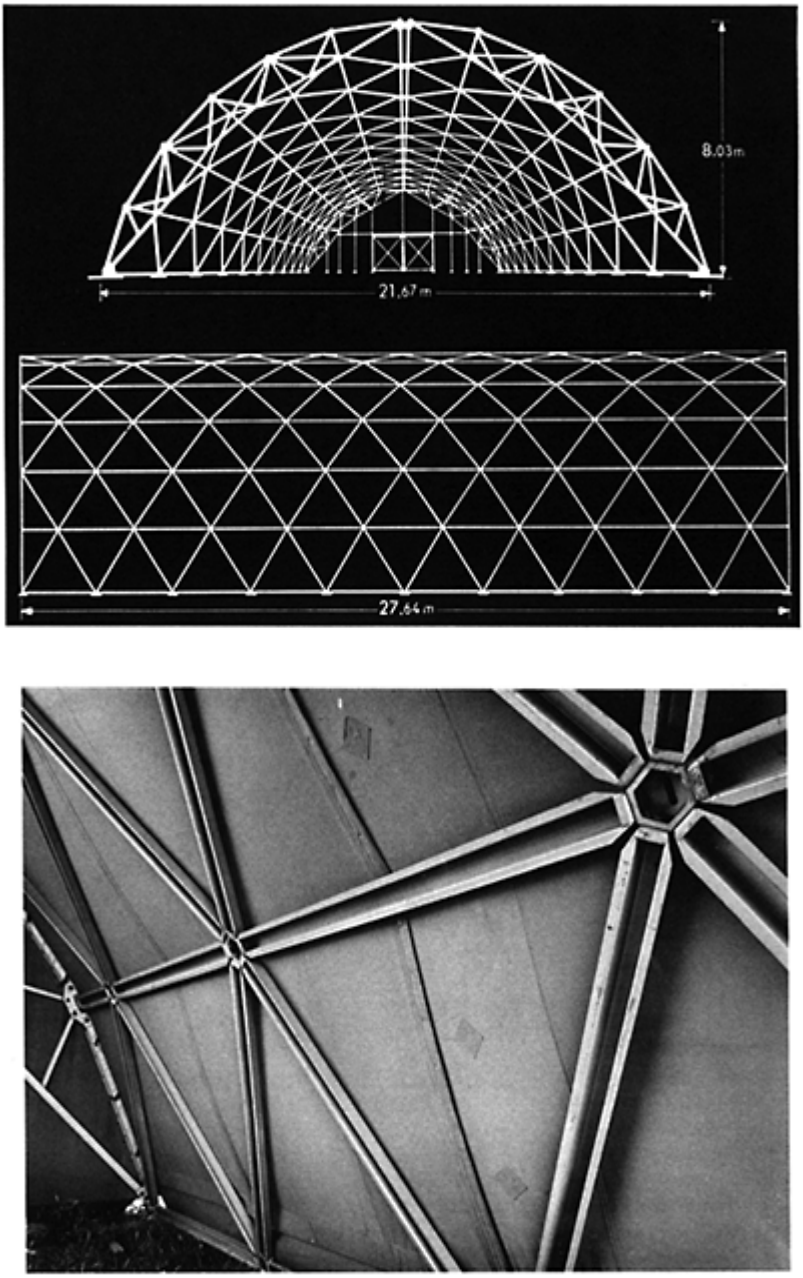

Fig. 1.28. Details of connection used in the TeZet barrel vaults.

@Seismicisolation

sports stadium in Berlin for an area of 59 m×75 m required a steel consumption for the roof structure of 21·38 kg/m^2.

Similarly favourable characteristics of structural steel requirements were obtained for two braced barrel vaults built in steel for sports stadia in Opole and Sosnowiec in Poland.

The single-layer braced barrel vault system 'Ruhland', developed in East Germany, requires only 12·4 kg steel per m^2 for a clear span of 17 m.

The prefabricated Wuppermann braced barrel vaults, at one time very popular in West Germany, and constructed in cold rolled steel sections, used 20·2 kg/m^2 of structural steel for a clear span of 22 m. This system, known in Germany as the TeZet barrel vault, consists of members, all of the same length, interconnected by bolting. Garages, workshops, exhibition pavilions and even hangars were covered in Germany using this system. Figure 1.28 illustrates the details of connection used in the TeZet barrel vaults.

8 ANALYSIS

The exact analysis of braced barrel vaults presented a difficult problem before the introduction of electronic computers. In the past these structures were analysed as pin-connected, but because of large numbers of constituent bars, the classical methods of analysis proved to be extremely tedious and time-consuming. The rigid joints have posed additional computational problems. Various attempts have been made to take into account a partial influence of rigidity of the longitudinal members. In this connection one should mention here the earlier techniques developed by Bleich[1] and Howley and Makowski.[7]

Their methods, by necessity, made simplified assumptions and certain approximations. Solutions have also been obtained using relaxation techniques or influence coefficients methods, but all these take far too long a time to be of any practical importance.

Shell analogies or folded plate analogies have been used in the past, but they provide only an approximation of the stress distribution in these structures and nowadays almost exclusively the analysis of braced barrel vaults is carried out by electronic computers. There are still some limitations imposed by the storage capacities of computers, though storage requirements are greatly reduced by utilising properties of symmetry, which the structure may exhibit. Normally, the stiffness method is applied.

The experimental and analytical work on braced barrel vaults carried out at the Space Structures Research Centre of the University of Surrey led to the production of a general computer program for the exact analysis of braced barrel vaults, assuming pin-connected or rigidly connected joints.

Subsequent studies emphasised the great influence of rigidity of joints on stress distribution in single-layer braced barrel vaults. The experiments show that large span slender single-layer braced barrel vaults are prone to instability, especially under the action of heavy unsymmetrical loads, and that the rigidity of joints exerts an important influence on the overall stability of the structure.

Rigid joints will modify greatly the deflections and the stress distribution in single-layer braced barrel vaults. The results obtained assuming pin-connected joints differ appreciably from those calculated for rigid joints. The percentage of the difference varies according to the different type of bracing, e.g. the three-way type grid shows much

@Seismicisolation

smaller differences than the rectangular type of bracing. There are, of course, certain types of barrel vault which cannot be analysed as pin-connected. They are unstable in this condition under unsymmetrical loads. Vaults having bracing arranged in a hexagonal regular pattern belong to this group. They must be analysed and constructed with rigid joints.

Detailed studies on braced barrel vaults carried out at the Space Structures Research Centre show that the behaviour of single-layer barrel vaults is affected appreciably by the imposition of different boundary conditions. The analyses show that the linear elastic analysis of pin-connected structures should be treated only as the first step in the determination of the load carrying capacity of braced barrel vaults. The work of Bligh in 1971 is of special relevance.[2]

Detailed studies of the three-way type of bracing carried out by Velankar[31] and King[8] contributed much to a better understanding of the behaviour of this type of barrel vault. King's work is particularly interesting as it deals with the effect of the rigidity of the end diaphragms or end trusses supporting the barrel vault upon the stress distribution in the structure. It shows that, contrary to previously held views, the provision of very rigid end trusses (which at one time were considered to be essential by many designers) does not improve the stress distribution or reduce deflection in single-layer barrels.

Although the elastic linear analysis of these systems can now be achieved relatively easily and cheaply by the use of electronic computers, it is still difficult to obtain a reliable assessment of buckling loads for these structures. This is one of the reasons for the use of double-layer braced barrel vaults for large spans. In such systems, due to their rigidity, the risk of instability may be almost eliminated. The determination of forces due to wind action requires further research and it is suggested that the existing codes of practice should turn their attention urgently to this problem.

REFERENCES AND BIBLIOGRAPHY

1. Bleich, F. *Stahlhochbauten* (Steel Structures). Springer Verlag, Berlin, 1933.
2. Bligh, J. Analysis of a braced barrel vault. MSc Thesis, University of Surrey, 1971.
3. Chiba, N., Tagawa, K., Yamamoto, N., Takashi, N. and Matsumura, K. Reticulated cylindrical steel shell composed of single-layer with wide-flange shapes. Proceedings of the IASS, Tokyo, 1972, pp. 931–944.
4. Dickie, J.F. and Broughton, P. Stability considerations in shallow vaults and shallow domes. Proceedings of the IASS, Tokyo, 1972, pp. 793–802.
5. Dziewolski, R. Computer-aided design and optimisation of structures. Proceedings of a Symposium on Industrialised Spatial and Shell Structures, Kielce, Poland, 1973, pp. 3–23.
6. Hosseinzadeh, H. Analysis of lamella structural systems with particular reference to lamella barrel vaults. MPhil Thesis, University of Surrey, 1967.
7. Howley, M. and Makowski, Z.S. The analysis of braced barrel vaults. Proceedings of the Institution of Polish Engineers in Great Britain, London, March 1957, pp. 11−39.
8. King, P.G. A study of the behaviour of braced barrel vaults. MSc Thesis, University of Surrey, 1974.
9. Lederer, F. Raumsysteme der Stahlkonstruktionen. Preliminary Report of the International Association for Bridge and Structural Engineering, Ninth Congress, Amsterdam, 1972, pp. 467–472.

@Seismicisolation

10. Lederer, F. Component system of a steel lamella vault. Proceedings of the Second International Space Structures Conference, University of Surrey, 1975, pp. 379–381.
11. Livesley, R. *Matrix Methods of Structural Analysis.* Pergamon Press, Oxford, 1969.
12. Mainstone, R.J. *Developments in Structural Form.* Allen Lane, London, 1975.
13. Makowski, Z.S. Analytical and experimental investigations of stress distribution in steel space frames. Proceedings of the Steel Congress, Luxembourg, 1964, pp. 581–603.
14. Makowski, Z.S.*Steel Space Structures.* Chapter 2 on braced barrel vaults, pp. 80–107. Michael Joseph, London, 1965.
15. Makowski, Z.S. Steel space structures in Japan—A review of their recent developments. *Building Specification,* May 1973, pp. 51–56.
16. Makowski, Z.S. Steel braced barrel vaults. *Building Specification,* October 1977, pp. 43–50.
17. Makowski, Z.S. and Wong, C-W. Stress analysis of braced barrel vaults subjected to wind loading. Proceedings of Sino-American Symposium on Bridge and Structural Engineering, Beijing, China, September 1982, pp. 3–13–1–3–13–23.
18. Matsuoka, O., Matsui, T., Kato, S. and Koide, H. Theoretical analysis of reticulated shells. Proceedings of the IASS, Tokyo, 1972, pp. 651–662.
19. Mavrikios, C.N. Analysis and design of an aluminium single-layer barrel vault. MSc Thesis, University of Surrey, 1971.
20. Mertol, A. Design of the braced barrel vault with hexagonal unit. MSc Thesis, University of Surrey, 1971.
21. Manohar, S.N. An experimental and theoretical analysis of braced barrel vaults with particular reference to the effect of edge conditions. MSc Thesis, University of London, 1958.
22. Nooshin, H. A technique for the analysis of structures having partially constrained joints. *Civil Engineering and Public Works Review,* May 1966, pp. 599–607.
23. Pagano, M. Designing a triangulated steel vault. *Acier, Stahl, Steel,* No. 4, 1960, pp. 159–164.
24. Pagano, M., Catanzaro, C. and Pedicini, G.C. The collapse load of braced translation vaults and cylindrical barrel vaults. Proceedings of the First International Space Structures Conference, Blackwell Scientific Publications, Oxford, 1967, pp. 502–524.
25. Peake, F.G. and Shewring, R.A. A multi-storey transit shed and warehouse for the Port of London Authority. Proceedings of the ICE Paper 7148, 1969, pp. 21–37.
26. Prynne, P. A computer investigation into the behaviour of a long braced barrel vault roof. Proceedings of the First International Space Structures Conference, Blackwell Scientific Publications, Oxford, 1967, pp. 361–369.
27. Smolett, D. The lamella roof. *The Engineer,* 29 January 1960.
28. Tanaka, Y. and Mashita, K. Study on circular cylindrical frame structures. Proceedings of the IASS, Tokyo, 1972, pp. 599–608.
29. di Tommaso, A. and la Tegola, A. Double-layer space frame shells. Preliminary Report of the International Association for Bridge and Structural Engineering, Ninth Congress, Amsterdam, 1972, pp. 517–522.
30. Watabiki, I., Satoh, M. and Onoe, H. Experimental research on a cylindrical structure consisting of intersecting two-way arches. Proceedings of the IASS Pacific Symposium on Tension Structures and Space Frames, Architectural Inst. of Japan, Tokyo, 1972, pp. 945–953.
31. Velankar, S.V. Barrel vaults having three-way grid type bracing. MSc Thesis, University of London, 1965.
32. Zeman, J. A remarkable steel structure for roofing a large sports hall in Czechoslovakia. *Acier, Stahl, Steel,* No. 4, 1968, pp. 181–188.
33. Zeman, J. Eine Serie von bogenartigen in der CSSR entwickelten Konstruktionen in Lamellen-bauweise. Proceedings of a Symposium on Mass-produced Steel Structures, Praha, 1971, pp. 191–203.

@Seismicisolation

2
Introduction to the Analysis of Braced Barrel Vaults

P.MULLORD
Space Structures Research Centre, University of Surrey, Guildford, UK

1 STRUCTURAL RESPONSE OF BRACED BARREL VAULTS

We start by considering how a braced barrel vault responds when subjected to loading. This question is fundamental as an engineer cannot design or analyse any structure until he has a clear qualitative understanding of how the structure will resist its design loading.

It is useful to consider first those barrel vaults which work as if they were thin isotropic or anisotropic shell structures. This means that the in-plane stiffness in any direction is considerably greater than the bending stiffness of the structure. Three principal modes of response have been identified for this type of barrel vault.

1 Arch mode

If the structure is only supported along its sides as shown in Fig. 2.1 then it works principally as an arch structure.

This class of structure relies on circumferential bending stiffness to resist displacement in the radial direction. This type of structure is a relatively soft structure.

2 Beam mode

If a barrel vault is only supported at its ends as shown in Fig. 2.2 then it works principally as a simple beam.

This class of barrel vault will have longitudinal compressive stresses near the crown of the vault, longitudinal tensile stresses towards the free edges and shear stresses towards the supports. In comparison to the arch structure this class of structure is relatively stiff and brittle. The end support could be provided by a thin diaphragm. If the diaphragm is rigid then the structure will behave as an encastre beam instead of a pinned beam. If the diaphragm is rigid but allowed to rotate then this will only effect stresses near the end of the structure due to the St Venant effect.

3 Shell mode

If a barrel vault is supported along both sides and both ends as shown in Fig. 2.3 then the structure responds as a thin shell.

This structure looks as if it is partly an arch and partly a beam; however, to work as an arch the structure must deflect radially but this is prevented by transverse shear in the shell. This means that the loads acting on the structure will be resisted by a complex system of forces acting tangentially to the surface of the barrel vault.

@Seismicisolation

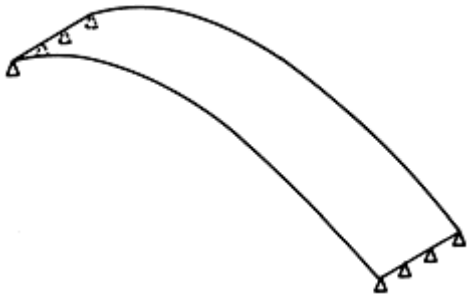

Fig. 2.1. Structure supported along sides.

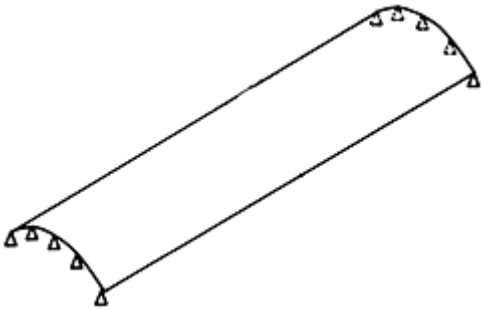

Fig. 2.2. Structure supported at each end.

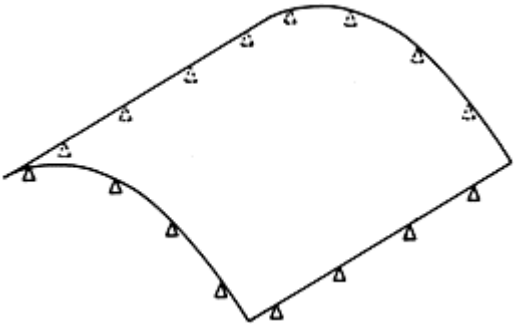

Fig. 2.3. Structure supported at both sides and ends.

A very long barrel vault supported along its sides will work partly as an arch and partly as a shell. A barrel vault supported along both sides and one end only will work as an

@Seismicisolation

arch. A barrel vault supported only at the corners will work both as an arch and as a beam.

The arch type shell barrel vaults work mainly by a system of shell bending stresses acting so as to deform the shell in a radial direction while the beam and shell vaults work mainly by in-plane shell forces. For these latter structures bending stiffness is required only to maintain the stability of those parts of the structure which work in compression.

Skeletal barrel vaults can be divided into those which are properly triangulated such as the example given in Fig. 2.4(a) and those which are not, such as the examples in Fig. 2.4(b) and (c).

Any barrel vault which is properly triangulated and also any with a stressed skin will behave essentially like the shell structures described above. Those which are not fully triangulated (and without a stressed skin) will have their own individual force distribution which will depend on the particular bracing configuration employed and will certainly include members working in flexure.

The failure mode of a braced barrel vault also depends on the configuration of the structure. The arch structures and those which are not properly triangulated will generally fail by members yielding due to bending stresses while those structures which are properly triangulated and acting as shells will generally fail by yield in tension

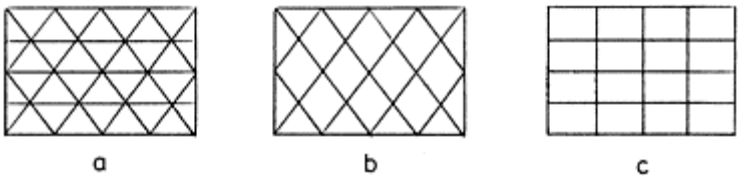

Fig. 2.4. Alternative bracing configurations.

members or instability in compression members. If the members are relatively long then the stability failure will be by simple member buckling while if the members are relatively short so that members meeting at a joint are nearly coplanar then a snap-through buckling mode involving more than one member will dominate. The buckling mode may involve just one node or a group of nodes or possibly the entire structure.

If the structure is likely to fail by snap-through instability then the designer must ensure that there is no possibility of movement occurring in the joints between erection and maximum load.

2 DESIGN OF BRACING

The simplest possible braced barrel vault is a single layer structure with bracing as shown in Fig. 2.4(c). This system is only suitable for small structures. A fully triangulated single layer barrel vault such as shown in Fig. 2.4(a) is a considerable improvement and fairly large structures of this type have been achieved.

@Seismicisolation

The use of single-layer structures is limited by stability problems. For larger structures a double-layer system should be employed. The simplest double-layer structure is probably one with simple latticed arches placed perpendicular to the longitudinal axis and linked by light longitudinal members. This type of structure will only work as an arch even when end diaphragms are available. For maximum efficiency the arches should be set at an angle to the longitudinal axis so that the structure becomes properly triangulated in the surface of the vault and full shell action can be exploited.

3 STRUCTURAL IDEALISATION FOR ANALYSIS

When we analyse any structure we first make physical approximations which lead to an idealised structure whose response can be described mathematically using differential equations or variational principals. We then use our mathematical skills to produce an algebraic or numerical solution to the problem; this generally involves further approximation.

There are two main physical idealisations in use for the analysis of braced barrel vaults. In the first approach the structure is represented by an 'equivalent shell' and in the second approach the structure is analysed directly as a general assembly of discrete simple members. This second approach is called the 'space frame' approach if the joints are assumed rigid or the 'space truss' approach if the joints are assumed pinned.

With the equivalent shell approach the members are assumed to be smeared over the surface of the barrel vault so as to produce a shell structure with the same stiffness as the original framework. The equivalent shell is then analysed algebraically or even possibly numerically. This approach is restricted to frameworks which are regular in both geometry and cross-section properties. For equivalent shell stiffnesses see, for example, Wright.[1]

If we analyse the structure as a general assembly of discrete members then we generally use the stiffness method to generate a large set of simultaneous equations. Each equation is an equilibrium equation for one of the force components at one of the nodes expressed in terms of the unknown nodal displacements. Compatibility is satisfied implicitly by defining a single set of nodal displacements.

There is a third approach known as the discrete field approach which exploits repetition in the structure to reduce the computer requirement in comparison to a stiffness method analysis. This technique has not yet been applied to non-linear analysis and is not considered further.

Double layer structures can be analysed in several ways. An equivalent shell can be produced and analysed, a full double-layer space frame or truss can be analysed while some double-layer structures can be replaced by an equivalent single layer structure which is then analysed as a single-layer space frame or truss.

It is useful to compare the equivalent shell and discrete space structure methods. The equivalent shell method can only be applied to regular structures while the stiffness method can handle an arbitrary structural configuration. The computation time is reasonable for an equivalent shell analysis while it may be enormous with a stiffness method analysis. The work involved in an equivalent shell analysis includes calculating the equivalent shell stiffnesses, calculating the forces in the equivalent shell and finally

@Seismicisolation

calculating the forces in the members. To carry out a stiffness method analysis one needs computer facilities and software and a data file must be generated describing the structure. Non-linear analysis is very limited with the equivalent shell approach while the stiffness method can handle all types of non-linearity. To summarise, the equivalent shell approach is probably best used for initial design while a stiffness method analysis should be used for a final design check.

4 COMPUTER IMPLEMENTATION OF THE STIFFNESS METHOD

A space frame analysis assumes rigid joints and requires six equilibrium equations at each node, while a space truss analysis assumes pinned joints and therefore only requires three equations at each node. If a structure with rigid joints is analysed as a space truss then the analysis will always underestimate the capacity of the structure. This applies to both linear and non-linear analysis.

The stiffness method produces a large set of simultaneous equations, and a computer is required to solve them. The size of computer required is related to the number of equations involved. As an example the structure shown in plan in Fig. 2.5 has 1250 nodes.

A frame analysis will be required as the bracing is not properly triangulated. There will be six equilibrium equations at each node which means 1250×6=7500 equations. If a standard disk-based banded equation solver is employed then the disk memory requirement will be $n \times b$ where n is the number of equations and b is the half bandwidth (maximum member node difference multiplied by the number of equations per node which is 6×(25+1)=156 for this example) and the main memory requirement will be $b^2/2$. Assuming 64 bit arithmetic and with some allowance for overheads this structure would require a computer with about 15 megabytes of free disk memory and about 200 kbytes of main memory.

It should be noted that the computer requirement increases rapidly as the number of

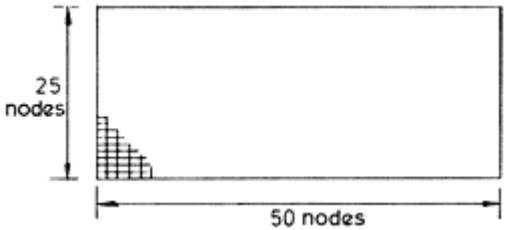

Fig. 2.5. Plan of a simple barrel vault.

nodes increases; also, a truss analysis is considerably cheaper than a frame analysis. Finally, symmetry can be exploited to reduce the number of equations.

The equivalent shell approach is normally used as an initial design method, or when computer facilities are not available, or when there are so many nodes that a space truss or space frame analysis becomes an avoidable extravagance.

@Seismicisolation

5 LINEAR AND NON-LINEAR ANALYSIS

Analysis methods can be categorised as either linear or non-linear. A simple linear analysis in association with appropriate permissible stresses can check for all types of member and joint failure. For members these are yield (axial and bending) and local buckling. For joints these are fracture, fatigue, yield and sliding within the joint. A first yield analysis is also a lower bound on the shakedown load which is a significant limit state when failure is by a plastic mechanism.

Non-linear analysis is needed to check for stability effects involving more than one member and can also exploit any post first yield strength that may be available in a redundant structure.

Non-linear analysis techniques can be divided into three main approaches. These are the plastic mechanism approach, the initial stability approach and finally a full non-linear analysis.

The plastic mechanism approach is only really appropriate for those braced barrel vaults which work as arches.

An initial stability analysis produces bifurcation buckling loads by solving the linear eigenvalue problem which represents equilibrium of the loaded structure in the undeformed position. In a shell barrel vault bifurcation buckling only occurs in limited circumstances such as a very long vault subjected to an internal vacuum. In general, instability of braced barrel vaults is likely to be of the snap-through variety which cannot unfortunately be detected by a conventional initial stability analysis.

Snap-through buckling is one of the more difficult problems in structural analysis. The equilibrium of the structure must be expressed in terms of the deformed geometry of the structure. This means that the analysis must inevitably include some sort of incremental and/or iterative procedure. The most popular approach is presently the updated Lagrangian incremental procedure which is now becoming available in some of the commercial Finite Element systems. Designers should be advised, however, that this type of non-linear analysis is still a fairly specialist activity. There are a number of areas of potential difficulty such as how to apply the loading, divergence of iteration procedures and movement along the wrong equilibrium path. The user must also ensure that the program employed is capable of detecting a snap-through buckling mode. The analysis may require several attempts before achieving a satisfactory analysis and this could be expensive if using a computer bureau.

In view of these difficulties we need some guide as to when non-linear analysis is required. One suggestion is to apply a fairly substantial point load to just one node and then to calculate the corresponding linear displacement. If there is any significant change in the direction of the members meeting at the node then a non-linear analysis should be performed. This type of approach is considered further in Wright.[1]

REFERENCE

1. Wright, D.T. Membrane forces and buckling in reticulated shells. *J. Struct. Div.*, PASCE, Feb. 1965.

@Seismicisolation

3
Formex Formulation of Barrel Vaults

H.NOOSHIN
Space Structures Research Centre,
University of Surrey, Guildford, UK

1 INTRODUCTION

The objective of the present work is to illustrate the application of formex algebra in formulating the interconnection patterns of a number of single-layer braced barrel vaults. The resulting formices may be used as data in conjunction with a suitable computer program for the purposes of structural analysis, or they may be employed in relation to automated graphics.

The number of possible interconnection patterns for a braced barrel vault is infinitely large. The number of patterns that are studied in the present work, on the other hand, is of necessity rather small. It is, however, clearly shown that whatever the interconnection pattern, it can be simply written down in terms of a formex.

In formulating an interconnection pattern, no consideration is given to such aspects as the jointing technique, support conditions and cladding and it is always assumed that a combination of reasons has given rise to the desirability of a particular configuration and the attention is entirely focused on the question of formex formulation of the configuration.

The reader is assumed to be familiar with the concepts of formex algebra, as described in the author's book *Formex Configuration Processing in Structural Engineering* (Elsevier Applied Science Publishers Ltd, London, 1984).

2 CASE STUDIES

The first case to consider is a barrel vault the interconnection pattern of which is given by the formex

$$B1 = E \# F$$

where

$$E = \sum_{i=0}^{14} \sum_{j=0}^{9} \text{tranid}\,(i,j)\,[1,1;2,1]$$

and

@Seismicisolation

$$F = \sum_{i=0}^{15} \sum_{j=0}^{8} \text{tranid}\,(i,j)\,[1,1;1,2]$$

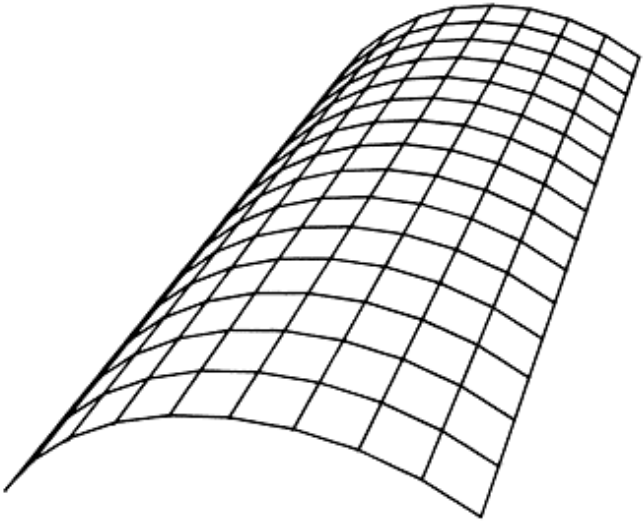

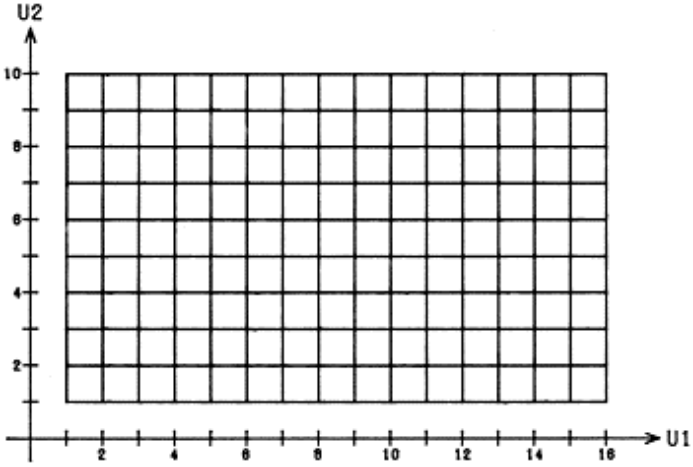

Fig. 3.1.

An intrinsic plot of *B*1 is shown in Fig. 3.1, where the following conventions are employed:

(1) The coordinate axes relating to the first and second direction uniples are denoted by *U*1 and *U*2, respectively.
(2) A signet is plotted as a point.

@Seismicisolation

(3) A cantle is plotted as a straight line connecting the points that represent its signets.
(4) No indication of the orderate of a cantle is included in the plot.
(5) No indication of the order of the appearance of the signets in a cantle is included in the plot.

A perspective view of the barrel vault under consideration is shown in Fig. 3.1. The geometric proportions in this perspective view are based on the assumption that the nodal points of the barrel vault lie on the surface of a right circular cylinder and the elements in the $U1$ direction are parallel to the generatrix of the cylinder.

A number of other barrel vault configurations are studied in the sequel and illustrated in Figs 3.2 to 3.24. Every one of these figures contains an intrinsic plot and a perspective view, where the intrinsic plot is drawn according to the retrocords described above and the perspective view relates to the geometric particulars described for the barrel vault of Fig.3.1.

The formex $B1$ that represents the interconnection pattern of the barrel vault of Fig. 3.1 has been obtained as the composition of two formices E and F, where E represents all the elements that are in the direction of $U1$ and F represents all the elements that are in the direction of $U2$. However, the interconnection pattern of the barrel vault of Fig. 3.1 may be formulated in many other ways.

For instance, each one of the formices

$$A1 = \text{pex}\,|\sum_{i=0}^{14}\sum_{j=0}^{8}\text{tranid}\,(i,j)\,|\,\text{rosid}\,(1\tfrac{1}{2},\ 1\tfrac{1}{2})\,|\,[1,1;2,1]$$

$$A2 = \text{vin}\,(1,1)\,|\sum_{i=1}^{16}\sum_{j=1}^{10}\text{projid}\,(i,j)\,|\,[0,0]$$

and

$$A3 = \text{rel}\,(EU1 < 17 \text{ AND } EU2 < 11)\,|\sum_{i=0}^{15}\sum_{j=0}^{9}\text{tranid}\,(i,j)\,|\,\{[1,1;2,1],[1,1;1,2]\}$$

provides a complete description of the interconnection pattern of the barrel vault of Fig.3.1.

Formex formulation of interconnection patterns may also be done generically, that is, one may write a formex in terms of some parameters and this would then provide a formulation for a family of configurations.

For instance, if m and n denote the numbers of divisions along the first and second directions, respectively, of a configuration of the type shown in Fig. 3.1, then generic formulations for this configuration may be written as

$$G1 = \text{pex}\,|\sum_{i=0}^{m-1}\sum_{j=0}^{n-1}\text{tranid}\,(i,j)\,|\,\text{rosid}\,(1\tfrac{1}{2},\ 1\tfrac{1}{2})\,|\,[1,1;2,1]$$

$$G2 = \text{vin}\,(1,1)\,|\sum_{i=1}^{m+1}\sum_{j=1}^{n+1}\text{projid}\,(i,j)\,|\,[0,0]$$

@Seismicisolation

or

$$G3 = \text{rel}\,(EU1 < m+2 \text{ AND } EU2 < n+2) \left| \sum_{i=0}^{m} \sum_{j=0}^{n} \text{tranid}\ (i,j) \right|$$

$$\{[1,1;2,1],[1,1;1,2]\}$$

The interconnection pattern of the barrel vault whose intrinsic plot and perspective view are shown in Fig. 3.2 may be obtained from $G1$, $G2$ or $G3$ by specifying m=14 and n=8. This interconnection pattern may also be obtained from a generic formulation which is based on formex $B1$ or may be independently written as

$$B2 = E \# F$$

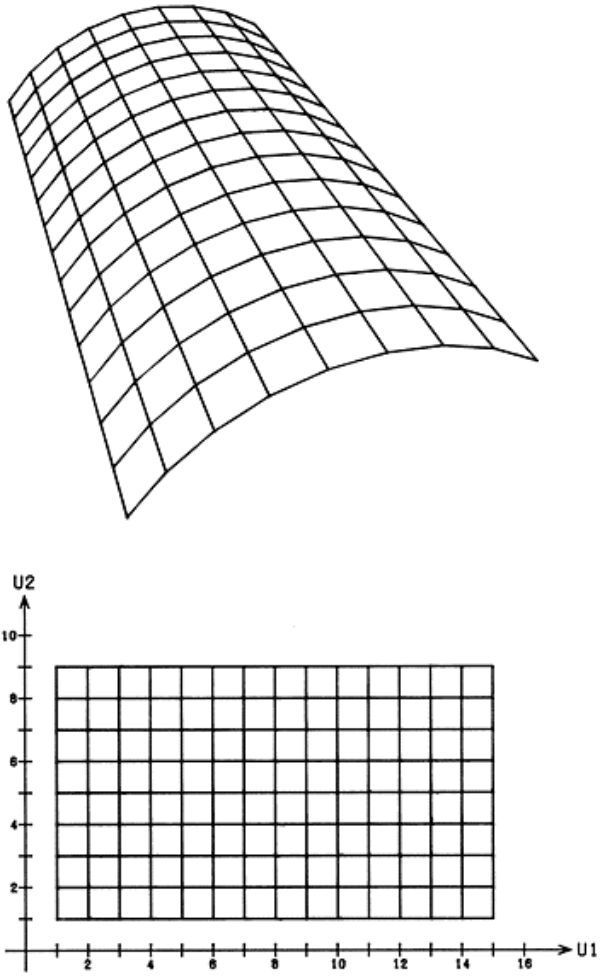

Fig. 3.2.

@Seismicisolation

where

$$E = \sum_{i=0}^{13} \sum_{j=0}^{8} \text{tranid}\,(i,j)\,{}_{|}^{|}[1,1;2,1]$$

and

$$F = \sum_{i=0}^{14} \sum_{j=0}^{7} \text{tranid}\,(i,j)\,{}_{|}^{|}[1,1;1,2]$$

In writing a formex formulation for the barrel vault of Fig. 3.3, one may notice that, except for some missing elements, the pattern is identical with that of the barrel vault of Fig. 3.1. Then, if a formex representing the configuration of the barrel vault of Fig. 3.1,

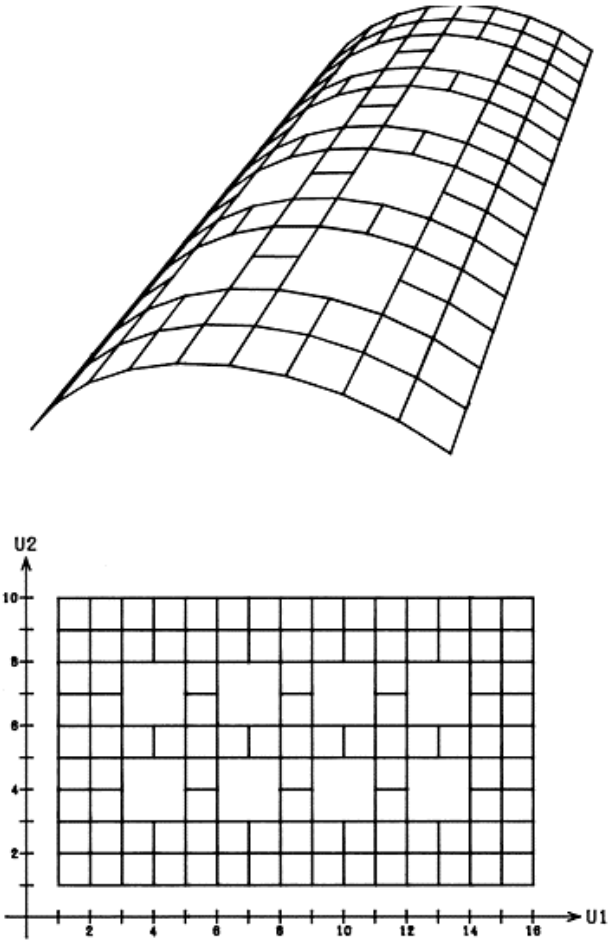

Fig. 3.3.

@Seismicisolation

such as $B1$, is in hand, one may write the interconnection pattern in terms of $B1$ as

$B3$ =lux (E)¦$B1$

where

$$E = \sum_{i=0}^{3} \text{tran}\,(1, 3i)\,¦\,\{[4, 4], [4, 7]\}$$

An alternative formulation for the interconnection pattern of the barrel vault of Fig. 3.3 may be given as

vin (1, 1)¦lux (E)¦F

where E is the formex given above and

$$F = \sum_{i=1}^{16} \sum_{j=1}^{10} \text{projid}\,(i, j)\,¦\,[0, 0]$$

@Seismicisolation

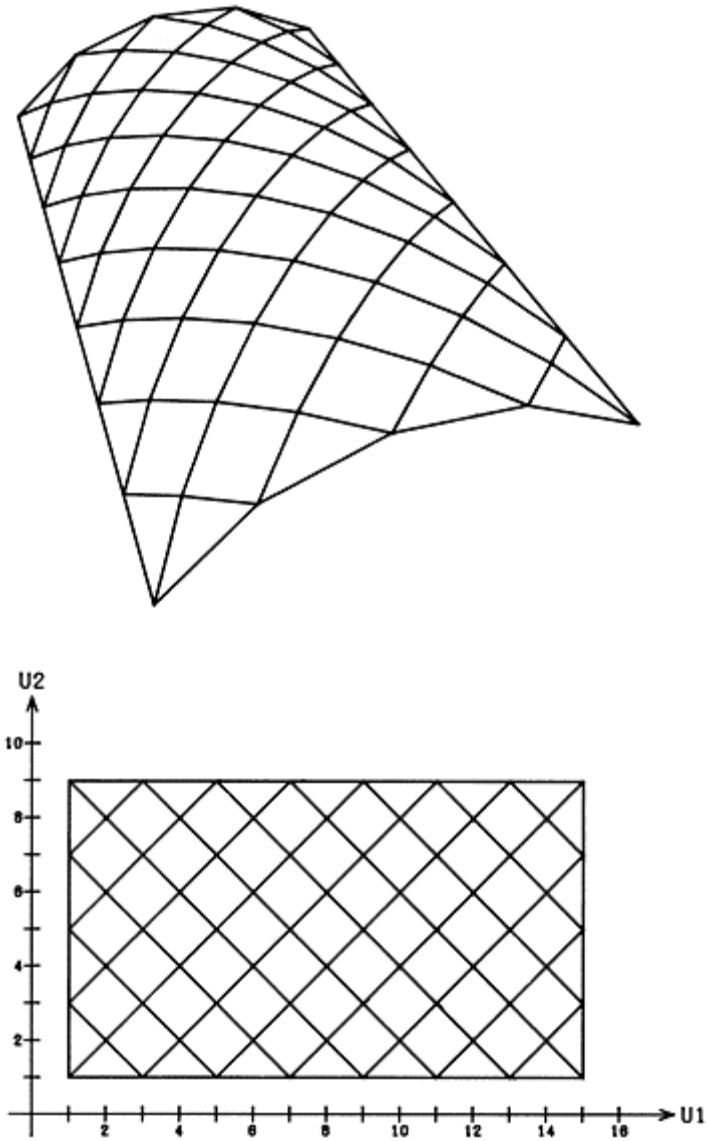

Fig. 3.4.

A formex formulation for the interconnection pattern of the barrel vault of Fig. 3.4 is given by

$$B4 = E \# F \# G$$

where

@Seismicisolation

$$E = \sum_{i=0}^{6} \sum_{j=0}^{3} \text{tranid}\,(2i, 2j)\,|\,\text{rosid}\,(2, 2)\,|\,[1, 1; 2, 2]$$

$$F = \sum_{i=0}^{6} \text{tran}\,(1, 2i)\,|\,\{[1, 1; 3, 1], [1, 9; 3, 9]\}$$

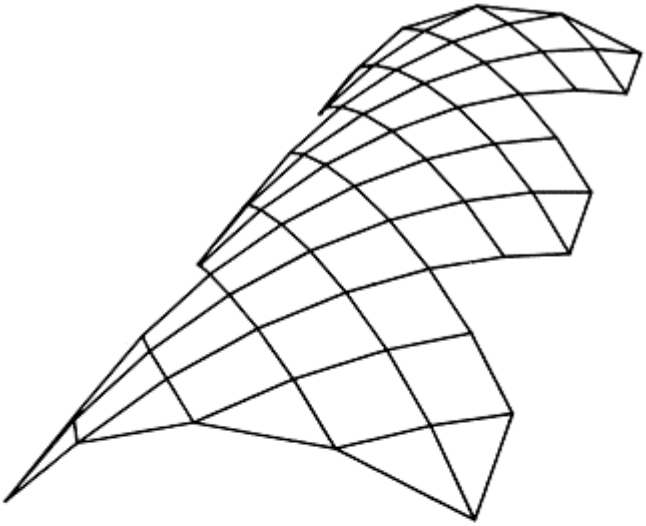

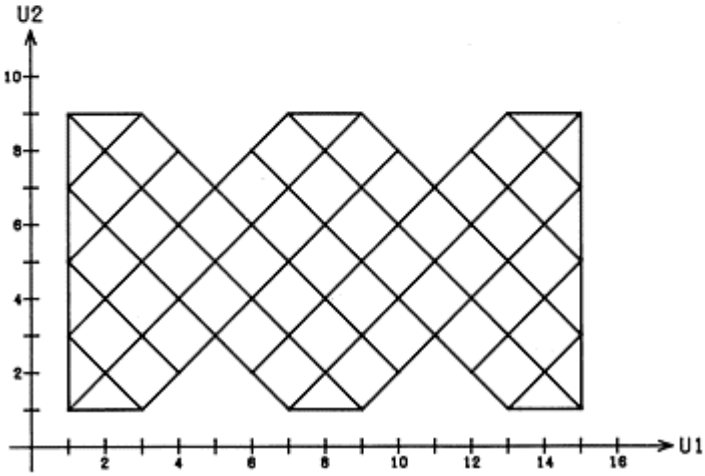

Fig. 3.5.

and

@Seismicisolation

$$G = \sum_{j=0}^{3} \text{tran}\,(2, 2j)\,|\,\{[1, 1; 1, 3], [15, 1; 15, 3]\}$$

With $B4$ in hand, the interconnection pattern of the barrel vault of Fig. 3.5 may be conveniently written as

$B5$=lux $(E)|B4$

where

E=lamid (8,5)|{[4, 1], [5, 1], [6,1], [5, 2]}

A formex formulation for the interconnection pattern of the barrel vault of Fig. 3.6 is given by

$$B6 = E \# F \# G \# H$$

@Seismicisolation

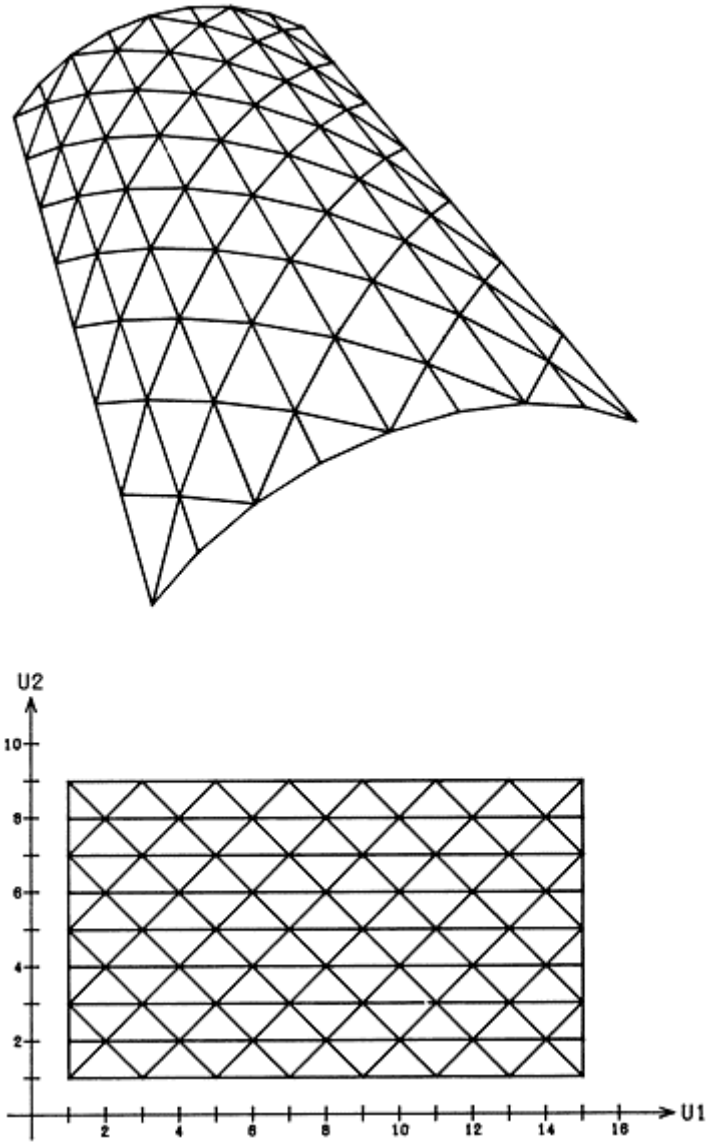

Fig. 3.6.

where

@Seismicisolation

$$E = \sum_{i=0}^{6} \sum_{j=0}^{3} \text{tranid}\,(2i, 2j)\,|\,\text{rosid}\,(2, 2)\,|\,[1, 1; 2, 2]$$

$$F = \sum_{i=0}^{6} \sum_{j=0}^{4} \text{tranid}\,(2i, 2j)\,|\,[1, 1; 3, 1]$$

$$G = \sum_{i=0}^{5} \sum_{j=0}^{3} \text{tranid}\,(2i, 2j)\,|\,[2, 2; 4, 2]$$

and

$$H = \sum_{j=0}^{3} \text{tran}\,(2, 2j)\,|\,\text{lam}\,(1, 8)\,|\,\{[1, 1; 1, 2], [1, 2; 1, 3], [1, 2; 2, 2]\}$$

@Seismicisolation

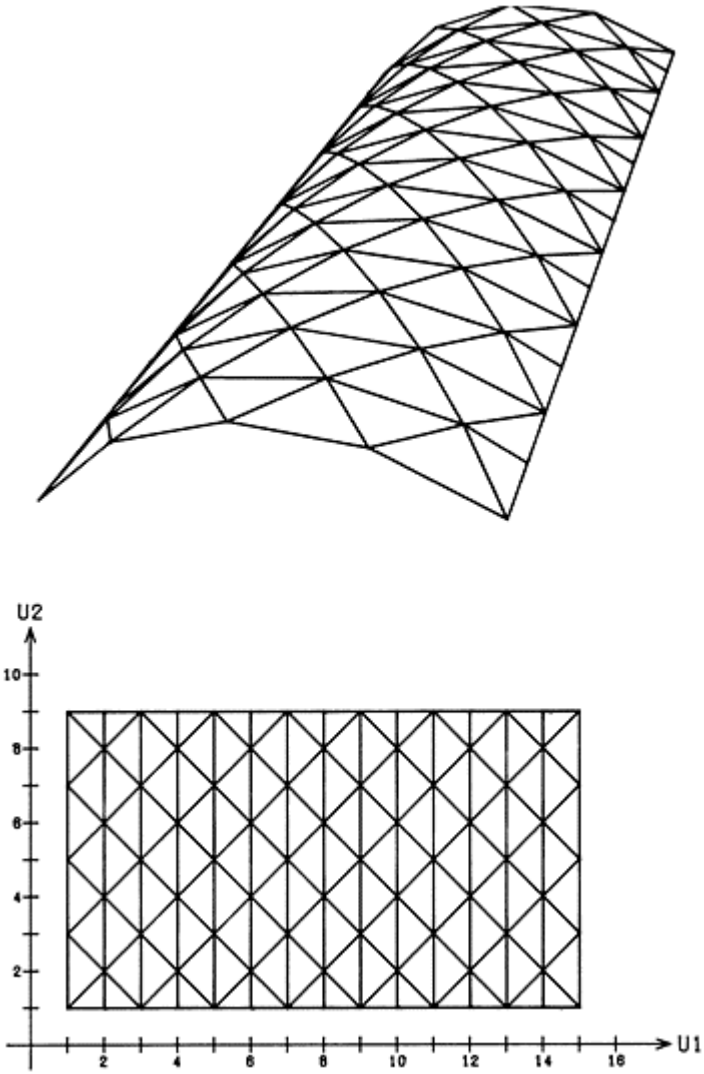

Fig. 3.7.

Similarly, a formex representing the interconnection pattern of the barrel vault of Fig. 3.7 may be written as

$$B7 = E \# F \# G \# H$$

where

@Seismicisolation

$$E = \sum_{i=0}^{6} \sum_{j=0}^{3} \text{tranid } (2i, 2j)\,|\,\text{rosid } (2,2)\,|\,[1,1;2,2]$$

$$F = \sum_{i=0}^{7} \sum_{j=0}^{3} \text{tranid } (2i, 2j)\,|\,[1,1;1,3]$$

$$G = \sum_{i=0}^{6} \sum_{j=0}^{2} \text{tranid } (2i, 2j)\,|\,[2,2;2,4]$$

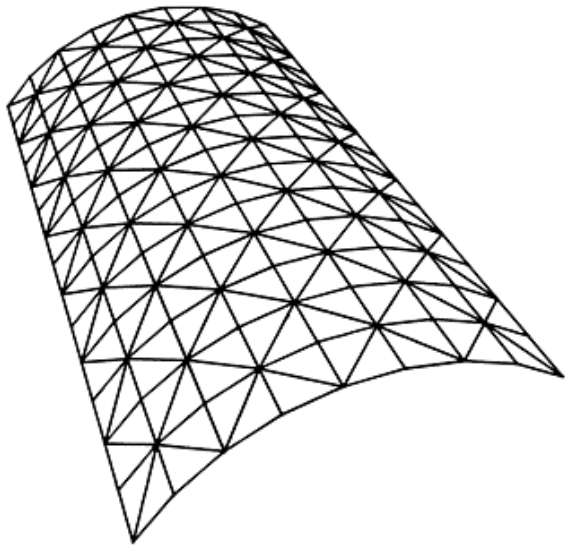

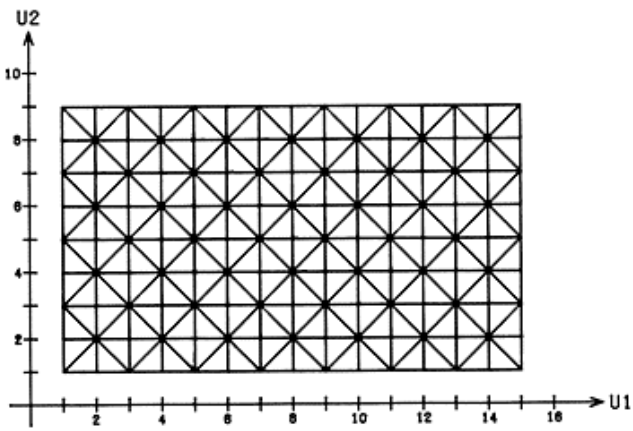

Fig. 3.8.

@Seismicisolation

and

$$H = \sum_{i=0}^{6} \text{tran}\,(1, 2i) \,|\, \text{lam}\,(2, 5) \,|\, \{[1, 1; 2, 1], [2, 1; 3, 1], [2, 1; 2, 2]\}$$

Taking advantage of the availability of formex *B2*, the interconnection pattern of the barrel vault of Fig. 3.8 may be written as

$$B8 = B2 \# E$$

where

$$E = \sum_{i=0}^{6} \sum_{j=0}^{3} \text{tranid}\,(2i, 2j) \,|\, \text{rosid}\,(2, 2) \,|\, [1, 1; 2, 2]$$

@Seismicisolation

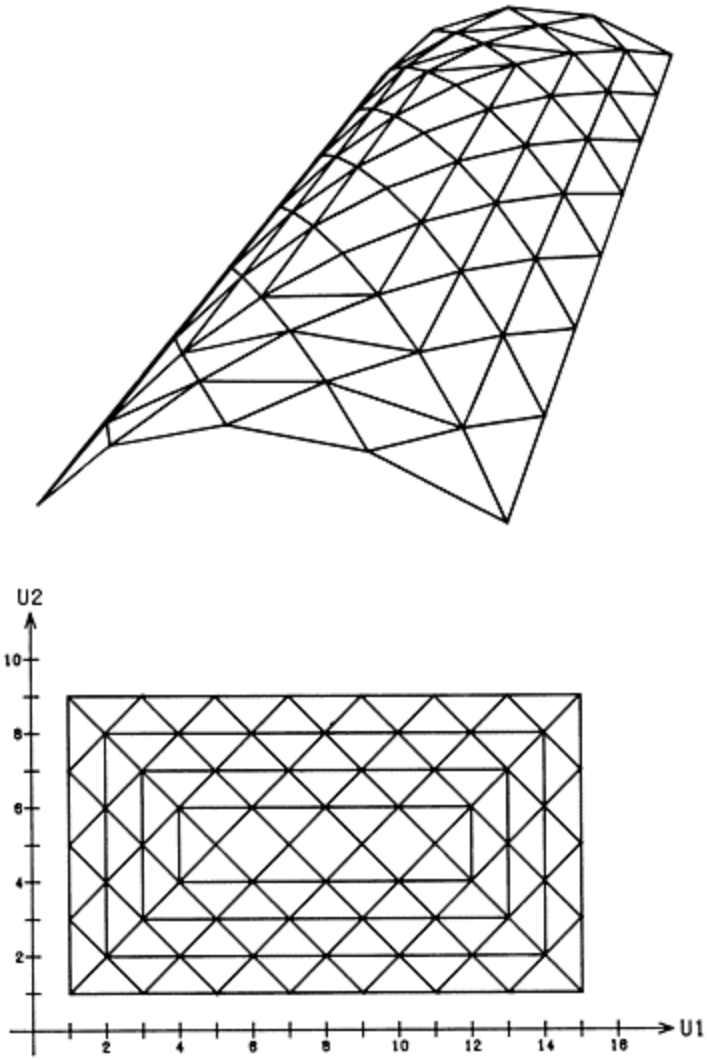

Fig. 3.9.

An alternative formulation for the interconnection pattern of the barrel vault of Fig. 3. may be written as

$$\mathrm{Pex}\,{}_{|}^{|}\sum_{i=0}^{6}\sum_{j=0}^{3}\mathrm{tranid}\,(2i,2j)\,{}_{|}^{|}\mathrm{rosid}\,(2,2)\,{}_{|}^{|}$$

$$\{[1,1;2,1],[1,1;1,2],[1,1;2,2],[1,2;2,2]\}$$

The interconnection pattern of the barrel vault of Fig. 3.9 may be formulated as

$$B9 = E \# F \# G$$

@Seismicisolation

where

$$E = \sum_{i=0}^{6} \sum_{j=0}^{3} \text{tranid}\ (2i, 2j)\,|\,\text{rosid}\,(2,2)\,|\,[1,1;2,2]$$

$$F = \text{lam}\,(2,5)\,|\,\sum_{j=0}^{3} \sum_{i=0}^{6-j} \text{tran}\,(1,2i)\,|\,[j+1, j+1; j+3, j+1]$$

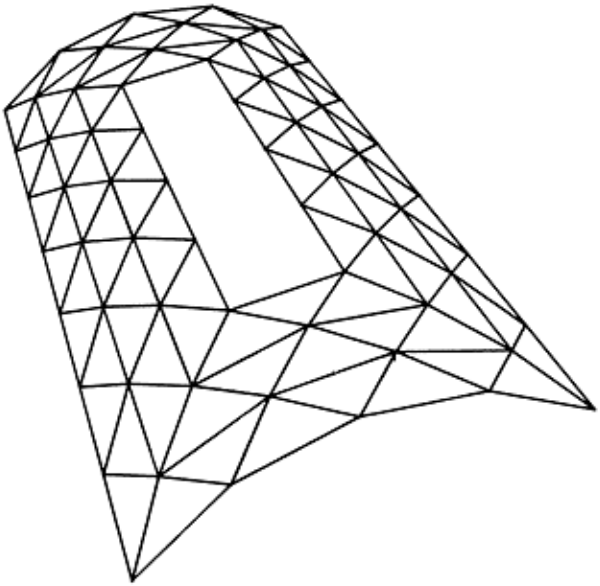

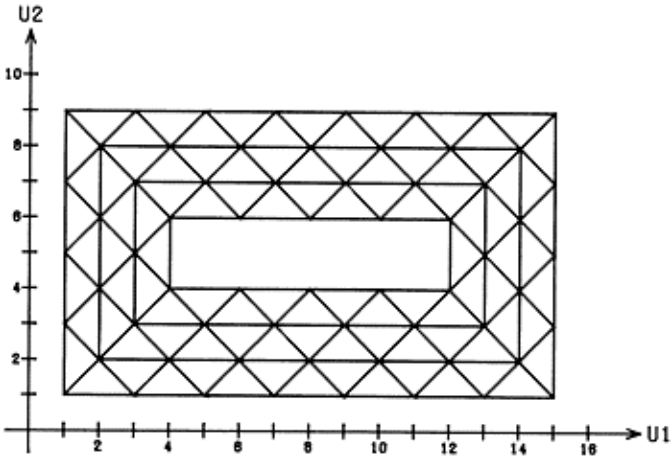

Fig. 3.10.

@Seismicisolation

and

$$G = \text{lam}\,(1,8)\,|\,|\sum_{i=0}^{3}\sum_{j=0}^{3-i}\text{tran}\,(2,2j)\,|\,|\,[i+1,i+1;i+1,i+3]$$

With the formex *B*9 in hand, the configuration of the barrel vault of Fig. 3.10 may be written as

*B*10=lux *(E)*|*B*9

where

$$E = \sum_{i=0}^{3}\text{tran}\,(1,2i)\,|\,|\,[5,5]$$

@Seismicisolation

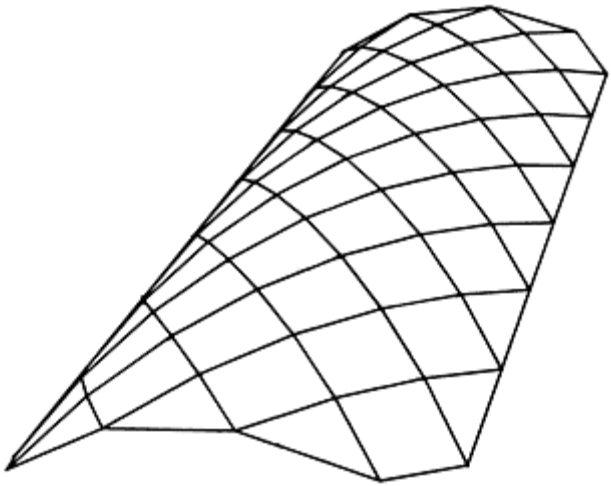

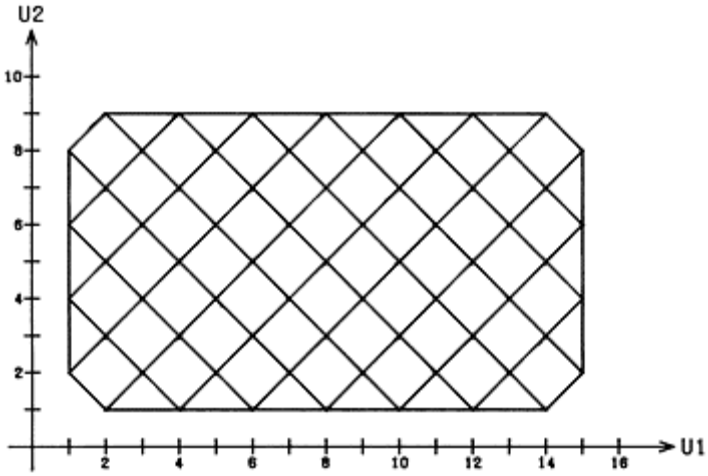

Fig. 3.11.

The configuration of the barrel vault of Fig. 3.11 may be formulated as

$$B11 = E \# F \# G$$

where

@Seismicisolation

$$E = \sum_{i=0}^{6} \sum_{j=0}^{3} \text{tranid}\ (2i, 2j)\,|\,\text{rosid}\,(2, 2)\,|\,[1, 2; 2, 1]$$

$$F = \sum_{i=0}^{5} \text{tran}\,(1, 2i)\,|\,\{[2, 1;\ 4, 1], [2, 9; 4, 9]\}$$

and

$$G = \sum_{j=0}^{2} \text{tran}\,(2, 2j)\,|\,\{[1, 2; 1, 4], [15, 2; 15, 4]\}$$

@Seismicisolation

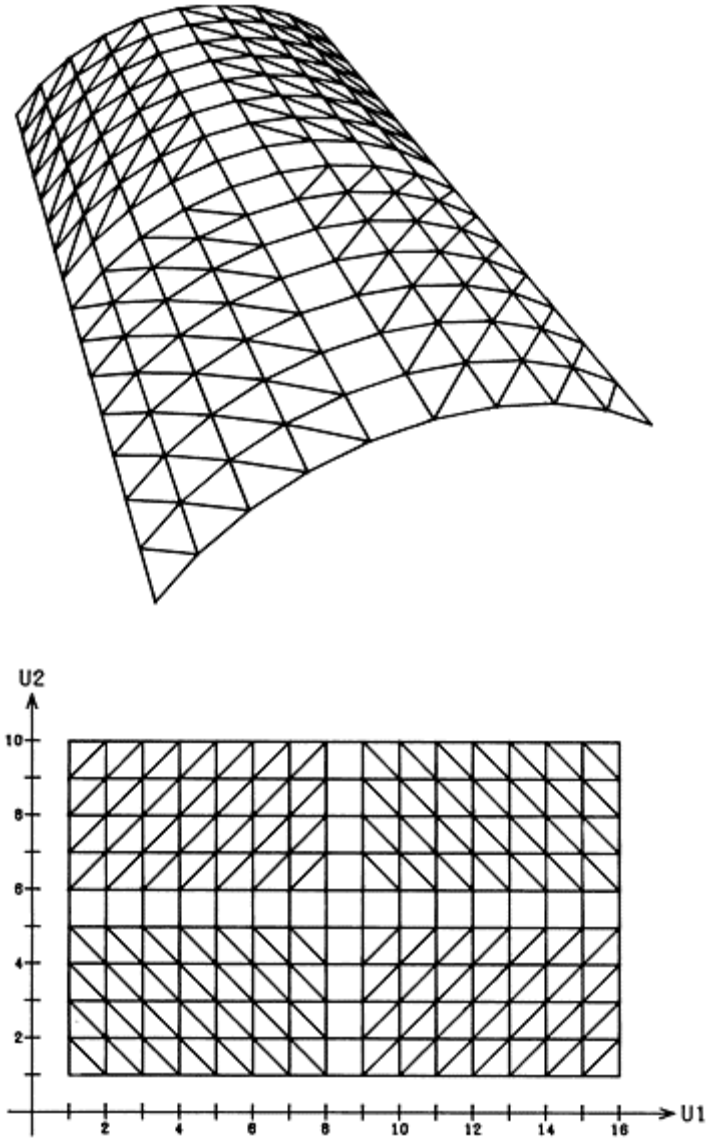

Fig. 3.12.

The interconnection pattern of the barrel vault of Fig. 3.12 may be given as

$$B12 = B1 \# E$$

where

@Seismicisolation

$$E = \text{lamid}\,(8\tfrac{1}{2}, 5\tfrac{1}{2})\,|\,\sum_{i=0}^{6}\sum_{j=0}^{3}\text{tranid}\,(i,j)\,|\,[1,2;2,1]$$

and where $B1$ is the formex representing the interconnection pattern of the barrel vault of Fig.3.1.

The interconnection pattern of the barrel vault of Fig. 3.13 can be written down as

$B13$=lux $(E)|B12$

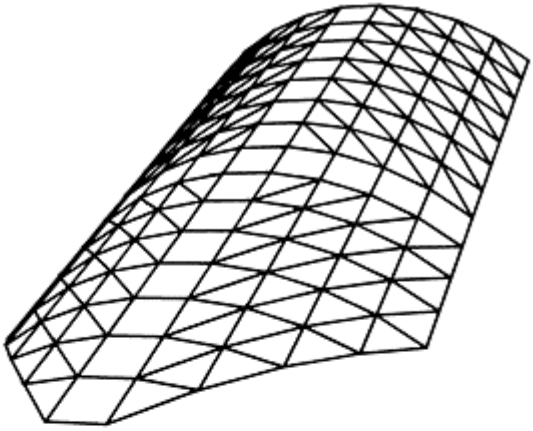

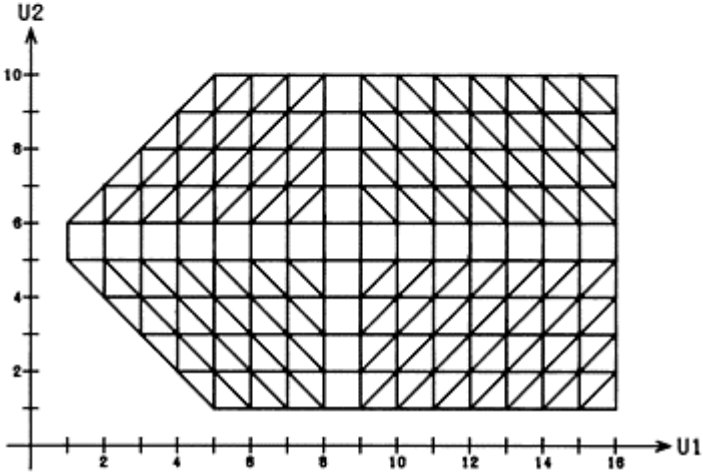

Fig. 3.13.

where

@Seismicisolation

$$E = \text{lam}(2, 5\tfrac{1}{2}) \sum_{j=0}^{3} \sum_{i=0}^{j} \text{tranid}(i,j)\,[1, 7]$$

and where *B*12 is the formex representing the interconnection pattern of the barrel vault of Fig. 3.12.

An alternative formulation for the interconnection pattern of the barrel vault of Fig. 3.13 may be given as

rel *(P)*B12

where *P* is a perdicant which, in brevic notation, is given by

$$(U11 + U12 > 5) \text{ AND } (U12 - U11 < 6) \text{ AND } (U22 - U21 < 6)$$

@Seismicisolation

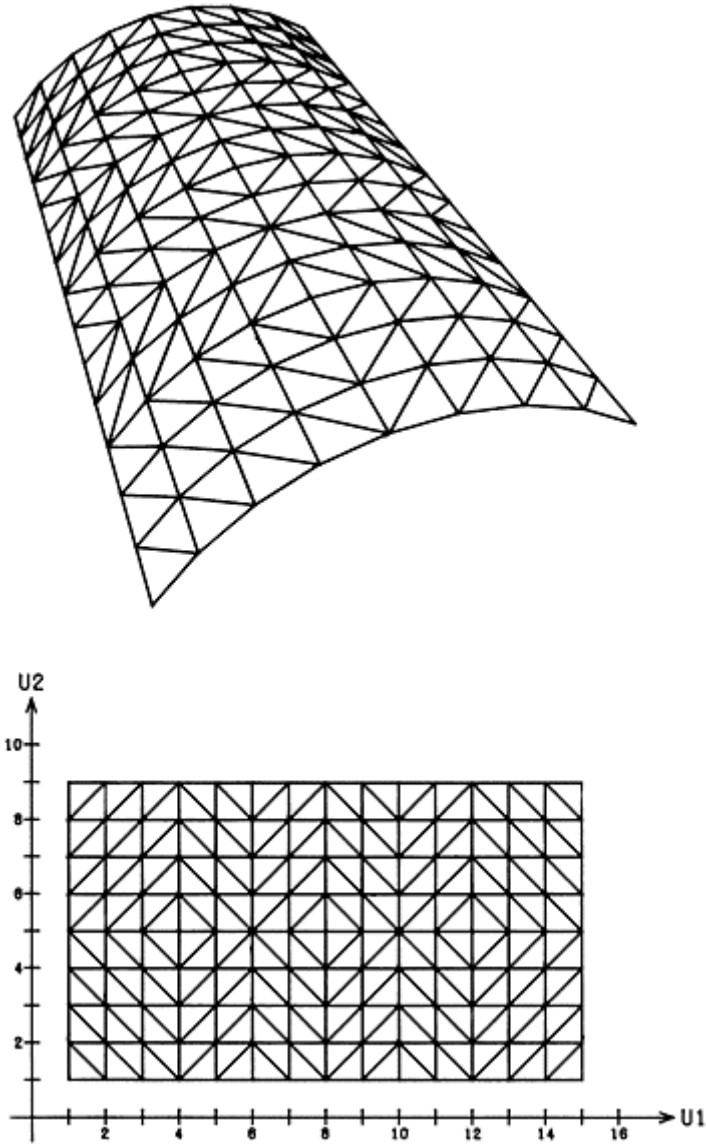

Fig. 3.14.

The interconnection pattern of the barrel vault of Fig. 3.14 may be given by

$$B14 = B2 \# E \# F$$

where

@Seismicisolation

$$E = \sum_{i=0}^{2} \text{tran}\,(1, 4i) \,|\, \text{lamid}\,(4, 5) \,|\, G$$

$$F = \text{lamid}\,(8, 5) \,|\, \sum_{j=0}^{3} \text{tran}\,(2, j) \,|\, [1, 2; 2, 1]$$

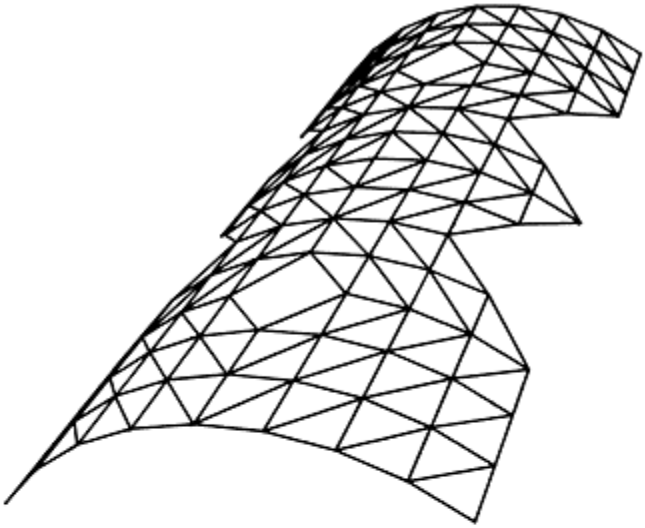

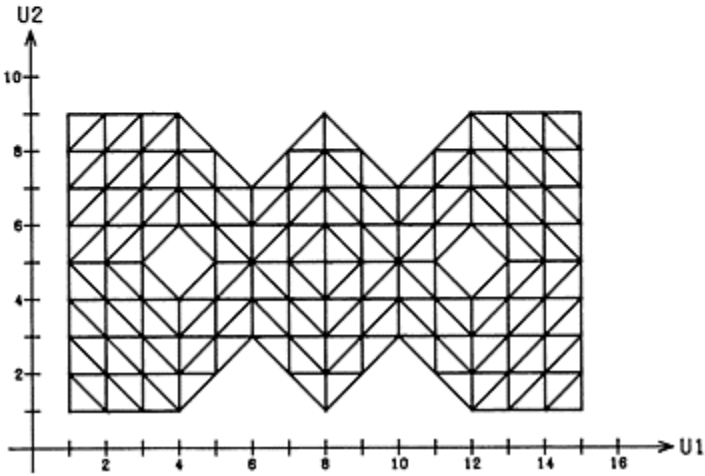

Fig. 3.15.

and

@Seismicisolation

$$G = \sum_{j=0}^{3} \text{tran}\,(2,j)\,|\,\{[2,2;3,1],[3,2;4,1]\}$$

The interconnection pattern of the barrel vault of Fig. 3.15 may be obtained as

$B15$=lux $(E)\,|\,B14$

where

$$E = \text{lamid}\,(8,5)\,|\,\{[4,5],[5,1],[6,1],[6,2],[7,1]\}$$

and where $B14$ is the formex representing the interconnection pattern of the barrel vault of Fig. 3.14.

@Seismicisolation

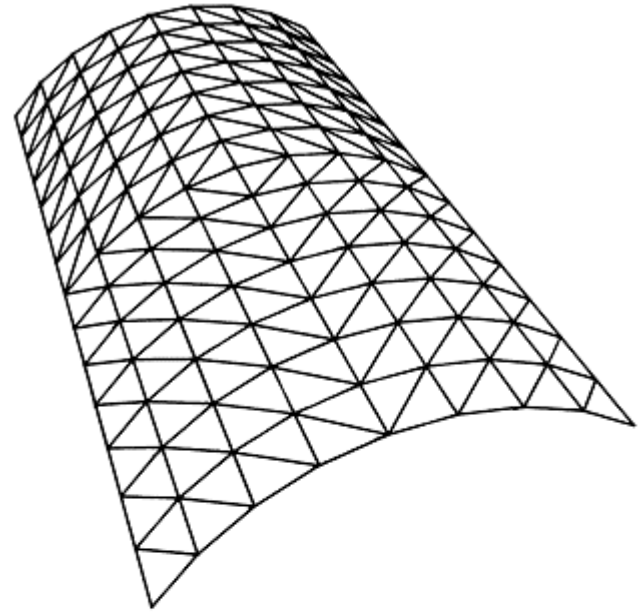

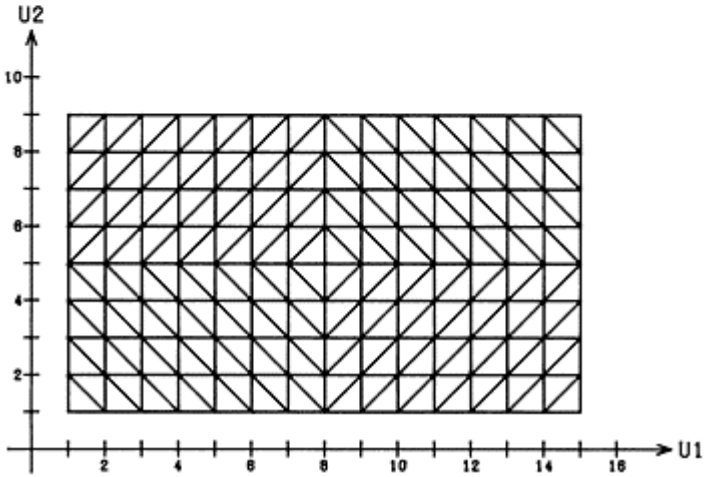

Fig. 3.16.

The interconnection pattern of the barrel vault of Fig. 3.16 may be written down as

$$B16 = B2 \# E$$

where

@Seismicisolation

$$E = \text{lamid}\,(8,5)\,|\sum_{i=0}^{6}\sum_{j=0}^{3}\text{tranid}\,(i,j)\,|\,[1,2;2,1]$$

and where $B2$ is the formex representing the interconnection pattern of the barrel vault of Fig. 3.2, as given earlier.

The interconnection pattern of the barrel vault of Fig. 3.17 may be obtained as

$$B17 = B1 \# E$$

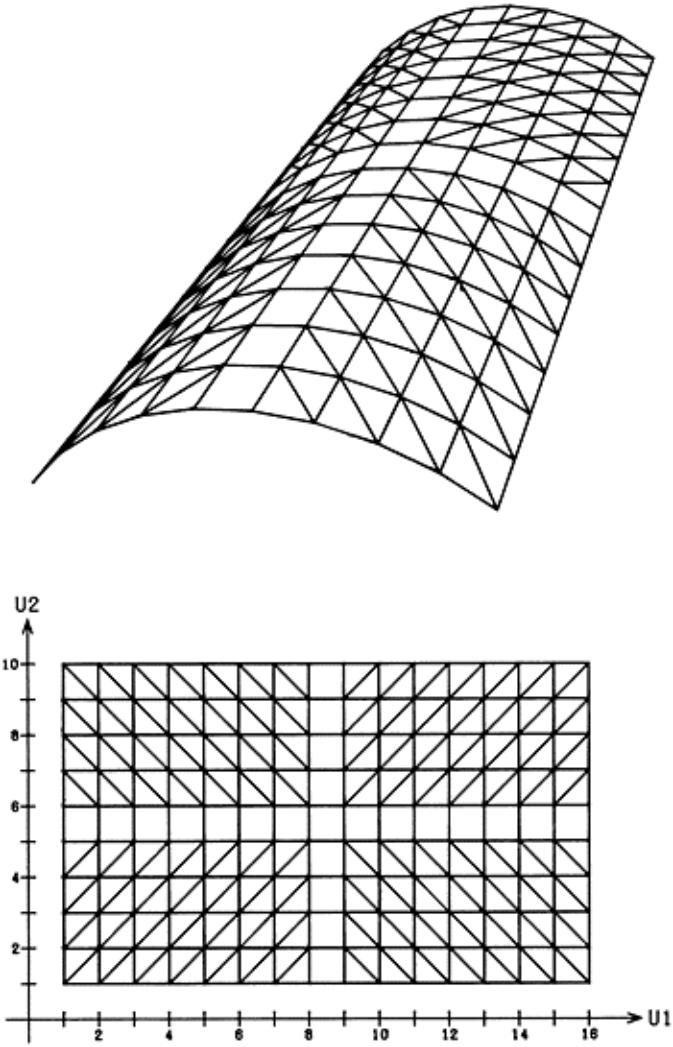

Fig. 3.17.

@Seismicisolation

where

$$E = \text{lamid}\,(8\tfrac{1}{2}, 5\tfrac{1}{2})\,\sum_{i=0}^{6}\sum_{j=0}^{3}\text{tranid}\,(i,j)\,[1,1;2,2]$$

and where $B1$ is the formex representing the interconnection pattern of the barrel vault of Fig.3.1.

With formex $B17$ in hand, the interconnection pattern of the barrel vault of Fig, 3.18 may be given as

$B18$ lux $(E)\,B17$

where

$$E = \text{lamid}\,(8\tfrac{1}{2}, 5\tfrac{1}{2})\,\{[1,4],[1,5],[4,3],[7,1],[8,1]\}$$

@Seismicisolation

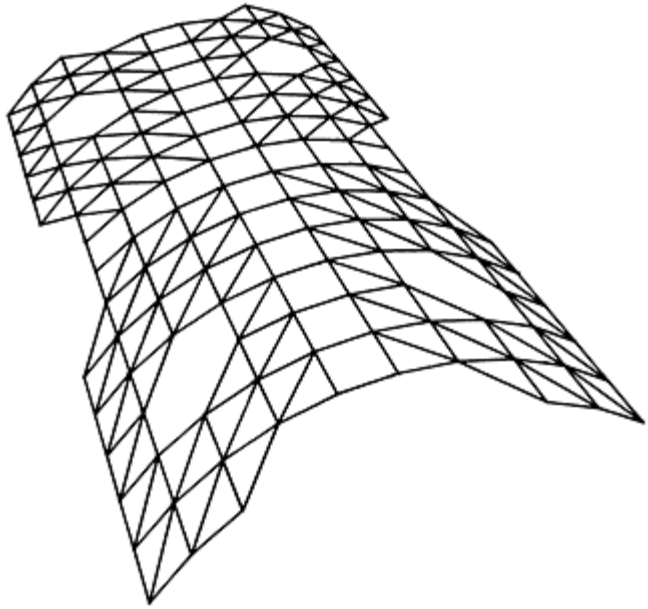

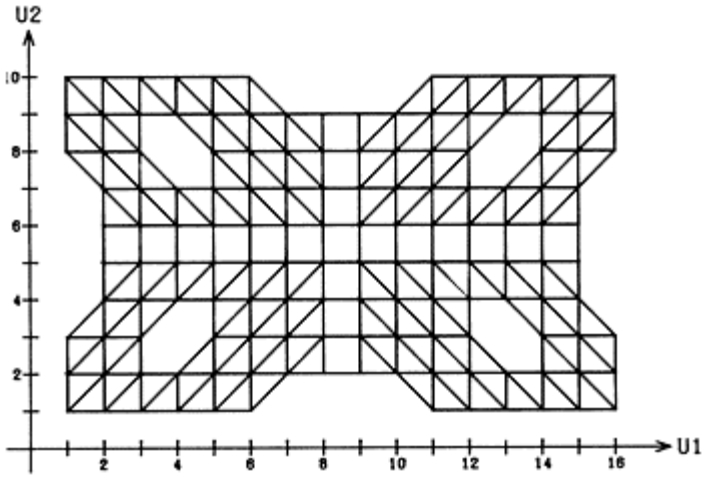

Fig. 3.18.

The interconnection pattern of the barrel vault of Fig. 3.19 may be written down as

$$B19 = B2 \# E$$

where

@Seismicisolation

$$E = \text{lamid}\,(8,5) \left| \sum_{i=0}^{6} \sum_{j=0}^{3} \text{tranid}\,(i,j) \right| [1,1;2,2]$$

and where $B2$ is the formex representing the interconnection pattern of the barrel vault of Fig. 3.2. Similarly, the interconnection patterns of the barrel vaults of Figs 3.20 and 3.21 may be written down as $B20$ and $B21$, respectively, as follows:

$$B20 = B2 \# E$$

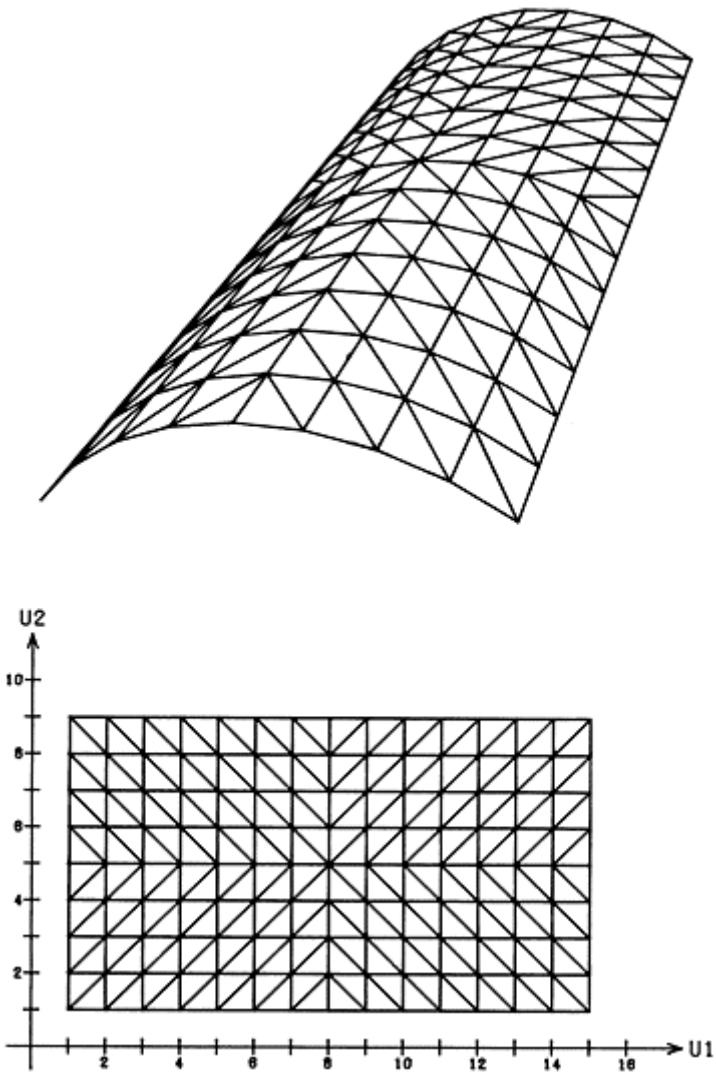

Fig. 3.19.

@Seismicisolation

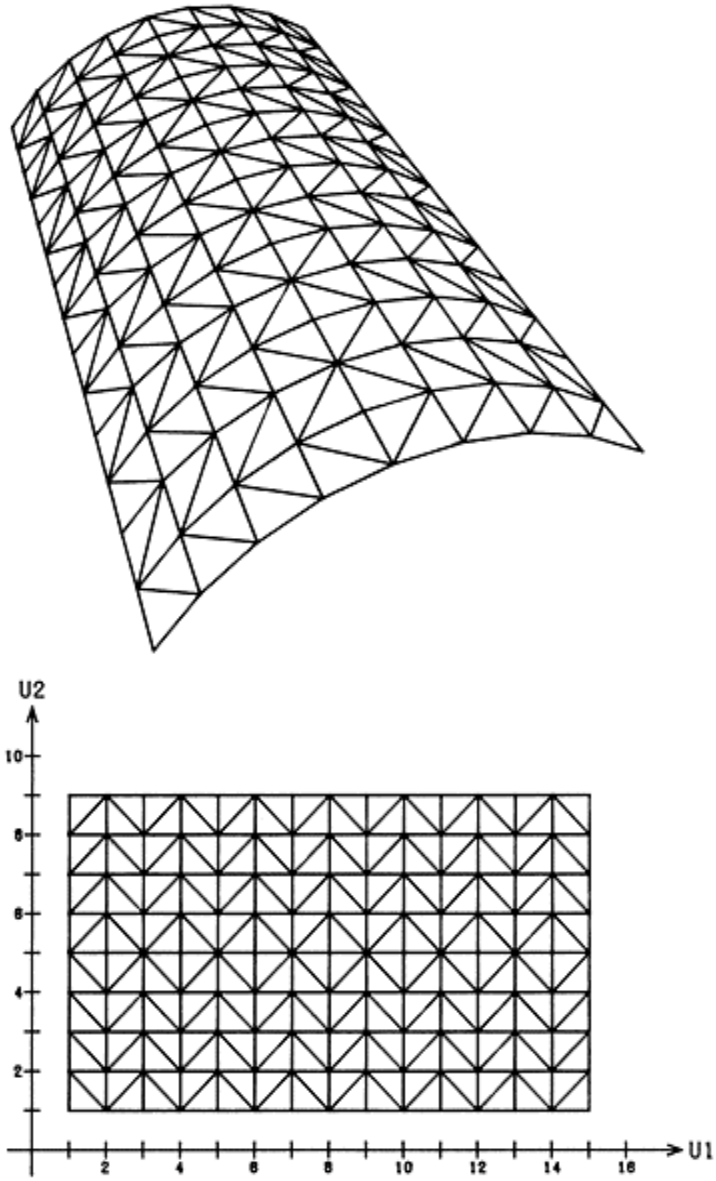

Fig. 3.20.

@Seismicisolation

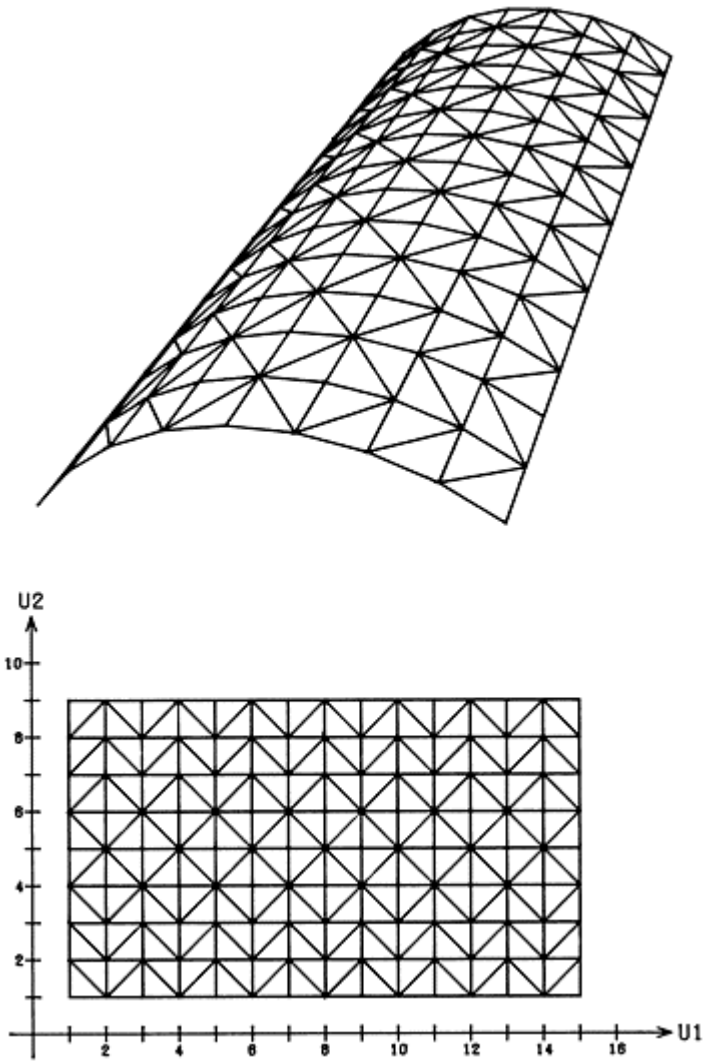

Fig. 3.21.

where

$$E = \text{lam}\,(2,5)\,|\,\sum_{i=0}^{6}\sum_{j=0}^{3}\text{tranid}\,(2i,j)\,|\,\{[1,2;2,1],[2,1;3,2]\}$$

and

$$B21 = B2 \# E$$

where

@Seismicisolation

$$E = \mathrm{lam}\,(2,5)\,|\,(F \# G)$$

and where

$$F = \sum_{i=0}^{6} \sum_{j=0}^{3} \mathrm{tranid}\,(2i,j)\,|\,\{[1,2;2,1],[2,1;3,2]\}$$

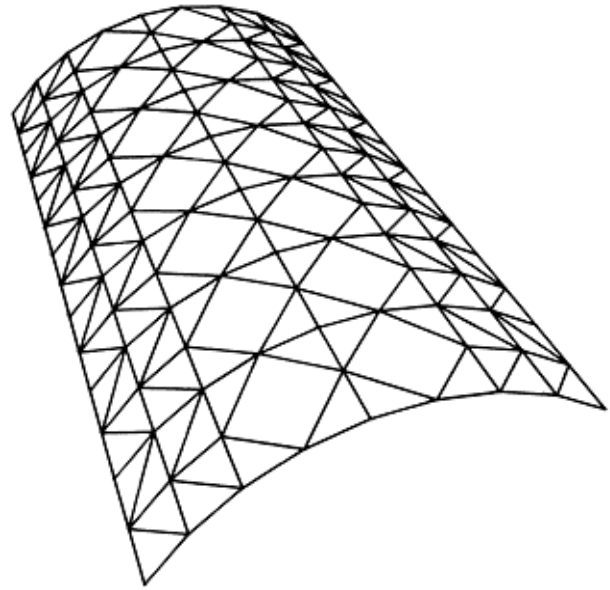

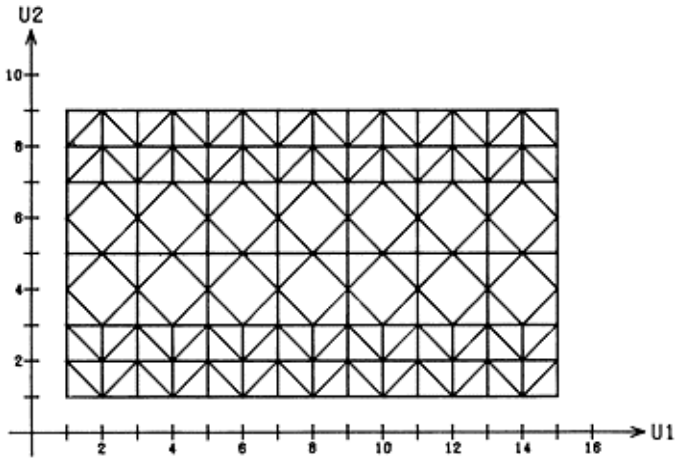

Fig. 3.22.

@Seismicisolation

and

$$G = \sum_{i=0}^{6} \text{tran}\,(1, 2i)\,{}_{|}^{|}\{[1, 4; 2, 5], [2, 5; 3, 4]\}$$

With formex *B*21 in hand, the interconnection pattern of the barrel vault of Fig. 3.22 may be written down as

*B*22=lux *(E)*$_{|}^{|}$*B*21

where

$$E = \sum_{i=0}^{6} \text{tran}\,(1, 2i)\,{}_{|}^{|}\{[2, 4], [2, 6]\}$$

@Seismicisolation

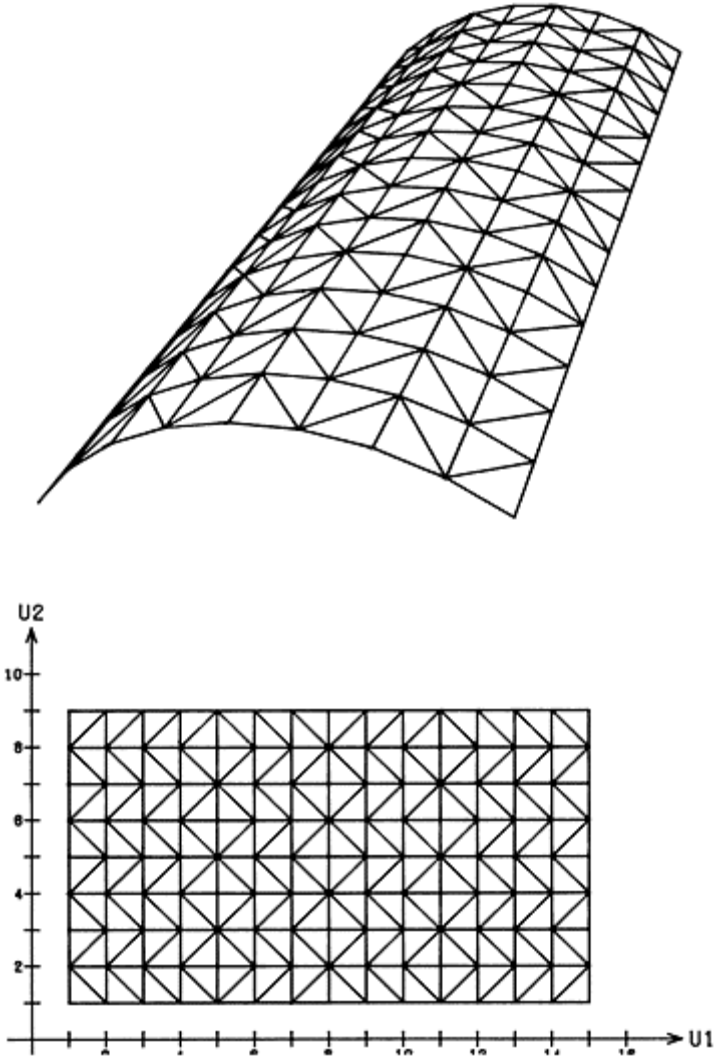

Fig. 3.23.

@Seismicisolation

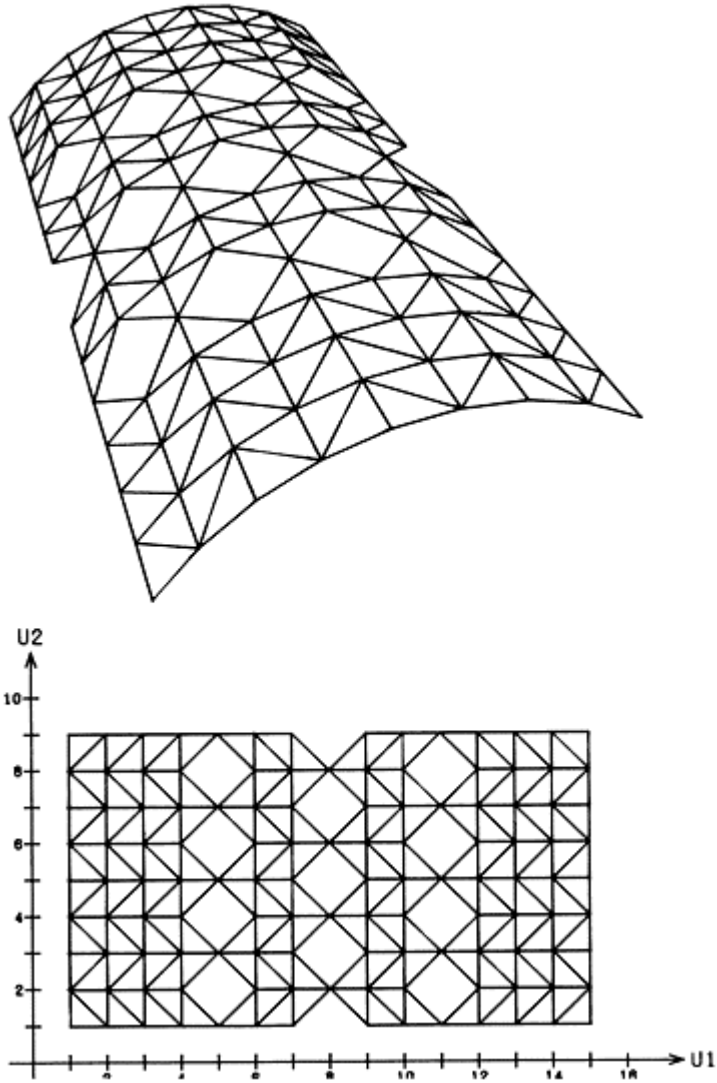

Fig. 3.24.

The interconnection pattern of the barrel vault of Fig. 3.23 may be obtained as

$$B23 = B2 \# E \# F$$

where

$$E = \text{lam}(1,8)\,|\,\text{lam}(1,5)\,|\,\sum_{i=0}^{2}\sum_{j=0}^{3}\text{tranid}(i,2j)\,|\,\{[3,1;2,2],[2,2;3,3]\}$$

@Seismicisolation

and

$$F = \mathrm{lam}\,(1,8)\,|\,\sum_{j=0}^{3} \mathrm{tran}\,(2,2j)\,|\,\{[2,1;1,2],[1,2;2,3]\}$$

and where *B*2 is the formex representing the interconnection pattern of the barrel vault of Fig. 3.2.

Finally, the interconnection pattern of the barrel vault of Fig. 3.24 may be written as

*B*24=lux *(E)*|*B*23

where

$$E = \sum_{j=0}^{4} \mathrm{tran}\,(2,2j)\,|\,\{[5,2],[8,1],[11,2]\}$$

and where *B*23 is the formex representing the interconnection pattern of the barrel vault of Fig. 3.23, as obtained above.

ACKNOWLEDGEMENTS

PAVO is the name of a research project which is currently in progress in the Space Structures Research Centre of the University of Surrey. The aim of the PAVO project is the development of concepts and associated computer software for automated engineering analysis and design, and the present work is an outcome of research in configuration processing within the scope of the PAVO project.

The PAVO project is partially supported through generous donations by Messrs. A. Sarshar, A.Jahanshahi, C.G.Abkarian, G.A.Mirzareza, M.S.Yazdani and J. Hassanein and their help in this regard is gratefully acknowledged.

In relation to the present work, the author wishes to thank Professor Z.S.Makowski for his encouragement and guidance, Mr P.L.Disney for his constructive suggestions and Mrs C.P.Young for her care and patience in typing the manuscript.

@Seismicisolation

4
Double-elliptic Vaults

P.HUYBERS and G.J.ARENDS*
Building Technology Group, Delft University of Technology, The Netherlands

1 INTRODUCTION

Vaults of roughly hemispherical shape and with a vertical axis of symmetry are defined by the vertical cross-section, coinciding with this axis, and by the horizontal cross-section which forms the basis of the vault.

The situation is considered where both cross-sections are ellipses. According to a suggestion by Kenner,[1] such an elliptic cross-section can be represented by an equation of the *nth* order. An enormous range of related shapes—but of greatly different appearance—is found by varying the power of *n* or the ratio of the long and short axes of the respective ellipses and by choosing various combinations. For the visual representation a computer program has been developed which produces the necessary data for isometric or perspective drawings with hidden line removal. For this purpose a triangular grid is projected upon the envelope.

The ellipse consists of basically four distinctive quadrants which are point or line-symmetric. Replacement of the four quadrants of the horizontal ellipse by a variable number of sectors offers another dimension in the generation routine of shapes.

2 BASIC GEOMETRY

Any point P on a hemisphere is defined by its polar coordinates: the horizontal angle ø (phi), the vertical angle θ (theta) and the radius R_p. They are indicated in Fig. 4.1 and their magnitudes can be derived from the formulae:

With

$$R_2 = R_1 E_2/(E^{n_2}\sin^{n_2}\theta + R_1^{n_2}\cos^{n_2}\theta)^{1/n_2}$$
$$R_1 = E_1/(E_1^{n_1}\sin^{n_1}\phi + \cos^{n_1}\phi)^{1/n_1}$$

E_1 and E_2 are the ratios of the maxima in the *x-y* plane and in the *y-z* plane respectively. The powers of the horizontal and of the vertical ellipse can be varied individually. Figure 4.2 shows the effect of various values of this power on the shape of the ellipse and also on the sign of its curvature. For n=1 four straight lines are found, which together form a rhombus. If n=2 a pure ellipse is found, and a circle if also E=1. Ellipses and circles with powers larger than 2 are usually referred to as superellipses or supercircles. A value of n=2·5 is commonly used in those cases where a better

@Seismicisolation

* *Present address:* J.van Beierenlaan 45, 2163 HZ Delft, The Netherlands

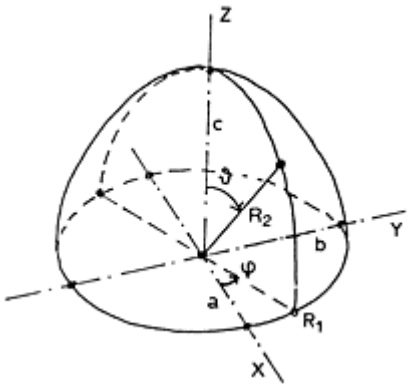

Fig. 4.1. Schematic sketch of double-elliptic hemisphere.

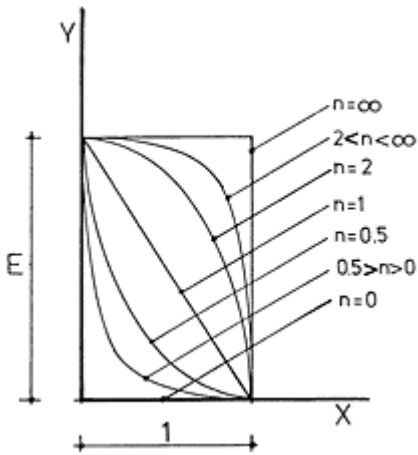

Fig. 4.2. Quarter part of ellipse with various values of *n*.

approximation of a square or a rectangular ground floor plan is wanted. If the value of *n* is still further increased, the ellipse forms more explicit ‘shoulders’ and coincides at last with the circumscribed rectangle or square. For values of $n<1$ the curve changes its sign and it nears the main axes *x* and *y* if *n* approaches zero.

@Seismicisolation

3 POSSIBLE COMBINATIONS

From Fig. 4.2 it can be seen that curves of completely different character are found if its power is varied within certain limits. It is interesting to study how the curvature of a shell is influenced by the combination of two of these curves in the horizontal and the vertical cross-section. If for instance four different ellipses are considered with values of *n* equal to 0·5, 1, 2 or 100 and which are of principally different character, as many as 16 different possible combinations are found for the horizontal and the vertical cross-section. This is demonstrated in the form of a matrix in Fig. 4.3. The variants F and H lead to virtually similar ground floor plans and hence to more or less similar shapes but they are derived in basically different ways.

4 METHOD OF SUBDIVISION

In order to visualise these shapes lines or grids have to be projected upon the surface. A great number of commonly used geodesic subdivisions has been described by J.D. Clinton.[2,3] In all of these cases a triangulated network is obtained, based on one of the three Platonic polyhedra that consist of regular triangles only, viz. the tetrahedron, the octahedron or the icosahedron. The polyhedron is positioned so that its centre coincides with the centre of the system (Fig. 4.4). The equilateral triangles are then subdivided into smaller triangles. The connecting lines of their respective corners and the centre of the system are protruded until the surface of the surrounding shell is intersected. The points found thus on the shell can be interconnected (Fig. 4.5). For the purpose of this exercise the octahedron has been chosen as the basis for the subdivision. This octahedron is positioned with each of its vertices upon one of the axes of the coordinate

@Seismicisolation

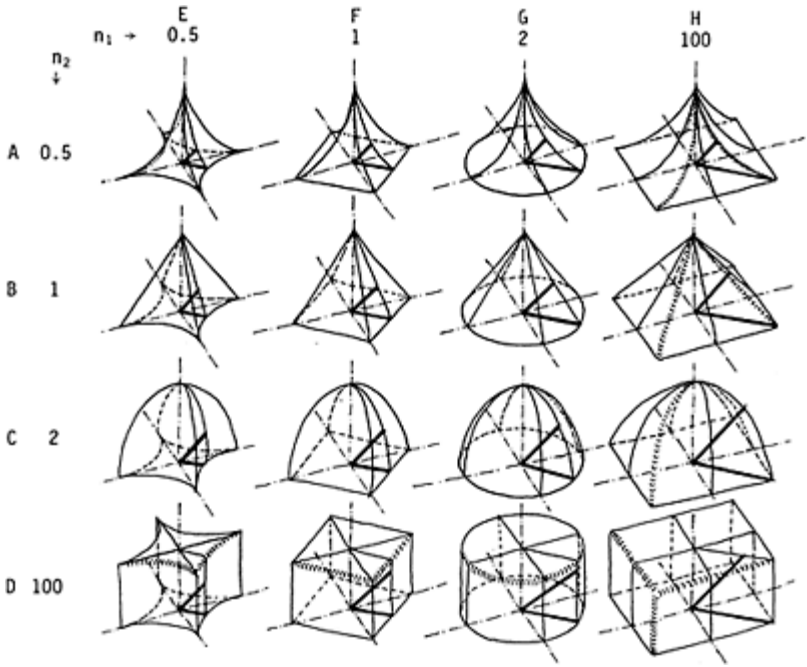

Fig. 4.3. Matrix of possible combinations for four different values of *n*1 and *n*2.

system and at a distance of $1/\sqrt{2}$ from the centre for the case that the original edge length=1. All triangles of the octahedron lie complete and alone in one of the octants. The polyhedron triangles are subdivided into identical, equilateral smaller triangles before projection upon the sphere. Clinton discerns many other possible subdivisions which also deliver triangulated patterns. The first one only has been incorporated in the program. Nevertheless, apart from the so-called ‘geodesic’ interconnection lines, another pattern called ‘antiprismatic’ has been introduced, using the same projection points (Fig. 4.5).

@Seismicisolation

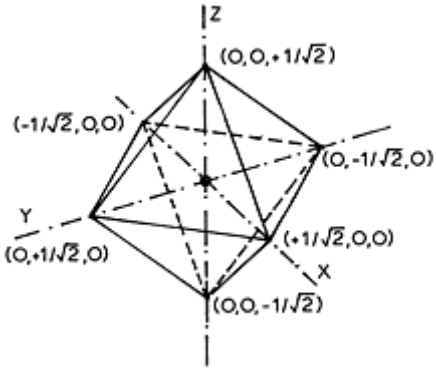

Fig. 4.4. Position of basic octahedron in the rectangular coordinate system.

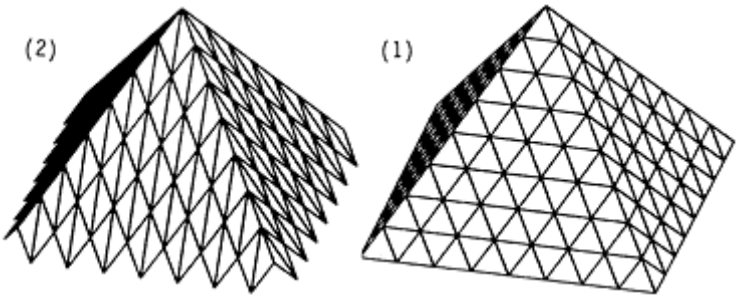

Fig. 4.5. Triangular subdivision of polyhedron triangle according to the 'geodesic' (1) and 'antiprismatic' (2) pattern.

5 COMPUTER PROGRAMS

Two computer programs have been developed, both of which require more or less the same input; the first produces a number of relevant alphanumeric geometric data, whereas the second provides the data necessary for the realisation of sketches. The latter has been inserted in the VISIPLOT system. With the help of this and of the IBM mainframe of the Delft University Computing Centre all sketches reproduced here have been made.

The required input data are:

FR=frequency of the subdivision,

E_1=ratio of long and short axes of ground ellipse,

E_2=ratio of long and short axes of vertical ellipse,

n_1 =exponent of ground ellipse,

@Seismicisolation

n_2=exponent of vertical ellipse,
FACTOR=magnification ratio,
n_3=number of sectors in ground floor plan,
TYPE=form of subdivision, viz. 1=geodesic and 2=antiprismatic.

The number of the sectors in the ground floor plan can mathematically be varied by multiplication of the original data of the octahedron (which has four sectors in the ground floor plan) with the factor $N3/4$ (Fig. 4.19). This has, of course, specific implications in the case that the horizontal ellipse has two different axes. Figure 4.6 shows an example of such an ellipsoid with the input FR=8, E_1=5, E_2=1, n_1=20, n_2=2, FACTOR=1, n_3=6, TYPE =1. This figure is produced with the help of the program SUPEREL.PUNCH.

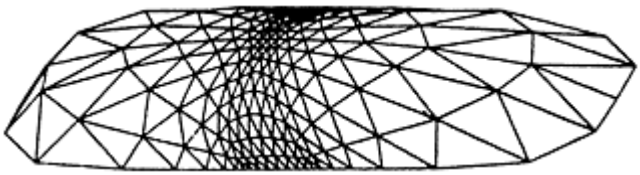

Fig. 4.6. Example of a superellipsoid with six horizontal sectors and with 8–frequency geodesic subdivision.

The alphanumeric program is called SUPERELLIPSOIDS and produces:

— cartesian and polar coordinates,
— lengths of the edges,
— face angles of the triangular elements,
— dihedral angles along the edges,
— angles between edge and radii at both of its ends,
— dihedral angles,
— area of each triangle and total area of hemisphere.
— volume of the hemisphere,
— statistical data of individual triangles.

The total area of the envelope is found by the summation of the areas of all individual triangles. Similarly the total volume is defined by the sum of all pyramids having the triangles as their basis and the system centre as their apex. Their magnitude may give information on some utility aspects of buildings thus formed, such as: amount of material used, heat loss, enclosed volume of air to be heated, etc. These data may therefore serve as tools for the optimisation of different solutions for one specifie case.

Being of special interest to the authors, a case had been studied for which a prismatic space of 40×60 cm in ground floor plan and with a height of 60 cm had to be circumscribed as closely as possible. Different solutions have been compared:

(1) sphere (i.e. groundcircle with vertical circle),
(2) groundcircle with vertical ellipse (n_2=2),
(3) groundcircle with vertical superellipse (n_2=2·5),

@Seismicisolation

(4) groundsuperellipse (n_1=2·5) with vertical superellipse (n_2=2·5),
(5) groundsuperellipse (n_1=100) with vertical superellipse (n_2=100).

In these five cases the data shown in Table 4.1 have been found for 1/8th sphere:

Table 4.1

Case	*Total area in cm²*	*Total volume in cm³*	
1	7597 (7697)	175404 (179595)	sphere
2	5887	112346 (115515)	ellipsoid
3	5567	102456	
4	5238	88046	
5	3345 (3600)	35460 (36000)	prism

If these two criteria are considered as decisive a clear preference is expressed, as expected, for the fifth case. This, however, is more or less of hypothetical value only as it represents a figure which is almost identical to the prismatic space itself to be circumscribed. The fourth case is more realistic. The results of the mathematical expression describing the pure sphere, ellipsoid or prism are given in parentheses, after the outcome of the program.

6 COMPUTER DRAWINGS

Figure 4.3 shows the theoretical number of possible combinations for four different curve types in both directions. Each item in this matrix in fact represents a whole group of forms

@Seismicisolation

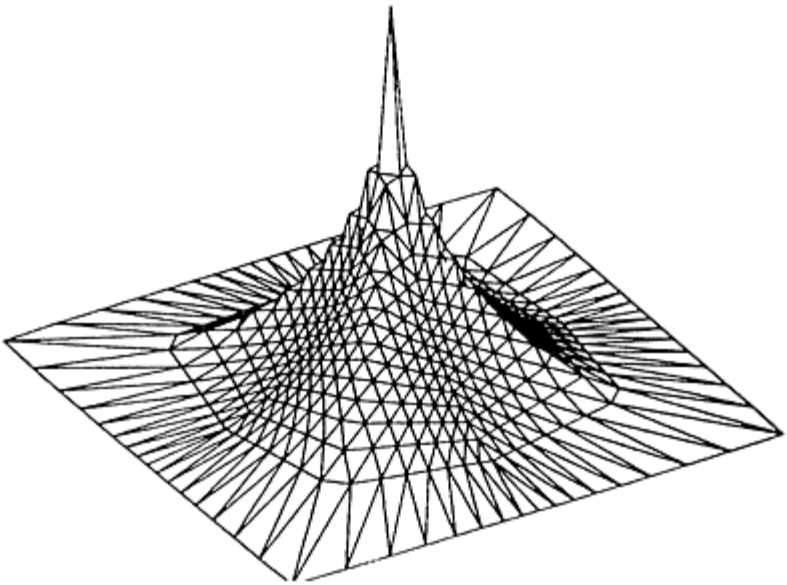

Fig. 4.7. Variant AH; inverted umbrella, n_1=100, n_2=0·5, E_1=1, E_2 $=1{\cdot}5\sqrt{2}$, FACTOR $=0{\cdot}5\sqrt{2}$, Freq.=24, n_3=4, TYPE=1.

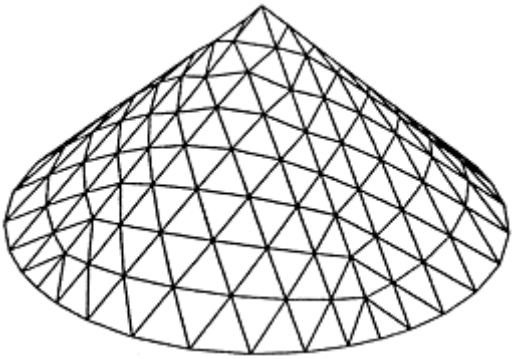

Fig. 4.8. Variant BG; cone, n_1=2, n_2=l, E_1=1, E_2=1, FACTOR=1, Freq.=8, n_3 =4, TYPE =1.

@Seismicisolation

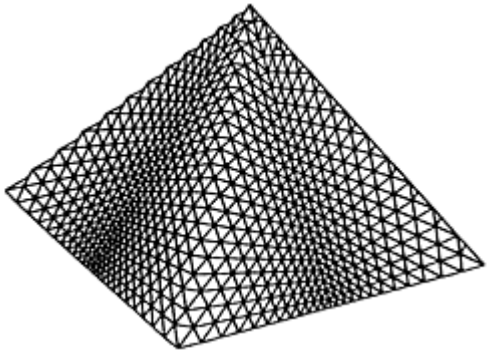

Fig. 4.9. Variant BH; pyramid, n_1 =100, n_2 =1 E_1=1, $E2=\sqrt{2}$, FACTOR $=0{\cdot}5\sqrt{2}$, Freq.=24, n_3=3, TYPE=1.

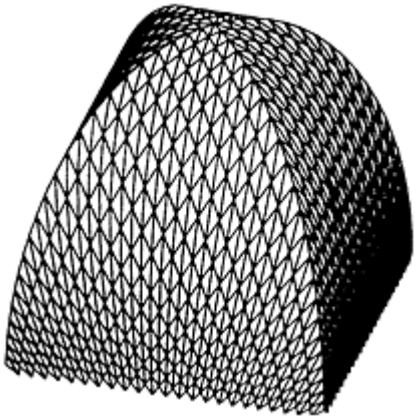

Fig. 4.10. Variant CF; cross vault, n_1=1, n_2=2, E_1=1, $E_2=\sqrt{2}$, FACTOR=$_1$, Freq.=8, n_3=4, TYPE=2.

@Seismicisolation

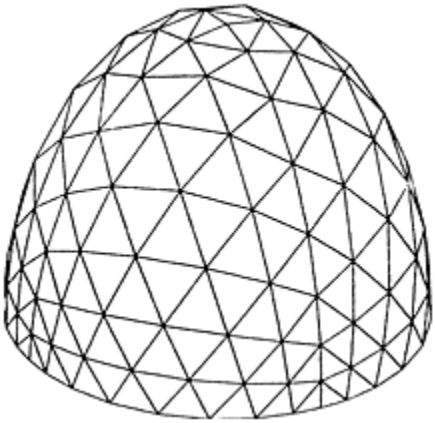

Fig. 4.11. Variant CG; pure rotation symmetric ellipsoid, n_1=2, n_2=2, E_1=1, E_2=1·5, FACTOR=1, Freq.=8, n_3=4, TYPE=1.

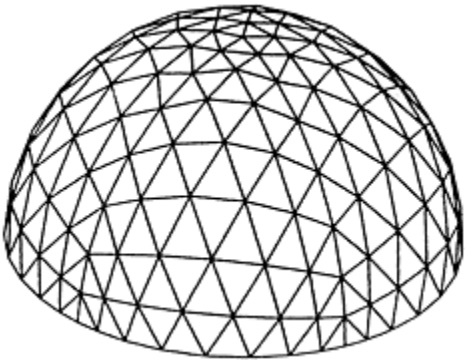

Fig. 4.12. Variant CG; pure sphere, n_1=1, n_2=2, E_1=1, E_2=1, FACTOR=1, Freq.=8, n_3=5, TYPE =1.

@Seismicisolation

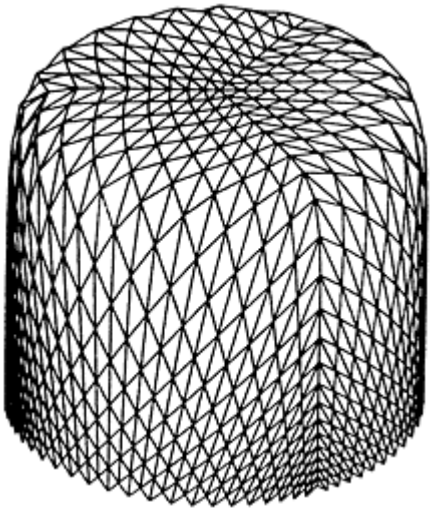

Fig. 4.13. Variant CG; ‘bowler hat’, n_1=2, n_2=10, E_1=1, E_2=1·5, FACTOR=1, Freq.=24, n_3=3, TYPE=1.

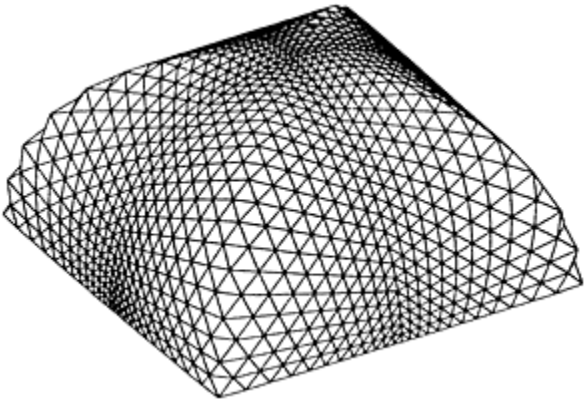

Fig. 4.14. Variant CH; cross vault, n_1=100, n_2=2, E_1=1, E_2=1, FACTOR=1, Freq.=24, n_3=4, TYPE=1.

@Seismicisolation

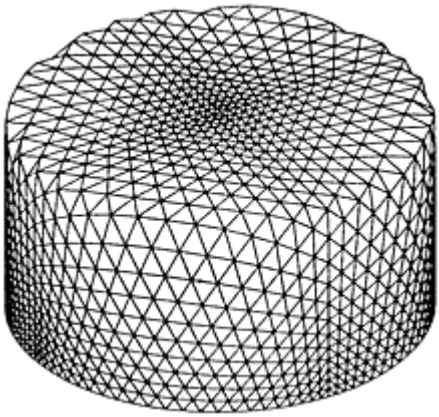

Fig. 4.15. Variant DG; cylinder, n_1= 2, n_2=100, E_1=1, E_2=1, FACTOR=1, Freq.=24, n_3=4, TYPE =1.

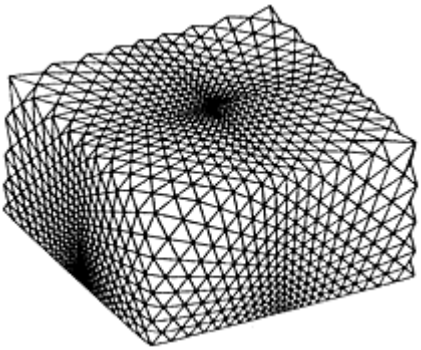

Fig. 4.16. Variant DH; cube, n_1=100, n_2 = 100, E1=1, E_2=1, FACTOR$=0{\cdot}5\sqrt{2}$, Freq.=24, n_3=4, TYPE=1.

@Seismicisolation

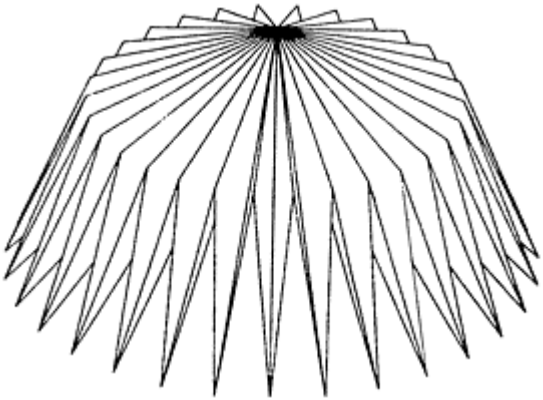

Fig. 4.17. Variant CG; folded plate shell, n_1=2, n_2=2, E_1=1, E_2=1, FACTOR=1, Freq.=2, n_3=30, TYPE=2.

with specific characteristics. Sketches of a number of those characteristic specimens have been made (Figs 4.7–4.17). In all these cases the subdivision has been done according to the method 1.

A somewhat unexpected shape is CG, which derives its folded surface from the conditions that it counts 30 sectors and that the subdivision is antiprismatic (see Fig. 4.17).

7 ADAPTATIONS

Programs like the one previously described can be changed according to specific wishes. If, for instance, cylinders are generated, they will appear in a vertical position and in the case that one uses only half of it this will cover a circular ground floor plan. It is possible, though, to generate a vertical half of it and to use this horizontally over a rectangular ground floor plan (Fig. 4.18). This is done by introducing a new variable n_4, which has some specific values.

As depicted in Fig. 4.19, the sectors in ground floor plan are generally mutually equal. Their number is given by the variable n_3.

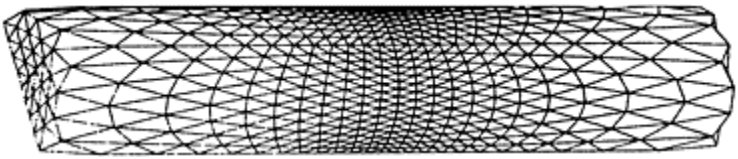

@Seismicisolation

Fig. 4.18. Cylinder, n_1=2, n_2=100, E_1=1, E_2=5, FACTOR=1, Method=1, Freq.=16, n_3=4, n_4=3, TYPE=1.

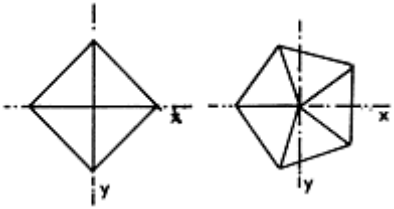

Fig. 4.19. Ground floor plan with numbers of sectors n_3 (octahedron: n_3=4).

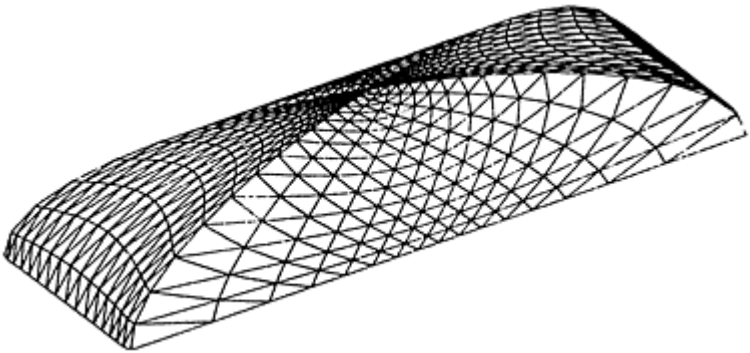

Fig. 4.20. Modified hipped barrel vault, n_1=100, n_2=2, E_1=3, $E_2 = \sqrt{2}$, FACTOR=1, Method=3, Freq.=16, n_3=4, n_4=0, TYPE=1.

@Seismicisolation

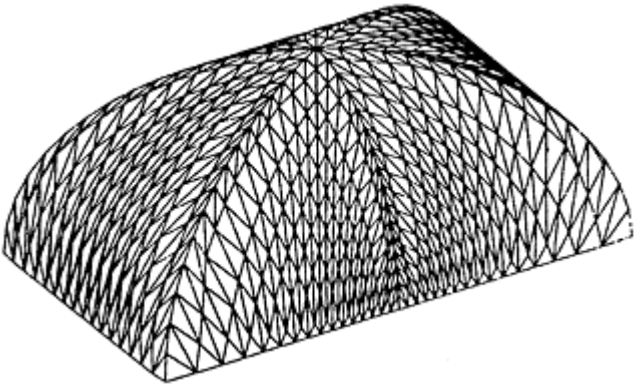

Fig. 4.21. Hipped barrel vault, n_1=100, n_2=2, $E1 = \sqrt{3}$, $E2 = \sqrt{2}$, FACTOR=1, Method=3, Freq.=16, n_3=6, n_4=1, TYPE=2.

Figure 4.20 shows a vault which covers a rectangular ground floor, although it counts 4 sectors. The sectors are in this case, however, not kept similar. A comparable effect is obtained in Fig. 4.21, where a structure is generated which is cylindrical in its longest horizontal direction merely by a proper choice of the variables.

8 POSSIBLE FUTURE DEVELOPMENTS

The described programs embody the present status quo in an ongoing research process. Further extensions could include:

— other classes of geodesic subdivision, [2]
— other basic polyhedra: tetrahedron and icosahedron as well as the three duals, viz. the cube, the rhombic dodecahedron and triacontahedron,
— eventual vertical shift of the projection centre of the subdivision pattern with respect to the system centre in order to be able to choose the base plane freely,
— truncations in horizontal or vertical sense with corresponding adaptation of adjacent vertices.

ACKNOWLEDGEMENT

Much support has been given by Ir. Jac. de Wilde of the Delft University Computing Centre. The authors wish to thank him cordially for his invaluable assistance.

REFERENCES

@Seismicisolation

1. Kenner, H. *Geodesic Math and How to Use it.* University of California Press, Berkeley, 1976.
2. Clinton, J.D. Advanced structural geometry studies, NASA Contract Report, CR1735.
3. Dome book 2, Pacific Domes, London, 1971.

@Seismicisolation

5
Analysis of Reticulated Shells by the Equivalent Continuous Method

CAO ZI and ZHANG SHAN-YU
Department of Civil Engineering, Beijing Polytechnical University, People's Republic of China

1 INTRODUCTION

The analysis of reticulated shells by the equivalent continuous method is an approximate practical method. It is based on the fact that the meshes of reticulated shells are of much smaller magnitude than their spans. Therefore, it can be approximately assumed that the stresses and strains in the bars of reticulated shells vary continuously, so that the models of the reticulated shells could be replaced by those of the continuous shells and analysed using the various methods of analysis of continuous shells. The internal forces and joint displacement of the bars are then derived.

In the past thirty years, there have been many papers, at home and abroad, dealing with the analysis of reticulated shells using the equivalent continuous method, and much experience has been gained in engineering practice as well. For medium and small size reticulated shells, the results obtained by using this method generally satisfy the requirements of engineering accuracy. Compared with other methods, it is simpler and more practical, and can be done manually or with a microcomputer. Therefore, even in countries where electronic computers are widely used, this method still has its practical value. But there also remain some problems to be solved in using the equivalent continuous method to analyse reticulated shells.

(1) How to replace the calculation model reasonably and quickly, i.e. how to determine the physical constants of equivalent continuous shells? This is a key problem of the equivalent continuous method.
(2) The equivalent shells, after replacement, are normally anisotropic. How to calculate the internal forces and displacements rapidly is another problem.
(3) In general, it is difficult to control the calculation accuracy.

In this paper, the authors make an investigation into the first two problems, using membrane flexibility a_{ij} and flexural stiffness coefficient d_{ij} as the basic physical constants, derive general formulae, and give physical constants with comparative accuracy for several generally adopted grids. The general formulae of internal forces and displacements are also given for orthogonal anisotropic cylindrical shells to facilitate both manual and computer computations.

@Seismicisolation

2 DETERMINATION OF PHYSICAL CONSTANTS

The physical constants are generally determined according to the principle that the internal forces and deformations or strain energy of the basic grid elements of the reticulated shells are equivalent to those of the corresponding continuous shells. The basic grid elements chosen must be of the simplest and representative ones, including all types of bar arrangement of the reticulated shells. There are many types of bar arrangement. For single-layer reticulated cylindrical shells, the common types of bar arrangement are: triangular grid pattern, single diagonal pattern in one direction, single diagonal pattern in two directions, cross diagonal pattern, rhombic grid pattern, etc. as

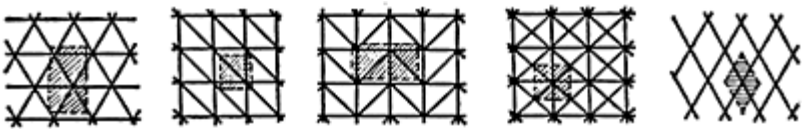

Fig. 5.1.

shown in Fig. 5.1. The choice of basic grid elements is also shown in Fig. 5.1. Grid bars are assumed to be subject to axial force only at their middle face (except rhombic grid pattern) and bending and torsion outside of the middle face.

2.1 Derivation of the General Formulae

2.1.1 The general formulae of flexural stiffness

Let *x*, *y* be the axes of the global coordinates of the structure as shown in Fig. 5.2. (The bars of the basic grid elements need not be parallel to the *x* or *y* axis, and may form any angle with the axes.) Let again φi be the angle between any arbitrary bar *i* of a basic grid element of any pattern and the positive direction of the *x* axis, *ei* be the spacing of bar *i*, local coordinate s_i axis coincides with bar i, and $\bar{s}_i$ axis be perpendicular to bar *i*.

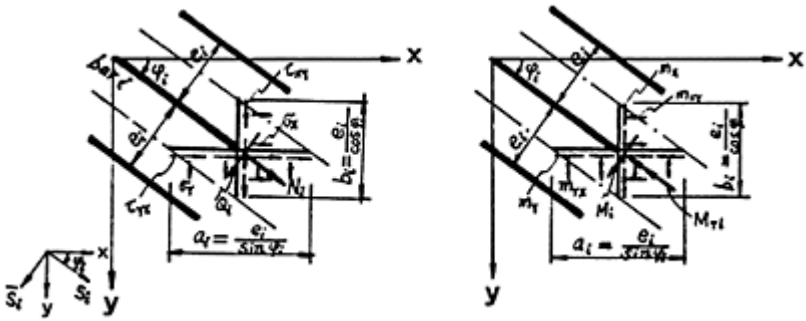

Fig. 5.2.

@Seismicisolation

Replace the internal forces of the pseudo bar i in Fig. 5.2(a) with distributed ones along the x and y directions respectively.

$$\left.\begin{aligned}
\sigma_x &= \frac{|\cos\varphi_i|}{e_i}(N_i\cos\varphi_i - Q_i\sin\varphi_i)\\
\tau_{xy} &= \frac{|\cos\varphi_i|}{e_i}(N_i\sin\varphi_i + Q_i\cos\varphi_i)\\
\sigma_y &= \frac{|\sin\varphi_i|}{e_i}(N_i\sin\varphi_i + Q_i\cos\varphi_i)\\
\tau_{yx} &= \frac{|\sin\varphi_i|}{e_i}(N_i\cos\varphi_i - Q_i\sin\varphi_i)
\end{aligned}\right\}$$

When φ_i is the angle obtained by revolving the positive x axis to the bar i direction $(0 \le \varphi_i \le 2\pi)$, the above expressions can be generalised to the following universal ones:

$$\left.\begin{aligned}
\sigma_x &= \frac{1}{e_i}(N_i\cos^2\varphi_i - Q_i\sin\varphi_i\cos\varphi_i)\\
\sigma_y &= \frac{1}{e_i}(N_i\sin^2\varphi_i + Q_i\sin\varphi_i\cos\varphi_i)\\
\tau_{xy} &= \frac{1}{e_i}(N_i\sin\varphi_i\cos\varphi_i + Q_i\cos^2\varphi_i)\\
\tau_{yx} &= \frac{1}{e_i}(N_i\sin\varphi_i\cos\varphi_i - Q_i\sin^2\varphi_i)
\end{aligned}\right\} \qquad (1)$$

Similarly we obtain

$$\left.\begin{aligned}
m_x &= \frac{1}{e_i}(M_i\cos^2\varphi_i - M_{\tau i}\sin\varphi_i\cos\varphi_i)\\
m_y &= \frac{1}{e_i}(M_i\sin^2\varphi_i + M_{\tau i}\sin\varphi_i\cos\varphi_i)\\
m_{xy} &= \frac{1}{e_i}(M_i\sin\varphi_i\cos\varphi_i + M_{\tau i}\cos^2\varphi_i)\\
m_{yx} &= \frac{1}{e_i}(M_i\sin\varphi_i\cos\varphi_i - M_{\tau i}\sin^2\varphi_i)
\end{aligned}\right\} \qquad (2)$$

If we transform equivalently M_i, $M_{\tau i}$ in all bar i (i=1, 2, …, n) of the basic grid element on to sections perpendicular to the x and y axes, we obtain the following sum of equivalent internal forces on these sections:

@Seismicisolation

$$\left.\begin{aligned} M'_x &= \sum_{i=1}^{n} \frac{1}{e_i}(M_i \cos^2 \varphi_i - M_{\tau i} \sin \varphi_i \cos \varphi_i) \\ M'_y &= \sum_{i=1}^{n} \frac{1}{e_i}(M_i \sin^2 \varphi_i + M_{\tau i} \sin \varphi_i \cos \varphi_i) \\ M'_{xy} &= \sum_{i=1}^{n} \frac{1}{e_i}(M_i \sin \varphi_i \cos \varphi_i + M_{\tau i} \cos^2 \varphi_i) \\ M'_{yx} &= \sum_{i=1}^{n} \frac{1}{e_i}(M_i \sin \varphi_i \cos \varphi_i - M_{\tau i} \sin^2 \varphi_i) \end{aligned}\right\} \tag{3}$$

When bar i has D_i and $D_{\tau i}$ as its flexural and twisting stiffnesses respectively, then its bending moment M_i and twisting moment $M_{\tau i}$ will have the following relations to its deformation:

$$M_i = -D_i \frac{\partial^2 w}{\partial s_i^2} \qquad M_{\tau i} = -D_{\tau i} \frac{\partial^2 w}{\partial s_i \partial s_i}$$

By coordinate transformation we get

$$\left.\begin{aligned} M_i &= -D_i\left[\cos^2 \varphi_i \frac{\partial^2 w}{\partial x^2} + \sin^2 \varphi_i \frac{\partial^2 w}{\partial y^2} + 2 \sin \varphi_i \cos \varphi_i \frac{\partial^2 w}{\partial x \partial y}\right] \\ M_{\tau i} &= -D_{\tau i}\left[-\sin \varphi_i \cos \varphi_i \frac{\partial^2 w}{\partial x^2} + \sin \varphi_i \cos \varphi_i \frac{\partial^2 w}{\partial y^2} + (\cos^2 \varphi_i - \sin^2 \varphi_i) \frac{\partial^2 w}{\partial x \partial y}\right] \end{aligned}\right\} \tag{4}$$

Let

$$K_x = -\frac{\partial^2 w}{\partial x^2} \qquad K_y = -\frac{\partial^2 w}{\partial y^2} \qquad K_{xy} = -2\frac{\partial^2 w}{\partial x \partial y}$$

then

$$M_i = D_i[\cos^2 \varphi_i K_x + \sin^2 \varphi_i K_y + \sin \varphi_i \cos \varphi_i K_{xy}]$$

$$M_{\tau i} = D_{\tau i}[-\sin \varphi_i \cos \varphi_i K_x + \sin \varphi_i \cos \varphi_i K_y + \tfrac{1}{2}(\cos^2 \varphi_i - \sin^2 \varphi_i) K_{xy}]$$

The internal force-strain relationships of the continuous shell element are

$$M_x = d_{11} K_x + d_{12} K_y + d_{13} K_{xy}$$

$$M_y = d_{21} K_x + d_{22} K_y + d_{23} K_{xy}$$

$$M_{xy} = d_{31} K_x + d_{32} K_y + d_{33} K_{xy}$$

According to the equivalent principle of internal forces between reticulated and continuous shell elements, we put

@Seismicisolation

$$M_x = M'_x \qquad M_y = M'_y \qquad M_{xy} = \tfrac{1}{2}(M'_{xy} + M'_{yx})$$

i.e. the internal forces M_x, M_y, M_{xy} in the continuous shell element are

$$\left.\begin{aligned} M_x &= \sum_{i=1}^{n} \frac{1}{e_i}[M_i \cos^2\varphi_i - M_{ti} \sin\varphi_i \cos\varphi_i] \\ M_y &= \sum_{i=1}^{n} \frac{1}{e_i}[M_i \sin^2\varphi_i + M_{ti} \sin\varphi_i \cos\varphi_i] \\ M_{xy} &= \sum_{i=1}^{n} \frac{1}{e_i}[M_i \sin\varphi_i \cos\varphi_i + \tfrac{1}{2}M_{ti}(\cos^2\varphi_i - \sin^2\varphi_i)] \end{aligned}\right\} \tag{5}$$

If we give differently the reticulated and continuous shell elements the same unit displacement, the flexural stiffness d_{ij} of the equivalent continuous shell of different grid patterns could be obtained.

$$\left.\begin{aligned} d_{11} &= \sum_{i=1}^{n} \frac{1}{e_i}[D_i \cos^4\varphi_i + D_{ti} \sin^2\varphi_i \cos^2\varphi_i] \\ d_{12} &= \sum_{i=1}^{n} \frac{1}{e_i}[D_i - D_{ti}] \sin^2\varphi_i \cos^2\varphi_i \\ d_{13} &= \sum_{i=1}^{n} \frac{1}{e_i}[D_i \sin\varphi_i \cos^3\varphi_i - \tfrac{1}{2}D_{ti} \sin\varphi_i \cos\varphi_i (\cos^2\varphi_i - \sin^2\varphi_i)] \\ d_{22} &= \sum_{i=1}^{n} \frac{1}{e_i}[D_i \sin^4\varphi_i + D_{ti} \sin^2\varphi_i \cos^2\varphi_i] \\ d_{23} &= \sum_{i=1}^{n} \frac{1}{e_i}[D_i \sin^3\varphi_i \cos\varphi_i + \tfrac{1}{2}D_{ti} \sin\varphi_i \cos\varphi_i (\cos^2\varphi_i - \sin^2\varphi_i)] \\ d_{33} &= \sum_{i=1}^{n} \frac{1}{e_i}[D_i \sin^2\varphi_i \cos^2\varphi_i + \tfrac{1}{4}D_{ti}(\cos^2\varphi_i - \sin^2\varphi_i)^2] \end{aligned}\right\} \tag{6}$$

Where φ_i is the angle between bar i and the positive direction of the x axis $(0 \le \varphi_i \le 2\pi)$.

To simplify calculation, if in the basic grid element, there are bars parallel to the x or y axis, we can move these terms to outside the summation symbol Σ, making it represent only the summation of all the oblique bars. Let j be the number of the oblique bar, and let

@Seismicisolation

D_H, $D_{\tau H}$, e_H and D_v, $D_{\tau v}$, e_v be respectively the flexural stiffness, twisting stiffness, and spacing of the bars parallel to the x or y axis; converting the angle φ_i between the oblique bar j and the x axis into an acute angle, then expressions (6) could be simplified to

$$\left.\begin{aligned}
d_{11} &= \frac{D_H}{e_H} + \sum_j \frac{1}{e_j}[D_j\cos^4\varphi_j + D_{\tau j}\sin^2\varphi_j\cos^2\varphi_j] \\
d_{12} &= \sum_j \frac{1}{e_j}[D_j - D_{\tau j}]\sin^2\varphi_j\cos^2\varphi_j \\
d_{13} &= \pm\sum_j \frac{1}{e_j}[D_j\sin\varphi_j\cos^3\varphi_j - \tfrac{1}{2}D_{\tau j}\sin\varphi_j\cos\varphi_j(\cos^2\varphi_j - \sin^2\varphi_j)] \\
d_{22} &= \frac{D_v}{e_v} + \sum_j \frac{1}{e_j}[D_j\sin^4\varphi_j + D_{\tau j}\sin^2\varphi_j\cos^2\varphi_j] \\
d_{23} &= \pm\sum_j \frac{1}{e_j}[D_j\sin^3\varphi_j\cos\varphi_j + \tfrac{1}{2}D_{\tau j}\sin\varphi_j\cos\varphi_j(\cos^2\varphi_j - \sin^2\varphi_j)] \\
d_{33} &= \frac{D_{\tau H}}{4e_H} + \frac{D_{\tau v}}{4e_v} + \sum_j \frac{1}{e_j}[D_j\sin^2\varphi_j\cos^2\varphi_j + \tfrac{1}{4}D_{\tau j}(\cos^2\varphi_j - \sin^2\varphi_j)^2]
\end{aligned}\right\} \qquad (7)$$

Where the sign of d_{13} and d_{23} is determined as follows:+for bars in direction as shown in Fig. 5.3(a),—for bars in direction as shown in Fig. 5.3(b).

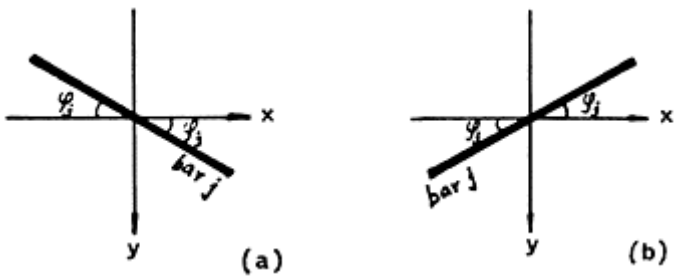

Fig. 5.3.

2.1.2 The general formulae of membrane stiffness

The same method for obtaining flexural stiffness d_{ij} may be used to find membrane stiffness b_{ij}. The general formulae of b_{ij} for different grid patterns (except the rhombic grid pattern) are obtained by substituting tensile stiffness B_i of bars into flexural stiffness and 0 into $D_{\tau i}$ on expressions (7).

@Seismicisolation

$$\left.\begin{aligned}
b_{11} &= \frac{B_H}{e_H} + \sum_j \frac{B_j}{e_j}\cos^4\varphi_j \\
b_{12} &= \sum_j \frac{B_j}{e_j}\sin^2\varphi_j\cos^2\varphi_j \\
b_{13} &= \pm\sum_j \frac{B_j}{e_j}\sin\varphi_j\cos^3\varphi_j \\
b_{22} &= \frac{B_v}{e_v} + \sum_j \frac{B_j}{e_j}\sin^4\varphi_j \\
b_{23} &= \pm\sum_j \frac{B_j}{e_j}\sin^3\varphi_j\cos\varphi_j \\
b_{33} &= \sum_j \frac{B_j}{e_j}\sin^2\varphi_j\cos^2\varphi_j
\end{aligned}\right\} \tag{8}$$

where φ_i is the acute angle between the oblique bar i and the x axis. The sign of b_{13}, b_{23} is determined as for flexural stiffness.

2.1.3 Calculation of membrane flexibility a_{ij}

Membrane flexibility a_{ij} may be expressed in terms of membrane stiffness:

$$a_{ij} = \frac{A_{ij}}{D} \qquad D = \begin{vmatrix} b_{11} & b_{12} & b_{13} \\ b_{21} & b_{22} & b_{23} \\ b_{31} & b_{32} & b_{33} \end{vmatrix} \tag{9}$$

where A_{ij} is the cofactor of determinant D.

After obtaining the membrane stiffness b_{ij} of various grid patterns, their flexibility a_{ij} is not difficult to obtain.

For statically determined grid elements, sometimes direct computation is also applicable to membrane flexibility. We will not discuss it in detail here, however.

@Seismicisolation

3 THE GENERAL FORMULAE OF PHYSICAL CONSTANTS FOR SEVERAL CONVENTIONAL GRIDS

3.1 The General Formulae of Physical Constants for Triangular Grids

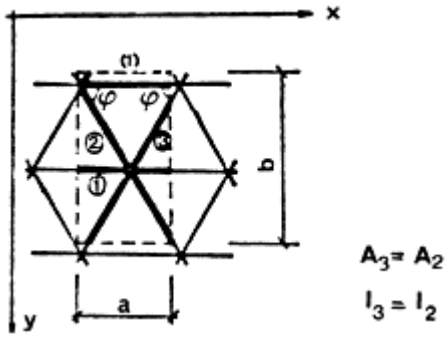

Fig. 5.4.

Table 5.1

Physical constant	*Arbitrary angle φ*	$\varphi = 60°$	$\varphi = 60°$ $A_1 = A_2 = A_3$ $I_1 = I_2 = I_3$
d_{11}	$\frac{2}{b}[D_1 + D_2\cos^3\varphi + D_{\tau 2}\sin^2\varphi\cos\varphi]$	$\frac{1}{4\sqrt{3}a}(8D_1 + D_2 + 3D_{\tau 2})$	$\frac{\sqrt{3}}{4a}(3D + D_\tau)$
d_{12}	$\frac{2}{a}(D_2 - D_{\tau 2})\sin\varphi\cos^2\varphi$	$\frac{\sqrt{3}}{4a}(D_2 - D_{\tau 2})$	$\frac{\sqrt{3}}{4a}(D - D_\tau)$
d_{13}	0	0	0
d_{22}	$\frac{2}{a}[D_2\sin^3\varphi + D_{\tau 2}\sin\varphi\cos^2\varphi]$	$\frac{\sqrt{3}}{4a}(3D_2 + D_{\tau 2})$	$\frac{\sqrt{3}}{4a}(3D + D_\tau)$
d_{23}	0	0	0
d_{33}	$\frac{1}{b}\left[\frac{1}{2}D_{\tau 1} + 2D_2\sin^2\varphi\cos\varphi + D_{\tau 2}\frac{(\cos^2\varphi - \sin^2\varphi)^2}{2\cos\varphi}\right]$	$\frac{1}{4\sqrt{3}a}(2D_{\tau 1} + 3D_2 + D_{\tau 3})$	$\frac{\sqrt{3}}{4a}(D + D_\tau)$
a_{11}	$\frac{a}{2B_1}tg\varphi$	$\frac{\sqrt{3}a}{2B_1}$	$\frac{\sqrt{3}a}{2B}$

@Seismicisolation

a_{12}	$-\dfrac{a}{2B_1 tg\varphi}$	$-\dfrac{a}{2\sqrt{3}B_1}$	$-\dfrac{a}{2\sqrt{3}B}$
a_{13}	0	0	0
a_{22}	$\dfrac{a\left(1+\dfrac{A_2}{A_1}\cos^3\varphi\right)}{2B_2\sin^3\varphi}$	$\dfrac{a\left(8+\dfrac{A_2}{A_1}\right)}{6\sqrt{3}B_2}$	$\dfrac{\sqrt{3}a}{2B}$
a_{23}	0	0	0
a_{33}	$\dfrac{a}{2B_2\cos^2\varphi\sin\varphi}$	$\dfrac{4a}{\sqrt{3}B_2}$	$\dfrac{4a}{\sqrt{3}B}$

3.2 The General Formulae of Physical Constants for Single Diagonal Patterns

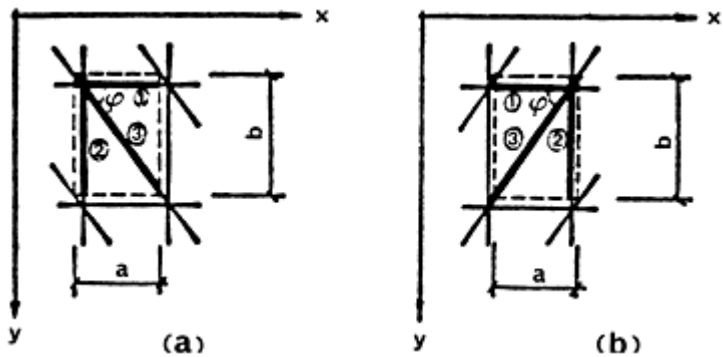

Fig. 5.5.

Table 5.2

Physical constant	*Arbitrary angle φ*	$\varphi \pm 45°$ $A_1 = A_2 = A; A_3 = \dfrac{A}{\sqrt{2}}$ $I_1 = I_2 = I; I_3 = \dfrac{I}{\sqrt{2}}$
d_{11}	$\dfrac{1}{b}[D_1 + D_3\cos^3\varphi + D_{\tau 3}\sin^2\varphi\cos\varphi]$	$\dfrac{5D+D_\tau}{4a}$
d_{12}	$\dfrac{1}{a}[D_3 - D_{\tau 3}]\sin\varphi\cos^2 x$	$\dfrac{D-D_\tau}{4a}$
d_{13}	$\pm\dfrac{1}{b}[D_3\sin\varphi\cos^2\varphi - \frac{1}{2}D_{\tau 3}\sin\varphi(\cos^2\varphi - \sin^2\varphi)]$	$\pm\dfrac{D}{4a}$

@Seismicisolation

d_{22}	$\frac{1}{a}[D_2 + D_3\cos^3\varphi + D_{\tau 3}\sin\varphi\cos^2\varphi]$	$\frac{5D + D_\tau}{4a}$
d_{23}	$\pm\frac{1}{a}[D_3\sin^2\varphi\cos\varphi + \frac{1}{2}D_{\tau 3}\cos\varphi(\cos^2\varphi - \sin^3\varphi)]$	$\pm\frac{D}{4a}$
d_{33}	$\frac{D_{\tau 2}}{4a} + \frac{1}{b}\left[\frac{D_{\tau 1}}{4} + D_3\sin^2\varphi\cos\varphi + \frac{1}{4}D_{\tau 3}\frac{1}{\cos\varphi}(\cos^2\varphi - \sin^2\varphi)^2\right]$	$\frac{2D_\tau + D}{4a}$
a_{11}	$\frac{b}{B_1}$	$\frac{a}{B}$
a_{12}	0	0
a_{13}	$\mp\frac{a}{B_1}$	$\mp\frac{a}{B}$
a_{22}	$\frac{a}{B_2}$	$\frac{a}{B}$
a_{23}	$\mp\frac{b}{B_2}$	$\mp\frac{a}{B}$
a_{33}	$\frac{a}{B_1 tg\varphi} + \frac{b tg\varphi}{B_2} + \frac{a}{B_3\sin\varphi\cos^2\varphi}$	$\frac{6a}{B}$

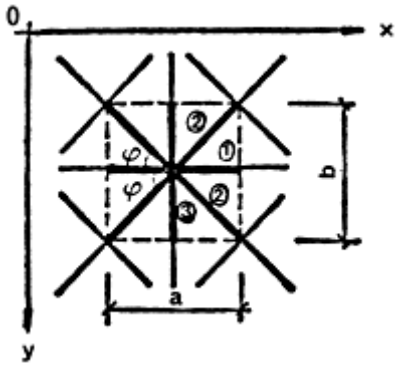

Fig. 5.6.

Note: The upper+sign is for the grid pattern shown in Fig. 5.5(a) and the lower—sign for the pattern shown in Fig. 5.5(b).

@Seismicisolation

3.3 The General Formulae of Physical Constants for Cross Diagonal Pattern

Table 5.3

Physical constant	*Arbitrary angle φ*	$\varphi = 45°$ $A_1 = A_3 = A;\ A_2 = \frac{A}{\sqrt{2}}$ $I_1 = I_3 = I;\ I_2 = \frac{I}{\sqrt{2}}$
d_{11}	$\frac{1}{b}[D_1 + 2D_2\cos^3\varphi + 2D_{\tau 2}\sin^2\varphi\cos\varphi]$	$\frac{1}{2a}(3D + D_\tau)$
d_{12}	$\frac{2}{a}[D_2 - D_{\tau 2}]\sin\varphi\cos^2\varphi$	$\frac{1}{2a}(D - D_\tau)$
d_{13}	0	0
d_{22}	$\frac{1}{a}[D_3 + 2D_2\sin^3\varphi + 2D_{\tau 2}\sin\varphi\cos^2\varphi]$	$\frac{1}{2a}(3D + D_\tau)$
d_{23}	0	0
d_{33}	$\frac{1}{4b}D_{\tau 1} + \frac{1}{4a}D_{\tau 3} + \frac{1}{b}\left[2D_2\sin^2\varphi\cos\varphi + \frac{1}{2}D_{\tau 2}\frac{1}{\cos\varphi}(\cos^2\varphi - \sin^2\varphi)^2\right]$	$\frac{1}{2a}(D + D_\tau)$
a_{11}	$\frac{b(B_3 + 2B_2\sin^3\varphi)}{B_1B_3 + 2B_1B_2\sin^3\varphi + 2B_2B_3\cos^3\varphi}$	$\frac{3a}{4B}$
a_{12}	$-\frac{2bB_2\sin\varphi\cos^2\varphi}{B_1B_3 + 2B_1B_2\sin^3\varphi + 2B_2B_3\cos^3\varphi}$	$-\frac{a}{4B}$
a_{13}	0	0
a_{22}	$\frac{a(B_1 + 2B_2\cos^3\varphi)}{B_1B_3 + 2B_1B_2\sin^3\varphi + 2B_2B_3\cos^3\varphi}$	$\frac{3a}{4B}$
a_{23}	0	0
a_{33}	$\frac{b}{2B_2\sin^3\varphi\cos\varphi}$	$\frac{2a}{B}$

@Seismicisolation

4 SOLUTION OF FUNDAMENTAL DIFFERENTIAL EQUATIONS AND FORMULAE FOR CALCULATING THE INTERNAL FORCES AND DISPLACEMENTS

It can be seen from the physical constants of the conventional reticulated shells that most basic grid elements belong to the orthogonal anisotropic type. Some do not, but for simplicity we often treat them as orthogonal anisotropic ones. Here, we only discuss the solution of fundamental differential equations for the case of orthogonal anisotropic cylindrical shells.

4.1 The Solutions of Homogeneous Equations

The characteristic equation of the homogeneous equations is

$$r^8+ar^6+br^4+cr^2+d=0 \tag{10}$$

in which

$$a=-\left[\frac{2(d_{12}+2d_{33})}{d_{22}}+\frac{2(a_{12}+a_{33})}{a_{11}}\right]k^2$$

$$b=\left[\frac{d_{11}}{d_{22}}+\frac{2(d_{12}+2d_{33})(2a_{12}+a_{33})}{a_{11}d_{22}}+\frac{a_{22}}{a_{11}}\right]k^4$$

$$c=-\left[\frac{(2a_{12}+a_{33})d_{11}}{a_{11}d_{22}}+\frac{2(d_{12}+2d_{33})a_{22}}{a_{11}d_{22}}\right]k^6$$

$$d=\left[\frac{a_{22}d_{11}}{a_{11}d_{22}}+\frac{R^2}{a_{11}d_{22}k^4}\right]k^8$$

$$k=\frac{\pi R}{l}$$

Let $r^2=\eta$ and substitute it into the above equation, to yield

$$n^4+an^3+bn^2+cn+d=0 \tag{11}$$

There are four solutions to eqn (11) as follows:

$$\left.\begin{aligned}\eta_{\frac{1}{2}}&=\tfrac{1}{2}\left(-\sqrt{f_1-b_0}\pm\sqrt{-f_1-b_0+2\sqrt{f_1^2-4d_0}}\right)-\frac{a}{4}\\ \eta_{\frac{3}{4}}&=\tfrac{1}{2}\left(\sqrt{f_1-b_0}\pm\sqrt{-f_1-b_0-2\sqrt{f_1^2-4d_0}}\right)-\frac{a}{4}\end{aligned}\right\} \tag{12}$$

@Seismicisolation

in which

$$f_1 = \sqrt[3]{-\frac{q}{2} + \sqrt{\frac{q^2}{4} - \frac{p^2}{27}}} + \sqrt[3]{-\frac{q}{2} - \sqrt{\frac{q^2}{4} + \frac{p^3}{27}}} + \frac{b_0}{3}$$

$$p = -\tfrac{1}{3}(b_0^2 + 12d_0) \qquad q = -\tfrac{1}{27}(2b_0^3 - 72b_0d_0 + 27c_0^2)$$

$$b_0 = -\tfrac{3}{8}a^2 + b \qquad c_0 = \tfrac{1}{8}a^3 - \tfrac{1}{2}ab + c$$

$$d_0 = -\tfrac{3}{256}a^4 + \tfrac{1}{16}a^2b - \tfrac{1}{4}ac + d$$

From this we obtain the following eight roots, $r = \pm\sqrt{\eta}$ of the characteristic equation (10):

$$\left.\begin{aligned} r_{1,2} &= \gamma \pm \beta i; & r_{3,4} &= \delta \pm \mu i \\ r_{5,6} &= -(\gamma \pm \beta i); & r_{7,8} &= -(\delta \pm \mu i) \end{aligned}\right\} \tag{13}$$

where γ, β, δ and μ are four shell constants only related to the physical constants, R and l of the shell.

When both the shell and loading are symmetric, the solution of the homogeneous equations may be written as

$$w = (A_1F_1 + A_2F_2 + A_3F_3 + A_4F_4)\cos k\xi \tag{14}$$

$$\begin{bmatrix} \varphi \\ N_x \\ N_y \\ w \\ M_x \\ M_y \\ \varepsilon_x \\ \varepsilon_y \end{bmatrix} = a_x[(B_1A_1 - B_2A_2)F_1 + (B_2A_1 + B_1A_2)F_2 + (B_3A_3 - B_4A_4)F_3 + (B_4A_3 + B_3A_4)F_4]\cos k\xi \tag{15}$$

$$\begin{pmatrix} Q_x \\ u \end{pmatrix} = a_x[(B_1A_1 - B_2A_2)F_1 + (B_2A_1 + B_1A_2)F_2 + (B_3A_3 - B_4A_4)F_3 + (B_4A_3 + B_3A_4)F_4]\sin k\xi \tag{16}$$

$$\begin{bmatrix} N_{xy} \\ M_{xy} \\ \gamma_{xy} \end{bmatrix} = a_x[(B_1A_1 - B_2A_2)F_5 + (B_2A_1 + B_1A_2)F_6 + (B_3A_3 - B_4A_4)F_7 + (B_4A_3 + B_3A_4)F_8]\sin k\xi \tag{17}$$

$$\begin{pmatrix} v \\ Q_y \end{pmatrix} = a_x[(B_1A_1 - B_2A_2)F_5 + (B_2A_1 + B_1A_2)F_6 + (B_3A_3 - B_4A_4)F_7 + (B_4A_3 + B_3A_4)F_8]\cos k\xi \tag{18}$$

where A_1, A_2,…are constants to be determined by the boundary conditions.

$$F_1 = \exp(-\gamma\phi)\cos\beta\phi \pm \exp(-\gamma\theta)\cos\beta\theta; \quad F_2 = \exp(-\gamma\phi)\sin\beta\phi \pm \exp(-\gamma\theta)\sin\beta\theta;$$

$$F_3 = \exp(-\delta\phi)\cos\mu\phi \pm \exp(-\delta\theta)\cos\mu\theta; \quad F_4 = \exp(-\delta\phi)\sin\mu\phi \pm \exp(-\delta\theta)\sin\mu\theta; \tag{19}$$

@Seismicisolation

ξ, $\varnothing$ and θ are dimensionless coordinates: $\xi = x/R\phi = y/R$. ϕ is the angle measured from the left and θ is the angle measured from the right, as shown in Fig. 5.7. Coefficients α_x, B_1, B_2, B_3, B_4 correspond to different internal forces and displacements can be obtained from the following Table 5.4.

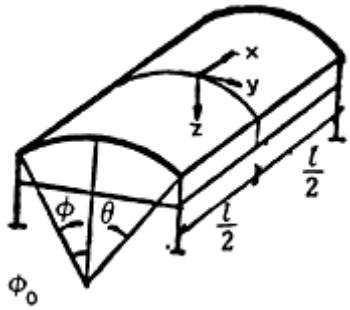

Fig. 5.7.

Table 5.4

	a_x	B_1	B_2
φ	-1	$\frac{1}{R}\left[\frac{d_{22}}{k^2}[(\gamma^2-\beta^2)^2-4\gamma^2\beta^2] - 2(d_{12}+2d_{33})(\gamma^2-\beta^2)-d_{11}k^2\right]$	$\frac{4\gamma\beta}{R}\left[\frac{d_{22}}{k^2}(\gamma^2-\beta^2)-(d_{13}+2d_{33})\right]$
N_x	$-\frac{1}{R^2}$	$(\gamma^2-\beta^2)B_1^{\varphi}-2\gamma\beta B_2^{\varphi}$	$(\gamma^2-\beta^2)B_2^{\varphi}+2\gamma\beta B_1^{\varphi}$
N_y	$\frac{k^2}{R^2}$	B_1^{φ}	B_2^{φ}
w	1	1	0
M_x	$-\frac{1}{R^2}$	$(\gamma^2-\beta^2)d_{12}-d_{11}k^2$	$2\gamma\beta d_{12}$
M_y	$-\frac{1}{R^2}$	$(\gamma^2-\beta^2)d_{22}-d_{12}k^2$	$2\gamma\beta d_{22}$
ε_x	$\frac{1}{R^2}$	$a_{12}k^2B_1^{\varphi}-a_{11}B_1^{N_x}$	$a_{12}k^2B_2^{\varphi}-a_{11}B_2^{N_x}$
ε_y	$\frac{1}{R^2}$	$a_{22}k^2B_1^{\varphi}-a_{12}B_1^{N_x}$	$a_{22}k^2B_2^{\varphi}-a_{12}B_2^{N_x}$
Q_x	$\frac{k}{R^3}$	$B_1^{M_x}+2d_{33}(\gamma^2-\beta^2)$	$B_2^{M_x}+4d_{33}\gamma\beta$
u	$\frac{1}{kR}$	$a_{12}k^2B_1^{\varphi}-a_{11}B_1^{N_x}$	$a_{12}k^2B_2^{\varphi}-a_{11}B_2^{N_x}$

@Seismicisolation

N_{xy}	$\frac{k}{R^2}$	$\gamma B_1^{\varphi} - \beta B_2^{\varphi}$	$\gamma B_2^{\varphi} + \beta B_1^{\varphi}$
M_{xy}	$-\frac{2kd_{33}}{R^2}$	γ	β
γ_{xy}	$\frac{ka_{33}}{R^2}$	$B_1^{N_{xy}}$	$B_2^{N_{xy}}$
v	-1	$\frac{1}{\gamma^2+\beta^2}\left(\frac{1}{R}(\gamma B_1^{\varepsilon_y} + \beta B_2^{\varepsilon_y}) + \gamma\right)$	$\frac{1}{\gamma^2+\beta^2}\left(\frac{1}{R}(\gamma B_2^{\varepsilon_y} + \beta B_2^{\varepsilon_y}) - \beta\right)$
Q_y	$-\frac{1}{R^3}$	$2d_{33}k^2\gamma - \gamma B_1^{M_y} + \beta B_2^{M_y}$	$2d_{33}k^2\beta - \beta B_1^{M_y} - \gamma\beta_2^{M_y}$

The expressions B_3 and B_4 correspond to those of B_1 and B_2, just to replace α, β in in B_1 and B_2 with δ, μ respectively.

4.2 The Particular Solution of Non-homogeneous Equations

In calculation, the membrane solution is often used instead of the particular solution. In the following, only results of the membrane solution under uniformly distributed transverse load are given. Loading diagrams are shown in Fig. 5.8. Loading

$$q_y = -p\cos(\phi_0 - \phi)\sin(\phi_0 - \phi)\cos k\xi$$
$$q_z = p\cos^2(\phi_0 - \phi)\cos k\xi \qquad (20)$$

Its membrane solutions are

@Seismicisolation

$$
\left.
\begin{aligned}
N_y &= -pR\cos^2(\phi_0-\phi)\cos k\xi \\
N_{xy} &= \frac{3pR}{2k}\sin 2(\phi_0-\phi)\sin k\xi \\
N_x &= -\frac{3pR}{k^2}\cos 2(\phi_0-\phi)\cos k\xi \\
e_x &= -pR\left(\frac{3a_{11}}{k^2}+a_{12}\right)\cos^2(\phi_0-\phi)\cos k\xi + \frac{3a_{11}pR}{k^2}\sin^2(\phi_0-\phi)\cos k\xi \\
u &= -\frac{PR}{k}\left(\frac{3a_{11}}{k^2}+a_{12}\right)\cos^2(\phi_0-\phi)\sin k\xi + \frac{3a_{11}pR}{k^3}\sin^2(\phi_0-\phi)\sin k\xi \\
\gamma_{xy} &= \frac{3pRa_{33}}{2k}\sin 2(\phi_0-\phi)\sin k\xi \\
v &= -\frac{pR}{k^2}\left[\frac{6a_{11}}{k^2}+a_{12}+\frac{3}{2}Ra_{33}\right]\sin 2(\phi_0-\phi)\cos k\xi \\
\varepsilon_y &= -pR\left[\frac{3a_{12}}{k^2}+a_{22}\right]\cos^2(\phi_0-\phi)\cos k\xi + \frac{3pRa_{12}}{k^2}\sin^2(\phi_0-\phi)\cos k\xi \\
w &= +\frac{pR}{k^2}\left[\frac{12a_{11}}{k^2}+(2+3R)a_{12}+a_{22}k^2R+3Ra_{33}\right]\cos^2(\phi_0-\phi)\cos k\xi \\
&\quad -\frac{pR}{k^2}\left[\frac{12a_{11}}{k^2}+(2+3R)a_{12}+3Ra_{33}\right]\sin^2(\phi_0-\phi)\cos k\xi
\end{aligned}
\right\} \tag{21}
$$

In the above solutions, there are four unknown integral constants, A_1, A_2, A_3, A_4 (in the case of symmetry) which are to be determined by the boundary conditions provided at the two longitudinal edges of the shell. The choice of the boundary conditions follows the

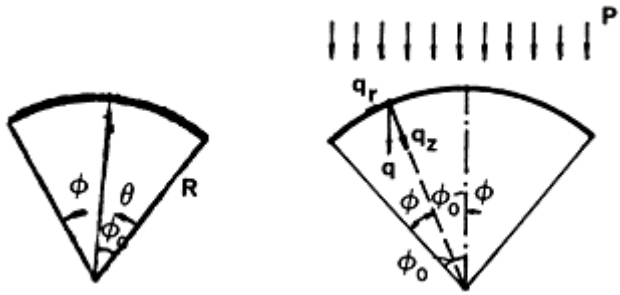

Fig. 5.8.

general shell theory. It need not be repeated here. According to the equivalent principle of the internal forces, the internal forces of the reticulated shell may be calculated by applying to its basic grid element the average values of internal forces of the corresponding equivalent shell element.

@Seismicisolation

BIBLIOGRAPHY

1. Matsushitaand Tsuge. A study of steel frame shell. *Transactions of the Architectural Institute of Japan*, 57, 1957.
2. Xue-Ren Hu. Theoretical analysis of reticulated shell. *Building Journal*, July 1960. The People's Republic of China.
3. Tien Lan, Shi-Lin Dong and Jing-Qian Xia. Analysis, design and testing of cylindrical reticulated shell. Research paper of Institute of Building Research, The People's Republic of China.
4. Masakazu Ozaki. A practical method for analysis of space truss shells structures. Building Research Institute, Ministry of Construction, Japanese Government, Sept. 1968.
5. Wright, D.T. Membrane forces and buckling in reticulated shells. *Journal of the Structural Division, ASCE*, 91, STI, February 1965.

@Seismicisolation

6
Comparison of the Structural Behaviour of Various Types of Braced Barrel Vaults

G.A.R.PARKE
Space Structures Research Centre, University of Surrey, Guildford, UK

1 INTRODUCTION

Braced barrel vaults are skeletal space structures similar in shape to cylindrical shell structures. This description of form does not limit barrel vaults to structures with only one radius of curvature but encompasses structures of double curvature and configurations with single, double or triple layers of members. Braced barrel vaults are usually of circular curvature and may be supported on end diaphragms, walls or trusses which follow the curvature of the vault. Alternatively the skeletal vault may be supported along the longitudinal horizontal boundaries or at corner locations, typically for vaults of double curvature.

Braced barrel vaults have been successfully used to cover a variety of spans but, similar to all space structures, barrel vaults are unlikely to prove economical when used to cover small floor areas. Previous experience has shown that the overall economy of the structure improves as the plan area approaches a square, although barrel vaults will provide economical roof structures covering large rectangular areas for length/width ratios of values up to 2.

Several different configurations of braced barrel vaults have been investigated using the stiffness methods of analysis. This analytical method results first in the determination of the nodal displacements and subsequently member forces. Three different. configurations have been analysed as shown in Fig. 6.1, each with five different span/height ratios and four different boundary conditions.

2 PRELIMINARY DESIGN OF BRACED BARREL VAULT MEMBERS

To enable a comparison to be made between the various configurations studied each vault has been preliminarily designed using a computer program in accordance with the normal laws of statics and to the limiting stresses permitted in BS449.[1] A flow chart outlining the program for the preliminary design of rigidly jointed space frame members is shown in Fig. 6.2. The vault members chosen are circular hollow sections in BS4360[2] grade 43C steel, and have been selected from predetermined groups of members. The members in each group have the same outside diameter but different wall thicknesses so that each particular vault may have a maximum of three different member thicknesses.

@Seismicisolation

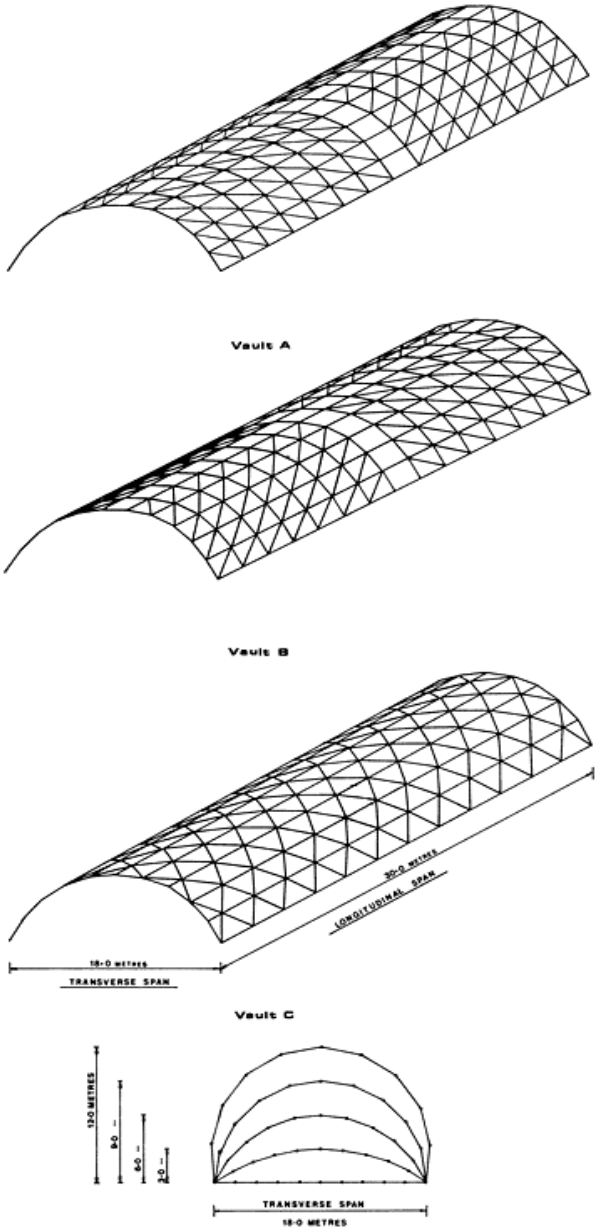

Fig. 6.1. Braced barrel vaults investigated by Parke.

@Seismicisolation

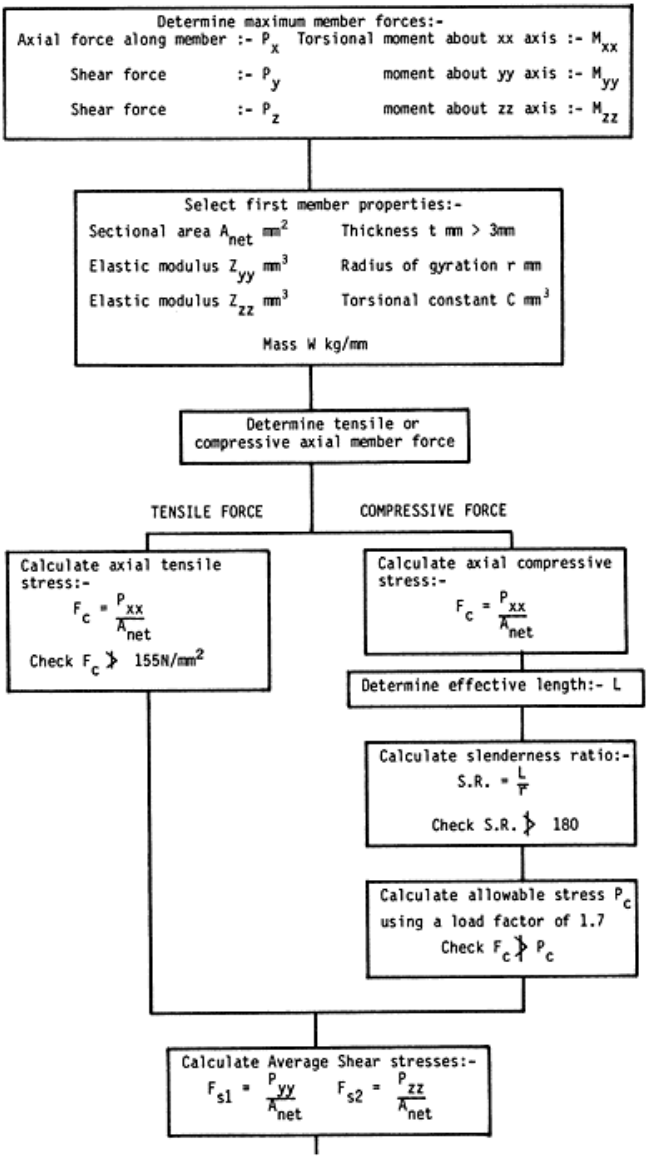

Fig. 6.2. Flow chart outlining the preliminary design of rigidly jointed space frame members. Designed using circular hollow sections in BS 4360 grade 43C steel to the stresses permitted in BS 449.

@Seismicisolation

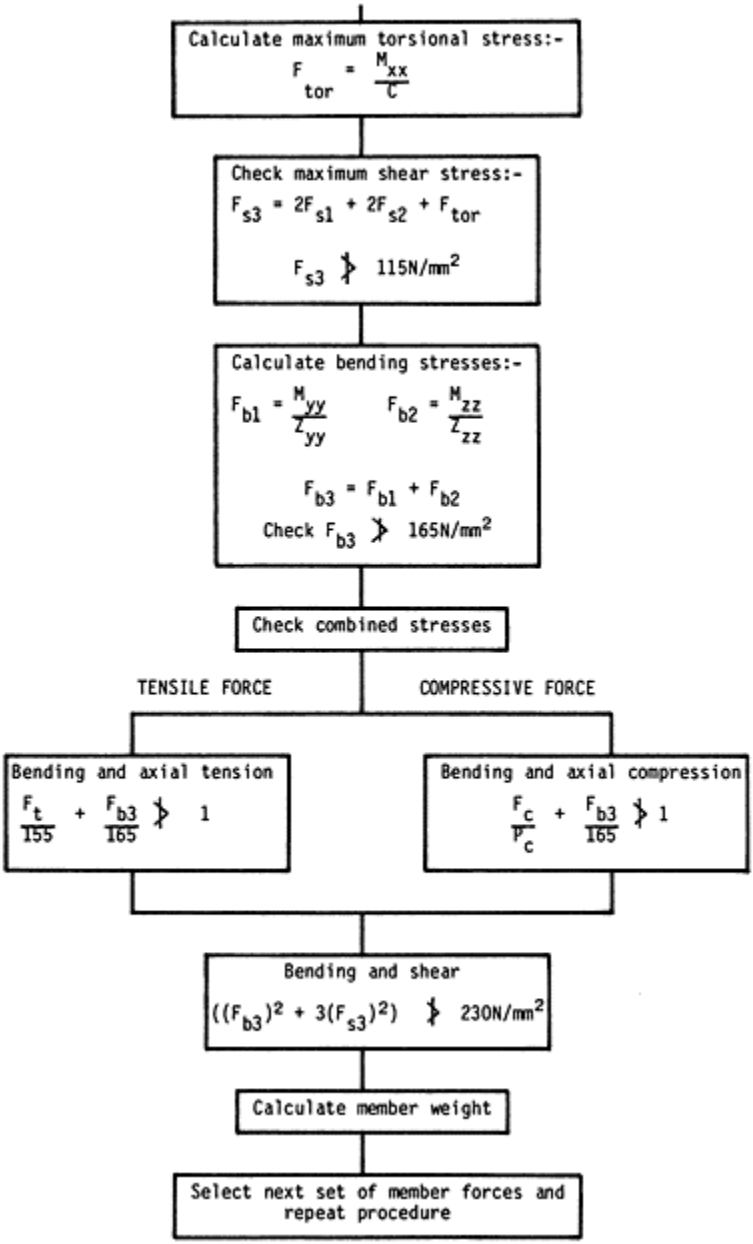

The selection of the most suitable group of members depends upon the experience of the designer and often the lightest sections may be rejected, due to many reasons which may include connection difficulties or long deliveries. To enable a free choice of member groups to be made, member properties were input into the program as separate data after completion of the stiffness analysis. After individual member design and calculation of

@Seismicisolation

the structure self weight, the initial member properties and dead load chosen for the first analysis were updated and the analysis and design repeated. A final deflection check was also incorporated to limit deflections to less than span/360.

2.1 Compression Member Design

The design of the compression members requires the determination of the effective length of the member which is directly related to the member end restraints, initial member imperfections, and overall stiffness of the structure. Braced barrel vault members considered fully fixed are subjected to complex stresses and the effective length should be taken as between 0·7 and 1·0 times the actual member length. For double- and triple-layer structures it is suggested that an effective length of 0·85 times the distance between centres of member intersection is appropriate. For single-layer barrel vaults the effective length of the member will also be affected by the span-to-height ratio of the structure. For shallow vaults with low out-of-plane stiffness it is proposed that the effective length of welded compression members should be taken as the actual length of the members. This assumption was used in the preliminary design of all the barrel vault configurations under investigation.

2.2 Investigation

The three single-layer vaults investigated are shown in Fig. 6.1. Types A and B are based on a rectangular configuration with diagonal bracing while type C is a three way lattice grid giving a structure in which all members are of equal length. The barrel vaults were first considered to be fully supported along only the horizontal longitudinal edge, and then taken as supported along the circular gable end also with horizontal restraint along the longitudinal edge. The last set of support conditions were used to simulate the restraints imposed on a single barrel remote from the ends of a continuous barrel vault system spanning longitudinally. The vaults were analysed as rigidly jointed structures but the support joints were considered both fixed and pinned in two separate groups of analysis.

The structures were preliminarily designed for each of the five different height-to-span ratios for an effective symmetric load of 1 kN at each internal node for longitudinally spanning vaults and 2 kN for the transversely spanning vaults, and also for a symmetrical snow load in accordance with CP3 chapter 5 part 1.[3] In addition each vault was preliminarily designed for a non-symmetric imposed load of effectively 1 kN for half of the vault nodes for the longitudinally spanning vaults, and 2 kN for the transversely spanning vaults.

3 BRACED BARREL VAULTS SPANNING TRANSVERSELY, SYMMETRICALLY LOADED

The barrel vaults under investigation were first considered spanning transversely with the longitudinal boundaries fully restrained against translational and rotational displacements. Figure 6.3 gives values of the total weight of the structure obtained from a

@Seismicisolation

preliminary design, for each of the five height-to-span ratios chosen. From these results it is evident that the most economical height-to-span ratio in relation to the weight of the structures is approximately 0·17. At this height-to-span ratio the lightest of the three configurations is the three-way diagonal grid structure type C which is only 2% lighter 0·5 the total weight of structure A has increased by 270% and structure C by 340%. At than configuration type B but 28% lighter than type A. At a larger height-to-span ratio of this height-to-span ratio of 0·5 configuration B gives the lightest structural weight but this is 240% greater than its structural weight at a height-to-span ratio of 0·17.

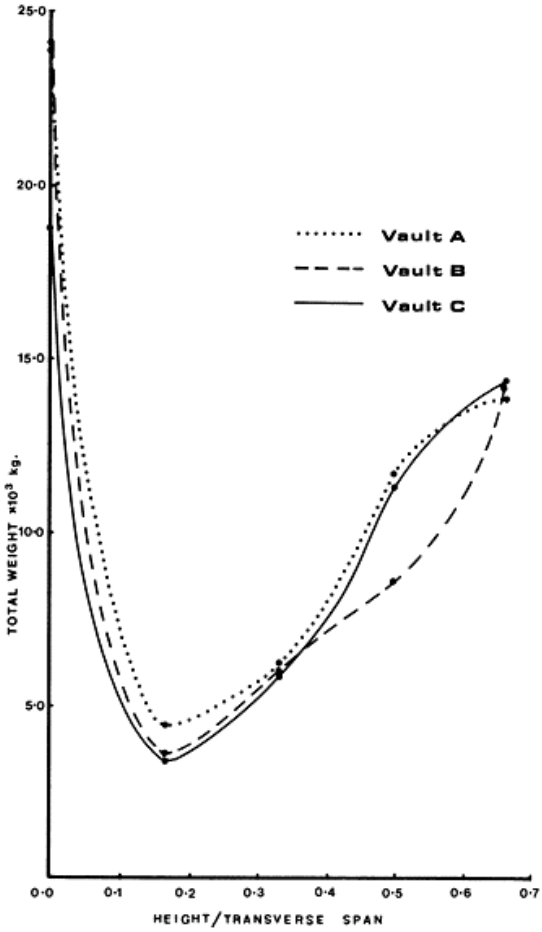

Fig. 6.3. Structural weight for height/transverse span ratios for transversely spanning vaults under an effective symmetrically imposed nodal load of 2·0 kN.

@Seismicisolation

Figure 6.4 shows how the values of the design axial force and moments change for three members in vault type C with increasing height-to-span ratios. It is evident that as the vault rises from the horizontal the major forces in the structure change from bending moments to axial. At the critical height-to-span ratio of 0·17 the bending moments in the three members are at a minimum while the axial forces are at a maximum. For height-to-span ratios greater than 0·17, bending moments increase and axial forces decrease with increasing height-to-span ratios. As the least structural weight for the vault was obtained at a height-to-span ratio of 0·17, it is evident from Fig. 6.4 that the value of the bending moments acting on the members tends to govern the vault design.

Figure 6.5 shows a section taken through the deflected profiles of the three vault

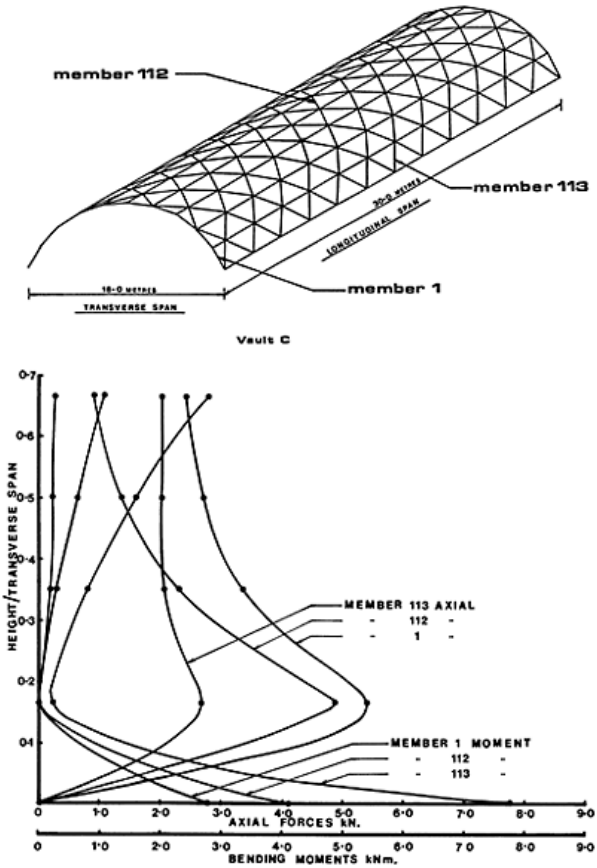

Fig. 6.4. Axial forces and moments for three members of vault C spanning transversely with fully fixed supports, under an effective symmetrically imposed nodal load of 1·0 kN.

@Seismicisolation

configurations. The minimum deflection obtained for all three vaults was at the height-to-span ratio of 0·17. When this ratio increased the deflections also increased. At a height-to-span ratio of 0·67 the maximum deflection for configuration B was 700% greater than the maximum deflection obtained at a ratio of 0·17.

Figures 6.6(A), (B) and (C) show the deflection contours, axial forces and moments for the three vault configurations at a height-to-span ratio of 0·17. From the contour plots it is evident that the most uniform deflection pattern is obtained with the diagonal grid type C. Both the braced rectangular grids type A and B exhibit greater deflections than type C, and the deflections of type B form a mirror image of the deflection obtained for type A.

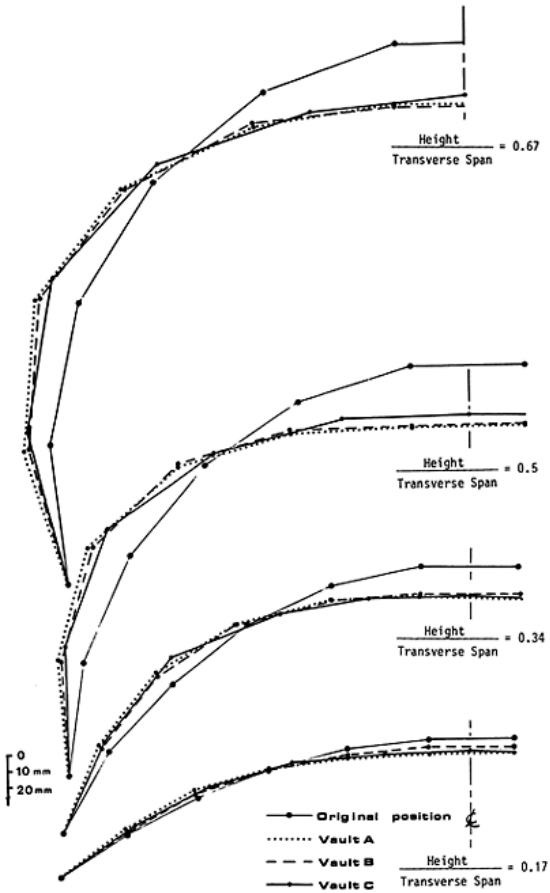

Fig. 6.5. Deflection profiles for transversely spanning vaults under an effective symmetrically imposed nodal load of 1·0 kN.

@Seismicisolation

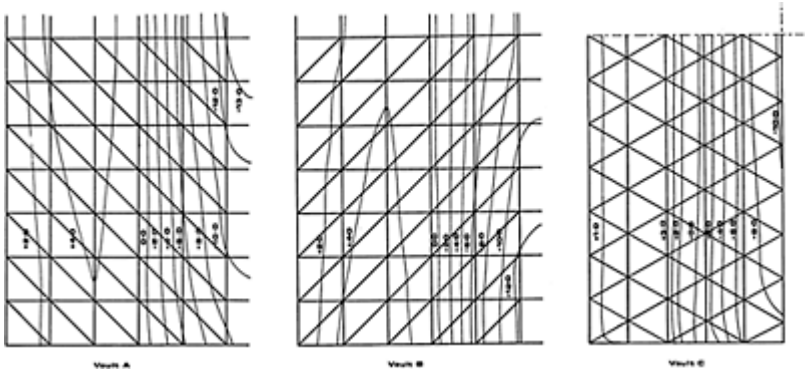

Fig. 6.6(A). Deflection contours in mm for transversely spanning vaults under an effective imposed symmetrical nodal load of 1·0 kN.

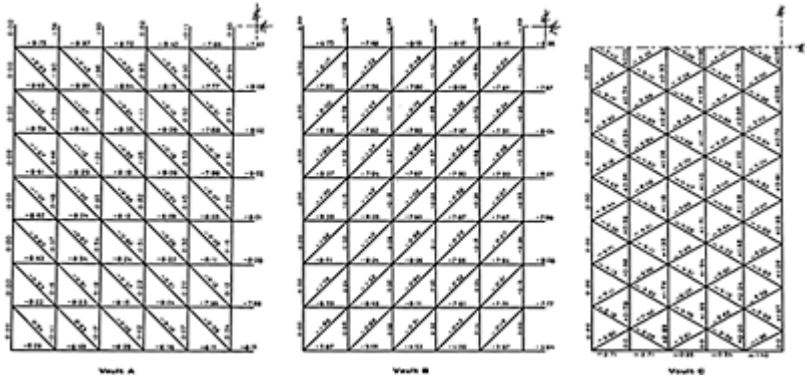

Fig. 6.6(B). Axial forces in kN for transversely spanning vaults under an effective imposed symmetric load of 1·0 kN (tension positive).

@Seismicisolation

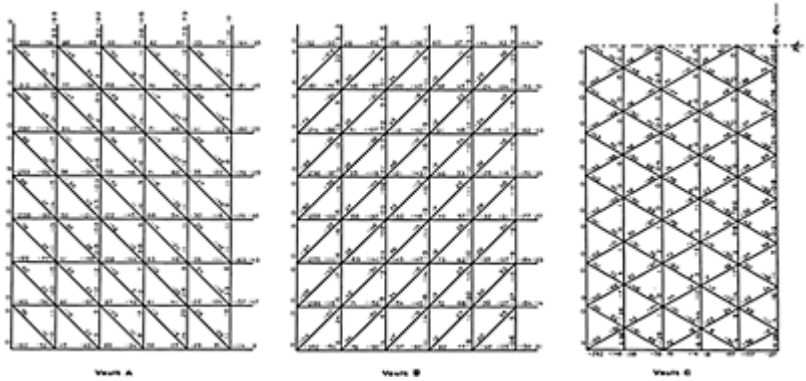

Fig. 6.6(C). Bending moments M_{zz} in kNm×10^{-3} for transversely spanning vaults under an effective imposed symmetrical load of 1·0 kN.

@Seismicisolation

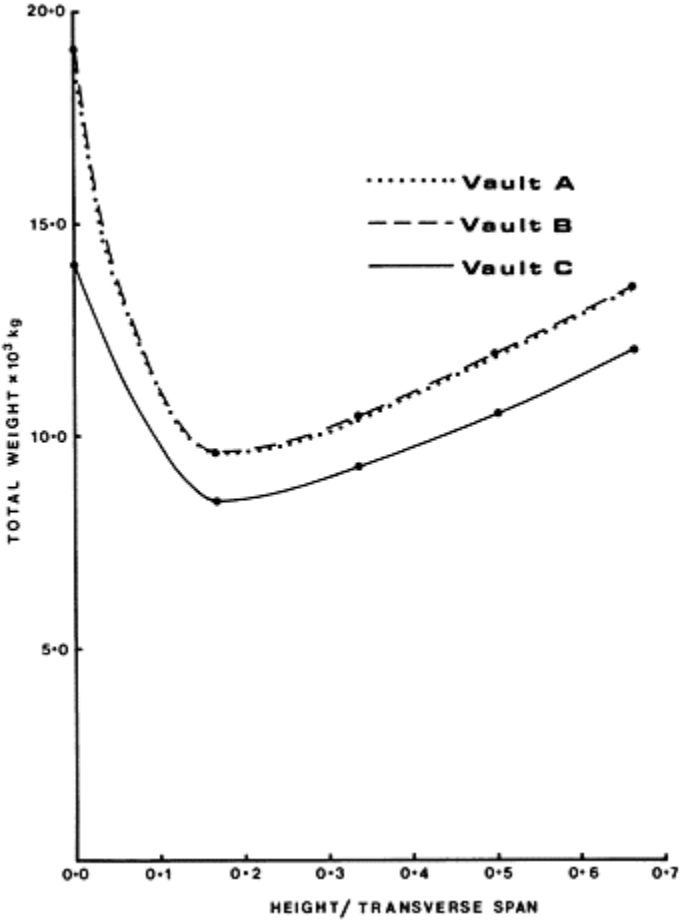

Fig. 6.7. Structural weight for height/transverse span ratios for transversely spanning vaults under an effective non-symmetrically imposed nodal load of 1·0 kN.

3.1 Transversely Spanning Vaults, Non-symmetrically Loaded

In addition to the symmetrical load cases, the vaults under investigation were considered spanning transversely under the action of a non-symmetrical imposed loading. Figure 6.7 gives values of the total weight of the three vault configurations obtained from a preliminary design for each of the five height-to-span ratios. It is apparent that for non-symmetric loading the most economic height-to-span ratio, in relation to structural weight, is again approximately equal to 0·17. Under the non-symmetrically imposed load

@Seismicisolation

the three-way diagonal grid vault C is consistently lighter than both vaults A and B. At the height-to-span ratio of 0·17 vault C is approximately 12% lighter than both vaults A and B.

Figure 6.8 shows how the axial forces and moments change for vault C as the height-to-span ratio increases. At a height-to-span ratio of approximately 0·17 the member forces are primarily axial and as the vault rises the member axial forces decrease while the member bending moments increase.

Figure 6.9 shows the deflected profiles for a cross-section through the three-way diagonal grid vault C. The lateral and vertical deflections of the vault increase considerably with respective increases in the height-to-span ratio. The average resultant

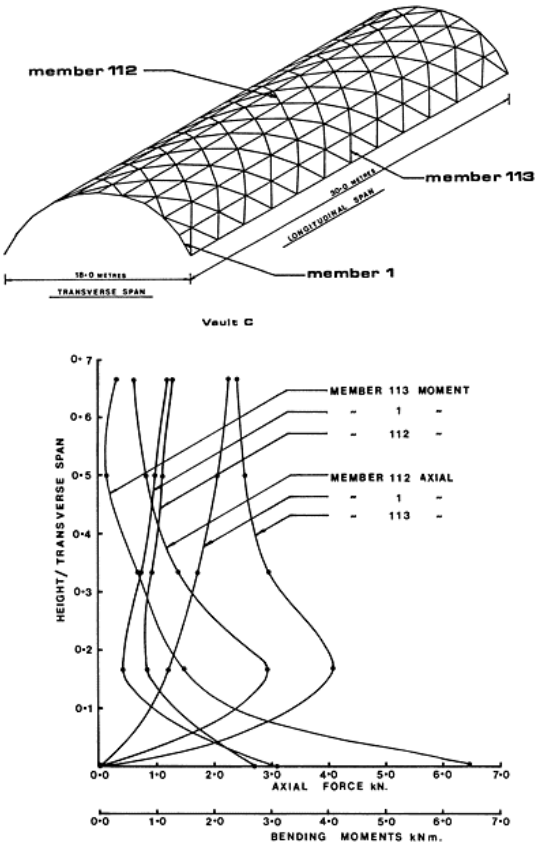

Fig. 6.8. Axial forces and moments for three members of vault C spanning transversely with fully fixed supports, under an effective imposed non-symmetrical nodal load of 1·0 kN.

@Seismicisolation

deflections at a height-to-span ratio of 0·67 are 200% larger than the deflections obtained at a ratio of 0·17.

3.2 Transversely Spanning Vaults with Pinned Horizontal Longitudinal Boundaries, Symmetrically Loaded

The major effects resulting from pinning the boundary supports were to increase the vault deflections on average by 200% and to change the boundary stress distribution. Figure 6.10 shows how the axial forces and design moments change for three members of vault

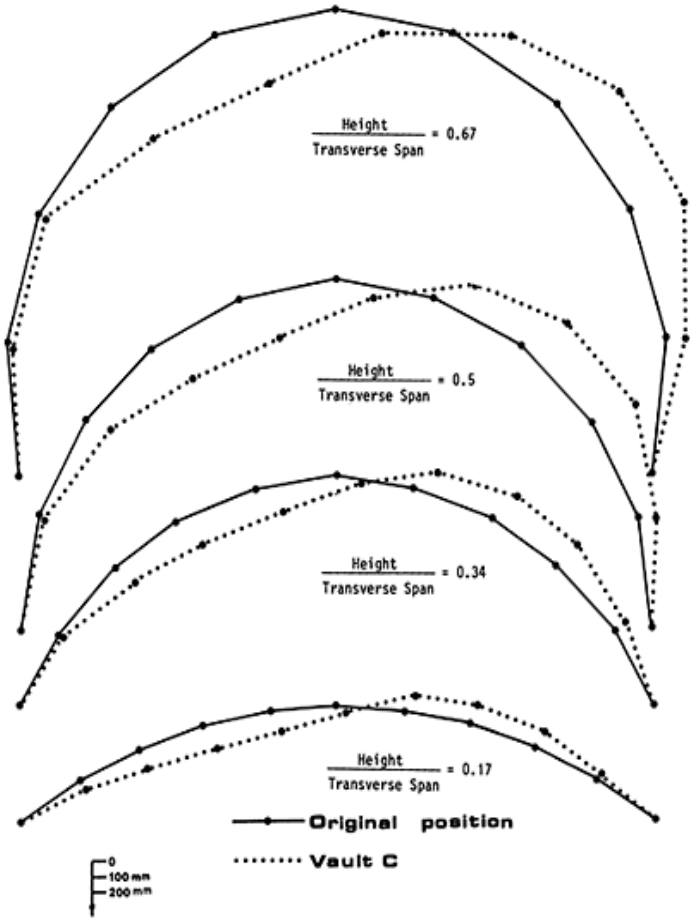

Fig. 6.9. Deflection profiles for vault C spanning transversely under an effective imposed non-symmetrical nodal load of 1·0 kN.

@Seismicisolation

type C with pinned supports as the height-to-span ratio increases. Similar graphs occur with both the pinned- and fixed-support conditions with the minimum design moments, and maximum axial forces, occurring at a height-to-span ratio of 0·17.

3.3 Transversely Spanning Vaults with Pinned Horizontal Longitudinal Boundaries, Non-symmetrically Loaded

Similar to the symmetrically-imposed loading case, the effect of pinning the boundary supports under non-symmetrical loading was to increase significantly the vault deflections on average by 190% and to change the boundary member forces. In addition, pinning the longitudinal boundary supports resulted in a relatively small average increase

@Seismicisolation

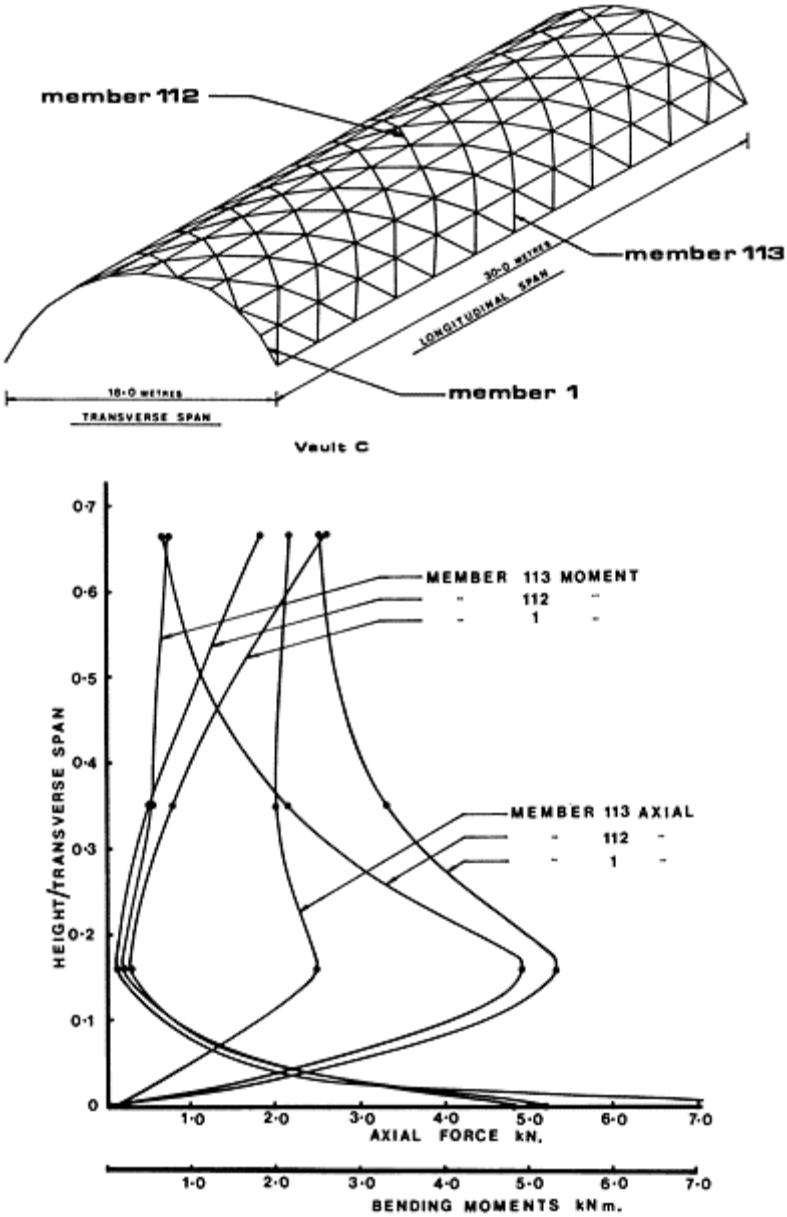

Fig. 6.10. Axial forces and moments for three members of vault C spanning transversely with pinned supports, under an effective imposed symmetrical nodal load of 1·0 kN.

@Seismicisolation

in the weight of the vault structures. For vault C at a height-to-span ratio of 0·17 this increase in weight was in the region of only 10%.

Both symmetrically and non-symmetrically loaded vaults spanning transversely, with both pinned and fixed longitudinal supports, behave in a similar mode. The structures generally act as an arch with nominal longitudinal distribution with the maximum moments and axial thrusts occurring in the transverse members following the circular profile over the span of the vault. The non-symmetrical load cases tend to govern the vault designs, with the three-way diagonal grid vault at a height-to-transverse-span ratio of 0·17 being the most efficient structural configuration of the three vault types considered.

As expected for pinned supports the boundary moments are greatly reduced, and the bending moments are redistributed towards the centre of the span with a resulting increase in deflection. The longitudinal members are generally nominally stressed, with axial forces and moments slowly increasing towards the centre of the vaults.

4 BRACED BARREL VAULTS SPANNING LONGITUDINALLY, SYMMETRICALLY LOADED

The three vault configurations under investigation were also preliminarily designed for the condition when the vault is rigidly connected to an unyielding circular gable support and restrained horizontally along the longitudinal boundaries. Figure 6.11 gives values of

@Seismicisolation

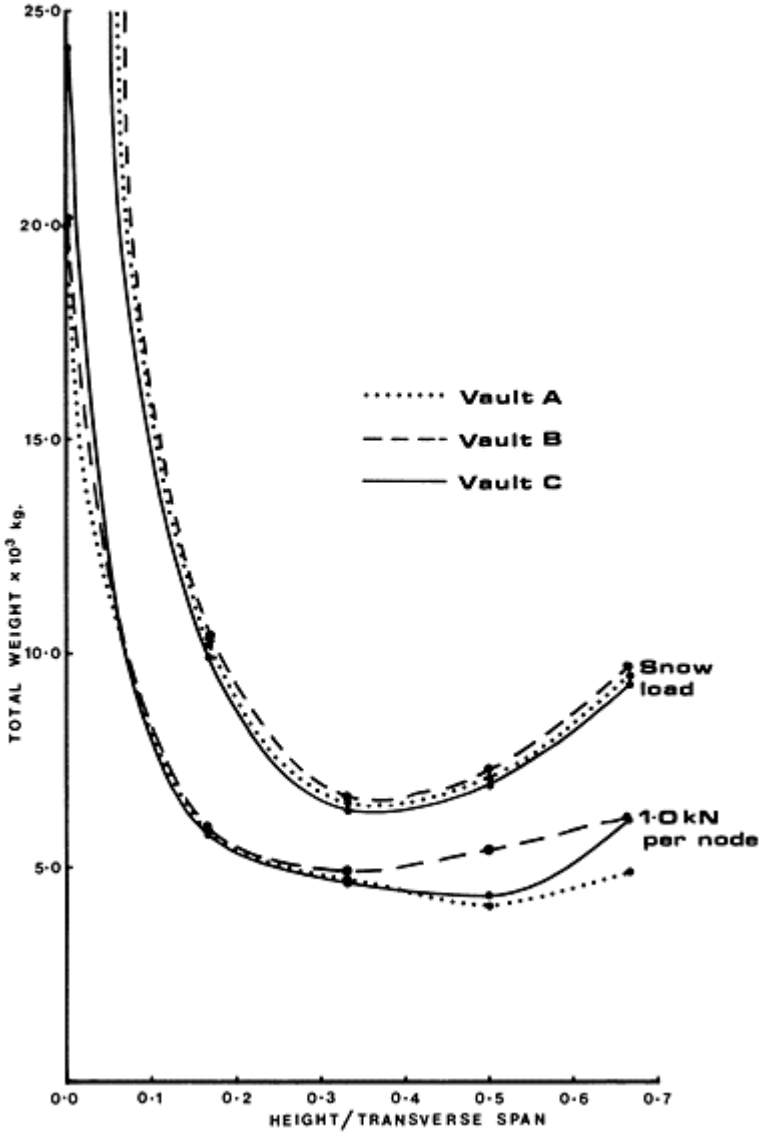

Fig. 6.11. Structural weight for height/transverse span ratios for longitudinally spanning vaults under an effective imposed symmetrical nodal load of 1.0 kN.

@Seismicisolation

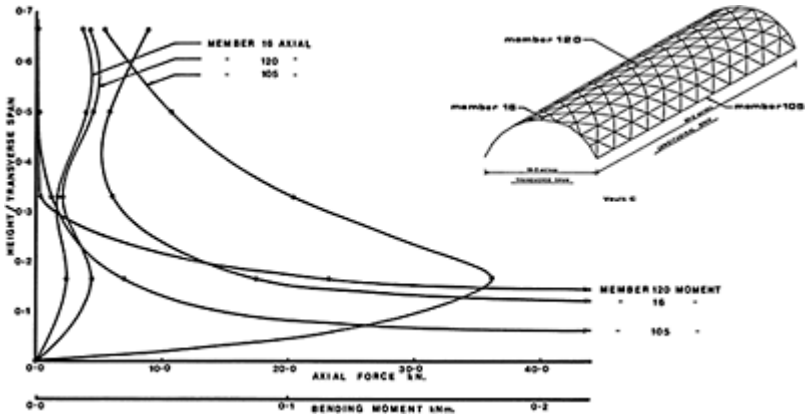

Fig. 6.12. Axial forces and moments for three members of vault C spanning longitudinally with fully fixed supports under an effective imposed symmetrical nodal load of 1·0 kN.

the total weight of the structure obtained from the preliminary design of each of the vaults for the five height-to-transverse-span ratios. A height-to-transverse-span ratio of 0·5 gave the minimum weight for the symmetrical load case of an effective load of 1 kN at each internal node while under snow loading, which was assumed to reduce as the vault rise increased, the minimum weight was obtained for all three vaults at a height-to-transverse-span ratio of approximately 0·34. At the height-to-span ratio of 0·5, vault A was the lightest structure, being only 1% lighter than type C but 21% lighter than type B.

Figure 6.12 shows how the axial forces and design moments vary for three typical members from configuration C, as the height-to-transverse-span ratio increases. For zero rise, and assuming small deflections, the applied loading is resisted by bending and torsion moments and shear forces only. As the rise increases, the bending and torsion moments significantly decrease and the axial forces increase.

At a height-to-transverse-span ratio of 0·5 the average resultant moments in the structure are at a minimum, and the axial forces are well below their maximum values. This combination of moments and axial forces resulted in the lowest structural weight for the vault type C.

Figure 6.13 gives deflection profiles across the width of the vault for each of the five height-to-transverse-span ratios. From the figure it is evident that the deflection decreases as the vault rise increases. Vault type C gave consistently smaller average deflections in comparison with types A and B, for height-to-span ratios up to 0·5, while, for the ratio of 0·67, vault type B gave the smallest average. Figures 6.14(A), (B) and (C) show the distribution of moments, axial forces and deflections for each of the vault types for the height-to-span ratio of 0·5. Vault type B has the lowest average compression and tensile force with an average force approximately 10% lower than configurations A and C. Although the average compressive force in vault B is the lowest of the three

@Seismicisolation

configurations, the longest members are in compression, while in vaults A and C the shorter members only are in compression.

For a height-to-span ratio of 0·5, bending and torsion moments acting in the structures are nominal in comparison with the member axial forces and, consequently, it is the selection of compression members which tends to govern the vault design under these support conditions.

4.1 Longitudinally Spanning Vaults, Non-symmetrically Loaded

The three vault configurations investigated were also preliminarily designed for the condition when the vault is spanning longitudinally with horizontal restraints along the longitudinal boundary, under a non-symmetrically imposed load. In this condition the vaults behave very similarly under both symmetric and non-symmetric loading. Figure 6.15 gives preliminary values of the total weight of the vault configuration for the five height-to-transverse-span ratios. The minimum weight was obtained for vault A at a height-to-transverse-span ratio of 0·5. The minimum weight for vault C was at a ratio of 0·34, and the minimum weight for vault B lies between the height-to-transverse-span ratios of 0·34 and 0·5. Very similar structural weights were obtained for the three vaults under both symmetric and non-symmetric loading.

Figure 6.16 gives the values of axial forces and maximum design moments for three members of vault C, for each of the five height-to-transverse-span ratios. Similar to the symmetrical loading case, as the vaults rise, the bending and torsion moments significantly decrease and the axial forces increase. For vault C the average design moments and axial forces for the complete structure are at a minimum at a height-to-transverse-span ratio of 0·34.

@Seismicisolation

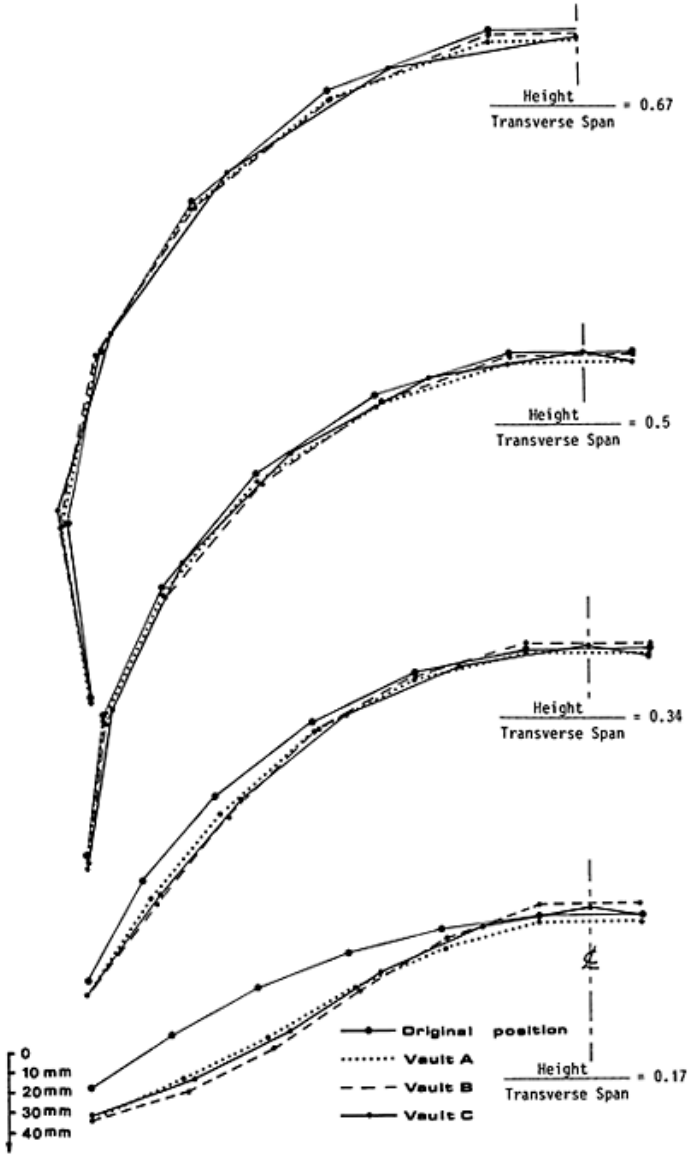

Fig. 6.13. Deflection profiles for longitudinally spanning vaults under an effective imposed symmetrical nodal load of 1·0 kN.

@Seismicisolation

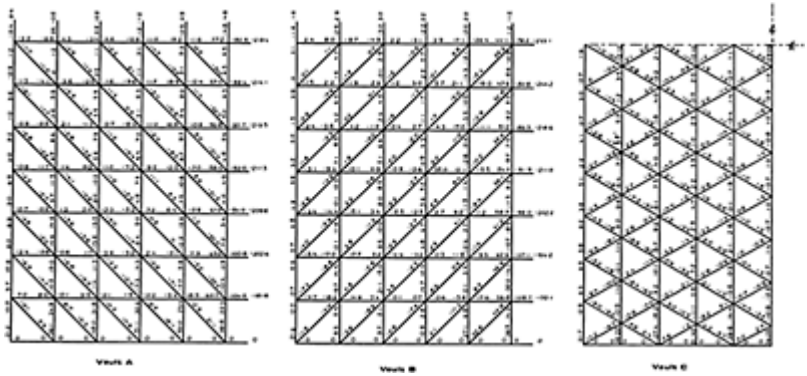

Fig. 6.14(A). Bending moments M_{zz} in kNm×10^{-3} for longitudinally spanning vaults under an effective imposed symmetrical nodal load of 1·0 kN.

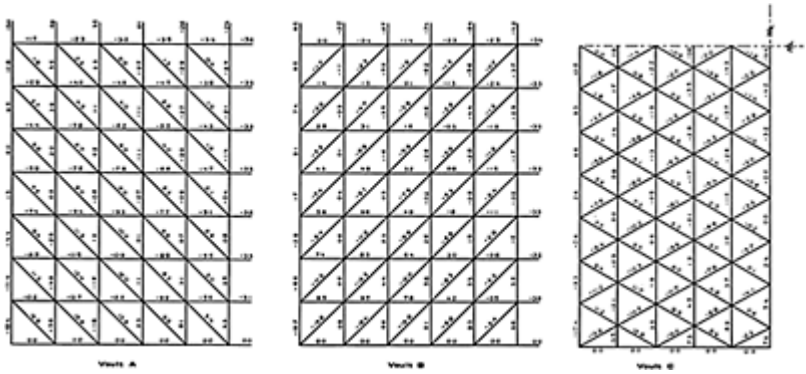

Fig. 6.14(B). Axial forces in kN for longitudinally spanning vaults under an effective imposed symmetrical nodal load of 1·0 kN (tension positive).

@Seismicisolation

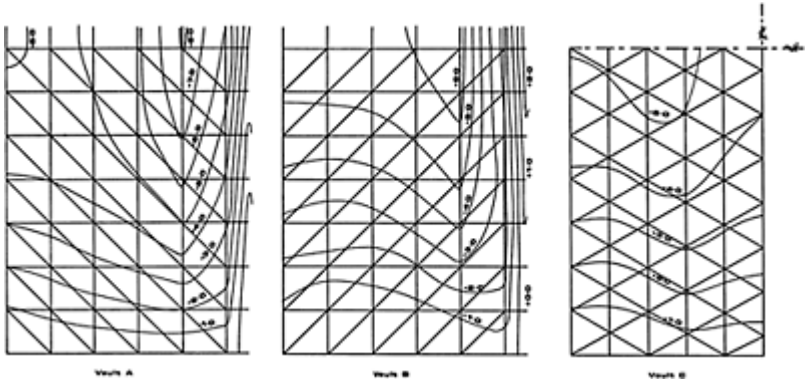

Fig. 6.14(C). Deflection contours in mm for longitudinally spanning vaults under an effective imposed symmetrical nodal load of 1·0 kN.

@Seismicisolation

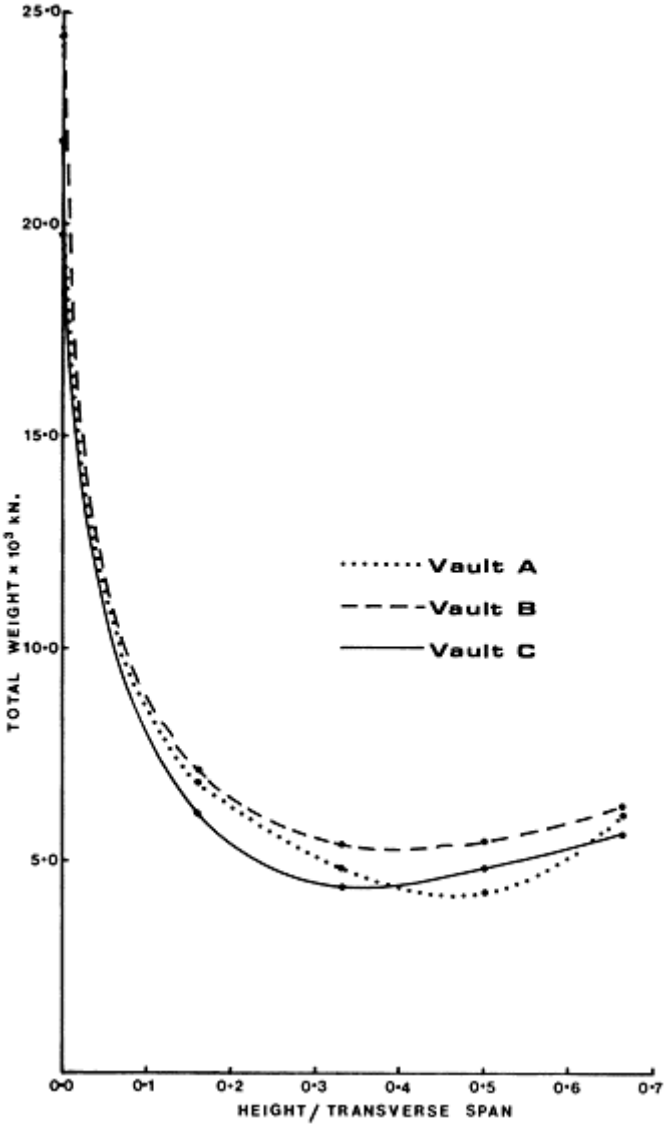

Fig. 6.15. Structural weight for height/transverse span ratios for longitudinally spanning vaults under an effective imposed non-symmetrical nodal load of 1·0 kN.

Figure 6.17 shows the deflections of a cross-section through vault C for each of the height-to-transverse span ratios for the non-symmetrically imposed loading case. Both

@Seismicisolation

the vertical and horizontal deflections greatly decrease as the height-to-transverse-span ratio increases up to a value of 0·5. The average deflections are of very similar magnitude for the two largest height-to-transverse-span ratios of 0·5 and 0·67.

4.2 Longitudinally Spanning Vaults with Pinned Gable End Supports, Symmetrically and Non-symmetrically Loaded

Pinning the gable end supports but maintaining the horizontal restraint along the longitudinal boundaries have very little effect on the distribution of moments and forces throughout the three vault configurations under investigation. Generally, the boundary

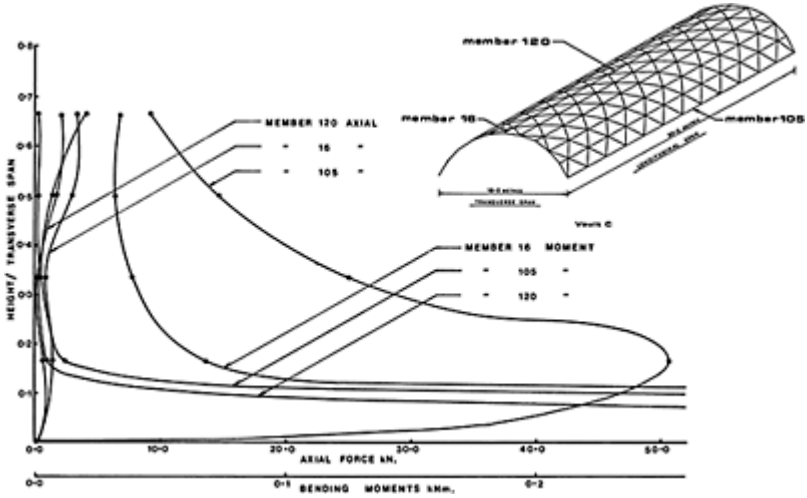

Fig. 6.16. Axial forces and moments for three members of vault C spanning longitudinally with fully fixed supports under an effective imposed non-symmetrical nodal load of 1·0 kN.

@Seismicisolation

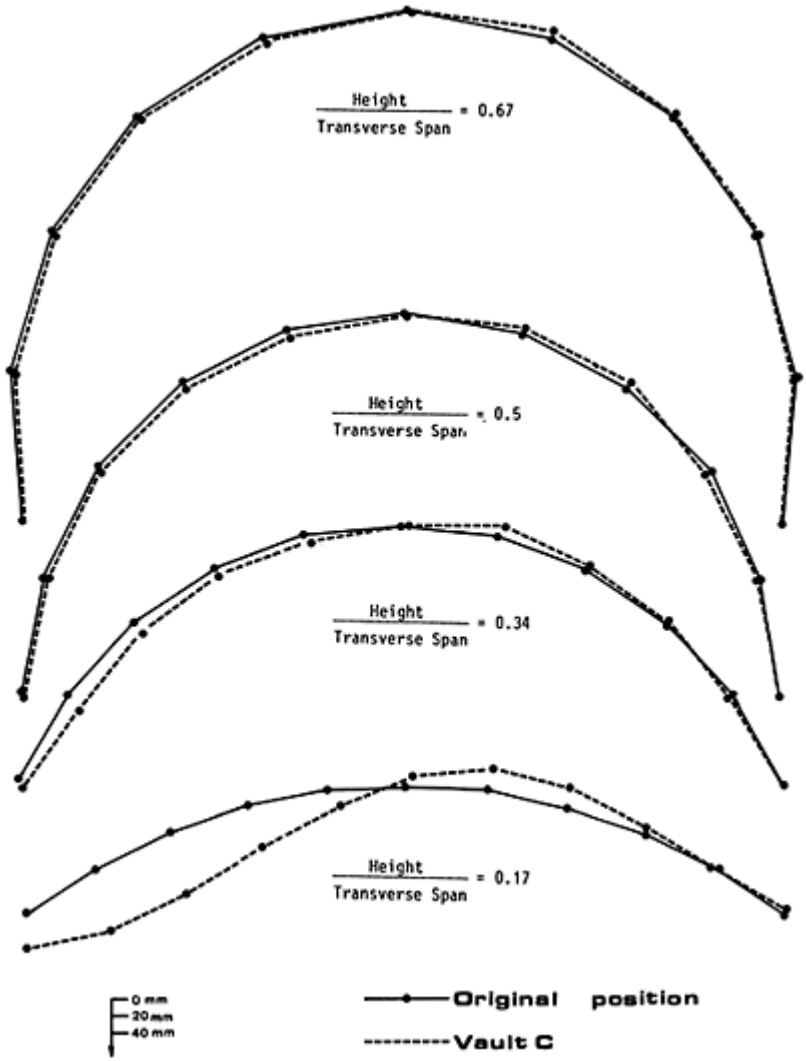

Fig. 6.17. Deflection profiles for vault C spanning longitudinally under an effective imposed non-symmetrical nodal load of 1·0 kN.

forces adjacent to the supports are reduced and redistributed towards the centre of the vault. For a height-to-span ratio of 0·5 the average deflections are approximately 1% greater for the pinned supports compared with deflections obtained from fully fixed supports. This small increase in deflections is also associated with a small increase, of the

@Seismicisolation

order of 2%, in the structural weight of the vault configurations. As the rise of the vault increases, the effects of pinning the supports decreases.

High-rise barrel vaults with fully fixed connections spanning longitudinally, and restrained against lateral movement, exhibit similar structural behaviour to rigidly connected trusses. The main forces in the members are axial tension and compression, the bending and torsion moments decreasing significantly as the rise of vault increases.

Under symmetrical loading the tensile and compression forces increase towards the centre of the structures for the longitudinal members, while the maximum axial forces in the diagonal members occur close to the corners of the vault and diminish towards the centre. For both symmetrically and non-symmetrically imposed loading, the diagonal configuration type C gives the most uniform deflection profile and, due to the reduced number of joints in comparison with types A and B, will almost certainly provide the most economical configuration for this type of structure.

5 SUMMARY OF EXISTING WORK ON BRACED BARREL VAULTS

Previous research work concerning the structural behaviour of barrel vaults has been undertaken at the Space Structures Research Centre by Makowski.[4] Several small scale model vaults were constructed each with a different configuration of members, some of which are shown in Fig. 6.18. Each of the models had the same overall dimensions with the bracing members arranged in such a manner as to give each model almost the same structural weight. The relative stiffness of the barrel vault types was investigated and it was found that the type of bracing used has a significant influence on the vault stiffness and stress distribution within the structure. The three-way braced vault was found to give

@Seismicisolation

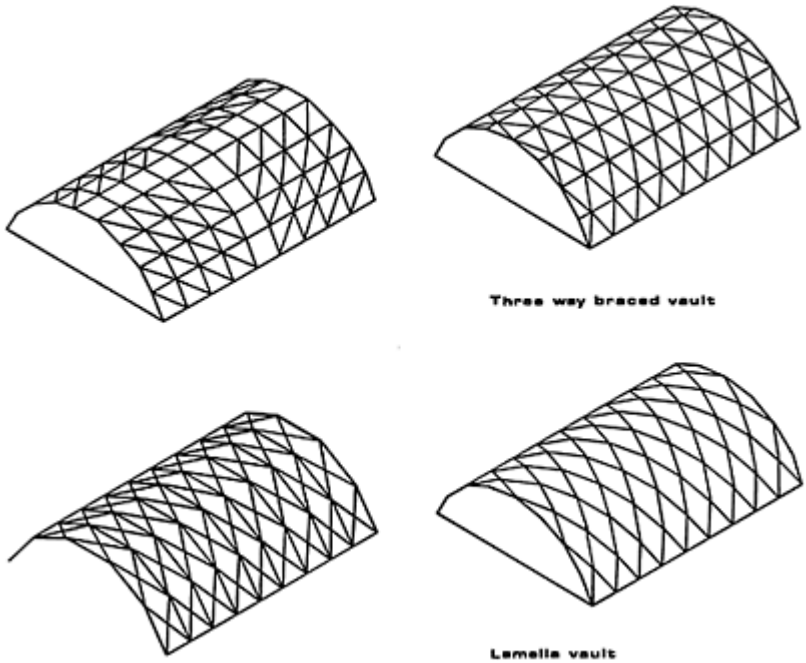

Fig. 6.18. Braced barrel vaults investigated by Makowski.

the most even force distribution throughout the structure under both symmetrical and non-symmetrical loading.

The lamella vault shown in Fig. 6.18 is kinematically unstable if the structure is considered pin-jointed. This configuration does become stable with fully fixed joints, which enable the structure to resist the applied loads by developing bending and torsion moments in the members and joints. This critical state for pin-jointed vaults is not so apparent in fully triangulated vaults, which can be kinematically stable with suitable boundary conditions, although instability is likely to occur in all pinned vaults with shallow rises. For this condition to prevail the vertical angles between the transverse members will become large with adjacent transverse members almost lying in the same plane, resulting in the likely formation of a 'toggle action' mechanism occurring in adjacent members.

Rigidly-jointed shallow vaults are also prone to instability with the possibility of snap-through buckling occurring chiefly under non-symmetrically imposed loading.

Vault type A (Fig. 6.1) has also been investigated by Bligh.[5] Several boundary conditions were studied under both symmetrical and wind loading. Analyses were carried out for both pinned and rigidly jointed vaults with two height-to-transverse-span ratios of 0·25 and 0·33. In all cases it was found that the stress distribution is extremely sensitive to boundary support conditions.

The assumption of rigid joints in the structure instead of pin-joints also changed the stress distribution in the vaults. The deflections obtained from the rigid joint analysis

@Seismicisolation

were between ten and twenty times smaller than similar deflections obtained for the pin-jointed vault, and generally the inclusion of fully fixed joints led to a more even stress distribution throughout the structure.

Bligh confirmed that under wind loading configuration type A (Fig. 6.1) is not structurally efficient. Stress reversals occurred in many members resulting in the diagonal members, which are in tension under symmetrical loading, taking compressive forces under wind and non-symmetrical loading. As the diagonal members are the longest

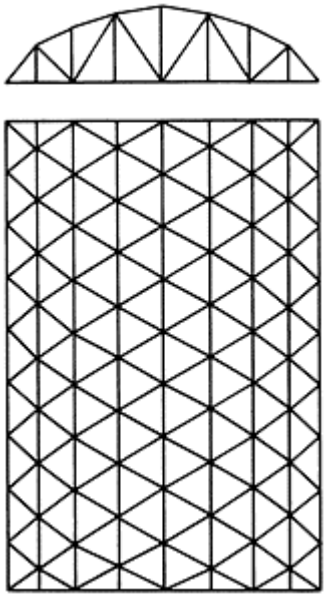

Fig. 6.19. Three-way braced barrel vault and gable bracing spanning longitudinally, investigated by King.

members in the particular vault configuration, an increase in section modulus may be necessary to enable the vault to carry non-symmetrical loading.

Additional work has been undertaken at the Space Structures Research Centre by King[6] who has investigated the effect which the stiffness of the end gable bracing has on the stress distribution in the three-way spatial grid barrel vault spanning longitudinally. The type of vault and gable bracing investigated are shown in Fig. 6.19. It was found that the stress distribution in the vault members was unaffected by any change in the area of the gable bracing provided the vault was pin-jointed. For stiff-jointed vaults there was a 1% change in the stress distribution in the vault members for a corresponding 100% change in the area of the gable bracing. This is to be expected as the stiffness of the gable bracing in relation to the stiffness of the curved vault is very low. If, however, the vault is assumed to be fully fixed along the transverse curved boundary, then both Bligh and King have confirmed that there are large reductions in the axial forces in the longitudinal

@Seismicisolation

boom members, while the axial forces in the remaining members are left almost unaltered. Even though gable bracing does not affect the stress distribution in the vault itself, it does provide an additional small restraint to reduce the possibility of instability occurring in shallow vaults.

Prynne[7] has also carried out an extensive analysis and preliminary design for a three-way braced barrel vault supported at only the four corners as shown in Fig. 6.20(A). This investigation has highlighted the structural weakness of barrel vault structure—that of high transverse flexibility when subjected to non-symmetrically imposed loading. In an attempt to increase transverse stiffness and hence improve the structural performance of the vault under non-symmetrical loading, Prynne considered the use of a hipped barrel vault shown in Fig. 6.20(B). This vault had additional vertical end supports, and a

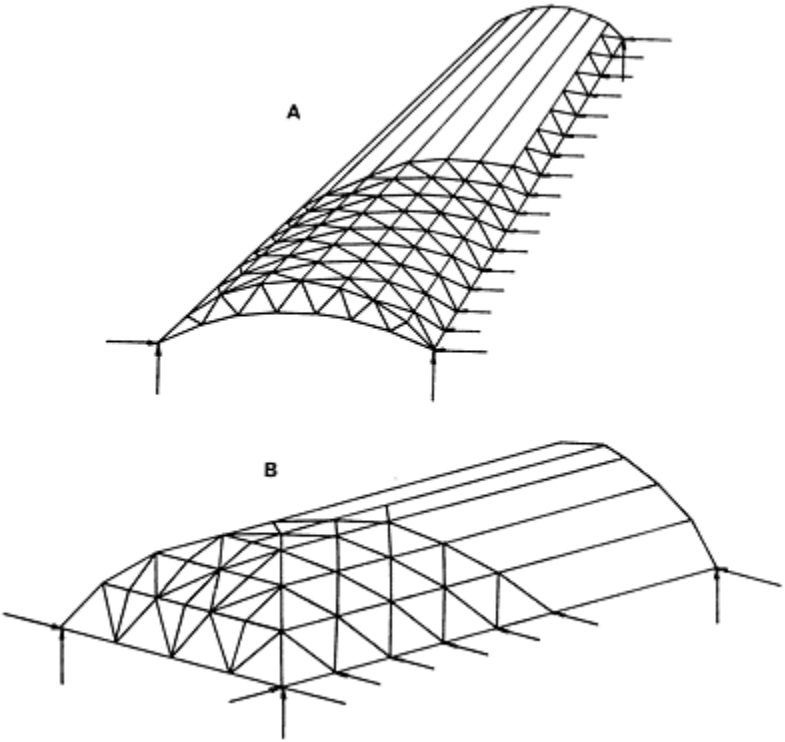

Fig. 6.20. Braced barrel vaults investigated by Prynne.

@Seismicisolation

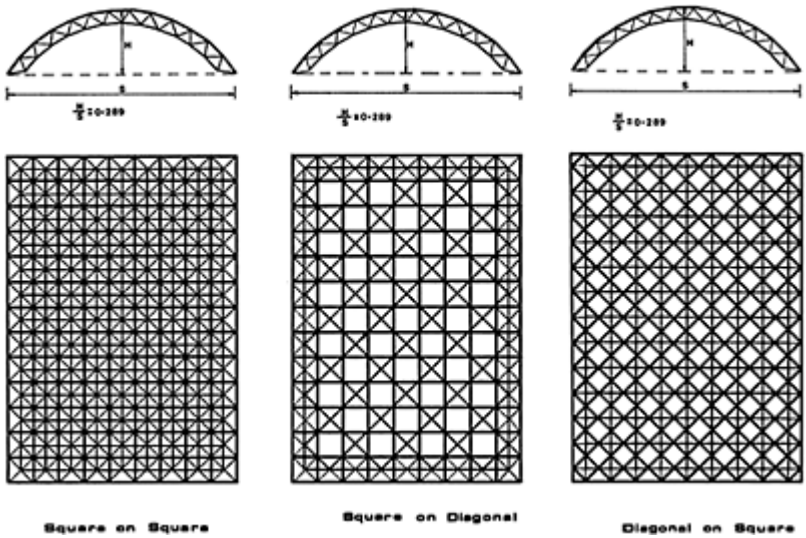

Fig. 6.21. Double-layer braced barrel vaults investigated by Wong.

redistribution of material. In a further analysis Prynne also considered a transversely stiffened barrel vault.

The introduction of hipped ends to the barrel vault substantially increased the axial forces and transverse end moments adjacent to the hipped end, and resulted in a general increase in deflections of the order of 10%. Three additional vertical restraints were introduced to support the node points at the hipped ends of the barrel vault; also, modifications were made to the member sizes at one end of the structure in an attempt to achieve an even stress distribution throughout the vault. Prynne found that neither of these modifications significantly altered the forces in the vault members, which is confirmed by the later work of Bligh and King. The incorporation of transverse stiffeners, placed symmetrically in long span barrel vaults, was first introduced by Makowski and Howley.[8] It was found by Prynne that inclusion of these stiffening ribs did improve the structural performance of the barrel vault under non-symmetrical loading. Local deflections and changes of shape were significantly reduced, resulting in a decrease in transverse bending moments in the bracing members.

To further improve the transverse rigidity of barrel vault systems and hence improve the stress distribution under non-symmetrical loading it is necessary to consider the performance of double-layer braced barrel vaults. Wong[9] has recently carried out an investigation at the Space Structures Research Centre to determine the stress distribution in three configurations of double-layer barrel vaults, each with two height-to-transverse-span ratios of 0·5 and 0·289. The configurations chosen were square on square, square on diagonal, and diagonal on square as shown in Fig. 6.21. These double-layer vault configurations were treated as pin-jointed and were analysed for dead load and two-wind load conditions. The vaults were considered supported along both the transverse and longitudinal edges. This investigation again highlighted the importance of considering

@Seismicisolation

non-symmetrical loading on barrel vault structures which produced stress reversals in many members and can consequently govern the vault design.

Wong found that, under the chosen support and load conditions, the diagonal on square configuration was not as efficient as the other two configurations in achieving an even stress distribution throughout the structure. Generally, the axial member forces in the square on diagonal system were found to be greater than the corresponding forces in the square on square type but, because of the reduction in member lengths and total joint numbers inherent with the former configuration, it is likely that the square on diagonal system would be the most economic.

6 SUMMARY

Braced barrel vault systems will provide long span economical roof structures to give large unobstructed floor areas. Many bracing configurations are available and each system will have a different stiffness and response to the imposed loading. The structures are sensitive to support conditions and also to non-symmetrically imposed loading which tends to govern the vault designs. The structural performance of long single-layer vaults is greatly enhanced by the inclusion of transverse stiffening ribs. Single-layer vaults primarily spanning longitudinally are more efficient at high height-to-transverse-span ratios and their behaviour is analogous to an assembly of trusses. For transversely spanning vaults the structure behaves similarly to an arch and the lower height-to-transverse-span ratio of 0·17 is recommended. Vaults with shallow rises must be checked to ensure that local and overall instability does not occur.

Of the single-layer barrel vaults analysed the three-way grid type has proved to give the most uniform stress distribution throughout the structure and, due to the low number of joints required in comparison with other configurations, should result in the most economical structural system.

The use of double-layer barrel vaults enhances the stiffness of the vault structure and will provide structural systems of great potential capable of spans in excess of 100 m.

REFERENCES

1. British Standard 449. The use of structural steel in building. British Standards Institution, London, 1969.
2. British Standard 4360. Weldable structural steels. British Standards Institution, London, 1979.
3. British Standard Code of Practice 3, Chapter V. Loading: Part 1, 1967: Dead and imposed loads (metric units).
4. Makowski, Z.S. Analytical and experimental investigation of stress distribution in steel space frames. Proceedings of the Steel Congress, Luxembourg, 1964, pp. 581–603.
5. Bligh, J. Analysis of a braced barrel vault. M.Sc.Thesis, University of Surrey, Guildford, 1971.
6. King, P.G. A study of the behaviour of braced barrel vaults. M.Sc. Thesis, University of Surrey, Guildford, 1974.
7. Prynne, P. A computer investigation into the behaviour of a long braced barrel vault roof. Chapter 31, Proceedings of the First International Space Structures Conference, 1967 (Ed. R. Davis). Blackwell Scientific Publications, Oxford, pp. 351–369.

@Seismicisolation

8. Makowski, Z.S. and Howley, M. The analysis of braced barrel vaults. *Journal of the Institution of Polish Engineers*, March 1957, pp. 11−39.
9. Wong, C.W. The structural behaviour of braced barrel vaults with particular reference to wind effects. Ph.D. Thesis, University of Surrey, Guildford, 1981.

@Seismicisolation

7
Determination of Wind Loads on Barrel Vaults

N.TOY
Department of Civil Engineering, University of Surrey, Guildford, Surrey

and
C.W.WONG
Department of Civil and Structural Engineering, Hong Kong Polytechnic, Hong Kong

NOTATION

C_d	Dimensionless drag coefficient.
C_p	Dimensionless pressure coefficient.
C_{pb}	Dimensionless base pressure coefficient.
C_{pm}	Dimensionless maximum negative pressure coefficient.
D	Diameter of circular curved barrel vault.
H	Height of structure or rise of barrel vault.
R	Radius of curvature of circular arc.
R_e	Reynolds number.
S_x	Length of barrel vault.
S_y	Chord of barrel vault.
V	Mean wind velocity.
V_0	Mean wind velocity outside the boundary layer.
ε	Effective height of roughness.
μ	Viscosity of air.
ρ	Density of air.
ψ	Angle of which the chord of the circular curved barrel vault subtends.

1 INTRODUCTION

In the initial design stage of light clad structures, the design engineer usually has to make an estimate of the types of loadings that will occur, both static and dynamic. One such load that he may be involved with is that due to the wind. In order to predict wind loads

@Seismicisolation

with confidence around a proposed structure, the engineer will turn first to the relevant code of practice for the particular country. In the case of barrel vaults, it is possible to find

American code (ANSI A58.1-1972)

TABLE 8

EXTERNAL PRESSURE COEFFICIENTS FOR ARCHED ROOFS, C_p

	Rise-to-Span Ratio, r	Windward Quarter	Center Half	Leeward Quarter
Roof on elevated structure	0<r<0·2 0·2≤r<0·3 0·3≤r≤0·6	-0·9 (1·5r-0·3)* (2·75r-0·68)	(-0·7-r)	-0·5 -0·5 -0·5
Roof springing from ground level	0<r≤0·6	1·42r	(-0·7-r)	-0·5

*When the rise-to-span ratio is (0·2≤r≤0·3), alternate coefficients given by (6r-2·1) shall also be used for the windward quarter.

Australian code (AS 1170, Part 2-1975)

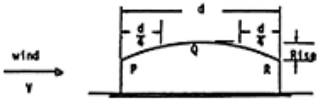

	Rise-to-span ratio, G	External pressure coefficients C_p		
Exposure	$(G = \frac{rise}{d})$	Windward quarter P	Centre half Q	Leeward quarter R
Roof on elevated structure	0<G<0·2 0·2≤G<0·3 0·3≤G≤0·6	-0·9 1·5G-0·3* 2·75G-0·675	-0·7-G -0·7-G -0·7-G	-0·5 -0·5 -0·5
Roof springing from ground level	0<G<0·6	1·4G	-0·7-G	-0·5

*The alternative coefficient 6G-2·0 shall also be used.

FIG. C8 CURVED ROOFS

Indian code (IS: 875-1964)

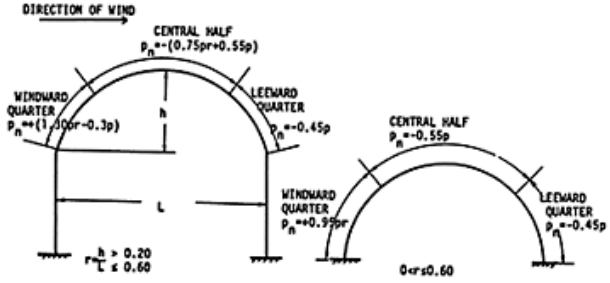

Fig. 7.1. Wind pressure distributions on curved structures, quoted from codes of practice.

@Seismicisolation

U.S.S.R. (BC & R II-A.11-62)

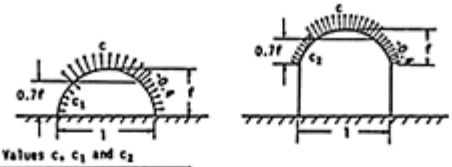

Values c, c_1 and c_2

f/l	c	c_1	c_2
0·1	-0·8	+0·1	-0·8
0·2	-0·9	+0·3	-0·7
0·3	-1·0	+0·4	-0·3
0·4	-1·1	+0·6	+0·4
0·5	-1·2	+0·7	+0·7

Remarks:

Aerodynamic coefficients for intermediate values f/l shall be determined by linear interpolation

TABLE 11 AERODYNAMIC COEFFICIENTS

U.K. Wind Loading Handbook (Newberry and Eaton, 1974)

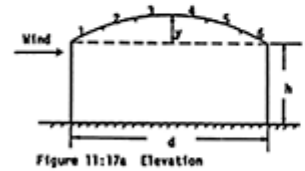

Figure 11:17a Elevation

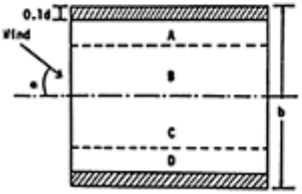

Figure 11:17b Plan

Table 11.5 C_{pe} for arched roof as in Figure 11:17 for wind angle $\alpha=0°$

Ratio y/d	Ratio h/d	C_{pe} for segments 1	2	3	4	5	6
1/5	0	+0·3	-0·3	-0·6	-0·7	-0·6	-0·2
	1/8	-0·5	-0·5	-0·7	-0·7	-0·5	-0·2
	1/4	-0·9	-0·6	-0·8	-0·8	-0·4	-0·2
	1/2	-1·2	-0·7	-0·9	-0·8	-0·3	-0·2
	1	-1·4	-0·8	-0·9	-0·9	-0·4	-0·4
	5	-1·8	-1·0	-1·1	-1·2	-0·8	-0·7
1/10	1/8	-1·0	-0·4	-0·4	-0·4	-0·4	-0·3
	1/4	-1·2	-0·5	-0·4	-0·4	-0·4	-0·3
	1/2	-1·5	-1·0	-0·7	-0·5	-0·4	-0·3
	1	-1·6	-1·0	-0·8	-0·6	-0·4	-0·3

NB All forces calculated from pressure coefficients should be assumed to act normal to the face.

Table 11.6 C_{pe} for arched roof as in Figure 11:17 for wind angle $\alpha=90°$

Section	C_{pe}
A	-0·8
B	-0·6
C	-0·3
D	-0·2

Local C_{pe} in hatched area of Figure 11:17b is -1·8

NB All forces calculated from pressure coefficients should be assumed to act normal to the face.

some information about wind pressures on a curved roof, either with an enclosure wall or springing from the ground surface, in several codes of practice. The wind pressures as given by the American code (ANSI A58.1–1972), Russian code (BC & R II-A. 11–62), Australian code (AS 1170, Part 2–1975), Indian code (IS: 875–1964) and the UK Wind Loading Handbook (Newberry and Eaton, 1974) are quoted[3–7] and shown in Fig. 7.1. These codes basically provide mean pressures for a variety of shapes in the form of non-dimensional pressure coefficients, and in order to predict the actual pressure and

@Seismicisolation

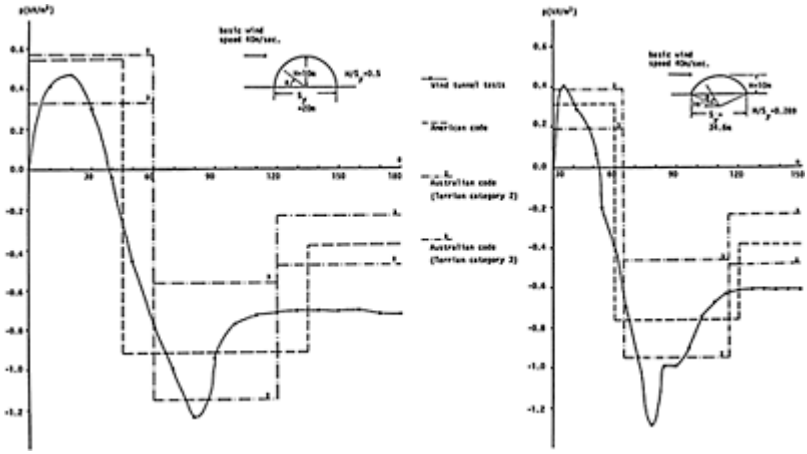

Fig. 7.2. Comparison of the present wind tunnel test results with the codes of practice.

consequently the load on the structure, they have to be multiplied by the dynamic head of the wind ($0{\cdot}5\,\rho U^2$), where U is the design wind speed. Although this design wind speed is known to be dependent on several parameters, such as terrain, building size, wind spectrum, etc., the magnitude of this speed may well be a somewhat uncertain element in calculating wind loads.

As an example of the complexity of estimating surface pressures for semi-cylindrical shaped bodies the wind pressure coefficient of a highly curved roof springing from the ground surface, as given by the different codes of practice (Fig. 7.2), shows that there is a high positive pressure on the windward side of the roof surface including the leading edge at ground level. Since the velocity in the boundary layer near the ground is small compared with the freestream velocity and theoretically approaches zero on the ground surface itself, the information in the codes of practice, being in themselves different, must be an oversimplification.

The major problem in trying to predict confidently wind loads on highly curved surfaces is the lack of experimental data of the flow characteristics on these types of structures. For sharp edged bodies the position of separation of the flow is predictable and therefore the pressure coefficients can be estimated with some confidence. Unfortunately, barrel vaults, by their very nature, may be of circular arc form or of elliptical curved form, either with supporting columns or simply springing from the ground surface, and do not allow such easy description. From our present knowledge of flows around circular cylinders, it is known that the effect of the Reynolds number of the flow may be pronounced in the case of the flow over curved surfaces because the flow can separate at different positions on the curved surface at different Reynolds number. Furthermore, the surface condition of the structure and the turbulence of the approaching flow can also produce flow separation at different positions at different Reynolds number.

@Seismicisolation

In reality, barrel vault type structures will have openings such as entrance doors, windows, ventilation systems, etc. so that internal pressures may be induced. The internal pressure in a structure usually depends on the relative ease of the inflow and outflow of the air and on the relative size and position of openings and leakage points in the roof relative to the external pressure distribution. The total wind pressure on the roof will then depend on the difference of pressure between the outer and the inner faces. In addition, it is also necessary to consider the disturbance of the flow by any particular neighbouring building.

As an example of the types of problems associated with understanding the fluid mechanics of the flow over highly curved surfaces, the surface pressure distribution of two different types of barrel vaults of different lengths has been measured in three different wind directions.

2 EXPERIMENTAL RIG

An investigation of the pressure distribution on the surface of two different types of semi-cylindrical models with different length/chord ratios were carried out in the Department of Civil Engineering's wind tunnel. This tunnel is a low-speed, blow-down, open circuit type with a working section of 1·372 m×1·067 m×9·0 m length, and is shown in diagrammatic form in Fig.7.3. Two thick turbulent boundary layers of different mean velocity and turbulent intensity were generated on the wall of the tunnel using a barrier fence and a set of velocity generators, similar to those described by Counihan.[1] Although these boundary layers may be described as turbulent, one of them was 'smooth' and the

@Seismicisolation

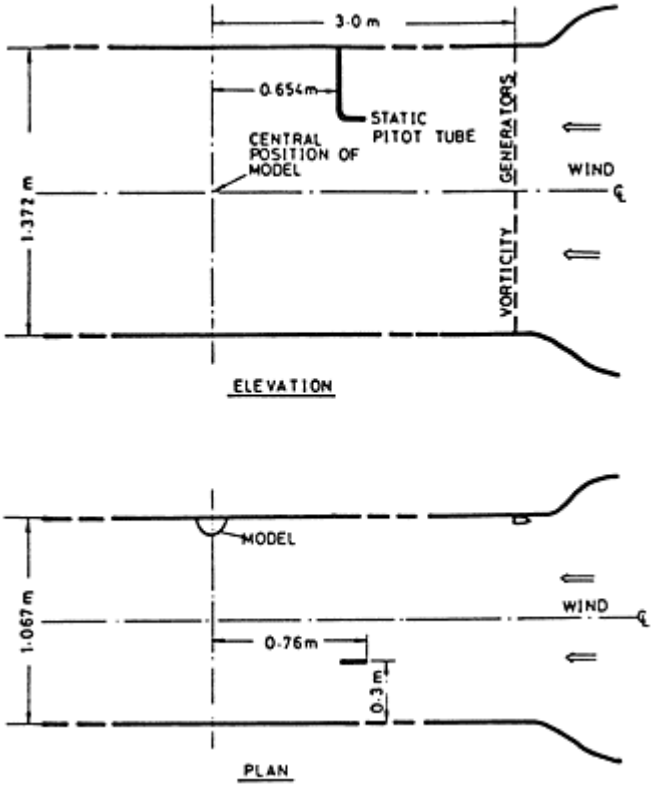

Fig. 7.3. Experimental arrangement of barrel vault mounted on the simulated boundary layer system.

@Seismicisolation

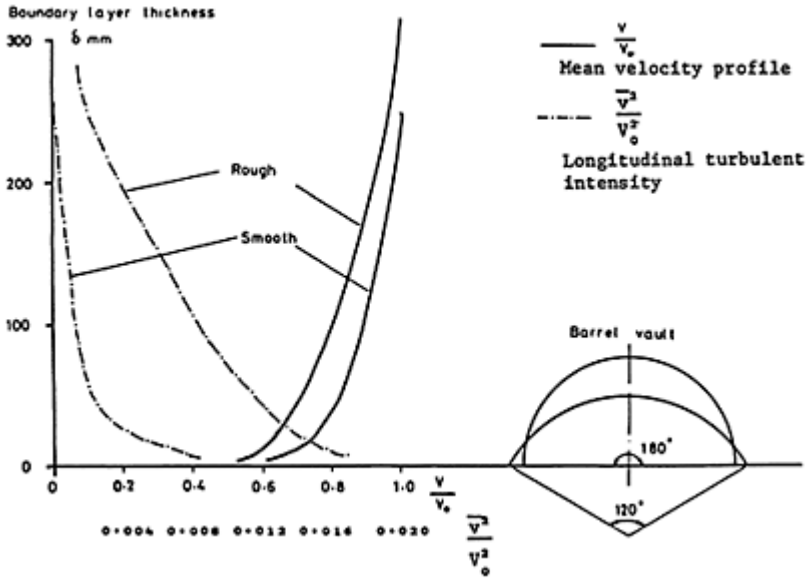

Fig. 7.4. Velocity profiles and longitudinal turbulent intensities of the ‘smooth’ and ‘rough’ boundary layers as they approach the barrel vaults.

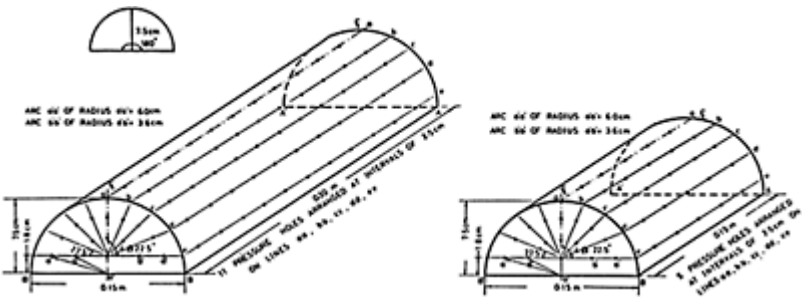

Fig. 7.5. Details of models with subtended angle of 180°.

@Seismicisolation

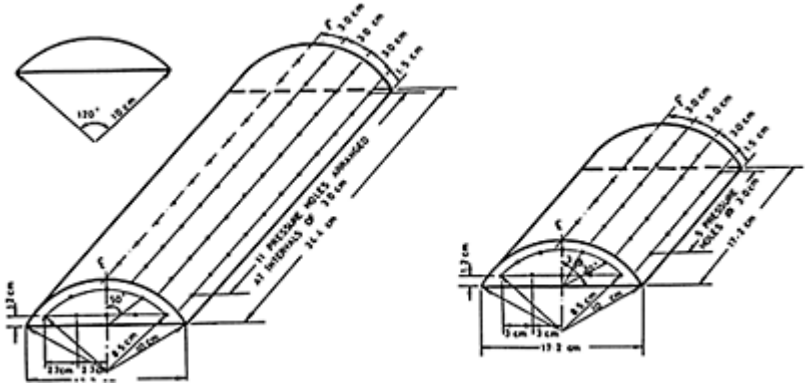

Fig. 7.6. Details of models with subtended angle of 120°.

other 'rough'. The smooth boundary layer was generated by allowing the flow to develop along the smooth surface of the wall of the tunnel; the rough boundary layer was obtained by allowing the flow to develop along the wall which was artificially roughened. The details of the two boundary layers are given in Table 7.1.

Table 7.1: Boundary layer details

	Thickness δ (mm)	*Displacement thickness δ* (mm)*	*Momentum thickness θ (mm)*	*δ*/θ*	*δ*/δ*	*θ/δ*
Smooth	265	32·6	25·45	1·27	0·121	0·096
Rough	360	64·77	44·52	1·46	0·180	0·124

These boundary layers were generated to simulate the lower part of the earth's natural boundary layer. The 'rough' boundary layer has a velocity distribution $V \alpha h^{1/4}$, similar to the distribution in suburban areas or small towns, whereas the velocity distribution for the'smooth' boundary layer is similar to that found over open fetch, where $V \alpha h^{1/7.}$

Barrel vaults of two different configurations were studied. The cross-section of the barrel vaults was a circular arc subtending an angle ψ at the centre; two different values of ψ were considered, ψ=180° and ψ=120°.

The two types of models were made from circular pipe of diameter 0·15 m and 0·20 m. For each type of model three different lengths were used, one having longitudinal length equal to the span of the tunnel so that two-dimensional flow conditions could be studied; the other two models were made so that their length/chord ratios were 2:1 and 1:1 respectively; these were chosen so that three-dimensional flow conditions could also be studied. In all cases the surface of the model was sand-roughened so that the flow conditions were similar to that which may be found in the super-critical regime for circular cylinders.[2] Figure 7.4 shows the height of the velocity profile and the magnitude of the turbulence intensity in the boundary layers as they approach the respective models.

@Seismicisolation

The magnitude of the turbulence intensity in the 'rough' boundary layer is some 3 to 4 times greater than that in the 'smooth' boundary layer.

In order to compute the wind loads on these models pressure distributions were obtained from measurements taken at a Reynolds number of $1{\cdot}0\times10^5$. This pressure distribution was obtained by pressure tapping the models in equal intervals over one half of the model, as shown in Figs. 7.5 and 7.6. For the case of the three-dimensional models

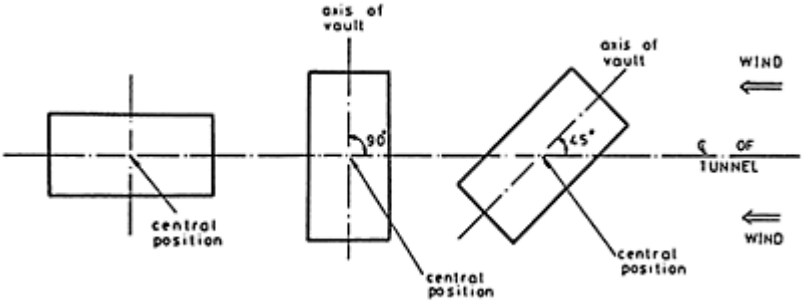

Fig. 7.7. Position of barrel vault under three different oncoming wind directions.

pressure distributions were obtained for the model in three different flow configurations: flow normal to the barrel vault, flow along the axis, and flow at 45° to the structure, shown diagrammatically in Fig. 7.7.

3 DISCUSSION

From a preliminary investigation of the pressure coefficient along the median line for the flow normal to the model it can be seen again from Fig. 7.2 that these coefficients as predicted by the different codes of practice may be seriously in error. The reason for the discrepancy between the present experimental results and the predicted values is probably due to the predicted values being obtained from the use of experimental data taken from a circular cylinder immersed in a uniform flow and then simplified.

To appreciate the extent of this problem in trying to predict accurately the pressure distribution and hence the wind loads on barrel vault type structures consider the present work in two parts: part (i) considers how the pressure distribution will vary over the two-dimensional model immersed in the two different boundary layers, and part (ii) will consider the pressure coefficients over the three-dimensional barrel vaults for different wind directions.

Part (i): In this case consider the pressure distribution along the median line for the semi-cyclindrical model with ψ=180° immersed in the two different boundary layers. These pressure coefficients are shown in Fig. 7.8 for a Reynolds number of 10^5 based on the freestream velocity and diameter of model. Furthermore, these coefficients are plotted

@Seismicisolation

using two different dynamic pressures. The crossed symbols relate to the dynamic pressure at the height of the model $0{\cdot}5\rho v^2_{(H)}$, whereas the open symbols relate to the

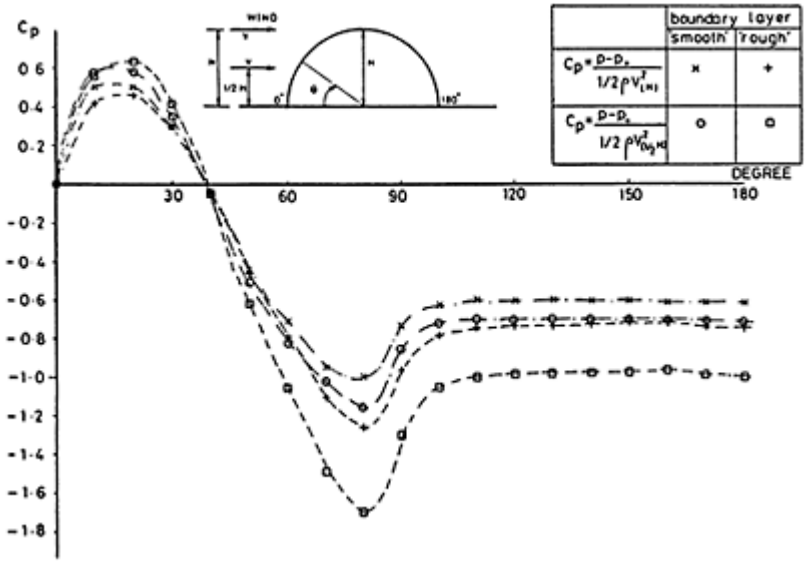

Fig. 7.8. Pressure distributions around the two-dimensional rough surface barrel vault with subtended angle of 180° and roughness ratio ε/D=7·3 ×10^{-3}~l.3×10^{-2} in the 'smooth' and 'rough' boundary layers at $Re \simeq 10^5$.

dynamic pressure obtained from the velocity in the boundary layer at half the height of the model $0{\cdot}5\rho v2_{(H/2)}$.

From these results it can clearly be seen that the distribution obtained in the 'rough' boundary layer has slightly lower positive pressure on the windward face of the model but much larger negative values over the rear surface than those given in the 'smooth' boundary layer. The differences in these distributions is even more accentuated if the dynamic pressure at half the height of the model is taken instead of the full height. This infers that the increased turbulence in the 'rough' boundary layer has an appreciable effect on the pressure distribution and hence on the wind loading. More information on this subject is required before accurate prediction methods can be devised.

Since it is known that the Earth's boundary layer has a turbulence intensity and length scales greater than that we have modelled as yet in our wind tunnel, it was decided that the following investigation of the effect of wind direction over the three-dimensional models would be performed in the 'rough' boundary layer only.

Part (ii): For the investigation of the pressure distribution over the three-dimensional models, the mean pressure distribution, based on freestream dynamic pressure, over the

@Seismicisolation

complete barrel vaults are shown as lines of constant pressure. Solid lines denote negative pressure regions and broken lines, positive pressure regions. Under different oncoming wind directions, the mean pressure distributions on the barrel vaults of the two different geometries, with different length-to-chord ratios, show a similar pattern but with some differences in detail.

With the oncoming wind blowing normal to the axis of the model, theoretically the pressure distribution should be symmetrical about the centre-line in the windward direction (Figs. 7.9 and 7.10). However, the present results show a pressure distribution that is not exactly symmetrical but only approximately so. This might be caused by the misalignment during the setting up of the models or the fact that the models might not be perfectly symmetrical. Observing the cross-sectional pressure distribution of each geometrical type of model, it is clearly seen that the distribution had pronounced similarities to the corresponding two-dimensional model. Near the centre part of the models, the cross sectional pressures were higher than the portion near the two ends and tended to become uniform. Since this portion was far from the two sides, the end effects are probably small. Detailed investigation of the pressure distribution on the two-dimensional models (i.e. of high length-to-chord ratios) and on the three-dimensional models shows that for the two different geometries the peak suction and the base pressure at the mid-span of the models were higher for the model of higher length-to-chord ratio. This indicates that the effect of three-dimensionality is more significant for a short vault.

With the oncoming wind blowing parallel to the axis of the barrel vault, the windward end wall experienced positive pressures and the leeward end wall experienced suctions (Figs. 7.11 and 7.12). Pressures on the cylindrical surface were all suctions with higher values at the leading part. This indicates that the flow first strikes the windward end wall and then separates at the edge of the wall.

With the wind at 45° to the axis of the model, the distribution patterns were absolutely different to the other two oncoming wind directions (Figs. 7.13 and 7.14). If a cross-section is taken from the upper windward corner along the wind flow direction, it could be observed that there were positive pressures at the front part with peak suction in the middle and the base pressure at the rear; it may be considered that in the portion of the body where the cross-section, in the direction of the wind, forms a complete curved surface elliptical rather than circular, the flow past that region must be in a generally

@Seismicisolation

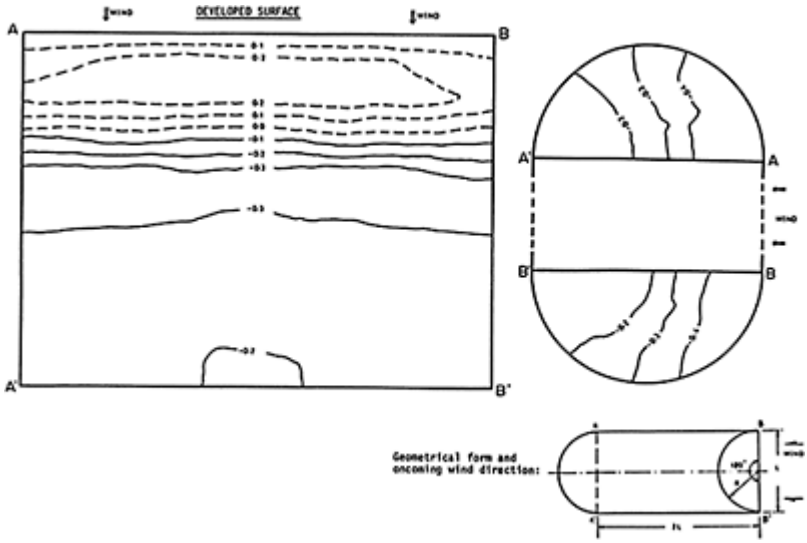

Fig. 7.9(a). Pressure distribution on barrel vault in 'rough' boundary layer. *Re* 10^5. ε/D: $7{\cdot}3\times10^{-3} \sim 1{\cdot}3\times10^{-2}$.

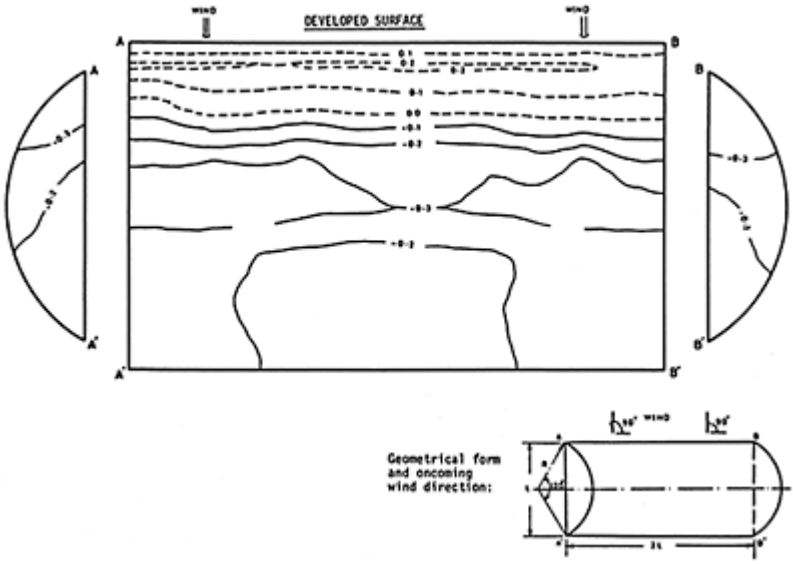

Fig. 7.9(b). Pressure distribution on barrel vault in 'rough' boundary layer. *Re* 10^5. ε/D: $5{\cdot}5\times10^{-3} \sim 1\text{–}0\times10^{-2}$.

@Seismicisolation

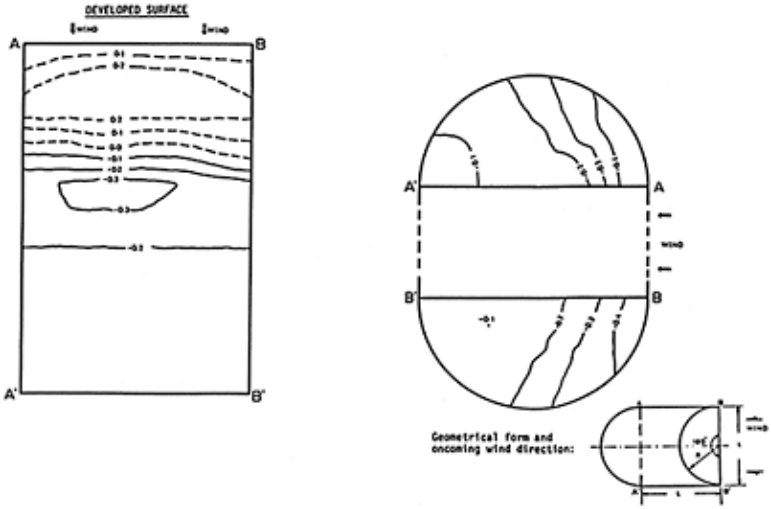

Fig. 7.10(a). Pressure distribution on barrel vault in 'rough' boundary layer. Re 10^5. ε/D: $7{\cdot}3\times10^{-3} \sim 1{\cdot}3\times10^{-2}$.

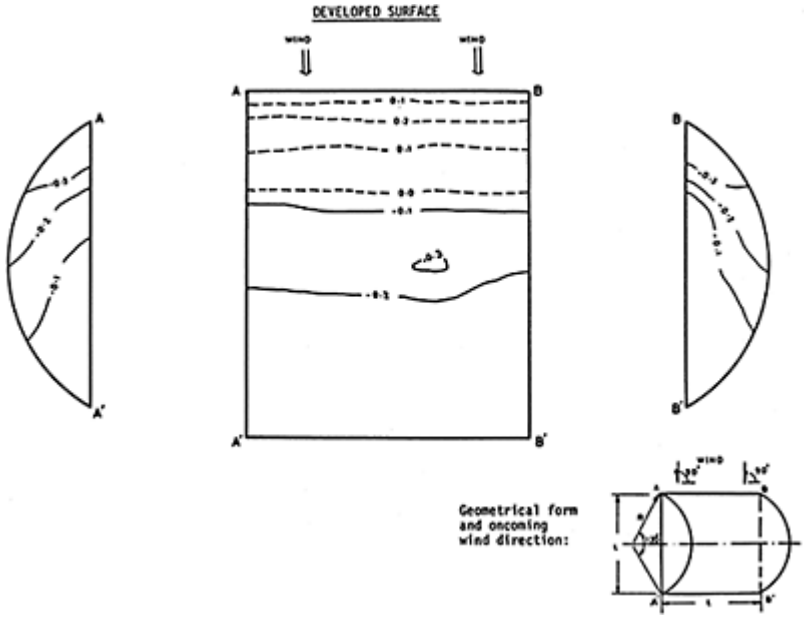

Fig. 7.10(b). Pressure distribution on barrel vault in 'rough' boundary layer. *Re* 10^5. *ε/D*: $5{\cdot}5\times10^{-3} \sim 1\text{–}0\times10^{-2}$.

@Seismicisolation

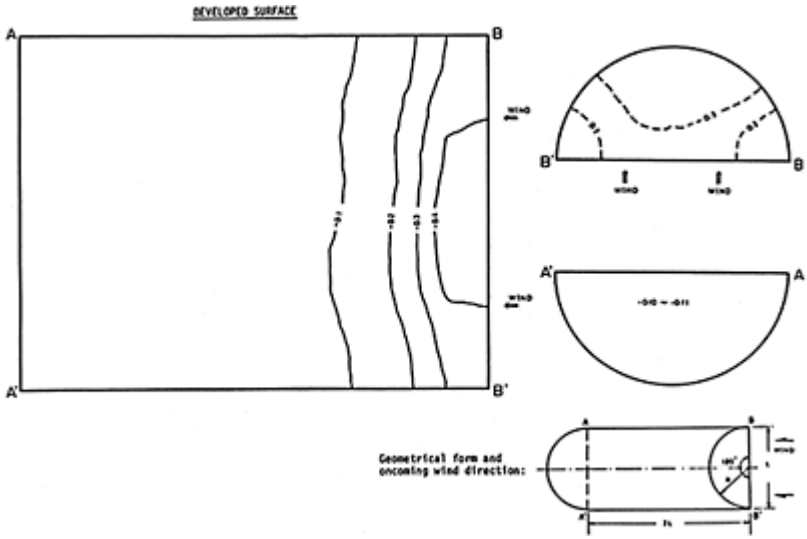

Fig. 7.11(a). Pressure distribution on barrel vault in 'rough' boundary layer. *Re* 10^5. ε/D:$7{\cdot}3\times10^{-3} \sim 1{\cdot}3\times10^{-2}$.

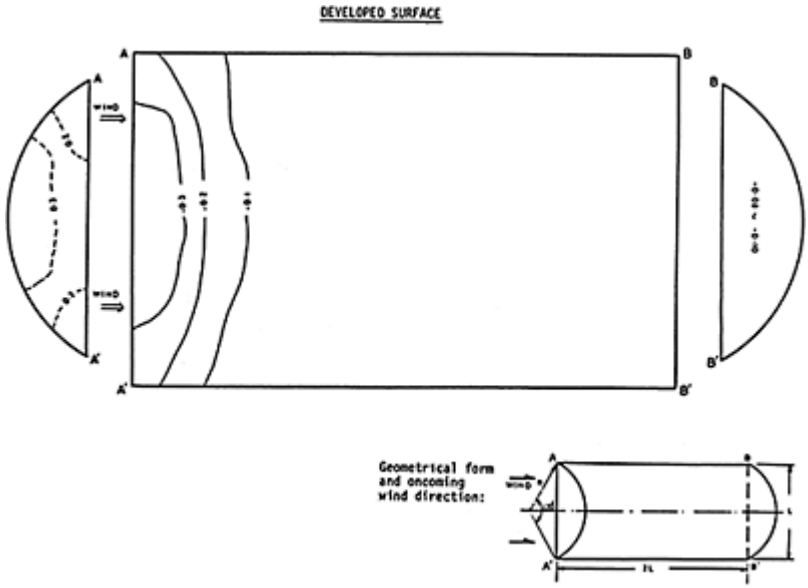

Fig. 7.1 1(b). Pressure distribution on barrel vault in 'rough' boundary layer. *Re* 10^5. ε/D: $5{\cdot}5\times10^{-3} \sim 1{\cdot}0\times10^{-2}$.

@Seismicisolation

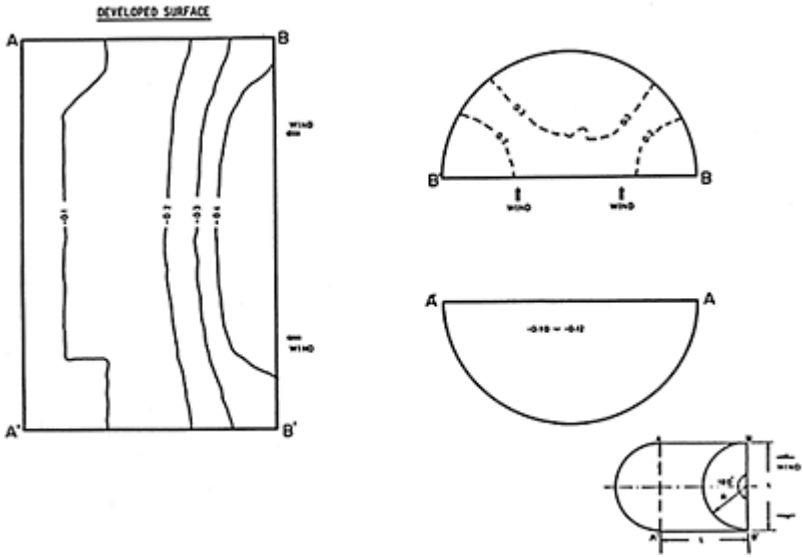

Fig. 7.12(a). Pressure distribution on barrel vault in 'rough' boundary layer. *Re* 10^5. ε/D: $7{\cdot}3\times10^{-3}$ ~$1{\cdot}3\times10^{-2}$.

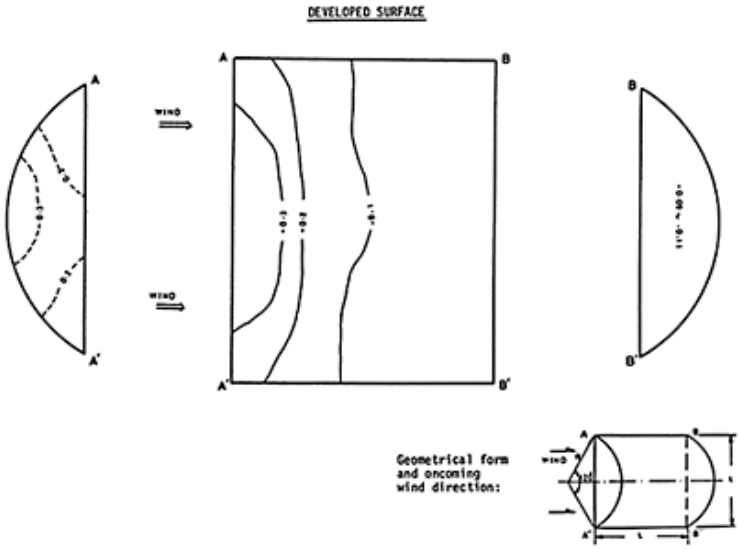

Fig. 7.12(b). Pressure distribution on barrel vault in 'rough' boundary layer. Re 10^5. ε/D: $5{\cdot}5\times10^{-3}$ ~ $1{\cdot}0\times10^{-2}$.

@Seismicisolation

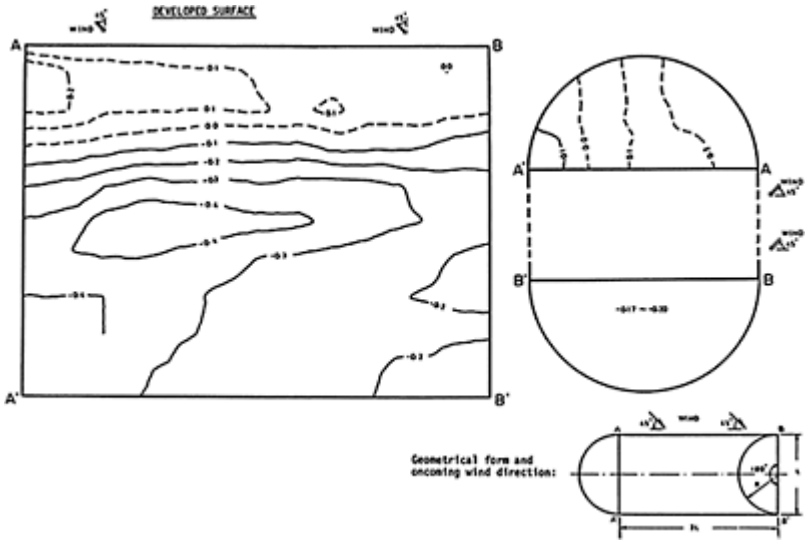

Fig. 7.13(a). Pressure distribution on barrel vault in 'rough' boundary layer. *Re* 10^5. ε/D: $7{\cdot}3\times10^{-3} \sim 1{\cdot}3\times10^{-2}$.

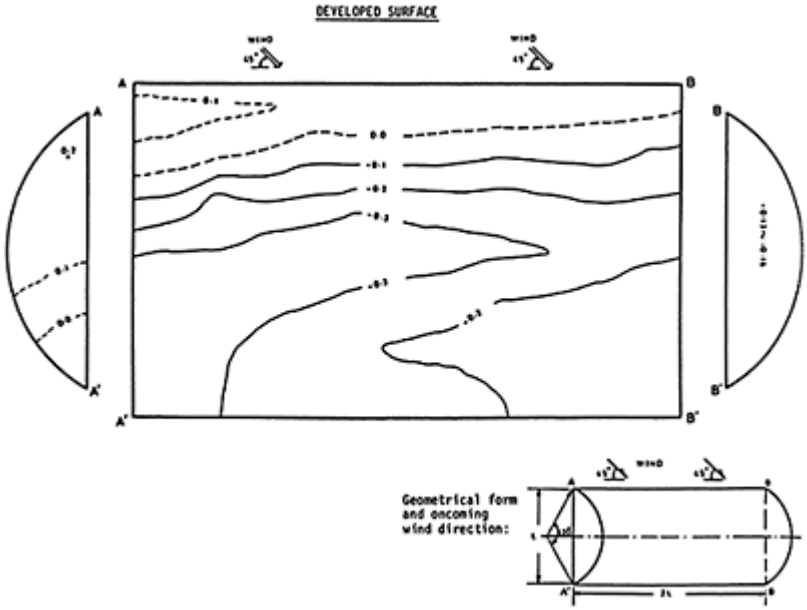

@Seismicisolation

Fig. 7.13(b). Pressure distribution on barrel vault in ‘rough’ boundary layer. *Re* 10^5. ε/D: $5{\cdot}5\times10^{-3} \sim 1{\cdot}0\times10^{-2}$.

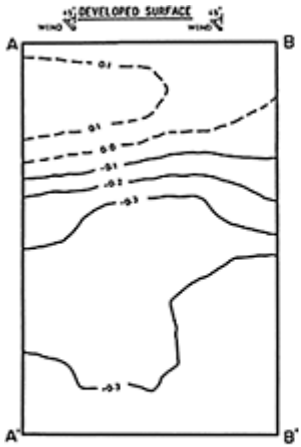

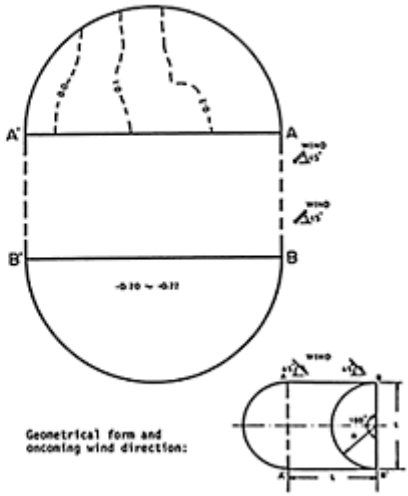

Fig. 7.14(a). Pressure distribution on barrel vault in ‘rough’ boundary layer. *Re* 10^5. ε/D: $7{\cdot}3\times10^{-3} \sim 1{\cdot}3\times10^{-2}$.

@Seismicisolation

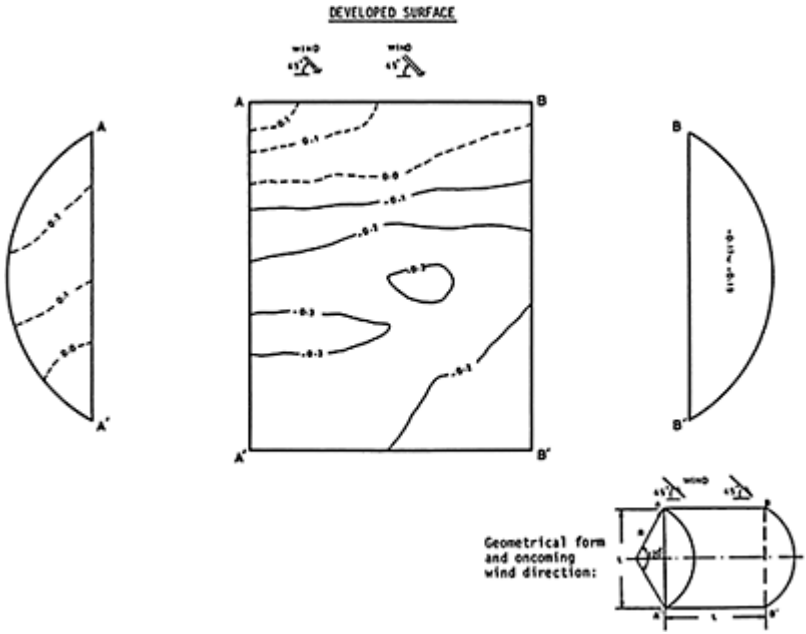

Fig. 7.14(b). Pressure distribution on barrel vault in 'rough' boundary layer. *Re* 10^5. ε/D: $5{\cdot}5\times10^{-3}$ ~ $1{\cdot}0\times10^{-2}$.

Table 7.2: Comparison of the pressure coefficients of rough surface barrel vaults with subtended angle of 180° and with roughness ratio ε/D=7.3×l0^{-3} ~1.3×l0^{-2} obtained in the 'smooth' and 'rough' boundary layers

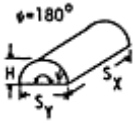	'smooth' boundary layer						'rough' boundary layer					
s_x/s_y	9.147		2		1		9.147		2		1	
$C_p$reference height	$C_{p(H)}$	$C_{p(\frac{1}{2}H)}$	$C_{p(H)}$	$C_{p(\frac{1}{2}H)}$	$C_{p(H)}$	$C_{p(\frac{1}{2}H)}$	$C_{p(H)}$	$C_{p(\frac{1}{2}H)}$	$C_{p(\frac{1}{2}H)}$	$C_{p(\frac{1}{2}H)}$	$C_{p(H)}$	$C_{p(\frac{1}{2}H)}$
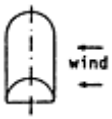												

@Seismicisolation

Vault surface max. +ve C_p	0.47	0.59	0.56	0.65	0.54	0.62	0.47	0.63	0.50	0.67	0.54	0.72
C_{pm}	−1.75	−2.02	−0.82	−0.95	−0.62	−0.71	−1.26	−1.70	−0.73	−0.98	−0.63	−0.85
C_{pb}	−0.53	−0.62	−0.40	−0.46	−0.33	−0.39	−0.71	−0.98	−0.48	−0.65	−0.34	−0.46
End walls max. -ve C_p			−0.98	−1.14	−0.98	−1.14			−0.94	−1.27	−0.82	−1.11
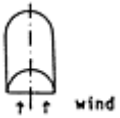												
Vault surface max. -ve C_p			−0.93	−1.07	−0.94	−1.09			−0.88	−1.19	−0.92	−1.24
End walls windward max. +ve C_p			0.77	0.89	0.78	0.90			0.73	0.98	0.75	1.01
leeward max. -ve C_p			−0.20	−0.23	−0.21	−0.25			−0.21	−0.28	−0.23	−0.31
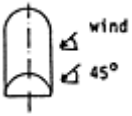												
Vault surface max. +ve C_p			0.47	0.54	0.43	0.50			0.38	0.52	0.32	0.44
C_{pm}			−0.87	−1.01	−0.70	−0.81			−0.94	−1.27	−0.73	−0.98
C_{pb}			−0.40	−0.46	−0.54	−0.62			−0.48	−0.65	−0.57	−0.78
End walls windward max. +ve C_p			0.59	0.68	0.51	0.59			0.55	0.75	0.50	0.67
leeward max. -ve C_p			−0.40	−0.46	−0.40	−0.46			−0.38	−0.52	−0.42	−0.57

similar pattern to the case of a circular curved body. Considering the region above that section, the flow first strikes the windward end wall and then separates at the edge of the wall. Therefore, positive pressures occurred at the windward end wall and suctions occurred on the vault surface. For the region further to the rear, the cross-section is still a curve but not so complete as in the middle portion of the body so that positive pressures occurred in a small area at the front part and a fairly uniform suction occurred on most of the surface. Further, comparing the positive pressure, the peak suction and the base pressure to those occurring with the wind direction normal to the axis of the barrel vault, it is found that the present wind direction gives a lower positive pressure but a higher peak suction and base pressure on the vault surface.

@Seismicisolation

To conclude this discussion, some overall results are shown in Table 7.2 of the maximum positive and negative pressures, maximum negative pressures and base pressures are shown for the Ψ=180° models immersed in both boundary layers and subjected to three wind directions. From this table, one can see at a glance that the overall pressure coefficient on a barrel vault type structure depends on:

(i) type of boundary layer,
(ii) position at which the dynamic pressure is recorded,
(iii) orientation of the wind.

Although these factors have to be taken into account when measuring pressure distributions on wind tunnel models, they are by no means the only important factors. For instance, shape, protuberances, surface roughness, etc. will all have to be taken into account if accurate pressure distribution and hence wind loads are to be made available to the design engineer.

4 CONCLUSIONS

Since little relevant work on wind pressure distributions on barrel vaults has been carried out, the present work is a first step in this type of investigation. From this work it has been shown that when designing these types of structures it is important to understand the significance of how the wind loads may be obtained and the difficulty in determining the accuracy of the wind loads from the codes of practice. To reiterate, this present work has shown that the pressure distribution over barrel vault type structures depends upon:

(i) freestream turbulence and length scale,
(ii) dynamic pressure,
(iii) wind direction,
(iv) shape of body,

and, to a more limited extent, it has emphasised that surface roughness, structural protuberances and location of the structure is of importance.

REFERENCES

1. Counihan, J. The structure and the wind tunnel simulation of rural and adiabatic boundary layers. Symposium on External Flows, University of Bristol, 1972.
2. Wong, C.W. The structural behaviour of braced barrel vaults with particular reference to wind effects. Ph.D. Thesis, Department of Civil Engineering, University of Surrey, 1981.
3. ANSI A58.1–1972. American national standard building code requirements for minimum design loads in buildings and other structures. American National Standards Institute, New York, 1972.
4. BC & R II-A.l1 1–62. Building code and regulations, Part II, Section A, Chapter 11: Loads and Effects. State Committee on Construction, Moscow, 1965.
5. AS 1170, Part 2–1975. Australian standard rules for minimum design loads on structures, Part 2 –Wind Forces. Standards Association of Australia, North Sydney, 1975.
6. IS: 875–1964. India standard code of practice for structural safety of building: Loading standard (revised). Indian Standards Institution, Delhi, 1964.

@Seismicisolation

7. Newberry, C.W. and Eaton, K.J. Wind loading handbook. Building Research Establishment Report, Department of the Environment Building Research Establishment, London, 1974.

@Seismicisolation

8
Stability Considerations in Barrel Vaults

JAMES F.DICKIE
Simon Engineering Laboratories, University of Manchester, UK

1 INTRODUCTION

Large span steel roof structures have been designed subject to a multitude of structural and financial restraints. They supply commercial and industrial needs such as exhibition halls, sports halls and airplane hangars. Building usage very frequently dictates a rectangular plan form. The larger spans suggest the adoption of a structural system that uses its profile to achieve primarily axial forces. These lead directly to 'arch' solutions and the Oxford dictionary defines the vault as

'arched roof, set or series of arches'.

The general surface of a vault may be technically defined as translating a curved generator along a generatrix. The straight line generatrix predominates and the resulting form is most commonly and simply described as a cylindrical or barrel vault with the shape illustrated in Fig. 8.1. The vault transfers load by a combination of longitudinal beam action and transverse arch action. In short barrels, with the arch radius/length< 0·6, the loads are carried essentially by arch action to the longitudinal edges whereas in longer barrels the vault behaves primarily as a beam of thin curved cross-section.

In the arrangement of individual members to form the surface three objectives affect the solution. Optimal patterns attempt to provide uniformly stressed members, sculptural patterns emphasise a particular repeated geometrical layout, and an adequate pattern is purely functional. Individual members between joints may be standard sections or of a truss nature. Connections for single-layered systems must possess substantial resistance against bending with minimum joint eccentricity. As spans have increased with markedly greater economy of material the dead load has decreased to as low as 20% of live loading. Figure 8.2 is indicative of the relationship between dead loading and span.

The present study describes basic form, loading patterns and analytical procedures; by contrasting two existing large spans the significance of these factors in stability and collapse are considered.

2 FORM

The Victorian era first saw the erection of vaults with a primary skeletal nature that incorporated many of the features seen today. The form was particularly favoured for

@Seismicisolation

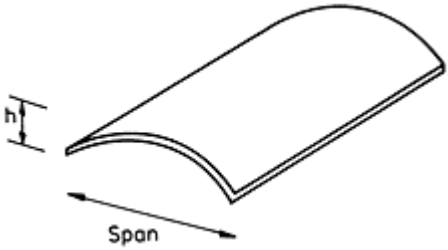

Fig.8.1

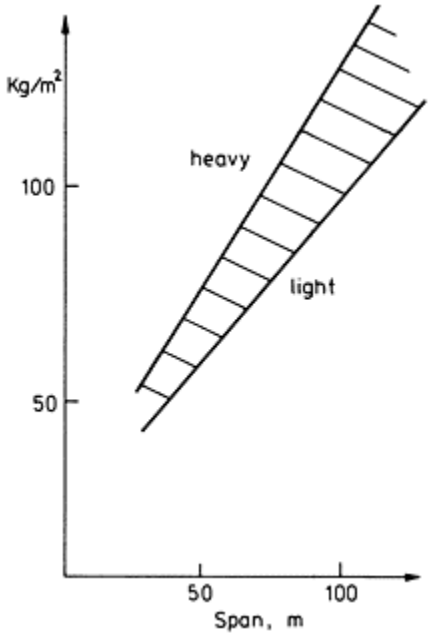

Fig. 8.2.

train shed roofs. The large span gave flexibility in the layout of the platforms and the high rise decreased exposure to acidic locomotive smoke.

Manchester Central Station,[2] built by the Cheshire Lines Committee, is one such example. The elevation is shown schematically in Fig. 8.3(i) and the plan form in Fig. 8.3(ii). A prestige motive was involved in order to match St Pancras station in London to and from which a connecting service was run. It is of interest to note that current plans for the refurbishment of the structure coincide with the erection of an attractive vault with domed ends for the 1984 Liverpool Garden Festival. The roof begun in 1876 is a series of wrought iron arches of 64 m span fixed at each abutment. There is no

@Seismicisolation

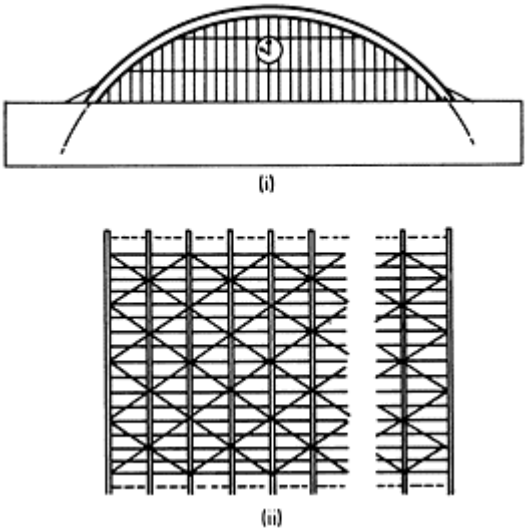

Fig. 8.3.

Fig. 8.4.

@Seismicisolation

Fig. 8.5. (By courtesy of Bethlehem Steel.)

tie and all the base thrust is taken by the vaulted masonry undercroft. In all there are 18 arch ribs, 10·6 m apart, excepting those at the ends supporting the gable screens that are 2 m apart. The profile is parabolic inducing a minimum of flexural forces during the most prevalent loading conditions.

The main arch ribs shown in Fig. 8.4 are 1·6 m deep overall and are singly triangulated. One of the design parameters for the rib calculation was

'the depth of the rib should be sufficient to contain all the lines of pressure generated by the dead load, snow and wind.'

The arch was designed to be capable of bearing an assumed load of 3·35 kN/m^2 on plan in addition to the weight of the principals.

The groined vault roof of Madison Square Garden, New York, shown in Fig. 8.5 is of a similar era and was a forerunner of the lamella diamond pattern used extensively today. It was recognised in the initial designs that adopted the lamella diamond configuration that the torsional forces would be particularly significant in skew arches of this form.

One of the earliest vaults to extend this principle in the United States was a temporary auditorium erected in Houston Texas for the National Convention of the Democratic Party in 1928. The vault spanned 37 m with a rise of 6m and was 75 m in length. Edge diaphragms were trusses supported on columns at 12·5 m centres. The columns also supported lateral trusses that stiffened the roof.

@Seismicisolation

The diamond lattice system was further developed by Nervi to provide aircraft hangars during World War II and were of the form shown in Fig. 8.6. Although the rise is relatively high the adoption of hipped ends and raked supports leads to a very favourable architectural solution to a rather dull fundamental form. His similar 'yoked' columns for

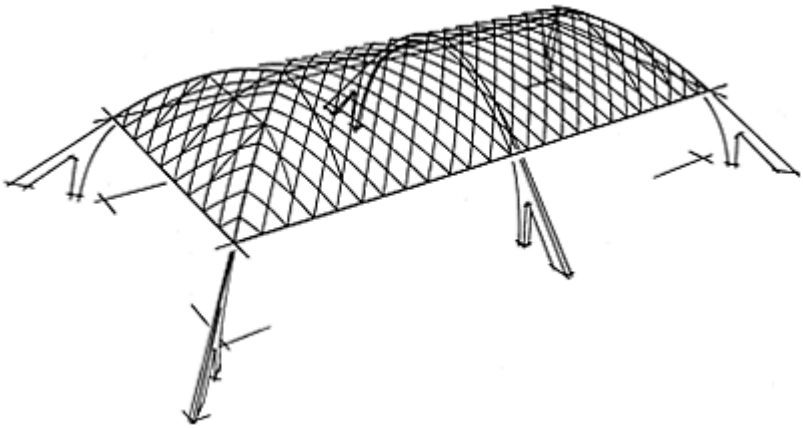

Fig. 8.6.

the domes 'Il Palazzetto Dello Sporto' has seen many imitations in both cylindrical vault and dome supports.

As an arch span or the subtended angle grows the loss of usable space diminishes as seen in the arched hangar for the Edwards Air Force Base, California;[1] the hangar with a relatively large span of 110 m was erected in 1956. The truss arches were 1·8 m in depth and possessed a rise of 29 m; eleven arches were placed at 12 m centres. The trusses were somewhat unusual as the chords were curved using a horizontal press.

Prynne[18] in a significant study examines vaults possessing a triangular skeletal structure. Although primarily concerned with a multibay system the analysis considered in some detail a single triangulated vault with a clear longitudinal arched span of 23 m and an associated rise of 5·5 m. The longitudinal edges of length 61 m were assumed to receive full lateral support from adjacent barrels. Amongst the conclusions reached were that:

(i) Owing to the transverse flexibility of the shell the long span, *unstiffened,* laterally supported barrel vault is not a structurally efficient means of resisting large bending moments or shear forces. Transverse stiffening at 10 m centres enhanced performance.
(ii) The reaction to a severe unbalanced snow requires careful examination.
(iii) The introduction of hipped ends requires additional stiffening.

The geometrical factors that influence the load diffusion characteristics of vaults are discussed by Gioncu.[10] The same arguments may be adopted in discussing the stiffening and end conditions as in (i) and (iii) above and Ref. 10 illustrates the use of stiffening arches very clearly. Makowski[17] in developing the form notes that the stiffness of very wide barrels can be increased by interweaving two sets of members or by corrugating

@Seismicisolation

them making the 'undulated' barrels very stiff. An alternative means of stiffening the longitudinal span is demonstrated in the vault designed by Matsushita for the Hachinoehe power station, an attractive structure in an unlikely setting. This coal storage area employs double curvature, as illustrated in Fig. 8.7, that not only stiffens but also considerably enhances its appearance. Three identical vaults each spanning 23·3 m are placed in parallel to cover an area 69·9 m×65 m. The individual vaults have a rise:span ratio of 1:6 for the shorter plan dimension and an effective rise of 1·84 m in the longitudinal span.

The Moscow (Idaho) stadium roof described by York[24] is an unusual timber vault using a stressed skin system to form the barrel shell roof. The basic structural element of

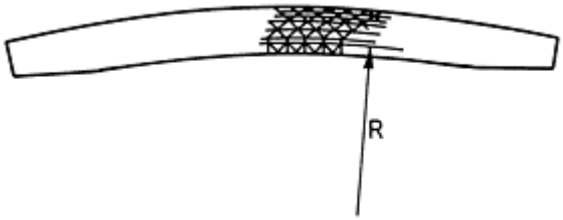

Fig. 8.7.

the shell is a 2 m deep open web trussed arch made up of 0·6 m wide laminated wood top and bottom chords connected with steel tube diagonals. The structure spans 122 m with a rise: span ratio of 1:4. Bracing was provided by designing the roof sheathing for the diaphragm shears.

3 LOADING

The form of loading on any roof structure is similar with magnitudes being related to the particular design. The following loads might be considered:

(1) dead load of the structure and the superimposed dead loads from mechanical equipment;
(2) uniform and non-uniform snow;
(3) wind;
(4) seismic;
(5) thermal.

Various combinations and forms of the above can be permutated; for the roof described in Ref. 24, twenty-nine loading conditions were considered. For linear analysis a large number of loading cases does not present a real problem. For a stability analysis that is non-linear, not simply an eigenvalue procedure, some discrimination is essential. Holzer[14] poses the problem succinctly. For stability considerations the spatial distribution of the external loads is usually specified. A single loading parameter that represents the magnitude of the load is then allowed to vary giving the buckling load. Multiple independent loading configurations are considered in Ref. 14 and the results presented

@Seismicisolation

using the concept of stability boundaries. These may be simply considered as interaction curves. For non-linear systems generalisation is not straightforward and a parametric study becomes necessary to construct the stability boundary. Shallow arches and vaults behave non-linearly and hence belong in this category. No new information was presented in Ref. 14 for this form of structure that readily assists the designer. The basic problem of the arch illustrates the difficulty of correctly defining the worst loading condition. Considerable literature on the shallow arch problem has, in the author's opinion, been given to problems amenable to solution rather than defining design parameters. Plaut[15] and Sundararajan[20] demonstrate the problem clearly and yet Deutsch[7] considered the case illustrated in Fig. 8.8 as long ago as 1940. The collapse of roofs during heavy snowstorms is clearly indicative of the problem that the practising engineer wishes to be confronted and hence provided with necessary design information.

Giroux and Bonnes[11] present a linear finite element analysis of shells under non-uniform snow loads that is particularly relevant. Four basic shapes are examined, all rectangular in plan; two are shown in Fig. 8.9(i). The finite element analysis adopted a curved triangle element with 9 degrees of freedom at each node. The 12×20 mesh results

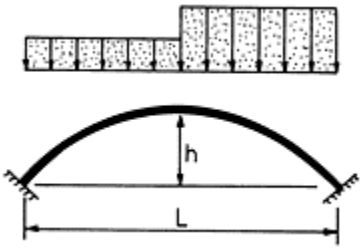

Fig. 8.8.

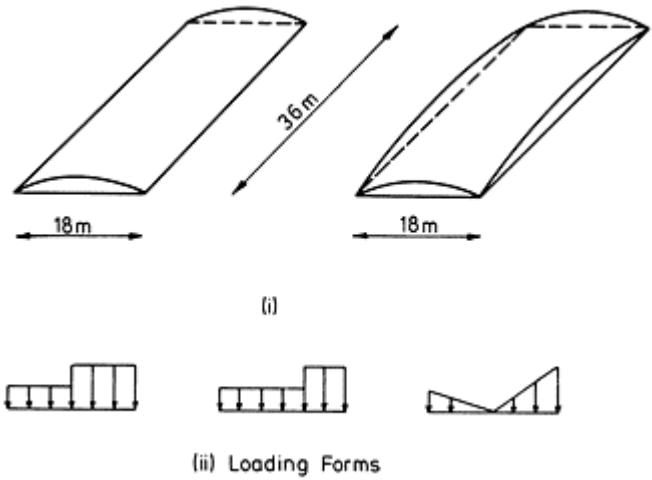

Fig. 8.9.

@Seismicisolation

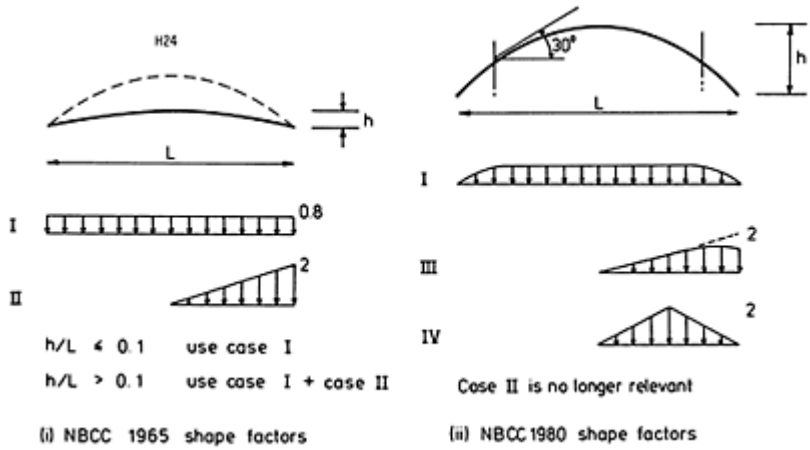

Fig. 8.10.

in 2457 degrees of freedom and serves to underline the numerical problem for a large displacement analysis. In all, eleven loading patterns of the form shown in Fig. 8.9(ii) were examined and as one would expect the cylindrical shell proved quite sensitive to non-uniform loading with significant stress reversals occurring. Loading patterns of the linearly varying form were most significant.

Templeton,[22] in discussing the drifting snow problem, presents the cylindrical shell loading as related to the National Building Code of Canada. The importance of drift loads is very significant and it is instructive to note these recent changes in the NBCC. Surveys of *actual* roof loads led to the introduction of 'snow load coefficients' or shape factors in the 1965 edition of the NBCC. These are illustrated in Fig. 8.10(i). More recent provisions are shown in Fig. 8.10(ii) and, as will be shown, are uncomfortably related to the stability problems of this structural form.

4 ANALYTIC PROCEDURES

Continuum methods[23] provide for the determination of thickness, elastic moduli and Poisson's ratio for an imaginary continuum that has the extensional, flexural, shearing and twisting resistances under external loading as the framework system in question. A membrane force system capable of resisting the external loads is then established and additional moments and forces are superimposed at discontinuities, i.e. boundaries as in conventional shell analysis. Continuum stress resultants are transposed to the frame to examine individual member behaviour. This method has been found satisfactory where the loading is uniform and the load transfer is predominantly through membrane action.

The attractiveness of continuum methods was in part due to the desire of designers to simplify a complex problem. The mathematical reduction enabled previously developed shell stability analysis to be adopted for design purposes and provided formulae incorporating basic parameters. For reticulated domes with continuous boundaries and large numbers of members the method was used by a number of authors to predict

@Seismicisolation

buckling loads. Reference 10 reports a stability analysis that uses an orthotropic equivalent continuum solution although a barrel vault has rather significant discontinuities. The problem illustrated in Fig. 8.11 is significant in that a number of finite element investigators have adopted it as a test case for their numerical procedures. The cylindrical edges are supported by diaphragms that are assumed infinitely rigid in their own plane whilst the straight edges are free. With a rise:span ratio of 1:3·4, $R/t=100$ and $\beta=40°$, both membrane and bending effects are of importance. It suffices to say that the large number of degrees of freedom necessary to obtain satisfactory convergence leads to reservations with regard to the application of the continuum methods for this type of problem.

Discrete field analysis[6] has been used in a number of latticed shell investigations. In the present problem the possibility of latticed irregularity or unusual boundary conditions presents considerable difficulties.

The results given subsequently use the method described in Ref. 9, a displacement matrix procedure that incorporates change of geometry.

The theoretical analysis incorporates

(a) effects of finite joint translation or rotation,
(b) change of member lateral stiffness,
(c) change of member length due to bowing.

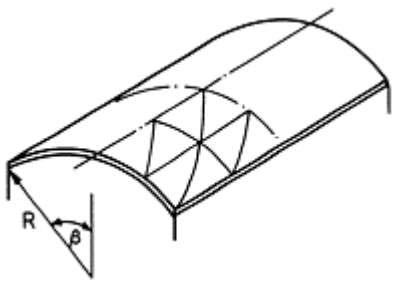

Fig. 8.11.

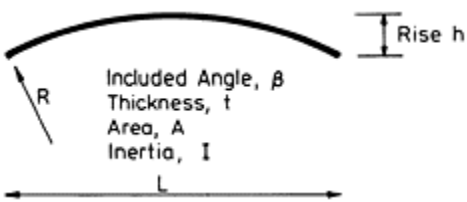

Fig. 8.12.

The method has been extensively compared with experimental results over a wide range of stability problems. As in all computational procedures, and to emphasise points made elsewhere, considerable care must be taken in assembling the mathematical model and in the interpretation of the results.

@Seismicisolation

The arch is very characteristic of the problem being considered here. In order to examine stability characteristics it is necessary to establish an acceptable subdivision of the arch that gives satisfactory convergence. Basic parameter definitions are given in Fig. 8.12. Ashwell and Gallagher3 describe a shallow arch of included angle 40° as being moderately thick if R/t=40 and moderately thin if R/t=320. Deep arch definitions are similar with an included angle of 180°. Using R/t=73 and an included angle of 30° under a central load pinned arch buckles unsymmetrically and a clamped arch, symmetrically. In both cases buckling loads obtained using nine elements were identical to those obtained from theory and for seven elements the buckling load and the deflections were within 5% of the theoretical values in both clamped and pinned cases. This would be adequate for design purposes.

Also significant was the result obtained by varying the load position and observing the arch response. Bearing in mind that the pinned case buckles unsymmetrically due to a vertical load at the crown it is found that the buckling load is reduced by 30% if the load is placed at the third point, $L/3$. This has originally been noted in Refs. 15 and 20, and is of significant influence to the critical loading distribution for the practical design case. Families of curves as illustrated in Fig. 8.13 may be derived.

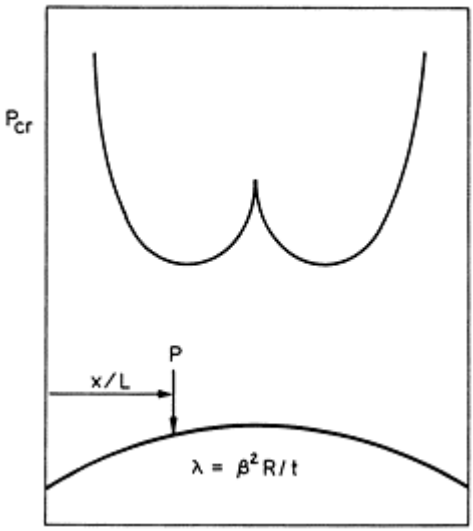

Fig. 8.13.

It is common to ‘tie’ the ends of the arch in order to accommodate the horizontal thrust. Numerous alternatives as discussed in Ref. 25 are adopted in practice to provide a horizontal support or to achieve a ‘tied’ effect. A considerable relaxation of the horizontal support stiffnesses from the fully restrained condition may be accommodated without significant loss in the load carrying capacity.

4.1 Zetlin’s ‘Arch’

@Seismicisolation

The design for the Niagara Falls Convention Center is described by Zetlin[26] and illustrates the simplest form of vault. The vaulted roof provides a column-free hall of approximately 8400 m^2. The principal structural members of the roof are trussed arches sitting on abutments seated on rock. The principal dimensions and structural members are given in Fig. 8.14. The basic design loadings were

195·3 kg/m^2 snow
44·5 kg/m^2 for the deck, insulation etc.
133·4 kg/m^2 wing pressure
50°F rise or fall of temperature
In all, nine loading combinations were examined.

The arched members were placed at 19·2 m centres. For a uniform load of 1 kN/m^2 on plan area each arch would carry 2100 kN plus self weight.

Calculated dead and live load deflections were of the order of 10 cm and a similar figure was obtained for deflection due to temperature variation. Very similar deflections were calculated for the roof described in Ref. 24 and referred to previously. As one would expect from these values, the structure is exceptionally stiff and it belies its appearance with bending action predominating although reduced by the curvature. Although structurally efficient the double layered system adds to the computation requirement. The principal members may be adequately represented by a single member of constant cross-section and moment of inertia. In this case the equivalent member for the truss has an effective moment of inertia of 2·45×10 cm^4 and an area equal to 1404 cm^2. A number of load cases were considered by the present author and, in all, local member failure would occur as a precursor of collapse. It is of interest to comment that inadvertently due to mishandling of data an arch truss was examined that placed the top and bottom chords

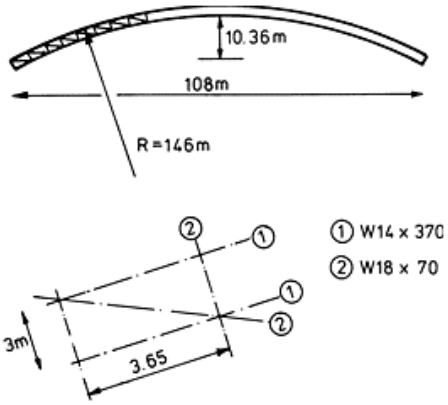

Fig. 8.14.

@Seismicisolation

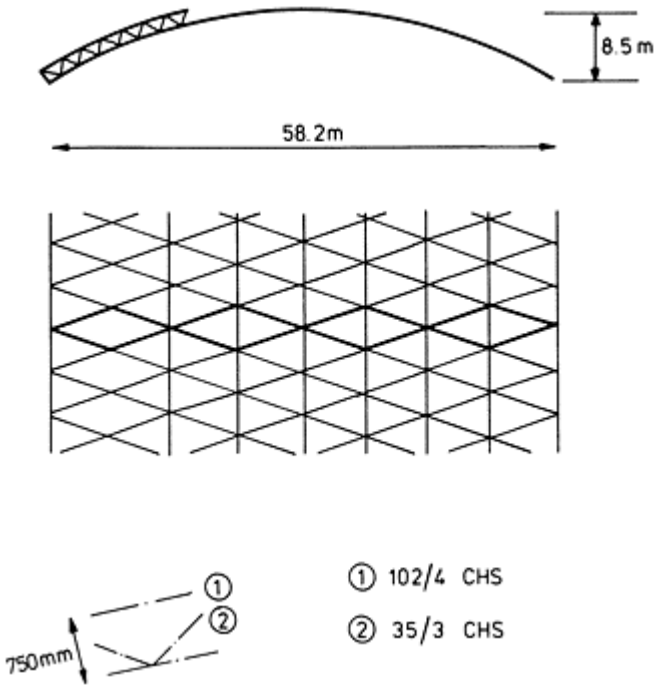

Fig. 8.15.

only 3 cm apart in the mathematical model. This naturally gives rise to an exceptionally slender arch. The structure as described, although quite non-linear, was found capable of supporting 50% snow loading over half the span before instability occurred.

4.2 Zeman's Arches

A number of noteworthy vaults are described by Zeman in Ref. 25. They are noteworthy in that the structural steel dead weight is very low. The basic parameters for one of the larger vaults reported are given in Fig. 8.15. Alternative means for providing the arch tie have been used. The modular system is easily stiffened by introducing crescent trusses to offer transverse support to members as indicated in Fig. 8.15. Stiffening similar to this in manner has been previously mentioned. An alternative means is demonstrated in Ref. 10, where 'external' arches at regular intervals stiffen a vaulted roof. Both Refs. 10 and 25 discuss arch orientation to provide both structural advantage and aesthetic improvements. Increases in overall buckling loads are not proportionally significant as a consequence of triangulation unless significant shear or point loading is present. Additionally the overall buckling or failure load is highly support dependent. Providing cross-sections of the structure are prevented from entering a post buckling configuration and hence shed load, additional loading can be diffused satisfactorily. Consequently the individual member characteristics will again be examined using the structure width as the span, that is 58·2 m. A nodal loading increment of 20 kN node was adopted. The steel dead weight being

@Seismicisolation

equivalent to 40% of this is extremely light at 21·38 kg/m^2. A primary question concerns whether the arch truss may be analysed as a single member for the buckling calculation. Various loading cases were examined as shown in Fig. 8.16. Single member representation was found adequate with nine elements being satisfactory for both the structural model and the loading representation. It should be borne in mind that both stiffness and loading need correct numerical idealisation. The lowest total buckling

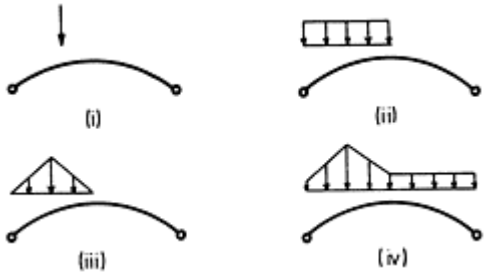

Fig. 8.16.

load is obtained for loading case one. This is not a particularly representative overall loading pattern; however, it indicates that lighting banks or other ancillary equipment should not be located in this vicinity. Apart from (i), the loading case (iv) gave the lowest overall buckling load and is, as previously mentioned, particularly realistic. The buckling load was 400 kN with the displacements at 368 kN being

U_{max}=0·83 m V_{max}=2·24 m

Axial force was 424 kN and the moment 16×10^2 kNm.

In the loading cases considered only the live load was varied. If the span increases to 63 m the buckling load decreases by approximately 15% and for 70 m span the decrease approaches 50%.

REFERENCES AND BIBLIOGRAPHY

1. Anon. *Engineering News Record*, 9 August 1956.
2. Anon. *The Engineer*, 27 Feb. 1880.
3. Ashwell, D.G. and Gallagher, R.H. *Finite Elements for Thin Shells and Curved Members.* Wiley, New York, 1976.
4. Bogusch, W. Timber structures. IABSE Structures C-6/78.
5. Coan, C.H. and Plaut, R.H. Dynamic stability of a lattice dome. *Earthquake Engineering and Structural Dynamics*, **11**, pp. 269–274, 1982.
6. Dean, D.L. and Penalba, C.M. Design formulae for latticed cylindrical shells. Proc. IASS Symposium on Industrialized Spatial and Shell Structures, Poland, June 1973, pp. 639–659.
7. Deutsch, E. Das Knicken von Bogenträgern bei unsymmetricher Belastung. Bauingenieur, December 1940, pp. 353–360.
8. Dickie, J.F. and Broughton, P. Shallow circular vaults. *Journal of the Engineering Mechanics Division, ASCE*, **99**, EMI, February 1973, pp. 1–12.
9. Dickie, J.F. and Broughton, P. Geometric non-linearity. *Journal of Structural Mechanics*, **1**(2), 1972.

@Seismicisolation

10. Gioncu, V. Recent examples of prefabricated steel vaults from Romania—their analysis, design and construction. Short course on the Analysis, Design and Construction of Braced Barrel Vaults, University of Surrey, September 1983.
11. Giroux, Y.M. and Bonnes, G. Finite element analysis of shells under non-uniform snow loads. Proc. IASS Symposium, Madrid, 1969.
12. Gregory, W.E. and Plaut, R.H. Dynamic stability boundaries for shallow arches. *Journal of the Engineering Mechanics Division, ASCE,* **108**, EM6, December 1982, pp. 1036–1050.
13. Haddow, T.H. The Roof of the East Kilbride swimming pool. *The Structural Engineer,* **145**(12), December 1967, pp. 435–441.
14. Holzer, S.H.*et al.* Stability of lattice structures under combined loads. *Journal of the Engineering Mechanics Division, ASCE,* **106**, EM2, April 1980, pp. 289–305.
15. Plaut, R.H. Stability of shallow arches under multiple loads. *Journal of the Engineering Mechanics Division, ASCE,* **104**, EM5, March 1978, pp. 1015–1026.
16. Makowski, Z.S. *Steel Space Structures.* Michael Joseph, London, 1965.
17. Makowski, Z.S. Steel braced barrel vaults. Building Specification, October 1977, pp. 43–50.
18. Prynne, P. A computer investigation into the behaviour of a long braced barrel vault roof. *Space Structures*(Ed. E.M. Davies), Blackwell, London, 1966, pp. 351–369.
19. Sherman, D.R. *et al.* Bibliography on latticed structures. *Journal of the Structural Division, ASCE,* **98,** ST7, July 1972, pp. 1545–1566.
20. Sundararajan, V. and Kumani, D.S. Dynamic stability of shallow arches under inclined load. *AIAA Journal,* **10**(8), 1972, pp. 1090–1091.
21. Sherman, D.R. *et al.* Latticed structures: State of the art. *Journal of the Structural Division, ASCE,* **102,** ST11, Nov. 1976, pp. 2197–2229.
22. Templeton, J.T. and Schreiver, W.R. Loads due to drifted snow. *Journal of the Structural Division, ASCE,* **108,** ST8, Aug. 1982, pp. 1916–1925.
23. Wright, D.T. Membrane forces and buckling in reticulated shells. *Journal of the Structural Division, ASCE,* **91,** ST1, Feb. 1965, pp. 173–201.
24. York, J.J. Moscow Stadium roof. IASS Congress on Space Enclosures, Montreal, 1976, pp. 1097–1105.
25. Zeman, J. A system for constructing lightweight roofs to various spans. *Acier-Stahl-Steel.* **No. 6**, 1973, pp. 270–281.
26. Zetlin, L. 360 ft span space frame for Niagara Falls Convention Center.

@Seismicisolation

9
Instability Behaviour of Triangulated Barrel Vaults

VICTOR GIONCU, NICOLAE BĂLUȚ, DORIN PORUMB and NICOLAE RENNON
Building Research Institute, Timisoara, Romania

1 INTRODUCTION

Although a great amount of research work has been carried out in order to determine the buckling load of cylindrical shell vaults, the available solutions[1] are less satisfactory than those concerning the complete circular cylinder, axially or radially loaded. In the case of reticulated barrel vaults the problem is more complicated by the following aspects:

(a) The effect of geometric non-linearity is very important; because of the small angles between the members, deflections and member forces are large and thus significant changes in the structural geometry occur.
(b) Several instability types may produce the collapse of the structure: member buckling, node buckling, line buckling and general buckling.
(c) Coupling of two or more instability types may occur: when the corresponding buckling loads have values close to each other the structure becomes more sensitive to geometrical imperfections.
(d) The effects of the less known loads are more important: since the dead loads of latticed structures are small, wind and snow loads are the main loads, but it is hard to predict their intensity and distribution.
(e) The behaviour of the structure is influenced by the joint system according to which the bars can be considered as pin-jointed, partially or completely restrained at the nodes.

Recent developments in computer techniques have resulted in new trends in analysis methods. The first attempts to apply the results available for solid shells to latticed shell-like structures were made by equivalent continuum methods.[2] New numerical processing techniques enable research workers to take into account more and more of the specific features of discrete structures as previously discussed.[3–5] However, the use of complex adequate computer programs is still limited by the following:

(a) The exact analysis of large structures needs computers with large memories and requires more computer time.
(b) Only a few design offices have access to complex computer programs.
(c) Very few computer programs can take into account all the above-mentioned structural features.

@Seismicisolation

On the other hand, it is very important for the designer to have simple methods which would allow him to understand the behaviour of the structure and to select the main factors which affect that behaviour. As Massonnet said,[6]

> …it must be recalled here that the majority of accidents in steel structures are due to instability. A large number of human lives have been lost due to such accidents during the last century. If ever the designer loses contact with physical reality because he believes blindly in computer results, new accidents will surely follow. It is up to you to judge if these considerations are a good justification for the search of safe, yet sufficiently accurate approximate methods that, in my opinion, are really the essence of engineering.

In this spirit, the present paper tries to study, using as simple models as possible, the instability phenomena, the factors that have influence on them and the corresponding conclusions from the designer's viewpoint.

2 MAIN TYPES OF BARREL VAULTS

For cylindrical vaults supported on end walls or arches only, one of the main factors which affects the structural behaviour is the ratio between the vault span l_1 and the girder span l_2. According to this ratio a cylindrical vault can be:

(a) *A short vault,* if $l_2/l_1<1$ (Fig. 9.1(a)); in such a latticed vault the diagonals carry greater member forces while in horizontal members only forces due to rigid end supports (walls or arches) occur. Instability phenomena occur mainly in the transverse direction.
(b) *A middle-length vault,* if $1<l_2/l_1<3$ (Fig. 9.l(b)); member forces in diagonals and horizontal bars are of similar magnitude and the instability can occur in both directions.
(c) *A long vault,* if $l_2/l_1>3$ (Fig. 9.1(c)); the greatest member forces occur in horizontal bars which are responsible for the structure instability.

@Seismicisolation

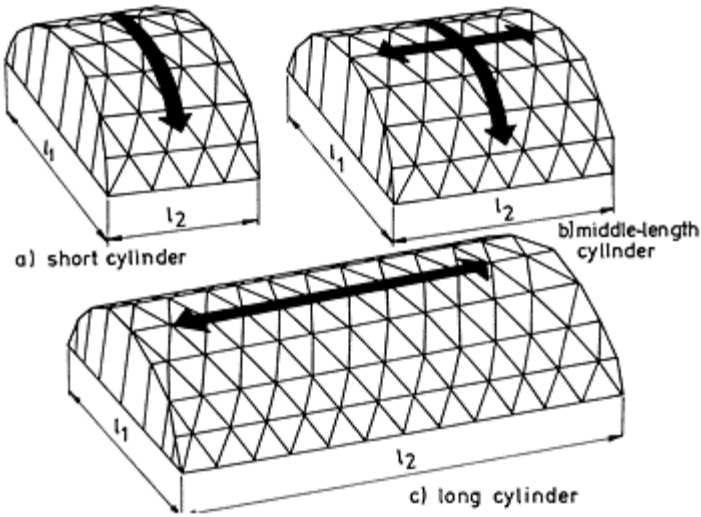

Fig. 9.1.

If the vault is supported along the horizontal edges too, the long barrel vault behaves similarly to an arch. Intermediate stiffening arches intended to improve the stability of the structure may change a long barrel vault into a structure composed of connected short vaults.

Due to the limited extent of this chapter, only the most frequent case of the short barrel vaults will be thoroughly discussed.

3 INSTABILITY TYPES

A single-layer latticed barrel vault can collapse according to the following instability types:

(a) *Member buckling* (Fig. 9.2(a)) occurs when an individual member buckles and the nodes and other members are not affected.
(b) *Node instability* (Fig. 9.2(b)) occurs when all connected bars undergo such axial strains that they cannot resist the node external load.
(c) *Line instability* (Fig. 9.2(c)) is specific for latticed cylindrical vaults and occurs when all the nodes of a generatrix line and the connected bars are involved.
(d) *General instability* (Fig. 9.2(d)) takes place when all the nodes and members of a major part of the structure including two or more lines are involved.

@Seismicisolation

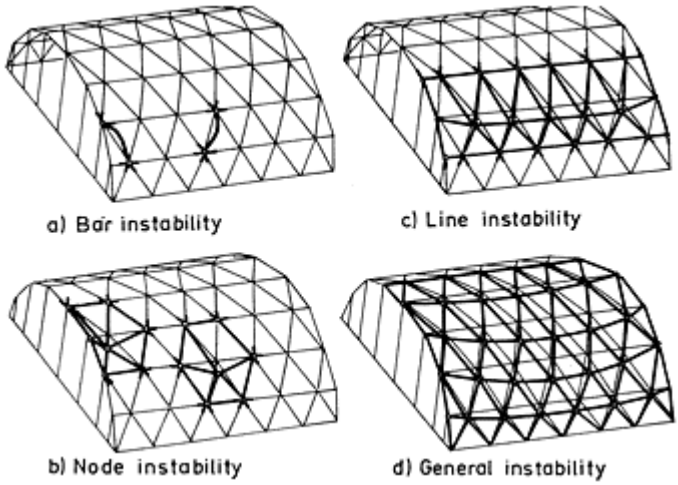

Fig. 9.2.

Besides these simple instability types there are also coupled instability phenomena if the bifurcation critical loads corresponding to simple instability forms take values close to each other. Of course two, three or all four instability types could be coupled.

In the following, each instability type will be studied.

4 MEMBER BUCKLING

Assuming approximately the cross-sectional characteristics of the bars, the designer has to perform a non-linear analysis which allows him to know the member forces and to take

@Seismicisolation

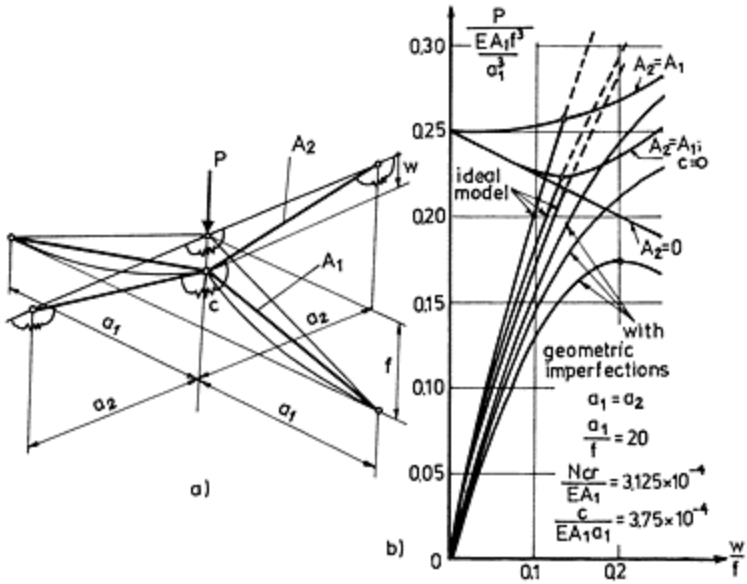

Fig. 9.3.

decisions concerning the final member sizes, geometry and topology of the structure. For these decisions the designer needs the answers to the following questions:

(1) Can the European Column Curves (ECC) be used for sizing the members?
(2) Can a partial end restraint of the bars be taken into account?

The first question arises from the fact that the European Column Curves were drawn for standard bars, i.e. single pin-ended bars, while the structural members can show different behaviour and increased imperfection sensitivity.[7] The answer is obtained by studying the post-critical behaviour of the structural member. If there is a stable post-critical range, the member is similar to the standard bar and the ECC are valid. If the post-critical behaviour is unstable, the imperfection sensitivity is increased and the ECC can be used only with higher safety factors.

The post-critical behaviour of a structural member in a latticed structure has not yet been studied as far as the authors know. In order to obtain a qualitative answer to this question, a simple model is used, as illustrated in Fig. 9.3(a). It consists of four members, two inclined bars representing the diagonals which buckle and two horizontal bars similar to those of the latticed vault. The bending spring models the end restraint of the horizontal bars. The equilibrium equation of the deflected model is:

$$P = \frac{EA_1 f^3}{a_1^3}\left[\frac{w}{f}\left(1-\frac{w}{f}\right)\left(2-\frac{w}{f}\right)+\frac{A_2}{A_1}\frac{a_1^3}{a_2^3}\frac{w^3}{f^3}+2\frac{c}{EA_1 a_1}\frac{a_1^2}{a_2^2}\frac{a_1^2}{f^2}\frac{w}{f}\right] \qquad (1)$$

where P is the load at the considered node, E is the modulus of elasticity, A_1, A_2 are the cross-sectional areas of the two categories of members, a_1, a_2 are respectively the

@Seismicisolation

horizontal projections of the bar lengths of the same members,fis the initial height of the node, w is its deflection and c is the elastic characteristic of the spring.

If the inclined bars have buckled under the member force N_{1cr}, eqn. (1) becomes

$$P = \frac{EA_1 f^3}{a_1^3}\left[2\frac{N_{1cr}}{EA_1}\frac{a_1^2}{f^2}\left(1-\frac{w}{f}\right)+\frac{A_2}{A_1}\frac{a_1^3}{a_2^3}\frac{w^3}{f^3}+2\frac{c}{EA_1 a_1}\frac{a_1^2}{a_2^2}\frac{a_1^2}{f^2}\frac{w}{f}\right] \qquad (2)$$

In Fig. 9.3(b) the curves corresponding to eqns. (1) and (2) are plotted for three cases:

(a) there are no horizontal bars;
(b) the horizontal bars are pin-jointed;
(c) the horizontal bars are elastically restrained at the ends.

One can see that for cases (a) and (b) the ultimate load (at the intersection of curves (1) and (2)) drops if the influence of deflections is taken into account, and that the horizontal bars have little effect. On the other hand, in case (c) the ultimate load increases significantly. In case (a) the behaviour of the structural member is unstable and the effect of the geometrical imperfections is much greater than for the standard bar. In this case, ECC should not be used for sizing the bar. In cases (b) and (c) the post-critical behaviour of the member is stable, similar to the standard bar, the elastic end-restraint of the horizontal bars being the main stabilizing factor.

Although quantitative conclusions cannot be drawn from this simplified model, it indicated the importance of the horizontal bars which the designer could be tempted to undersize, due to their reduced member forces. It is recommended that these members be continuous and have the largest possible radius of gyration in the radial direction of the vault.

The answer to the other question—whether the structural members could be considered as elastically end-restrained—depends on the joint system and should be experimentally checked. Generally, the bolted connections should be considered as hinged. For welded nodes, since no studies are available for latticed structures, those for plane trusses provide some information.

It is known that design codes allow a reduction of the effective length for the stability analysis in the plane of the truss of the web members. For tubular web members, due to their torsional stiffness, an elastic end restraint normal to the truss plane could be considered.[8] Professor Massonnet's opinion must be mentioned,[6] that the reduction of the effective length is not permissible when ECC are used because in the common slenderness range of the diagonals these curves allow a compression force increased by 30 to 40% as compared to the old column curves.

The authors' opinion is that, in the case of latticed structures, where more members are connected in a node than in the case of a plane truss, the elastic end restraint could be considered. Further research work is needed in this field to provide a correct solution.

5 NODE INSTABILITY

The basic cell for latticed cylindrical structures is the hexagon shown in Fig. 9.4. The general case is considered when all the nodes are loaded with the force P, except the node

@Seismicisolation

0 which is loaded with the force P_m. A similar case for a spherical structure was studied in Ref. 9. The loads are supposed to be directed radially and to be applied in two steps (Fig. 9.5(a)). First, all the nodes are loaded with a force P. The loads are resisted by the bars 01, the bar shortenings Δl and node displacements u being

$$u_{1(1)} = \Delta l_{1(1)} = -\frac{Pl_1^2}{4EA_1 f} \qquad u_{2(1)} = \Delta l_{2(1)} = 0 \tag{3a,b}$$

where l is the bar length, the first subscript indicating the bar category and the second subscript in parentheses indicating the loading step. The other notations are similar to those in the previous model and are clearly explained in Fig. 9.4. In the second step, the

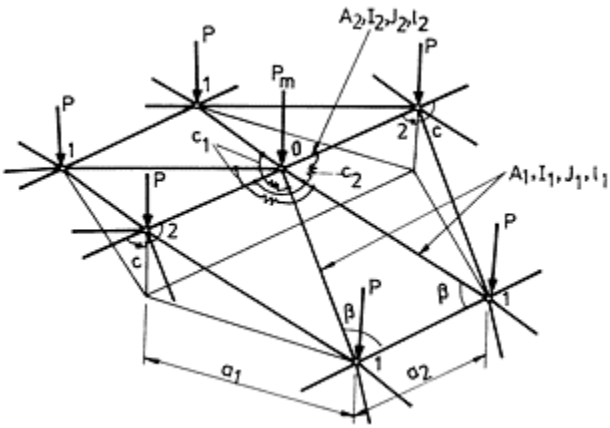

Fig. 9.4.

load in the node 0 is increased from P to P_m and produces the displacements $u_{1(2)}$ and $u_{2(2)}$ which depend on the stiffness of the neighbouring structural zone around the considered cell. If the bars 01 are considered separately and loaded by unit forces F=1, the displacements of the bar ends are u_{1c} (Fig. 9.5(b)). If the same forces F=1 are applied in the nodes 1 of the remaining structure, these nodes have the displacements u_{1m}. A similar procedure is applied to the bars 02.

The relative rigidity factors of the cell with respect to the surrounding structure are

$$K_1 = -\frac{u_{1c}}{u_{1m}} \qquad K_2 = -\frac{u_{2c}}{u_{2m}} \tag{4a,b}$$

where the negative sign shows that the two displacements have different signs. The horizontal displacements of nodes 1 and 2 can be written as

$$u_{1(2)} = -\frac{\Delta l_{1(2)}}{K_1} \qquad u_{2(2)} = -\frac{\Delta l_{2(2)}}{K_2} \tag{5a,b}$$

@Seismicisolation

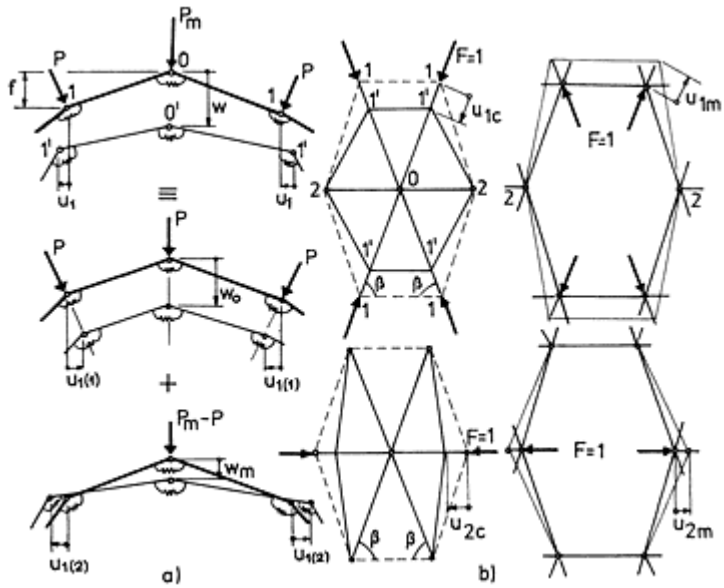

Fig. 9.5.

Due to vertical deflections, the shortenings of the bars are

$$\Delta l_{1(2)} = \sqrt{a_1^2 + (f - w_m)^2} - l_1 + u_{1(2)} \simeq -\frac{l_1}{2}\frac{w_m(2f - w_m)}{a_1^2} - \frac{\Delta l_{1(2)}}{K_1} \tag{6a}$$

$$\Delta l_{2(2)} = \sqrt{a_2^2 + w_m^2} - l_2 + u_{2(2)} \simeq \frac{l_2}{2}\frac{w_m^2}{a_2^2} - \frac{\Delta l_{2(2)}}{K_2} \tag{6b}$$

Thus,

$$\Delta l_{1(2)} = -\frac{1}{1 + \frac{1}{K_1}}\frac{l_1}{2}\frac{w_m(2f - w_m)}{a_1^2} \qquad \Delta l_{2(2)} = \frac{1}{1 + \frac{1}{K_2}}\frac{l_2}{2}\frac{w_m^2}{a_2^2} \tag{7a,b}$$

Knowing that

$$\Delta l_1 = \Delta l_{1(1)} + \Delta l_{1(2)} \qquad \Delta l_2 = \Delta l_{2(1)} + \Delta l_{2(2)} \tag{8a,b}$$

the member forces are obtained:

$$N_1 = \frac{EA_1 \Delta l_1}{l_1} = -EA_{1r}\frac{w_m(2f - w_m)}{2a_1^2} - \frac{Pl_1}{4f} \tag{9a}$$

$$N_2 = \frac{EA_2 \Delta l_2}{l_2} = EA_{2r}\frac{w_m^2}{2a_2^2} \tag{9b}$$

@Seismicisolation

where

$$EA_{1r} = \frac{EA_1}{1 + \frac{1}{K_1}} \qquad EA_{2r} = \frac{EA_2}{1 + \frac{1}{K_2}} \tag{10a,b}$$

are the reduced member stiffnesses due to the elasticity of the surrounding structure.

The factors K_1 and K_2 could be approximated from the strains of the cell contour bars as follows:

$$K_1 = \frac{1}{1 + 2\frac{A_1}{A_2}\frac{a_2}{a_1}\cos^2\beta} \qquad K_2 = 2\frac{A_1}{A_2}\frac{a_2}{a_1}\cos^2\beta \tag{11a,b}$$

the angle β between the bars being shown in Fig. 9.4.

From the equilibrium equation of node 0, it can be seen that

$$P_m = -4N_1\frac{f - w_m}{a_1} + 2N_2\frac{w_m}{a_2} + 4c_1\frac{w_m}{a_1^2} + 2c_2\frac{w_m}{a_2^2} \tag{12}$$

where c_1 and c_2 are the spring characteristics and N_1 and N_2 can be substituted from eqn. (9):

$$P_m = P\left(1 - \frac{w_m}{f}\right) + \frac{EA_{1r}f^3}{a_1^3}\left[2\frac{w_m}{f}\left(1 - \frac{w_m}{f}\right)\left(2 - \frac{w_m}{f}\right) + \frac{A_{2r}}{A_{1r}}\frac{a_1^3}{a_2^3}\frac{w_m^3}{f^3}\right] + \left(4\frac{c_1 f}{a_1^2} + 2\frac{c_2 f}{a_2^2}\right)\frac{w_m}{f} \tag{13}$$

If the loads are considered as

$$P_m = P_{mN} + P_M \qquad P = P_N + P_M \tag{14a,b}$$

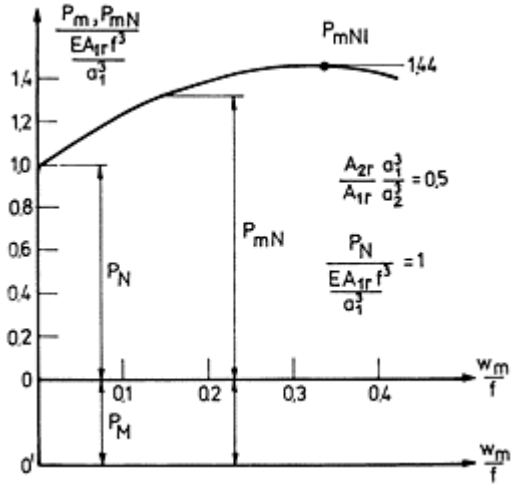

Fig. 9.6.

@Seismicisolation

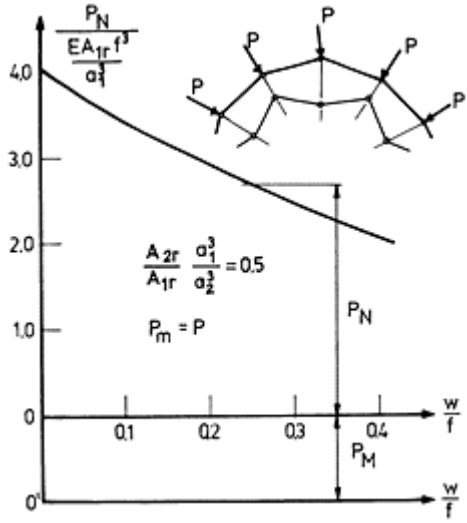

Fig. 9.7.

i.e. they are decomposed in parts resisted by axial member forces P_{mN} and P_N and by bending moments P_M, one can write

$$P_M = 4\frac{c_1 f}{a_1^2} + 2\frac{c_2 f}{a_2^2} \tag{15a}$$

$$P_{mN} = P_m - \frac{4c_1 f}{a_1^2} - \frac{2c_2 f}{a_2^2} \tag{15b}$$

$$P_N = P - \frac{4c_1 f}{a_1^2} - \frac{2c_2 f}{a_2^2} \tag{15c}$$

Equation (13) can be now written as

$$P_{mN} = P_N\left(1 - \frac{w_m}{f}\right) + \frac{EA_{1r}f^3}{a_1^3}\left[2\frac{w_m}{f}\left(1 - \frac{w_m}{f}\right)\left(2 - \frac{w_m}{f}\right) + \frac{A_{2r}}{A_{1r}}\frac{a_1^3}{a_2^3}\frac{w_m^3}{f^3}\right] \tag{16}$$

Equations (13) and (16) are plotted in Fig. 9.6 in the coordinate systems P-w/f and P_N-w/f respectively. One can see that to find the maximum values, only eqn. (16) need be analysed, being simpler than eqn. (13). The maximum condition is $dP_{mN}/dw_m=0$ which has solutions only if

$$\frac{A_{2r}a_1^3}{A_{1r}a_2^3} \le \frac{3}{1 - \frac{P_N a_1^3}{4EA_{1r}f^3}} - 2 \tag{17}$$

and in the case of $P_N=0$ only if

@Seismicisolation

$$\frac{A_{2r}a_1^3}{A_{1r}a_2^3} \leq 1 \tag{18}$$

If condition (17) is not fulfilled, there is no instability phenomenon.

A particular solution is obtained when all the nodes are loaded with the same force (P_m=P). From eqn. (16) it can be seen that

$$P_N = \frac{EA_{1r}f^3}{a_1^3}\left[2\left(1-\frac{w_m}{f}\right)\left(2-\frac{w_m}{f}\right)+\frac{A_{2r}}{A_{1r}}\frac{a_1^3}{a_2^3}\frac{w_m^2}{f^2}\right] \tag{19}$$

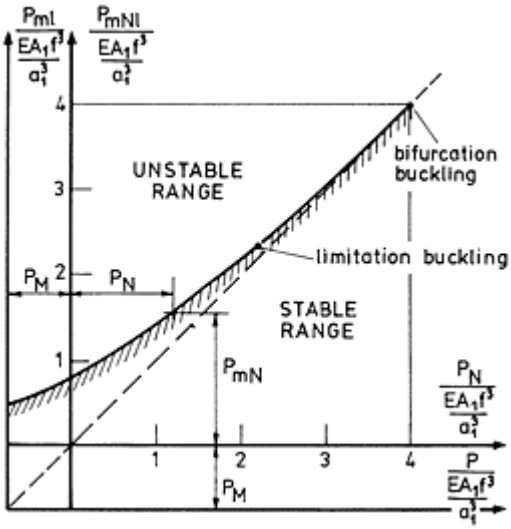

Fig.9.8.

Equation (19) is plotted in Fig. 9.7. Unlike the general case where instability occurs by limitation when the load increases to a limit value, in this case instability takes place by bifurcation under the critical load:

$$P_{Ncr} = \frac{4EA_{1r}f^3}{a_1^3} \tag{20}$$

As the post-critical behaviour is unstable, the structure is imperfection sensitive.

In Fig. 9.8 an interaction curve between P_m and P is plotted. One can see that if the loads P are below those corresponding to the bifurcation instability, the central node of the cell can be further loaded up to the limitation value P_{ml}.

@Seismicisolation

6 LINE INSTABILITY

The line 0–0 which becomes unstable is shown in Fig. 9.9. All the nodes on this line are loaded with a force P_m greater than the forces P in the remaining nodes. Furthermore, this line has an erection imperfection w_i with respect to the ideal position. As the distance between the end walls is large enough, in the central zone several nodes will show equal displacements normal to the roof surface and therefore the effect of the horizontal bars is insignificant and can be neglected. Thus the structure resists loads only in the transverse direction, i.e. only the 01 members will be stressed. In the following, a similar procedure to the case of node instability will be adopted. The loads are presumed to be normal to the roof surface and will be applied in two steps. In the first step, (Fig. 9.10(a)) the nodes are loaded with forces which produce only radial displacements. Equilibrium is possible only if the nodes 0 are loaded by the forces

$$P_1 = P\frac{f - w_i}{f + w_i} \simeq P\left(1 - 2\frac{w_i}{f}\right) \tag{21}$$

The horizontal displacement of the nodes 1 and the shortening of the bars 01 in this loading step are

$$u_{1(1)} = \Delta l_{1(1)} = -\frac{Pl_1^2}{4EA_1(f + w_i)} \tag{22}$$

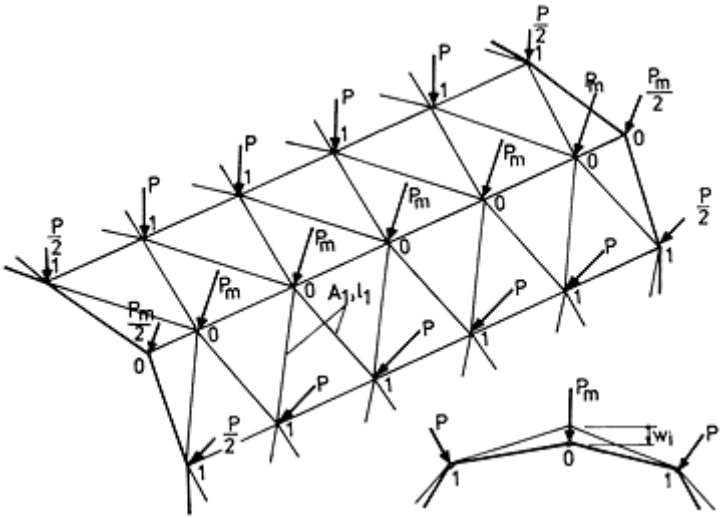

Fig. 9.9.

Similarly to the node instability case, in the second step the nodes 0 are loaded with the remaining forces P_m -P_1, but their deflection will be f– w_1 instead of f. The shortening of the bars 01 are

@Seismicisolation

$$\Delta l_{1(2)} = -\frac{1}{1+\frac{1}{K_1}}\frac{l_1}{2}\frac{w_m(2f-2w_i-w_m)}{a_1^2} \tag{23}$$

and the corresponding member forces are

$$N_1 = \frac{EA_1\,\Delta l_1}{l_1} = -EA_{1r}\frac{w_m(2f-2w_i-w_m)}{2a_1^2} - \frac{Pl_1}{4(f+w_i)} \tag{24}$$

where EA_{1r} is given in eqn. (10a). For the approximate calculation of K_1 only the bars with the same directions as bars 01 need be considered (Fig. 9.10(b)) and thus K_1=1 and $EA_{1r}=0.5EA_1$. Writing the equilibrium equation for a node 0,

$$P_m = -4N_1\frac{f-w_i-w_m}{a_1} + 4c_1\frac{w_m}{a_1^2} \tag{25}$$

and substituting here eqn. (24),

$$P_{mN} = P_N\left(1-\frac{2w_i+w_m}{f}\right) + 2\frac{EA_{1r}f^3}{a_1^3}\frac{w_m}{f}\left(1-\frac{w_i+w_m}{f}\right)\left(2-\frac{2w_i+w_m}{f}\right) \tag{26}$$

where, similarly to eqn. (15) but with c_2=0,

$$P_{mN} = P_m - P_M = P_m - 4\frac{c_1 f}{a_1^2} \qquad P_N = P - \frac{4c_1 f}{a_1^2} \tag{27}$$

Equation (26) is plotted in Fig. 9.11 where one can see that the limit load decreases seriously due to the erection imperfection. In Fig. 9.12 the interaction curve between P_m and P is plotted in the case of an erection imperfection wi/f=0·1. One can see that only below the value $P_{mN}/(EA_{1r}f^3/a_1^3) \simeq 1{\cdot}12$ could the loads in the nodes 0 be greater than those of the nodes 1. At this value, $P_{mN}=P_N$, i.e. all the nodes should be equally loaded at

@Seismicisolation

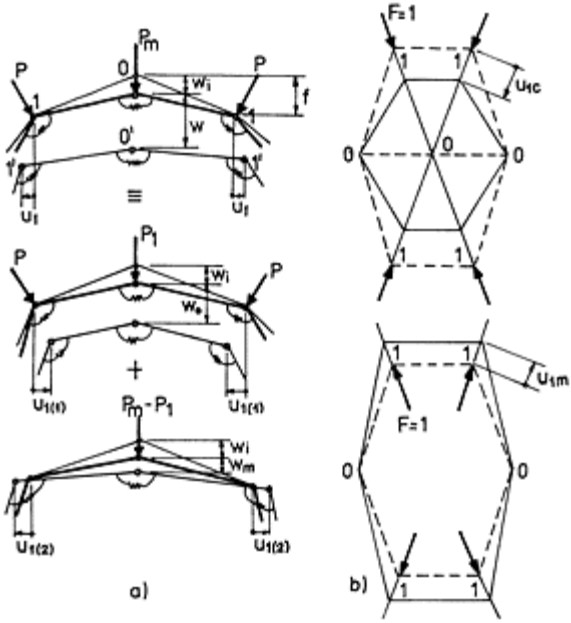

Fig. 9.10.

a significantly lower load value as compared to the perfect structure. One can see also that up to a value of $P_N/(EA_{1r}f^3/a_1^3) \leq 3{\cdot}2$ the nodes 0 can be further loaded over the value P_1 given in eqn. (21). Over this value, which is

$$P_N \geq 4\frac{EA_{1r}f^3}{a_1^3}\left(1-\frac{w_m}{f}\right)^2 \tag{28}$$

the slope of the PmN-w curve becomes negative and the equilibrium is unstable. In the range between 1·12 and 3·2 the loads in nodes 0 must always be smaller than in the nodes 1.

@Seismicisolation

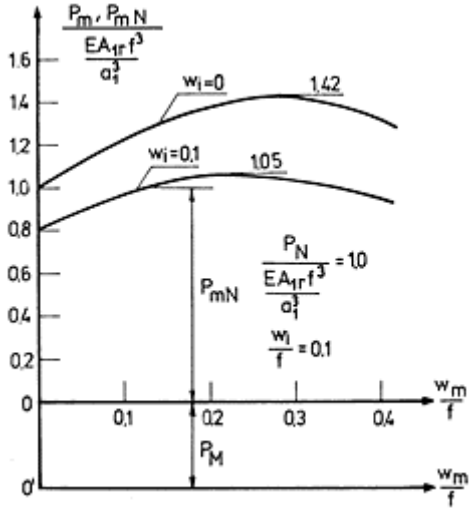

Fig. 9.11.

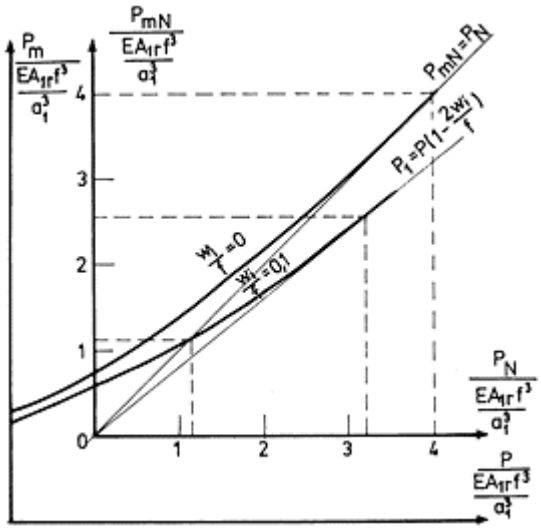

Fig. 9.12.

@Seismicisolation

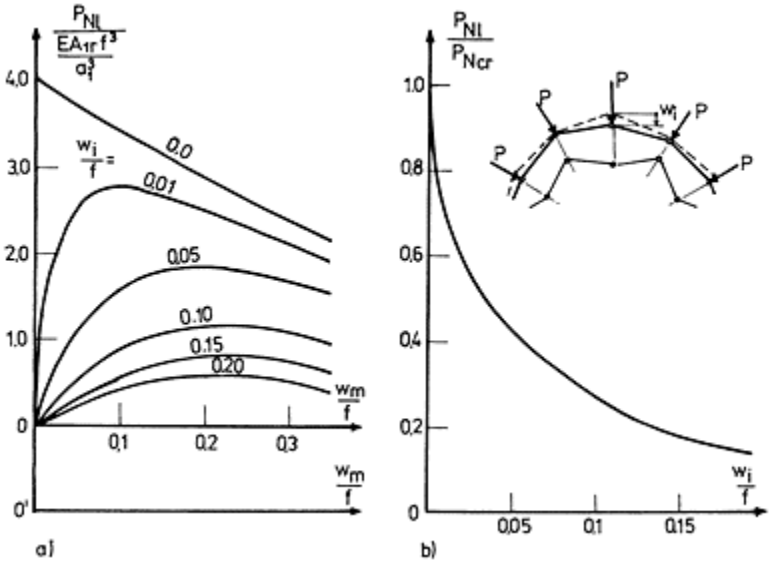

Fig.9.13.

If all the nodes have equal loads, $P_{mN}=P_N$, it can be seen from eqn. (26) that

$$P_N = 2\frac{EA_{1r}f^3}{a_1^3}\frac{\frac{w_m}{f}\left(1-\frac{w_i+w_m}{f}\right)\left(2-\frac{2w_i+w_m}{f}\right)}{\frac{2w_i+w_m}{f}} \tag{29}$$

Equation (29) is plotted in Fig. 9.13(a). The curve corresponding to $w_i=0$ shows an unstable post-critical behaviour, while the other curves show an important imperfection sensitivity. Figure 9.13(b) shows the reduction of the critical bifurcation load due to geometrical imperfections. As can be seen, an erection imperfection of *wi/f*=0·1 yields a reduction of 72% of the critical load. This reduction would be less severe if the joint stiffness were taken into account.

7 GENERAL INSTABILITY

General instability occurs when a relatively large portion of the latticed structure becomes unstable. The problem of determining the ultimate load in this case is very intricate and therefore only some essential aspects will be discussed here.

The designer of a latticed barrel vault should have clear information about:

(a) the loads acting on the structure;
(b) which type of instability could occur;

@Seismicisolation

(c) what analysis methods are available;
(d) the reliability of the calculated values.

The loading conditions in countries with a severe climate, like Romania, and for lightweight roofs such as latticed ones are mainly provided by snow. The design codes specify for barrel vaults two load distributions for snow, on the roof portions with slopes not exceeding 60° (Fig. 9.14). As the dead load distribution is symmetrical, the critical

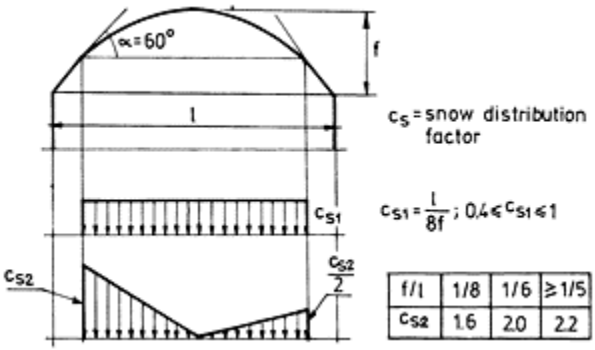

Fig. 9.14.

load must be determined for two loading cases, one symmetrical and the other highly unsymmetrical.

The ultimate load for the symmetrical case of uniformly distributed load can be calculated in two ways: either the bifurcation critical load of the ideal perfect structure is calculated and then reduced in accordance with the geometrical imperfections, or the limit load is determined directly for the real imperfect structure (Fig. 9.15(a)).

In the case of unsymmetrical loads, the limitation load has to be determined (Fig. 9.15(b)).

Since many solutions for the bifurcation critical load of cylindrical solid shells can also be used for latticed barrel vaults, the behavioural peculiarities of the two types of structure must be thoroughly discussed.

@Seismicisolation

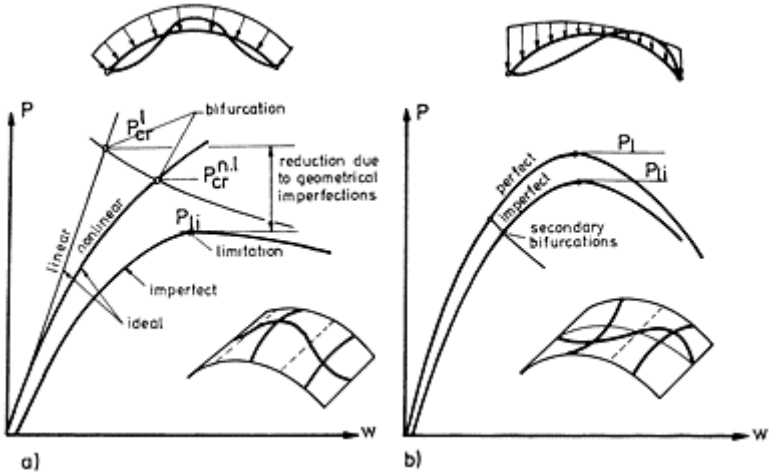

Fig. 9.15.

First, the bifurcation critical load of a continuous cylindrical shell is determined for radial loads, i.e. normal to the surface, while the loads acting on latticed roofs are mainly vertical. In Ref. 10 it is shown that the ratio between the two critical loads is

$$\frac{(p_{cr})_{rad}}{(p_{cr})_{vert}} = \frac{\varphi_0}{\sin\varphi_0}\,\frac{\left(\dfrac{2n\pi}{\varphi_0}\right)^2 - 1}{\left(\dfrac{2n\pi}{\varphi_0}\right)^2 + \dfrac{2\pi^2}{3} - 2} \tag{30}$$

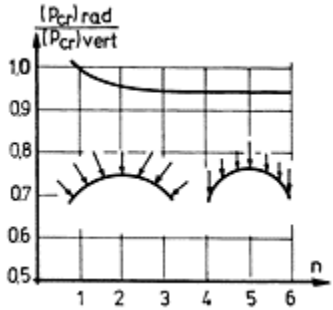

Fig. 9.16.

where φ_0 is the subtending angle of the circular vault and n is the number of buckling half-waves. This ratio is plotted in Fig. 9.16 for $\varphi_0 \geq 71°$ as a function of the number of buckling half-waves. One can see that considering the load to act radially instead of vertically is on the safe side.

Another important aspect is that for continuous shells the bifurcation load is determined assuming a linear pre-critical behaviour while latticed structures show a

@Seismicisolation

definite non-linear pre-critical behaviour (Fig. 9.15(a)). Even a qualitative statement is difficult to make; Fig. 9.17, according to Ref. 11, shows the ratio between the bifurcation critical load of a latticed cylinder and that of a continuous shell, as a function of the slenderness ratio of the latticed structure members. For latticed structures the reduction in critical load is drastic, especially when the members are slender and thus provoke a markedly non-linear behaviour.

The third problem in using the bifurcation critical load for design purposes is its reduction as an effect of geometrical imperfections. It is known that the bifurcation critical load is partially resisted by axial forces P_{crN} and the other fraction of it, P_{crM}, is resisted by bending moments:

$$P_{cr}=p_{crN}+p_{crM} \tag{31}$$

This relationship is similar to eqn. (14).

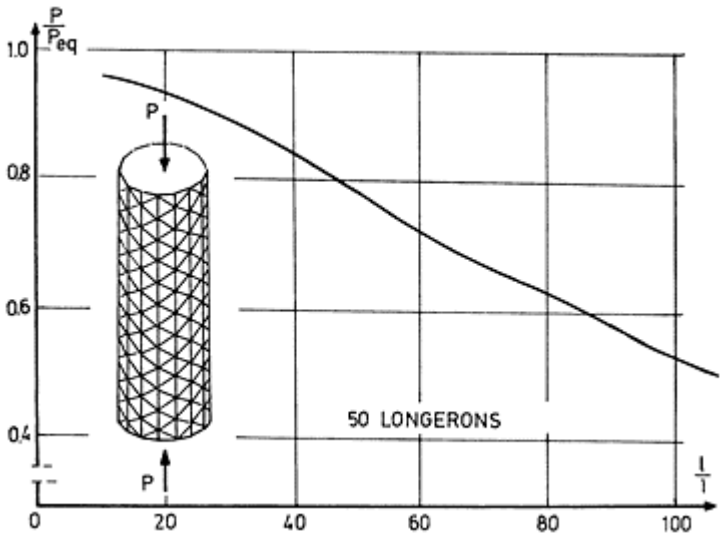

Fig. 9.17.

@Seismicisolation

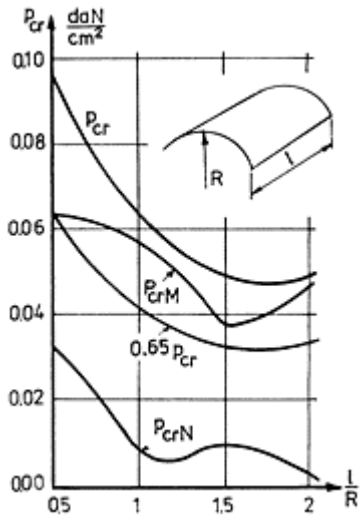

Fig.9.18

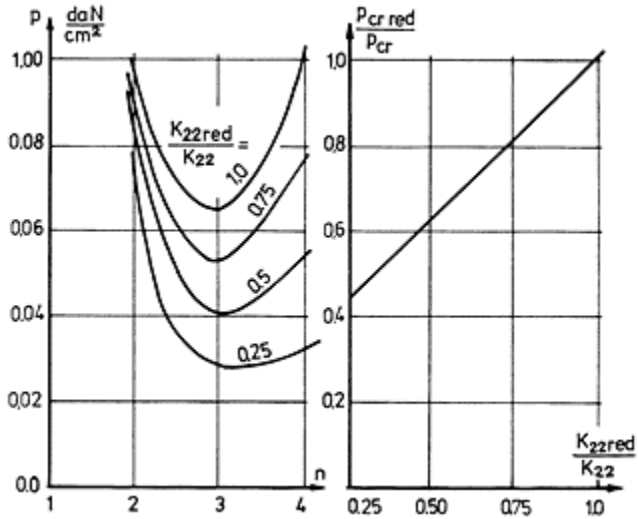

Fig. 9.19.

As shown in the preceding sections, only the axial force resisted fraction P_{crN} is eroded by geometrical imperfections. The two components of critical load were separated in Ref. 10 and it was shown that, in the case of latticed barrel vaults, the fraction P_{crM} is predominant and the reduction in the total critical load due to imperfections is not as severe as for an axially loaded latticed cylinder. For latticed barrel vaults, assuming a reduction of 35% of the bifurcation critical load due to imperfections, i.e.

@Seismicisolation

$$p_{cri}=0{\cdot}65p_{cr} \tag{32}$$

seems to be sufficient (Fig. 9.18).

On the other hand, the type of connections in the nodes has great influence on the critical load by its effects on the bending stiffness of the structure. If the nodes are hinged in the transverse direction the critical load is severely reduced (Fig. 9.19). This effect was checked experimentally[10] on a roof model composed of bolted prefabricated triangles, the experimental values being very close to the theoretical ones. If the ultimate load is determined by a limitation analysis (Fig. 9.15(a)) the imperfection magnitudes and the shape of the erection imperfections must be known. The estimation of these parameters is almost impossible because the number of similar completed structures is small and each case is unique by its general dimensions and constructional solution. Hence the designer must assume the worst situation, i.e. the deviations from the perfect surface have the same shape as the overall buckling shape of the structure. That is why the information provided by bifurcation analysis is also very useful in limitation analysis.

For unsymmetrical loads, as in Fig. 9.15(b), the limit load can be obtained only by a non-linear analysis of the discrete structure. In this case, the effect of geometrical imperfections is less important because of the unsymmetrical load distribution. A difficult problem is that of some bifurcations which could start from the equilibrium curve if the erection geometrical imperfections or the initial deflections due to the unsymmetrical loads are not similar to the overall bifurcation deflections. Such secondary bifurcations could be the line instability phenomena as discussed in the preceding section.

The methods of analysis may be divided into two main categories according to the way the discrete structure is considered. The first category would include the equivalent continuum methods. The mechanical characteristic features of the equivalent continuum depend on the lattice peculiarities as angles between the bars, cross-sectional areas and radii of gyration of the members, etc. The general case is that of an orthotropic equivalent continuum, but in special cases it may be isotropic. If the discrete triangulated structure corresponds to an orthotropic equivalent continuum, an approximate analysis can be performed considering an isotropic equivalent continuum characterized by the equivalent depth and Young's modulus:[2]

$$\delta_e = 2\sqrt{3}i \qquad E_e = \frac{EA}{3ia} \tag{33a}$$

or equivalent depths specific to axial forces and to bending moments:[12]

$$\delta_N = \frac{2}{\sqrt{3}}\frac{A}{a} \qquad \delta_M = \sqrt[3]{9\sqrt{3}\frac{I}{a}} \tag{33b}$$

or different axial and bending stiffnesses:[13]

$$(E\delta)_e = \frac{2EA}{\sqrt{3}a} \qquad K_e = \frac{\sqrt{3}EI}{4a}\left(3+\frac{GJ}{EI}\right) \tag{33c}$$

@Seismicisolation

where the notations are similar to those used previously. If an isotropic equivalent continuum can be adopted, the main advantage of the method is that the results known for solid shells can be used.

A better approximation is obtained when an orthotropic equivalent continuum is considered,[1,10,14] and the following differential equations are obtained:

$$\nabla_r^2 F - [K_{11} w'''' + 2(K_{12} + K_{33}) w^{\cdot\cdot\cdot\cdot} + K_{22} w^{\cdot\cdot\cdot\cdot}] + L(F, w_i + w) + p = 0 \tag{34a}$$

$$\frac{D_{11}}{D_{11}D_{22} - D_{12}^2} F'''' + 2\left(\frac{1}{2D_{33}} - \frac{D_{12}}{D_{11}D_{22} - D_{12}^2}\right) F^{\cdot\cdot\cdot\cdot} + \frac{D_{22}}{D_{11}D_{22} - D_{12}^2} F^{\cdot\cdot\cdot\cdot} + \nabla_r^2 w + \frac{1}{2} L(w, 2w_i + w) = 0 \tag{34b}$$

where w are the deflections normal to the shell surface and F is the Airy stress function. The notations

$$\nabla_r^2(\quad) = \frac{1}{R_x}(\quad)^{\cdot\cdot} - \frac{2}{R_{xy}}(\quad)^{\cdot\prime} + \frac{1}{R_y}(\quad)'' \tag{35a}$$

$$L(A, B) = A''B^{\cdot\cdot} + A^{\cdot\cdot}B'' - 2A^{\cdot\prime}B^{\cdot\prime} \tag{35b}$$

are the differential operators, where

$$\frac{\partial(\quad)}{\partial x} = (\quad)'; \qquad \frac{\partial(\quad)}{\partial y} = (\quad)^{\cdot}$$

The axial stiffnesses are

$$D_{11} = \frac{EA_1}{a_1} \frac{\frac{A_2}{A_1} + \cos^3\beta}{\sin\beta} \qquad D_{12} = \frac{EA_1}{a_1} \sin\beta\cos\beta \tag{36a,b}$$

$$D_{22} = \frac{EA_1}{a_1} \frac{\sin^3\beta}{\cos\beta} \qquad D_{33} = \frac{EA_1}{a_1} \sin\beta\cos\beta \tag{36c,d}$$

and the bending stiffnesses are

$$K_{11} = \frac{EI_1}{a_1} \frac{\frac{I_2}{I_1} + \cos^3\beta + \frac{GJ_1}{EI_1}\cos\beta\sin^2\beta}{\sin\beta} \tag{37a}$$

$$K_{12} = \frac{EI_1}{a_1} \sin\beta\cos\beta\left(1 - \frac{GJ_1}{EI_1}\right) \tag{37b}$$

$$K_{22} = \frac{EI_1}{a_1} \frac{\sin^3\beta + \frac{GJ_1}{EI_1}\sin\beta\cos^2\beta}{\cos\beta} \tag{37c}$$

$$K_{33} = \frac{EI_1}{a_1} \frac{1}{\sin\beta\cos\beta}\left[\sin^2\beta\cos^2\beta + \frac{1}{2}(\cos^2\beta - \sin^2\beta)^2 \frac{GJ_1}{EI_1} + \frac{1}{2}\frac{GJ_2}{EI_1}\cos\beta\right]$$

@Seismicisolation

The notations of the geometrical characteristics are shown in Fig. 9.4. Equations (34) were used for plotting the curves in Figs. 9.16, 9.18 and 9.19.

The main drawback of the equivalent continuum-based methods is that they cannot take into account the bar stiffness reduction near the critical load. The reduction is clearly shown in Fig. 9.17, drawn up according to Ref. 11. This is an interaction problem between two instability types which will be thoroughly discussed in the next section.

The second category of analysis methods includes discrete analysis methods which properly reflect the real structure. These methods are generally composed of two sub-processes: in the first one the non-linear deflections and member forces are determined under a given load and in the second the ultimate load which produces instability is calculated.

To determine the deflections and member forces under a certain load several methods are used:

(a) The search for the node equilibrium can be achieved as in Ref. 3, starting with a common linear analysis which leads to the equation system

$$[K_0]\{d_0\} = \{P\} \tag{38}$$

where $[K_0]$ is the stiffness matrix of the unloaded structure, $\{d_0\}$ is the displacement vector and $\{P\}$ the load vector, external forces being applied to the nodes. The stiffness matrix is then modified, according to the displacements, into a new one, $[K_1]$. In this stage the node equilibrium equations will not be satisfied and the unbalanced node forces $\{\Delta P_1\}$ are considered as external loads for a new linear calculation:

$$[K_1]\{\Delta d_1\} = \{\Delta P_1\} \tag{39a}$$

where, from the displacement corrections, $\{\Delta d_1\}$ are obtained. The new displacement vector will be

$$\{d_1\} = \{d_0\} + \{\Delta d_1\} \tag{39b}$$

Displacements $\{d_1\}$ lead to a new stiffness matrix $[K_2]$ and a new unbalanced force vector $\{\Delta P_2\}$; the linear analysis is repeated until, at the ith iteration,

$$[K_i]\{\Delta d_i\} = \{\Delta P_i\} \qquad \{d_i\} = \{d_{i-1}\} + \{\Delta d_i\} \tag{40a,b}$$

the equilibrium is considered as satisfactory in any node and any direction, i.e. each component of the vector $\{\Delta P_i\}$ is below a chosen value. Other similar procedures are presented in Refs. 5, 15 and 16. *(b) The search for the potential energy*, which avoids the node equilibrium equations by determining the minimum of the potential energy equation

$$V = \sum_1^M U_m - \sum_1^N W_n \tag{41}$$

@Seismicisolation

where U_m is the strain potential energy of the *m*th bar in the structure and W_n is the mechanical work of the external load in the *nth* node (the total number of bars is *M* and of loaded nodes is *N*).

The minimum of a function such as that expressed in eqn. (41) is known from the optimization analysis of structures.[17] Let us consider the equipotential curves calculated for a given load and various restraint-compatible deflections (Fig. 9.20). The minimum

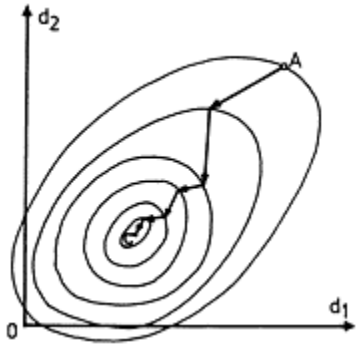

Fig. 9.20.

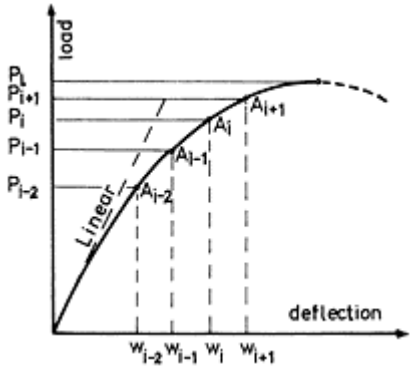

Fig. 9.21.

potential energy is in the centre C of the concentric curves and this point corresponds to the equilibrium solution. For the starting values, corresponding to the point A, calculated for example by a linear method, the potential energy is not the minimum one and the path towards the point C must be found. This is performed by the gradient or the conjugate gradient method; in Refs. 4 and 18 the conjugate gradient method was used. In these methods the most favourable path towards the point C is determined so that the number of iterations is minimum. According to Ref. 4 the potential energy method is much simpler than the node equilibrium method and requires fewer iterations.

The next problem to be discussed is the calculation of the ultimate load of the structure. With that end in view, the load is increased step by step until the tangent to the

@Seismicisolation

load-deflection curve becomes horizontal (Fig. 9.21), by using a constant load increment or a constant deflection increment. The minimum number of iterations at each loading step is obtained if the initial node deflections can be approximated to be as close as possible to the final ones. For this reason it is recommended[3] to choose the point A_{i+1} (Fig. 9.21) by equal deflection steps, extrapolating on the parabola meeting the points A_{i-2}, A_{i-1}, A_i.

The flow-chart of the computer program NELIN developed at the Building Research Institute Timişoara, Romania, is shown in Fig. 9.22. Details concerning the non-linear analysis of braced barrel vaults with the program NELIN are given in Refs. 3, 19 and 20.

The last problem is that of the reliability of calculated values and of an appropriate safety factor. Its solution depends on the correct estimation of the imperfection magnitudes and on the information about the effect of some imperfections exceeding the prescribed tolerances. What values the imperfections should take into account in the stability analysis is not stated yet even for continuous shells. For latticed structures these

@Seismicisolation

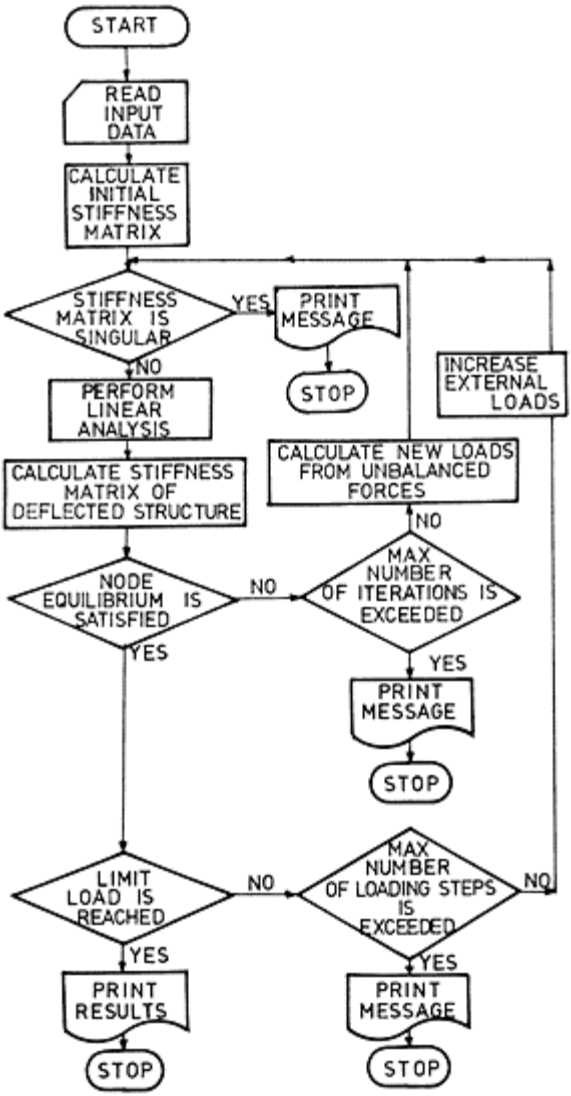

Fig. 9.22.

values could be related to the erection tolerances prescribed by the designer. The imperfection sensitivity of latticed barrel vaults could be estimated by similarity to the continuous shells from where it is known that under radial pressure the imperfection sensitivity is less important than in the case of axially loaded cylinders. The influence of imperfections can be expected to be even smaller in the case of very unsymmetrical specified snow loads.

@Seismicisolation

8 INTERACTION BETWEEN DIFFERENT INSTABILITY TYPES

Little research work deals with the complex problem of the interaction between several instability types. For circular latticed cylinders axially loaded the interaction between member buckling and overall instability is discussed in Refs. 11 and 13. Interaction

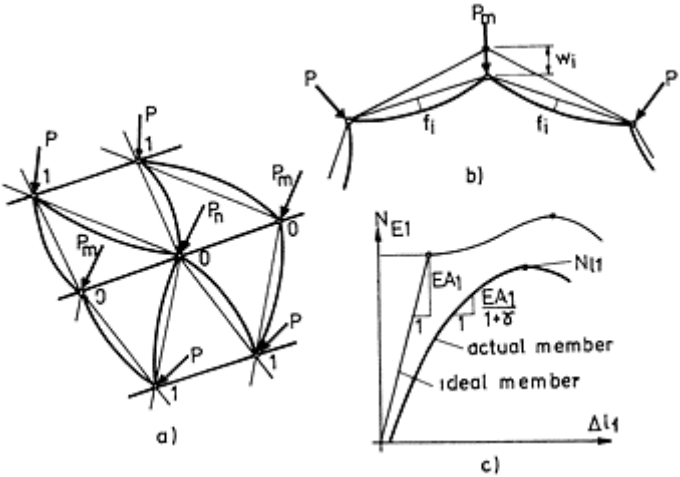

Fig. 9.23.

between member buckling and node buckling is studied in Refs. 20 and 21 for spherical structures. In the following, the interaction between member buckling, line buckling and general instability will be studied.

For the interaction of member buckling with line instability the node in Fig. 9.23(a) is studied where members 00 do not take any loads, as was shown in Section 6. It is assumed that all bars 01 have the same imperfections fi (Fig. 9.23(b)) and the same loading level N_1/N_{1E}, where N_{1E} is the Euler force of the bar 01 (Fig. 9.23(c)). The end displacement of bar 01 is

$$\Delta l1=\Delta l_{1N}+\Delta l_{1f}=\Delta l_{1n}(1+\gamma) \tag{42}$$

where

$$\Delta l_{1N}=\frac{N_1 l_1}{EA_1} \qquad \Delta l_{1f}=\frac{\pi^2 f_i^2}{4l}\left[\frac{1}{(1-n_1)^2}-1\right] \qquad n_1=\frac{N_1}{N_{1E}} \tag{43a,b,c}$$

Δl_{1N} is the bar shortening due to the axial load and Δl_{1f} is the end displacement due to the imperfection fi calculated as the difference between the arc length and the chord length. In eqn. (42),

$$\gamma=\frac{1}{4}\frac{2-n_1}{(1-n_1)^2}\frac{f_i^2}{i^2} \tag{44}$$

@Seismicisolation

The magnitude of f_i was determined in Ref. 20 from the European Column Curves and for circular tubes it was

$$\frac{f_i}{i} = 1{\cdot}6074\left(\frac{1}{\varphi} - 1\right)\left(1 - \frac{N_{1l}}{N_{1E}}\right) \tag{45}$$

where N_{1l} is the ultimate load of the bar (Fig. 9.23(b)); a plasticity reduction factor was considered. Equation (45) is plotted in Fig. 9.24 for two steel grades (with yield limits of 230 and 260 N/mm^2 respectively) as a function of the slenderness ratio $\lambda = l_1/i_1$·One can see that for tubes in the range 60<A<160, eqn. (45) is closely approximated by

$$\frac{f_i}{i} = 0{\cdot}007\lambda - 0{\cdot}27 \tag{46}$$

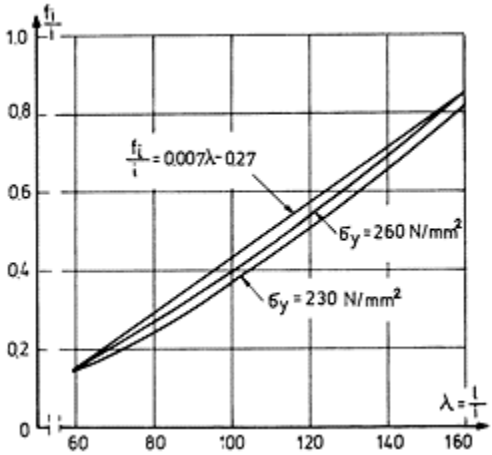

Fig. 9.24.

As in the case of line instability and taking into account eqn. (42), the bar shortening in the first step is

$$u_{1(1)} = \Delta l_{1(1)} = -\frac{Pl_1^2}{4EA_1}\frac{1+\gamma_{(1)}}{f+w_i} \tag{47}$$

where $\gamma_{(1)}$ is calculated for the first loading step. If the load in the node 0 increases from P_1 to P_m the bar shortening in the second loading step is given in eqn. (23), the factor K_1 being the same. The total bar shortening is

$$\Delta l_1 = \Delta l_{1(1)} + \Delta l_{1(2)} = -\frac{Pl_1^2}{4EA_1}\frac{1+\gamma_{(1)}}{f+w_i} - \frac{1}{1+\dfrac{1}{K_1}}\frac{l_1}{2}\frac{w_m(2f-2w_i-w_m)}{a_1^2} \tag{48}$$

and the member forces in the bars 01 are

@Seismicisolation

$$N_1 = \frac{EA_1}{1+\gamma_{(2)}}\frac{\Delta l_1}{l_1} = -\frac{EA_{1r}}{1+\gamma_{(2)}}\frac{w_m(2f-2w_i-w_m)}{2a_1^2} - \frac{Pl_1}{4(f+w_i)}\frac{1+\gamma_{(1)}}{1+\gamma_{(2)}} \tag{49}$$

The equilibrium equation for the node 0 will be

$$P_m = -4N_1\frac{f-w_i-w_m}{a_1} \tag{50}$$

and substituting eqn. (49),

$$P_m = P\frac{1+\gamma_{(1)}}{1+\gamma_{(2)}}\left(1-\frac{2w_i+w_m}{f}\right) + 2\frac{EA_{1r}}{1+\gamma_{(2)}}\frac{f^3}{a_1^3}\frac{w_m}{f}\left(1-\frac{w_i+w_m}{f}\right)\left(2-\frac{2w_i+w_m}{f}\right) \tag{51}$$

$\gamma_{(1)}$ and $\gamma_{(2)}$ are calculated for the loading levels

$$N_{(1)} = \frac{Pl_1}{4(f+w_i)} \qquad N_{(2)} = \frac{P_m l_1}{4(f-w_i-w_m)} \tag{52a,b}$$

Equation (51) can be solved by iteration only. In the most significant case, when all the nodes are equally loaded, P_m=P, it can be seen from eqn. (51) that

$$P = 2\frac{EA_{1r}}{1+\gamma_{(2)}}\frac{f^3}{a_1^3}\frac{\frac{w_m}{f}\left(1-\frac{w_i+w_m}{f}\right)\left(2-\frac{2w_i+w_m}{f}\right)}{\frac{\gamma_{(2)}-\gamma_{(1)}}{1+\gamma_{(2)}}+\frac{2w_i+w_m}{f}} \tag{53}$$

and the ratio between the loading steps will be

$$\frac{N_{(2)}}{N_{(1)}} = \frac{f+w_i}{f-w_i-w_m} \simeq 1+2w_i+w_m \tag{54}$$

One can see that if there is no erection imperfection, the bifurcation critical load is obtained for w_m=0 and because $\gamma_{(2)}$=$\gamma_{(1)}$=γ from eqn. (53) it can be seen that

$$P_{crc} = 4\frac{EA_{1r}}{1+\gamma}\frac{f^3}{a_1^3} \tag{55}$$

This relationship is plotted in Fig. 9.25 as a function of the stress level of the bars. One can see the significant reduction of the bifurcation critical load due to member imperfections.

@Seismicisolation

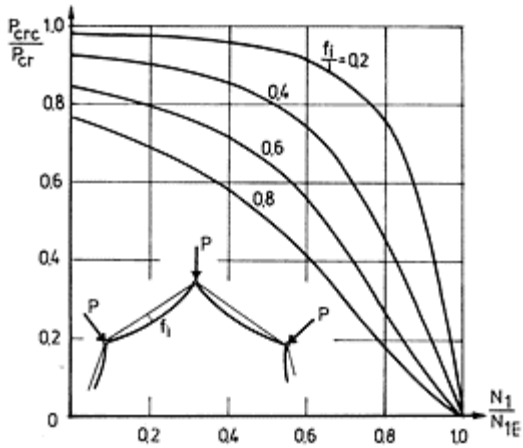

Fig.9.25

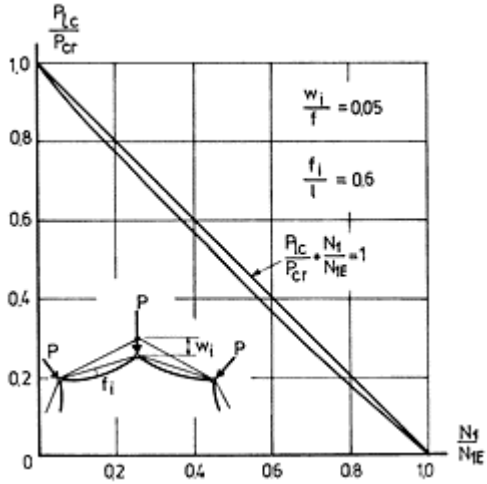

Fig. 9.26.

The ultimate load curve of a structure affected by both member and erection imperfections is plotted in Fig. 9.26 as a function of the stress level and using eqn. (53). One can see that the relationship

$$\frac{P_{lc}}{P_{cr}} + \frac{N_1}{N_{1E}} = 1 \tag{56}$$

approximates with good accuracy the exact curve.

@Seismicisolation

The study of the interaction between member buckling and general instability would be very complex and there are no satisfactory solutions as yet. In Ref. 22 an interaction relationship is suggested:

$$\frac{p_{cr}}{p_{crg}} + \frac{p_{cr}}{p_c} = 1 \tag{57}$$

where P_{crg} is the critical load for general instability and p_c is the one corresponding to member buckling or yielding. This empirical equation is properly satisfied in the case of line instability, as is seen in eqn. (56); therefore, it could also be used in the case of coupling member buckling with general instability.

9 CONCLUSIONS

The main instability types which may occur in latticed barrel vaults were presented in order to help the designer to understand the structure behaviour, to choose properly the proportions of its elements and to evaluate qualitatively the computer results. Approximate methods cannot replace exact computer-aided analysis which should take into account the interaction between various instability types and the effects on the load bearing capacity of the structure.

Moreover, it must be borne in mind that a bifurcation analysis under symmetrical loads cannot alone supply a sufficient basis for the practical design of a barrel vault. Instability is likely to occur in most cases by equilibrium limitation under unsymmetrical loads, although the effect of erection imperfections is expected to be smaller than by symmetrical loading.

REFERENCES

1. Gioncu, V. and Ivan, M. *Buckling of Shell Structures* (in Romanian). Editura Academiei, Bucureşti, 1978.
2. Wright, D.T. Membrane forces and buckling in reticulated shells. *J. Struct. Div.*, ST1, 1965, p. 173.
3. Băluţ, N., Porumb, D. and Rennon, N. Nonlinear analysis of reticulated shells (in Romanian). The 2nd Conference on Steel Structures, Timişoara, 11 Oct. 1979, vol. 1, p. 88.
4. Monforton, G.R.and El-Hakim, N.M. Analysis of truss-cable structures. *Comput. and Struct.* 11**,** 1980, p. 327.
5. Supple, W.J. Stability and collapse analysis of braced domes, in *Analysis, Design and Construction of Braced Domes*(Ed. Z.S.Makowski), Granada, London, 1984, pp. 143–159.
6. Massonnet, Ch. The collapse of struts, trusses and frames: A survey of up-to-date problems. Proceedings of IUTAM Symp. Collapse: The Buckling of Structures in Theory and Practice, London, August 1982.
7. Gioncu, V. New conceptions, trends and perspectives in the theory of postcritical behaviour of structures. General Report. The 3rd International Colloquium on Stability, Timişoara, 16 Oct. 1982.
8. Resinger, F. Zur Stabilität von torsionssteifen Fachwerkfüllstäben, insbesondere aus Rundstahl. *Der Stahlbau,* No. 1, 1963, p. 18.

@Seismicisolation

9. Lind, N.C. Stability criteria for reticulated shells. IASS Congress, Leningrad, 1966, Large Span Shells, vol. 1, p. 173.
10. Matescu, D., Gioncu, V. and Konrad, C. Stability of symmetrical loaded latticed cylindrical roofs. The 3rd International Colloquium on Stability, Timişoara, 16 Oct. 1982.
11. Anderson, M.S. Buckling of imperfect periodic lattice structures. Proceedings of IUTAM Symp. Collapse: The Buckling of Structures in Theory and Practice, London, Aug. 1982.
12. Buchert, K.P. *Buckling of Shell and Shell-like Structures.* K.P.Buchert and Assoc., Columbia, 1973.
13. Forman, S.T. and Hutchinson, J.W. Buckling of reticulated shell structures. *Int. J. Solids and Structs.*, 7, 1970, p. 909.
14. Gioncu, V. Stability of reticulated cylindrical roofs (in Romanian). Proceedings of Symp. Problems and Trends in Steel Structures, Timişoara, 17 April 1976, p. 46.
15. Tezcan, S.S. and Ovunc, B. An iteration method for the nonlinear buckling of framed structures. *Space Structures* (Ed. E.M.Davies), 1966, p. 491.
16. Rothert, H., Dickel, T. and Renner, D. Snap-through buckling of reticulated space trusses. *J. Struct. Div.*, ST1, 1981, p. 129.
17. Popescu, H. and Chiroiu, V. *Optimum Design of Structures* (in Romanian). Editura Academiei, Bucureşti, 1981.
18. Mallet, R.H. and Schmit, Jr., L.A. Nonlinear structural analysis by energy search. *J. of Struct. Div.*, ST3, 1967, p. 221.
19. Gioncu, V., Băluţ, N., Porumb, D. and Rennon, N. Recent examples of prefabricated steel barrel vaults from Romania, this book, Chapter 22, pp. 354–366.
20. Gioncu, V., Băluţ, N., Porumb, D. and Rennon, N. Interaction between different instability modes of latticed roof structures. The 3rd International Colloquium on Stability, Timişoara, 16 Oct. 1982.
21. Galoussis, E.G. Snap-through buckling of elastically restrained imperfect system. The 3rd International Colloquium on Stability, Timişoara, 16 Oct. 1982.
22. Pagano, M., Catanzaro, C. and Pedicini, G.C. The collapse load of braced translation vaults and cylindrical vaults. *Space Structures* (Ed. E.M.Davies), 1966, pp. 502–524.

@Seismicisolation

10
The Elastic and Post-buckling Analysis of Braced Barrel Vaults Manufactured from Fibre/Matrix Composite Materials

L.HOLLAWAY and A.RUSTUM
Department of Civil Engineering, University of Surrey, Guildford, UK

1 INTRODUCTION

The use of glass fibre reinforced polyester matrix (GRP) in construction, although not widespread, is now well established. One of the principal uses of the material in this field has been in the form of repeatable units of both load bearing and infill type that can be assembled to form a structure. The technique for jointing these units is also well established. GRP in the form of rods and tubes has not yet been seriously used; this is due mainly to the difficulty of jointing tubular members at nodal points.

Recently the crimped and bonded joint technique has been patented by the Fulmer Research Institute and the Royal Aircraft Establishment and has been used in this investigation to make an end connection to a GRP pultruded member which may then be screwed into an aluminium node joint. This invention has opened up a whole new field in skeletal structural systems which can be manufactured from fibre/matrix composites; one of these systems is the barrel vault.

The pultrusion technique is a mechanised process for producing GRP tubes by the closed mould system. There are no physical limits to the size of tube that can be produced, but for economic reasons they generally vary from 25 mm diameter with a wall thickness of 2 mm up to 150 mm diameter and wall thickness of 5 mm. The fibre/matrix percentage ratio by weight can have a wide range of values with an upper limit of about 70/30. The pultruded tube is an ideal unit with which to manufacture skeletal systems of the double-layer and braced barrel vault types, because of the inherent stiffness of these geometrical configurations. The modulus of elasticity for the upper limit of the fibre/matrix ratios would be of the order of 25 GN/m^2. This quantity is relatively low compared with that of steel but, if members which are highly loaded in a skeletal system require greater stiffness to prevent buckling, a hybrid composite of glass and carbon fibre in a polyester matrix could be used. An acceptable fibre/matrix ratio from an economic viewpoint would be 33·3/33·3/33·3% by weight of glass/carbon fibre/polyester resin and the modulus of elasticity would be of the order of 50 GN/m^2.

The problems associated with a braced barrel vault manufactured from a fibre/matrix composite material are clearly different to those encountered when the structure is made from steel. The GRP material with a high fibre/matrix ratio has tensile loading characteristics which are practically linear to failure. A member under a compressive

@Seismicisolation

force will buckle gradually due to small eccentricities, the causes of which were developed during its manufacture. However, once buckled and the load removed the member will show no permanent deformation and this loading process can be repeated many times without the material showing any signs of damage. Because of these specific material characteristics the barrel vault will have its own unique deformation properties as failure under increasing load progresses.

The current problem examines theoretically the elastic and post-buckling analysis of a barrel vault manufactured from a composite of glass fibre and polyester resin with a fibre/matrix percentage ratio of 60/40.

Four span-to-rise ratios are investigated; these are 8000/4000, 8000/2000, 8000/1000 and 8000/500, and are called types 1, 2, 3 and 4 respectively. This chapter will analyse the structural deformations of these barrel vaults as they are loaded to failure.

The barrel vault configuration was the same for the four types, and consequently the longitudinal members were constant but the length of all other members increased as the rise of the structure increased; the overall number of members and nodes of the vaults were constant.

2 THE BARREL VAULT STRUCTURE

The finite element method was used to study linear and non-linear parameters of the barrel vault on various span-to-rise ratios for a constant span of 8000 mm. The members of the structure were assumed to have been manufactured from 50 mm external diameter, 2 mm wall thickness pultruded tubes with a glass fibre/polyester matrix percentage ratio by weight of 60/40. Aluminium tubes were assumed to have been crimped and bonded on to the pultruded tubes and the ends threaded; these would then be screwed on to the aluminium node to form the nodal joint. A photograph of a Perspex model of the barrel

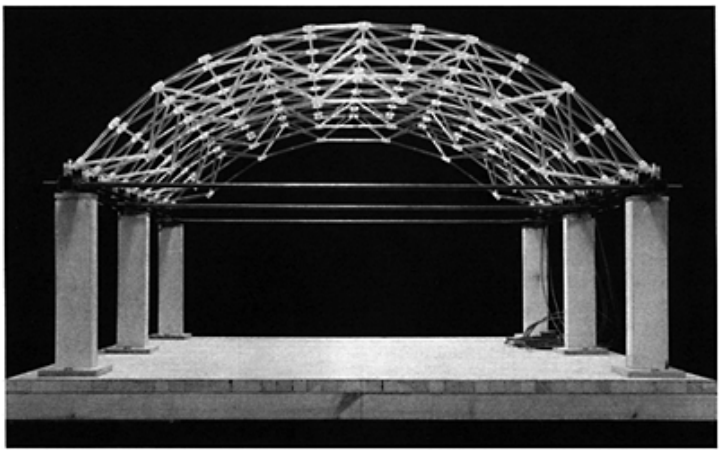

Fig. 10.1. Photograph of Perspex model of braced barrel vault.

@Seismicisolation

vault with a span-to-rise ratio of 4/1 is shown in Fig. 10.1 and an example of an aluminium tube which has been crimped and bonded on to a pultruded tube is shown in Fig. 10.2. It will be seen that the barrel vault has four double-layer skeletal beams throughout its length. These are to stiffen the overall structural system; for a single-layer braced barrel vault the relatively low modulus material was able to support only a fraction of the working load before deforming excessively.

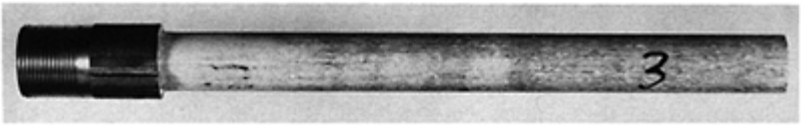

Fig. 10.2. Aluminium tube crimped and bonded on to a pultruded tube.

For the analysis the structure was position fixed but not direction fixed in the *X*, *Y* and *Z* cartesian coordinate directions at the various nodal joints around its free edges.

The barrel vaults were analysed by applying a uniformly distributed snow load of 718 N/m^2 over plan area of the structure, and in addition this magnitude of load was applied to half plan area of the span over its full length.

3 THEORETICAL ANALYSIS

A non-linear analytical analysis was required to study the behaviour of the fibre/matrix composite barrel vault structure up to failure. The analysis was to include the effects of imperfections of the structure on the ultimate failure load. The linear analysis cannot include changes in geometry and hence values of internal stresses.

A linear and a non-linear analytical analysis were undertaken on the fibre/matrix structure. The latter analysis was performed in order to study its characteristics as a change in geometry took place during loading up to failure. In addition the effects of certain imperfections on the behaviour and on the value of the ultimate load were investigated.

The non-linear method of analysis takes geometric non-linearity only into account as the material, from which the space structure was manufactured, has a linear stress-strain to failure.

The fundamental methods used in the analysis and the computer implementation are briefly summarised:

(a) In the strain displacement relationship of the members non-linear terms were retained.
(b) Displacement mode functions were selected for the members. A cubic function and a linear function in *X* were chosen for the transverse and axial deformations respectively.
(c) Partial differentiation with respect to the nodal point displacements (according to Castigliano's theorem) yield the stiffness coefficients which are the elements of the non-linear member stiffness matrix.

@Seismicisolation

The non-linear member stiffness matrix, which is a function of the nodal displacements and the internal forces, represents the basis for a computer program. As an incremental iteration technique is used the first step is to assemble an overall tangent stiffness matrix from the member stiffness matrices, taking as zero both the nodal displacements and internal stresses. (The implementation of the external constraints is achieved by using standard well-established techniques.) The solution for the first load increment displacements and the internal forces are used for the formulation of the new tangent stiffness matrix. A further load increment is applied and the same procedure is repeated. Iterations take place after each load increment to obtain equilibrium and to avoid departing from the equilibrium path; during this process the tangent stiffness matrix is not updated. The deformed configuration of the structure must be used when considering equilibrium and therefore it is updated during each load increment.

It should be mentioned that in this analysis the control parameter is not the load but the length of the equilibrium path, and therefore an extra constraining equation is used. During the iterations the load increment is modified. Also, the modified Choleski method is used during the solution of the system of equations (i.e. tangent stiffness matrix is decomposed to LDL^{t}). This method has the advantage in that changes in sign of any of the diagonal matrix elements D are used to detect changes in sign of the stiffness matrix and consequently changes in sign of the applied load increment. This then follows the equilibrium path in the event of snap through buckling.

The non-linear analytical analysis detailed above has been applied to types 1, 2, 3 and 4 braced barrel vaults. Figure 10.3 shows a plan and elevations of the four barrel vaults. The detailed results have been limited to an investigation of (i) the load factors, expressed in terms of snow loading, versus vertical displacements for skeletal nodal points, and (ii) load factors versus skeletal member forces. Four nodal point positions were investigated; two were on the centre line and two were in an area of the structure exposed to high deformations.

Four loading cases were considered, viz:

(a) a uniformly distributed load throughout the structure and acting vertically downwards;
(b) a uniformly distributed load thoughout the structure and acting vertically upwards;
(c) a uniformly distributed load on half the structure and acting vertically downwards;
(d) a uniformly distributed load on half the structure and acting vertically upwards.

In the following sections the items (a) and (b) above will be referred to as the full load conditions and items (c) and (d) the half load conditions.

As is usual when analysing skeletal systems, the external loads to the structure are assumed to be concentrated loads applied through the nodal points; these forces were derived from the uniformly distributed loads acting on equivalent areas of the structure.

Advantage was taken of the symmetry of the structure and for cases (a) and (b) above only one-quarter of the structure was considered, whereas for cases (c) and (d) one-half of the barrel vault was analysed.

Figures 10.4, 10.5, 10.6 and 10.7 show the linear and non-linear relationships between the load factor and displacements for the loading case (c) above. Each figure gives these relationships for the four nodal points A, B, C and D. The sign convention used in this analysis is that the vertically downward displacements are assumed negative and the upward displacements positive.

@Seismicisolation

Figure 10.8 shows the relationship between the load factor and vertical displacement of node point D. The graph enables a comparison to be made between the overall stiffness and the degree of non-linearity for the four types of structures as the span-to-rise ratio

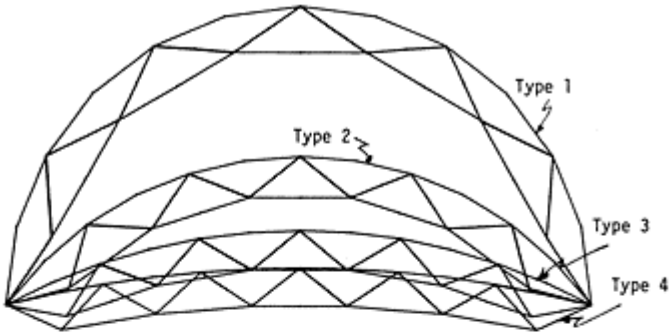

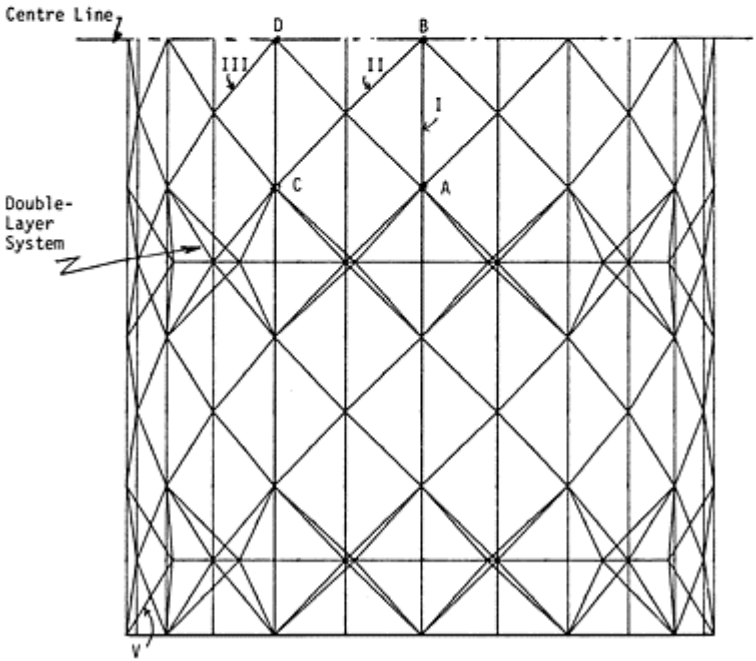

Fig. 10.3. (a) Comparative elevations of types 1, 2, 3 and 4 braced barrel vaults. (b) Plan of type 1 barrel vault (half length).

@Seismicisolation

varies. It is shown that as the rise decreases the structure becomes more flexible and the degree of non-linearity increases.

The linear and non-linear load factors plotted against vertical displacement for node point D is shown in Fig. 10.9. Three sets of curves are drawn, each giving the behaviour of the node under full and half load (load types (a) and (c)) for barrel vault types 2, 3 and 4. The graph for barrel vault type 2 shows that for both linear and non-linear analyses, displacement under half load is larger than that under full load. Type 3 barrel vault shows a similar linear behaviour when considering full and half load conditions, whereas under low loads placed on half span only the non-linear behaviour shows displacements larger than those for full load conditions. However, for the high external load values the situation is reversed, with the full load condition having the larger deflection value for the same applied load. In the type 4 barrel vault, which is a very low rise structure, the

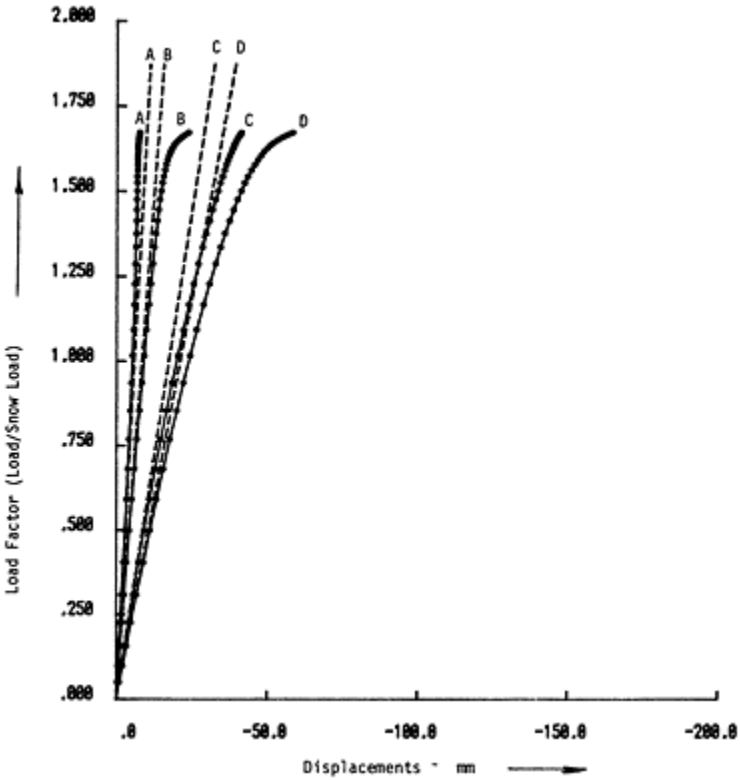

Fig. 10.4. Load factor-displacement of node points A, B, C and D for type 1 barrel vault (load case (c)).

@Seismicisolation

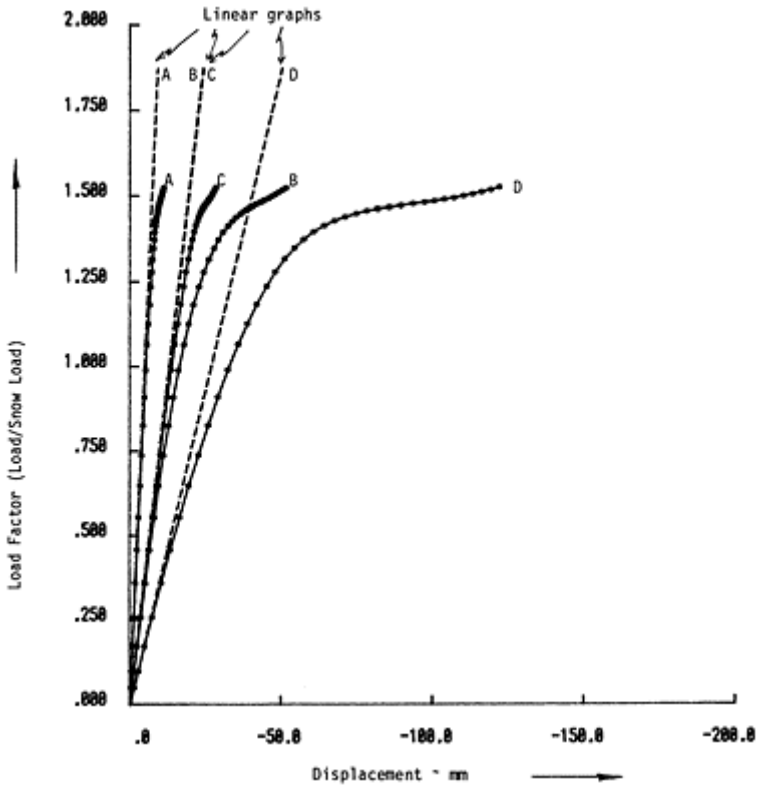

Fig. 10.5. Load factor-displacement of node points A, B, C and D for type 2 barrel vault (load case (c)).

@Seismicisolation

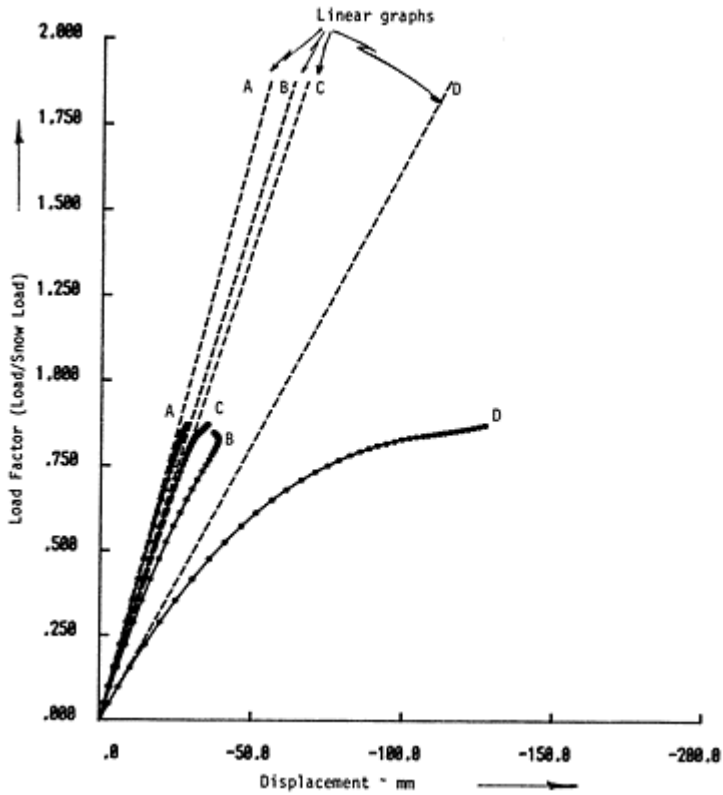

Fig. 10.6. Load factor-displacement of node points A, B, C and D for type 3 barrel vault (load case (c)).

@Seismicisolation

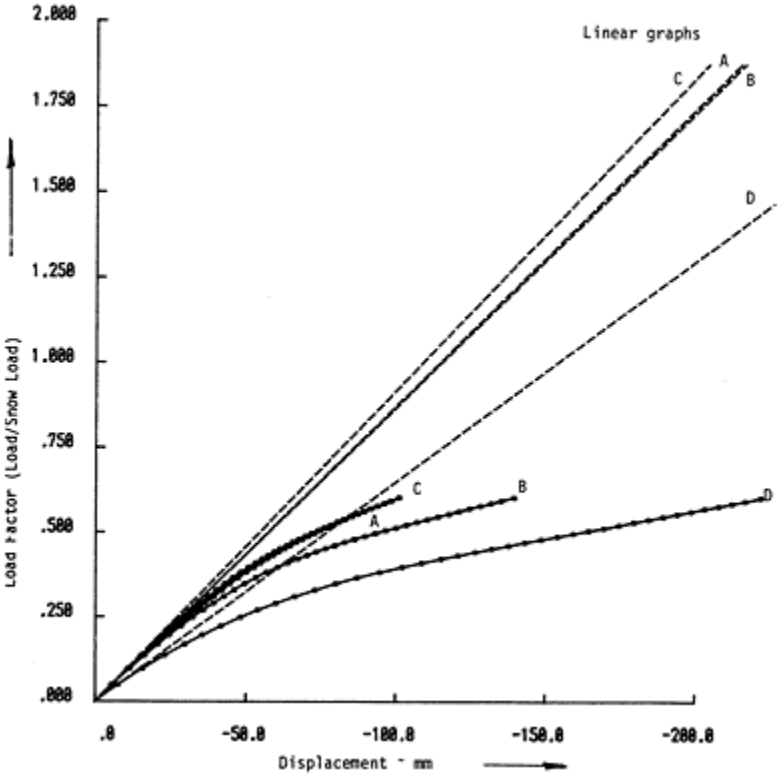

Fig. 10.7. Load factor-displacement of node points A, B, C and D for type 4 barrel vault (load case (c)).

@Seismicisolation

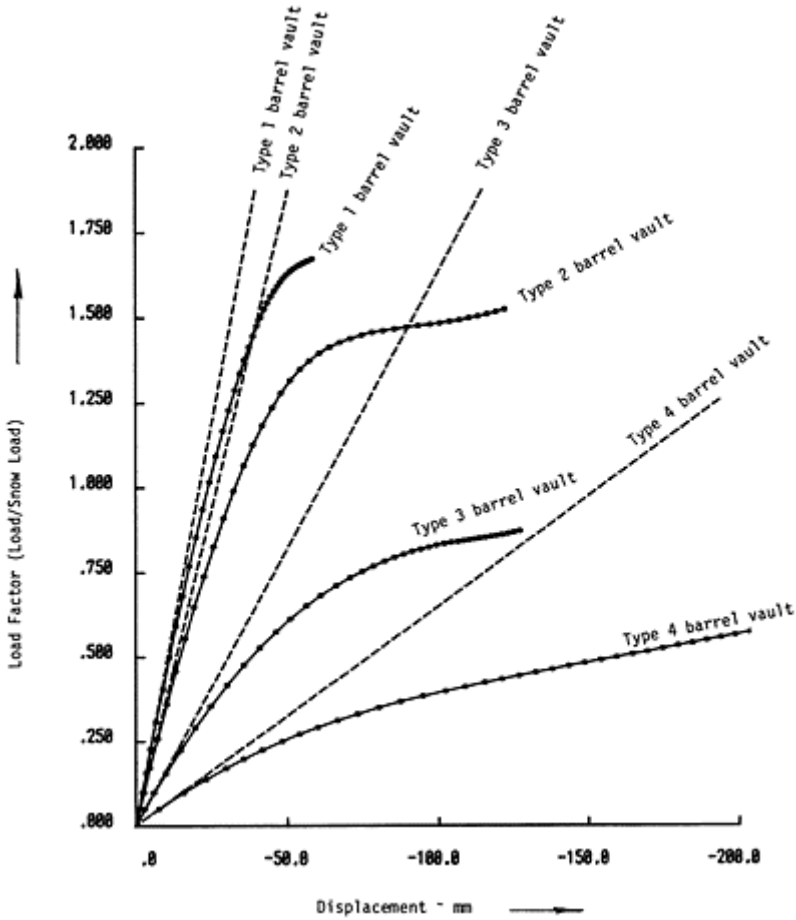

Fig. 10.8. Load factor-displacement of node point D for types 1,2, 3 and 4 barrel vaults (load case (c)).

@Seismicisolation

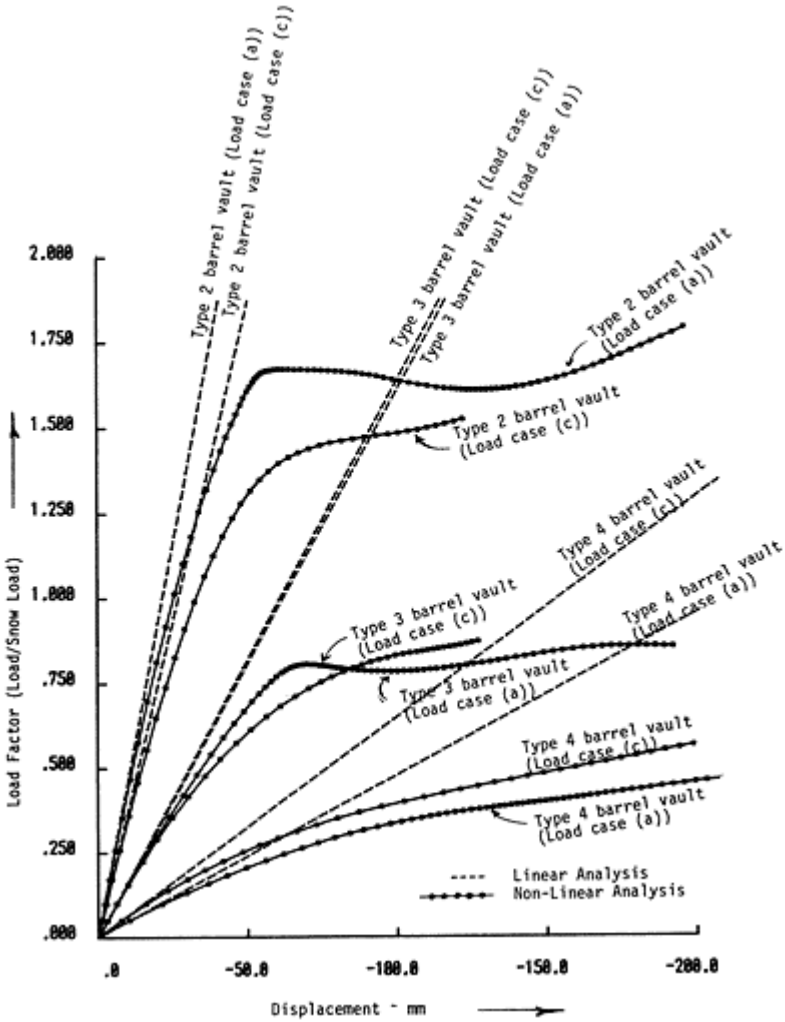

Fig. 10.9. Load factor-displacement of node point D for barrel vaults types 2, 3 and 4 (load cases (a) and (c)).

@Seismicisolation

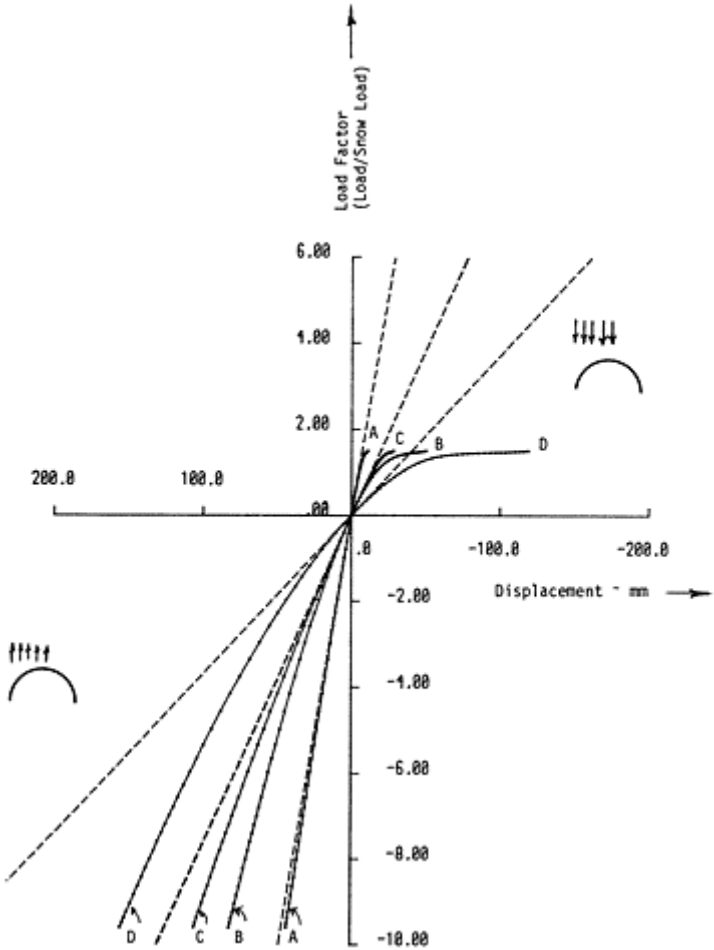

Fig. 10.10. Load factor-displacement of nodes A, B, C and D for type 2 barrel vault (load cases (c) and (d)).

displacements under the applied load for both the linear and non-linear analyses are greater than those under similar loadings applied on only half the span of the structure.

For barrel vault types 2 and 3, a local snap through instability occurs under full load conditions, whereas under the half loading condition the rate of deformation increases as the higher loads are applied, although no instability is evident. Both the full load and half load investigations of the barrel vault type 4 were stopped after large displacements had been recorded. It was felt that this particular structure at this time did not warrant the large amount of computer time required to cause snap through buckling to occur.

Figure 10.10 shows the relationship between load factor and vertical displacements at positions A, B, C and D in the type 2 barrel vault. The two loading cases considered are a

@Seismicisolation

positive and negative half load (load cases (c) and (d)). It may be clearly seen that the linear analysis underestimates deformation when analysing a positive loading condition and overestimates it when analysing a negative loading condition.

Figures 10.11 and 10.12 show the load factor plotted against displacement of nodal point D for the barrel vault types 2 and 3. The graphs compare the results for one position on the vault (node D) under loading cases (a), (b), (c) and (d). It may be seen that for the linear curves of both graphs and the non-linear curves of Fig. 10.11, the displacement

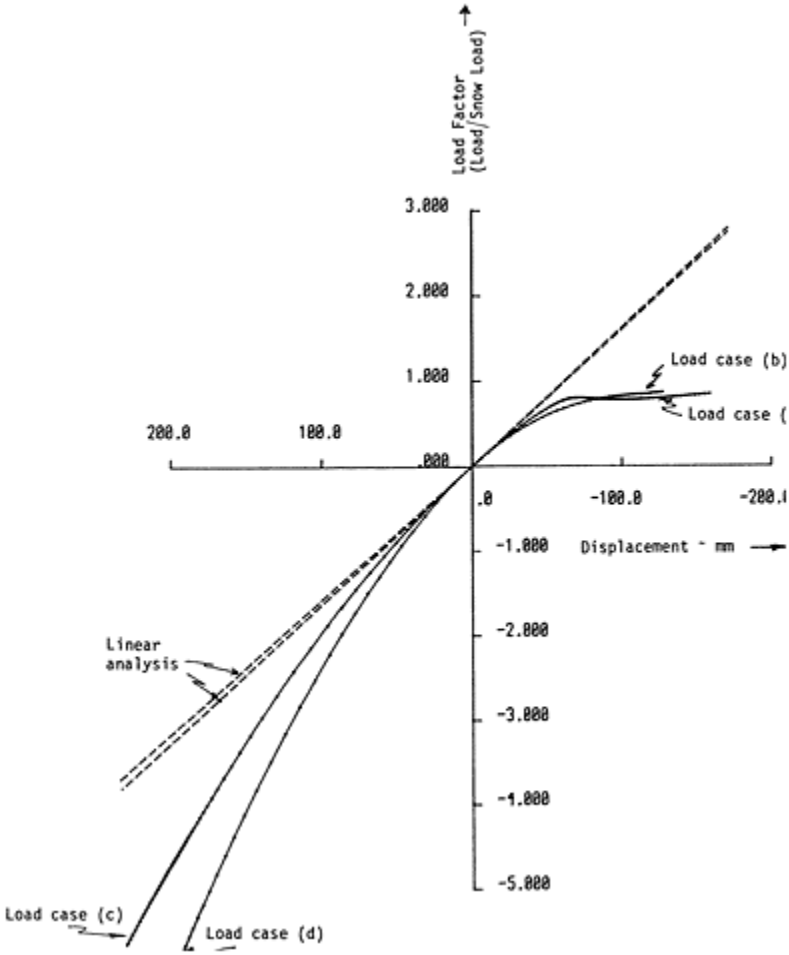

Fig. 10.11. Load factor-displacement of node D for type 3 barrel vault (loading cases (a), (b), (c) and (d)).

@Seismicisolation

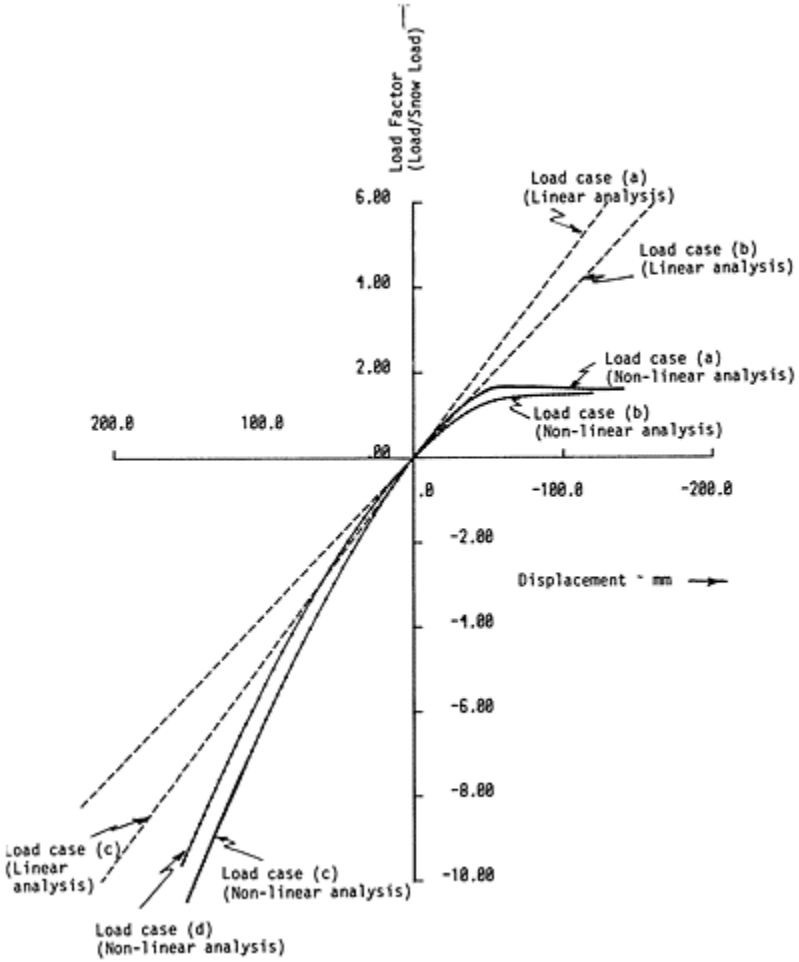

Fig. 10.12. Load factor-displacement of node D for type 2 barrel vault (loading cases (a), (b), (c) and (d)).

@Seismicisolation

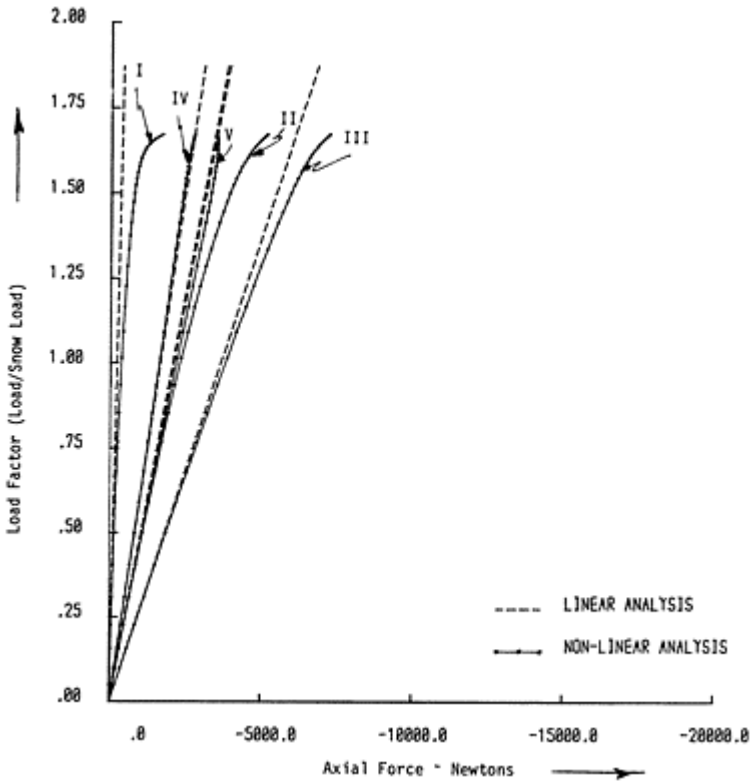

Fig. 10.13. Load factor-axial forces for type 1 barrel vault (members I to V, load case (c)).

@Seismicisolation

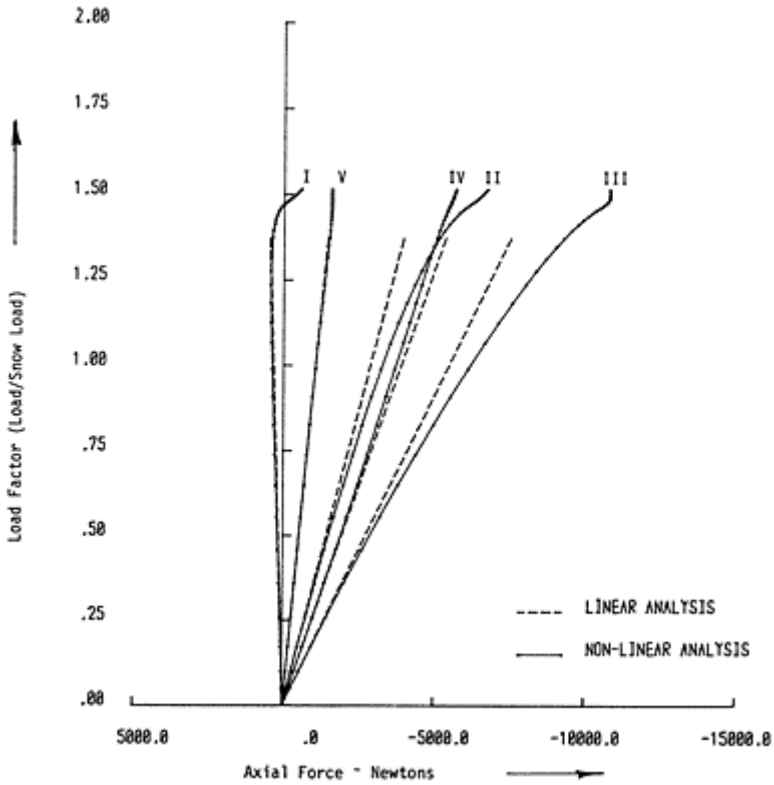

Fig. 10.14. Load factor-axial forces for type 2 barrel vault (members I to V, load case (c)).

@Seismicisolation

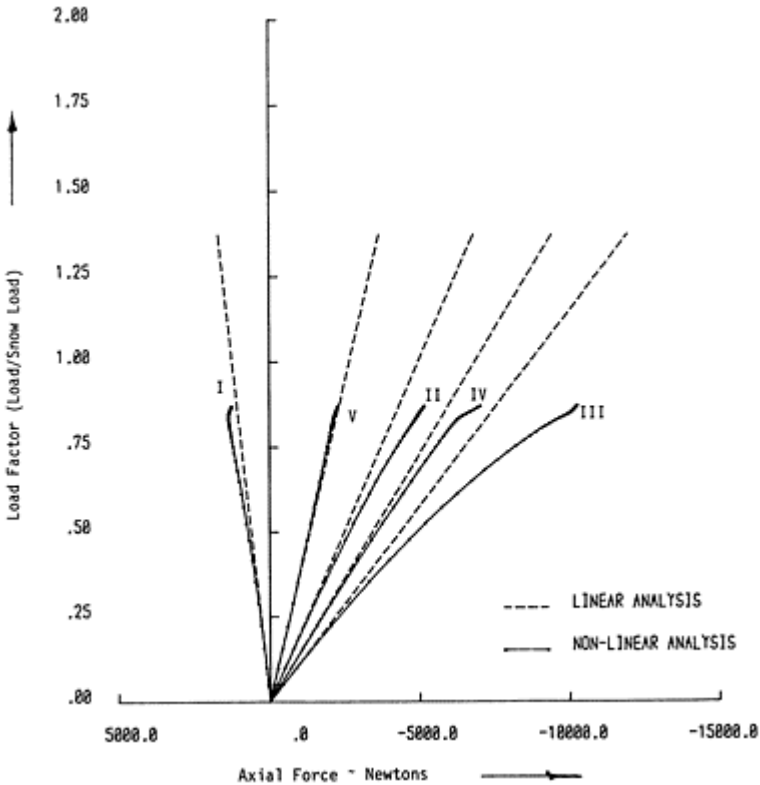

Fig. 10.15. Load factor-axial forces for type 3 barrel vault (members I to V, load case (c)).

@Seismicisolation

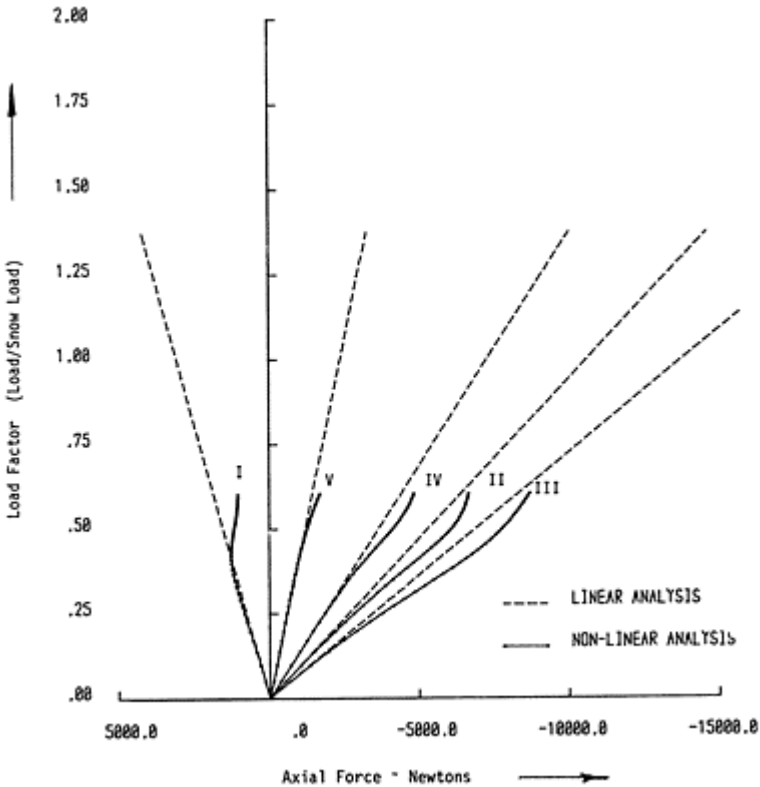

Fig. 10.16. Load factor-axial forces for type 4 barrel vault (members I to V, load case (c)).

under half loading is larger than that under full load. However, this is not so for the non-linear behaviour shown in Fig. 10.12.

The criterion for design of fibre/matrix skeletal systems is invariably the deflection; to gain an appreciation of the general behaviour of the overall structure, especially in the non-linear region, an investigation of the deformation of the entire structure is generally undertaken. The non-linear behaviour of the internal forces is a direct consequence of geometric non-linearity and therefore in this study only the results of members I to V (Fig. 10.1) will be given. Figures 10.13 to 10.16 show the relationships between the internal applied load, in terms of load factor, and the axial forces for the five members of barrel vault types 1 to 4 under load case (c).

@Seismicisolation

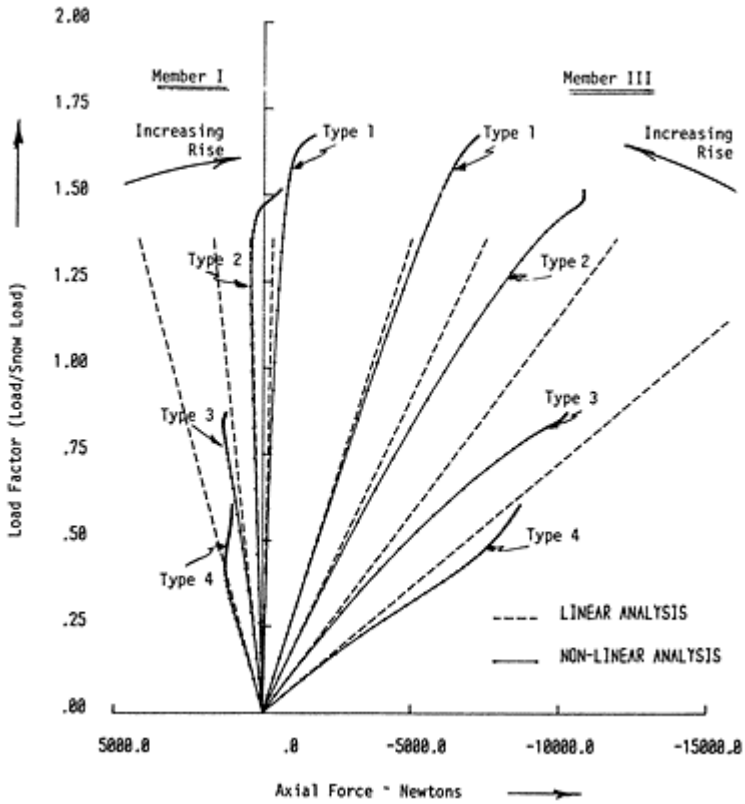

Fig. 10.17. Load factor-axial force for types 1, 2, 3 and 4 barrel vaults (members I and II, load case (c)).

There are two main points to be noted from the four figures. First, the degree of non-linearity of the internal forces increases as the span-to-rise ratio of the barrel vault increases (i.e. the height of the barrel vault decreases). Second, the effect that the geometry of the barrel vault has on the internal forces: it will be seen that as the rise of the structure decreases, internal forces increase in certain members and decrease in others. The general trend is that an increase occurs in the members which are highly stressed. The results also show that the divergence of the axial forces between the high stressed and the low stressed members in any particular barrel vault becomes larger as the rise decreases; this is clearly shown in Fig. 10.17.

4 OBSERVATIONS

To reduce the flexibility of the barrel vaults which have been manufactured from a low modulus fibre/matrix composite, stiffening ribs were placed along the length of the

@Seismicisolation

vaults. These types of systems have a local instability rather than a general instability problem, and it has been shown that the greater the rise of the barrel vault, the better is the structural performance of the system in relation to the load carrying capacity. The structures investigated showed that, for span-to-rise ratios greater than 8/1, more flexible behaviour was apparent when a uniformly distributed load was applied to half span of the structure in a vertically downward direction than under a uniformly distributed load applied to the full span. For span-to-rise ratios of less than 8/1 the reverse was shown to be true.

As would be expected, the low rise barrel vaults had higher member forces associated with them than the high rise vaults.

@Seismicisolation

11
Basic Principles in the Design and Construction of Steel Braced Barrel Vault Roofs

H.B.WALKER
Constructional Steel Research and Development Organisation, London, UK

1 INTRODUCTION

The barrel vault, as a form of construction, is extremely old, being extensively built in masonry since Roman times and before. It followed the natural principle of the arch but in three-dimensional form. With the advent of materials capable of resisting tension forces the barrel vault was used for very large structures in the last century, particularly railway stations and large assembly halls. These applications normally used a series of cast iron or steel arches interconnected with lattice girders and were not fully three-dimensional structures. The full principle of the modern three-dimensional barrel vault did not come into use until the braced barrel vault became a practical form of construction.

The full potential of braced barrel vault structures has not yet been realised in the UK although there is a renewed interest, particularly, for the roofs of the atriums of some of the newer multi-storey building developments.

With all three-dimensional structures, jointing of the members represents a high cost feature of the construction and it is this area that will be most fruitful for detailed investigation in the future.

2 TYPES OF STRUCTURAL ARRANGEMENT

The purpose of the structure is to support the outer protective membrane or cladding so that the climate within the structure is controlled. The form of structure, being essentially cylindrical in shape, can be generated by many different structural arrangements. When considering the various options available, the simplest possible design approach usually is the most economic, bearing in mind factors such as location of the site, size of the structure, possible size of individual members, location of works, transport to site, erection equipment and methods, and the type of labour which is available.

The simplest barrel vaults can be constructed using single curved members of the longest lengths possible. This type of structure is one where the fabricating works and the site are likely to be close together with good roads between and the appropriate cranage

@Seismicisolation

available. Where transport over a long distance is required, perhaps by ship, the structural components would need to be broken down to small elements, preferably to sizes that could be packed into the standard international container.

Some of the options available to the designer are illustrated in Figs. 11.1 to 11.5.

2.1 Single Layer

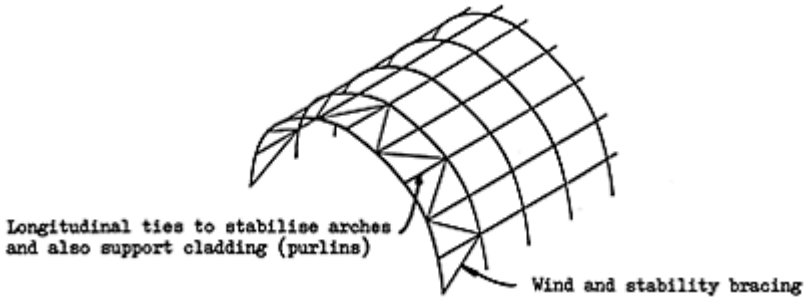

Fig. 11.1. Simple arch.

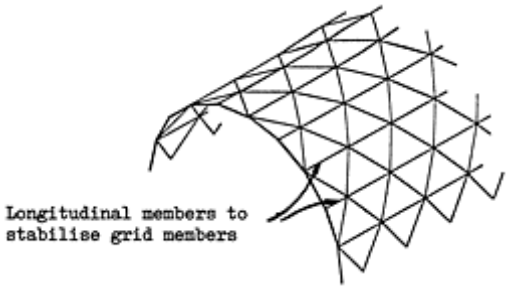

Fig. 11.2. Braced vault.

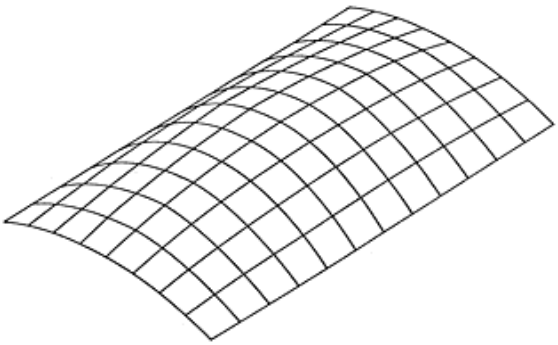

Fig. 11.3. Simple 2-way grid.

@Seismicisolation

2.2 Double Layer

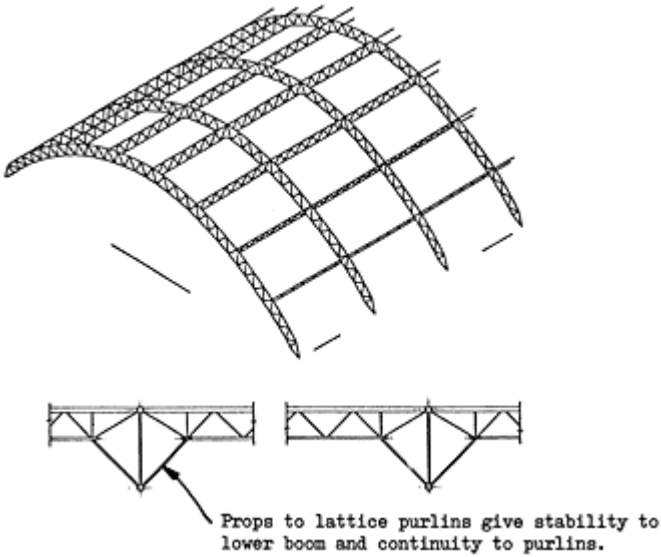

Fig. 11.4. Braced truss arch.

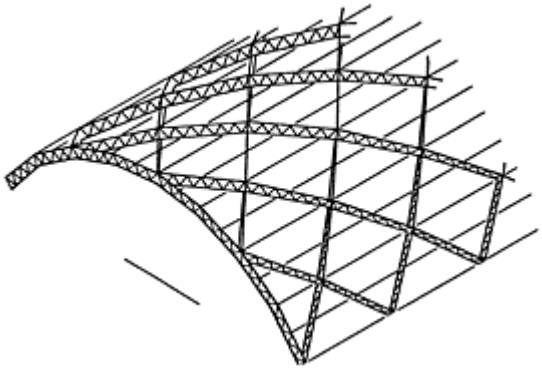

Fig. 11.5. Lamella frame.

3 DESIGN LOADS

The design loads which will need to be considered for barrel vault roofs are:

(i) *Dead loads*

This includes self weight of structure, cladding, glazing, services, etc.

(ii) *Imposed loads*

@Seismicisolation

This includes the weight of snow (or dust), non-permanent services such as flood lights, special heating and ventilation, maintenance equipment and operators, point loads from hoists and special requirements for exhibitions and sports.

(iii) *Wind loads*

The wind can blow in any direction although there are usually prevailing winds in known directions. Local effects, due to mountains or valleys, should always be considered.

When considering the design loads special consideration will need to be given to imposed loads due to snow, to wind loads and their combined effect. By their nature barrel vaults perform best under balanced loading systems. When the loading is asymmetric high local moments and deflections may be caused.

4 IMPOSED LOADS CAUSED BY SNOW (OR DUST)

In the UK reference should be made to CP.3 Chapter V, Part 1, Dead and Imposed Loads.

In locations subject to heavy snowfalls special consideration should be given to the effects of accumulation of snow in roof valleys and due to drifting. The following data (Figs. 11.6 and 11.7) taken from Draft ISO/DIS 4355 forms a basis for determining asymmetric loading requirements.

@Seismicisolation

4.1 Light or No Wind Condition

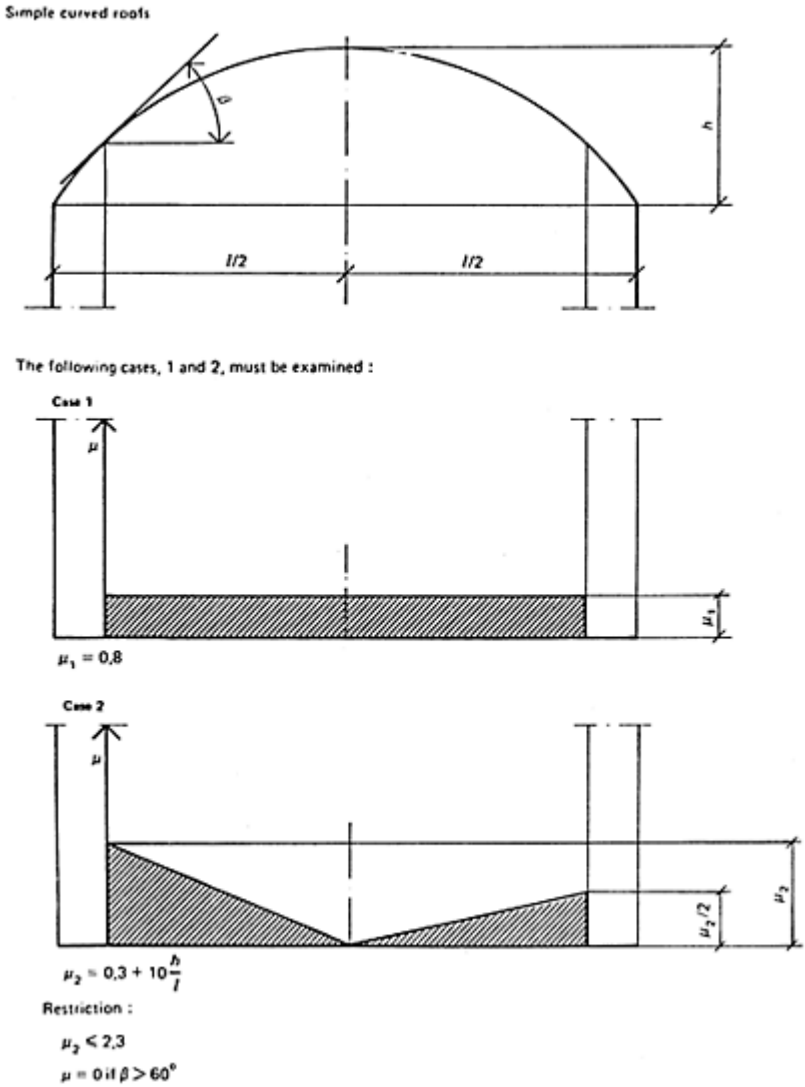

Fig. 11.6. Imposed load.

4.2 Multi-bays and Strong Winds

Snow can accumulate to one side of a barrel vault or it can accumulate m the valleys between barrel vaults in a multi-bay roof. The snow can accumulate for two reasons:

@Seismicisolation

either it can slide down the roof surface and accumulate at the sides or in the valleys, or it can be blown there by high winds.

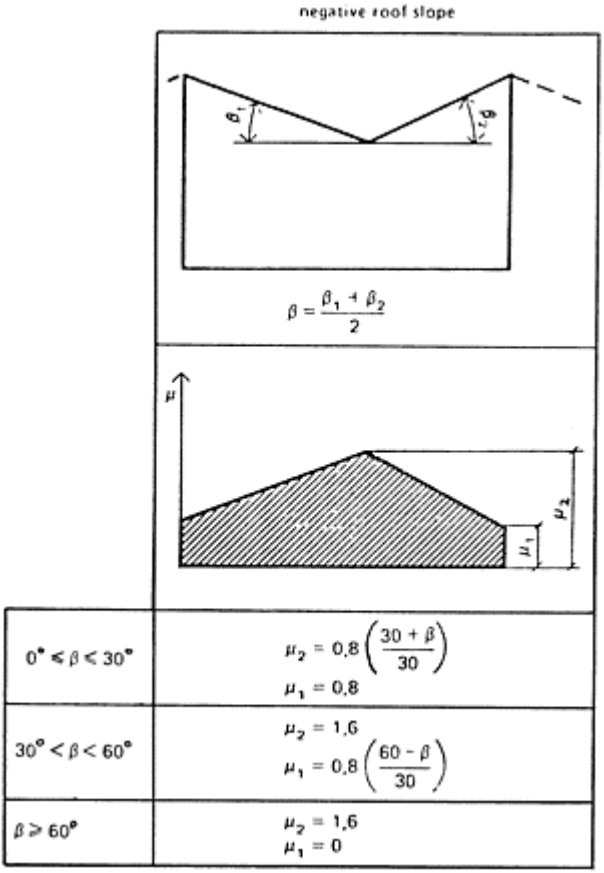

Fig. 11.7. Imposed loads, drifting and multi-bay. Nominal snow load=S=S_0. S_0 is the characteristic intensity of snow on the ground, and μ is the shape coefficient noted above.

4.3 Wind Loads

The loads due to wind forces acting on a barrel vault roof are given in Fig. 11.8. The data have been obtained from the ECCS publication, 'The Recommendations of ECCS Technical Committee T.12—Wind Effects'.

Where wind tunnel test data is available for the particular roof under consideration, then this should be used in preference.

@Seismicisolation

5 CONSTRUCTION

As previously noted there are many different forms of structure which will generate the barrel vault shape. Simple construction methods are usually best and give the least cost, as

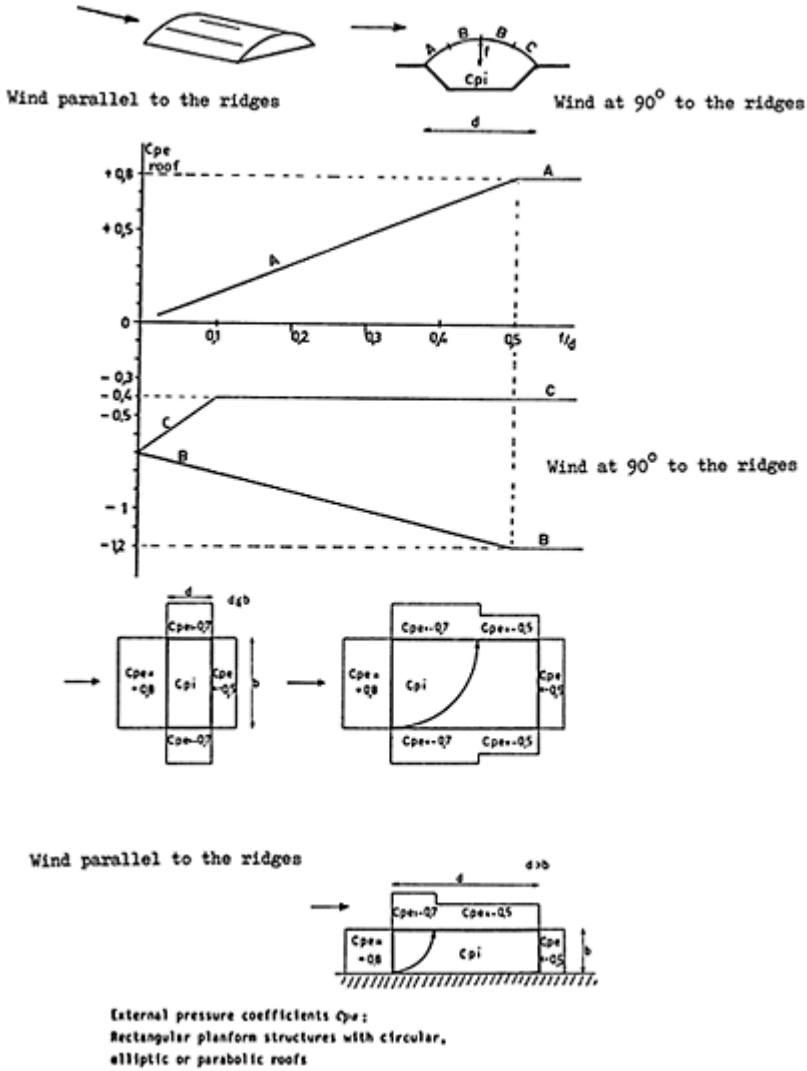

Fig. 11.8. Wind loads.

@Seismicisolation

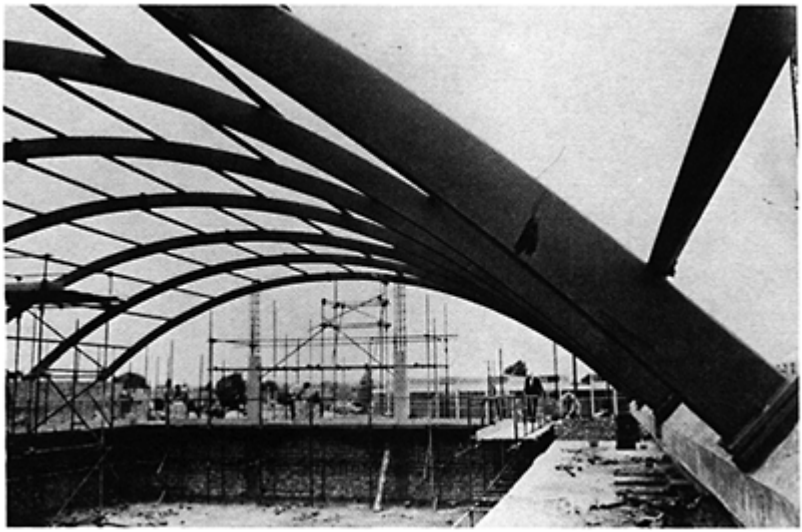

Fig. 11.9. Sports hall, Swindon. 27 m span, 3-pin arch.

shown in Fig. 11.9. Least weight solutions are rarely also the least cost solutions. Systems with a multiplicity of members are costly to fabricate and protect. The erection methods to be used will also play a very significant part in the design process as these, again, must be as simple as possible so that the minimum time is involved. Steel is the preferred material for barrel vault structures; it gives the best strength/cost ratio and long-term integrity characteristics and there is no shortage of design and fabrication expertise. Long life can be guaranteed by adopting the correct surface protection systems for the environmental conditions and, provided adequate maintenance is given, a steel structure should last forever.

6 CLADDING

There should be no problems in cladding a barrel vault. Many systems are available and they are all readily adaptable to the curved form. It is only on small structures with a tight curvature that special rolled bending of the cladding sheets may be required. As far as possible long sheets should be used—12/14 m or longer—to reduce the number of overlap joints. Roof lights can be incorporated as required. Where indoor sports are to be played, where a ball may be played high in the air, shutters may be required across the roof lights to prevent dazzle in the daytime.

@Seismicisolation

7 CONSTRUCTION USING PRE-FABRICATED TRUSS PANELS

It will be of interest to consider a multi-span braced barrel vault which was constructed in London some years ago for the Port of London Authority, shown in Fig. 11.10. This is known as the M-shed and is situated in what was then the South Dock of the

Fig. 11.10. M-shed, 7-bay braced barrel vault roof.

West India Docks. It is a multi-storey building with an elevated roadway at first floor level and was used for the handling of general cargo from import vessels.

The roof is of prime interest to us as it is a 7-bay braced barrel vault, each bay spanning 22·8 m×53.6 m long to cover a total area of 8554 m^2. Supports were provided by steel posts in the gable walls at 44·7 m centres and by concrete beams with infill brickwork to like the end thrusts. The roof extended over the elevated roadway by 8·9 m to give weather protection to the loading operations.

The roof itself was constructed from structural hollow sections and involved the shop fabrication of over 200 lattice frames each 3 m wide by approximately 10 m long. The main boom members in the valley trusses were 127 mm×51 mm×6.4 mm 4·9 mm and 3·6 mm RHS in high tensile steel while the boom members for the upper trusses were 102 mm×51 mm×4·9 mm and 4·6 mm RHS m mild steel. The bracing members varied between 102 mm×102 mm×6.4 mm RHS in high tensile steel to 76 mm×76 mm×3·6 mm RHS in mild steel.

Assembly of the structure on site was carried out on scaffolding formmg a series of arches on to which the truss units were placed for *in situ* welding.

@Seismicisolation

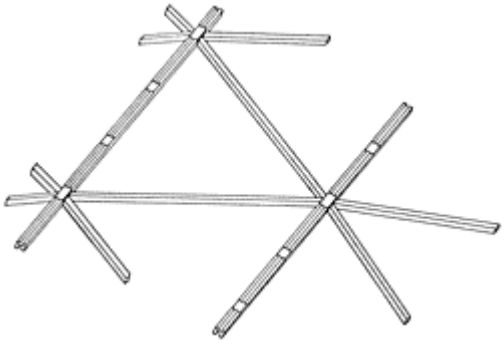

Fig. 11.11. M-shed. Arrangement of roof frames.

The welders had to pass tests for both works and site welding and a representative number of joints were subsequently radiographed to ensure that a high standard was maintained.

The structural members were galvanised, the welds being cleaned and painted with two coats of zinc-rich paint. Additionally, a calcium plumbate primer and two coats of alkydresin paint was also applied.

8 NODUS JOINT SYSTEM FOR BRACED BARREL VAULTS

For braced barrel vaults up to approximately 40 m span, depending upon the span/rise ratio and the loading, a single-layer frame using the NODUS Joint System can offer a very practical and economic solution. The structural members are small individual units which are easily transported and handled.

A very clean joint (Fig. 11.12) is obtained by using two plain half casings only held together by a high-strength centre bolt. The chords, which can be circular or square hollow sections, are welded on to the chord connectors at an angle appropriate to the curvature of the roof using the standard assembly jig. The use of the jig will guarantee a high degree of accuracy. Provided that the profile of the roof forms an arc of constant radius about the longitudinal axis, the angle between each chord connector and the chord will be the same. This will ensure that fabrication problems will be reduced to a minimum and erection on site will be straightforward.

@Seismicisolation

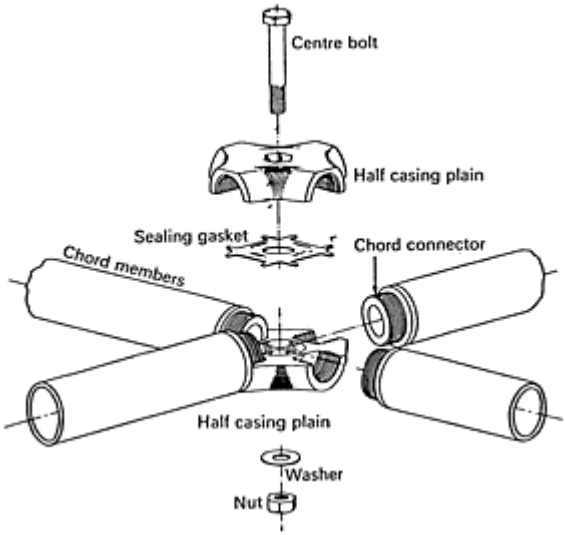

Fig. 11.12. NODUS joint.

A braced barrel vault, using the NODUS Joint System, is shown in Fig. 11.13; comparative studies have been carried out to determine the effect of the longitudinal purlin members. To reduce the number of members in the structure consideration was given to a braced framework without longitudinal members. With this arrangement the cladding would span at right angles to the chord members taking a diagonal path over the roof. This structural arrangement was analysed and it was found that high moments were generated at the joints, particularly in the plane of the structure. An indication of the

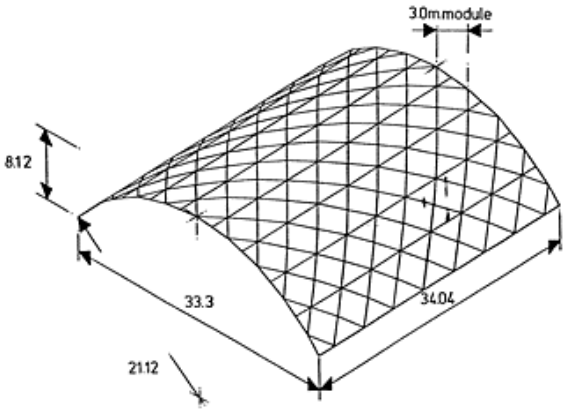

Fig. 11.13. Braced barrel vault with NODUS joint.

@Seismicisolation

magnitude of these moments is shown in Fig. 11.14. A further analysis was carried out with longitudinal members as indicated in Fig. 11.13 and the effect of these members on the in-plane moments is shown in Fig. 11.15. The longitudinal members, which also act as purlins to support the cladding, stiffen the structure to a very considerable extent and allow a much more economic structure to be designed. The deflections at the joints are also considerably reduced, as shown in the table in Fig. 11.16.

Large moments and deflections at the joints would make cladding fixings vulnerable to damage and, unless the roof cladding was designed to operate as a stressed skin, would cause difficulties when the maximum snow and wind loads were applied.

It is interesting to note that the dimensions of the NODUS braced barrel vaults under consideration would meet specified requirements for an indoor tennis court. The floor level would be lowered to improve the visual aspect and to ensure that the side thrusts can

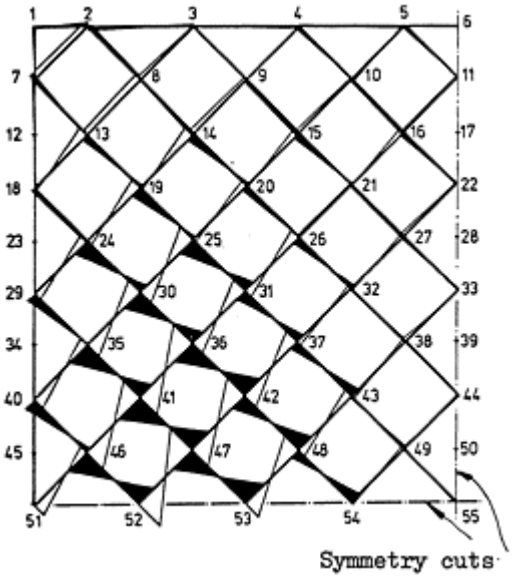

Fig. 11.14. In-plane moments, no longitudinal members.

@Seismicisolation

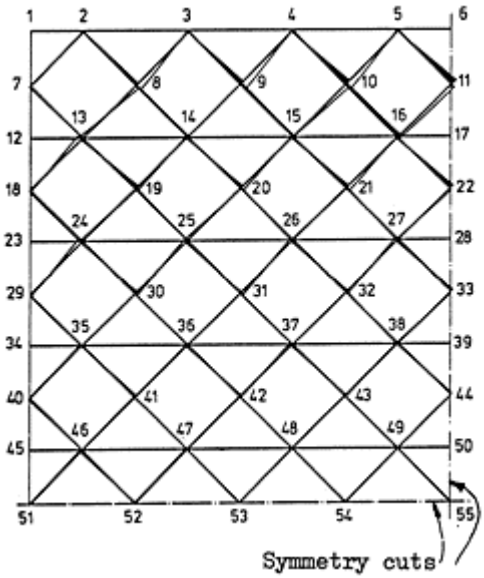

Fig. 11.15. In-plane moments with longitudinal members.

@Seismicisolation

JOINT NO.	X-DEFLN. (CM)	Y-DEFLN. (CM)	Z-DEFLN. (CM)
1	- 0.84	0.00	0.00
2	- 0.84	0.00	0.00
3	- 0.69	0.00	0.00
4	- 0.45	0.00	0.00
5	- 0.15	0.00	0.00
6	0.00	0.03	0.02
7	- 1.08	0.19	0.00
8	- 0.85	- 5.77	- 5.10
9	- 0.61	- 6.88	- 6.13
10	- 0.32	- 6.14	- 5.54
11	0.00	- 5.65	- 5.13
12	- 1.84	0.25	0.00
13	- 1.48	- 6.04	- 6.20
14	- 0.84	-11.61	-11.43
15	- 0.43	-11.53	-11.42
16	- 0.13	-10.41	-10.41
17	0.00	0.00	-10.23
18	- 2.82	0.30	0.00
19	- 1.85	-11.07	-12.31
20	- 0.65	-13.39	-14.19
21	- 0.16	-12.10	-12.68
22	0.00	-11.29	-11.83
23	- 4.78	0.27	0.00
24	- 3.99	- 6.84	- 9.48
25	- 1.80	-13.01	-15.74
26	- 0.28	-12.19	-13.10
27	0.02	-10.49	-10.55
28	0.00	0.00	-10.19
29	- 6.26	0.24	0.00
30	- 4.34	- 9.44	-14.21
31	- 1.29	-10.35	-11.69
32	0.05	- 7.93	- 5.33
33	0.00	- 6.72	- 2.87
34	- 8.60	0.19	0.00
35	- 7.43	- 4.74	-10.32
36	- 3.71	- 8.38	-13.37
37	- 0.61	- 6.31	- 2.94
38	0.15	- 3.93	5.01
39	0.00	0.00	6.06
40	- 9.59	0.13	0.00
41	- 6.97	- 4.99	-13.32
42	- 2.48	- 4.65	- 4.15
43	- 0.09	- 2.18	10.63
44	0.00	- 1.00	16.76
45	-11.22	0.06	0.00
46	- 9.82	- 1.64	-10.29
47	- 5.27	- 2.73	-10.22
48	- 1.19	- 1.53	7.22
49	0.06	- 0.29	21.40
50	0.00	0.00	23.36
51	-10.94	0.00	0.00
52	- 8.09	0.00	-12.68
53	- 3.07	0.00	- 0.51
54	- 0.30	0.00	18.59
55	0.00	0.00	26.94

JOINT NO.	X-DEFLN. (CM)	Y-DEFLN. (CM)	Z-DEFLN. (CM)
1	- 0.70	0.00	0.00
2	- 0.70	0.00	0.00
3	- 0.56	0.00	0.00
4	- 0.36	0.00	0.00
5	- 0.12	0.00	0.00
6	0.00	0.03	0.02
7	- 0.87	0.20	0.00
8	- 0.66	1.56	1.20
9	- 0.48	2.34	1.84
10	- 0.25	2.79	2.21
11	0.00	2.96	2.34
12	- 0.70	0.30	0.00
13	- 0.70	0.32	- 0.18
14	- 0.53	1.72	1.08
15	- 0.33	2.38	1.60
16	- 0.11	2.77	1.92
17	0.00	0.00	1.96
18	- 0.69	0.38	0.00
19	- 0.49	0.71	- 0.18
20	- 0.35	1.31	0.15
21	- 0.17	1.64	0.29
22	0.00	1.77	0.35
23	- 0.42	0.37	0.00
24	- 0.42	- 0.55	- 2.10
25	- 0.29	- 0.17	- 2.15
26	- 0.18	- 0.11	- 2.62
27	- 0.05	- 0.03	- 2.76
28	0.00	0.00	- 2.77
29	- 0.36	0.35	0.00
30	- 0.22	- 0.31	- 2.32
31	- 0.13	- 0.32	- 2.99
32	- 0.06	- 0.37	- 3.55
33	0.00	- 0.38	- 3.72
34	- 0.22	0.28	0.00
35	- 0.22	- 0.53	- 2.98
36	- 0.10	- 0.52	- 3.52
37	- 0.04	- 0.60	- 4.25
38	- 0.01	- 0.63	- 4.59
39	0.00	0.00	- 4.64
40	- 0.21	0.20	0.00
41	- 0.11	- 0.21	- 2.50
42	- 0.04	- 0.18	- 2.73
43	- 0.00	- 0.19	- 3.08
44	0.00	- 0.19	- 3.19
45	- 0.17	0.10	0.00
46	- 0.17	- 0.17	- 2.93
47	- 0.06	- 0.14	- 2.91
48	- 0.01	- 0.12	- 3.03
49	- 0.00	- 0.12	- 3.08
50	0.00	0.00	- 3.09
51	- 0.20	0.00	0.00
52	- 0.10	0.00	- 2.20
53	- 0.03	0.00	- 1.94
54	- 0.00	0.00	- 1.95
55	0.00	0.00	- 1.94

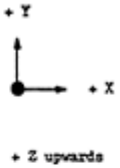

Fig. 11.16. Comparison of joint deflections.

easily be catered for by moderate abutments. Gable end treatment can be arranged in various ways, probably incorporating restaurants, bars and changing rooms.

9 CONCLUSIONS

It can be seen that barrel vaults can be treated as relatively simple structures and that there are many different structural arrangements which can be used. The designer should always consider the economics of the particular project and should take account of location, transport and the type of labour available. The braced barrel vault is a visually attractive structure as well as being cost-effective and it is confidently anticipated that, with the increased use of computer techniques, it will be used to a much greater extent m the future.

@Seismicisolation

12
Some Possibilities Offered by Braced Vault Construction

F.E.S.WEST*
PRC Engineering (UK) Ltd, London, UK

1 INTRODUCTION

There are various design advantages which skeletal vault construction could obtain over continuum vaults. In the construction of continuum vaults (which are invariably in reinforced or prestressed concrete) it is very difficult to alter the shell thickness appreciably in order to vary its stiffness to suit stability requirements. As the construction is invariably *in-situ* and 'wet', requiring centering and shuttering, single curvature formwork is expensive to place and double curvature formwork wildly expensive unless inflatable forms are used. Inflatable formwork can only be economical if intended for multiple re-use on a grand scale. Therefore in shell vaults one is left with three basic components which are capable of manufacture by normal civil engineering methods:

(a) Edge beams Which may be precast with starter bars left protruding
(b) End diaphragms Which may be precast with starter bars left protruding
(c) A shell which is almost always cast *in-situ* on to formwork which allows it to merge into components (a) and (b). (It should be noted that some small shells have been precast and grouted to edge beams and diaphragms *in-situ*.)

The analysis of continuum vaults has traditionally been restricted to the differential equations for the flexure of a continuous membrane for which the boundary conditions can never be represented adequately and, for unsymmetrical forms and loadings (particularly point loads), can hardly be modelled at all.

Finite element (FE) methods have largely superseded the difference methods then used, and FE methods are used for both shell and discrete (beam) element structures. Although discrete element structures can be accurately and economically modelled for strength, stiffness and stability (including local buckling stability), the solution of continuum structures by FE methods has not been put to general use for the following reasons.

(1) A good FE model for a practical continuum structure must contain significant section changes where the edge beams and diaphragms merge and must generally contain the areas in which the highest stresses may be expected; this becomes a very expensive model to compile, let alone to solve for an adequate number of loading conditions.

* *Present address:* 2 Hove Court, Raymond Road, London SW19 4AG, UK.

@Seismicisolation

(2) The actual medium (*in-situ* cast concrete) is in itself not amenable to the changes of shape and stiffness which enable the optimum form to be achieved. In fact one is constrained to the original form of shell, edge beams and diaphragms as the only practical solution—one which allows little possibility for development.

To overcome these stultifying defects and progress to a form worthy of development, the use of skeletal support is as natural as that of a leaf or a bat's wing; in fan vaulting it was used in building before architecture became a profession.

In this chapter the author wishes to suggest paths by which design and construction methods for braced vaults may be improved and polished and their advantages maximised, to enable them to regain their place as beautiful and useful elements of construction.

2 ADVANTAGES OF THE BRACED VAULT FORM

These can be summarised as follows:

(1) Any shape can be developed in terms of nodal coordinates of the surface. Such a shape need not conform to a simple mathematical equation of curvature, but may be a composite of several, may imply flatness, single or double curvature and may not consciously have a simple mathematical basis at all but be the subject of logical and organic development as was the fan vault.

(2) Any discrete member or superelement comprising discrete members can be given the stiffness it requires to fulfil its purpose within the overall structure. If required, a superelement member can comprise a latticed plane or three-dimensional structure itself.

The forces transferred at joints of these members may be analysed to give finite values from which the strength of the joint can be designed with confidence. In fact logical development of shape can be analysed and supported by mathematical theory.

(3) The same computer program can be used to assess and draft the geometry of each component, draft the complete form of the structure, perform a structural analysis for strength and stability, and list (and possibly detail) the components required, giving the weight of each.

(4) The strength, stability and stiffness of the structure can be accurately established for any combination of applied loads.

The advantages of the skeletal form incur some disadvantageous side effects and it is in countering these that new developments and techniques in construction must be pursued. These disadvantages and possible means of overcoming them are listed from here on.

@Seismicisolation

3 COUNTERING DISADVANTAGES IN THE SKELETAL VAULT FORM

(1) Covering curves and doubly curved surfaces can be uneconomical, unsightly and difficult to weatherproof unless membrane weathering techniques are employed. Self supporting trough sheeting relying on laps or even sealed laps are generally unsatisfactory in all the above respects. Sheet bonded membranes have a comparatively short life and their replacement incurs a heavy maintenance cost; in any case they need to be fully supported. To counter these problems, modern

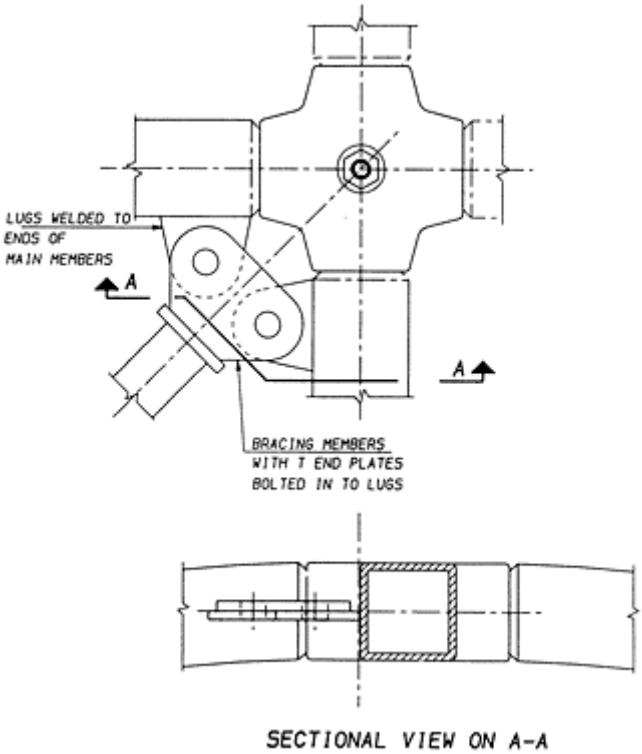

Fig. 12.1. NODUS joint adapted to take in-plane bracing.

pumping and spraying techniques now enable ‘wet’ construction and finishes to be applied at moderate cost.

For example, lightweight concrete reinforced with glass or polypropylene fibres can provide a durable deck structure with excellent thermal insulation and fire resistance. As composite construction, such deck structures can make a significant contribution to the strength of the construction. If a logical sequence is developed for the application, the skeletal frame can be designed to act as permanent shuttering without adding appreciably to its cost and weight.

@Seismicisolation

The top surface of the deck can be finished to provide a good surface to receive one of the sprayed membrane covers which have been developed by the major oil companies.

(2) Discrete members (particularly lattice members) protruding beneath the vault soffit can be unsightly and give rise to corrosion and other maintenance problems at the concrete/steel interfaces.

To counter this these members can be boxed in to provide fire protection and additionally provide service ducting.

(3) Curved and, more particularly, doubly curved members can raise some difficult jointing problems and it is doubtful if computer graphics in its present state of development can handle the detailed design of such complex joints.

Provided symmetrical sections are employed and convergent members are made to meet tangentially to the roof surface of curvature at joints, such connections should not be more difficult to design than joints in a plane grillage (see Fig. 12.1).

(4) More analytical effort would be needed to assess the structure initially as skeletal, than as supporting wet construction and finally as composite construction.

For smaller structures it would probably be uneconomical to carry out the last named analysis, but for major structures the cost of additional analyses would be more than offset in the final construction cost, and a better, more cost effective, structure would result.

4 CONSTRUCTION

The most important factor in the fabrication and construction of braced vaults is accuracy. Effects such as dead load displacements should be carefully considered in design, bearing in mind that the most visible and derogatory defects to final appearance may be edge displacements if the outer edge beams have insufficient stiffness in the horizontal direction.

There would appear to be no great advantage derived from fabricating long narrow panels as advocated in Fig. 12.2(a) and (b). The cost of delivery of such large flimsy panels, coupled to the danger of damage in transit, makes this method unattractive.

@Seismicisolation

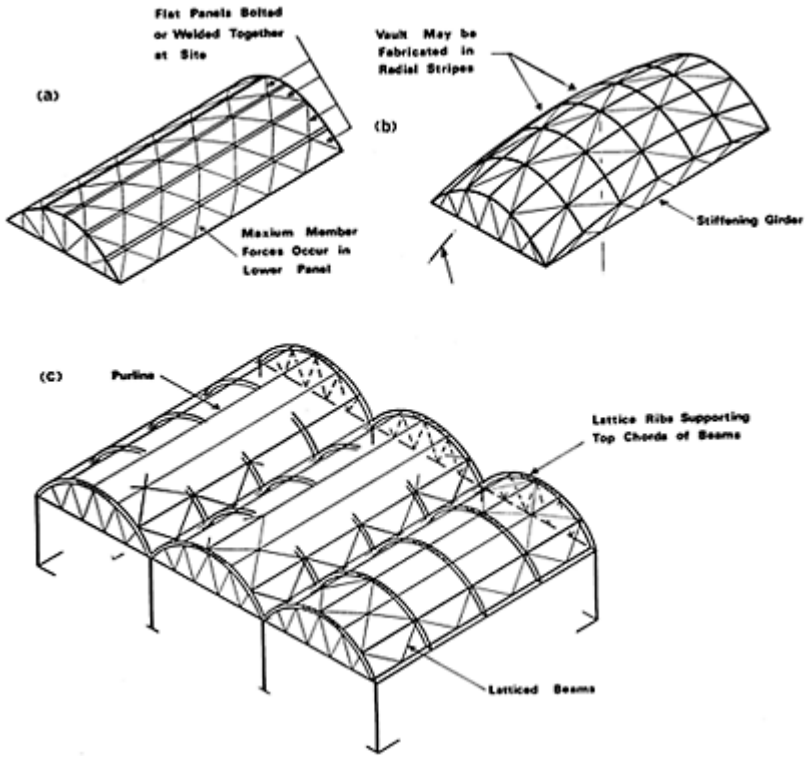

Fig. 12.2. (a) Braced vault made from longitudinal panels. (b) Braced vault from a surface of revolution. (c) Braced vault of sloping beam and rib form.

@Seismicisolation

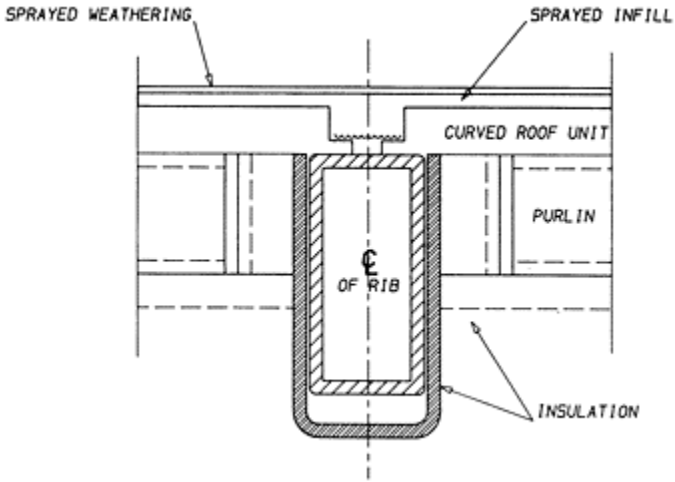

Fig. 12.3.

For type 2(a) the main longitudinal members may be fabricated in lengths of 10 to 15 m with piece-small bracings clipped in at site with mechanical connectors. In this way all welding may be carried out in the fabrication shops.

For type 2(b), as all members with the exception of the stiffening girder and the end diaphragms comprise only three lengths and sections, the use of a standard grid connector appears attractive. By use of accurate jigs the longitudinal, radial and bracing members can be fabricated to close tolerances and connected at site as indicated in Fig. 12.1.

The NODUS connection is used in this illustration but the idea could be adapted to many other standard connectors. It will be noted that only the cover (topmost) units of the joints are used and the bracing members are connected to the radial and longitudinal joints by simple bolted joints. The slight surface curvature theoretically required over the joints will not be noticeable to the eye as the actual joint is very compact. The joint is not detailed in full as its actual format is well documented by the promoters.

Type 2(c) requires longer and more complete members to be sent to site. These could be joined by site welding or bolting; if the former method is used, the site welding should be carried out in a jig specially set up at site.

Figure 12.3 indicates a way in which the joints could be neatly covered and smooth finish applied to the vault soffit.

As all the members in each of the structures illustrated are acting as load bearing members in a skeletal space structure the actual forces to be transferred will be quite small. The shop welds required would probably not be greater than 4·5 millimetre fillet welds and butt welds made on members of less than 6 mm.

5 CONCLUSIONS

For the whole of this century in Britain structural design has been relegated to the rank of pawn to fabrication and construction interests; this is particularly so in the case of the

@Seismicisolation

steel industry. The latter two interests have dominated design, and under this oppression design standards reached their nadir at about the time when welding first became an acceptable fabrication technique. The long, dour rearguard action fought by works managers against such an obviously desirable change as that from gusseted and riveted construction to welding is now past history, but obsolete and unimaginative attitudes persist to dog the British steel fabrication industry. It is true that most steel design is unimaginative in conception, and this is due to the severe discipline imposed on the designer by the necessity of working with prescribed prismatic sections. One should consider that the poetic form most rigidly structured is that of the sonnet; it nevertheless produces the most sparkling and moving lines of all poetry.

Space structures are one path by which the designer can transmute pieces of steel into constructions of great beauty. The braced vault and the dome are the forms which offer the greatest scope to provide beautiful structures; the vault can provide the more practical and flexible covering medium of the two. Even so, unless every small detail is considered carefully in design, to guard against apparent or illusory deflections, patterned weather staining and ugly and obtrusive gutter and downpipe details, some of the beauty will be lost.

Among the many lines written by Alexander Pope, apparently as explicit advice to the design engineer, some of the most apposite must be:

> But of this frame the bearings, and the Ties,
> The strong connections, nice dependencies,
> Gradations just, has thy pervading soul
> Look'd thro'; and can a part become the whole?

Only if affirmatively answered can your structures be as beautiful as his lines.

@Seismicisolation

13
Analysis, Design and Construction of 'Diamond Truss' Type of Three-way Grid Barrel Vaults

F.MATSUSHITA
Tomoegumi Iron Works Ltd, Tokyo, Japan

1 INTRODUCTION

The 'Diamond Truss' system was developed by the Tomoegumi Iron Works Company to satisfy the demand for large span prefabricated structures. Since 1933 thousands of buildings have been constructed in Japan and abroad using the 'Diamond Truss' system. This term covers several types of structures designated as 'Diamond Truss', 'Diamond Shell', New Diamond' and Tomoe Unitruss'.

2 FEATURES

'Diamond Truss' is a grid space framework composed of uniform triangles. As the basic element of structure is a triangle, which is the simplest and most stabilised, this space structure has equal rigidity in every direction, and all structural members of it are in service at all times. It does not require any uneconomical secondary members such as diagonal bracing, tie beam, etc. which are commonly used in conventional truss structures and are put in service only when the structure receives wind pressure or unusual loads of short duration as in earthquakes, etc. The triangle-composing main structural members of 'Diamond Truss' space framework are effectively in service under all load conditions, eliminating uneconomical secondary members and saving the quantity of steel members.

Furthermore, as described later, a 'Diamond Truss' structure is erected without scaffolding, and this is extremely advantageous in erecting a large span structure for economising on the cost of construction, shortening the length of work and removing dangers to which workers would be exposed.

3 ANALYTICAL THEORY

The exact analysis can be carried out by means of the usual stiffness method using a computer. In practice various approximations are used. Normally 'Diamond Truss'

@Seismicisolation

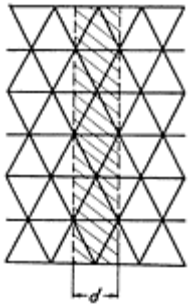

Fig. 13.1. Diamond-shape chain arch.

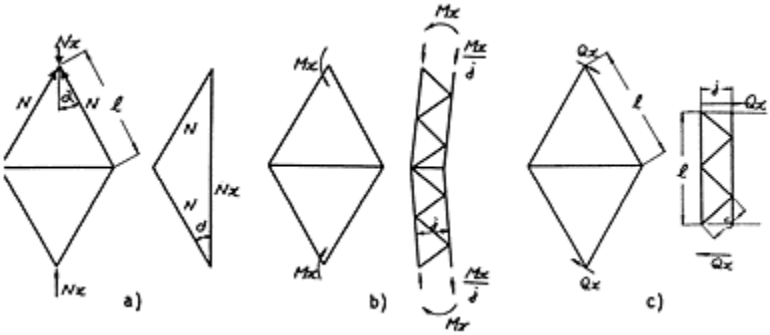

Fig. 13.2. Stress distribution due to (a) axial force, (b) bending moment, (c) shearing force.

structure is regarded as an assembly of many diamond-shape chain arches, the portion enclosed by dotted lines in Fig. 13.1. A diamond-shape chain arch is replaced by an equivalent arch extended in plane, and the stress at each point is calculated. The amount of stress thus obtained for each point is distributed in a diamond-shape arch and the stress of each member is calculated.

First, a diamond-shape chain arch is regarded as an equivalent arch extended in plane, having a width d in Fig. 13.1 as loading reign, and about such a replacement, respective amounts of stress, N_x, M_x and Q_x are obtained according to the ordinary rigid frame calculation. These amounts of stress (N_x, M_x and Q_x) are distributed in the diamond-shape chain arch as follows.

Against the axial force N_x, the stress N in a member of an elemental shape of chain arch shown in Fig. 13.2(a) is obtained by

$$N = \frac{N_x}{2} \times \frac{1}{\cos\alpha}$$

and for consideration of upper and lower chords, the stress N in any one of these two is

@Seismicisolation

$$N = \frac{N_x}{4} \times \frac{1}{\cos\alpha}$$

The bending moment M_x can be treated in a manner similar to the case of axial load when M_x is divided by the distance j shown in Fig. 13.2(b), which is a distance between the centre of gravity of the upper chord and that of the lower chord, and the stress N in a member is obtained by

$$N = \frac{\pm\frac{M_x}{j}}{2} \times \frac{1}{\cos\alpha} = \pm\frac{M_x}{2j} \times \frac{1}{\cos\alpha}$$

Consequently, the stress N in any one of the upper and lower chords is

$$N = \frac{1}{2\cos\alpha}\left(\frac{N_x}{2} \pm \frac{M_x}{j}\right)$$

The shearing force Q_x is countered by the lattice bars of the chain arch, and the stress Q in a lattice bar is obtained by

$$Q = \frac{Q_x}{2} \times \frac{S}{j}$$

(see Fig. 13.2(c)). There are more than ten different shapes of 'Diamond Shell' structures though the three-way cylindrical braced barrel vault is probably the most commonly used in practical applications. The analysis of structures of this type is frequently carried out by the shell analogy in which the actual space grid steel framework is replaced by an equivalent shell. This technique, developed by the author, is known as the Equivalent Shell Replacement method.

In Fig. 13.3 the hatched portion is regarded as a structural element, and an imaginary shell having the same height, width and thickness as the said element is considered. The respective modulus of elasticity is calculated, and the imaginary shell is made to be elastically equal to the element. Such a modulus is termed a 'modulus of equivalent elasticity'.

First, the equivalent Young's modulus is obtained as follows.

In Fig. 13.4 the external force P is applied to the element and the amount of displacement δ is calculated. Then the Young's modulus of elasticity for a shell having the same height, width and thickness as the element is calculated to satisfy the condition that the same amount of displacement δ will be caused in the shell by the same external force P. This is the equivalent Young's modulus. In the same manner, G and v are obtained using the following expressions developed by the author.

@Seismicisolation

$$E_\varphi = \frac{E_s A_s \cos^3 \alpha}{hl \sin \alpha (1 + \sin^3 \alpha)} = E$$

$$E_x = \frac{E_s A_s}{hl \cos \alpha} = KE$$

$$\frac{G_{\varphi x}}{G_{x\varphi}} = \frac{E_s A_s \sin \alpha \cos \alpha}{hl} = G$$

$$\nu_\varphi = \frac{\sin \alpha \cos^2 \alpha}{1 + \sin^3} = \nu$$

$$\nu_x = \tan^2 \alpha = k^\nu$$

$$k = \frac{\sin \alpha (1 + \sin^3 \alpha)}{\cos^4 \alpha}$$

where E_s=Young's modulus of a truss member (2100 tons/cm^2), A_s=sectional area of a truss member (the sectional area of member No. 3 only is regarded as $2A_s$), E_φ=Young's modulus of equivalent shell in the φ direction, E_x=Young's modulus of equivalent shell in the x direction, ν_φ=Poisson's ratio of equivalent shell in the φ direction, ν_x=Poisson's ratio of equivalent shell in the x direction, G=modulus of rigidity of equivalent shell, and h=thickness of equivalent shell.

With these moduli, the stress calculation is made for the equivalent shell, and by applying such results to the said structural element, the stress in each member of the element can be obtained.

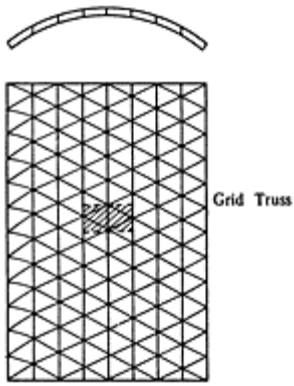

@Seismicisolation

Fig. 13.3. A typical three-way single-layer braced barrel vault of cylindrical shape.

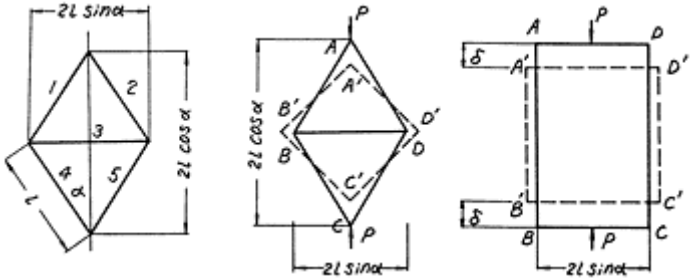

Fig. 13.4. Deformations of truss and imaginary shell.

4 METHOD OF CONSTRUCTION

The diagonally crossing members in ‘Diamond Truss’ structure consist of those alternately extending in the upper left direction and in the upper right direction, and each one member has the length extending over three crossing points (Fig. 13.5).

In constructing this structure, the main side columns, girders, gable columns and gable beams are first erected, and then the erection of the Diamond Truss frame is started from

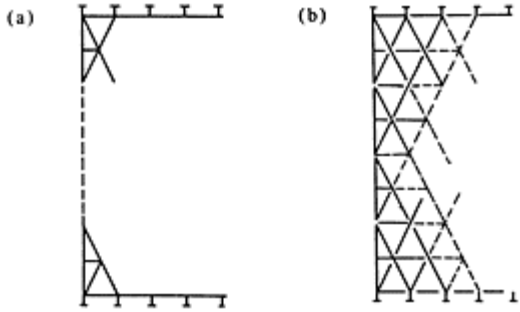

Fig. 13.5. Sequence of erection of ‘Diamond Truss’ structure.

respective corners as shown in Fig. 13.5(a). After erecting the portions shown with the solid line in Fig. 13.5(b), the workers can climb such erected portions, which are sufficiently stable, for continuing the erection work thereafter without the necessity of scaffold. This is what we term a ‘no-scaffold’ erection method.

@Seismicisolation

5 PRODUCTION TECHNIQUES

The design techniques of 'Diamond Structures' have been described by the author elsewhere[1] and therefore the purpose of this chapter is to emphasise the production methods used by the author's company and to describe the future development.

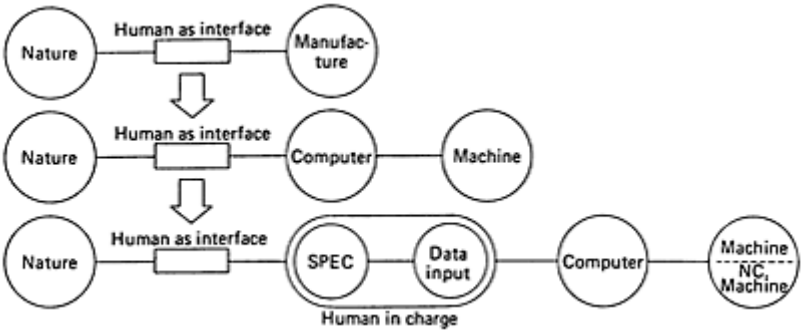

Fig. 13.6. Future prospect of human part in manufacturing activity.

5.1 Improvements in Production of Space Structures by Means of Automatic Machines

It is only a dozen or so years since numerically controlled (NC) machines were introduced into steel workshops. In the meantime the prices of NC machines, robots and conveyors have fallen so sharply that many firms are now able to improve their production methods by using these machines. This development changes in a significant way the interface between Man and Machine. Man can be completely freed from manual work, though process management and information control still depend upon technical manpower (Fig. 13.6).

The introduction of automatic production machines means that Man's task is to prepare production design specifications and input data for the computer leading to an automatic flow production. The interesting point, which has to be emphasised, is that complex space structures consist of members which may be different from each other and joined at different angles. The manual production and assembly of such systems is obviously very expensive. On the other hand, NC machines may produce both the identical or different members in about the same time and at the same cost. It is obvious, therefore, that in order to maintain and extend the market for space structures, a fully automatic production method has to be adopted.

5.2 Production Methods

Figure 13.7 illustrates the interaction between the requirements (specifications), control and error checks for multiformity structures.

@Seismicisolation

Present production methods are divided into four classes according to the product and its quantity, as shown in Fig. 13.8.

One piece of one type should be made by means of individual manufacturing, but five pieces of the same type can be made through lot manufacturing. As the production

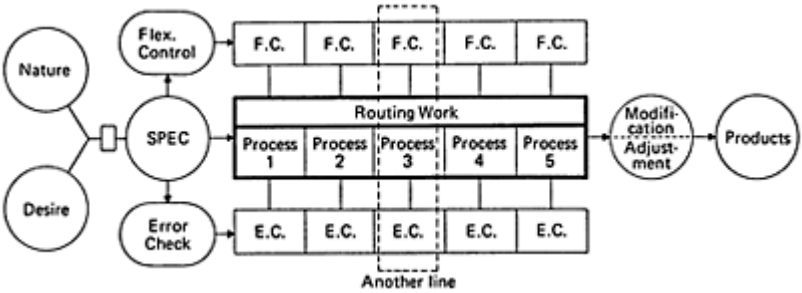

Fig. 13.7. Production method for multiformity of structure.

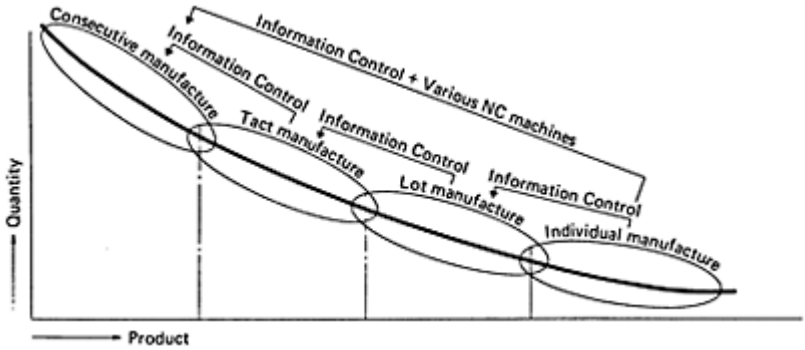

Fig. 13.8. Consecutive manufacture by information control and NC machines.

increases, the tact manufacture method is applied in which materials are fixed at a place for a limited time and are removed to another after finishing the operation. In the case of mass production, a consecutive manufacturing method such as the conveyor system can be applied. As a matter of course, the productivity becomes higher in the order outlined above, i.e. first individual manufacture, lot manufacture, tact manufacture and finally consecutive manufacture.

It is possible to advance the production method step by step. For example, as mentioned above, NC machines can produce ten pieces of one type and ten-type pieces in almost the same time. If the member information for five-type pieces is obtained by computer and is output as NC tape for manufacture, the productivity for five-type pieces is much the same as that for five pieces of one type. Consequently, the individual

@Seismicisolation

manufacturing method can be promoted to the lot manufacture method, the method one step higher.

Further, by installing various NC machines with the same manufacturing process but different functions, in addition to the information control, the individual manufacturing method can be advanced directly to the consecutive manufacturing method, though the paths of members are different from each other.

Next, the important thing in the production method for multiformity is that in preparing the specification and production facilities line, the routine work, the fixed and regular specification (given in the middle of Fig. 13.7), is of no use.

Each of the partial manufacturing processes must be separated from the others and controlled flexibly. The specification should be divided into several parts having a partial manufacturing process independent of the others and controlled flexibly. It is quite useless to amend the whole process resulting from alternations in the product.

Similarly, the error check, independent of the whole process, should be incorporated into each partial process. But for the error check in a partial process, some troubles would not be found until the assembling reached its final stage and the check would be made over the whole process. In the production methods, in addition to the routine work, the independent line of the flexible control and error check will be necessary.

5.3 Production Method of 'Diamond Structure'

At present our 'Diamond' system has structures of 17 shapes, and 'Unitruss' system developed recently has structures of several shapes. As shown in Fig. 13.9(1), the structures with double curvature are more complicated than those with single curvature, and the compound structures are more intricate still. The structures with free form are the

@Seismicisolation

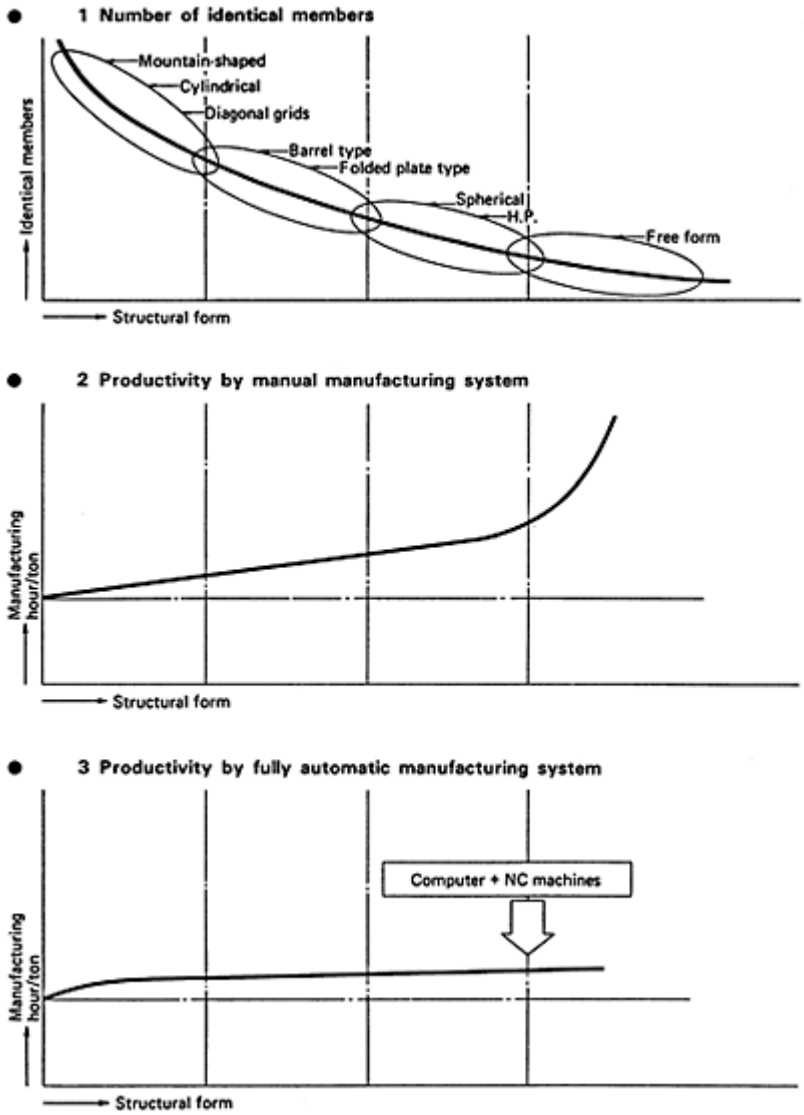

Fig. 13.9. Production cost of 'Diamond Truss' system.

most complicated of all, and it is impossible to control the production information of the members without a computer, and to manufacture the members without NC machines.

Figure 13.9(2) shows a model of productivity by manual manufacturing system. As mentioned above, the structures with free form are too intricate to be manufactured manually, and therefore the plot is a purely imaginary line. By applying the production method for multiformity to space structures, it is presumed that production by a fully

@Seismicisolation

automatic manufacturing system can be obtained as in Fig. 13.9(3). Here, interpolation is made because all structures have not yet been manufactured using this method. The manufacturing cost for the structure with free form does not increase so much compared

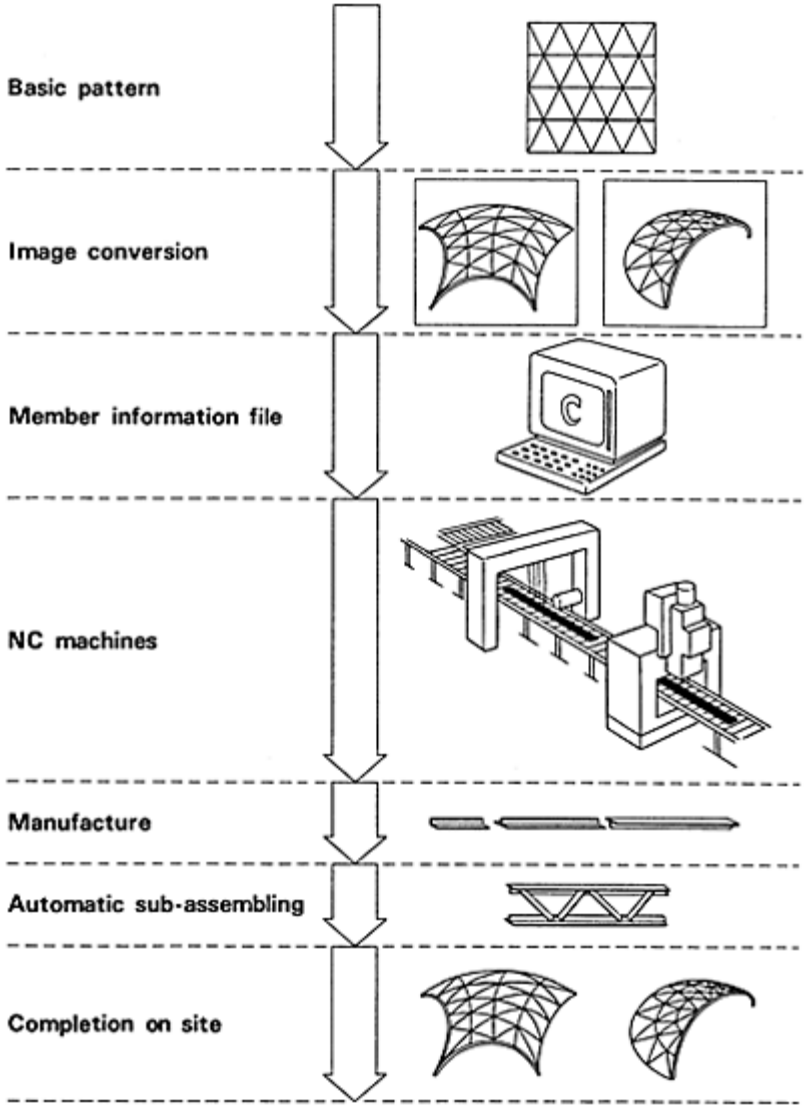

Fig. 13.10. Flow of automatic design and manufacture for 'Diamond Truss' system.

@Seismicisolation

with that for the other structures, and there is little difference among them. The reason for this is that nowadays almost all products of our firm are manufactured by a fully automatic manufacturing system. In the case of the structure with free form, the 'Unitruss' system is frequently used and the material cost of metal fittings at the joints increases sharply.

Figure 13.10 shows the flow of automatic design and manufacture for 'Diamond Structures'. First, basic patterns are defined on the plane and they are then changed into the desired shape by means of image conversion. Second, manufacturing information of members is obtained by computer and is output as NC tape for manufacture; then the NC tape is input to NC machines in the automatic production line to work the members of structures. When a simple steel member is being wrought, factory workers can understand only the member sign but cannot understand what shape the structure is as a whole. Lastly, after parts are manufactured, necessary parts are collected and an automatic sub-assembling is made through member information of an assembled member. Thus, manufacturing in a factory is completed.

The steel members are sent to a building site, and erection work is executed there. However, it is still very difficult to automate the working process on site, unlike in a factory; therefore conventional erection methods are still being used.

REFERENCE

1. Matsushita, F. Diamond dome systems, in *Analysis, Design and Construction of Braced Domes* (Ed. Z.S.Makowski). Granada Publishing, London, 1984, Chapter 17, pp. 487–520.

@Seismicisolation

14
Architectural Aspects of Braced Barrel Vaults

S.DU CHÂTEAU
Institut le Ricolais, IRASS, Paris, France

1 INTRODUCTION

The application of the concept of cylindrical barrel vaults requires an insight into the inter-relationship of their topological, aesthetic and structural properties, as well as an investigation into their specific form and an architectural justification for their use.

Architecture is concerned with enclosing space, and therefore its principal objective is the investigation of the use of volume which is created by the building and its architectural function. ‘ln the research, what drives us mostly is the urge to fill the existing gap in our knowledge’, said Le Ricolais.

The means to fill such a gap or to organise and to arrange space are of secondary importance and can be envisaged as a material constraint, imposed by technological or economic considerations.

In research, reflection and ingenuity are essential to produce optimum solutions. One encounters curved surfaces of circular cross-sections in Nature. They are created by insects and animals, in most cases beneath the surface of the earth. Such a typical example is the surface produced by a mole, which consolidates the friable soil by means of its own back. Other animals dig out their shelters in the form of underground passages producing functional space for their dwellings which protect and safeguard them.

Probably the most astonishing and remarkable is the ingenuity of a small predatory crab of Malaya, which constructs its own shelter in the form of a regular barrel vault (shown in Fig. 14.1), where the dimensions as well as the created form represent a truly striking example of a three-dimensional arrangement of space. One finds similar examples in human activities. An early cave dweller found in his cavern, often through chance, all the basic conditions of a shelter allowing him to develop the sedentary family, as well as a community lifestyle.

And so this enabled the first relationship to be formed between his life and his gradual progress. In addition the interior space forming his shelter is also the first manifestation of the architectural necessity, in its most intimate aspect. Thus through thousands of years of development of human life, we are bequeathed objects illustrating Man’s life, art and civilisation.

It is obvious that as soon as Man left his cave, he had to start constructing his shelter.

@Seismicisolation

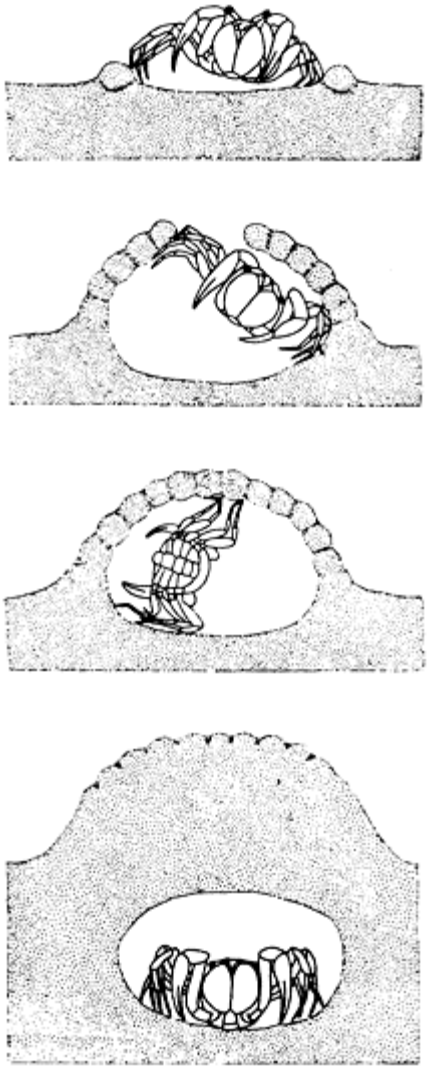

Fig. 14.1. Construction of a three-dimensional shelter by a crab native to Malaya (after D. Hancocks—*Animals and Architecture*).

Originally it was built with the same material and had an identical form, by virtue of placing stone upon stone in the form of an arch. Typical examples of this type of structure are preserved in Provence and Tuscany (Fig. 14.2), as well as the Aztec Temples from Central America. Thousands of years were required to achieve the perfect regular geometry of the masonry vault. The precise stereotomy of the appropriately

@Seismicisolation

proportioned stone blocks permit the gradual and gentle flow of forces in such systems, even in the case of great spans achieved for monumental structures.

The introduction of reinforced concrete shells and the technique of prestressing concrete have permitted an evolution towards greater lightness and larger spans which has led to the practical achievement of structures of very large dimensions.

Nowadays it is necessary to realise that the solutions in steel skeletal systems allow even greater spans and permit the designer outstanding performances in the sense of a bold structural approach and very large, clear spans.

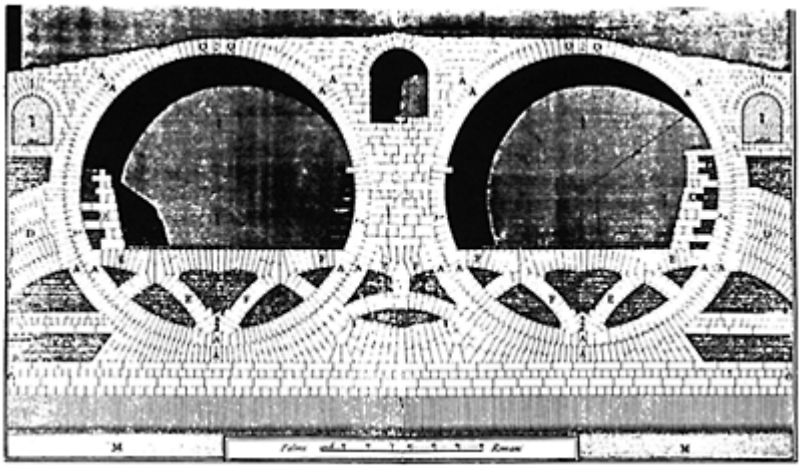

Fig. 14.2. Consolidation of foundations for a bridge through arch construction (after Piranesi).

2 RETICULATED BARREL VAULTS

Considering the possible general geometries of barrel vaults, one normally distinguishes two main types:

(i) cylindrical barrel vaults of rectilinear grids which are developable;
(ii) structures of double curvature, not developable, and usually of the toroidal shape.

There are, of course, other possible geometries, but as they do not lead to regular arrangements of members they are rarely used in practice. To give overall stability to the structure, end diaphragms have to be provided; they can be of different configurations. Their geometry influences in a significant way the visual effect of the architecture of such structures through their rhythm of expression, as they are visible not only from the outside but also from the inside.

There is no doubt that the type of roof covering on the exterior of a barrel vault is responsible for the final aesthetics of the structure. Lightweight steel barrel vaults often

@Seismicisolation

provide the most efficient solution, and in addition give the required stability to the structure. In a way their action is similar to a three-dimensional truss working under flexure and supported at its two ends. On the other hand, barrel vaults supported longitudinally exhibit the characteristics of the stress distribution of an arch.

3 PRACTICAL APPLICATIONS

3.1 A Braced Barrel Vault Stabilised with Two Triangulated End Diaphragms over the Tennis Court SNCF in Paris (Fig. 14.3)

The principle of a rigidly connected three-directional single-layer grid of a cylindrical form, having its stability provided by the end diaphragms, has been applied to the construction of a covered tennis court for the SNCF at Paris-Vaugirard.

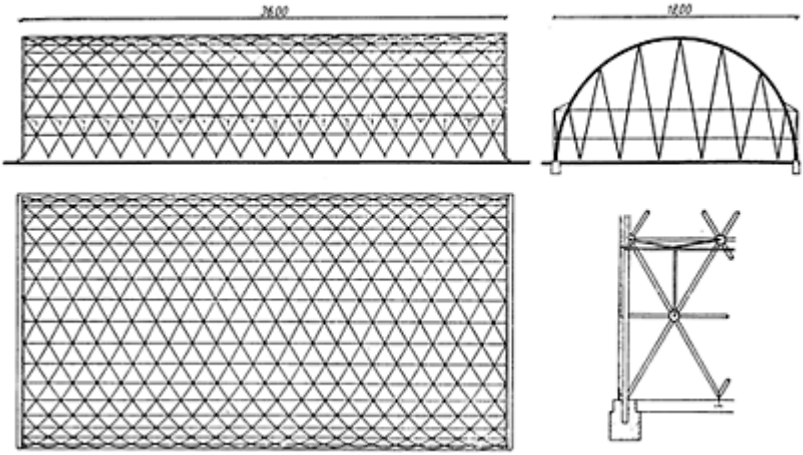

Fig. 14.3. The plan and elevations of the braced barrel vault at Paris-Vaugirard.

This building has a width of 18 m and a length of 36 m; its height is 9 m. The structural framework is in the SDC system. The OD of the tube members used in this case is 60 mm, the thickness of the web is 5 mm and the nodes are provided by a special type of connector produced in weldable cast steel (Figs. 14.4 and 14.5). This structure was prefabricated at the works in longitudinal elements having a width of two modules and a length of 9 m.

Such prefabricated welded units are fixed in position on site using the minimum of support; they are interconnected with intermediate tubular members inserted on site into the connectors and welded into a completely rigid structure (Fig. 14.6).

@Seismicisolation

The covering is made from overlapping curved thin corrugated sheets of polyvinyl following the curvature of the barrel vault. The sheets are restrained by means of cables which are fixed at their ends to the longitudinal strip foundation along the sides of the

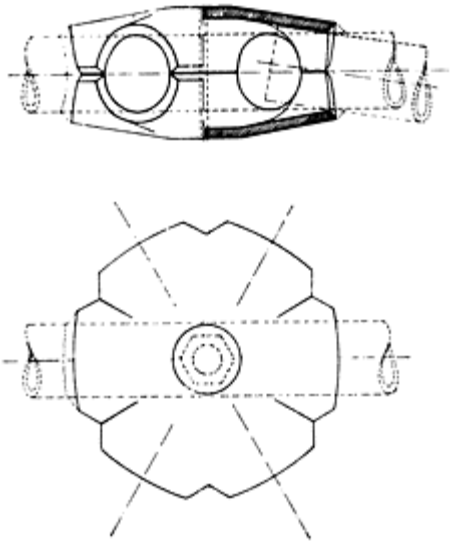

Fig. 14.4. The SDC joint.

@Seismicisolation

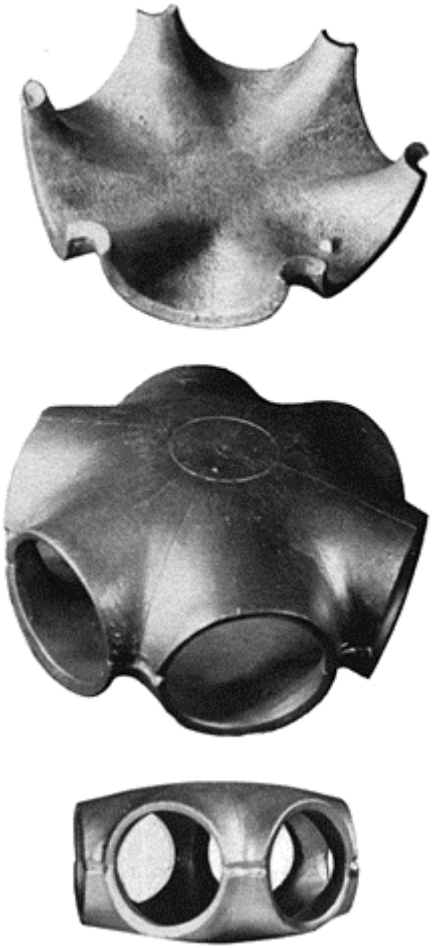

Fig. 14.5. Component parts of the SDC joints.

structure. In this way the plastic covering is waterproof and retains complete freedom of thermal expansion (Fig. 14.7).

The structural simplicity, the exceptional lightness and pleasant aesthetics of its external appearance are the main characteristics of this structure (Fig. 14.8). The SDC nodal connector in cast steel allows a simple connection of tubular members which after the required adjustments are then welded to the connector. Figure 14.9 gives the internal view of the structure.

@Seismicisolation

3.2 Barrel Vault for the Academy of Montpellier—The University Sports Centre of the Motte Rouge in Montpellier (Architects P.Jaulmes and J.C.Deshon)

In this case a circular braced barrel vault has been used with conoidal end diaphragms. The central part of the circular barrel vault has a length of 39 m and a width of 22·8 m, enclosed at its ends by two conoidally-shaped triangulated trusses extending the full length of the structure to 44 m (Fig. 14.10).

The plastic covering is supported by additional transverse elements and fixed to r.c. strip foundations. The structural framework also supports the ventilation and lighting equipment suspended under the structure. The steel frame consists of prefabricated tubular elements of square shape, 2·12 m wide, manufactured in rectangular hollow

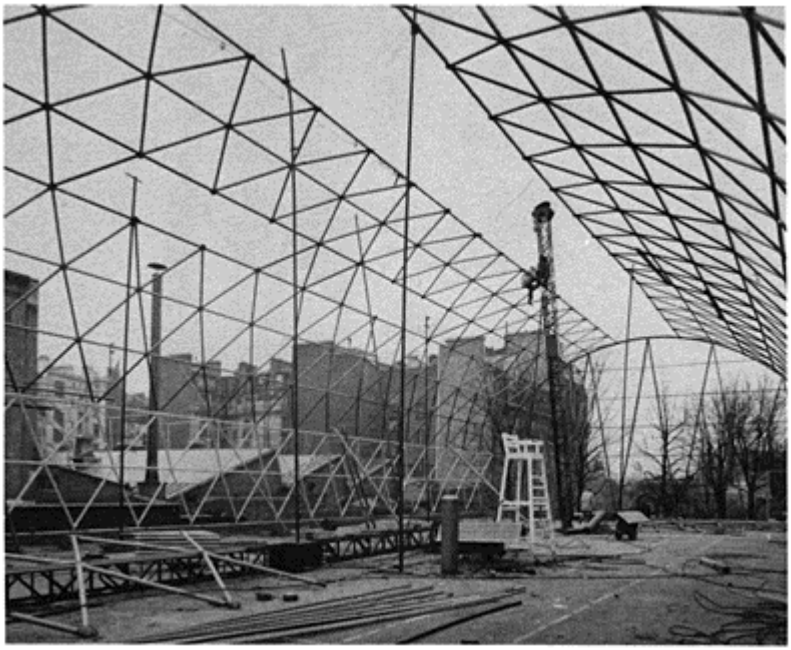

Fig. 14.6. Site erection of the Vaugirard barrel vault.

@Seismicisolation

Fig. 14.7. Inside view of the barrel vault during construction.

Fig. 14.8. The inside view of the finished structure.

@Seismicisolation

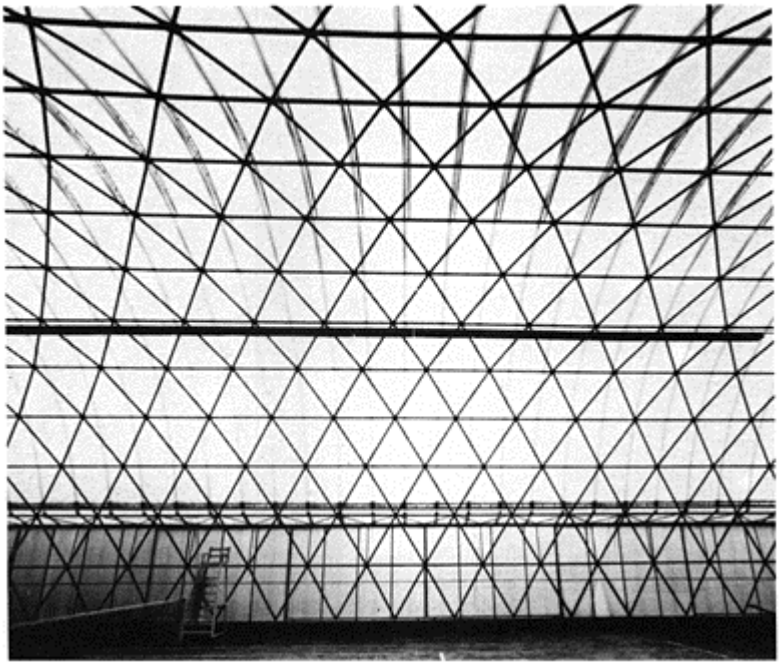

Fig. 14.9. The side view of the barrel vault covered with corrugated translucent plastic sheeting.

@Seismicisolation

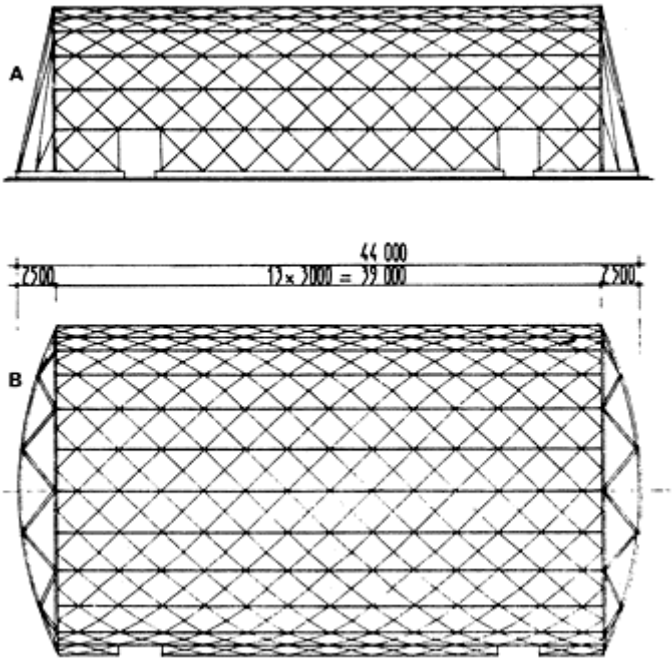

Fig. 14.10. The elevation (A) and plan (B) of the Montpellier barrel vault.

sections 80×40×4 mm and arranged after bolting into a two-way truss running in the longitudinal direction and connected to two adjacent continuous I sections (60 mm high) by means of high tensile bolts.

At the gables the main framework is supported at the boundary by an arch stiffened by inclined diagonals forming a fully triangulated stiff end diaphragm (Fig. 14.11). At the north side of the barrel vault are two openings protected by steel door frames built into the inclined surface of the structure. The assembly of the structure has been carried out with high tensile bolts. The protection of the surface of all the steel elements is performed by hot galvanisation undertaken after the welding in works. The prefabricated elements, when bolted together, automatically produce the required curvature of the barrel vault (Fig. 14.12).

The material used for covering the structure is a fabric made from glass fibre reinforced polyester and coated on each side with PVC.

@Seismicisolation

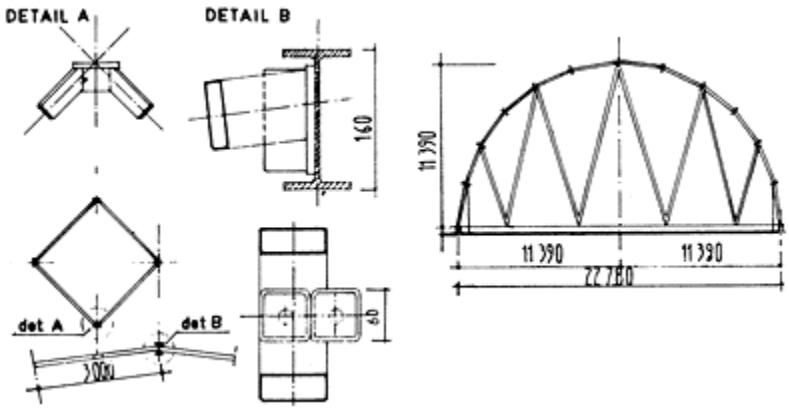

Fig. 14.11. Details.

Fig. 14.12. Inside view of the Montpellier barrel vault.

The roof covering to the structure consists of four separate segments in the longitudinal direction together with two separate fabrics over the conoidal gable ends. On the cylindrical part the roof covering is supported by tensile cables fixed at their ends to the foundation blocks. On the conoidal end diaphragms the fabric is fixed to the structure by means of hangers and connected to hooks embedded in the r.c. foundation. The wind loading is resisted by the main structural frame. The tensile wind forces developed in the

@Seismicisolation

fabric are resisted by the additional transverse members and carried to the main structure. At all contact points between fabric and frame special attention has been given to the production of smooth edges so as to prevent any danger of damage to the fabric.

3.3 The Barrel Vaults over the Gymnasium for a Grammar School in Carpentras

(Architects A.Gregoire and Biscop)

The structure consists of five braced barrel vaults, each having a rectangular arrangement of longitudinal members and ribs, stiffened by additional slender diagonals forming, in effect, a four-way single-layer grid. In contrast to the formal and rather restrained shape of the main buildings of this school, the architects have treated the gymnasium in a very dynamic fashion by covering the gymnasium without any internal supports by means of a series of five interconnected barrel vaults, each of double curvature and having an unsupported length of 18 m and width of 6 m (Fig. 14.13). The covering in this case consists of ceramic tiles. The transverse arches of the barrel vaults are of rectangular hollow sections 30×60 mm, whereas the longitudinal members are made with tubes of circular cross-section ø 50/60 mm and welded at the joints (Fig. 14.14).

The diagonals are steel rods of appropriate sizes to ensure the stability of the structure, not only under the vertical load, but also under wind action, the intensity of which has been assumed in the analysis to be 200 kg/m2.

@Seismicisolation

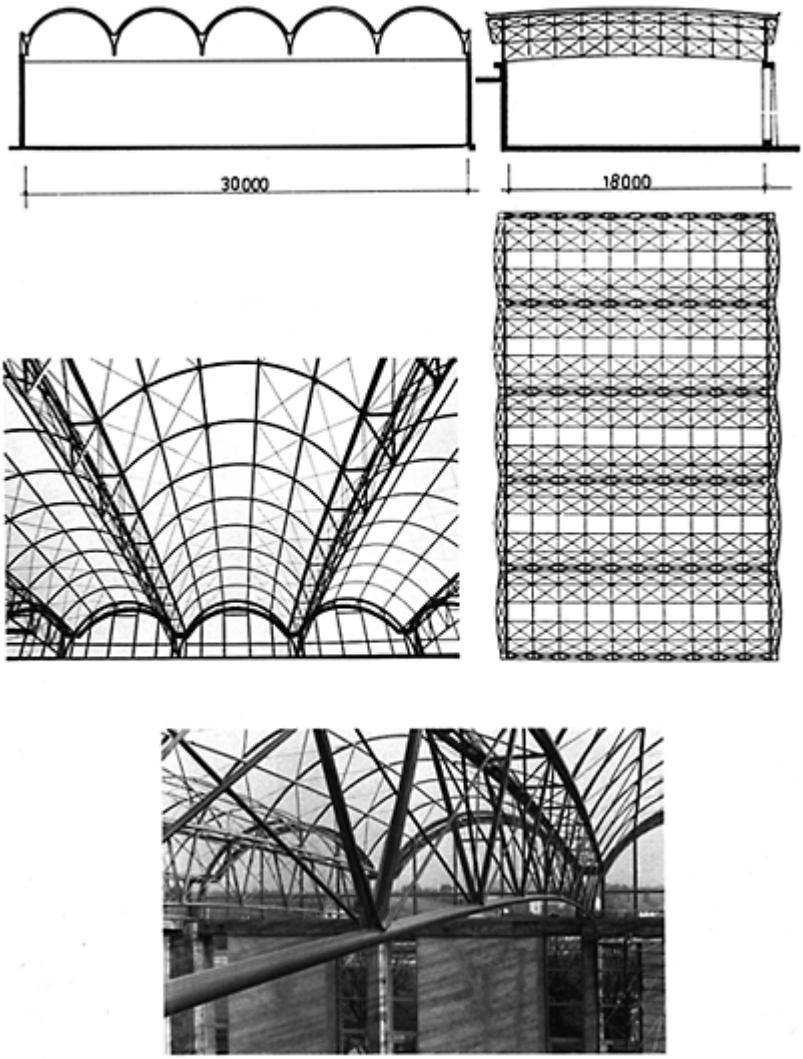

Fig. 14.13. Plan, elevation and view of the five barrel vaults covering the gymnasium at Carpentras.

@Seismicisolation

Fig. 14.14. Longitudinal view of the barrel vaults.

The diagonals are interconnected in each trapezium creating a light but strong four-way grid bracing.

Gutters are formed at the junctions of barrel vaults, which are not only cylindrical in the transverse direction, but also curved in the longitudinal direction, facilitating the removal of rain water from the roof surface.

The framework has been prefabricated in the works in panels consisting of double modules and assembled on site by welding into a rigid frame. (Figure 14.15 gives the internal view of the gymnasium.) The glazing of the vertical diaphragms lets the light into the interior of the structure, which, because of the absence of any protruding bracing members, creates visually an extremely pleasant view. Externally the architectural treatment provides a structure which is rational and logical from the structural point of view. The stress analysis of this structure, assuming rigid joints, was carried out by Z.S. Makowski.

@Seismicisolation

Fig. 14.15. The internal view.

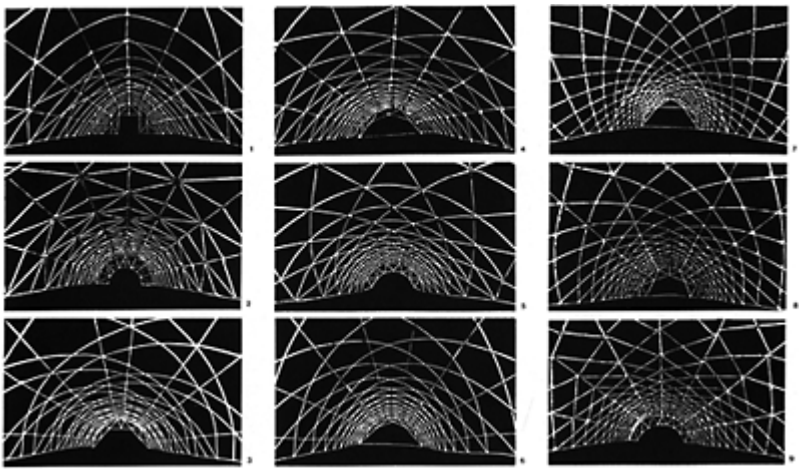

Fig. 14.16. Fifteen types of bracing used in the experimental studies of braced barrel vaults.

@Seismicisolation

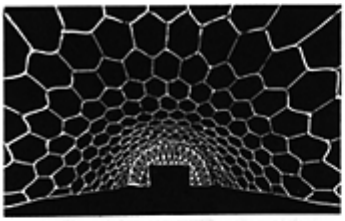
10

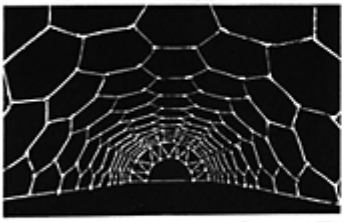
11

12

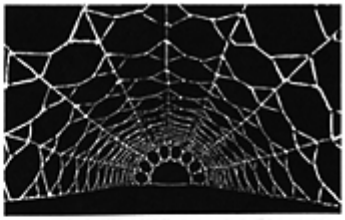
13

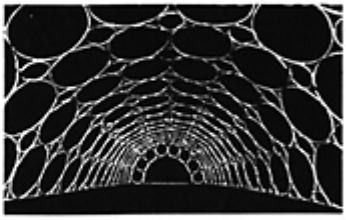
14

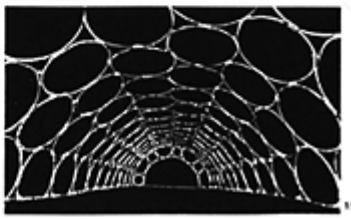
15

4 RESEARCH

The studies illustrated in the following figures and carried out under the guidance of the author are the results of 15 investigations undertaken by architectural students of the UPA7 (Paris 6e) School. The object of this research was the experimental analysis of the stability behaviour of braced barrel vaults in relation to their consumption of structural material. The illustrations included in this section refer to small scale models, each 60 cm long and 20 cm wide, built and tested by the students. Altogether 28 different types of bracings were investigated during this experiment, to obtain an optimum system of bracing for steel braced vaults.

The models, subjected to vertical loading, were supported only at four corners. All of them are stiffened by end diaphragms. During this investigation, special attention was paid to:

— number of bars,
— number of nodes,
— total length of members,
— total weight,
— time required to produce a model.

The comparison of deflections of the models under the applied loading, the same for all models, gave an indication of relative stiffness of the structure. During the investigation, models undergoing large deformations were strengthened by the successive addition of bracing members. This allowed a comparison of the improvement in the overall

@Seismicisolation

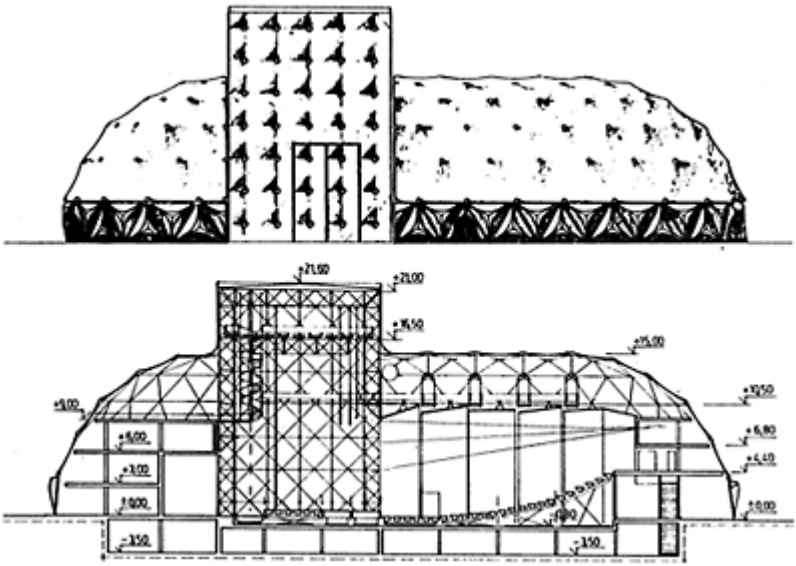

Fig. 14.17. A design proposal for a theatre to be covered with a tubular barrel vault.

rigidity—an exercise extremely useful to the students who took part in this exercise. Figure 14.16 (1–15) illustrates fifteen different types of bracing investigated in this study.

Figure 14.17 illustrates a design proposal for a theatre covered with a tubular braced barrel vault. In this case the Spherobat connector was envisaged for the structure. The central part of the building, housing a raised podium, is of double-layer construction. The barrel vault proper is of single-layer three-way grid type.

@Seismicisolation

15
MERO Braced Barrel Vault Structures

HERBERT KLIMKE and HELMUT EBERLEIN
MERO-Raumstruktur GmbH & Co., Würzburg, West Germany

1 INTRODUCTION

Barrel vault structures were first used in the nineteenth century to cover large span cast iron greenhouses, and many of them were built in this material at that time, especially in Great Britain.

In Germany thin reinforced concrete barrel vault shells were introduced by W. Bauersfeld and F.Dischinger in the 1920s. These two designers developed the famous Zeiss-Dywidag system for the construction of domes and barrel vault concrete shells, using a special type of braced steel scaffolding. Their first large span structure of this type was built over the market in Frankfurt/M. in 1927.

The MERO building system was introduced in 1940 by Dr Max Mengeringhausen[1] as a solution for structural problems related to the design of three-dimensional space structures through the development of a simple connector allowing the interconnection of up to 18 members in space. The MERO system was initially applied to various types of plane and space grid frameworks, especially in the field of double-layer grids. Only recently its use has been extended to braced domes and double-layer barrel vaults. Important examples of their application include grandstands covering stadia in Berlin, Germany and Split, Yugoslavia, and a large span convention hall in Münster, Germany, as well as several gymnasia in Japan.

2 STRUCTURAL ANALYSIS ASPECTS

It was A. Föppl[2] who discovered the influence of cross bracing on the behaviour of braced barrel vaults. This was the key factor in the understanding of the structural load carrying capacity of barrel vaults as space structures.

Using cross bracings all loads are transferred to the supports by shear only, i.e. the structure can have no bending stiffness. Without cross bracings a non-symmetrical load can only be transferred by a rigid arch type structure. Most barrel vaults built, especially those by MERO, provide a combined load carrying capacity corresponding to those two types of structural behaviour.

The approximate analysis of braced barrel vaults can be performed by the shell analogy. The differential equations describing the membrane behaviour of barrel vault shells were developed by Bauersfeld in 1923. The bending theory was developed by Finsterwalder in 1930.[3]

@Seismicisolation

Nowadays, finite element approaches are used for the analysis of braced barrel vaults. They are commonly based on the stiffness method. MERO uses the MEFA (MERO Elastic Frame Analysis) program for linear and non-linear analysis. Non-linear analysis is becoming necessary for the solution of stability problems of single-layer membrane or double-layer wide span structures.[4] MEFA is part of the MERO program for the computer aided design (CAD) of MERO space trusses.

3 MERO APPLICATIONS

3.1 Berlin Olympic Stadium Roof

The problem consisted of designing two space structure roofs to cover an approximate ground area of 17 000 m^2, which had to be adjusted to an existing stadium structure. The stadium was originally built for the 1936 Olympic Games by Professor W. March and was at one time going to be used for the soccer world championship in 1974 (Fig. 15.1).

Fig. 15.1. General view of the Berlin Olympic stadium roofs.

The design involved a number of problems regarding the geometry of the structure, which had to match the existing structural boundary conditions of the stadium, and had to satisfy the demand for material optimisation of the space structure.

The solution, once found, was relatively simple: the geometry of the space trusses had to be developed on conoidal surfaces with a common apex. These surfaces provided two advantages:

(1) The circular basic edge of the inner cone could be adjusted approximately to the existing stadium edge. The remaining differences could be resolved by using a supporting frame structure as shown in Fig. 15.2, where the edge nodes have been moved on to the cantilevers of the frames and the trapezoidal columns moved on to the supporting beams, which were anchored each on two of the stonework columns of the existing stadium structure.

@Seismicisolation

(2) A trapezoidal $\frac{1}{2}$O+T-based truss geometry consisting of half octahedra and tetrahedra could be optimised so that only one node type (angles of connecting members) became necessary for the bottom and top chords, respectively. This was possible by developing the chord member lengths with a geometrical series (Fig 15.3).

Fig. 15.2. Supporting frame structure for the rear edge.

@Seismicisolation

Fig. 15.3. Curvature and inclination of one roof.

@Seismicisolation

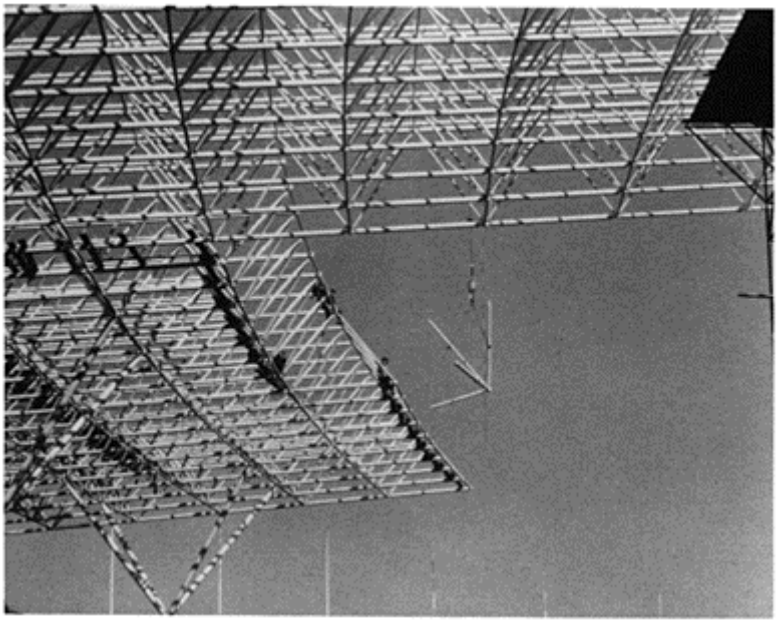

Fig. 15.4. Erection by free cantilevering.

The 55·5 m cantilevered roof is supported by a number of very slender columns (full circular steel sections with a diameter of 270 mm). Each column is connected to the structure by four members, forming a half octahedron. The free cantilevering length of the roof was thus reduced to 37·7 m. To take the tension of the cantilever action, prestressing cables had to be placed inside a specially drilled circular shaft hole in each of the 16m high stonework columns, which form the back of the stadium.

The erection was carried out using three different methods: first, preassembly of the rear parts and lifting them into place; second, free cantilevering (Fig. 15.4); and, finally, assembly of the front parts on scaffolding. The cladding elements are transparent acrylic barrel vaults.

The solution proved that the use of curved space trusses can solve the problems of adjusting and optimising geometry at the same time. This investigation was done by Professor Dr H.Emde at the University of Darmstadt, West Germany.

3.2 Split Stadium Roof

Two wide span double-layer barrel vaults were built by MERO[5] in 1979 (Fig. 15.5). The two structures together cover a ground area of 13600 m2 600 m^2, providing a maximum span of almost 215 m at the ends of a roof s edge. Geometrically, each roof surface is cut from a slightly inclined circular cylinder of 226 m radius by a series of ellipses. The space frame is based on a 3×3 m module with a 2·3 m structural depth, which leads to an *l*/*h* ratio of about 90. Each roof consists of 1730 spherical nodes and 6191 tubular

@Seismicisolation

members of 839 and 1143 different types respectively. The distribution of member sizes is given in Fig. 15.6 and a view of the skeletal structure in Fig. 15.7. The structural analysis has shown (see Fig. 15.6) that the system is mainly acting as an arch with only small bending moments. The stability check became the key problem of the analysis. A 'Modified Newton-Raphson' approach[6] was chosen for the non-linear analysis of the structure, considering geometrical and structural imperfections.

The structure demonstrates the important contribution of computer aided design (CAD) methods for the design, analysis and construction of space trusses. In particular,

Fig. 15.5. Bird's eye view of the Split stadium.

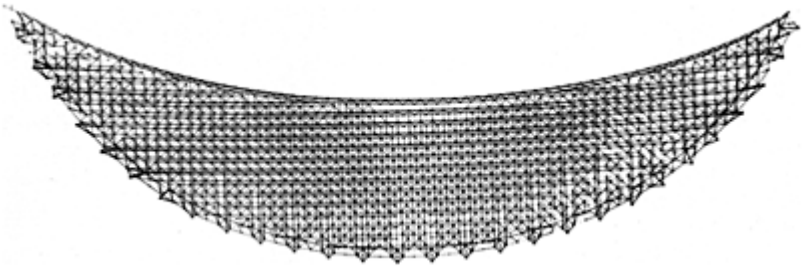

Fig. 15.6. Member arrangement of the Split stadium roof structure.

@Seismicisolation

Fig. 15.7. One completed roof structure including transparent cladding.

Fig. 15.8. Erection procedure of the Split stadium roof.

the decision (and necessity) to produce a regular cylindrical mesh compatible with the edge curves of the given stadium geometry required a powerful tool for solving the problems of structural optimisation and construction; for example, Fig. 15.6 was used to

@Seismicisolation

find an appropriate arrangement for the supporting members. The ‘smooth’ flow of forces shown in Fig. 15.6 is the result of the optimisation process.

The erection started at the centre of each roof. Scaffolding was used to assemble a middle section, which enabled the remaining side parts of the structure to be erected by free cantilevering. The free edge was supported by temporary towers (Fig. 15.8) which were removed after completion. This operation proved to be the most critical of the whole erection procedure.

Transparent acrylic (Lexan) vaulted units (similar to the ones in Berlin stadium roof) were chosen for the cladding of the roofs.

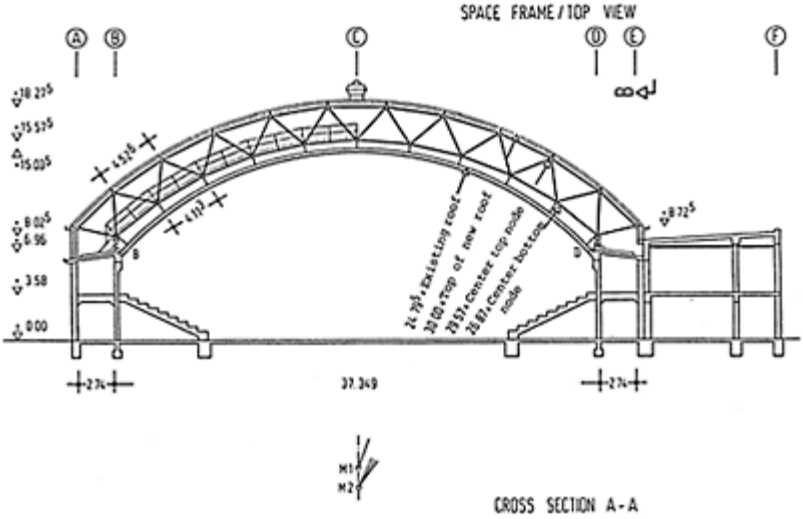

Fig. 15.9. Cross-section of the Münsterland convention hall.

@Seismicisolation

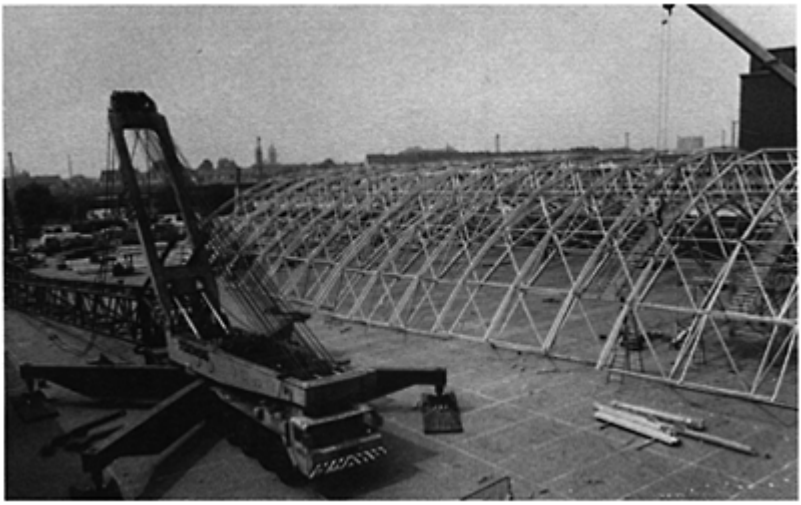

Fig. 15.10. Preassemblage of the MERO space frame units.

3.3 A MERO Space Frame Barrel Vault Preserves a Timber Zollinger Lamella Roof

The Münsterland convention hall (Münster, Germany), built in 1928, was initially covered with a steel roof. After the Second World War, the destroyed roof was replaced by a Zollinger lamella timber roof. The roof's load carrying capacity turned out to be insufficient for modern requirements. In 1982, a supporting MERO space frame provided the best solution to preserve the old timber structure and increase the load carrying capacity at the same time.[7] The roof covers an area of 37×80 m without any intermediate columns (Fig. 15.9).

The weakness of the existing roof had to be considered in the erection procedure and, consequently, the new supporting structure was preassembled on a car park beside the

@Seismicisolation

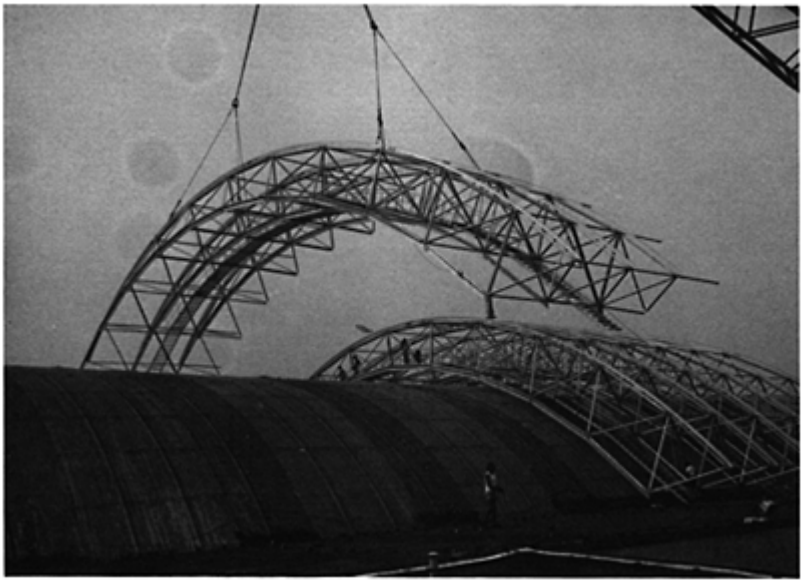

Fig. 15.11. Lifting of one preassembled space frame unit.

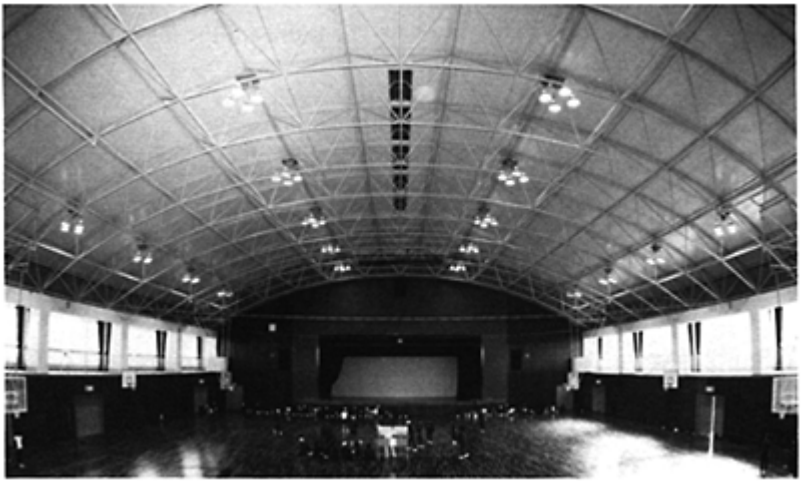

Fig. 15.12. The Shingu High School gymnasium.

hall (Fig. 15.10). Three module-width arches were lifted one by one and connected together at the top of the convention hall (Fig. 15.11). Statically, the system behaves as a curved truss due to the chosen plate-type boundary conditions.

@Seismicisolation

3.4 MERO Barrel Vault Roofing Structures in Japan

A number of space frame barrel vaults have recently been built in Japan under MERO licence by Taiyo Kogyo Corp.

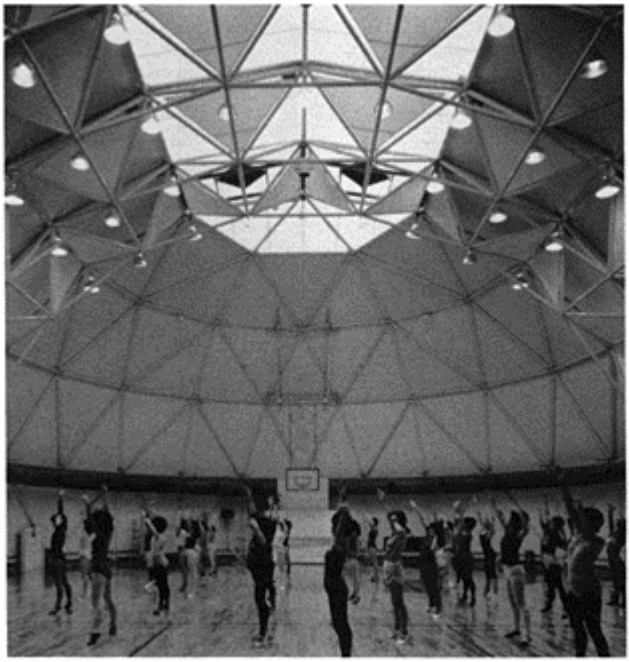

Fig. 15.13. The Tamagawa Takashimaya gymnasium.

3.4.1 Shingu High School gymnasium (Fig. 15.12)

This structure covers an area of 36·3×52 m. The radius of the inner surface cylinder is 35 m, which yields to a rise of about 5 m.

3.4.2 Tamagawa Takashimaya Shopping Centre gymnasium (Fig. 15.13)

This structure consists of a small double-layer barrel vault (10×20 m) and two attached half single-layer hemispherical domes with 10 m radius. The task of the barrel vault is obviously the stabilisation of the dome halves.

4 CONCLUSION

A number of double-layer barrel vault space.frames have been built by MERO in recent years. This shows that, after a period of neglect, steel braced barrel vaults are becoming

@Seismicisolation

popular again in Germany. These structural forms are being used for different types of sport buildings and convention halls as a solution to geometrical, structural and, last but not least, architectural problems.

REFERENCES

1. Mengeringhausen, M. *Raumfachwerke aus Knoten und Stäben.* Bauverlag, Wiesbaden and Berlin, 1975.
2. Föppl, A. *Vorlesungen über Technische Mechanik*, Bd. II, p. 266. Leipzig and Berlin, 1920.
3. Finsterwalder, U. Die querversteiften zylindrischen Schalengewölbe mit kreissegmentförmigem Querschnitt. *Ingenieur-Archiv*, **4**, 1933.
4. McConnel, R. and Klimke, H. Geometrically nonlinear pin-pointed space frames. Proceedings of the International Conference on Numerical Methods for Nonlinear Problems, University College Swansea, 1980, pp. 333–42.
5. Klimke, H., Kliem, A. and McConnel, R. Die Dachkonstruktion für das Stadion der Stadt Split. *Bauingenieur*,**55**, 1980, pp. 211–18.
6. Livesley, R.K. *Matrix Methods of Structural Analysis.* Pergamon Press**,** Oxford, 1975.
7. Kliem, A. Sanierung der Halle Münsterland in Münster. *Bauingenieur*, **58,** 1983, pp. 285–8.

@Seismicisolation

16
Triodetic* Aluminium and Steel Braced Barrel Vaults

H.G.FENTIMAN
Triodetic Structures Ltd (International), Ottawa, Canada

1 STRUCTURAL COMPONENTS

The performance of structural connections has been the subject of intensive research for some time. In steel butt-welded joints, full tensile strength, or 100% efficiency, has been established; however, similar techniques applied to aluminium structural alloys lead to unavoidable annealing and reduced efficiency. In aluminium and steel-bolted or riveted joints, efficiencies of up to 75% only can be achieved.

Precision manufactured components have now been developed that allow easy assembly with unskilled labour. Using Triodetic, aluminium or steel tubular structural members can be fabricated to precision lengths with the coined keyways on either end at the required angle. These are fitted into hub or node points forming continua of triangles. triangles.

The connectors or node points have been developed to the point where not only different diameters, but different wall thicknesses (usually tubes) can be effectively joined (see Figs. 16.1 and 16.2).[1,2]

As more projects are undertaken, new details of connections between three-dimensional structures and conventional forms of construction are being developed. Tests of the actual elements (aluminium and steel) are used to validate the behaviour under tensile, compressive and combined loading. These continue to show an average efficiency of Triodetic joints well in excess of 90% of ultimate under direct tension loadings, with deviations of approximately 6%.[2,3]

2 STAGE SHELL BARREL VAULT

The Central Canada Exhibition Authorities had a requirement to cover an 18 m×18 m outdoor stage to protect the performers and their instruments from the elements. They also required that the enclosure should be erected and dismantled quickly and easily, and that the view from all grandstand seats remain unobstructed.

* Triodetic is a Registered Trademark of Triodetic Structures Ltd, Ottawa, Canada.

@Seismicisolation

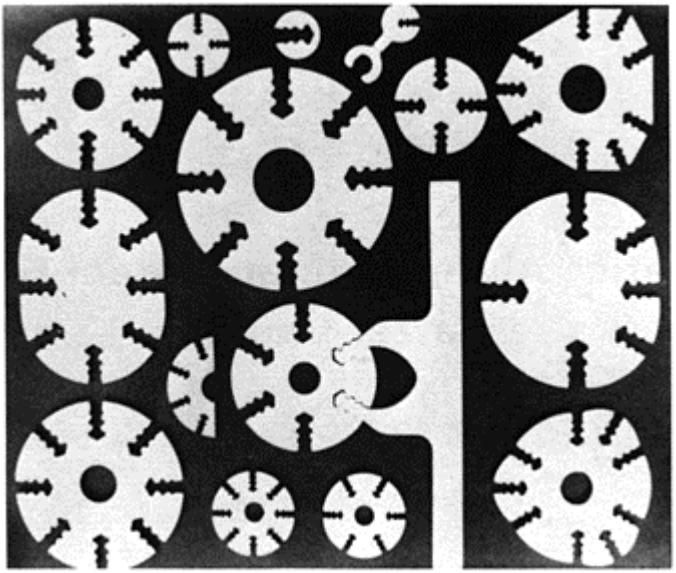

Fig. 16.1. Typical Triodetie connector shapes.

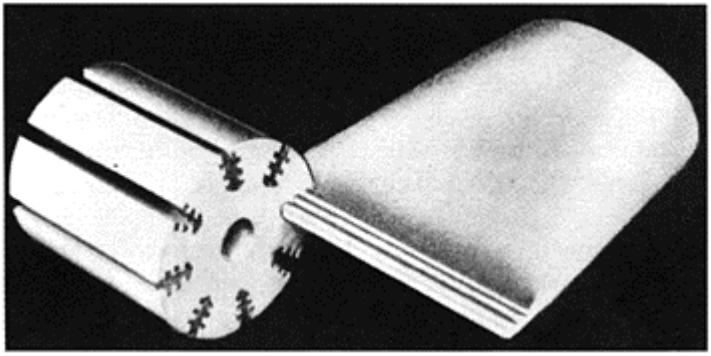

Fig. 16.2. Triodetic tube hub connection.

@Seismicisolation

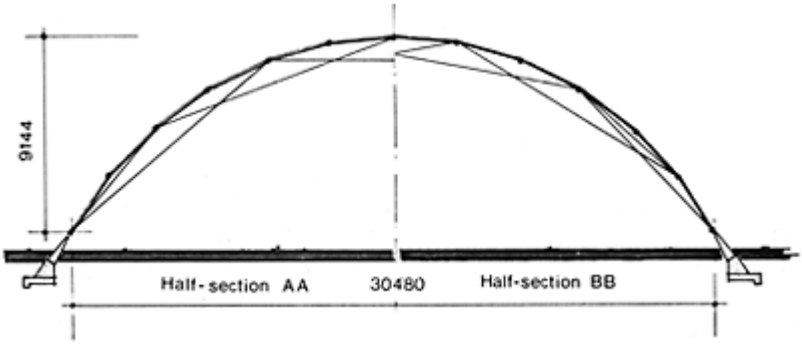

Fig. 16.3. Sections—stage shell barrel vault.

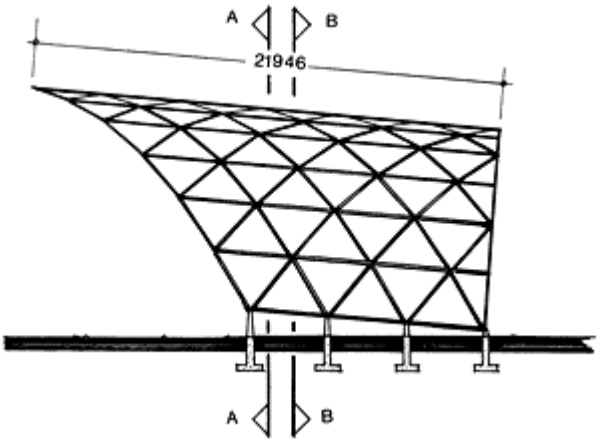

Fig. 16.4. Elevation—stage shell.

To satisfy these requirements, a pre-stressed barrel vault with a cantilevered front lip was designed. The structure had a 30·5 m span and a 9 m rise with an overall depth of 21 m at zenith. The principal framing used 3·6 m lengths of aluminium tubes, 89 mm dia.×3 mm wall. Structural connection of tubing was by the use of standard extruded aluminium 6–slot Triodetic connectors. Tolerance between the tube and the connector permits easy erection and dismantling. Light blows with a soft-faced hammer are all that is needed to assemble the elements.

Critical design condition was under wind, with unequal loads (pressure on one side and suction on the other) tending to cause bending. This was offset by continuous loops of 8 mm dia. 7×19 flexible steel aircraft cable (Fig. 16.3). Attachment of the cable was made by looping each end over an extension of the connecting rods and securing it in place with a through-pin. The pre-stressing was accomplished by placing 32 mm dia.×2

@Seismicisolation

mm wall thickness aluminium spreader bars at the centre of each cable loop. With the cable elements preloaded, bending of either side could be tolerated.[4]

Eight individual concrete footings were placed below the frost line and brought up to within 200 mm of grade. Boxes were placed above the footings, so that the anchor bolts would be readily accessible. Only 600 mm of turf need be removed at each footing in order to expose the lids of the boxes; this turf is easily replaced upon dismantling the structure.

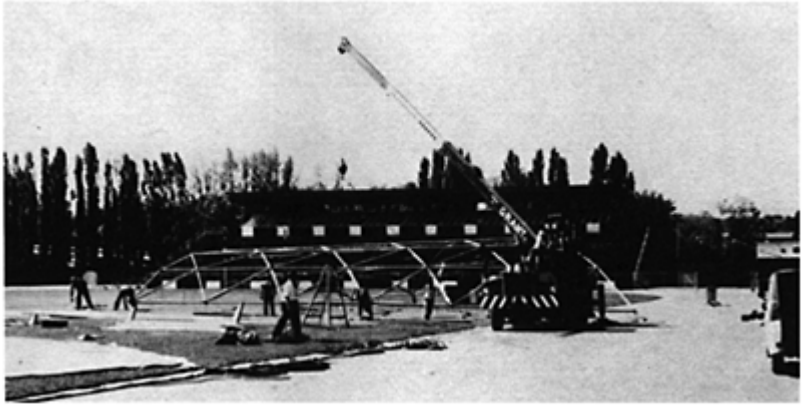

Fig. 16.5. Ground assembly—stage shell.

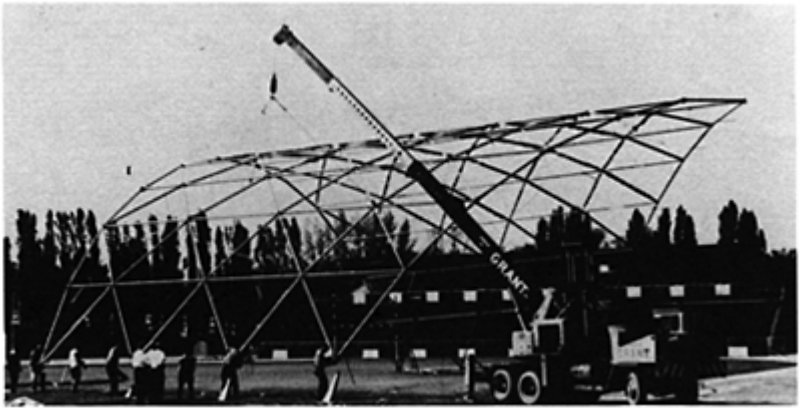

Fig. 16.6. Near completion—stage shell.

Tapered box section steel supports were provided to connect the structure to the footings. They were manufactured in varying lengths in order to tilt the structure lip upward (Figs. 16.3 and 16.4).

@Seismicisolation

In order to facilitate assembly and erection of this structure, special hinged connections were provided at the top of the tapered box supports. This allows the assembly connection of the various structural elements at ground level. After three or four sections have been erected on the ground, a light crane is brought into use. This crane is used to lift the open side of the barrel vault allowing ground assembly to proceed, until the final connection is achieved on the opposite side of the 30 m arch. The cable loops are placed over the node points as construction proceeds, with a final tensioning after the skeleton framework is secured (Figs. 16.5 and 16.6). The entire structure has a shipping weight (including the canvas) of approximately 1750 kg. It is interesting to note that this structure has been in use for 15 consecutive summers (Fig. 16.7).

The success of this structure led to an additional one being provided for an outdoor theatre in Quebec City as protection over a theatre stage. In this instance, the forward or cantilevered lip had twin tubes installed to provide adequate support for an elaborate system of stage lighting.

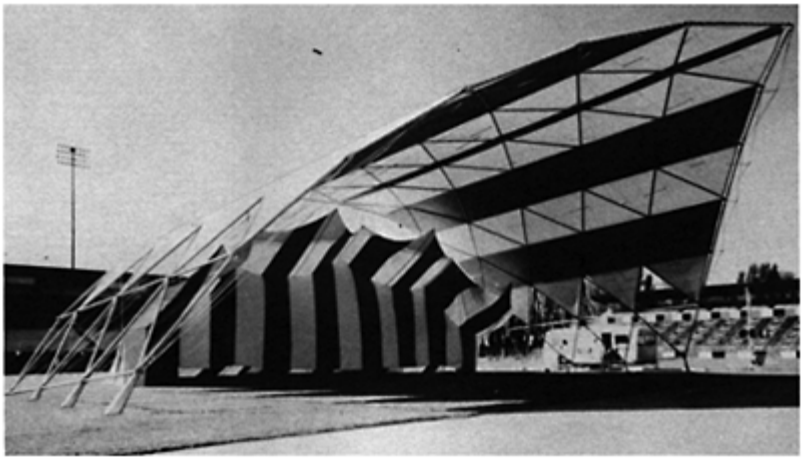

Fig. 16.7. Completed stage shell barrel vault.

3 ST MARK'S ACADEMY, SOUTHBORO, MASS., USA

St Mark's Academy's Board of Directors was faced with a requirement for a new building that could be used as a skating rink for 8 months, and for other recreational activities in the remaining 4 months of each year. The land available placed restrictions upon the shape of the building. The owners and their architects selected a braced barrel vault to satisfy their requirements. The design of the structure was realised by arranging the support system in the line of the radius of the barrel (Fig. 16.8).

In this instance, the cylindrical shell or barrel vault is achieved as a series of arches, each in itself a plane structure with all stresses guided along the linear access to the

@Seismicisolation

abutment. In choosing this form, the object was to eliminate all bending moments, to direct all primary external forces in the form of direct stresses in the arch to the abutment.

The building had a clear span width of 30·4 m and a length of 67 m. Site conditions negated the use of pre-fabricated rigid frames, which lead to the use of Triodetic prefabricated components that could be erected *in situ*. As a consequence, all the components required to construct the vault comprised less than one full tractor load.

A typical attachment of the column support to the base concrete pier is shown in Fig. 16.9. This arrangement ensured that vertical and horizontal reactions were minimised. Once the support system had been installed, a number of rolling scaffolds were put into place at one end of the building. As each arch was completed in the form of a curved folded plate (Fig. 16.10), scaffolds were moved forward until the entire vault was

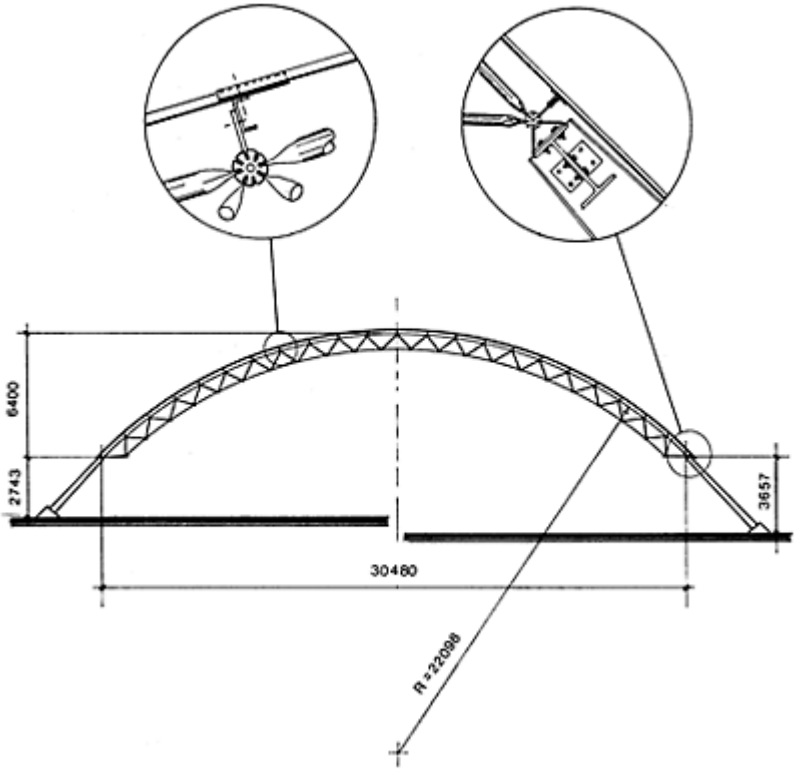

Fig. 16.8. Section and details—St Mark's Academy.

@Seismicisolation

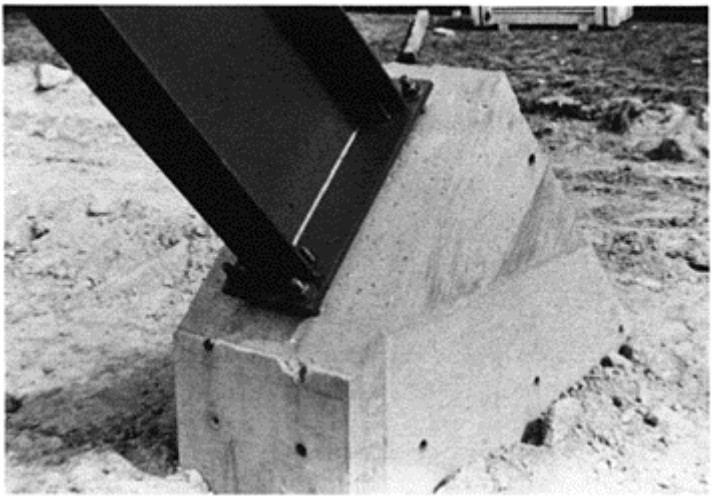

Fig. 16.9. Base support—St Mark's Academy.

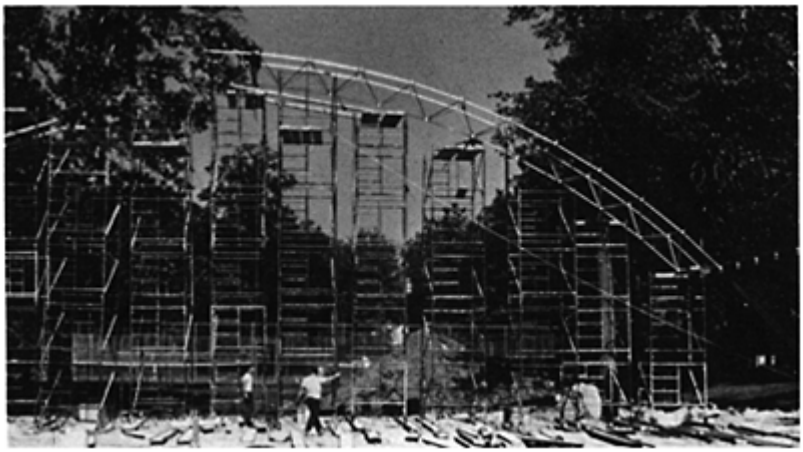

Fig. 16.10. Construction scaffold—St Mark's Academy.

@Seismicisolation

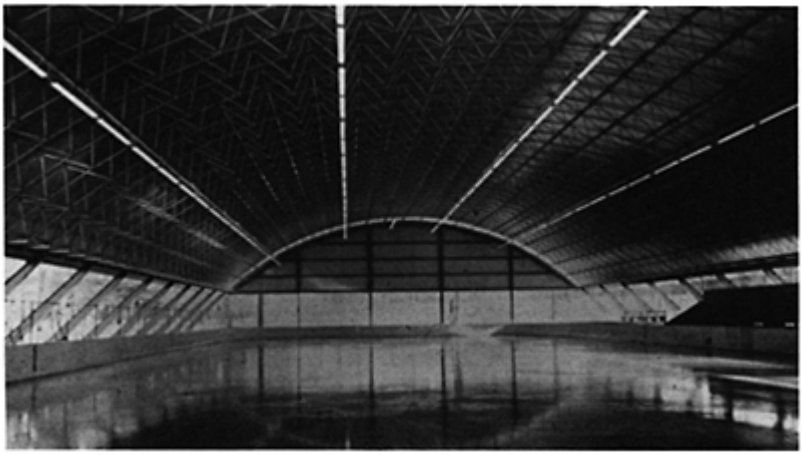

Fig. 16.11. Completed structure—St Mark's Academy.

completed. The scaffolds were staggered to permit access to all levels of the arch for assembly of the components.

A special connector at the spandrel beam was fabricated, using two coined plates fastened to the connector and bolted to the beam. The third coined plate was then inserted to receive the longitudinal purlins, to which the roof decking was applied (Fig. 16.8).

This structure provided a satisfactory solution for the special requirements of the owners (Fig. 16.11).

4 NUCLEAR PLANT BARREL VAULT

The inclement weather, heavy snows and cold temperatures of the Canadian climate render winter construction very difficult. The Ontario Government's Nuclear Electric facility at Pickering required a versatile type of cover for their winter construction work. It was to be used over reinforced concrete installations that were poured during this period.

The owners wanted the structure to be sectionalised and of a very light weight, so that the sections could be readily transported, and used in various applications and configurations. In that the application of the structure would vary, it was designed for full snow loading in accordance with the National Building Code of Canada, 1965, which called for a dead load of 20 kg per square metre, a snow load of 245 kg per square metre, and a wind load of 100 kg per square metre, basic pressure. The structure was designed as a three-pinned arch composed of plane frames, which were tied together on the outer surfaces with cross bracing and purlins, and on the inner surface with longitudinal ties and a single bay of cross bracing.

While the structure provided was made up of individual aluminium Triodetic hubs and tubes, and was completely demountable (into individual pieces), the intention was to

@Seismicisolation

build 15 m×15 m sections used in combinations to produce 15, 30, 45 and 60 m lengths. The sections could also be assembled to provide 15 m×15 m, or 30 m×30 m enclosures for the protection of related equipment (Figs. 16.12, 16.13 and 16.14).

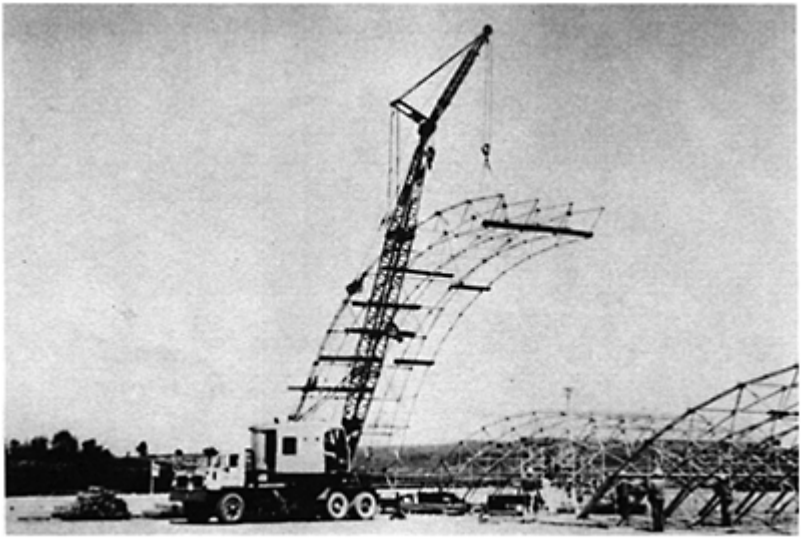

Fig. 16.12. 15 m×15 m sections—nuclear plant barrel vault.

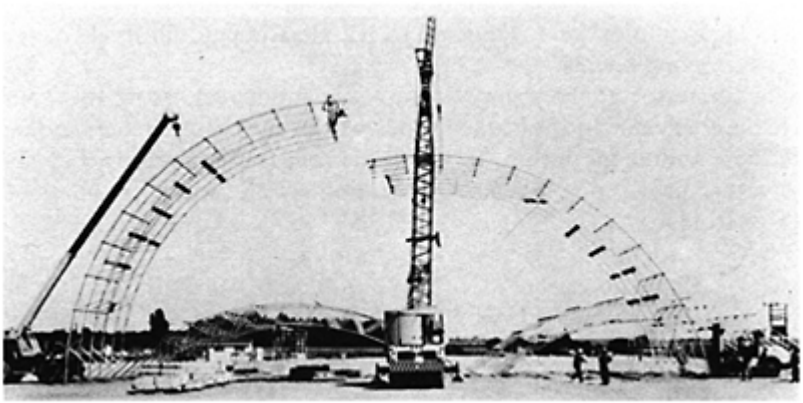

Fig. 16.13. Positioning 15 m×15 m sections—nuclear plant barrel vault.

The material selected was Alcan 755T4 extruded aluminium, which was heat-treated to the T6 state after coining. The extruded Triodetic connectors were Alcan B51S T6, and the bracing components were 65S T6.

@Seismicisolation

The principal span of the total structure was 30 m between base supports with a height at the apex of 14 m. The depth of the arch frames was 1 m centre to centre of hubs, and the spacing was 2 m on centre. The arch top chord members were 76 mm diameter by 3 mm wall, with the bottom members being 83 mm diameter by 3 mm wall. All connectors were specially designed 8-slot by 2 mm and 3 mm with all slots oriented in such a manner as to avoid any bending to the ends of the structural Triodetic tubing components.

The completed 30 m span section shown (Fig. 16.14), is 15 m deep and the quantity and material in the foreground is the total required to erect an identical section of the building. The simplicity of the framing is such that unskilled labour can be used for primary assembly.

It is interesting to note that, once the sections had served their initial purpose as temporary enclosures for construction, the entire structure (30 m square) was then reerected on site, clad with timber and water-proofed. It served as a semi-permanent storage building for servicing construction machinery until the project was completed.

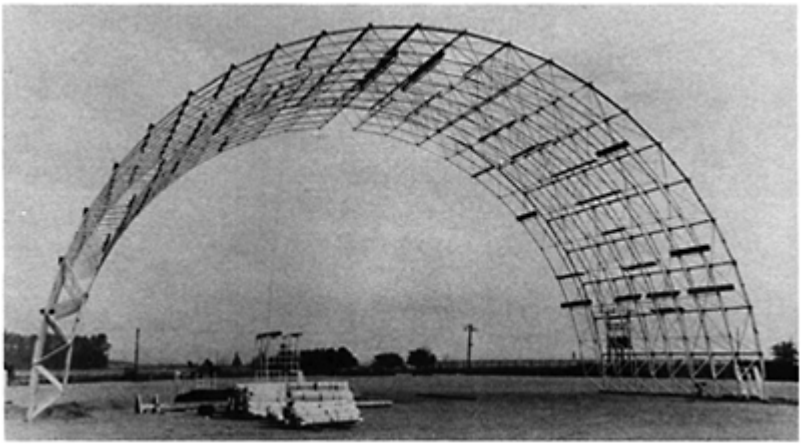

Fig. 16.14. Completed 30 m×15 m sections—nuclear plant barrel vault.

5 EQUESTRIAN RIDING RING

In Canada, there has been an increasing interest in recent years in equestrian facilities and associated riding schools. In most parts of the country, the inclement winter weather, with its accompanying heavy snowfalls, make year-round participation in this sport extremely difficult, if not impossible, without enclosed facilities. As a result, there has been an increasing requirement for fully enclosed riding rings built to Olympic standards. In many cases, such schools or clubs are enterprises with only modest capital, and do not have the economic means to enable them to acquire or construct commercial structures. To meet this need, the inventor of the Triodetic system devised a structure that would

@Seismicisolation

allow the assembly and construction of a riding ring to be undertaken by the owners and operating personnel of the facility.

The concept was to use a system of inter-connected arches, placed 3 m apart and having a span of 33·5 m to provide a building of any desired length (Figs. 16.15 and 16.16).

The truss design incorporated varying tube diameters and used double tubes in the same slot in highly stressed areas. A simple assembly drawing identified the various tubular structure components, each clearly marked for assembly on site.

The supporting wall for the structure consisted of 300 mm reinforced concrete placed on footings 1·4 m below grade. Such footings are necessary in Canada to prevent possible frost heave caused by severe climatic conditions. A series of 18-tonne ground anchors (one for each arch) were sunk at a 45° angle below grade and connected to the supporting foundation walls at each arch base plate. These were used to counteract the horizontal reaction of the individual arches (Fig. 16.17).

In order to minimise the total span, as well as providing the necessary height for both horse and rider to perform equestrian jumps, the arches were cranked downward at each end (Fig. 16.17). Each arch was assembled on the ground in three sections. Pyramid-type gantries were then assembled to hold the central section in place until the lower sections were added. Once the two trusses were in place and adequately braced, the gantries were

Fig. 16.15. Assembly of arches—equestrian riding ring.

@Seismicisolation

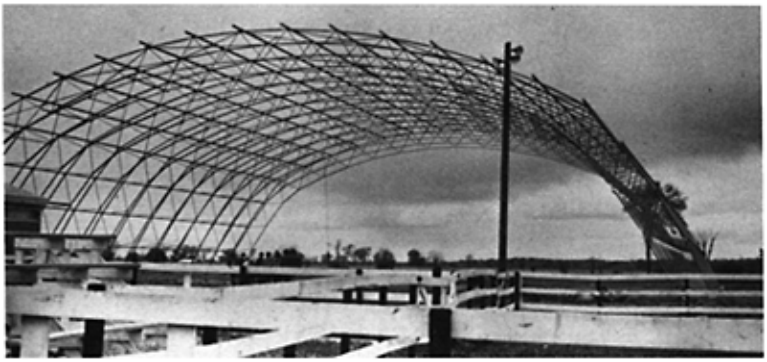

Fig. 16.16. Structural frame—equestrian riding ring.

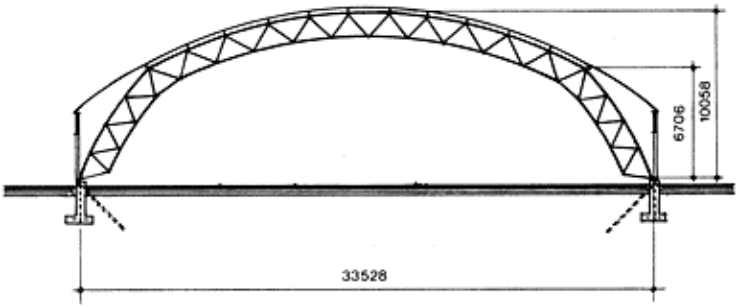

Fig. 16.17. Section—equestrian riding ring.

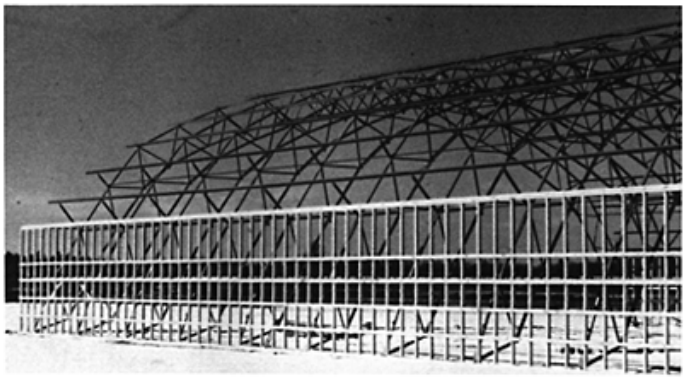

Fig. 16.18. Vertical side wall—riding ring.

@Seismicisolation

merely towed horizontally as each consecutive arch was lifted and the lower sections added. It was then braced and connected into place. The longitudinal purlins served as bracing as well as fastening sections for the corrugated metal trough roof sheeting (Fig. 16.15).

For aesthetic reasons, and to facilitate storage and spectator accommodation, the perimeter walls were erected vertically using standard timber construction (Figs 16.17 and 16.18).

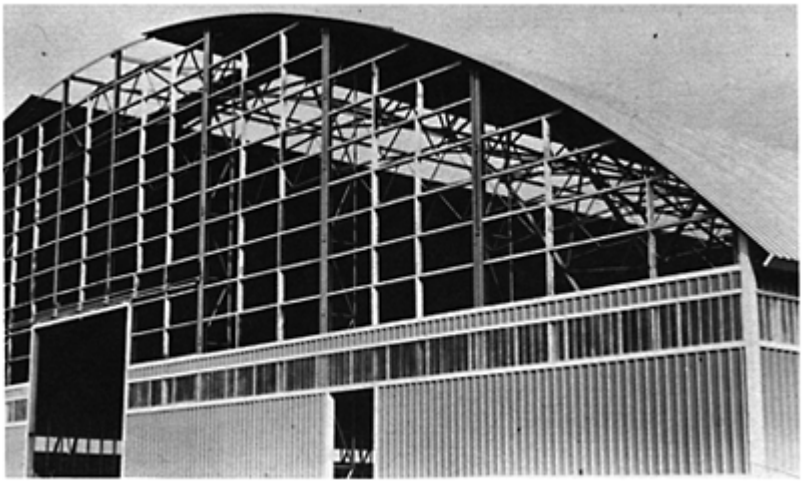

Fig. 16.19. End wall—riding ring.

The end walls were moveable in case an extension to the structure might be required. They consisted mainly of simple vertical Triodetic trusses, infilled with standard timber. The finished roof line of the barrel continued the circle to the walls, which were vertically sheeted with standard trough sheeting. Lighting from the exterior was achieved with a band of matching fibreglass contour (Figs. 16.17 and 16.19).

The entire structure was built rapidly and very economically without any heavy equipment other than three standard one-tonne chainblocks.

6 CASTANO

One further area of interest in the utilisation of continuous barrel vaults has been advanced by Engineer Francisco Castano of Triodetic de Mexico, s.a. Developed in conjunction with his spectacular and highly efficient water towers, continuous concrete sluiceways have been constructed using the Triodetic system.

A single layer shell is constructed over a base concrete sluiceway, which has plywood formwork attached to and slightly below the Triodetic network (Fig. 16.20). Transverse reinforcing rods are added to the upper surface. The network and rods are then

@Seismicisolation

encapsulated with poured concrete. Using this method, continuous sluiceways are very economically realised.

7 CONCLUSION

It seems clear that with the generally growing acceptance of three-dimensional space structures, and the particular attractiveness of braced barrel vaults with their many applications, a much wider use of this type of structure will be seen in the future.[5]

The techniques developed using Triodetic components offer a significant contribution to the realisation of practical, latticed and metal-framed braced barrel vaults.[6]

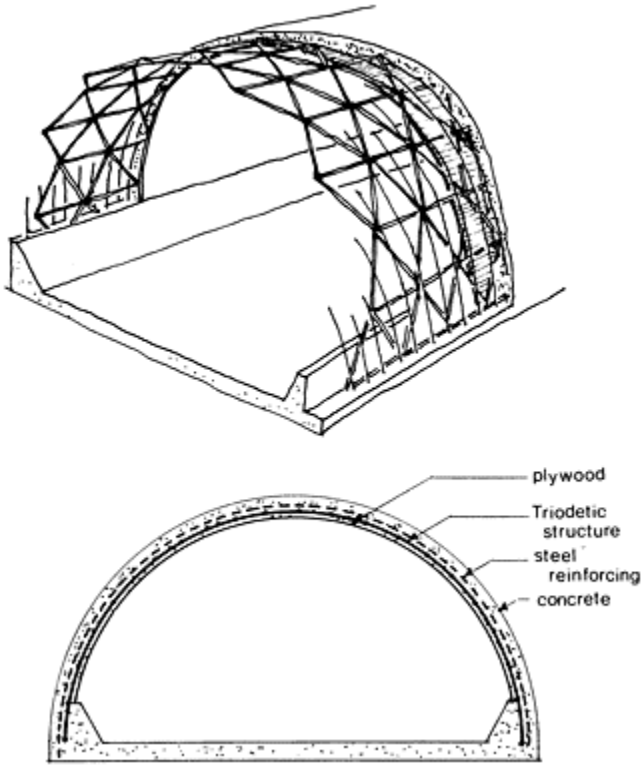

Fig. 16.20. Continuous barrel vault sluiceway, Mexico.

REFERENCES

1. Makowski, Z.S. Aluminium space structures. Symposium on Aluminium in Structural Engineering, London, 11–12 June 1962, pp. 195–207, 313–315.

@Seismicisolation

2. Fentiman, H.G. Triodetic connections in space frame structures. Part II, Tension Structures and Space Frames. IASS Pacific Symposium, Tokyo and Kyoto, Japan, 17–23 October 1971, pp. 855–863.
3. Fentiman, H.G. Development in Canada for the fabrication of three-dimensional structures using the Triodetic system. International Conference on Space Structures, London, 1966.
4. Wright, D.T Metal Frame Space Structures. Bulletin of the International Association for Shell Structures, No. 17, Madrid,September 1960.
5. Makowski, Z.S. Space structures. International Association for Bridge and Structural Engineering, Amsterdam, Holland, 8–13 May, 1972, pp. 127–149.
6. Fentiman, H.G. Examples of three-dimensional (Triodetic) structures. ASCE/EIC/RTAC, Joint Transportation Engineering Meeting, Montreal, Canada, 15–19 July, 1974.

@Seismicisolation

17
Design and Construction of Steel Barrel Vaults for Buildings of Medium and Large Spans

J.ZEMAN
Prague, Czechoslovakia

1 GENERAL ASPECTS OF DESIGN OF LARGE SPAN ROOFS IN STEEL STRUCTURES

At the design stage of large span structures, the designer has to pay special consideration not only to the structural and architectural aspects of his structure, but he has also to aim towards simple fabrication and ease of erection. The recent trends put an increasing emphasis on the optimisation of the structural material. Nowadays maximum exploitation of material combined with minimum use of energy becomes a focal point of interest. This explains the great interest in the design of structures with minimum unit weight per square area. At the same time attempts are made to simplify the fabrication with a saving in all kinds of energy during the construction.

Lamella steel vaults undoubtedly belong to the most effective systems of this kind. Their main roof shape is characterised by the form of a barrel vault. Their basic form can, of course, be adapted in various ways to different purposes and requirements of the actual structure. Some possibilities will be demonstrated in this chapter with steel barrel vaults designed by the author.

2 REVIEW OF DEVELOPMENTS

Several of the structures of this type were designed and erected some time ago and were described in earlier publications.[1,2] In this chapter the author wishes to draw attention to the fundamental principles used in his designs and refer to more recent structures. Experience shows that all the structures built so far have proved to be eminently suitable for projects involving medium and large spans, mainly because of their significant economy in material consumption, satisfying architectural appearance and also due to their effective fabrication and easy erection.

A considerable amount of practical experience has been obtained on a series of realisations over the last few years and significant progress has been achieved in improving the design and construction of such systems. Two references given at the end of this chapter contain detailed information about the previously constructed lamella barrel vaults designed by the author, and the following pages contain details of recently

@Seismicisolation

built barrel vaults emphasising some new aspects experienced in their design. The progress achieved shows that these structural systems can satisfy many of the requirements of modern design.

3 SOME REMARKS ON THE COMPOSITION OF THE STRUCTURAL SYSTEM

3.1 The System as a Whole

The design of main arched ribs in the diagonal form rather than the supposedly simpler system of parallel arches may seem, at first sight, to be more complicated, especially during the fabrication of structural steelwork, than the more conventional systems. However, practical experience gained during the construction of numerous structures of this type has shown that the mass production of identical or similar main lamella elements for the spatial arrangement used in this design did not present any special difficulties in the workshop. On the contrary, the prefabrication showed that it had many advantages, especially as the interconnection of assembled units lead to a very uniform stress distribution in the resulting structure (Fig. 17.1).

The resulting great rigidity of these small prefabricated units, slender in themselves, but extremely stiff when interconnected into a three-dimensional framework, can be

@Seismicisolation

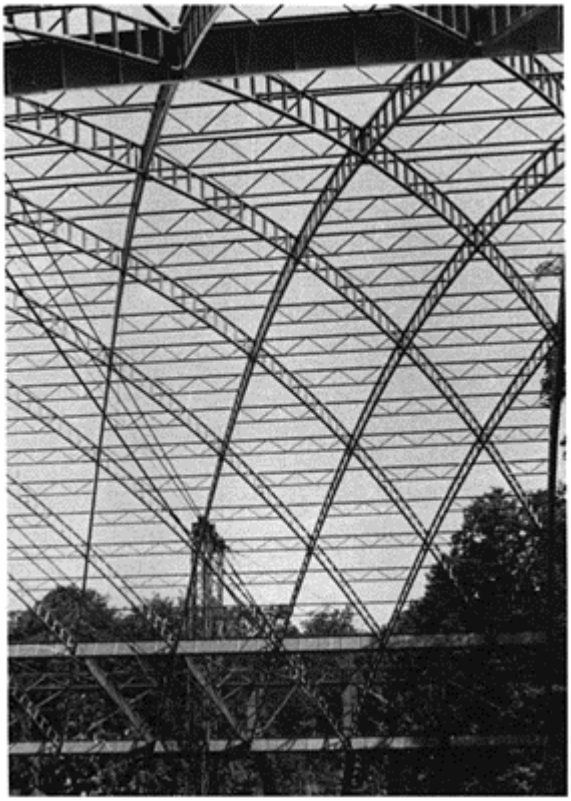

Fig. 17.1. Structural system of braced lamella barrel vault.

@Seismicisolation

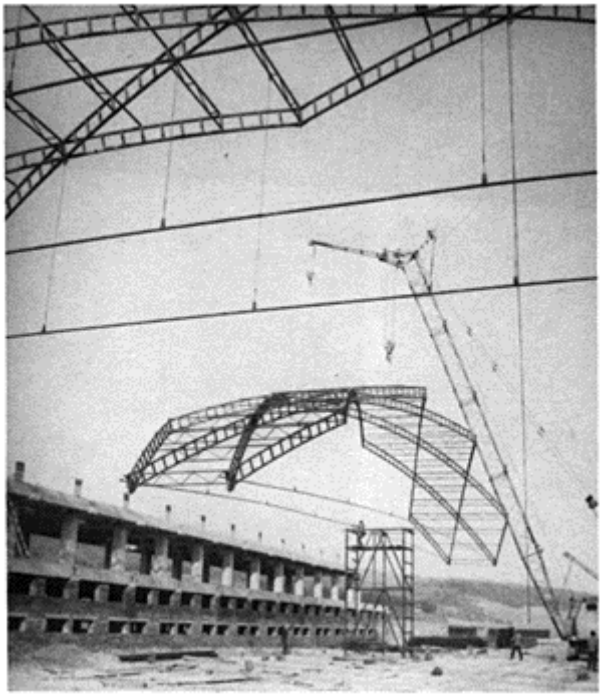

Fig. 17.2. The erection of a hall in Poprad from assembled large component parts—the span is 45 m.

appreciated during the erection. The spatial interconnection of these modular units leads to a substantial advantage expressed in reduced structural weight (Fig. 17.2).

3.2 The Jointing Details

The development of a simple joint in which six structural elements are connected together in one point represents the main reason for the success of the system (Figs. 17.3 and 17.4).

A direct contact, where the main elements run into a continuous fashion through the joint and carry their compressive forces by bearing, is fundamental in achieving simple erection and providing a satisfactory structural solution. At the same time, the connection of six components in a single joint is obtained with a minimum number of bolts. In certain cases this connection could be made by means of one bolt only.

Asymmetrical loads acting on cylindrical roofs could lead to bending moments and subsequently to tension forces occurring at the joints. In such a case the use of high-tensile bolts and the introduction of pre-stressing of the contact surfaces will take care of this situation. This is also why the thickness of the structural material in the contact areas

@Seismicisolation

must not be too small, in order to avoid deformations and greater elasticity of the whole connection.

It is obvious that such joints are not only suitable for easy erection, but also that they are equally simple when dismantled. Thus the whole structure could be moved to another place and re-erected there, if necessary, without undue difficulties.

3.3 The Structural Composition, Size of the Basic Module of the System and Dimensions of the Modular Units

The choice of the size of the cross and longitudinal modules of this system, as well as the size of the main basic elements, lies generally in the hands of the designer. A skilled

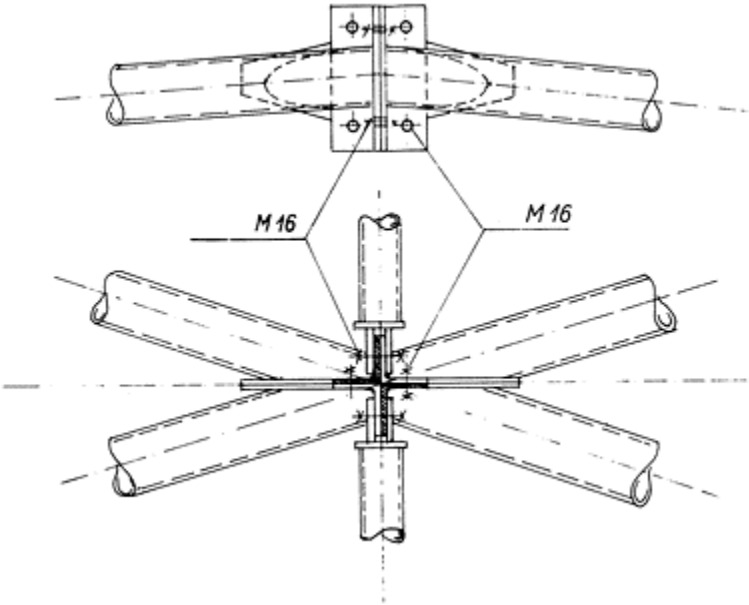

Fig. 17.3. The plan and elevation of a typical ‘cross’ joint for a single-layer lamella structure. 4 main elements and 2 secondary lateral units are interconnected at the joint.

designer can succeed in the choice of the optimum proportions for each relevant span (Fig. 17.5).

Generally, the longitudinal module, i.e. the cross distance of the arched ribs, depends on the distance of the supports; on the other hand the cross module is dependent on the span *and* the number of lamella subdivisions projected over the whole span. This choice will also influence the geometry of the ‘cross joints’.

@Seismicisolation

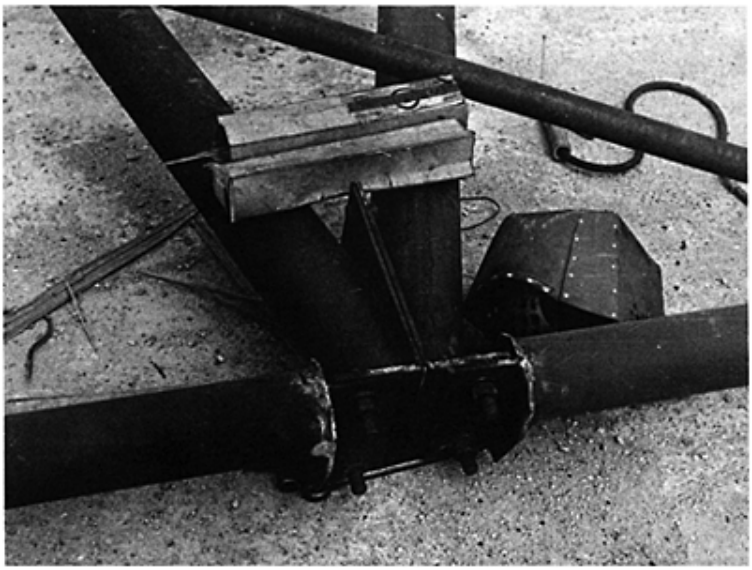

Fig. 17.4. A view of a joint during the erection.

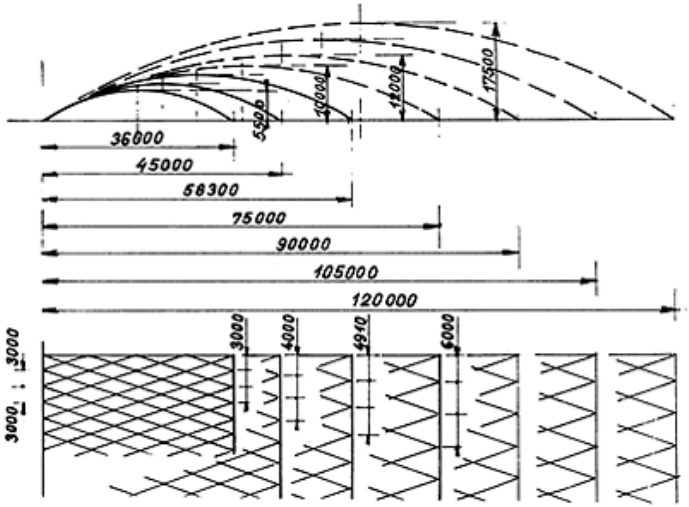

Fig. 17.5. Structural arrangements of lamella barrel vaults for different spans.

@Seismicisolation

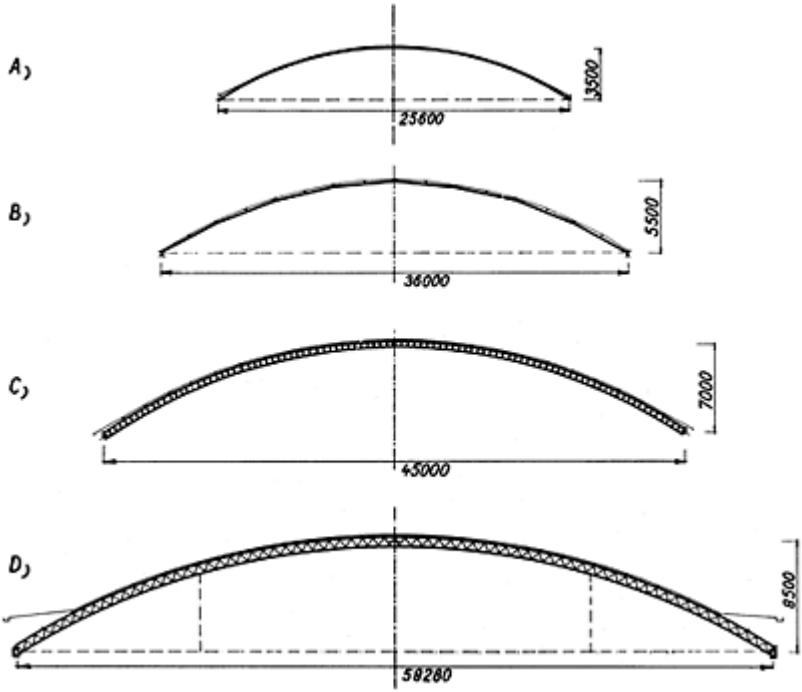

Fig. 17.6. Cross-sections for typical ‘single-’ and ‘double-layer’ lamella barrel vaults.

@Seismicisolation

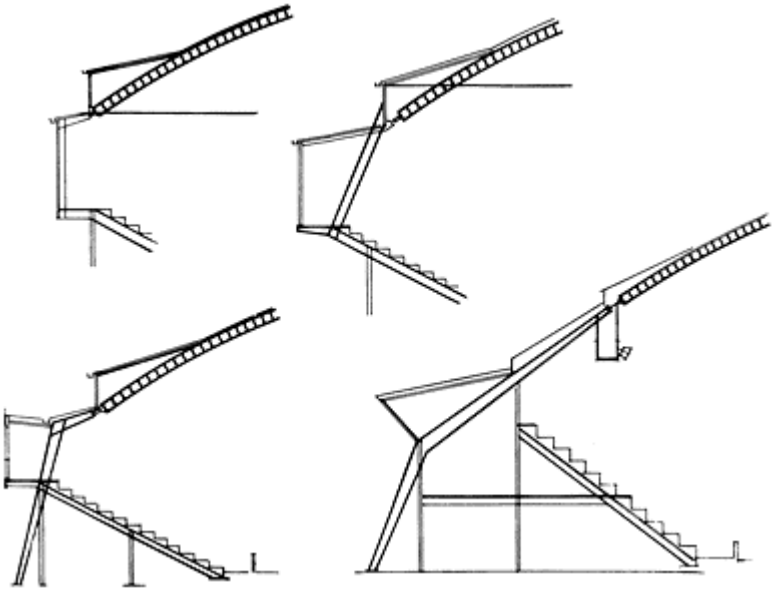

Fig. 17.7. Different solutions for the supporting structure of the lamella barrel vaults.

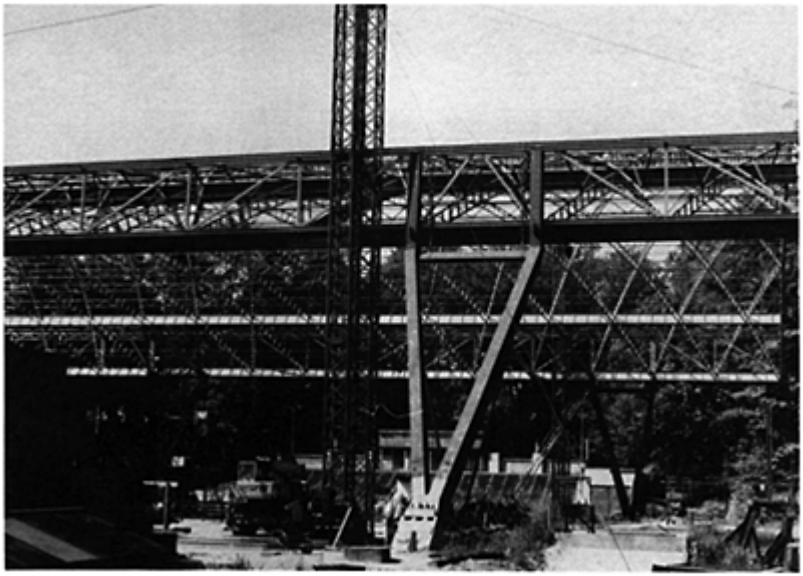

Fig. 17.8. V-shaped support of the ice rink in Havlíčkův Brod.

@Seismicisolation

The magnitude of the span also affects the detailed solution of the basic lamella elements. For spans up to 36 m, it is possible to design the lamella as a simple bar and then to design the whole barrel vault as a 'single-layer' slender shell which works mainly in tension and compression without bending moments (Fig. 17.6). For spans exceeding the previously mentioned limit, the lamella vaults have to be designed as 'double-layer' lamella grids, which behave as two-hinged arches taking into account the additional stiffness due to their three-dimensional interaction.

The form of the basic elements can be either straight or curved—bow-shaped, following directly the curvature of the barrel vault. Such a continuous curvature, though it may be more appropriate for architectural reasons, brings, however, a slight complication in the fabrication, as an element with curved chords requires more time during production. However, due to the modular nature of the basic elements and the possibility of their mass production, the complication produced by the introduction of curvature affects only very slightly the final economy in fabrication.

3.4 The Supporting Systems of Barrel Vaults

The designer has some freedom in choosing the correct arrangement of the supports, not only taking into account the structural factors, but also the architectural aspects of the whole design, and hence influencing the external appearance of the building (Fig. 17.7).

It is possible, for example, to design the supports of the roof in different materials and in various ways. The structural function can be influenced by adding ties. Sometimes it is possible to obtain a special solution with the minimum number of supports, adjusting the main support system, as has been achieved in the construction of the barrel vault covering the ice rink in Havlíčkův Brod, as illustrated in Fig. 17.8 and in Fig. 17.20.

3.5 The Modification of the Overall Shape of Vaults Through the Introduction of Hipped Ends

The cylindrical form is generally of particular interest to architects, because of its characteristic contour. However, it does not always provide the best architectural solution and its use depends on circumstances and environment. In most typical cases a braced barrel vault is closed at both ends by vertical gable walls (Fig. 17.9).

@Seismicisolation

Fig. 17.9. The simple architectural treatment of the lamella barrel vault over the ice rink in Kopřivnice.

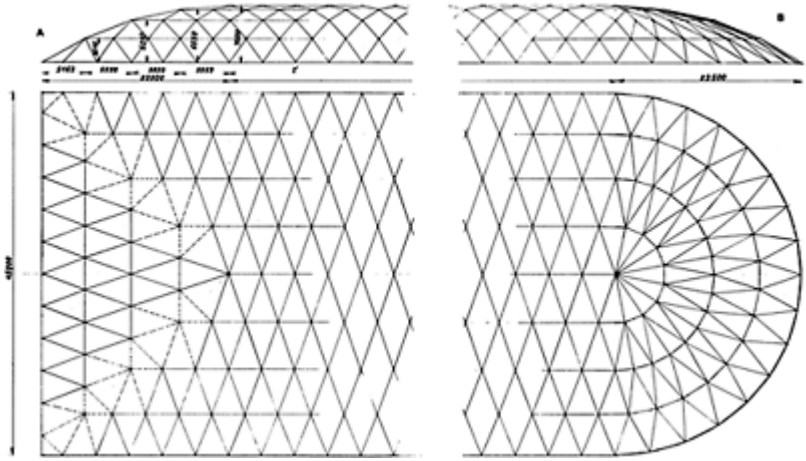

Fig. 17.10. Plans of two possible variants for the end parts in a hipped barrel vault.

In certain cases the designer can modify the support conditions and, by adjusting the shape of the ends, help the architect. The usual approach is by the introduction of inclined hipped ends as illustrated in Figs. 17.10(A) and 17.10(B). It should be noted that, although the modification of the end walls may complicate slightly the geometry, as a rule it does not complicate too much the production or the mass fabrication of the required elements. It should be added that often the introduction of hipped ends will

@Seismicisolation

reduce the maximum stresses in the barrel vault, leading to a more uniform stress distribution.

4 MATERIALS ECONOMY OF THE LAMELLA VAULTS

The previous notes dealt with the most characteristic features of lamella braced barrel vaults, with some remarks added on their development and practical experience gained during their construction. To end this part it would be useful and instructive to report here some data obtained through practical experience concerning the economy and steel consumption of these structural systems. The actual figures quoted later in this paper are based on structures designed and built by the author within the last few years.

In general, it can be stated on the basis of a large number of actual realisations that for lamella braced barrel vaults designed for medium and large spans, the unit steel consumption for enclosures with light roof covering is from 20 to 25 kg/m^2 of covered ground plan.

This fact illustrates clearly the extremely efficient material economy for structures of this type. At the same time, we can add the indisputable advantages of their possibilities in the mass production of modular elements, the easy handling of space saving stocks, easy transport conditions of lightweight elements and, last but not least, the exceptionally simple erection (or dismantling when necessary). All this allows us to speak of a really impressive final economy. This surely should be brought to the attention of the building industry and engineers involved in the design of similar constructional projects, especially now when the maximum economy of material and saving of energy receive the utmost priority.

5 DESCRIPTION OF SOME REALISATIONS

It is possible to divide the realised structures into two groups according to the size of their clear spans.

(i) Lamella barrel vaults constructed as a ‘single-layer’ system, for spans between 20 and 36 m, as a rule as cylindrical shells (Fig. 17.11).
(ii) Lamella barrel vaults as ‘double-layer’ systems, for greater spans, working usually as two hinged interconnected space arches (Fig. 17.12).

Details of some of the formerly constructed structures of these types have already been published. Good results and experience gained with the previous realisations evoked an interest in the further use of lamella vaults for other structures. This resulted in the construction of similar structures during recent years, often of almost identical shape, though some projects involved further development of the original ideas. Some new applications will be demonstrated in the following pages.

@Seismicisolation

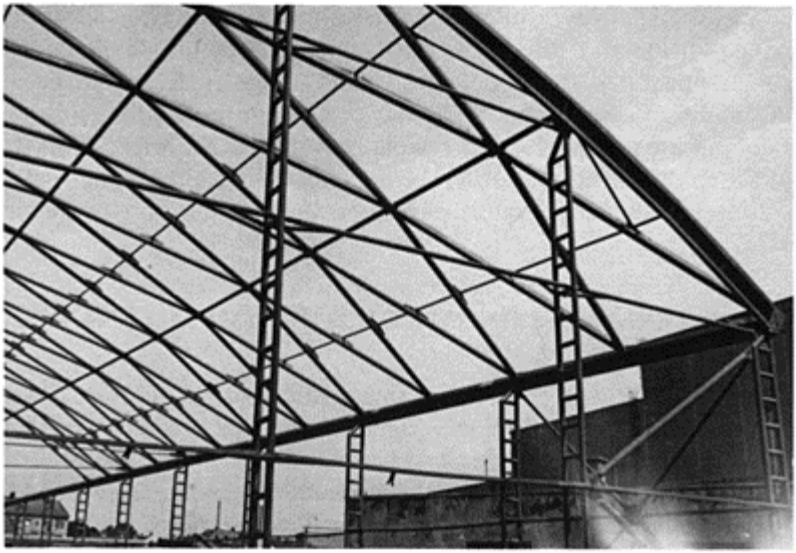

Fig. 17.11. A typical example of a slender single-layer lamella barrel vault.

5.1 Triangulated shells

A great deal of practical experience has been gained with this extremely slender type of steel shell through the erection of two halls, each with spans of 36 m, in Berlin (Fig. 17.13) and in Ostrava (Figs. 17.14(A) and (B)). The unit steel consumption is as follows:

Shell 36 m span in Ostrava, covering an area of 72 m×36 m=2600 m^2. Lamella roof, 45000 kg, 17·49 kg/m2. The steel in the whole structure including the supporting columns weighs 69560 kg; hence total unit steel consumption is 26·75 kg/m^2.

@Seismicisolation

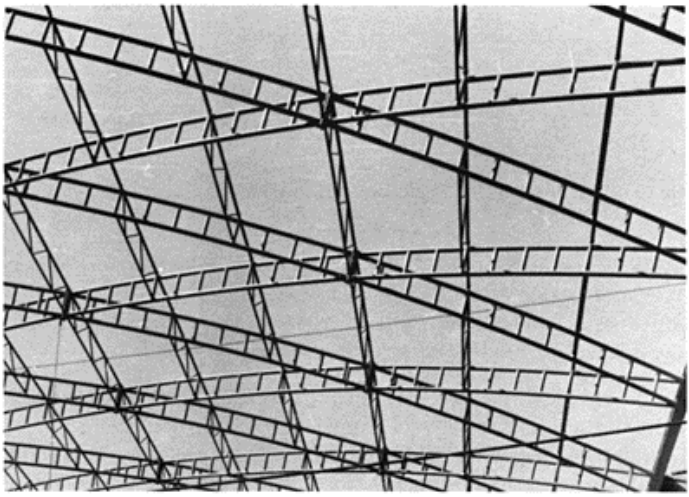

Fig. 17.12. The internal view of the interconnected mass produced modular lamella units in the structure over the ice rink Ždár nad Sázavou. An example of a double-layer system.

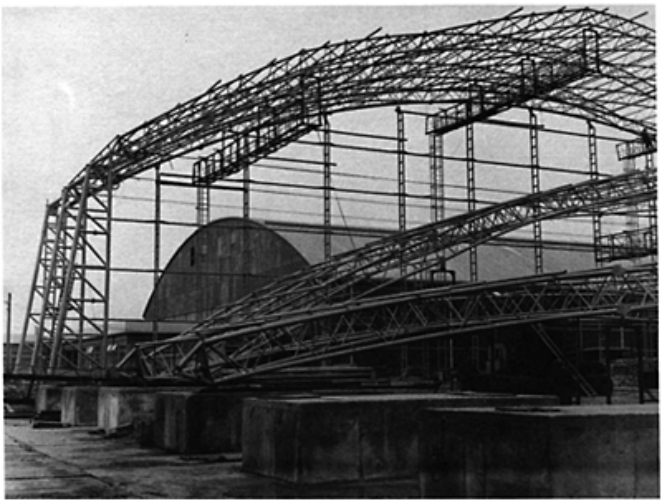

Fig. 17.13. Lamella latticed barrel vault for greater spans (the Berlin ice stadium).

@Seismicisolation

Shell 36 m span in Berlin, covering an area of 127 m×36 m=4560 m2.

Roof weighs	95960 kg	21·05 kg/m^2.
Walls	50411 kg	11·05 kg/m^2.
	146371 kg	

Hence total unit steel consumption is 32·10 kg/m2.

The same type of structure has been projected for the ice rink in Popovice, near Prague, with an area of 2500 m^2; with total steel consumption of 52710 kg for the roof structure, the unit steel consumption would be 21·08 kg/m^2 of the ground area. Unfortunately, this object was finally realised in a slightly modified type of structural framework.

For structures of such spans the main lamella elements are very simple and slender. In the case of a cross module of 3 m, the lamella is represented by a simple circular tube having a cross-section of 128·4 mm and 5 m length.

The whole erected structure over the span of 36 m is, of course, extremely slender and elastic.

The erection of such slender elements in space appears to be one of the greatest problems. The assembly of these so extraordinarily elastic units into their final three-dimensional rigid framework requires some attention.

The actual realisation of the above-mentioned two halls proved that such erections are possible and real, although in each case the erection proceeded in a slightly different way.

During the assembly, maximum care should be exercised in order to avoid introducing residual stresses into the erected structure.

The erection procedure is important; otherwise some undesirable pre-stressing may lead to a possible reduction of the future load carrying capacity of the completed structure.

A mass production of a similar lightweight lamella shell suitable for spans of about

@Seismicisolation

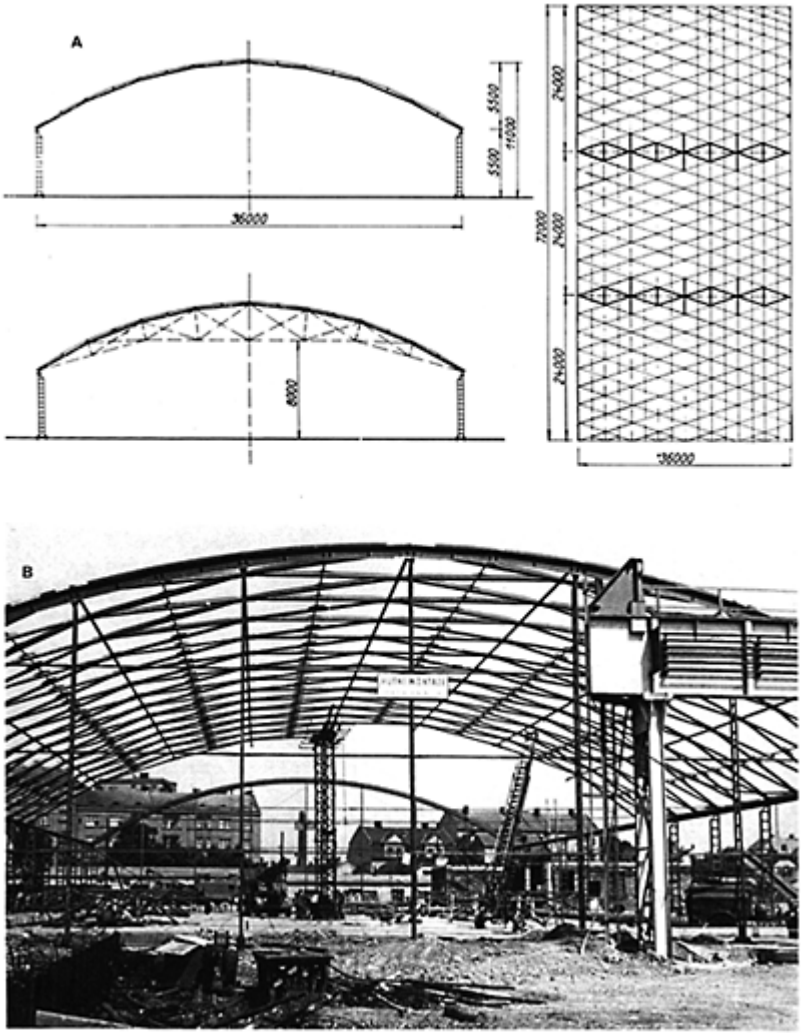

Fig. 17.14. (a) Plan and elevation of the lamella barrel vault in Ostrava. (b) View of the Ostrava barrel vault during erection.

@Seismicisolation

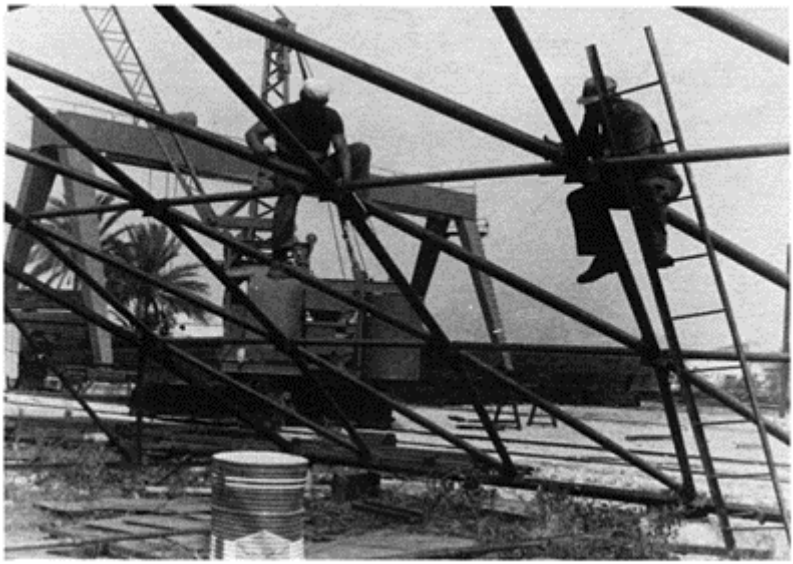

Fig. 17.15. The experimental prototype barrel vault erected for testing in Ondara, Spain.

30 m has been carried out by the Spanish firm of Caselles from Valencia. This small manufacturing firm of steel structures, in close collaboration with the Czechoslovakian design office, decided to produce first a prototype shell having a span of 30 m and a length of 20 m in scale 1:1 and to test the structure in their workshop to the full designed load. The supervision of the test was done by a competent and authorised institute in Madrid before issuing a certificate allowing the intended mass production. The fabrication, erection and controlled load test of this experimental shell structure provided a good opportunity to obtain a detailed picture of the behaviour of such a slender structure under closely controlled conditions.

For an area of 600 m^2 covered by the shell having a span of 30 m and a length of 20 m the steel consumption was

For the roof	4300 kg kg	7·17 kg/m^2
For gable walls and columns	3200 kg	5·33 kg/m^2
Hence in total		7500 kg or 12·50 kg/m^2

After the successful completion of tests on the prototype (Figs. 17.15 and 17.16), the firm Caselles in Valencia and Ondara is producing nowadays in Spain these structures in a mass series for Spanish industry and agriculture.

@Seismicisolation

5.2 'Two-layer' Lamella Barrel Vaults Consisting of Latticed Elements

This form proved to be especially popular and frequently used in practice during the last few years. It has been used mostly for the roofs of sports halls and ice rinks, mainly for spans of 45 m. The first realisation of this type was over the ice rink in Kopřivnice (span 45 m with ties, covered area of the roof 2700 m^2, total area of the building 3940 m2, steel for the roof 56800 kg, i.e. 21·00 kg/m2, total amount of steel including the supporting structure 109000 kg, hence the unit steel consumption 27·65 kg/m^2) (see Fig. 17.9).

The second equally interesting application has taken place at Popgrad (main span 45 m, extended to 70·60 m by means of slender steel cantilevers, area of the main roof

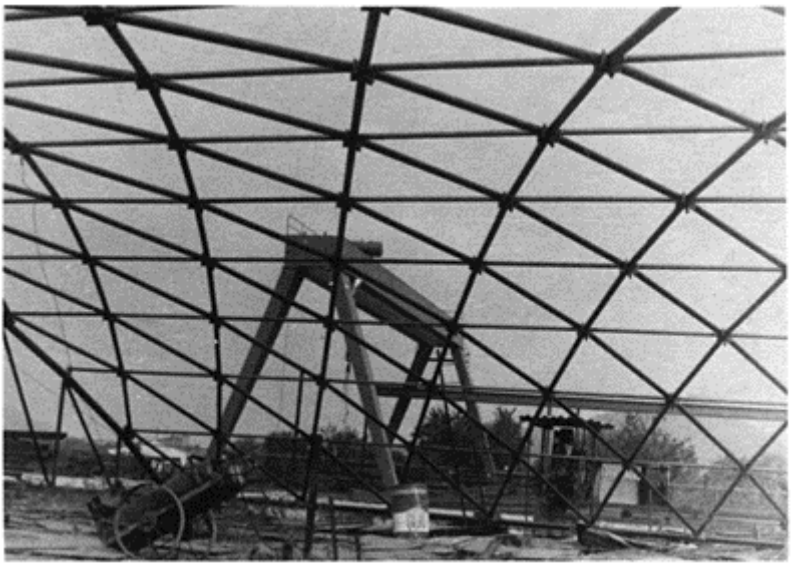

Fig. 17.16. Another view of the experimental barrel vault.

3980 m^2, total area of the whole structure 6248 m^2, steel for the roof 78880 kg, i.e. 19·59 kg/m^2, total steel for the whole building 217000 kg or 34·83 kg/m^2) (see Fig. 17.17).

Several other projects followed and the realisation of this type for ice stadiums in Uherský Brod, Uničov should receive special attention. There is a similar project now in preparation for Orlova.

All these structures have a special solution of their supports. The vaults are lying on the oblique cantilevers which at their upper ends are connected by means of ties, thus reducing the horizontal thrust from the vaults.

There are also barrel vaults without ties constructed recently for the halls in Kroměříž, Žďár nad Sázavou (area 3240 m^2, the weight of the steel roof structure is 75374 kg or

@Seismicisolation

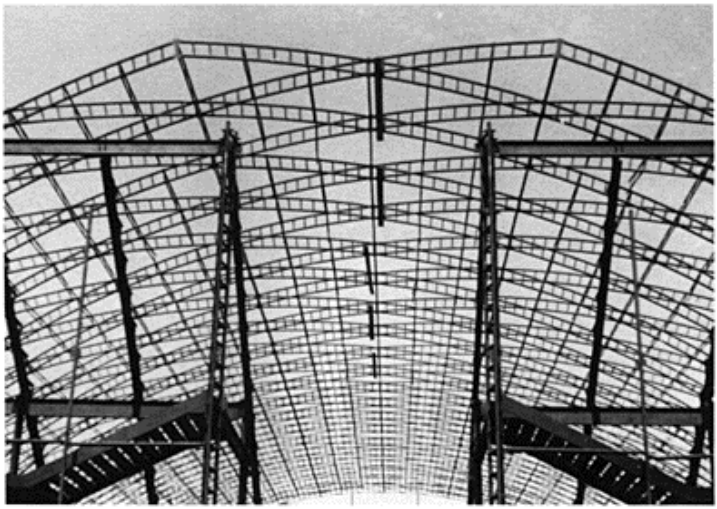

Fig. 17.17. The ice rink barrel vault at Poprad, during construction.

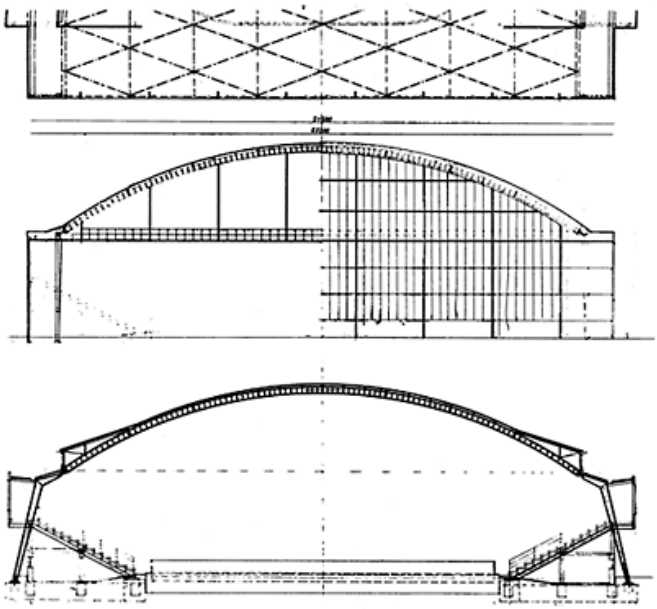

Fig. 17.18. Plan, elevation and cross-section of the double-layer lamella barrel vault in Kroměříž.

@Seismicisolation

23·26 kg/m^2) (Fig. 17.18). The type of bracing used in these structures has been illustrated already in Fig. 17.12. In these cases the main structural framework is covered with a wooden roofing, which gives an extremely pleasant internal appearance of the halls. This is shown in Figs 17.19(a) and 17.19(b).

The ice stadium in Havlíčkův Brod (illustrated in Figs. 17.20 and 17.21) presents a further modification of the supporting system, different from that used in previous cases. In this structure the axis of the main vault, with a length of 56 m, is orientated in the cross direction to the ice rink area having the dimensions 60 m×30 m. Here the vault is supported only at four points, by means of oblique stanchions in the form of a 'V'. The whole span of the main bearing vault is enlarged by means of these oblique supports to 58 m.

Supporting such a large vault at only four points, 36 m apart, required the longitudinal side parts of the main lamella vault to be reinforced. The most stressed latticed lamella units have been strengthened by means of the plate girder filler introduced between the chords. A project now receiving the attention of the author deals with the design of a lamella barrel vault having a length of 100 m, with ties arranged 5·0 m apart and resting on a

@Seismicisolation

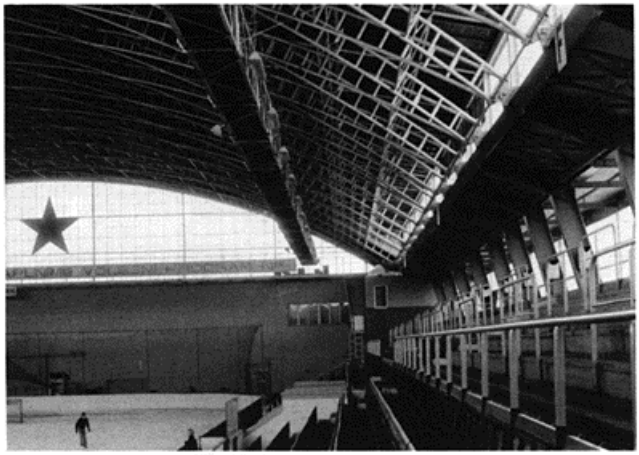

Fig. 17.19. Internal views of the ice rink in Žďár nad Sázavou.

@Seismicisolation

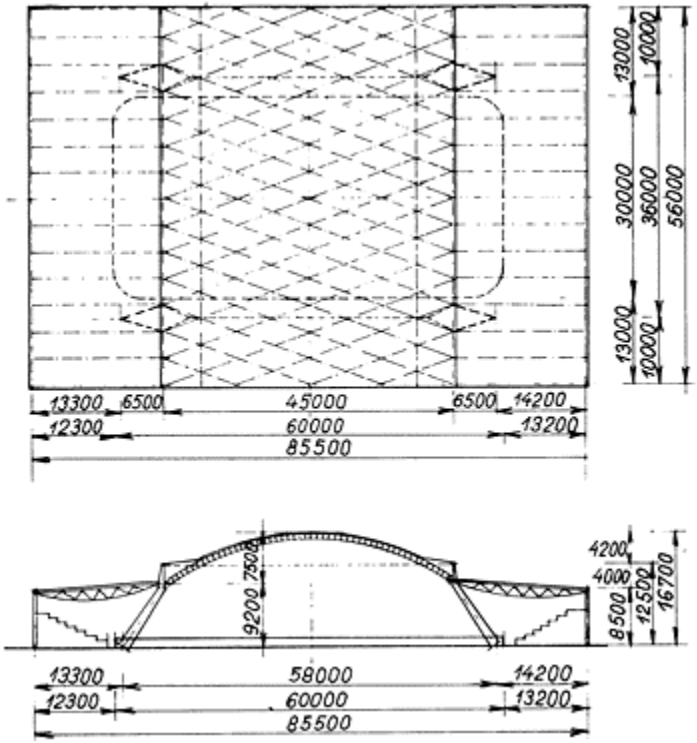

Fig. 17.20. Plan and cross-section of the barrel vault for an ice rink in Havlíčkův Brod.

@Seismicisolation

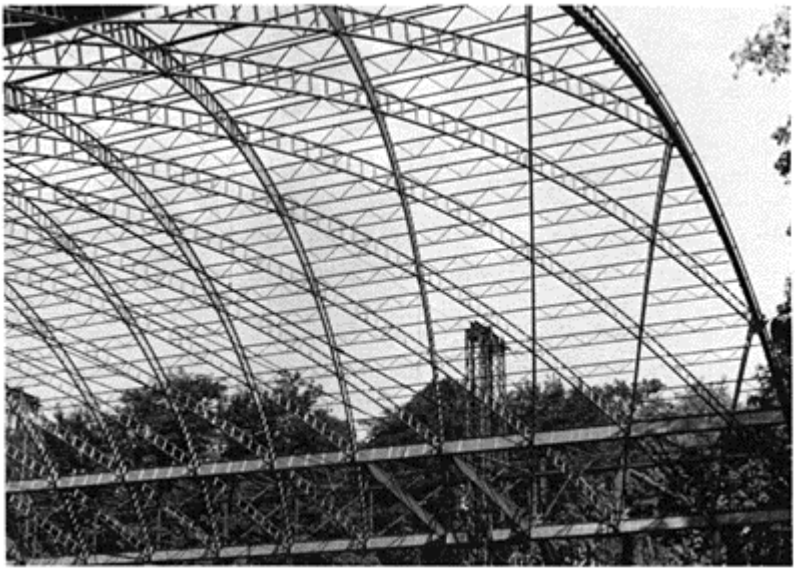

Fig. 17.21. The erection of the barrel vault in Havlíčkův Brod.

@Seismicisolation

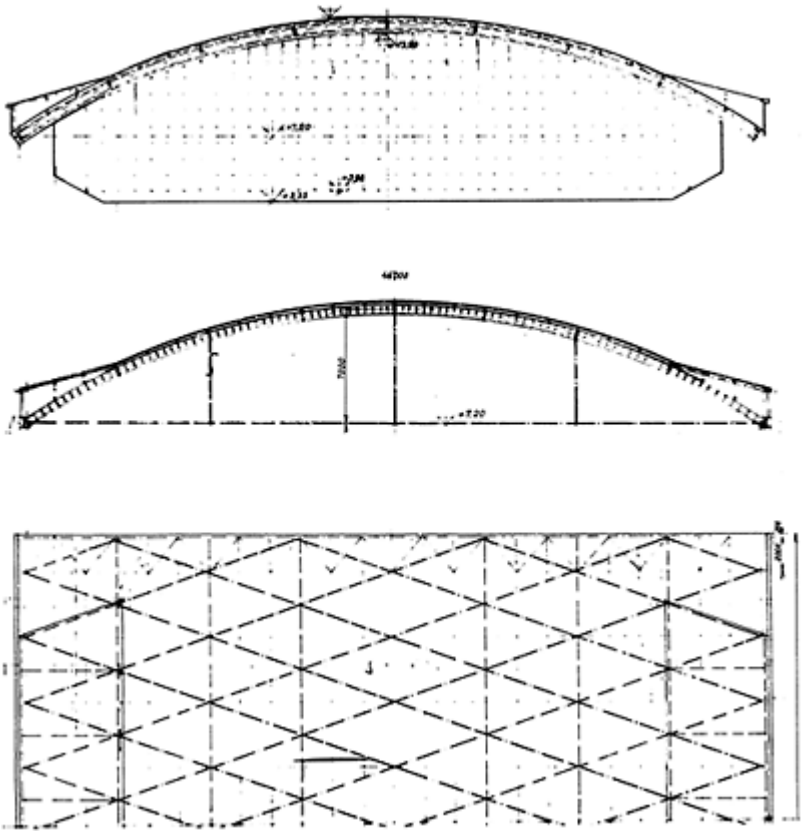

Fig. 17.22. Plan, cross-section and elevation of the barrel vault for the riding school in Motěšice.

massive building. This structure will cover a riding school in a small village, Motěšice, near Trenčín (Fig. 17.22). The steel consumption for this lamella roof over a ground plan of 4650 m^2 is 84978 kg, i.e. 18·29 kg/m^2, for the whole structure the steel will weigh 133721 kg, i.e. 28·78 kg/m^2.

5.3 Other Recent Applications of the Lamella System

Another interesting example where the lamella vault system could usefully be applied was the roof over a large span sports hall in Valencia, Spain (Fig. 17.23).

In this case, the lightweight steel lamella barrel vault has a span of 43·20 m and covers, like a great hat, the central part of the roof over a large sports hall.

The remaining surrounding periphery of the whole structure of oval shape is formed by the massive concrete cantilevers covering the tribunes for spectators. The central part

@Seismicisolation

of this structure is in steel, and has a total length of 79·45 m with its ends spatially formed in the shape of two hemi-domes.

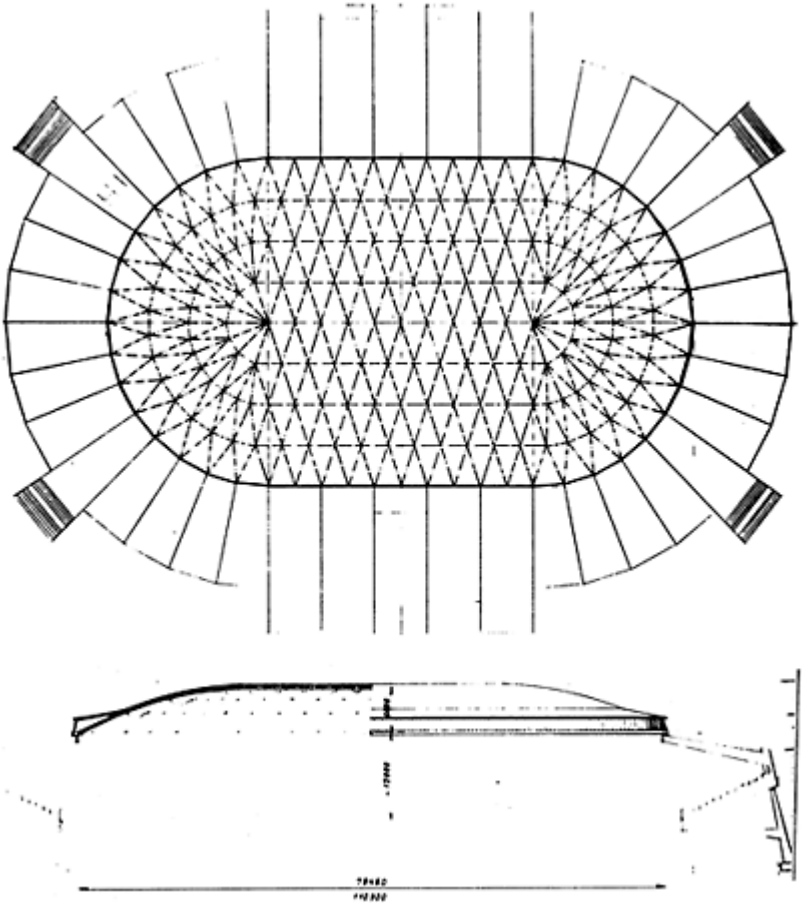

Fig. 17.23. Plan of the barrel vault erected over the sports hall in Valencia, Spain.

The lamella steel space structure lies along its whole periphery on massive concrete framed cantilevers, spaced 7·25 m apart. Figure 17.24 provides details of the supports used for this structure.

Over its supports the lamella roof is glazed by a horizontal strip of windows that follows the inner oval ground form plan of the surrounding massive concrete roof parts. This shape forced the design of the barrel vault to close both its ends by semi-domical structures. These two parts consist of lamella units, similar to those used for the central

@Seismicisolation

cylindrical part of the lamella vault, though their dimensions vary, whereas the main structure is formed by members of identical length.

It is possible to provide many other examples. Some of them are under active considerations for even bigger spans than those already achieved in practical applications (Figs. 17.25 and 17.26). These studies and projects of application of lamella-type roofs are for large span structures, such as sports halls, football stadiums, halls over gymnasia, cycling and speed-skating.

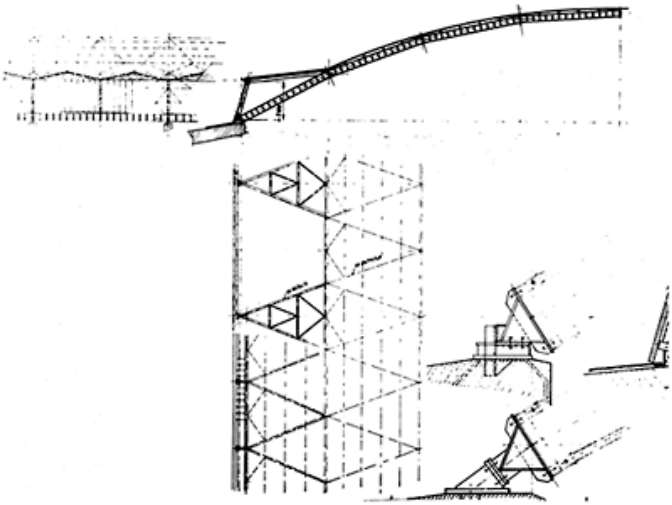

Fig. 17.24. The details of supports used for the Valencia Hall.

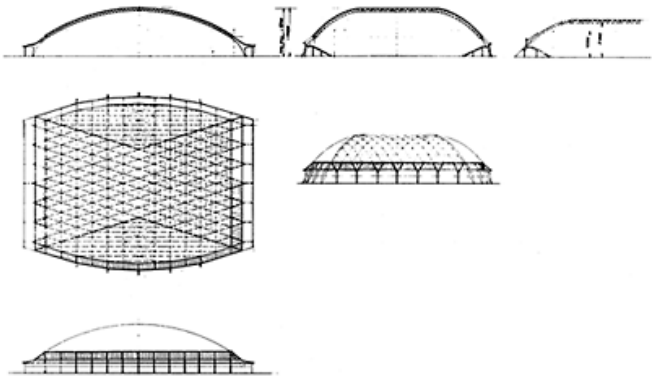

Fig. 17.25. Examples of projects now under active consideration for large span braced barrel vaults.

@Seismicisolation

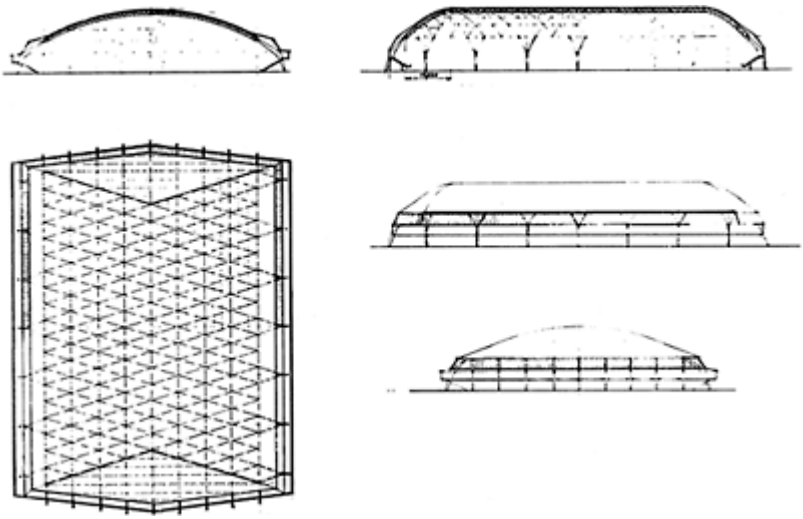

Fig. 17.26. A project for a lamella barrel vault for a sports hall of 98 m span.

The enclosed line drawings and photographs give some ideas and demonstrate the structural and architectural potential of such systems. The calculations proved that even for those large span lamella barrel vault structures the steel consumption lies between 25 and 35 kg/m^2 of the ground plan area. This, surely, can be declared to be very satisfactory.

REFERENCES

1. Zeman, J.Zwei neue Sporthallen in der CSSR. *Stahlbau*, **8**, 1973, pp. 252–254.
2. Zeman, J.A system for constructing light-weight roofs for various spans. *Acier-Stahl-Steel*, **6**, 1973, pp. 270–281.

@Seismicisolation

18
Structural Analysis of Reticulated Vaults

M.PAGANO and P.LENZA
Cattedra di Complementi di Tecnica delle Costruzioni,
Facoltà di Ingegneria, University of Naples, Italy

1 INTRODUCTION

Since 1952 the Engineering Faculty of Naples University has been carrying out studies on membrane and bending theory for single and double curvature vaults. Chapters 18 and 19 are the result of an extensive investigation made over a number of years under the guidance of Professor Michele Pagano at the University of Naples by a team of research workers consisting of G.C.Catanzaro, E.De Nardo, A.Ghersi, E.Giangreco, A. Giliberti, C.Greco, P.Lenza, M.Pagano, A.Pedecini and R.Sannino.

These studies have provided membrane solutions for translational as well as spherical vaults, identifying the static behaviour of slender barrel vaults with respect to various conditions along the two free edges.

In 1958 a triangular reticulated vault was designed for the Experimental Centre for Tests on Models of the Istituto di Tecnica delle Costruzioni. It appears to be one of the first examples of roofing a square plan with such a type of framework. The concept of shifting from continuous shells to discontinuous braced barrel vaults was introduced in this design and in the following years the Naples research team tackled the problem of non-linear behaviour, improving the analysis technique and completing the study of the behaviour of such structures under static conditions subjected to asymmetric loads, temperature effects and geometrical irregularities. This research was carried out both analytically and experimentally. Tests were performed not only using small scale models but also investigating full size prototypes; the latter tests, however, sometimes involved considerable difficulties.

The analysis of single curvature vaults is undoubtedly very complex. For structures of this type the problem of stability in non-linear conditions has great relevance and the elastic and plastic effects are receiving special attention.

This chapter provides the opportunity to sum up the results and to evaluate them as well as to consider further possible developments. Initially, then, it seems appropriate to present an exhaustive picture of the work carried out to date.

It should be pointed out that, as a result of architectural and social changes now taking place, more emphasis is being placed on the development of prefabricated systems, of which braced barrel vaults are exceptionally good examples.

@Seismicisolation

2 DOUBLY CURVED RETICULATED VAULTS

2.1 The Construction of Doubly Curved Experimental Vaults

The establishment of the Experimental Centre for testing models and structures at the University of Naples provided the opportunity to construct two laboratory buildings to house the testing equipment needed to carry out research work on full scale and small scale models of structures.

As these structures had to be erected in an area which is also used for annual exhibitions, their construction, beyond meeting the functional requirements, had also to satisfy a particular aesthetic quality. This has led to choosing shells of double curvature

Fig. 18.1. The doubly curved reinforced brick vault.

(Fig. 18.1), whose theoretical and practical analysis has been included in the research programme which the Centre has been carrying out under the auspices of the Italian National Research Council.

The methods of analysis used to find the stress distribution in the doubly curved reinforced brick vaults have been presented elsewhere.[1] They are based on the classical assumption that the shells behave as pure membranes. The solution of the indeterminate system of equilibrium equations for these structures has been obtained by approximate methods.

As a first step, it has been assumed that the boundary arches, supporting the structure, are not capable of withstanding loads normal to their plane. As a second step, on the other hand, it has been assumed that the system of arches is capable of applying a series of forces to the vault, which will re-establish the equilibrium at the four corner vertices.

@Seismicisolation

The resulting stress distribution in the shell is shown in Fig. 18.2, illustrating the principal forces.

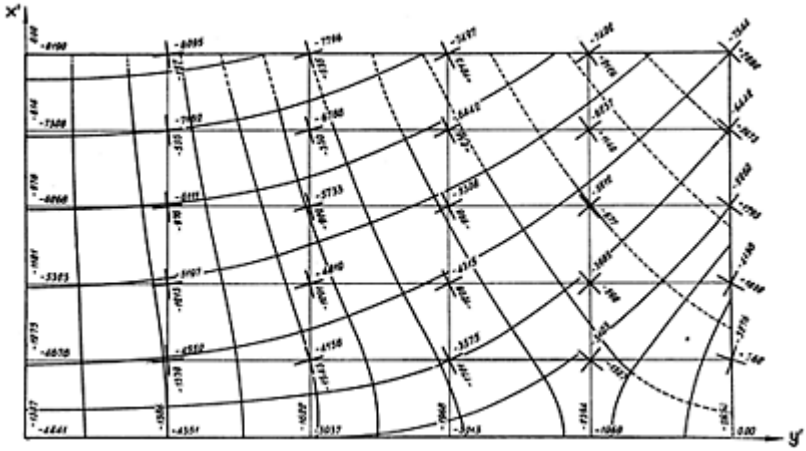

Fig. 18.2. The directions and values of the principal stresses in the vault shown in Fig. 18.1.——, Compression;——, tension.

2.2 Reticulated Steel Vault (see Fig. 18.3)

This structure has been analysed under two loading conditions:

(a) superimposed load of 200 kg/m^2, uniformly distributed over the horizontal area,
(b) wind pressure of 100 kg/m^2, uniformly distributed over half of the vault and 20 kg/m2 of dead weight.

The loads are assumed to be concentrated at the nodes. The boundary structure is unable to withstand forces acting normally to the plane of the vault, but is assumed to be able to resist symmetrical and asymmetrical forces transmitted by the vault, as well as a horizontal force, acting in the plane of the vault, due to the wind pressure acting on the total horizontal projected area.

@Seismicisolation

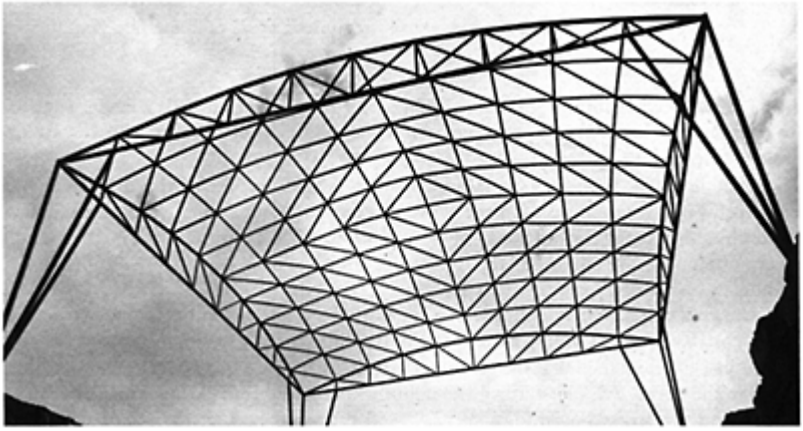

Fig. 18.3. The full-size reticulated steel barrel vault.

Fig. 18.4. Various stages of erection of the braced barrel vault.

Assuming that the structure consists of pin-connected members, the stress distribution may be obtained by the application of the usual equations of static equilibrium at joints.

@Seismicisolation

2.3 Method and Details of Construction

The construction of the reticulated steel barrel vault has been carried out according to the design drawings prepared by the Centro Carpenteria Tubolare of Dalmine, S.A., of Milan. This firm has fabricated the structure in several parts in their workshop. The size of the prefabricated parts has been chosen to allow for easy transportation and for simple erection on site. All the members have been connected by welding. This jointing technique and the use of tubular members greatly simplified the construction.

Figure 18.4 illustrates various stages in the erection of the structure.

3 THEORETICAL AND EXPERIMENTAL RESEARCH ON TRIANGULATED STEEL BARREL VAULTS[2,3]

The triangulated steel vault shown in Fig. 18.3 consists of a lattice framework over a translation surface and provides a satisfactory solution to the problem of roofing a square or rectangular area, or, in general, any polygonal area.

The roof diagrams, shown in Fig. 18.5, seem to be the most suited for a square or rectangular area. They consist of two series of polygonal arches at right angles to each other and parallel to the perimeter, and form a series of squares on plan.

These are stiffened by diagonal bars, placed in such a manner as to be in tension under the dead load.

The calculation of stress distribution in this barrel vault was based on the assumption that the members were pin-jointed at their nodal points. It was also assumed that the supporting spandrels were incapable of producing stress components in a direction normal to their plane.

The analysis of such a structure, in accordance with the above-mentioned hypotheses, may be carried out by applying the normal conditions for static equilibrium at the joints. These may be written as follows:

$$\sum_j S_{ij} \cos \alpha_{ij} + X_i = 0 \tag{1}$$

$$\sum_j S_{ij} \cos \beta_{ij} + Y_i = 0 \tag{2}$$

$$\sum_j S_{ij} \cos \gamma_{ij} + Z_i = 0 \tag{3}$$

where X_i, Y_i and Z_i are the component of load P_i in relation to a system of axes x, y, z; S_{ij} are the stresses in members linking joint i to all adjacent joints j, and α_{ij}, β_{ij} and γ_{ij} are the angles formed by member ij with the axes.

Stresses in all members, including spandrel members, can be determined by using eqns. (1), (2) and (3). For the perimeter joints, eqns. (1) and (2) will enable the determination of forces in the lower boundary of the spandrels.

@Seismicisolation

The results produced by symmetrical uniform loading are given in Fig. 18.6. Figures 18.7 and 18.8 give the results due to the asymmetrical and semi-symmetrical loading cases.

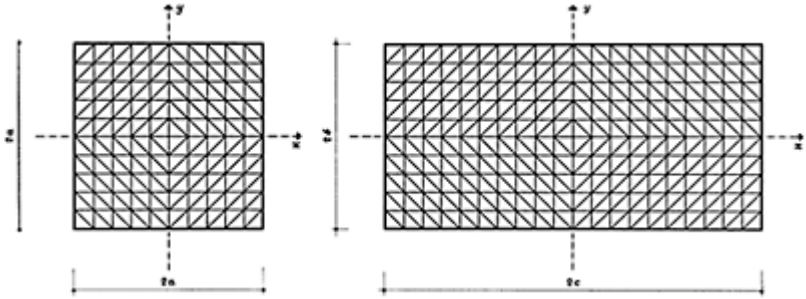

Fig. 18.5. Diagrams of bracing used for square and rectangular areas.

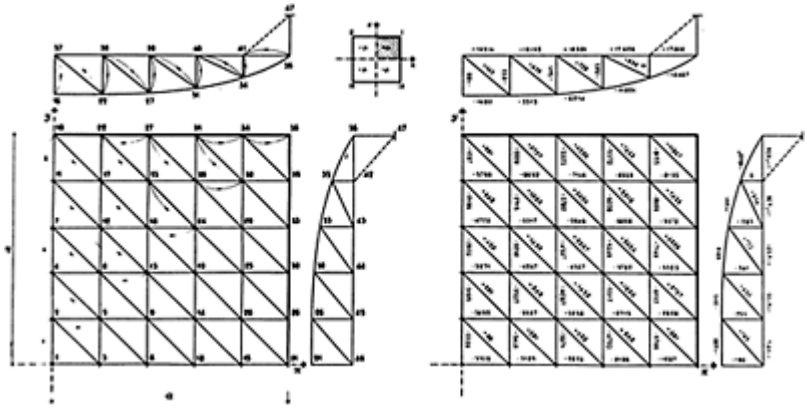

Fig. 18.6. Forces in the structure under symmetrical uniform loading. The diagram on the left shows the order in which the joint equilibrium has to be considered.

@Seismicisolation

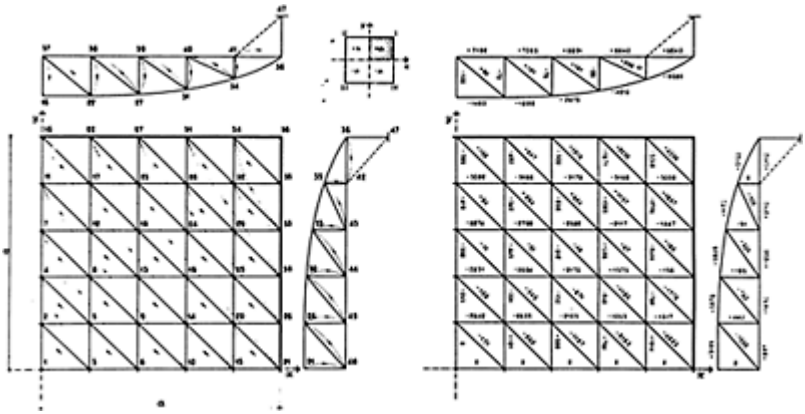

Fig. 18.7. Forces due to loading acting on one quadrant of the structure.

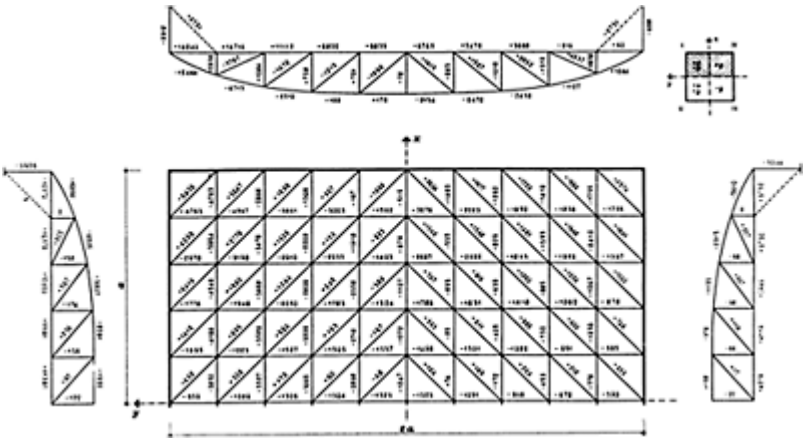

Fig. 18.8. Forces induced by loading acting on half of the structure.

In the case of fully symmetrical loading, because of the symmetry of the considered structure, only $\frac{1}{8}$ of the frame has be be considered during the analysis (Fig. 18.6).

The analysis is commenced at joint 1 which is the highest point of the vault and where the application of eqn. (3) suffices to define the forces in the members meeting at this joint. At joints 2 and similarly at points 4, 7 and 11, eqn. (1) is immediately satisfied by the symmetry, and the two remaining equations (2) and (3) are no longer sufficient to determine the three unknown forces at the joints. It is therefore necessary to express these as a function of one of them. As an example the stress in the member 2–4 may be taken as

$S_{2-4}=A$

@Seismicisolation

In 5, as in 13, 24 and 32, eqns. (1) and (2) coincide and give rise to a single condition, which, with eqn. (3), allows the two unknown forces to be determined. Continuing in the same way we reach joint 7, where a new unknown must be introduced, e.g. $S_{7-11}=B$.

Next we arrive without further difficulty at the periphery, where the stresses in the spandrel members appear in eqns. (1) and (3), and are calculated separately: if the peripheral members belonging to the spandrel are considered, eqn. (2) alone is sufficient to deduce at 16 the only unknown stress in the member 16–17.

After following through 17, 18, 24 and 23 we reach the perimeter again at joint 22, where the first of the two equations linking the values of A and B results as eqn. (2), since the stresses in 22–17 and 22–23 are known. This equation, with the one that may be written for joint 31, allows the values A and B to be determined, and consequently the values for the stresses in any member of the vault.

It should be noted that, given that the conditions imposed along the perimeter are arbitrary, equilibrium must be satisfied in each joint of the vault for any values of A and B: it is thus possible to ensure the equilibrium by assigning arbitrary values to A and B.

Stresses in the spandrel members are determined by applying eqns. (1) and (3) to the joints of the roof grid in conformity with the usual analytical method. Equation (2) is not involved because of the hypothesis that the curved members have no resistance in a transverse direction.

In the four corners, account is taken of the vertical upright alone, which thus supports a quarter of the total load. The loads applied to the upper joints of the curved units are added to the stresses transmitted by the vault members. Testing of local and general equilibrium serves as a check on the validity of this procedure.

The method of calculation described above, and carried out by the normal procedure for lattice frames, is undeniably a long and laborious one. The possibility of simplifying it, by making use of the calculation for the continuous membrane covering the vault, is therefore to be exploited, if offered.

When the membrane calculation is available the stresses in all members can be determined in a matter of hours, as against the many days needed with the procedure based on eqns. (1), (2) and (3). As is known, the membrane hypothesis implies satisfying the three indeterminate equilibrium equations (Fig. 18.9):

$$\frac{1}{8} \tag{4}$$

$$\frac{\partial n_1}{\partial x}+\frac{\partial S}{\partial y}+X=0 \tag{5}$$

$$\frac{\partial n_2}{\partial y}+\frac{\partial S}{\partial x}+Y=0 \tag{6}$$

Following the usual notation, the components of the external load are given as X, Y and

@Seismicisolation

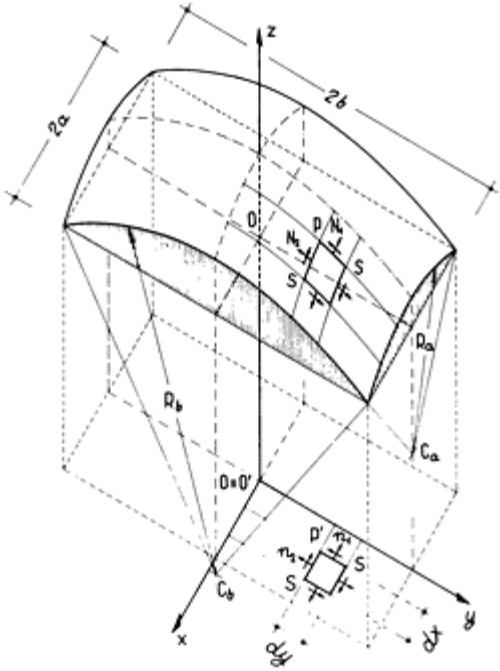

Fig. 18.9. Translational surface of a vault over a rectangular area.

Z; n_1, n_2 and S are the components of tension referred to the projection of the element on the plane x, y; p, q, r, s, t are the derivatives of the function $z=f(xy)$, representing the membrane surface. Expressions (4), (5) and (6), written for translational shells, can be used to calculate the stresses by means of the relaxation method, for which a suitable potential function should be introduced.

For simplification, it is generally assumed that boundary stresses are zero. This implies that spandrels are completely flexible transversely, and only capable of absorbing shear stresses transmitted by the vault in their plane.

Given the difficulties of exactly integrating eqns. (4), (5) and (6), a number of approximate methods have been put forward. This rapid evaluation of stresses is highly useful, not only for the initial design but also for the final design, provided it is possible to establish that the behaviour in fact differs slightly from that of a membrane.

The following is a summary of the approximate method proposed. The case taken is a translation vault roofing a rectangular area, with sides $2a$ and $2b$, circular directrices of radius R_a and R_b, and loaded by dead weight g and uniform over p. Introducing the derivatives of the surface function

$$z=\sqrt{R_b^2-y^2}+\sqrt{R_a^2-x^2}-R_a \tag{7}$$

the system of equations (4), (5) and (6) may be written as follows:

@Seismicisolation

$$\frac{\partial n_1}{\partial \xi}+\frac{\partial S}{\partial \eta}=0 \qquad \frac{\partial n_2}{\partial \eta}+\frac{\partial S}{\partial \xi}=0-n_1\frac{\rho_a^2}{(\rho_a^2-\xi^2)^{3/2}}-n_2\frac{\rho_b^2}{(\rho_b^2-\eta^2)^{3/2}} \tag{8}$$

$$=pa+ga\sqrt{1+\frac{\xi^2}{\rho_a^2-\xi^2}+\frac{\eta^2}{\rho_b^2-\eta^2}}$$

where

$$\xi=\frac{x}{a} \qquad \eta=\frac{y}{a} \qquad \rho_a=\frac{R_a}{a} \qquad \rho_b=\frac{R_b}{a} \qquad \sigma=\frac{b}{a}$$

For an approximate solution of eqn. (8), for the shear value we may assume the following semi-symmetrical polynomial expression:

$$S=[K_1\xi\eta+K_2(\xi\eta^3+\eta\xi^3)+K_3\xi^3\eta^3](pa+ga) \tag{9}$$

Differentiating, substituting in eqn. (8), and taking $n_1=n_2=0$ at the edge, we get

$$n_1=\left\{K_1\frac{1-\xi^2}{2}+K_2\left(\frac{1-\xi^4}{4}+\tfrac{3}{2}\eta^2(1-\xi^2)\right)+K_3\tfrac{3}{4}\eta^2(1-\xi^4)\right\}(pa+ga) \tag{10}$$

$$n_2=\left\{K_1\frac{\sigma^2-\eta^2}{2}+K_2\left(\frac{\sigma^4-\eta^4}{4}+\tfrac{3}{2}\xi^2(\sigma^2-\eta^2)\right)+K_3\tfrac{3}{4}\xi^2(\sigma^4-\eta^4)\right\}(pa+ga) \tag{11}$$

The three unknowns K_1, K_2 and K_3 are determined by assuming that eqns. (8) are satisfied at three suitable points on the vault. K_1, K_2 and K_3 are then obtained for dead weight and superimposed load as follows:

$$\text{self weight}\begin{cases} K_1=\dfrac{(\rho_a\rho_b/\sigma)[(\gamma_2+5)-\sigma^2(\gamma_1+5)]+[\sigma^3\rho_a^2\gamma_2-(\rho_b^2/\sigma^3)\gamma_1]}{2{\cdot}5(\sigma^2-1)(\rho_b/\sigma+\sigma\rho_a)} \\ K_2=-0{\cdot}8\dfrac{\rho_a\gamma_2-(\rho_b/\sigma^2)\gamma_1}{\sigma^2-1} \\ K_3=-\dfrac{(\rho_a\rho_b/\sigma)[5\sigma^2(\gamma_1-1)-\gamma_2(\sigma^2+5)+\gamma_1+5]+6\sigma[(\rho_b^2/\sigma^2)\gamma_1-\rho_a^2\gamma_2]}{3{\cdot}75\sigma^2(\sigma^2-1)(\rho_b/\sigma+\sigma\rho_a)} \end{cases} \tag{12}$$

$$\text{uniform super load}\begin{cases} K_1=\dfrac{-6(\rho_a\rho_b/\sigma)(\sigma^2-1)+\sigma^3\rho_a^2-\rho_b^2/\sigma^3}{2{\cdot}5(\sigma^2-1)(\rho_b/\sigma+\sigma\rho_a)} \\ K_2=-0{\cdot}8\dfrac{\rho_a-\rho_b/\sigma^2}{\sigma^2-1} \\ K_3=\dfrac{(\rho_a\rho_b/\sigma)(\sigma^2-1)-6\sigma(\rho_b^2/\sigma^2-\rho_a^2)}{3{\cdot}75\sigma^2(\sigma^2-1)(\rho_b/\sigma+\sigma\rho_a)} \end{cases} \tag{13}$$

where ρ_a, ρ_b and σ are designated as specified, representing the characteristics of the structure, and γ_1 and γ_2 have the values

$$\gamma_1=\frac{\rho_a}{(\rho_a^2-1)^{1/2}} \qquad \gamma_2=\frac{\rho_b}{(\rho_b^2-\sigma^2)^{1/2}}$$

@Seismicisolation

Substituting eqn. (12) or (13) in eqns. (9), (10) and (11), the relation produces

$$N_1=n_1(\beta_1/\alpha_2) \tag{14}$$

$$N_2=n_2(\alpha_2/\beta_1) \tag{15}$$

giving the whole system of stresses.

The stresses obtained for the membrane can be used to good advantage in determining the stresses in the members of the braced barrel vault. Considering each square of the roof grid together with the corresponding portion of the membrane (Fig. 18.10), we may

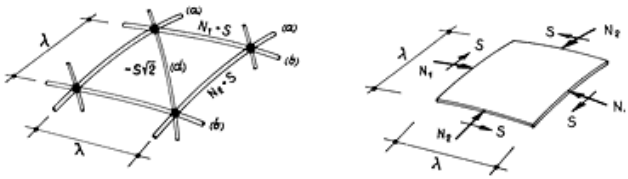

Fig. 18.10. Axial forces in the element of the braced barrel vault on the left and stresses in the equivalent shell portion on the right.

assume that the normal stresses *(N_1, N_2)* and shear stresses (S) would be absorbed by members (a) and (b) of the mesh. Normal stresses N_1 and N_2 are directly opposed and hence in equilibrium, whereas, on the hypothesis of pin-jointed members, the shear stresses *S* tend towards kinematic deformation of the mesh. As shown in Fig. 18.11, the diagonal bars absorb the resultant of shear and prevent this deformation. The diagonal is subjected to tension or compression in the two cases shown in the figure.

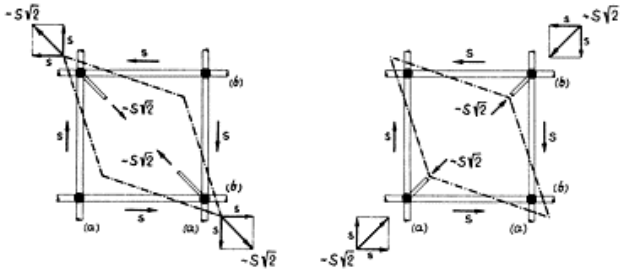

Fig. 18.11. The diagram shows how the diagonal member absorbs shear stresses *S;* the diagonal member is in tension on the left and in compression on the right.

@Seismicisolation

On the basis of the foregoing it is possible to obtain the normal stresses in the members parallel to the sides of the roofed area as the sum of two terms, one corresponding to the axial stresses in the membrane *(N_1, N_2)*, and the other to shear stresses in the membrane (S). Normal stress in diagonal members is obtained by vectorial composition of shear stresses (S). For a good degree of approximation it seems advisable to determine normal stresses *(N_1, N_2)* at the middle point of members (a) and (b), and shear stresses at the middle point of each diagonal (d).

For the structure in question, use was made of Tables 18.1 and 18.2. These give coefficients for determining N_1, N_2 and S with a uniform over-load acting on the vault

Table 18.1: Values of S/ga

η \ ξ	*0·00*	*0·20*	*0·40*	*0·60*	*0·80*	*1·00*
0·00	0·000000	–	–	–	–	–
0·20	0·000000	0·137971	–	–	–	–
0·40	0·000000	0·267502	0·528143	–	–	–
0·60	0·000000	0·380152	0·775065	1·199495	–	–
0·80	0·000000	0·467482	1·001404	1·668202	2·534316	–
1·00	0·000000	0·521051	1·200733	2·195945	3·666184	5·769215

Table 18.2: Values of *N1/ga* and *N_2/ga*

N1/ga	*N_2/ga*						
η \ ξ	η \ ξ	*0·00*	*0·20*	*0·40*	*0·60*	*0·80*	*1·00*
0·00	0·00	1·500000	1·433078	1·235647	0·917884	0·497348	0·000000
0·20	0·20	1·563792	1·499488	1·307448	0·990302	0·552436	0·000000
0·40	0·40	1·753321	1·696805	1·520812	1·205528	0·716175	0·000000
0·60	0·60	2·062972	2·019219	1·869545	1·557406	0·983937	0·000000
0·80	0·80	2·483170	2·456822	2·343079	2·035430	1·347825	0·000000
1·00	1·00	3·000000	2·995217	2·926066	2·624348	1·796375	0·000000

joints. The values for N_1 and N_2 given in Fig. 18.12 were obtained by multiplying the coefficients in Table 18.1 by the factor $pa\lambda$ ($\lambda/2$ for the perimeter members) and then taking the mean between the two joints at the end of each member.

The figure, Fig. 18.12, gives the values of S for each diagonal, obtained by multiplying the table coefficients by $pa\lambda$ and then taking the mean of the mean of the four corners for each square.

Figure 18.13 shows, for each member of type (a) and (b), the mean of the two S values for the two adjacent squares.

@Seismicisolation

Figure 18.14 gives, for each diagonal, the values of *S* multiplied by $\sqrt{2}$(sufficiently accurate in view of the shallowness of the vault) and, for each member of type (a) and (b), the sum of the values shown in Figs. 18.12 and 18.13. The result s of the normal method of calculation for a lattice structure are given in brackets for comparison.

For a similar comparison in the case of perimeter members it is first necessary to make allowance for the additional spandrel stresses, to be determined separately. This calculation was carried out following the standard method for thin shells. The boundary shears of the membrane were applied to the spandrel joints, and the stresses in its

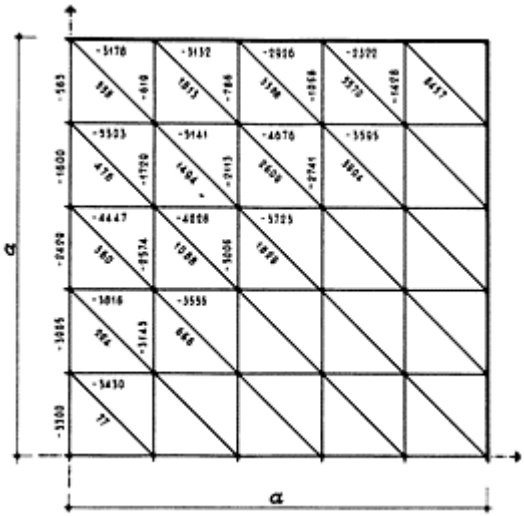

Fig. 18.12. Normal stresses of the continuous membrane evaluated at the mid-point of the member of type (a) and (b), and shear stresses evaluated at the centre of each elemental square.

@Seismicisolation

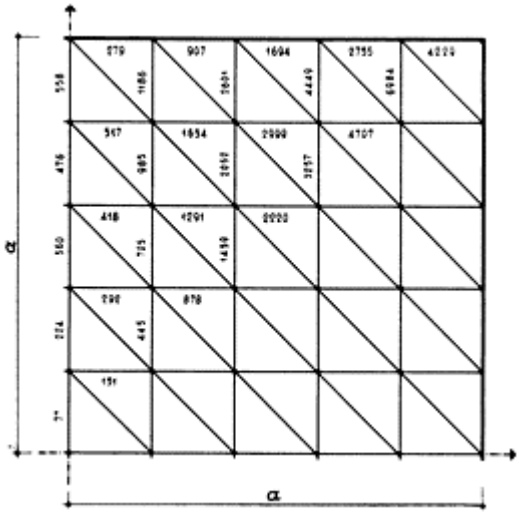

Fig. 18.13. Medium values of shear stresses relative to two adjacent squares.

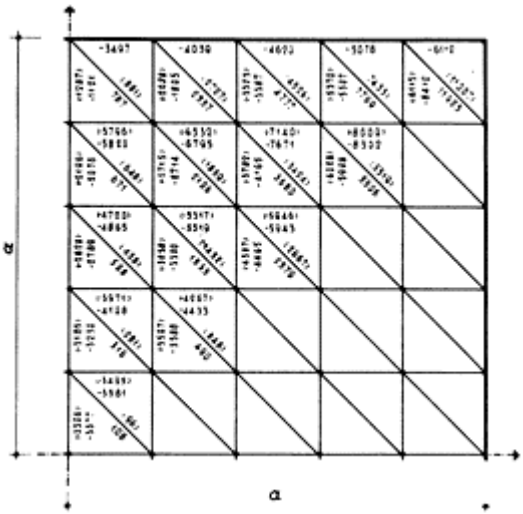

Fig. 18.14. Total stresses in members of triangulated vault; brackets contain values from Fig. 18.6.

@Seismicisolation

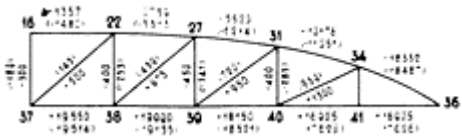

Fig. 18.15. Stresses in the gable truss; brackets contain values from Fig. 18.6.

individual members were calculated by assuming the isostatic scheme of a simply supported lattice beam.

The value thus obtained for the members linking vault and spandrel were then added to those already determined for vault members. The totals can then be compared with the results obtained by the usual theoretical method (given in brackets in Fig. 18.15).

As can be seen from Figs. 18.14 and 18.15, the results in general tally well, except for inclined spandrel members, for which stresses are very small and the graphic method adopted here consequently gives a less accurate degree of approximation.

The method of calculating the covering membrane, as described in the foregoing, is open to several criticisms. To begin with, it makes no allowance for bending, which may have considerable effects both near the edges and at the rigid spandrel joints. Furthermore, at the perimeter corners eqn. (6) is only solvable for zero load. Lastly, the assumption of complete transverse flexibility for the spandrels certainly does not hold good at the corners, where each spandrel is rigidly connected with the adjacent ones.

These criticisms are valid enough to justify further theoretical and experimental research in order to establish how far the membrane calculation holds good. Work along these lines is now being carried out on a 1:10 scale model of the actual structure (Fig. 18.16).

These experiments, which aim at a comparison between the results obtained by the foregoing calculation and those measured on the model, are complicated in this case by the fact that, in the actual structure, the spandrels are supported not only by vertical columns at the four corners but also by inclined bars to withstand transverse wind action. This invalidates the original hypothesis, and a fresh calculation for the spandrels has had to be made on the assumption of a triangulated portal pin-jointed at the bottom.

The complete research programme envisages a series of tests on the actual building, but numerous difficulties have arisen to prevent this and have likewise slowed down the progress of laboratory work. Too few members have been tested, and too few checks carried out on test loadings, for us to express a final opinion as yet, though some interesting results have already emerged. To give an overall picture of the agreement

@Seismicisolation

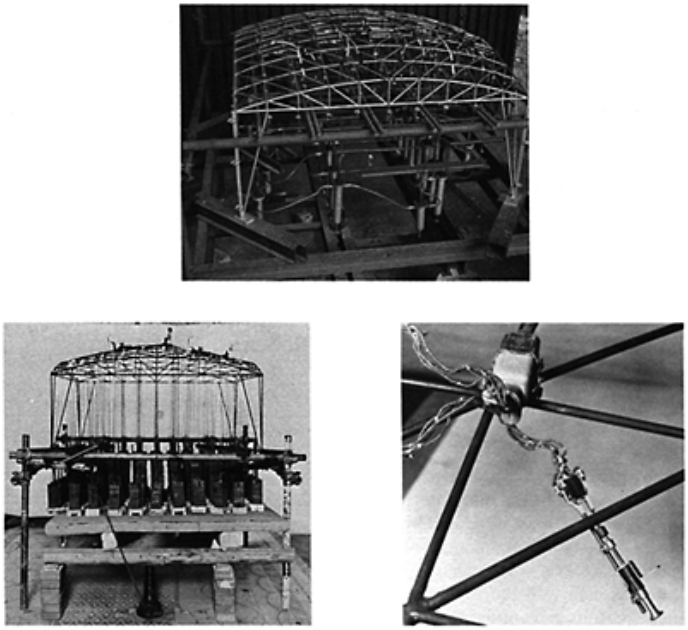

Fig. 18.16. Structural model of the triangulated barrel vault, made in scale 1:10, under test loading. Strain measurements have been taken with electric resistance strain gauges.

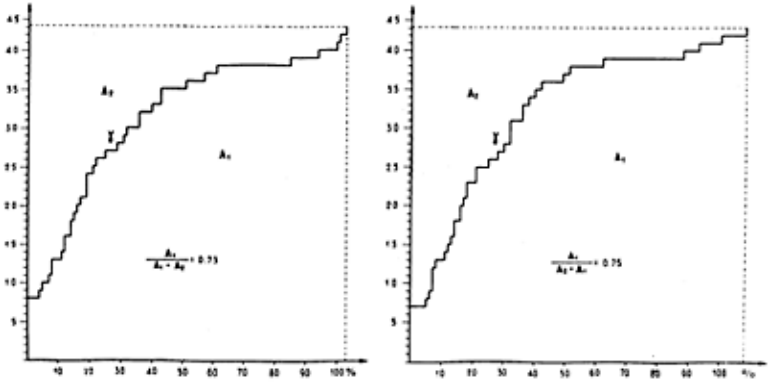

Fig. 18.17. Diagrams illustrating the accordance between theory and experiment.

@Seismicisolation

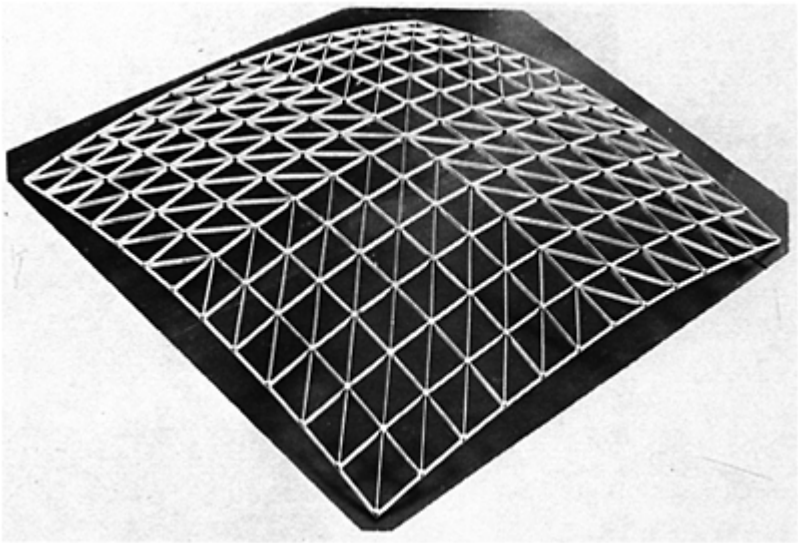

Fig. 18.18. A model of a plywood reticulated vault.

between experimental and theoretical results in the two cases assumed for the spandrels we refer the reader to the diagrams in Fig. 18.17.

On the vertical axis is shown the number of measured members in which the discrepancy between experimental and theoretical results is less than the corresponding figure (expressed as a percentage) on the horizontal axis. Discrepancies of slightly over 100% are taken in, and almost all test results are included, with the obvious exception of anomalous results and scatter. For the purposes of the comparison we have allowed for a small plus or minus error in measurement in every case, and the discrepancy is taken as the minimum value offered by this range.

The curves in Fig. 18.17 have been plotted on this basis. Where there is complete agreement area A_2 vanishes. The ratio of areas A_1:(A_1+A_2) can thus be taken as an 'index of agreement' between theory and test. On the basis of results so far, as shown in Fig. 18.17, this agreement varies around 75%, though it is not considered that sufficient measurements have been taken yet to convalidate this figure.

The high cost of construction and experimentation with reticulated vaults has reduced to a minimum the number of reticulated models and has obliged us to effect the greater part of the experimentation on continuous vaults. The research programme has been limited to only three models of reticulated vaults: the small scale model already mentioned (Fig. 18.16), the corresponding full scale model (Fig. 18.3) and a plywood model in which the diagonals have turned through 90° in respect of the preceding model (Fig. 18.18).

@Seismicisolation

REFERENCES

1. Pagano, M. and Greco, C. Sul calcolo delle volte di translazione. *Giornale del Genio Civile*, Dec. 1958, Rome.
2. Pagano, M. Studio di una volta reticolare in acciaio. *Acciaio*, No. 4, 1960, Rome.
3. Pagano, M. Theoretical and experimental research on triangulated steel vaults. Proceedings of the IASS colloquium, Paris, July 1962.

@Seismicisolation

19
Theoretical Studies and Experimental Research on Structural Behaviour of Reticulated Vaults

M.PAGANO and P.LENZA
Cattedra di Complementi di Tecnica delle Costruzioni,
Facoltà di Ingegneria, University of Naples, Italy

1 INTRODUCTION

All investigations reported so far in Chapter 18 have been carried out using the structural method of analysis, formulated in the 1950s and supplemented by specially prepared tables.

In this technique the authors adopted approximate polynomial expressions discussed in the previous chapter, for the solution of the differential equations which describe the stress distribution in the shell vaults.

The earlier theoretical and experimental investigations into the static behaviour have emphasised an obvious need for more exhaustive theoretical studies. This could lead to the extension of the range of various types of barrel vaults covered by the described structural analysis, and could satisfy the demand by designers for a reliable method of analysis of steel reticulated vaults. The stress equations have been improved, therefore, by replacing the polynomial terms by trigonometric ones easily adaptable for tabulation and leading to a determination of stress distribution which appears to be more consistent with the actual behaviour of these structures, in particular in the zones adjacent to the four apexes, where the previously described theory has failed altogether.

Thus the use of the continuum shell analogy for the reticulated barrel vaults has appeared to be more consistent with the actual behaviour provided by the experimental studies.

2 DERIVATION OF THE SURFACE OF THE TRANSLATION VAULT

The translation vault (shown in Fig. 18.9) roofing a rectangular plan having as sides $2a$ and $2b$ and as circular directrix radii R_a and R_b and being under dead load g and uniform superimposed load p can have its surface represented by the following equations:

$$z = \sqrt{R_b^2 - y^2} + \sqrt{R_a^2 - x^2} - R_a \tag{1}$$

@Seismicisolation

This becomes
where

$$\left.\begin{aligned}
&\frac{\partial n_1}{\partial \xi}+\frac{\partial S}{\partial \eta}=0\\
&\frac{\partial n_2}{\partial \eta}+\frac{\partial S}{\partial \xi}=0\\
&-n_1\frac{\rho_a^2}{(\rho_a^1-\xi^2)^{3/2}}-n_2\frac{\rho_b^2}{(\rho_b^2-\eta^2)^{3/2}}=pa+ga\sqrt{1+\frac{\xi^2}{\rho_a^2-\xi^2}+\frac{\eta^2}{\rho_b^2-\eta^2}}\\
&\xi=\frac{x}{a}\qquad \eta=\frac{y}{a}\qquad \rho_a=\frac{R_a}{a}\qquad \rho_b=\frac{R_b}{a}\qquad \sigma=\frac{b}{a}
\end{aligned}\right\}\tag{2}$$

For the approximate solution of eqns. (2) the following hemi-symmetric expression for the shear characteristic is proposed:

$$S=\left[\sum A_m(\xi^i\eta^j+\xi^j\eta^i)+\sum B_n \operatorname{sen}\frac{n\pi\xi}{2}\operatorname{sen}\frac{n\pi\eta}{2\sigma}\right](p+g)a \tag{3}$$

where, i,j and n are odd numbers. By substituting in the first two equations of (2), where the usual edge conditions hold (n_1=n_2=0 for ξ=1 and η=σ), the following expressions are obtained:

$$\left.\begin{aligned}
n_1=&-\left\{\sum A_m\left[\frac{j}{i+1}(\xi^{i+1}-1)\eta^{j-1}+\frac{i}{j+1}(\xi^{j+1}-1)\eta^{i-1}\right]\right.\\
&\left.-\sum\frac{B_n}{\sigma}\cos\frac{n\pi\xi}{2}\cos\frac{n\pi\eta}{2\sigma}\right\}(p+g)a\\
n_2=&-\left\{\sum A_m\left[\frac{i}{j+1}(\eta^{j+1}-\sigma^{j+1})\xi^{i-1}+\frac{j}{i+1}(\eta^{i+1}-\sigma^{i+1})\xi^{j-1}\right]\right.\\
&\left.-\sum B_n\sigma\cos\frac{n\pi\xi}{2}\cos\frac{n\pi\eta}{2\sigma}\right\}(p+g)a
\end{aligned}\right\}\tag{4}$$

where A_m and B_n are unknown dimensional coefficients that can be determined by satisfying the local equilibrium in characteristic points of the vault through the third equation of eqns. (2). Expressions (2), (3) and (4) offer the advantage of a considerable convergence so that the first terms of each summation are sufficient for reaching a good approximation; moreover, the terms of the second summation of the eqn. (4) are null at the boundary; therefore in the third equation of system (2) written for the selected boundary points, the B_n terms disappear. It is thus convenient to assume a number of terms from the first summation equal to the number of selected boundary points and a number of terms from the third summation equal to the internal points.

@Seismicisolation

In short, the A_m values are determined by a system of equations the order of which is equal to m; the B_n values are determined in the same way once the A_m have become known, i.e. when the number of points grows, the order of the system does not grow correspondingly. However, the chosen expressions do not permit one to comply with the apex equilibrium conditions (ξ=1, η=σ) due to the preset assumption that tympana are incapable of exerting normal forces upon the vault.

2.1 Influence of the Tympana upon the Stress Distribution in the Shell

To take into account the real ability of the tympana to exert normal forces near the apexes we propose the overlapping of further stress conditions with the values of n_1 and n_2 different from zero along the edges. The following expressions, subject to the local equilibrium in the apex (ξ=1, η=σ), satisfy the first two equations everywhere and supply rapidly decreasing stress values towards the medians where they become zero.

where

$$\left.\begin{aligned}
S &= \left[\frac{4}{3}n^*\xi^3\eta^3 + \sum C_k\left(\frac{k+1}{k}\xi^k\eta^k - \frac{k+3}{(k+2)\sigma^2}\xi^{k+2}\eta^{k+2}\right)\right](p+g)a \\
n_1 &= -\left[n^*\xi^4\eta^2 + \sum C_k\left(\xi^{k+1}\eta^{k-1} - \frac{1}{\sigma^2}\xi^{k+3}\eta^{k+1}\right)\right](p+g)a \\
n_2 &= -\left[n^*\xi^2\eta^4 + \sum C_k\left(\xi^{k-1}\eta^{k+1} - \frac{1}{\sigma^2}\xi^{k+1}\eta^{k+3}\right)\right](p+g)a \\
n^* &= \frac{pa + ga\left[1 + \frac{1}{\rho_a^2 - 1} + \frac{\sigma^2}{\rho_b^2 - \sigma^2}\right]^{1/2}}{(pa+ga)\left[\frac{\rho_a^2\sigma^2}{(\rho_a^2-1)^{3/2}} + \frac{\rho_b^2\sigma^4}{(\rho_b^2-\sigma^2)^{3/2}}\right]}
\end{aligned}\right\} \qquad (5)$$

and

k=5+4r r=0, 1, 2…

Such a damping effect can be distributed along the edges so as to take into account particular characteristics of the tympana through the summation terms. For example the forces n_1 and n_2 become zero in an arbitrary number of points in addition to the intersection points of the medians for which the above condition has already been satisfied.

As regards pre-stressed vaults, an arbitrary stress distribution along the edges can be reproduced. Indeed, through such a technique it seems possible to have concordance between the static and structural models. This is in fact the object of the present theoretical and experimental investigations.

What was stated above has been applied to a vault roofing a rectangular plan having the following characteristics

@Seismicisolation

$$\frac{R_a}{a}=2, \qquad \frac{R_b}{b}=2, \qquad \frac{b}{a}=2$$

for the over-load only, and to a vault roofing a square plan the characteristics of which are R/a=2 with reference to the dead load and the superimposed load, by only considering the first terms of the system of equations (4) and (5) written for the apex (0,0) and for points (1,0) and (0, σ). Tables 19.1,19.2 and 19.3 give the stress values for the considered rectangular translation vault.

To estimate the degree of approximation of the method the load surface has been determined by formulae (4) and (5). Analytically eqns. (4) and (5) are substituted in the left-hand side of the third equation of the eqns. (2) which thus supplies function $P(\xi,\eta)$ and $g(\xi, \eta)$ for which the equilibrium condition is fulfilled in all points of the vault. It is clear

Table 19.1: Rectangular translation vault (*ba*=2; *Ra/a*=2; R_b/b=2); values of *S/pa* (uniform superimposed load)

η \ ξ	*0*	*0·2*	*0·4*	*0·6*	*0·8*	*1·0*
0	0	0	0	0	0	0
0·4	0	0·08311	0·1690	0·2615	0·3639	0·4652
0·8	0	0·1846	0·3777	0·5906	0·8318	1·1137
1·2	0	0·3232	0·6652	1·0538	1·5150	2·0456
1·6	0	0·5181	1·0728	1·7200	2·4890	3·4230
2·0	0	0·7888	1·6418	2·6598	3·8904	5·4204

Table 19.2: Rectangular translation vault *(ba=2; R_a/a=2; b=2)*; **values of N_1/pa (uniform superimposed load)**

η \ ξ	*0*	*0·2*	*0·4*	*0·6*	*0·8*	*1·0*
0	0·5332	0·5106	0·4435	0·3335	0·1837	0
0·4	0·5936	0·5685	0·4940	0·3729	0·2106	0·0150
0·8	0·7793	0·7462	0·6488	0·4941	0·2929	0·0612
1·2	1·1050	1·0577	0·9204	0·70611	0·4368	0·1415
1·6	1·5982	1·5295	1·3311	1·0268	0·6544	0·2618
2·0	2·3088	2·2091	1·9230	1·4882	0·9657	0·4330

@Seismicisolation

Table 19.3: Rectangular translation vault (*ba=2; Ra/a=2; b* = 2); **values of** N_2/pa **(uniform superimposed load)**

η \ ξ	*0*	*0·2*	*0·4*	*0·6*	*0·8*	*1·0*
0	2·9328	2·9855	3·1504	3·4476	3·9150	4·6179
0·4	2·8374	2·8884	3·0474	3·3338	3·7843	4·4612
0·8	2·5381	2·5845	2·7301	2·9910	3·40011	4·0130
1·2	1·9982	2·0413	2·1756	2·4149	2·7862	3·3331
1·6	1·1679	1·2136	1·3547	1·6035	1·9829	2·5343
2·0	0	0·0603	0·2449	0·5660	1·0474	1·7320

that the approximation is evaluated on the basis of the deviation between absolute uniformity, that remains a theoretical schematisation, and the one obtained. The percentage differences and the load surfaces calculated for this example are clearly a sign of the reliability of the obtained approximation (Fig. 19.1).

Therefore the application of the proposed formulae holds if the predicted stress distributions in correspondence of the edges have been actually realised. For the sake of comparison as regards the square vault we have diagrammatically reported with respect to the dead load the stresses calculated for the edge conditions corresponding to the first term of eqn. (5) only, the stresses for edges that are completely unable to resist normal forces and Flugge's stresses.

The first diagram of Fig. 19.2 depicts the stress distributions predicted at the edges in the above three cases. The distribution, that only corresponds to the first term of eqn. (5), follows the parabolic law and its value is zero at the centre; for the edges unable to resist

η \ ξ	0	0·2	0·4	0·6	0·8	1·0
0	1·0000	1·0031	1·0123	1·0235	1·0272	1·0000
0·4	1·0191	1·0217	1·0283	1·0352	1·0332	0·9988
0·8	1·0704	1·0706	1·0705	1·0662	1·0487	0·9960
1·2	1·1303	1·1279	1·1199	1·1021	1·0662	0·9925
1·6	1·1462	1·1429	1·3322	1·1101	1·0688	0·9908
2·0	1·0000	1·0027	1·0101	1·0179	1·0194	1·0000

(a)

η \ ξ	0	0·2	0·4	0·6	0·8	1·0

@Seismicisolation

0	1·0000	1·0163	1·0585	1·1048	1·1124	1·0000
0·2	1·0163	1·0310	1·0685	1·1082	1·1094	0·99511
0·4	1·0585	1·0685	1·0930	1·1145	1·0987	0·9819
0·6	1·1048	1·1082	1·1145	1·1114	1·0753	0·9658
0·8	1·1124	1·1094	1·0987	1·0753	1·0322	0·9603
1·0	1·0000	0·9951	0·9819	0·9658	0·9603	1·0000

(b)

η \ ξ	0	0·2	0·4	0·6	0·8	1·0
0	1·0000	1·0202	1·0710	1·1236	1·1268	1·0000
0·2	1·0202	1·0380	1·0825	1·1264	1·1219	0·9939
0·4	1·0710	1·0825	1·1096	1·1301	1·105 8	0·97711
0·6	1·1236	1·1264	1·1301	1·1208	1·0744	0·9577
0·8	1·1268	1·1219	1·1058	1·0744	1·0237	0·9527
1·0	1·0000	0·9939	0·9771	0·9577	0·9527	1·0000

(c)

Fig. 19.1. Percentage errors of local equilibrium corresponding to the stresses reported in Tables 19.1–19.3 and in the examples of Figs. 19.2 and 19.3.

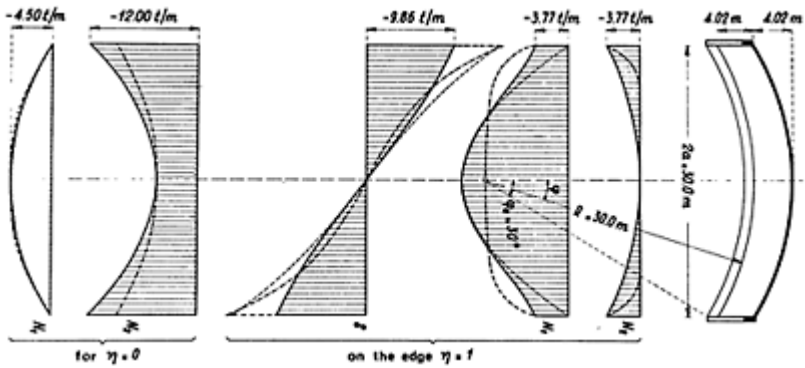

Fig. 19.2. Square vault: membrane forces diagram.–·–·–, Flügge's example (g=0·3 t/mq);——, formulae (3), (4) (g=0·3t/mq);——, formulae

@Seismicisolation

(3), (4)+ (5) (g=0·3t/mq). For the proposed formulae only the first term of each summation has been used: the percentage error of local equilibrium is shown in Fig. 19.1(c).

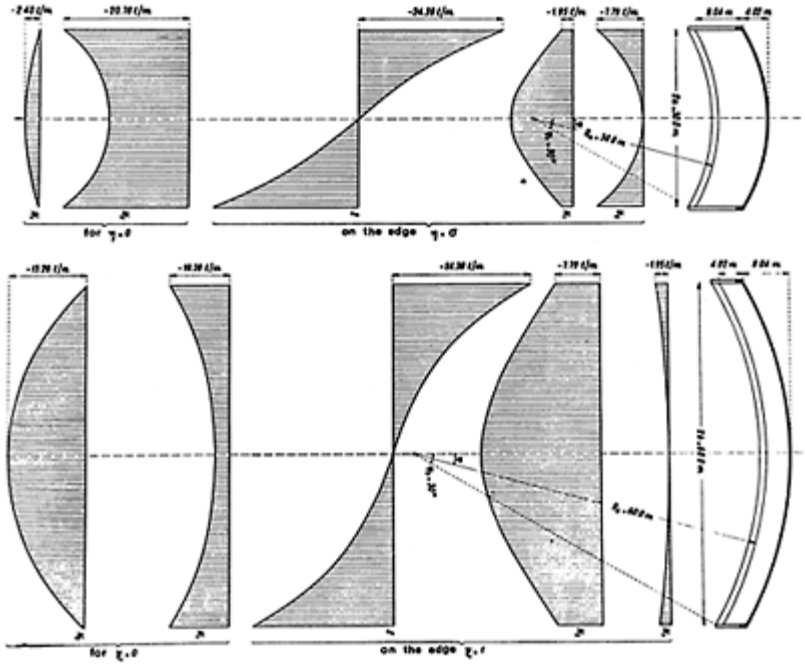

Fig. 19.3. Rectangular vault: diagrams of membrane forces for p=0·3 t/mq supplied by (3), (4)+(5). The percentage error of local equilibrium is shown in Fig. 19.1(a).

@Seismicisolation

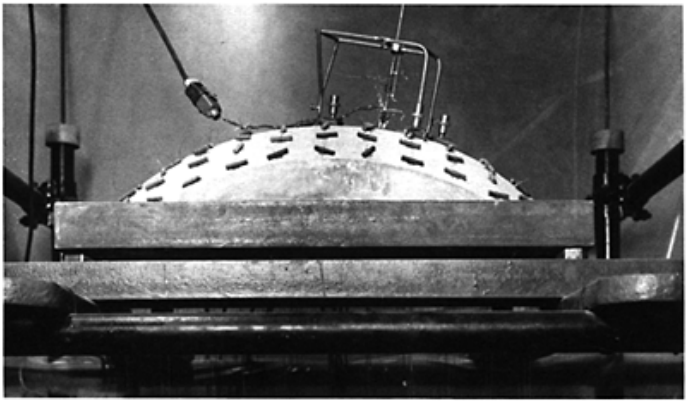

Fig. 19.4. Experimental equipment.

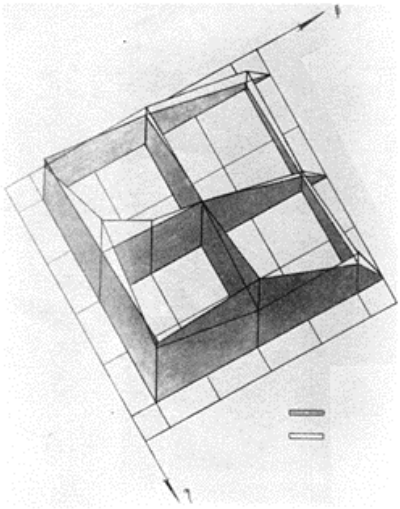

Fig. 19.5. Values of theoretical and experimental strains measured in the ξ direction; the experimental values correspond to tympana which are mobile on the supporting plane. The experimental curves have been assigned an edge value of zero: the extrapolation does not appear to be allowable near the apex.

@Seismicisolation

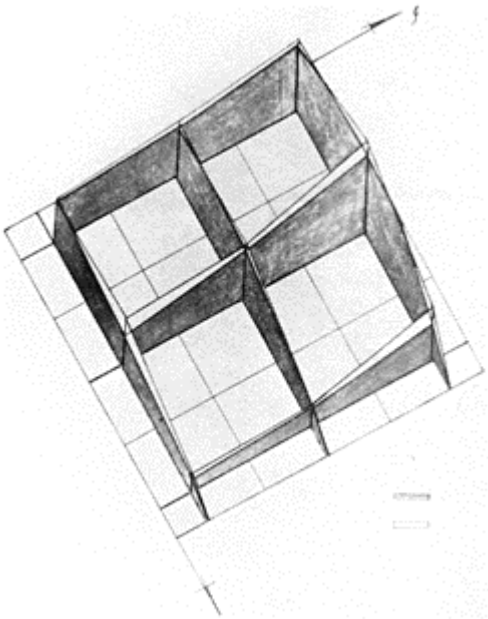

Fig. 19.6. Values of theoretical and experimental strains measured in the η direction; the experimental values correspond to tympana mobile on the supporting plane. The experimental curves have been assigned an edge value of zero; the extrapolation does not appear to be allowable near the apex.

normal forces all the values are zero. Finally, according to Flügge, the values of the edge reactions exhibit an intermediate behaviour and tend to zero near the apex.

The following diagrams clearly show the influence of the edge conditions of the vault stress system; it does not affect the medians while becoming relevant near the edges.

Figure 19.3 depicts the diagrams calculated for the rectangular vault described earlier, to which we have applied the proposed formulae; as concerns eqns. (5) for characterising the edge stress system, only the first term has been chosen.

Intuitively it appears clear that at least on the long side the actual diagram of edge stresses should exhibit values which are only sensitive near the apex; to this and the successive terms of eqn. (5) could be used.

The set of comments and criticisms that can be applied to the theoretical treatment (already mentioned), in particular with reference to the assumptions and the scheme underlying the calculations, requires the construction of these types of structures to be

@Seismicisolation

supported by experimental investigations. Hence a series of tests have been made aiming at investigating the static behaviour of a very wide range of vaults and the advantages that can be derived by using the pre-stressing technique.

The results are summarised now concerning asbestos-concrete models (Fig. 19.4). The tests were made at the Istituto di Scienza delle Costruzioni of Naples University. The stresses are obviously affected by the actual boundary conditions of tympana: the zero edge condition determined by the extrapolation (Figs. 19.5–19.8) appears never allowable

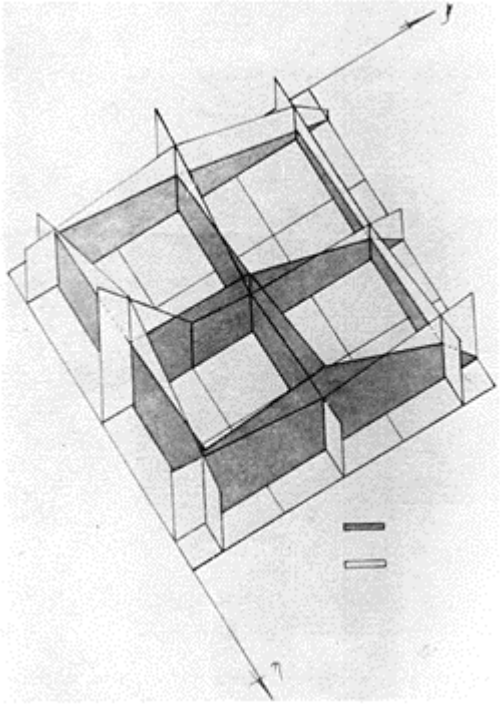

Fig. 19.7. Values of theoretical and experimental strains measured in the ξ direction; the experimental values correspond to tympana fixed in the supporting plane of the model (at the level of the apexes).

@Seismicisolation

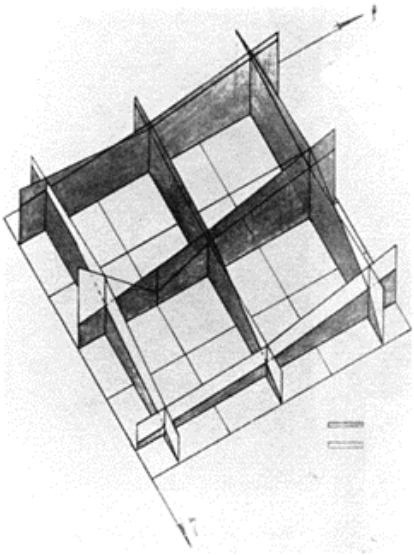

Fig. 19.8. Values of theoretical and experimental strains measured in the η direction; the experimental values correspond to tympana fixed in the model supporting plane.

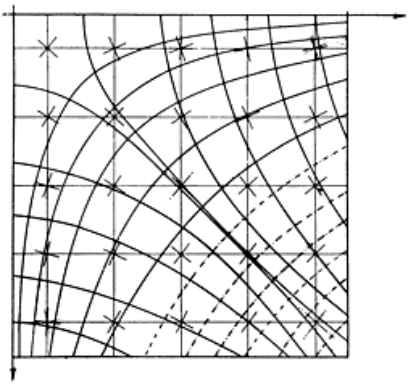

Fig. 19.9. Isostatic curves estimated for the model of Fig. 19.4. In some points the dotted curves stand for the experimentally determined main

@Seismicisolation

directions.——, stressed; –·–·–, tensioned.

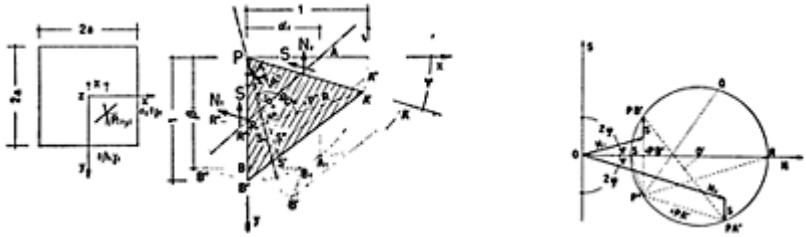

Fig. 19.10. Research for the main forces and directions by means of Mohr's circle.

in the proximity of the apex and quite reliable for the supported tympanum. Figure 19.9 also depicts the behaviour of the isostatic lines in the vault. The main forces have been determined through the well-known construction of Mohr's circle (Fig. 19.10), which has remained conceptually the same, concerning the vault element vertically projected on the tangential plane.

The comparison must still be refined, but it is already clear that theoretical and experimental results agree to a sufficient extent so as to permit their practical application.

3 ASYMMETRIC UNIFORM LOAD CONDITION[7]

3.1 Generalities

The model of uniformly distributed load certainly cannot exhaust all design investigations on the membrane system. In fact it is well known that in the structure lifetime it may happen that the vault pitches are differently loaded; this may be due to the effect of wind or to the snow that usually covers the windward pitch; and during construction and maintenance. To take these effects into account, though within the limitations of a technical schematisation, partial load models or, at any rate, pitch differentiated models must be studied.

To emphasise the importance of such models for a reticulated vault roofing a square

@Seismicisolation

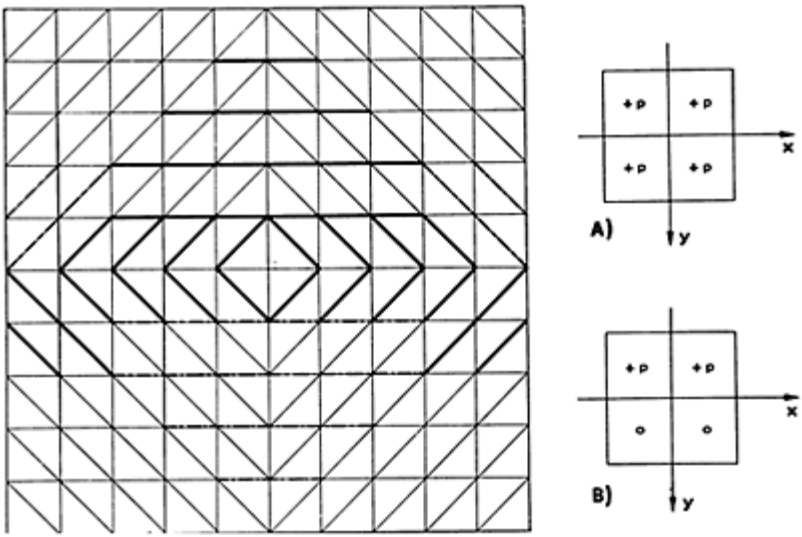

Fig. 19.11. Comparison of the static conditions corresponding to the uniform load acting on the entire surface (scheme A) and those of partial load (scheme B) for a reticulated translation vault roofing a square plan (ρ=2·97). The bold face denotes the most stressed bars of the second scheme while the dashed lines stand for the bars whose static function is reversed (from tie-rods to rafters or vice versa).

plan, the static conditions have been compared (Fig. 19.11) corresponding to the overload distributed along the entire surface and that distributed on half of it only. The comparison shows that many bars are more stressed in the partial load assumption while others even reverse their static function from tension to compression. Since the solution to such load models must be found by overlapping the appropriately partitioned effects of the symmetric load scheme and those of the hemisymmetric scheme (Fig. 19.12), such results could be useful for the designer.

3.2 Hemisymmetric Load Model*

The already known methods of finite differences and the 'analogous' reticulated structures lead to the solution of the hemisymmetric load model through lengthy procedures that provide a degree of approximation as high as desired; as an alternative, a

@Seismicisolation

methodology is now set out capable of solving the problem in an approximate, workable and technically acceptable way. Each structure that belongs to the typology under investigation can be represented by three geometrical parameters (ρ_a, ρ_b, σ) which, theoretically, can take up any value but are in reality limited by static opportunity conditions.

The following intervals have been assumed:

$1{\cdot}5 \leq \rho a \leq 3{\cdot}5$

$1{\cdot}5 \leq \rho b \leq 3{\cdot}5$

$0{\cdot}5 \leq \sigma \leq 2$;

The domain of the typology is represented by a parallelepiped (Fig. 19.13) in a space of

* Note that here: $\rho_b = R_b/b$; $\eta = y/b$; $\sigma = a/b$.

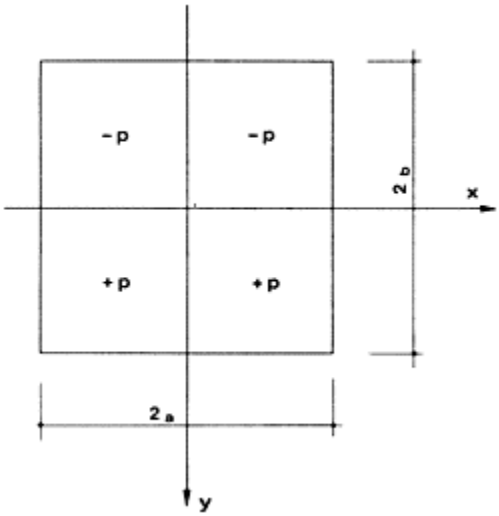

Fig. 19.12. Hemi-symmetric load scheme.

@Seismicisolation

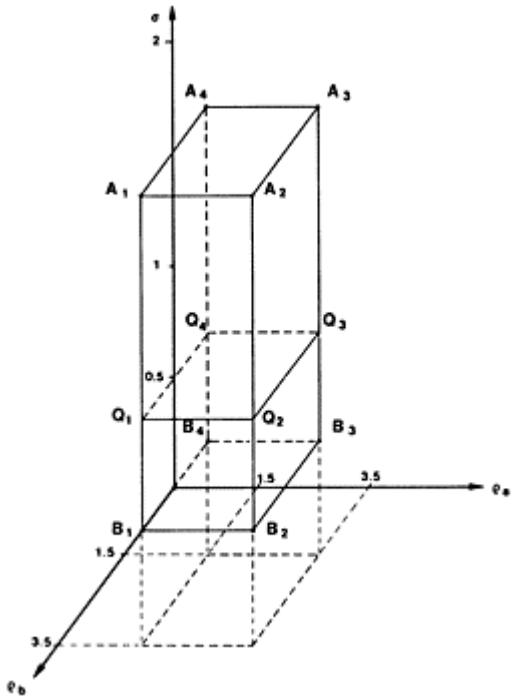

Fig. 19.13. The domain of the structural typology under examination can be represented in a space of axes ρ_a, ρ_b, σ, by a parallelepiped.

axes. By using the results of the study carried out for a reticulated vault roofing a square plan p=2·97, and passing from a continuous to a discontinuous set, the behaviour of the membrane forces in the continuous analogous structure was determined.

Since it was evident that such a behaviour would not qualitatively change with the variation of the geometric parameters of the structure (ρ_a, ρ_b, σ), the research has aimed at determining, with a sufficient degree of exactness, the numerical incidence of the change in geometrical parameters so as to supply a solution which, though approximate, could be applied to the entire typology.

In the search for the forces, thanks to the particular symmetry conditions of this load model, it has been possible to make reference to one-fourth of the structure surface ($0 \leq \xi \leq 1$; $0 \leq \eta \leq 1$).

Before expounding the proposed formulations that will be set out in the form of alignment charts and tables, the assumed approximations should be stated exactly so as to permit the operators critically to apply these formulations in relation to the degree of exactness required by their own conceptual problems.

Therefore the solution proposed, to be technically acceptable, had to rigorously satisfy the boundary conditions and the first two equations of system of eqns. (2). Moreover, the

@Seismicisolation

third equation had to be fulfilled for a loading that, though not uniform, was globally equal to the uniform one (one has to remember that reference is still made to the one-fourth of the structure).

Hence, having rigorously determined the overall equivalence of the load, the only approximation left would be its lack of uniformity that, especially when its value is low, does not hinder any technical applications, as already stated.

In order to quantify such a characteristic the authors propose to use as an

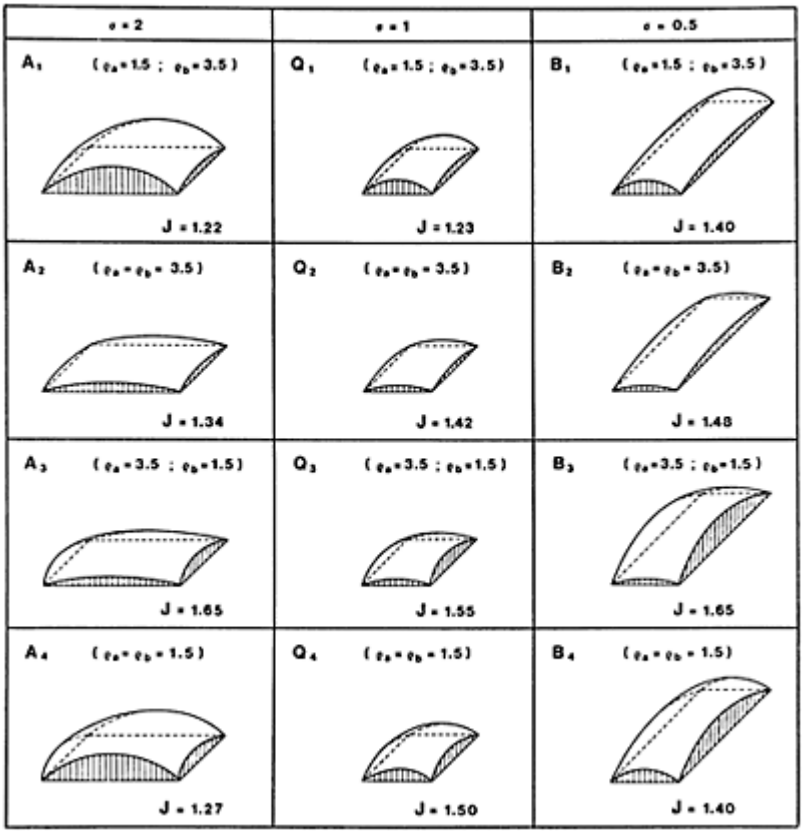

Fig. 19.14. Some values of the approximation index J computed for structures on the frontier of the domain of the typology concerned.

'approximation index' *(J)* the highest ratio of the effective load to the theoretical one, i.e. (q_{eff}/q_{theor}) max.

As regards the typology under consideration, the above formulation has yielded values of *J* ranging from 1·20 to 1·65. It should be noted that the highest value (equal to 1·65) was only found on the frontier of the domain in correspondence with the corner of the

@Seismicisolation

parallelepiped denoted by ρ_a=3·5; ρ_b=1·5 corresponds to geometrical characteristics that the designer is very unlikely to encounter in the real practice. Figure 19.14 sets out the values of *J* estimated for structures placed on the frontier of the domain.

3.3 Tables for the Solution of Hemisymmetric Load Model

The domain of the structural typology has been divided into two parts, separated by a surface that can be considered as a plane (Fig. 19.15); a different formulation is put forward for each of them.

The values of $\bar{N}_\xi$, $\bar{N}_\eta$, $\bar{N}_{\xi\eta}$ in the validity range
$\sigma \geq 0{\cdot}35\rho_a - 0{\cdot}43\rho_b + 1$ $0 \leq \xi \leq 1$ $0 \leq \eta \leq 1$

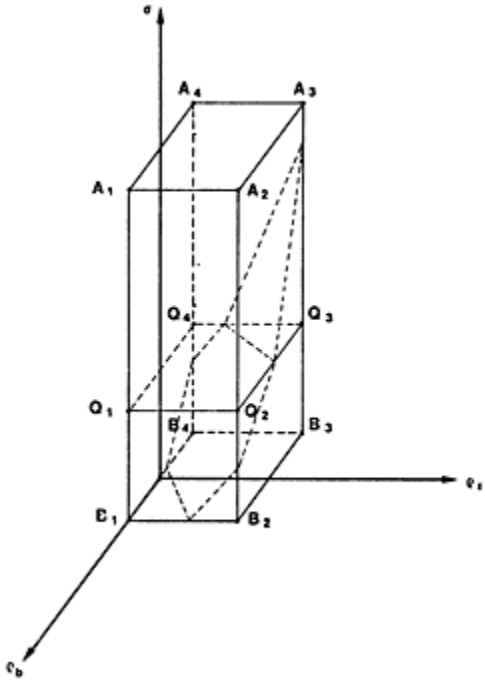

Fig. 19.15. The dominion of the structural typology under investigation has been subdivided into two parts by means of a surface similar to a plane. For each part a different formulation has been proposed for the solution of the hemi-symmetric load model.

@Seismicisolation

are derived, for the loading scheme represented in Fig. 19.12, from eqn (6) as a function of the load and the geometry of the structure.

$$\left.\begin{aligned} \bar{N}_\xi &= -p\frac{a^2}{aK(\rho_a)+b\lambda(\rho_b)}A(\xi)B(\eta) \\ \bar{N}_\eta &= -p\frac{b^2}{aK(\rho_a)+b\lambda(\rho_b)}C(\xi)D(\eta) \\ \bar{N}_{\xi\eta} &= -p\frac{ab}{aK(\rho_a)+b\lambda(\rho_b)}E(\xi)F(\eta) \end{aligned}\right\} \qquad (6)$$

$K(\rho_a)$ and $\lambda(\rho b)$ are derived from the chart depicted in Fig. 19.16 while the functions $A(\xi)$,

Table 19.4

$\xi=\eta$	$A(\xi)$	$B(\eta)$	$C(\xi)$	$D(\eta)$	$E(\xi)$	$F(\eta)$
0	–8·19	–1·9	8·94	0	0	1·20
0·2	−8·03	–2·26	7·70	0·20	−1·54	0·78
0·4	−7·54	−2·53	14·11	0·31	−3·60	0·30
0·6	–6·46	–2·72	28·07	0·32	−7·67	–0·22
0·8	–4·24	−2·83	49·61	0·22	−15·30	−0·78
1·0	0	−2·85	78·74	0	−27·90	−1·35

Note: $A=(7{\cdot}9x^4-4{\cdot}18x^3+4{\cdot}47x^2-8{\cdot}19)$ $C=(94{\cdot}8x^2-25x+8{\cdot}94)$ $E=(-31{\cdot}6x^3+12{\cdot}55x^2-8{\cdot}94x)$ $B=(1{\cdot}05y^2-2y-1{\cdot}9)$ $D=(0{\cdot}08y^4-0{\cdot}33y^3-0{\cdot}95y^2+1.2y)\cdot 2y)$ $F=(0{\cdot}35y^3-y^2-1{\cdot}9y+1{\cdot}2)$

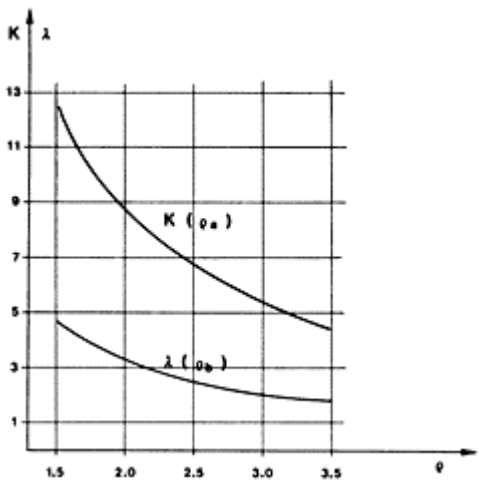

Fig. 19.16. Chart for the computation of $K(\rho_a)$ and $\lambda(\rho_b)$.

@Seismicisolation

B(η), C(ξ), D(η), E(ξ), F(η), the analytical expression of which is reported in the footnote, are shown in Table 19.4.

The values of $\bar{N}_\xi$, $\bar{N}_\eta$, $\bar{N}_{\xi\eta}$ in the validity range
$\sigma \leq 0{\cdot}35\rho a - 0{\cdot}43\rho b + 1$ $0 \leq \xi \leq 1$ $0 \leq \eta \leq 1$

are derived, for the loading scheme represented in Fig. 19.17, from eqn. (6) as a function of the load and the geometry of the structure.

$$\left.\begin{aligned} \bar{N}_\xi &= -p\frac{a^2}{aK'(\rho_a)+b\lambda'(\rho_b)}A'(\xi)B(\eta) \\ \bar{N}_\eta &= -p\frac{b^2}{aK'(\rho_a)+b\lambda'(\rho_b)}C'(\xi)D(\eta) \\ \bar{N}_{\xi\eta} &= -p\frac{ab}{aK'(\rho_a)+b\lambda'(\rho_b)}E'(\xi)F(\eta) \end{aligned}\right\} \tag{7}$$

K'(ρ_a) and *K'(ρ_b)* are drawn from the chart of Fig. 19.18, while functions *A'(ξ), C'(ξ),*

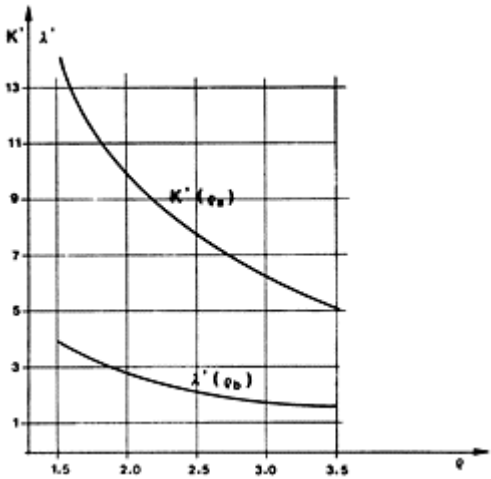

Fig. 19.17. Chart for the calculation of *K'(ρ_a)* and *λ'(ρb)*.

@Seismicisolation

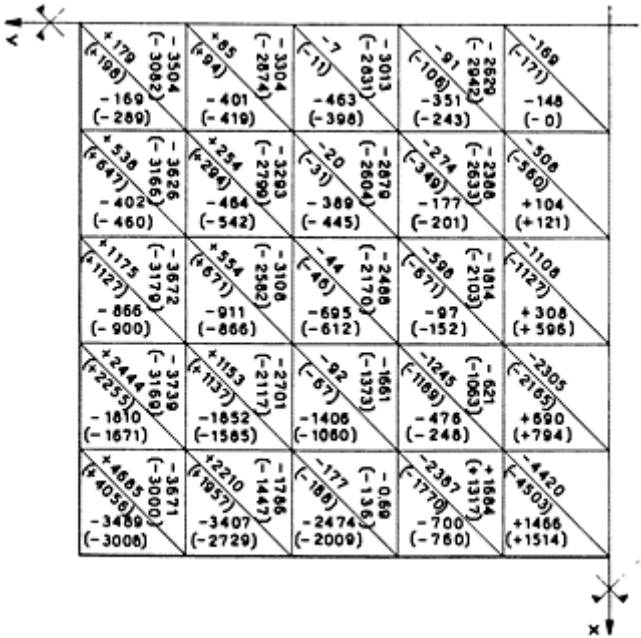

Fig. 19.18. Comparison between the values of bar forces obtained by the solution of a space reticulated system (in parentheses) and those computed by the proposed formulation by shifting from a continuous to a discontinuous set.

E'(ξ), the analytical expression of which is provided in the footnote, are shown in Table 19.5.

3.4 A Numerical Example

As an example of the proposed formulation we report the solution for a reticulated vault roofing a square plan. For the sake of a fruitful comparison the authors report the results of the calculations of the vault as a space reticulated structure hinged at its nodes.

Square reticulated vault
Scheme: (Fig. 19.12)
Load=p =100 kg m^{-2}
ρ=2·97
σ=1
Figure 19.20 provides the comparison of axial forces in the bars of the barrel vault.

@Seismicisolation

Table 19.5

ξ	$A'(\xi)$	$C'(\xi)$	$E'(\xi)$
0	−10·32	22·00	0
0·2	−9·91	18·68	−4·01
0·4	−8·74	18·72	−7·69
0·6	−6·81	22·12	−15·51
0·8	−3·99	28·88	−16·74
1·0	0	39·00	−23·45

Note: $A'=(3{\cdot}5x^4-4{\cdot}18x^3+11x^2-10{\cdot}32)$
$C'=(42x2^{-}25x+22)$
$E'=(-14x^3+12{\cdot}55x^2-22x)$

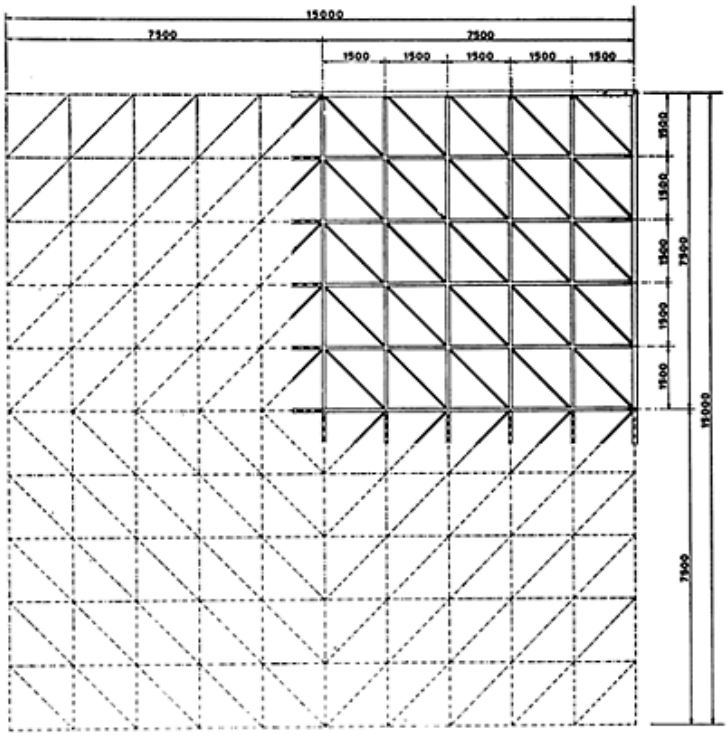

Fig. 19.19. Plan of the reticulated vault, which is the object of the experimental study.

@Seismicisolation

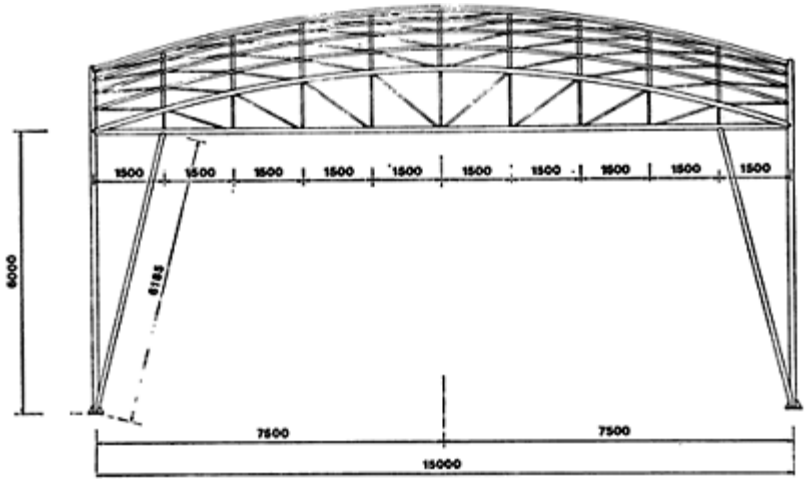

Fig. 19.20. Layout of the reticulated vault, which is the object of the experimental study.

4 SECONDARY STRESS STATE OF BENDING SHEAR AND TWIST; THERMAL EFFECTS AND GEOMETRICAL FAULTS; TESTING OF REAL STRUCTURES

The confidence with which members of widely used structural typologies—such as the structures of a normal building—are dimensioned and tested is based on the coexistence of the three following conditions: (i) exhaustive studies on theoretical models, (ii) experimental evidence of their results, and (iii) the presence in the field of several structures which, dimensioned on the basis of such models, have in time offered a satisfactory degree of safety concerning the ultimate and operating limit states and good serviceability. All this can be summarised in the statement that in designing a structure the choice of models must be made on the basis of the generally accepted technical literature encompassing the entire technical and scientific knowledge.

The present study on reticulated vaults has been carried out in the light of such a philosophy with a view to evaluating the fitness of the available analytical instruments and to highlighting the problems solved while identifying those for which a satisfactory solution has still to be found.

4.1 Description of the Structural Typology and of the Experimental Model

The reticulated vault, which has been the object of this experimental study, develops in a translation surface covering a square plan having a side of 15 m. It is formed by a double series of polygonal arches which are circular in shape and mutually orthogonal,

@Seismicisolation

constituting a square mesh lattice of a 1·50×1·50 m modulus stiffened by a diagonal that, due to the uniform load condition, results to be tensioned (Figs. 19.19 and 19.20).

The curvature radius of the circular section measures 22·28 m and has a deflection of 1·30 m. In the perimeter four reticulated ribs perform the function of tympana and again the load is carried by uprights each of which consists of a tripod-shaped strut, where the adjacent tympana meet, anchored in the reinforced concrete foundation.

All the bars of the structure consist of tubes, particularly suitable when axial forces prevail and for the easy realisation of complex three-dimensional nodes. As a whole the geometry of this typology presents remarkable aesthetic and static advantages.

The tested structure was constructed by using completely welded joints, producing the various parts in the workshops subject to the transport limitations (piers, tympana ends, vault tympana without their ends) and then by assembling them on site.

Later this structure had to be moved so that it was cut and assembled elsewhere, unluckily this resulted in considerable displacements compared to the original surface of the layout. To a certain extent this proved to be useful for a theoretical and experimental evaluation of the effects of faults in the assembly upon the structure.

4.2 Theoretical Investigation: Discontinuous Bending Model (Space Frame)

The previously described models, which are all different from each other except for the basic assumption of their non-flexural behaviour, yield almost the same results. To consider the structure as a space frame with monolithic nodes means to discard these simplifying assumptions, which is already a significant progress. In such a case the investigation, being very complex, requires the support of a computer. For this study the program IBM-STRUDL has been used which is capable of making a complete analysis of the stress and strain state, also taking into account the deformability due to twisting, shear and stretching always under rigorously linear-elastic conditions.

This program has been used to analyse the structure as regards both the geometry of

@Seismicisolation

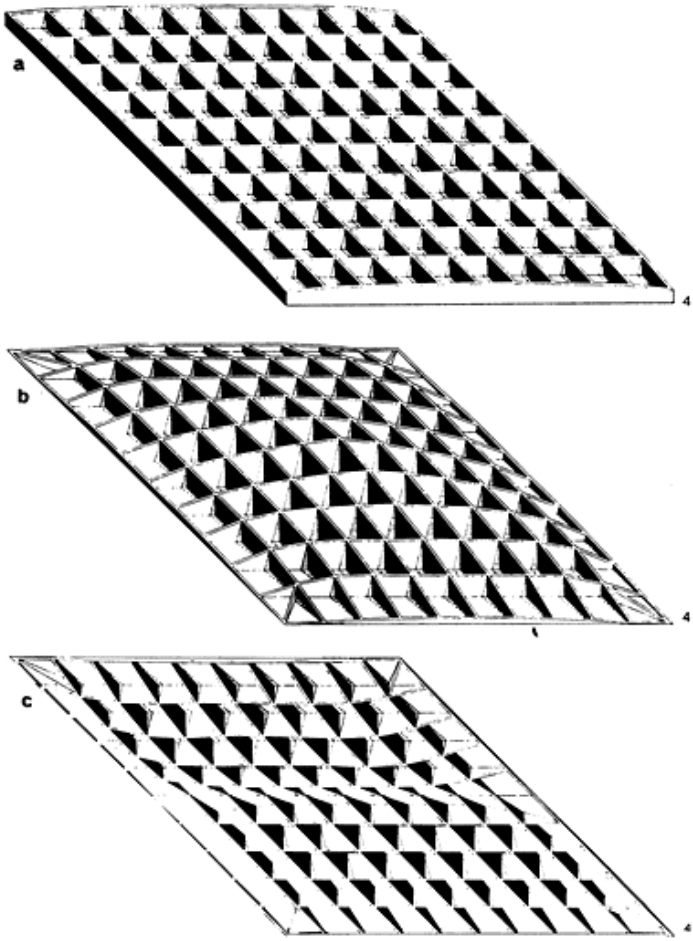

Fig. 19.21. The most exhaustive results of theoretical investigations were attained by analysing the structure as a space frame: (a) depicts the vault's elastic surface for a positive and uniform thermal change, (b) represents the elastic surface for a vertical uniform and symmetric load, and (c) denotes the elastic surface for a vertical uniform and hemi-symmetric load with respect of an axis.

@Seismicisolation

the design and that of the measurements made after dis-assembly and re-assembly in the final location site. Several load conditions have been studied, in particular that of a uniform variation of temperature.

From the rational standpoint such a procedure is much more satisfactory than the two preceding ones; however, to apply it in practice is much more costly and always confined to the linear system (Fig. 19.21). In short it can be argued that of the three theoretical models set out so far, the first two can be used for the general design stage and for dealing with dimensioning problems, while the third one can be used for more detailed investigations which are indispensable when dealing with large structures where, as the size grows, the material's exploitation reaches the limit point set by theoretical investigations. Hence the risk exists that due to the very high values reached by secondary stresses the latter can also give rise to dangerous phenomena of instability.

In the case of small spans, where the size of many bars is only decided on the basis of an economically necessary standardization of the sections adopted, this more accurate investigation can be superfluous.

4.3 Experimental Investigation: Tests on Full Scale Model

The development of theoretical studies has gone hand in hand with experimental investigations on full scale models and measurement testing. Compared to small scale models this experience is much more exhaustive and is deemed to represent a better term of comparison with the available theoretical information. It is in fact well

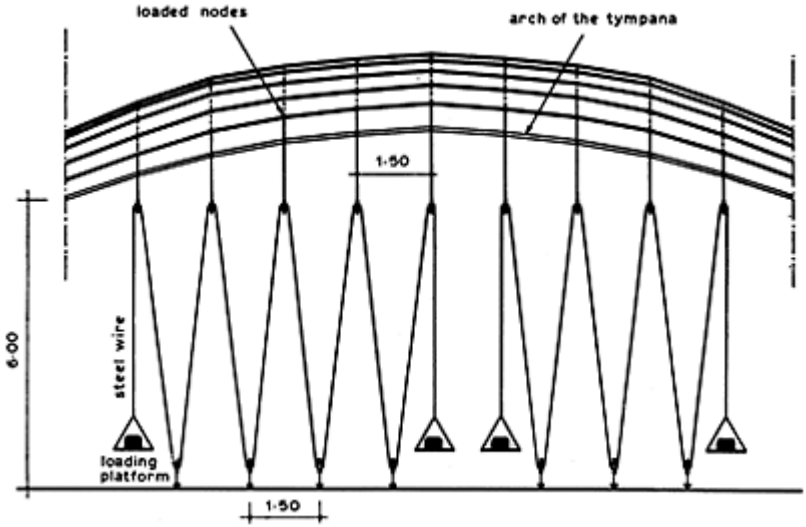

Fig. 19.22. Layout of the loading device: thanks to this system the number of necessary weights has been considerably reduced.

@Seismicisolation

known that when real structures are tested measurement errors are smaller. However, other difficulties arise, not only of an organizational and economic nature, but also of a scientific kind. The most relevant ones are (i) the greater impact of thermal changes upon measurements; (ii) the amount of load to be applied; (iii) the length of measurement time due to the quality of the available equipment. To overcome these difficulties, with a view to attaining sufficiently reliable loading schemes that could be compared with theoretical models, a device has been used consisting of a double pull system (Fig. 19.22) connected in its upper part with the nodes of the structure and with its lower end pinned in the ground. These pulleys permit one to reduce the number of weights; in fact 36 weights were used to load the 81 nodes of the vault, excluding those of the lower stringer of the tympana, thus fulfilling the uniform load condition on the structure.

Such equipment permitted us to take the measurements for the charts described in Fig. 19.23. Schemes A and B aim at determining the effects of thermal changes during day and night time. In the period when the trials were performed weather conditions remained constant, with a cloudless sky and regular temperature diagrams. The values of daytime deformations were affected in an uncontrollable way; disturbances were unacceptable for they were of the same magnitude as load-induced deformations. On the other hand, night-time disturbances were equal to about one-tenth of the maximum strains corresponding to the four other loading tests. Starting from an unloaded structure, those

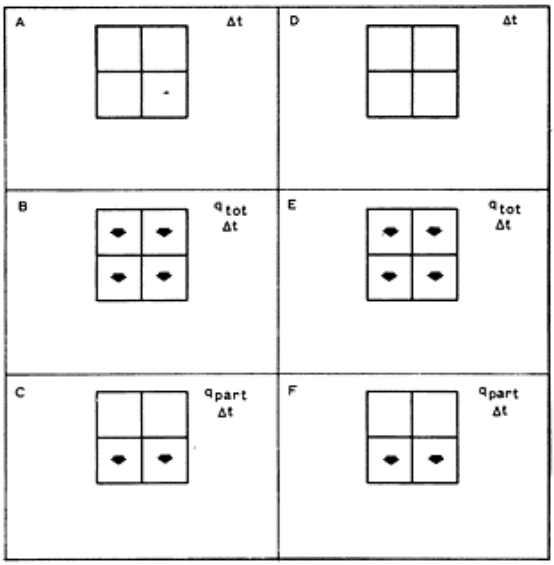

Fig. 19.23. Schemes of trials made on the structure. (A) Behaviour of the unloaded structure with respect to daytime thermal variations. (B) Uniform load condition during daytime. (C) Partial load condition

@Seismicisolation

during daytime. (D) Behaviour of the unloaded structure with respect to night-time thermal variations. (E) Uniform load condition during night-time. (F) Partial load condition during night-time.

four tests applied a load of 240 kg in two proportional stages going through the same stages as in the unloading operations. For each of these stages measurements were taken of the strains of the bars, the displacements of several nodes as well as the variation of the ambient temperature and of the structure.

The deformations have been measured by applying electroresistant strain-gauges to 120 bars; for each of them the reading basis is formed by three strain gauges placed on the circumference of the perimeter at a distance of 120° the one from the other. The average of the three readings directly provides the axial deformation cleared of the bending effects. Vertical displacements have been surveyed by means of a dumpy level attached to stadia suspended at 25 nodes from the structure. The horizontal displacements of six points of the two orthogonal tympana have been measured by a tachometer (Fig. 19.24). Because of the complexity of measurements the entire loading cycle took 5 hours as an average. Under these conditions thermal effects on measurements should be taken into consideration. As regards the increase in strain, it is well known that, for a uniform change of temperature, the problem is solved by using a dummy gauge placed on an unstressed specimen. But even if this condition is fulfilled, which is not easy, it is impossible to determine the effects of temperature on the hyperstatic structure. Therefore the considerable differences between the results provided by the daytime trials (B, C) and those of the night-time trials (E, F) are undoubtedly to be ascribed to the thermal effects of the sun producing large differences of temperature that vary in time and space between the active strain gauges and the dummy gauge.

The behaviour of this type of structure in relation to thermal effects can now be defined. Reticulated vaults are in fact hyperstatic and thus, strictly speaking, sensitive to thermal changes. However, if the latter are distinguished into local variations which vary due to

@Seismicisolation

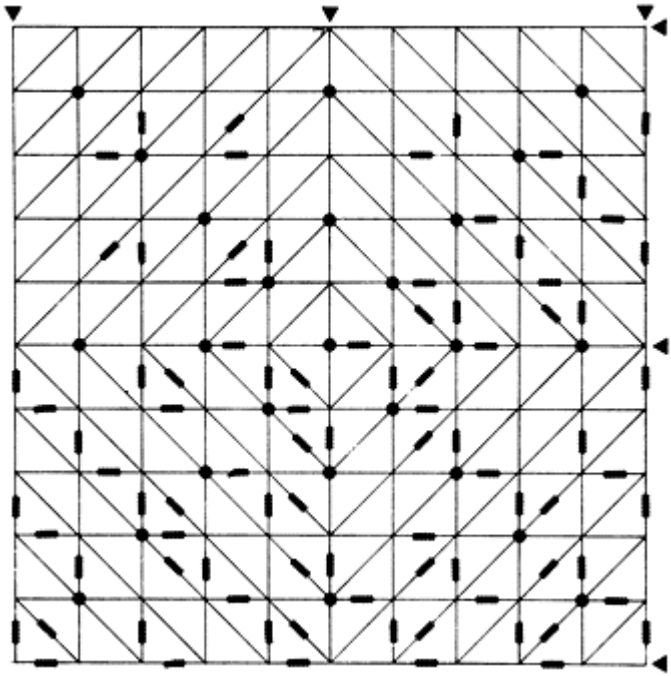

Fig. 19.24. Arrangement of strain gauges to evaluate the stress state of the structure. The black dots stand for the sagging joints, the black triangles stand for the measurements of horizontal displacements.

the direct impact of sun rays and thermal variations that affect all the structure, it can be argued that, because of the high level of deformability of perimetral connections consisting essentially of uprights, only the former considerably disturb the internal stress state. On the other hand, the latter variations do not affect the structure to a great extent since it is sufficiently capable of accommodating to thermal changes. Evidence of this fact has been provided by the computer which, for a model of space frame subjected to a uniform variation of 1°C, supplies stress values that only in some girders of the tympana reach the level of 1–2 kg per cm^{-2} and are usually much lower.

The actual possibilities offered by the existing testing equipment, which unfortunately is not the best available, have not permitted us to connect the 360 strain gauges with the central strain recorder. The connection took place by means of bush and plug commutators which subjected measurements to the influence of possible variations of local contact resistance. To evaluate possible surveying errors an experimental control was made: the maximum error amounted to 20×10^{-6}. As a conclusion it can be stated that the main causes of indeterminacy of strictly static investigations (schemes B, C, E, F)

@Seismicisolation

were thermal changes and defects of measurement devices. For the night-time trials (schemes E, F) the overall maximum incidence has been estimated which, expressed in stress terms, was then assumed to be equal to 50 kg cm^{-2}.

4.4 Comparison Between Theoretical and Experimental Results; Membrane Conditions

The results of the five theoretical and experimental investigations described so far, expressed in stress attributes for several bars and in mostly vertical node displacements, have been used for comparing the theoretical system with the experimental one in order to assess the validity of the analytical models reviewed. From the static viewpoint, taking

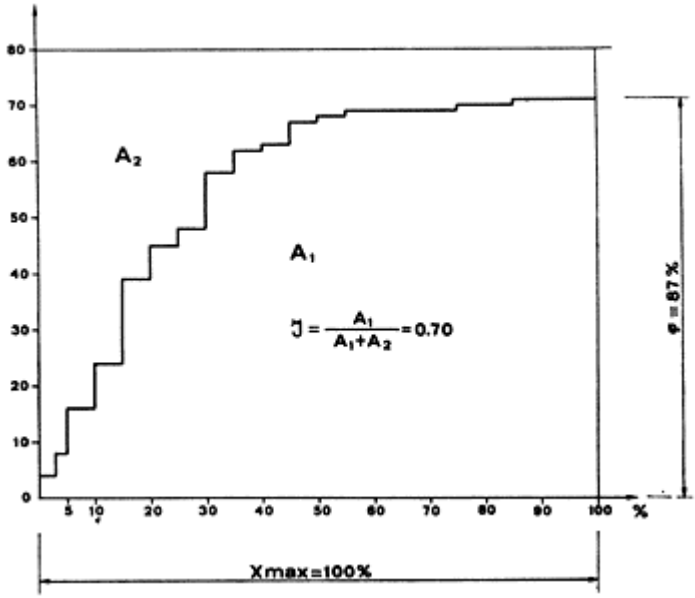

Fig. 19.25. Index of concordance between theoretical and experimental results; comparison of membrane system (uniform load condition), theoretical model of space frame.

@Seismicisolation

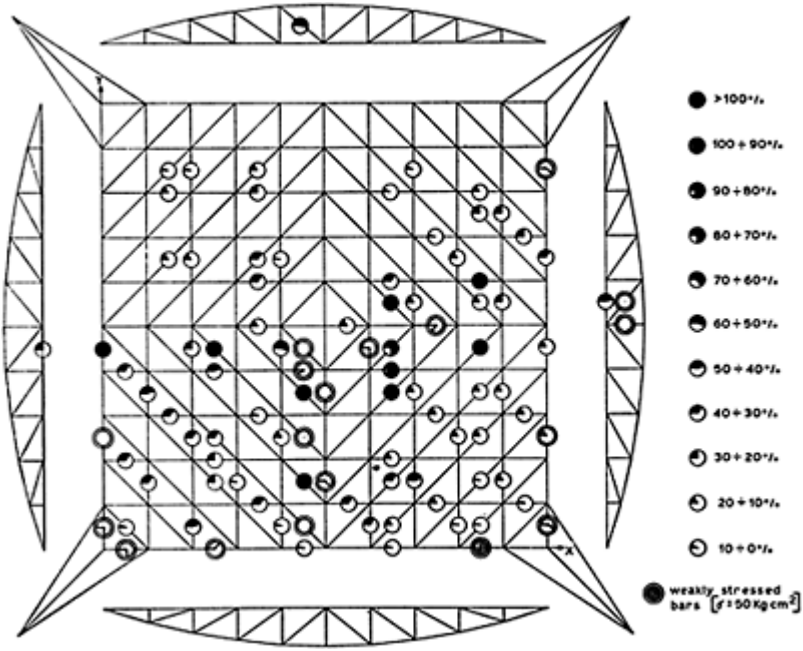

Fig. 19.26. Graphical representation of the local discordance values of theoretical and experimental results. The former concern the space frame model (effective geometry); the latter refer to the structure loading trial (scheme E); moreover the weakly stressed bars have been identified.

into account the prevailingly membrane nature of the structure, the authors deemed it significant to compare the axial forces' values for the uniform load condition. The following methodology deals with the definition and evaluation of three interrelated indices:

X, local percent discordance < X_{max};

ψ, comparability index;

l, index of overall agreement.

Having assigned various sets of comparable results it is necessary to define some preliminary criteria. First of all a subset of values has to be found, the magnitude of which, in absolute terms, is the same as that of the unavoidable errors; the values which are mostly affected by those errors should be removed from the comparison.

It is thus necessary to define a preliminary criterion of comparability for deciding whether an overall numerical comparison between two sets of results is significant for our technical purposes. Because of the fact that when, for all the couples of results, the

@Seismicisolation

percent discordance *(X)* is extremely high a numerical comparison is meaningless, such a criterion could well consist in defining a 'comparability index' (Ψ) expressed as the mean of the couples of results whose percent discordance is less than a predetermined ceiling discordance. In other words, it would be possible to make a numerical comparison only if the comparability index is greater than a preset limit value.

As regards the problem under examination, as the highest 'percent discordance' the authors propose Xmax=100 %, and as limit value of the comparability index $\Psi_{lim} = 75\%$. The adopted methodology is based on the following procedure: taking the trial's values as a reference point for each bar *i,j*, the discordance X_{ij} is supplied by the following relationship:

$$X_{ij} = \left| \frac{\text{theoretical datum} - \text{experimental datum}}{\text{experimental datum}} \right| \times 100$$

Hence the diagram is constructed where on the ordinates appear the number of bars exhibiting a discordance lower than or equal to each given value of X that appears on the abscissae. The curve identifies two areas A_1 and A_2. The index of overall concordance is defined as the ratio $A_1/(A_1+A_2)$ (Fig. 19.25).

In such a way the sets of axial forces determined on the basis of the three theoretical models have been compared to those determined on the basis of results of the night-time loading trial (scheme E) because the latter test has been considered as the most exhaustive and feasible among the experimental investigations performed. The results achieved are as follows:

continuous membrane model Ψ=76%, *I*=59%

discontinuous membrane model Ψ=77%, *I*=59%

discontinuous bending model Ψ=87%, *I*=70 % (space frame)

In making the comparison low stressed bars have not been taken into account ($\sigma_{theor.} < 50$ kg cm $^{-2}$), since they are not very statistically significant while being mostly affected by unavoidable errors.

The overall static comparison made by means of the space frame model has yielded almost the same results both in the case of design geometry and of the effective one. With reference to the latter, Fig. 19.26 depicts the discordance values of single bars to permit also the local visualisation of the comparison.

Comparisons have then been extended to elastic surface (Fig. 19.27). In such a case the

@Seismicisolation

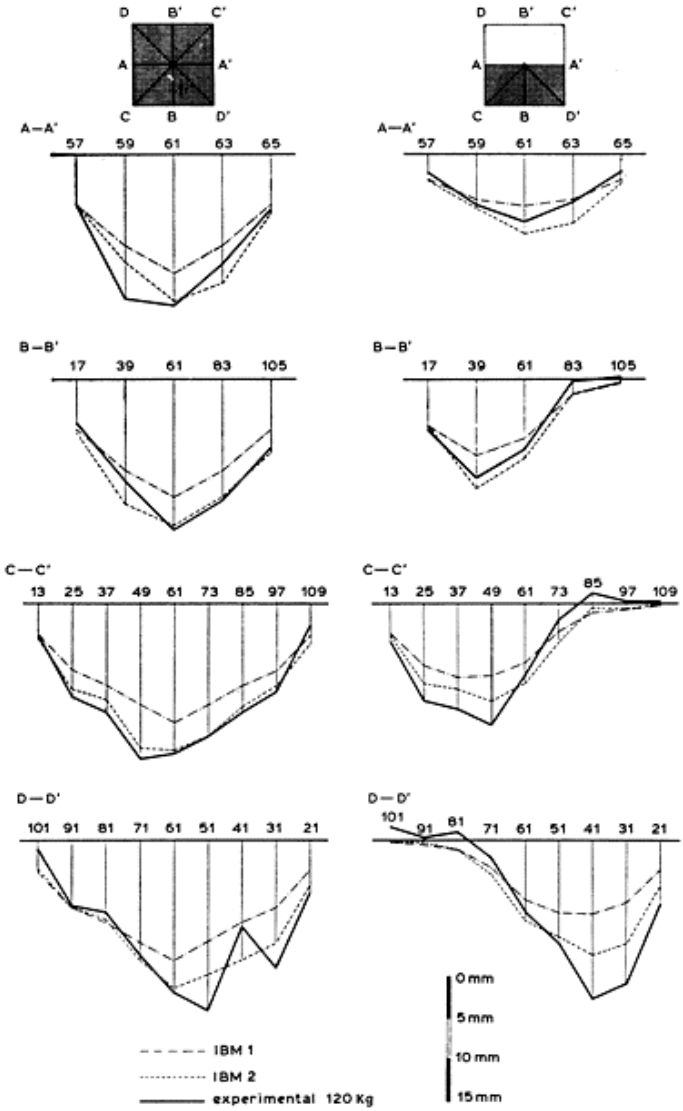

Fig. 19.27. Comparison between theoretical and experimental deflection curves. IBM1 and IBM_2 stand for the results of the space frame theoretical model that takes into consideration both the design and the effective geometries.

@Seismicisolation

only available theoretical values are those concerning the space frame model. The same methodology has then been used for the comparison between theoretical and experimental deflections; for the uniform load condition the results have been as follows (Figs. 19.28 and 19.29):

Discontinuous bending model (space frame)	
design geometry	Ψ=96%, *I*=72 %
Discontinuous bending model (space frame)	
effective geometry	Ψ=96 %, *I*=80 %

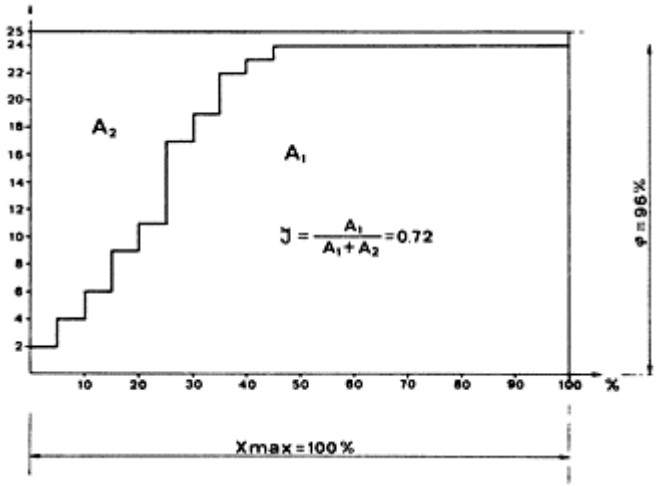

Fig. 19.28. Index of concordance between theoretical and experimental results: comparison of elastic surfaces (the theoretical results concern the design geometry).

Those who deal with theoretical-experimental investigations know well that deflection comparisons yield more fruitful results.

It is also necessary to test the experimental behaviour of the structure in relation to the linear elasticity hypothesis that underlies all theoretical models reviewed so far. To this end, Fig. 19.30 depicts the load-strain diagrams for some significant point of the vault. The almost linear behaviour of the graphs proves that also from this standpoint and within the limits of the loads employed there is a reasonable agreement between the theory and the actual behaviour of the structure.

It can thus be argued that the calculation models described, in particular the space frame model, are useful instruments for analysing the prevailing static conditions which for this type of structure are represented by the axial forces. In fact a static concordance of 70% is quite a good result. The remaining 30% that separates the theoretical conditions

@Seismicisolation

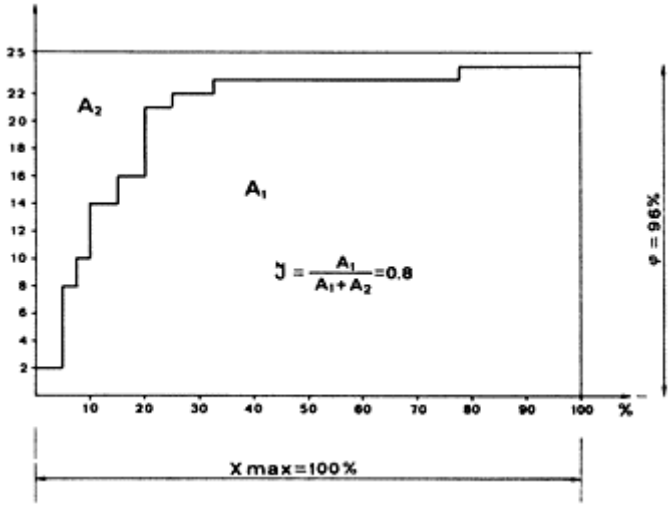

Fig. 19.29. Index of concordance between theoretical and experimental results: comparison of elastic surfaces (the theoretical results concern the effective geometry).

@Seismicisolation

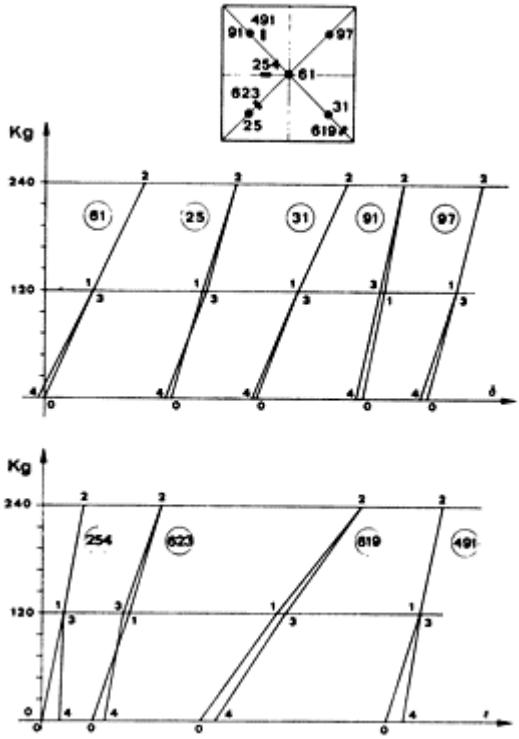

Fig. 19.30. Verification of the elastic behaviour of the tested structure: diagrams of loading-deflection for some nodes and of loading-deformation for some bars.

from the experimental ones is to be attributed to structural faults (imperfect arrangement of bars, imperfect welding of connections), to self-stresses, which in a welded structure are always considerable, and finally to measurement errors due to the faulty functioning of the various devices. However, even by assuming the worst, the latter could not account—as already explained—for more than 15% of such a difference.

4.5 Static Conditions of Bending, Shear and Twisting

The space frame model does not limit itself only to the system of axial forces, but for each bar it yields six values of forces and strains, i.e. all that complex bending, shear and twisting state that overlaps with and changes the undoubtedly prevailing membrane system as it has also been confirmed by the various trials. The critical investigation of these theoretical values has been carried out for the uniform load condition acting on the

@Seismicisolation

entire vault and has led to the estimate of its incidence with respect to the axial forces' principal static condition.

It is first of all useful to consider the qualitative and quantitative variations of the bending moment in relation to the normal force. Moving along an arch from the edges towards the centre the normal force increases, reaching its maximum almost at the centre of the structure while the bending moment rapidly decreases with a sudden recovery in the central node. On the diagonals, on the other hand, always going from the edges toward the centre both the moment and the normal force decrease rapidly. Briefly it can be said that the value of the eccentricity in all the bars of the structure has been determined. This has permitted us to verify that the pressure lines are always located in the core of the section except for tympana, the zones in their proximity and for the central node.

Moreover, in order to determine the punctual increment of tension caused by the bending moment with respect to the mean value, having considered the well-known expression

$$\sigma_{\max} = \frac{N}{A}\left(1 + \frac{e\, y_{\max}}{\rho^2}\right)$$

for all the bars of the structure, the value of $k=ey_{max/p}^2$ has been determined which represents the percentage increase in tension with respect to the mean value.

These values are depicted in the graphs of Fig. 19.31. It should be pointed out that (i) the highest value of K equal to 2·77 is reached in the upper stringer of the tympanum in the proximity of the angles, (ii) in the arches the value of *K* is usually lower than 1 (except for the bars near the edges and for the central node) and on the diagonals it assumes values which are considerably lower than 1, reaching the value of 0·7 at most. Such a result obtained for the reticulated vaults indicates a behaviour basically similar to that of continuous vaults exhibiting bending moments near the edges which cause the membrane state to change considerably. This observation is particularly relevant because it justifies the use of all the models which take into account the bending state both for the continuous and the discontinuous system in perfect analogy. This happens not only for the determination of the static state of one of them when the analogous condition is known, but also for the instability analysis.

It is indeed unusual that such a disturbance should also involve the central node of the vault. This can be accounted for by the fact that such a point represents an irregularity in the topological network of the structure since, together with the four corners, it is the only node where no diagonals converge; the phenomenon could be ascribed to the greater deformability of this part of the structure. On the other hand the shear forces effects estimated by the theory are quite negligible.

The torsional moments are also negligible; they produce appreciable effects only near the corners of the structure (Fig. 19.32). As a criterion of evaluation of their incidence on the static conditions for each bar the ratio of ideal tension to the maximum tension due to the compound bending is used. By assuming the following expression for the ideal tension:

$$\sigma_{id} = \sqrt{\sigma + 3\tau^2}$$

@Seismicisolation

that ratio takes completely negligible values for the entire vault. Only in the proximity of the corners does it acquire non-negligible values (a ceiling of 1·18 in the case under examination) as, on the other hand, could be expected from the analogy with the well-known slab behaviour. Eventually the complex state of bending shear and twisting, as can be derived from theoretical analysis, is shown to be of secondary importance compared to the membrane state. In fact also a considerable increase in punctual tension with respect to the mean value, which only occurs in limited areas of the structure, can concern us only in view of such a punctual verification (allowable tension), but not for the purpose of a more realistic testing of the ultimate breaking stage of the section, because for the tubular section the breaking moment is twice that of incipient plasticisation.

So far the approach has been solely theoretical. Its experimental testing has not permitted a comparison as accurate as the previous one, but it allowed the reading of the 360 strain gauges fitted in the centre-line sections of 120 bars and to affirm that for 5 bars of the vault surface and for 5 others belonging to the tympana it is necessary to realise the influence of a force eccentricity greater than the core of inertia in order to justify the readings

@Seismicisolation

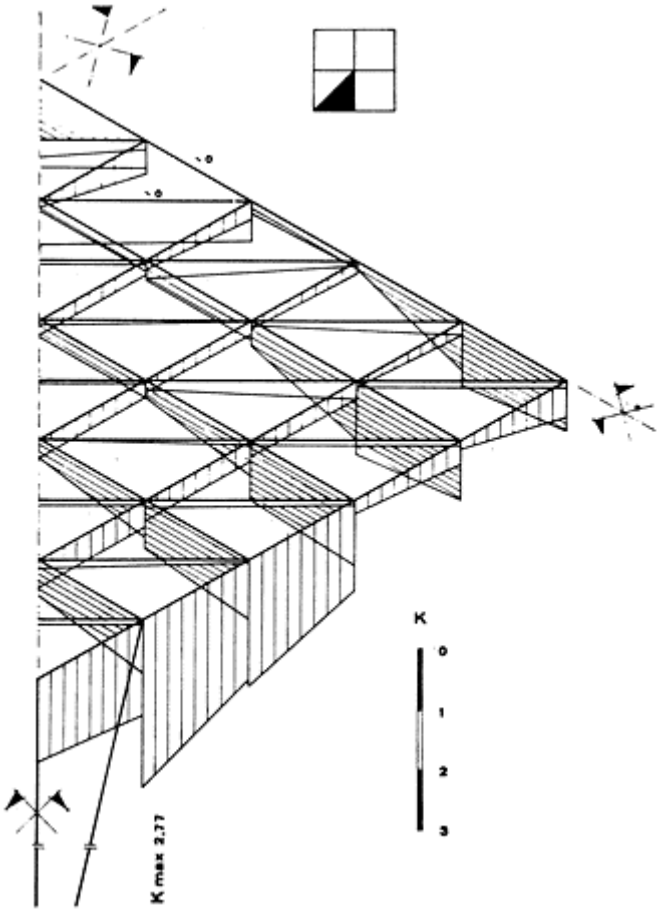

Fig. 19.32. Graphical representation of the distribution of the twisting moment (results of the space frame theoretical model for a uniform load of 100 kg m^{-2}).

@Seismicisolation

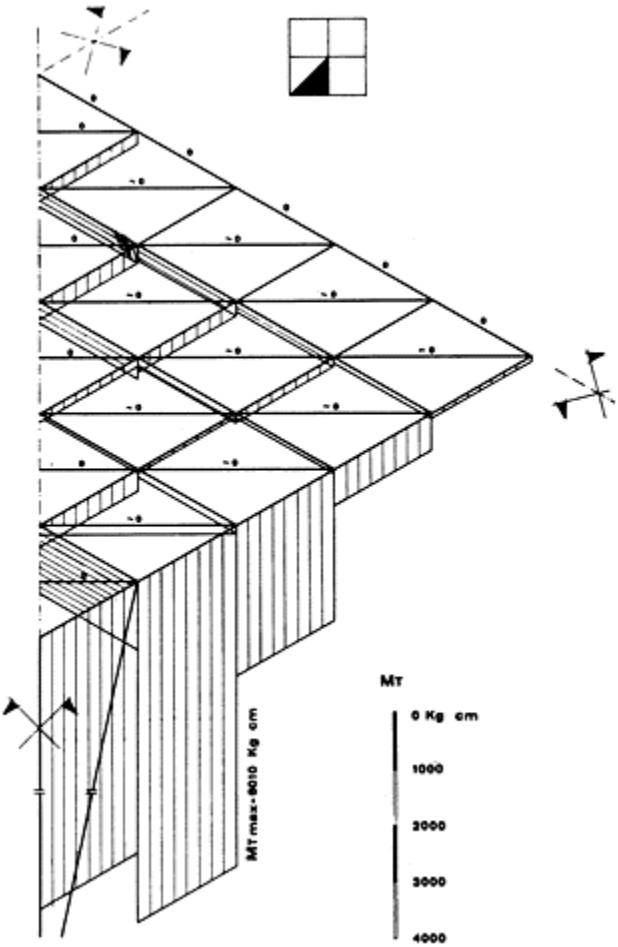

Fig. 19.31. Punctual increment of the average stress caused by the bending moment: graphical representation of the values of *K*.

@Seismicisolation

Fig. 19.33. The spatial reticulated structure described can be seen in this view. It is basically a triangulated network stretched over a translation surface with circular directrices.

themselves. Therefore it seems that the bending state derived from the trials has more modest effects than the theory had predicted; this is also likely to be due to the lower effective rigidity of nodes compared to theoretical stiffness.

5 THE COLLAPSE LOAD OF BRACED TRANSLATION VAULTS: ROUGH CALCULATIONS AND EXPERIMENTAL TESTS[6]

The behaviour of spatial reticulated structures having the form of translation vaults is difficult to predict. An expression is proposed to deal with the problem in which an approximation to the collapse load is expressed as a function of the plastic limit load, the local instability limit load and the overall instability load. For the values of the limit loads a possible theoretical analysis is provided, while, for the overall instability load, the formula proposed is based on experimental observation. The first results are given from the experimental programme whose purpose is to check the validity of the expression proposed.

@Seismicisolation

List of Symbols

2_a	The length of one side of the translation vault
2_b	The length of the other side of the translation vault
E	Young's modulus of elasticity
f	The rise of the translation vault
K	Safety factor
L	Span of the barrel vault
Q_{crit}	Uniform critical load distributed per unit of length of the barrel vault
Q^*	$4a^2q$
q	Uniformly distributed external load
q'	Load producing material failure
q''	Load producing local instability
q'''	Load producing overall elastic instability
q^*	Actual collapse load uniformly distributed
q_{amm}	Maximum permitted load
R_a, R_b	Curvature radii of the vault directrices
s	Thickness of the vault
a	Experimental coefficient for the evaluation of the overall critical load
β	Ratio of a to b

Braced translation and cylindrical barrel vaults

δ	Parameter representing the deformation of the vault
ζ	Parameter representing faults of construction, design and materials
η	Ratio between y and b
θ	The angle that the tangent at the vault contained in a plane parallel to yz forms with y
λ	The angle that the tangent at the vault contained in a plane parallel to xz forms with x
λ	Edge of each square of the roof grille
ν	Poisson coefficient
ξ	Ratio between x and a
ρ_a	Ratio between R_a and a
ρ_b	Ratio between R_b and b

@Seismicisolation

At the present stage, the collapse load of spatial reticulated vaults cannot be rigorously defined theoretically. The aim of the research at present in progress is to seek, by theoretical and experimental means, an approximate expression for the effect of such a load, supposedly distributed uniformly in the horizontal plane, for a reticulated vault of square plan, according to a translation surface with circular directrix.

For such a surface, the following can be separately calculated:

(a) The load corresponding to failure of the material along the most heavily loaded member (limit plastic load≡*q*').
(b) The load which determines buckling of a compressed member (local instability limit load≡*q*").
(c) The load which produces overall instability (overall instability load≡*q'"*).
(d) Faults in construction, design or quality of materials.

It is not difficult to evaluate, to an acceptable degree of approximation, the forces in the members of the reticulated shell, through the membranal stresses of the analogous continuous shell.

One can then determine the load *q'* which, according to membrane theory, induces stresses in the vault sufficient to cause the material to fail or to render it plastic (limit plastic load). Such failure can occur in members both in compression and in tension. For vaults with very flexible roofing and for uniformly distributed loads, the increase in stresses caused by flexural theory is not high and can be ignored.

Only in compressed members can local instability occur. One can determine the value *q"*of the load which, in membrane theory, gives an axial force that is critical, at least for a single member. In this calculation, it is assumed that the members are equal in length to the distance between the nodes, in the hypothesis that the nodes are rigid, but free to move normally at the shell surface. In practice applying *q"* more than one beam joined at one node reaches the critical load at the same time.

In continuous vaults of double curvature (Gaussian positive) it is only in large spans that overall elastic instability manifests itself. The load bearing material continuously stretched over the double-curvature vault gives that vault a high degree of rigidity, which, in turn, reduces the danger of overall elastic instability.

On the other hand, it is evident that for discontinuous reticulated vaults the critical load is lower; this is made clear by the results obtained by Wright, in which the reticulated vault is equivalent to a continuous vault constructed in a rather spongy material that is of low elastic modulus and rather thick.[12]

In general, it is certainly possible with this new type of structure to achieve spans much greater than with other traditional systems because it gives a considerable reduction in weight and because it is possible to increase significantly the rigidity by using multi-layer lattices. Nevertheless, for this type of vault in general, there is the probability that overall instability may occur in the elastic field. On the value of the overall critical load *q'"* some approximative expressions are proposed, as follows.

It is opportune here to point out that to obtain sufficient resistance to local and overall instability, it is necessary to have rigid nodes. In other words, it is necessary to avoid deformable joints which would be theoretically acceptable only in a strictly membrane type of behaviour.

@Seismicisolation

Both from the theoretical and physical standpoints the phenomena defined above are inextricably linked; a rigorous theory should determine the deformations *(δ)* corresponding to their reciprocal influence as a function of the external load *q* and determine the actual collapse load as the extreme of the function *q=q(δ)*. For the sake of completeness it would be necessary to introduce into this theory a fourth cause of increase in deformation caused by local faults indicated symbolically by *ζ*.

Under this load must be included play in the nodes, inaccuracies in assembly, misalignment of the nodal axes, internal tensions generated in welding, etc. Such faults are difficult to identify and to fit into the theory. Therefore, while it is to be expected that the builders would do their best to ensure perfect assembly and the designers to achieve rigid and perfectly aligned joints, it seems reasonable to allow for this complex of faults by giving a suitable value to a safety coefficient *K*.

However, not even in the completely abstract hypothesis of a total absence of faults has a non-linear unitary theory yet been formulated in the elasto-plastic field. Only experimentally is it possible to determine that the function *q=q(δ,ξ)* is not linear and appears to be of the type shown in Fig. 19.34. It can be presumed, then, that for the time being we must fall back on approximate formulae that have been proved valid in other structural fields. Among these it is logical to adopt an expression of the type

$$\frac{1}{q^*} = \frac{1}{q'} + \frac{1}{q'''}$$

in which *q** is the actual collapse load, $q' \leq q'$ is the load causing material failure, $q' \leq q''$ is the load causing the instability of a member between two consecutive nodes, and *q'''* is the overall instability load of the vault considered perfectly elastic.

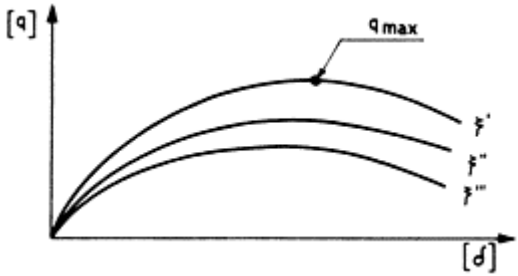

Fig. 19.34. The ordinates *q* represent symbolically the external load; the abscissae represent symbolically deformations of the structure. Structural faults are symbolically represented by the parameter *ζ*. With increase in the number of faults the value of the maximum load which the structure can bear is decreased. The

@Seismicisolation

descending arc of the curve can be followed only experimentally by arranging adequate supports to enable the structure to collapse slowly enough for measurement.

The value of the safety coefficient *K*, which gives us the acceptable load

$$q_{amm} = \frac{q^*}{k}$$

depends, case by case, on the considerations set out above concerning faults in building, in design and in the quality of the materials.

REFERENCES AND BIBLIOGRAPHY

1. Pagano, M. Industrializzazione e scienza dell'edilizia. *Casabella* 474/475, Nov.-Dec. 1981.
2. De Nardo, E., Giliberti, A. and Pagano, M. Strutture spaziali—Sperimentazione e teoria a diversi livelli di industrializzazione. *Costruzioni Metalliche*, 2, 1979.
3. Giangreco, E. and Pagano, M. Theoretical-experimental research on circular and linear generator vaults. Congresso di Madrid, 1960.
4. Pagano, M. Theoretical and experimental research on triangulated steel vaults. Atti Colloquium IASS—Parigi, luglio, 1962.
5. Pagano, M. and Greco, C. Sul calcolo delle volte di traslazione. *Giornale del Genio Civile*, fasc. 12, Dec. 1958.
6. Pagano, M., Catanzaro, C. and Pedicini, G. The collapse load of braced translation vaults and cylindrical barrel vaults. International Conference on Space Structures, London, September 1966, pp. 502–524.
7. Lenza, P. Volte di traslazione soggette a carico simmetrico od emisimmetrico. *Giornale del Genio Civile*, fasc. 7–8–9, 1977.
8. Lenza, P. Validità dei modelli per la progettazione di volte reticolari. *Costruzioni Metalliche*, No. 1, 1977.
9. Ghersi, A. and Lenza, P. Analysis models for the instability limit state of double-curvature translation vaults. *Costruzioni Metalliche*, No. 4, 1981.
10. Pagano, M. Contributo teorico sperimentale al calcolo delle volte autoportanti. *Atti dell'Accademia Pontaniana*, vol. IV, 1953.
11. Pagano, M. and Sannino, R. Contributo teorico-sperimentale al problema dell'instabilità delle volte travi. *Giornale de Genio Civile*, fasc. 7–8, 1961.
12. Wright, D.T. Membrane forces and buckling in reticulated shells, *J. Struct. Div. Am. Soc. Civ. Engrs*, 91(ST1) (1965) 173–201.

@Seismicisolation

20
Probability Analysis of Braced Barrel Vaults Composed of Elements of Random Strength

ANTONIO LA TEGOLA
Department of Structures, University of Calabria, Cosenza, Italy

1 INTRODUCTION

The advantages given by braced barrel vaults are well known both from the architectural and the economic point of view, especially as these structures often consist of mass produced prefabricated modular elements. However, when the use of standard elements is considered, great importance must be given to the problem of assuring, under a given risk and in relation to actions given in a deterministic or probabilistic way, adequate performances joined to service or ultimate limit states. The behaviour of highly statically indeterminate reticular structures is strongly influenced by geometrical and mechanical non-linearities and by the presence of imperfections of different natures distributed at random in all the structure rods. In the analysis of these structures, no reliable results can be obtained if both the aspects of non-linearities and imperfections are not taken into account. So far, for high redundant structures with random imperfections, the only method able to provide useful results is numerical simulation. Modern multivectorial processors make easier both the non-linear discrete analysis of complex reticular structures and the use of numerical simulation statistical methods.

The present work, referring to more detailed studies mentioned in the references, aims at providing a basic formulation necessary for the study of these structures from the probability point of view.

2 NON-LINEAR BEHAVIOUR AND RANDOM IMPERFECTIONS

2.1 Non-linear Behaviour

At present, there are various methods of carrying out the structural analysis, taking into account both the geometrical and the mechanical non-linear behaviour, and there are different structural materials which require the consideration of such behaviours. In the previous papers[1–7] we have mentioned calculation methods for double- and single-layer space reticular structures, which can be used also for braced barrel vaults.

@Seismicisolation

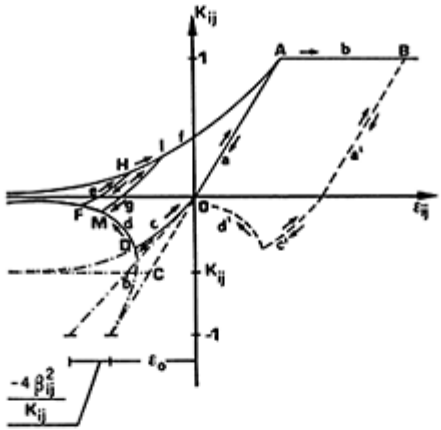

Curve	*Incremental stress–strain relations* $(\dot{K}_{ij}) = \lambda(\dot{\varepsilon}_{ij})$	*Constraints*	*Behaviour*
a	$\lambda_a = \frac{1}{\varepsilon_0}(\varepsilon_{ij})^0$	$0 < K_{ij} < 1;\ \varepsilon_{ij} < \varepsilon_0$	Elastic
b	$\lambda_b = 0$	$K_{ij} = 1;\ (\varepsilon_{ij}) > 0$	Plastic
c	$\lambda_c = \frac{(K_{ij}^{B} - K_{ij})^3}{\varepsilon_0(K_{ij}^{E} - K_{ij})^3 - 4(K_{ij}\beta_{ij})^2}$	$K_{ij}^{D} < K_{ij} < 0$ $\varepsilon_{ij}^{D} < \varepsilon_{ij} < 0$	Elastic
d	$\lambda_d = \frac{1}{\varepsilon_0 + 4\gamma_{ij}^2 \frac{1 + K_{ij}}{K_{ij}^3}}$	$(\dot{\varepsilon}_{ij}) < 0$	Plastic
e	$\lambda_e = \frac{1}{\varepsilon_0 + 4\gamma_{ij}^2\left(1 + \frac{1}{K_{ij}^{E}}\right)^2 \frac{(K_{ij}^{E} - K_{ij}^{E})^2}{(K_{ij} - K_{ij}^{E})^3}}$	$K_{ij}^{E} < K_{ij} < K_{ij}^{H}$	Elastic recovery
f	$\lambda_f = \frac{1}{\varepsilon_0 + 4\gamma_{ij}^2 \frac{1 - K_{ij}}{K_{ij}^3}}$	$K_{ij} < 1;\ (\dot{K}_{ij}) > 0$ $(\dot{\varepsilon}_{ij}) > 0$	Plastic
g	$\lambda_g = \frac{1}{\varepsilon_0 + 4\gamma_{ij}^2 \frac{(K_{ij}^{A} - K_{ij}^{E})^2}{(K_{ij} - K_{ij}^{E})^3}\left(1 - \frac{1}{K_{ij}^{A}}\right)^2}$	$K_{ij}^{M} < K_{ij} < K_{ij}^{A}$	Elastic recovery

ε_0 = the yielding strain

$\varepsilon_{ij} = \frac{\Delta l_{ij}}{l_{ij}} =$ the ratio between the variation of length in the i-j bar and its actual length

$K_{ij}^{E} = \frac{N_{ij}^{E}}{N_{ij}^{0}} =$ the ratio between the critical Eulerian force in the i-j bar and the ultimate axial force in the same bar

$K_{ij} = \frac{N_{ij}}{N_{ij}^{0}} =$ the ratio between the normal force N_{ij} in the i-j bar and the ultimate axial force N_{ij}^{0} in the same bar

$\gamma_{ij} = \frac{|M_{ij}^{0}|}{l_{ij}N_{ij}^{0}} =$ where $|M_{ij}^{0}|$ is the absolute value of the ultimate bending moment in the i-j bar

Fig. 20.1.

@Seismicisolation

An incremental stress-strain relation for reticular structure rods, which takes into account the post-critical behaviour with decreasing stiffness and the elastic perfectly-plastic behaviour in traction, is shown in Fig. 20.1. [3]

An incremental analysis of pin-joined structures can be carried out by means of the following procedure.

2.2 Incremental Analysis

In the case of pin-joined space reticular structures, the equilibrium equations written at any step in the *i* joint having *k* bars (*j*=1…*k*) referring to the changed shape and to the fixed axes of displacements are:

$$\sum_{j=1}^{k} (\alpha_x)_{ij} N_{ij} + X_i = 0 \qquad (1)$$

$$\sum_{j=1}^{k} (\alpha_y)_{ij} N_{ij} + Y_i = 0$$

$$\sum_{j=1}^{k} (\alpha_z)_{ij} N_{ij} + Z_i = 0$$

or even, in the incremental form:

$$\sum_{j=1}^{k} (\alpha_x)_{ij} \dot{N}_{ij} + \sum_{j=1}^{k} (\dot{\alpha}_x)_{ij} N_{ij} + \dot{X}_i = 0 \qquad (2)$$

.....

.....

The expressions of the geometrical terms in the eqns. (2) are:[6] $(\alpha_x)_{ij} = (x_j - x_i)/l_{ij}$ and similar with $l_{ij} = \sqrt{(x_j - x_i)^2 + (y_j - y_i)^2 + (z_j - z_i)^2}$ and also in a symbolic form:

$$\begin{vmatrix} (\alpha_x)_{ij} \\ (\alpha_y)_{ij} \\ (\alpha_z)_{ij} \end{vmatrix} = \frac{1}{l_{ij}} \begin{vmatrix} [1-(\alpha_x)_{ij}^2] & -(\alpha_x)_{ij}(\alpha_y)_{ij} & -(\alpha_x)_{ij}(\alpha_z)_{ij} \\ -(\alpha_y)_{ij}(\alpha_x)_{ij} & [1-(\alpha_y)_{ij}^2] & -(\alpha_y)_{ij}(\alpha_z)_{ij} \\ -(\alpha_x)_{ij}(\alpha_z)_{ij} & -(\alpha_z)_{ij}(\alpha_y)_{ij} & [1-(\alpha_z)_{ij}^2] \end{vmatrix} \begin{vmatrix} \Delta\dot{u}_{ij} \\ \Delta\dot{v}_{ij} \\ \Delta\dot{w}_{ij} \end{vmatrix} \qquad (3)$$

where $\Delta\dot{u}_{ij} = (\dot{u}_j - \dot{u}_i)$ etc.

The adequate constitutive laws in the incremental form must be joined to eqns. (2) which is linear in the ui, vi, wi unknown quantities. Given $K_{ij} = N_{ij}/N_{0ij}$ and

@Seismicisolation

$\dot{K}_{ij} = \dot{N}_{ij}/N_{0ij}$, between the normal stress's increases and the deformation's increases there is the law:

$$\dot{K}_{ij} = \dot{\varepsilon}_{ij}\lambda_h\rho_{hk} \tag{4}$$

with *(h,k=a…g)* and p_{hk}=1 for $h=k$, p_{hk}=0 for $h\neq k$. The values of the coefficient λ_h are supplied in the table of Fig. 20.1. In eqn. (4) it is: $\dot{e}_{ij} = \Delta\dot{l}_{ij}/l_{ij}$ with

$\Delta l_{ij}=(\alpha_x)_{ij}\,\Delta u_{ij}+(\alpha y)_{ij}\,\Delta v_{ij}+(\alpha_z)_{ij}\,\Delta w_{ij}$

Equations (2) written in the form:

$$\sum_{j=1}^{k}(\alpha_x^{(r-1)})_{ij}\delta N_{ij}^{(r)} + N_{ij}(\delta\alpha_x^{(r)})_{ij} + \delta X_i^{(r)} = 0 \tag{5}$$

.....

.....

where $\delta N_{ij} = \dot{N}_{ij}\,\delta t$ and $(\delta\alpha_x)_{ij} = (\dot{\alpha}_x)_{ij}$ can be solved by finished increases of the load, supposing as linear the structure's response at each step.

At the beginning of the rth generic step, we know the vector:

$$(N_{ij}, X_i, Y_i, Z_i, \alpha_{xij}, \alpha_{yij}, \alpha_{zij})^{r-1}$$

and linking to each bar the component λ_{hk} of the constitutive law in function of $N_{ij}^{(r-1)}$, from the solution of the linear system (5) we obtain the unknown quantities

$$\delta_{ui}^{(r)} \qquad \delta_{vi}^{(r)} \qquad \delta_{wi}^{(r)}$$

being $\delta_{ui} = \dot{u}_i\,\delta t$ and similar.

The correction of the error due to the non-linearity in the step is carried on through the theory shown in Ref. 4.

As to the following step, eqns (5) are modified through the relations:

$$N_{ij}^{(r)} = N_{ij}^{(r-1)} + \delta N_{ij}^{(r)} \qquad X_i^{(r)} = X_i^{(0)} + \sum_{1}^{r}\delta u_i$$

and similar, and the computation is carried on for a new increase of the exterior load.

The inversion of the sign of the system's determinant between two subsequent steps singles out the collapse load. Further details are shown in Refs. 3 and 6.

2.3 Imperfections

Imperfections of geometric kind essentially concern: (1) the area of the section; (2) the imperfect rectilinearity; (3) the length of the bar. Imperfections of mechanical kind concern: (4) the yield strength and (5) the ultimate tensile strength.

@Seismicisolation

Imperfections 1, 4, 5 can be described only by one random variable which refers to the strength under the bar tension; the probability distribution of this may be obtained starting from the p.d.f.* of 1, 4, 5. Imperfections 1, 4, 5 can be well represented by a random variable with Gaussian distribution Γ. Imperfections 2 and 3 are better represented by γ distribution function, whose p.d.f.* is:

$$p(\delta) = \frac{1}{\Gamma(a+1)b^{a+1}} \delta^a \exp\left\{-\frac{\delta}{b}\right\} \tag{6}$$

Given the mean δ_m and the standard derivation σ_δ of the member imperfection, the coefficients a and b may be calculated as follows:

$$b = \frac{\sigma_\delta^2}{\delta_m} \qquad a = \frac{\delta_m^2}{\sigma_\delta^2} - 1$$

* p.d.f. is the abbreviation for probability density function.

Introducing the new random variable $\beta=\delta/\delta_m$ and the coefficient $\alpha=\delta_m/\sigma_\delta$, the ratio $P(\delta)/P_{max}$ may be calculated through the expression

$$(b' \leq \bar{p}),\ \delta \tag{7}$$

which allows one to assign to each member a random imperfection δ Moreover, for prefabricated mass produced structures, it is better to perform the direct construction of the p.d.f. of each imperfection, by using cumulative histograms carried out from highly numerous populations. The consideration of all the random variables allows us to supply indications about the structure behaviour only in particular cases, by using direct probability methods. In most cases, the problem has no solution and, consequently, information of a probabilistic nature can be obtained by using numerical simulation methods.

The reliability of such methods has been tested in Refs. 8, 9 and 10. These methods consist essentially in the generation of pseudo-random structures, each of which must be analysed in a deterministic way.

3 NUMERICAL SIMULATION METHODS

The first step in the numerical simulation method consists in the generation of pseudorandom structures, by using techniques of the Monte-carlo kind.

3.1 Generation of Pseudo-random Structures

A sample value δmax is chosen for δ so that its probability of occurrence is very small and a rectangular domain is chosen in the plane $\delta, p(\delta)$ as $\Omega=(0, \delta_{max})\times(0, P_{max})$, P_{max} being the maximum value of the p.d.f.

Setting $a' = a\delta_{max}$, $b' = bP_{max}$, all points (a', b') such that $0 \leq a \leq 1$, $0 \leq b \leq 1$ belong to the domain Ω

@Seismicisolation

After a couple of pseudo-random numbers *(a, b)* is generated, we $\bar{\delta} = a' = a\delta_{max}$ setand $\bar{p} = p(\bar{\delta})$.

The couple $(\bar{\delta}, \bar{p})$defines the point P_0 on the curve *p(δ)* (Fig. 20.2). $(\bar{\delta}, \bar{p})$represents point $\bar{p}_1$if $b' \leq \bar{p}$ b' or point $\bar{p}_2$ if $b' \geq \bar{p}$.In the former case $(b' \leq \bar{p})$, δrepresents a pseudorandom variable with p.d.f. *p(δ).*

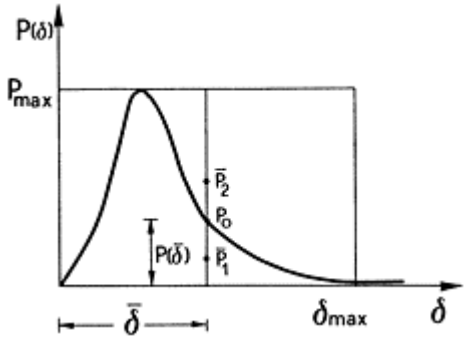

Fig. 20.2.

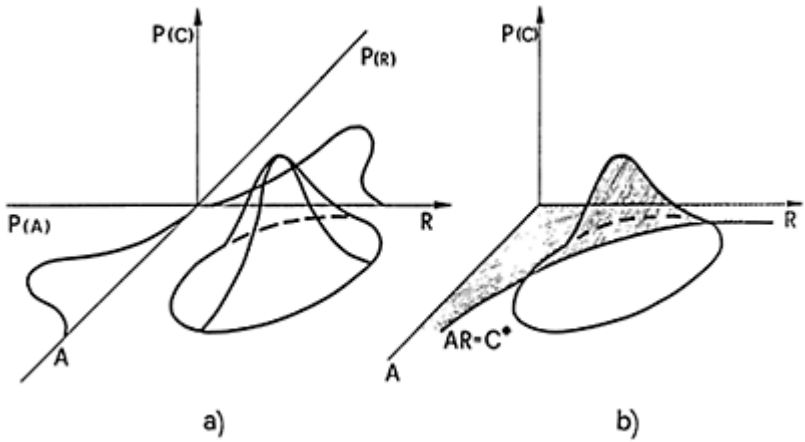

Fig. 20.3.

In the latter case a new couple *(a, b)* of pseudo-random numbers is generated, and so on, until the condition $b' \leq \bar{p}$ is satisfied.

For the simulation of a random structure, the previous procedure is applied to each random variable which occurs in the definition of the structure itself.

3.2 Reliability of the Simulation Method

@Seismicisolation

In order to assess its reliability the simulation method has been applied to a model involving only two random variables. Given two independent random variables A, R with probability density functions $p(A)$ and $p(R)$, the p.d.f. of the random variable $C=A\ R$ is given by

$$p(C) = p(A)p(R) \tag{8}$$

The probability of C being less than a given value, say C^*, is given by

$$P(C \le C^*) = \int_{-\infty}^{C^*} p(C)\,\mathrm{d}C \tag{9}$$

This can be evaluated directly or through the simulation method. Given $A \ge 0$, $R \ge 0$ it turns out that (Fig. 20.3)

$$P(C \le C^*) = \frac{\int_0^{\infty} p(A')\left[\int_0^{C^*/A} p(R)\,\mathrm{d}R\right]\mathrm{d}A}{\int_0^{\infty} p(A)\left[\int_0^{\infty} p(R)\,\mathrm{d}R\right]\mathrm{d}A} \tag{10}$$

If A and R have Gaussian distributions with mean values μ_A, μ_R and standard deviations σ_A, σ_R, their p.d.f.s are

$$P(A) = \frac{1}{\sigma_A\sqrt{2\pi}} \exp\left\{-\frac{1}{2}\left(\frac{A-\mu_A}{\sigma_A}\right)^2\right\} \tag{11}$$

$$P(R) = \frac{1}{\sigma_R\sqrt{2\pi}} \exp\left\{-\frac{1}{2}\left(\frac{R-\mu_R}{\sigma_R}\right)^2\right\} \tag{12}$$

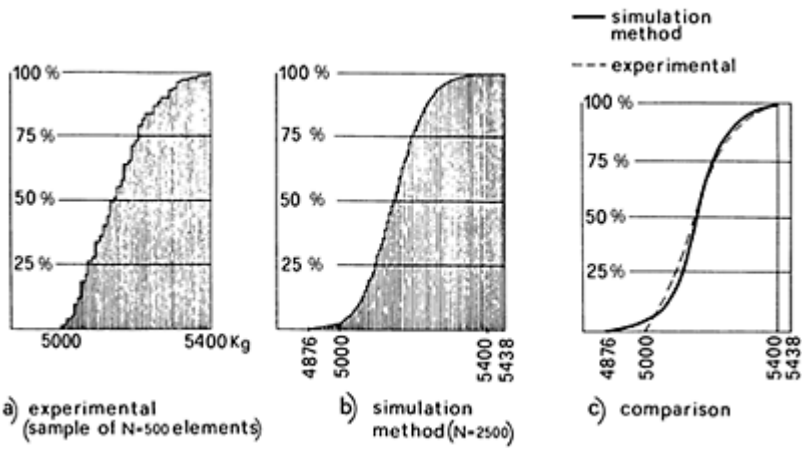

Fig. 20.4.

@Seismicisolation

Using eqns. (11) and (12) in eqn. (10) after having set $\mu_A=\mu_R=1$, $\sigma_A=O_R=1/100$, $C=0{\cdot}99$, it turns out that $P(C \leq 0{\cdot}99)=0{\cdot}235$. In order to provide an experimental check a sample of 500 steel bars has been analysed by measuring for each one the area of the cross-section, the yield stress and the yield load. The cumulative frequency histogram obtained is shown in Fig. 20.4(a).

By assuming a normal distribution for the area of the cross-section and for the yield stress with mean and standard deviation equal to that of the sample, the numerical simulation method has been applied for the generation of a sample of 2500 values of the yield load, which have been reported in the cumulative frequency histogram of Fig. 20.4(b). The superposition of the histograms of Fig. 20.4(c) shows the good qualities of approximation of the method.

3.3 Statistical Analysis of the Pseudo-random Structure Group

A large group of pseudo-random structures can be generated by the method shown in Section 3.1 and tested in Section 3.2. Each element of the group must be analysed through the structural analysis method of the deterministic kind. If 0 is the aim function (performance) under observation, from the statistical analysis of the results given by N deterministic analyses, we can easily obtain the p.d.f. $V(0)$. The use of very large N does not always have an economic justification. In those cases, the theory of statistical inference of small samples may be used by estimating the mean value and standard deviation of the variables of interest.

To these estimates are then applied the significance tests, the Student's t test to the mean and the Pearson's x^2 test to the standard deviation.

In detail, given the confidence interval θ, the value γ of the random variable having probability p of being exceeded, or more specifically the load Q having probability p of producing the collapse of the structure, is given by

$$\gamma_k = \bar{\gamma} - K(p)\sigma \tag{13}$$

where $\bar{\gamma}$ is the mean value, σ its standard deviation and $K(p)$ a Student's coefficient for

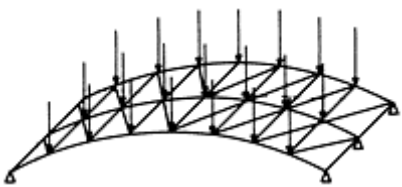

Fig. 20.5.

$N=\infty$ reported in textbooks on statistics. Having a small sample (N) and for the given confidence interval θ the theory of statical inference furnishes:

$$\gamma = \bar{\gamma}_m - K^*(N,\theta,p)s_\gamma \tag{14}$$

@Seismicisolation

with

$\bar{\gamma}_m = \dfrac{\sum \gamma_i}{N}$ the mean of the sample

$s_\gamma = \sqrt{\dfrac{\sum (\bar{\gamma}_m - \gamma_i)^2}{N-1}}$ its standard deviation

and

$$K^*(N,\theta,p) = \frac{t_{n,\theta}}{\sqrt{N}} - K(p)\sqrt{\frac{N-1}{\chi^2_{n,\theta}}}$$

a coefficient dependent on the size *(N)* of the sample, the confidence interval θ and on the pre-fixed probability *p*.

The variables $t_{n,\theta}$ $\chi^2_{n,\theta}$

with $n=N-1$ are reported in textbooks on statistics.

The above-mentioned method has been applied for the evaluation of the collapse load of the braced barrel vault of Fig. 20.5 with bars having imperfections of geometric nature. Constitutive laws of Fig. 20.1 have been assumed and the incremental analysis summarised in Section 1 has been carried out over a sample of 150 pseudo-random structures. Figure 20.6 shows respectively the histogram of the cumulative frequencies (20.6(a)) and the characteristic values of the collapse load (20.6(b)) obtained by applying the small samples theory with 5% collapse probability and confidence interval θ=95%.

The results obtained confirm that the small samples theory always gives precautionary values and that the analysis of a sample of a few elements is enough to supply reliable information.

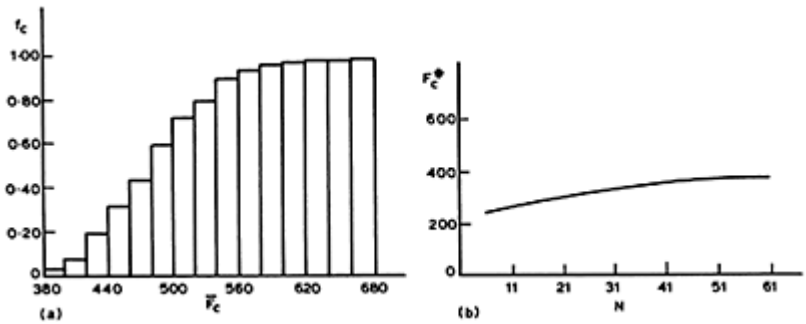

Fig. 20.6.

REFERENCES

1. Di Tommaso, A. and La Tegola, A. Double-layer space frame shells. Ninth Congress IABSE, Amsterdam, 1972.
2. La Tegola, A. and Oliveto, G. Premessa allo studio delle strutture reticolari spaziali in fase post-critica. Report for the CNR group meeting Plasticity, Milan, 1972.

@Seismicisolation

3. La Tegola, A. Analisi incrementale di strutture reticolari metalliche in campo plastico con aste in regime post-critico. *Giornale del Genio Civile*, No. 7–8-9, 1972.
4. La Tegola, A. Contribution to the Incremental Solution of Elastoplastic structures geometrically nonlinear. *Mechanics Research Communications*, vol. 1, Pergamon Press, Oxford, 1974.
5. La Tegola, A. and Sara, G. Seismic response of reticular elastoplastic structures.5 WCEE Earthquake Engineering, Rome, 1973.
6. La Tegola, A. and Sara, G. Analisi dinamica di strutture reticolari elastoplastiche soggette ad azioni di tipo sismico in regime geometricamente non lineare. Colloque RILEM-CISM, Udine, 1974.
7. La Tegola, A. Design problems of space reticular structures. 2nd International Conference on Space Structures, University of Surrey, Guildford, 1975.
8. La Tegola, A. II carico di collasso delle strutture con imperfezioni random. *Giornale del Genio Civile*, Rome, 1979.
9. La Tegola, A. Simulation methods for the analysis of pin-jointed structures with randomly imperfect members. Innovative Numerical Analysis for the Applied Engineering Sciences, Montreal, June 1980.
10. Badala, A. and La Tegola, A. Sul carico di collasso delle strutture costituite con materiale a resistenza random. Report No. 40, Department of Structures, University of Calabria, 1981.

@Seismicisolation

21
Recent Research on Timber Lamella Barrel Vaults

CLAUS SCHEER and JEFFREY PURNOMO
Technical University of Berlin, West Germany

On the initiative of the Timber Construction Development Association (EGH) and with the financial support of the Baden-Württemberg Ministry of Economy, the research project on 'Further Development of the Zollinger Lamella Construction Type with Determination of Simplified Design Methods and Statical Checks' was carried out in the Department of Structural Engineering at the Technical University of Berlin.

1 DESCRIPTION OF THE ZOLLINGER LAMELLA CONSTRUCTION TYPE[1–5]

The Zollinger Lamella roof (named after its inventor, who was a municipal building surveyor of Merseburg) is an arched network consisting of single lamellae arranged in rhombic form. The construction principle illustrated in Fig. 21.1 was developed about 1920 from the 'curved plank rafter' and found manifold application in the following years as pointed, round or segmental arches (Fig. 21.2). By separating the curved planks at the points of contact by an angle of a and the arrangement of several such systems alongside each other, one obtains a meshlike spatial frame with rigid joints; this arrangement is known as the Zollinger lamella roof. The lamellae are cut to size in curved form on one side in accordance with the shape of the roof and bevelled at the ends. At the joints there are always three lamellae bolted together. This joint and the connection of the lamellae to the support may be seen in Fig. 21.3. As a rule the roof construction has to be stiffened at the gable ends. For the cladding of the roof bricks, shingles, slate panels, straw or composition roofing on battens or boarding are used.

2 STRUCTURAL ANALYSIS OF THE ZOLLINGER LAMELLA ROOF

2.1 Approximate Method of R.Otzen[6,7]

The Zollinger lamella roof is a system that internally and externally is statically indeterminate to a high degree. In order to calculate the stress distribution in such a roof Robert Otzen developed an approximate method of analysis frequently used by practical

@Seismicisolation

designers. This method first of all determines the force magnitudes either for a statically determined three-hinged arch or for a statically indetermined two-hinged arch or

Fig. 21.1. Segmental timber shell using Zollinger lamella construction type.

hingeless arch for a unit strip of width *b* equal to the rhombus width. The slanting position of the lamellae was taken into account by resolution of the force magnitudes into the given lamella direction. For the bending stress M_0 in a loading strip only one lamella section was taken into account to determine the bending stresses; the normal forces were distributed over two lamellae and the transverse forces were in general left out of account. The torsional stress about the arch axis—determined by the resolution of the bending stress—was not particularly investigated, as it was assumed that the approximate approach used in this method describes in an adequate way the equilibrium of forces in the structure.

As the force magnitudes determined were greater than the stresses actually encountered in a rhombic system, Otzen introduced a correction factor for the determining moment stress in the case of unilateral load, the so-called 'rigidity coefficient'. This rigidity coefficient is the ratio of the deformation of a rhombic model of round bars to the deformation obtained by the approximate analysis of the arch. By taking the rigidity of

@Seismicisolation

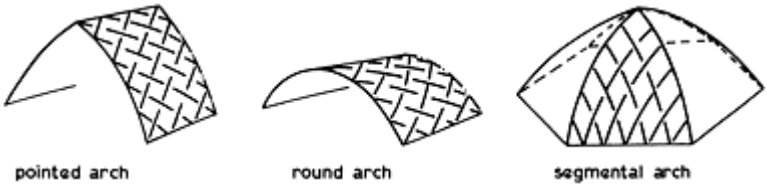

Fig. 21.2. Variants of Zollinger lamella construction type.

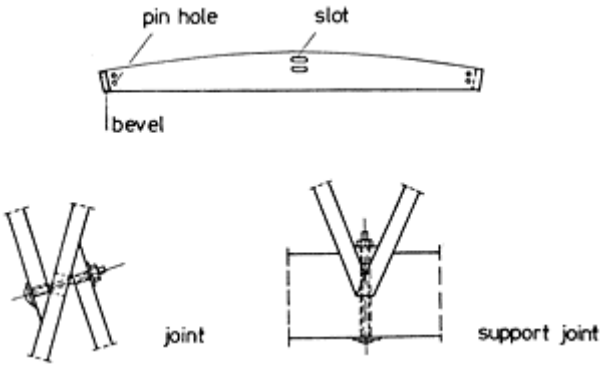

Fig. 21.3. Lamellae and joints used in the Zollinger lamella construction type.

the structure into account it was possible to determine the moment stress of the individual lamellae as follows:

(a) Without gable bracing

$$M_0 = \frac{M_a}{\rho_0 \cos\frac{\alpha}{2}} \qquad \rho_0 = \frac{\Delta}{\delta_0}$$

(b) With gable bracing

$$M_m = \frac{M_a}{\rho_0 \rho_m \cos\frac{\alpha}{2}} \qquad \rho_m = \frac{\delta_0}{\delta_m}$$

where M_0 or M_m=design moment of one lamella of a Zollinger lamella roof without or with gable bracing; M_a=moment obtained by the approximate analysis of an equivalent arch; α=aperture angle of the rhombic system (inclination of the lamellae to each other); Δ=deformation obtained using the approximate arch analysis; δ_0 or δ_m=measured deformation on a model of round bars without or with gable bracing.

@Seismicisolation

Zollinger lamella roofs were designed, analysed and constructed by Otzen for spans up to 30 m using this approximate method. At that time the design of these structures was carried out by engineers who used their instinct in determining the actual load carrying behaviour of the Zollinger lamella roofs rather than an exact calculation of stress distribution, which at that time, anyway, would have been very costly and very difficult to perform.

A further contribution to the treatment of spatial networks of circular cylindrical form as continuous systems was made by May and Nowack.[9]

2.2 Computation Using the Finite Element Method

To obtain a more exact picture of the load carrying and deformation behaviour of the Zollinger lamella roof construction type, hereinafter referred to as the rhombic lamella roof, electronic computations were carried out with the aid of the Finite Element Program SAP IV. The SAP (Structural Analysis Program) has been under development since 1970 by E.Wilson and co-workers at Berkeley, University of California.[8]

The calculation uses first-order theory and assumes linear elastic material behaviour by considering the equilibrium conditions at the joints and subsequently determining the elemental forces or stresses. In the course of the present investigation the material constants used were those of DIN 1052, Part 1, 1969 edition—Holzbauwerke, Berechnung und Ausführung (Timber Construction, Calculation and Execution).

The element type of a rhombic lamella roof is described in terms of the joints of the spatial system and leads to the numbering of joints *m* and of bar elements *n* shown in Fig. 21.4, representing a side ratio *L:B*=1:1. As a result of the adoption of straight bar elements a polygonal row arose approximating the cross-section shape. The bar elements, cut on one side to an arch shape in order to avoid the emergence of buckling points in the roof area, are assumed to have a variable section, which was taken into account by the adoption of equivalent section values for the determination of respective bar rigidities.

In the case of the connections a distinction was made between a hinged and a rigid joint.

The roof covering nailed on to the lamellae was assumed approximately to be an elastically supported single bar between the joints. In combination with the lamellae this single bar forms a triangulated system with a bracing effect. The yielding of the joints in connection with the rigidity of boarding was allowed for by the adoption of an equivalent rigidity determined from the following expression:

$$EF_{\mathrm{id}} = \frac{1}{\sum \frac{1}{nCl} + \frac{1}{EF}}$$

where *E* is the modulus of elasticity of the wood of the roof boarding, *F* is the crosssectional area of the roof boarding, *C* is the modulus of translation of the fasteners, *n* is the number of fasteners, and *l* is the interval between joints (bar length).

The influence of the structure geometry on the force magnitudes and the deformation behaviour was studied by adopting various arch forms, e.g.

circular arch

parabolic arch

@Seismicisolation

arch formed according to pressure line as a result of permanent load
and variants of the ratio of roof length *L* to roof width *B:*
L:B=1·0:1
L:B=1·25:1
L:B=1·5:1
L:B=2·0:1

In the attempt to find the influence of gable construction a distinction was made between an end arch frame (elastic support) and an end arch sheet (rigid support).

2.3 Analytical Results

The analytical results illustrated in the enclosed diagrams refer to a circular cylindrical rhombic lamella roof with a span of B=21 ·5 m, an arch aperture angle of β=120° and a rhombus aperture angle of α=60°. The lamellae were 3·0 m long and had a section of 10/22 cm. The lamella connections were assumed to be hinged.

No comprehensive calculations were undertaken for roofs that were parabolic or formed according to the pressure line, as some comparative calculations showed that these roof forms only yielded slight section savings for the lamellae and that the circular arch offered advantages over other roof forms with regard to execution and cost economy.

@Seismicisolation

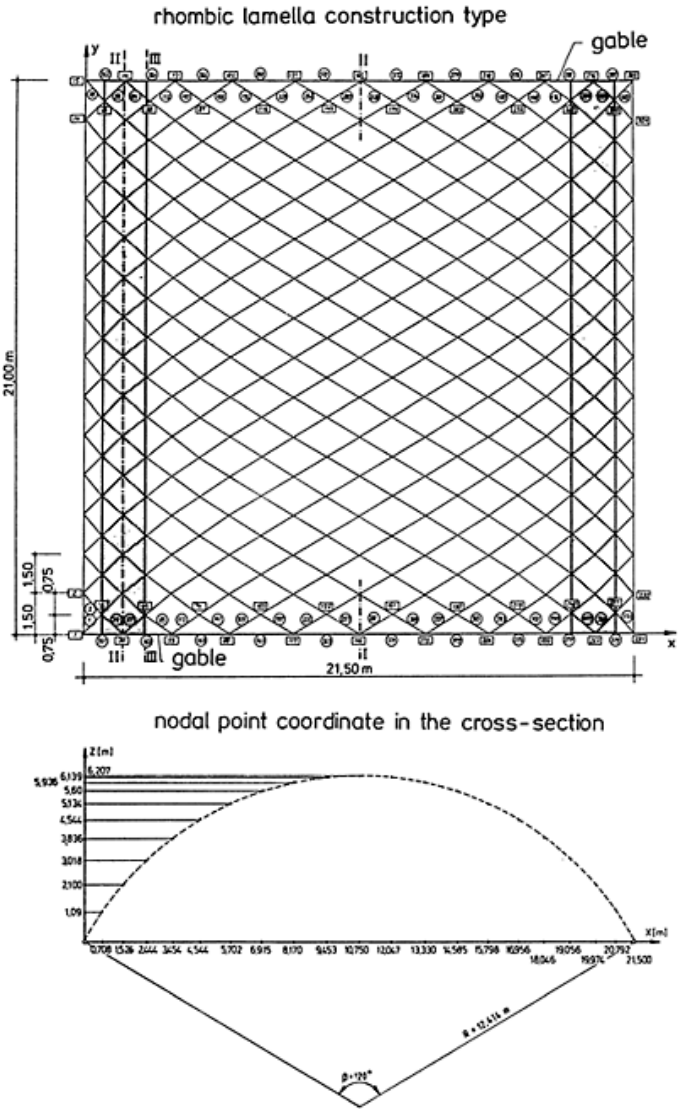

Fig. 21.4. Dimensions, plan view of the rhombic lamella roof nodal point coordinate in the cross-section. Ground plan aspect ratio $L:B \approx 1:1$. ⓜjoint numbers; ⓝbar element numbers. Shaded regions indicate range of determining strain.

@Seismicisolation

The decisive force magnitudes for rhombic lamella roofs of various ground plan side ratios were derived from

the load case with asymmetrical loads in the case of construction with elastic gable arches;

the load case with symmetrical loads in the case of constructions with rigid gable ends.

This is explained by the fact that the rigid gable supports reduce deformation of the lamella construction in the case of asymmetrical load.

In the case of lamella structures with roof covering, investigations have shown that the normal forces and bending moments about the strong axis are of primary importance for the design of the lamellae. Transverse forces, torsional moments and moments about the weak axis have only a secondary significance. The bending stress about the weak axis is important only in the case of constructions without roof boarding. This stress can be reduced by the use of tiebacks.

The normal forces in the individual lamellae increase from the hall centre to the gables and from the apex of the structure diagonally along the given lamella chain to the points of support. They hardly alter their maximum values at all in the case of symmetrical load and various ground plan side ratios.

The maximum bending moments occur in the case of all ground plan sides in the 2nd and 3rd rows of bars from the support in the centre of the hall length. In the case of lamella constructions with roof covering the bending stress increases with increasing side ratios; in the case of constructions without roof covering the bending stress changes only slightly.

The vertical deformation of the rhombic lamella roof increases steadily in the case of structures with roof covering in the longitudinal direction of the hall, and reaches its maximum in the hall centre. The maximum deformations are doubled in the case of an alteration of the ground plan side ratios from *L:B*=1:1 to *L:B*=2:1. In the case of

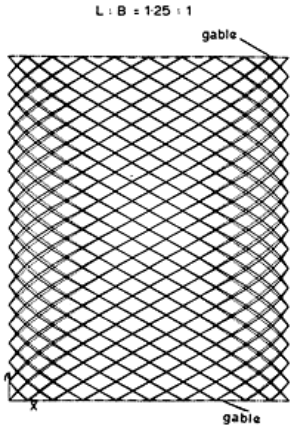

Fig. 21.5. Horizontal deformation of rhombic lamella structure with roof boarding.

@Seismicisolation

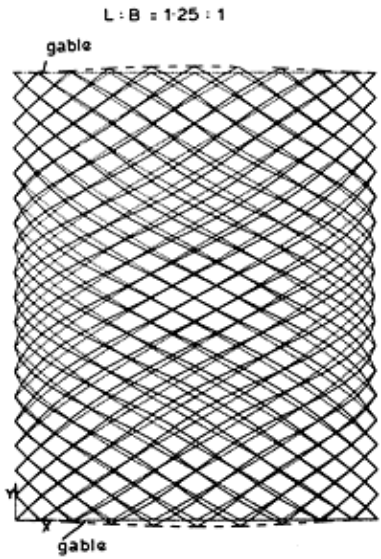

Fig. 21.6. Horizontal deformation of rhombic lamella structure without roof boarding.

structures without covering under the loading the roof is deforming with a maximum deflection in the vicinity of the gable.

The horizontal deformation may be seen from Figs. 21.5 and 21.6. They illustrate the deformations in the projection plane *x-y* for a structure with a side ratio *L: B*=1·25:1, assuming elastic end arch frames and with or without roof covering under symmetrical load. It is quite clear from the study of these figures that the rigidity of lamella roofs relies to a great extent on the roof covering.

3 LARGE-SCALE EXPERIMENTS

3.1 Experimental Set-up and Execution of Tests

In addition to the mathematical investigations, eight large-scale models and prototypes have been built and experiments carried out at the Federal Institute for Material Testing (BAM) on a specially constructed test rig for the application of loads and experimental determination of strains and deflections. The intention was to compare the experimental results with those obtained by mathematical theory. Figure 21.7 shows a test model, dimensioned to represent a structure in a ratio of 1:4, on which the analysis has been carried out. The model covered an area of 5·51 m×5·61 m, with an arch aperture angle of β=120° and a radius of 3·17 m.

@Seismicisolation

The timber lamellae were fastened together with 2·5 mm thick steel plates, inserted in the slots, and nails N25×55 as well as with steel sheet preforms at the supports and armature nails 40×50.

The load was applied to the structure unilaterally at the joints by means of linen sacks filled with steel weights (Fig. 21.8) in three equal load increments. With the third load stage a working load of 1·2 kN/m^2 for the overall area was reached.

The deformation behaviour of the structure was determined by means of electric displacement transducers (potentiometers; Fig. 21.9) in combination with a data logger

Fig. 21.7. Top view of the test stand in the **BAM**.

@Seismicisolation

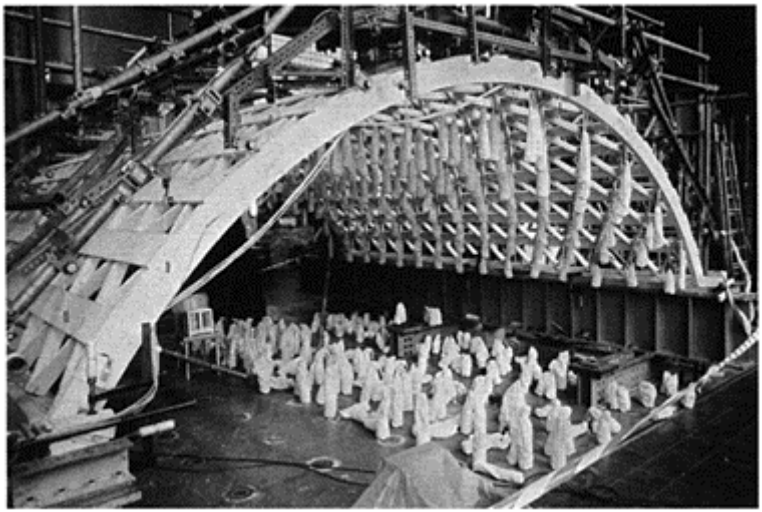

Fig. 21.8. Test sample with load stage 1.

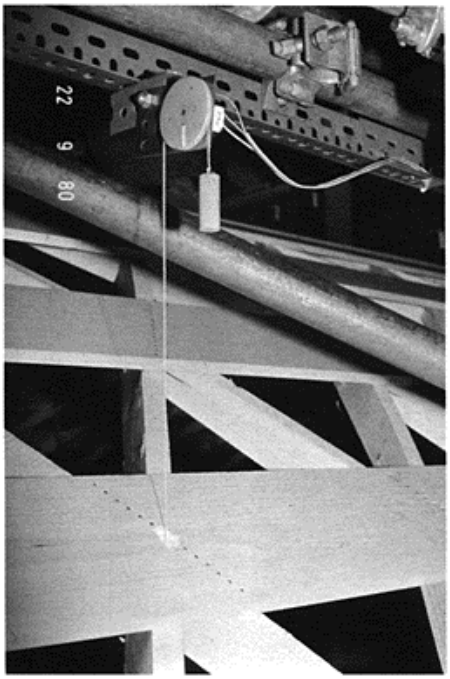

Fig. 21.9. Displacement measurement with potentiometer.

@Seismicisolation

Fig. 21.10. Enhancing the gable rigidity with framework.

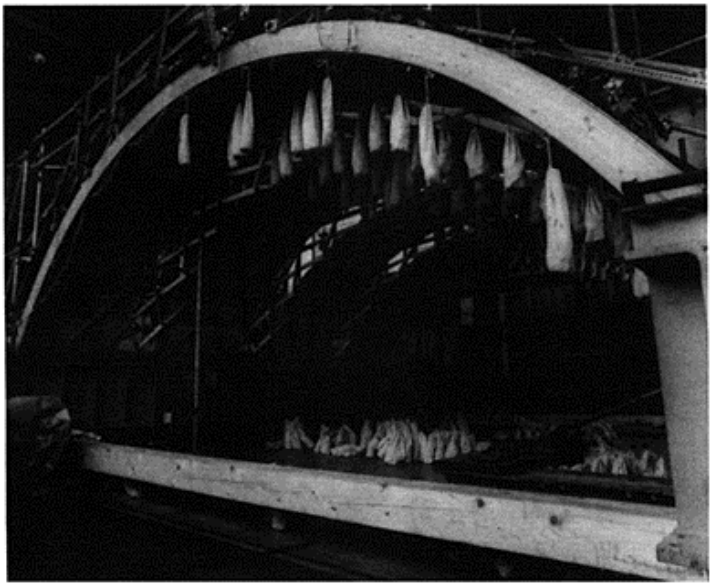

Fig. 21.11. Test sample with strip-line fixtures.

@Seismicisolation

(multi-digit measuring unit p.d.p. 11/05) and mechanical displacement transducers (dial gauges).

3.2 Results of the Experiments

The experimental investigations made it possible to measure the deformation behaviour of a rhombic lamella structure for different gable rigidities (Fig. 21.10), and allowed the influence of roof covering to be taken into account. A comparison of the experimental results with those of the analytical calculations on the basis of the material characteristics and translation values of the joints yielded a comparable deformation behaviour within the normal limits of accuracy. This experimental result confirmed the assumptions used in the calculations.

The tests allowed us also to determine the influence of strip-line fixtures (Fig. 21.11) upon the reduction of the longitudinal rigidity of the structure.

4 TYPES OF JOINT

In the case of structures built so far using the rhombic lamella construction method, with the exception of the construction according to Ref. 10, the individual bars in the joints were fastened with bolts.

@Seismicisolation

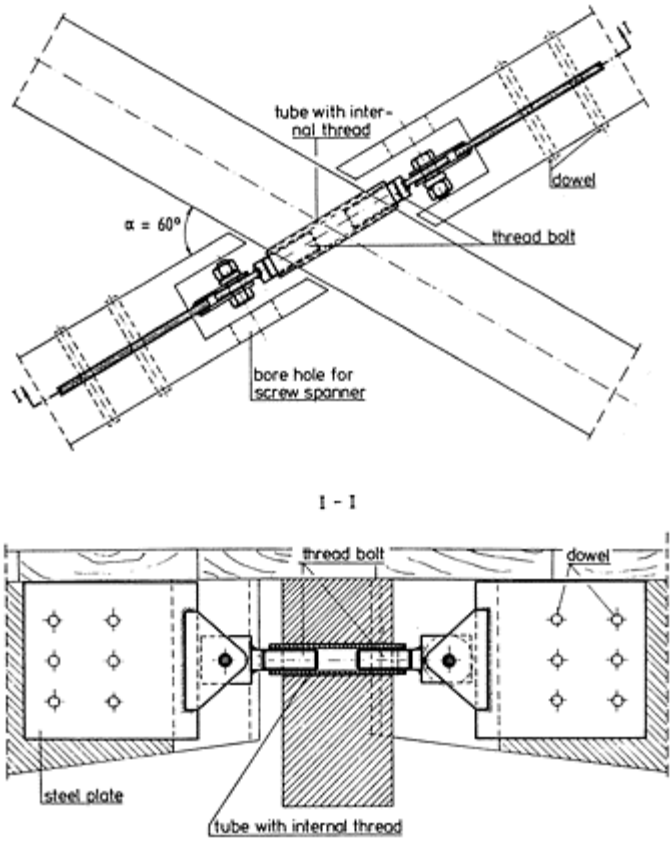

Fig. 21.12. New development of a joint for a rhombic lamella structure.

@Seismicisolation

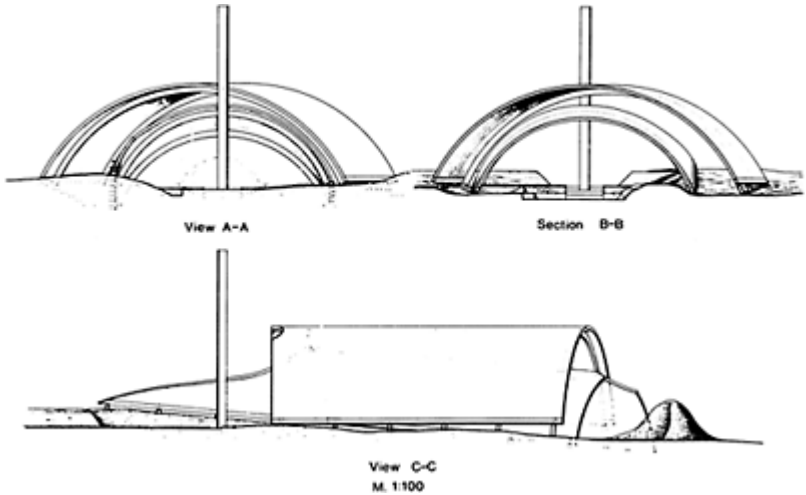

Fig. 21.13. Architectural concept for the 'Church Amid Greenery'.

As bolts in accordance with DIN 1052 may only be used in permanent structures for load transmission under certain conditions and the eccentricity of the connections leads to additional stresses, new developments regarding the formation of the joints are required. One possibility is presented in Fig. 21.12. This joint is adjustable and detachable.

5 CONCLUSIONS

The mathematical and experimental investigations of rhombic lamella structures have shown that the influence of the roof covering and of the gable construction on the stress of the lamella and on the deformation behaviour of the joints is considerable.

The investigations carried out show a circular cylindrical rhombic lamella structure with a ground plan side ratio of $L: B$=1:1, roof covering and a braced gable to be an optimal solution. In the case of longer halls intermediate arches should be used at intervals corresponding to the hall width B.

For structures without boards covering the roof tiebacks should be used in the roof plane in the longitudinal direction of the hall.

6 PRACTICAL APPLICATION OF THE RESEARCH RESULTS

The architectural and practical evaluation and application of the research results found their implementation in the planning of the 'Church Amid Greenery' for the Federal Garden Show to be held in Berlin in 1985 (BUGA 85) (Fig. 21.13). The design was by architects Dr Peter Stürzebecher and Mr Kenji Tsuchiya, Dipl. Ing. Figure 21.14 shows a model of the proposed structure.

@Seismicisolation

The structural design was made by Mr Manfred Wunderlich, Dipl. Ing., of the Consulting Engineering office of Prof. Claus Scheer.

The church consists of two superimposed rhombic lamella structures whose external forms correspond to that of a cylinder segment. A computer has been used to determine

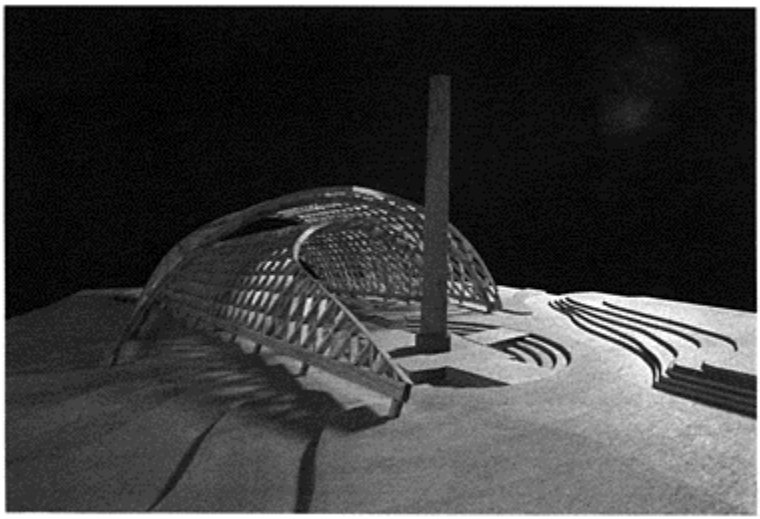

Fig. 21.14. Model of the planned structure.

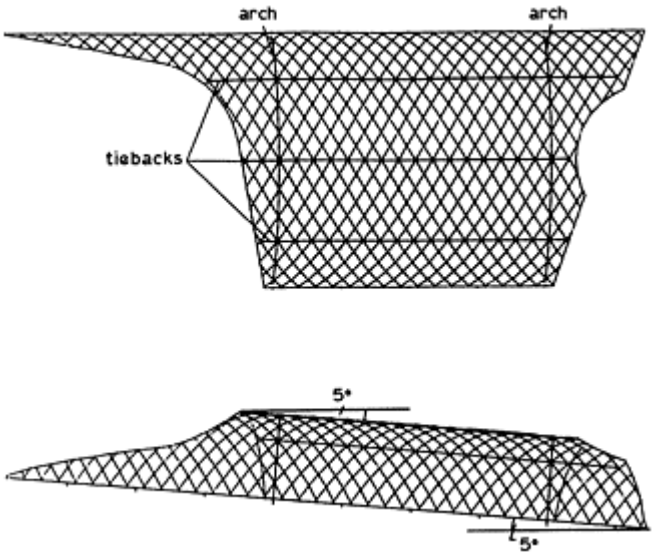

@Seismicisolation

Fig. 21.15. Graphic representation of the inner shell.

the stress distribution in the elements of the structure, and its deformation (Fig. 21.15) illustrates the bracing arrangement.

The outer shell has been designed without roofing and provided with greenery in the shape of creeper plants, while the inner shell has a covering of transparent foil.

The bracing of the structures is provided by two arches in each case and, due to the absence of rigid roofing covering, ties in the roof plane which link the two arches with each other.

REFERENCES AND BIBLIOGRAPHY

1. Gesteschi, Th. *Der Holzbau.* Verlag J. Springer, Berlin, 1926.
2. Kress, F. *Der Zimmerpolier—Ein Lehr- und Konstruktionsbuch.* Otto Meier Verlag, Ravensburg, 5. Auflage, 1938.
3. Kersten, C. *Freitragende Holzbauten.* Verlag J. Springer, 2. Auflage, Berlin, 1926.
4. Eiselen, F. Das Zollbau-Lamellendach. *Holzbau.* (Beilage der Deutschen Bauzeitung), No. 13, 27.10.1923.
5. Hofmann, E. Das Zollinger-Lamellendach als freitragende Dachkonstruktion für Wohnhäuser, Siedlungsbauten, Hallen, Fabrikanlagen, Feldscheinen und Ausstellungsgebäuden. Bauzeitung 1923.
6. Otzen, R. Die statische Berechnung der Zollbau-Lamellendächer. *Der Industriebau* 1923, Heft VIII/IX.
7. Gesteschi, Th. Hölzerne Dachkonstruktionen—Ihre Ausbildung und Berechnung; Verlag W. Ernst & Sohn; 5. Auflage 1938; S. 199–208.
8. Wilson, E.L., Bathe, K.-J. *et al.* SAP—Ein Programmsystem zur linearen statischen und dynamischen Berechnung von Tragwerken. University of California, Berkeley; eingeführt von Wunderlich, W., Ruhr-Universität Bochum; September 1973.
9. May, B. and Nowack, B. Zur Berechnung kreiszylindrischer Netzwerkschalen. Der Stahlbau 8/1971.
10. Nowack, B. and Brunotte, R. Netzwerkkonstruktionen im modernen Ingenieurholzbau. Bauen mit Holz, Heft 5/1974.
11. Scheer, C. and Purnomo, J. Weiterentwicklung der Zollinger-Lamellenbauweise mit Ermittlung von vereinfachten Berechnungsverfahren und statischen Nachweisen. Forschungsbericht Fachgebiet Baukonstruktionen, Technische Universität Berlin (in Vorbereitung).
12. Beiträge zur Bautechnik. Robert von Halasz zum 75. Geburtstag gewidmet; herausgegeben von Jürgen Bauer, Claus Scheer und Erich Cziesielski; Verlag W. Ernst & Sohn; Berlin, München, 1980.
13. Scheer, C. and Purnomo, J. Weiterentwicklung der Zollinger-Lamellenbauweise mit Ermittlung von vereinfachten Berechnungsverfahren und statischen Nachweisen. Bauen mit Holz, Heft 6/1981.

@Seismicisolation

22
Recent Examples of Prefabricated Steel Barrel Vaults from Romania: Their Analysis, Design and Construction

VICTOR GIONCU, NICOLAE BĂLUȚ, DORIN PORUMB
and NICOLAE RENNON
Building Research Institute, Timişoara, Romania

1 INTRODUCTION

During the last eight years a joint research team from the Building Research Institute Timişoara and from the Department of Civil Engineering, Polytechnic Institute of Timişoara, Romania, was involved in the study of various types of latticed space structures.

In this chapter only cylindrical latticed structures will be discussed and some details given of several barrel vaults recently built in Romania. The above-mentioned research team had to accomplish several tasks.

First, comparative studies were carried out to provide information about the structural behaviour, analysis methods, constructional problems and economic aspects related to this type of structure. Second, a reliable analysis tool was needed, including computer programs and stability analysis methods. These problems are thoroughly discussed in Ref. 2. The third task was to satisfy immediate design needs with a view to stimulate designers' interest in braced barrel vaults.

2 STUDIES ON PREFABRICATED BARREL VAULTS

2.1 Lamellar Barrel Vault

The first studied structure was the 36 m span roof intended for sports halls, industrial buildings and warehouses. The general geometry of the roof is shown in Fig. 22.1. The reticulated structure is composed of two families of intersected arches and of longitudinal purlins. The angle between the intersecting arches is 35°. Both the arches and the purlins are obtained by connecting plane prefabricated trusses made of thinwalled cold-formed steel members with 0·5 m depth and a maximum length of 5·0 m (Fig. 22.2(a)).

@Seismicisolation

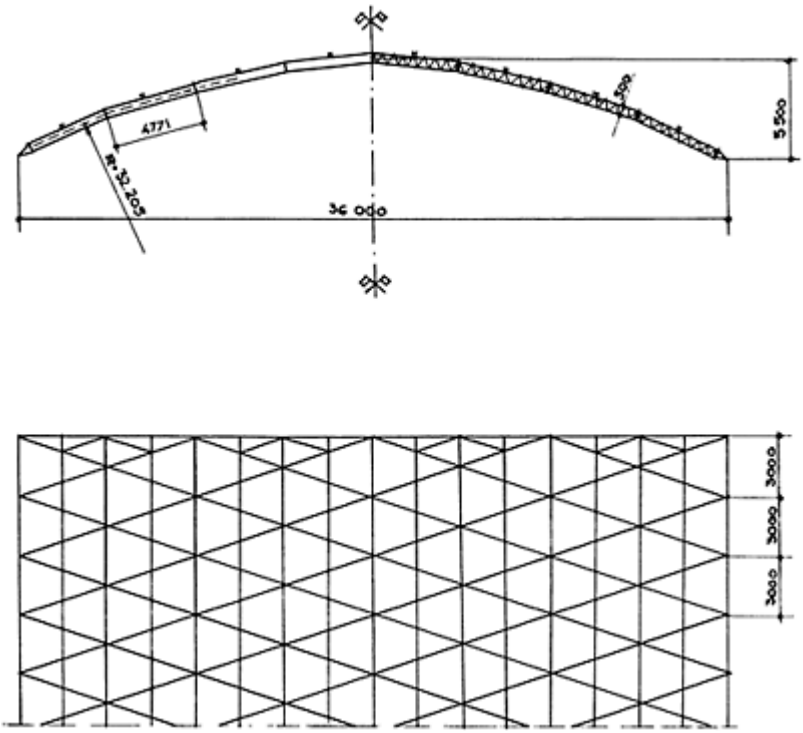

Fig. 22.1.

The main purlins connect the arch intersections and the secondary ones provide lateral support at midspan of each arch segment preventing lateral buckling. High-strength pre-stressed bolts were used for obtaining node joints as rigid as possible (Fig. 22.2(b)). Node deformability was experimentally studied for both top and bottom joints (Fig. 22.3). Laboratory results were satisfactory and the recorded deformations are presumed not to affect the structural stability.

The structure was analysed by the equivalent continuum method (Refs. 1 and 2) considering an orthotropic equivalent continuous shell. General buckling under symmetrical loads showed two half-waves as for arches, denoting little effect of the end walls.

The estimated steel consumption was 17·9 kg/m^2.

2.2 Single-layer Barrel Vault with Stiffening Arches

A multi-purpose cylindrical demountable roof was intended for temporary lightweight buildings. The maximum span of 21·0 m of the vault (Fig. 22.4) is obtained when 10 identical adjacent prefabricated plane trusses are used, but some of them could be omitted

@Seismicisolation

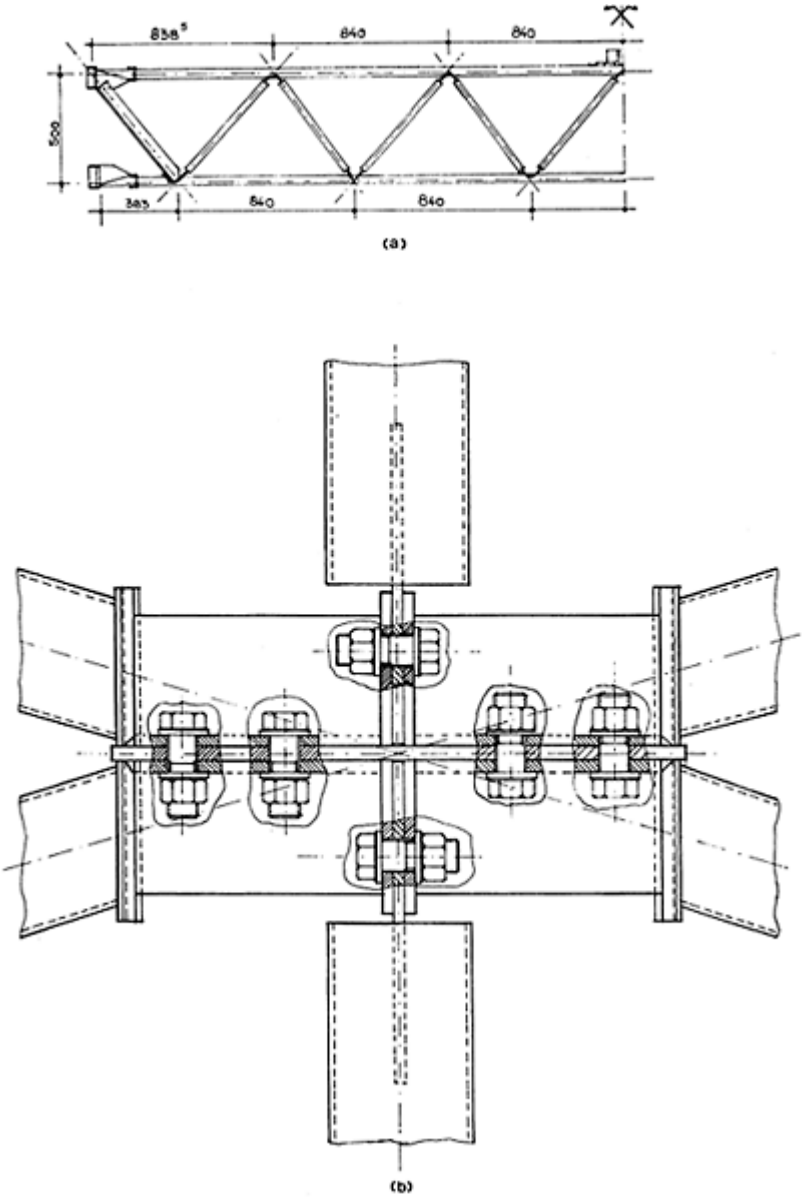

Fig.22.2.

@Seismicisolation

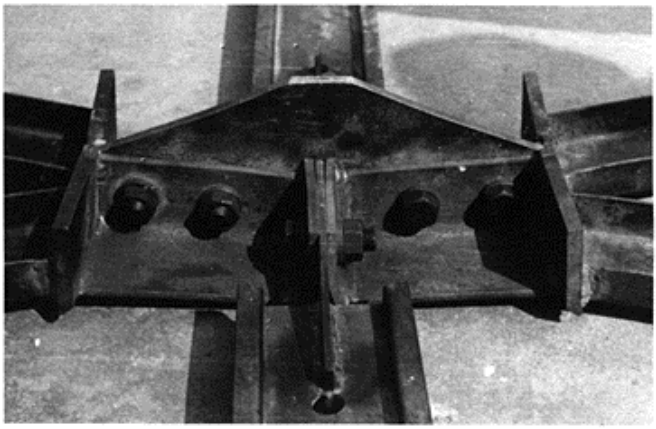

(a)

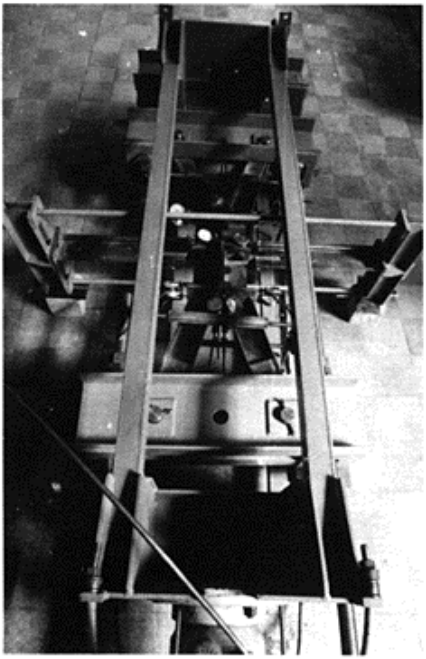

(b)

Fig. 22.3.

@Seismicisolation

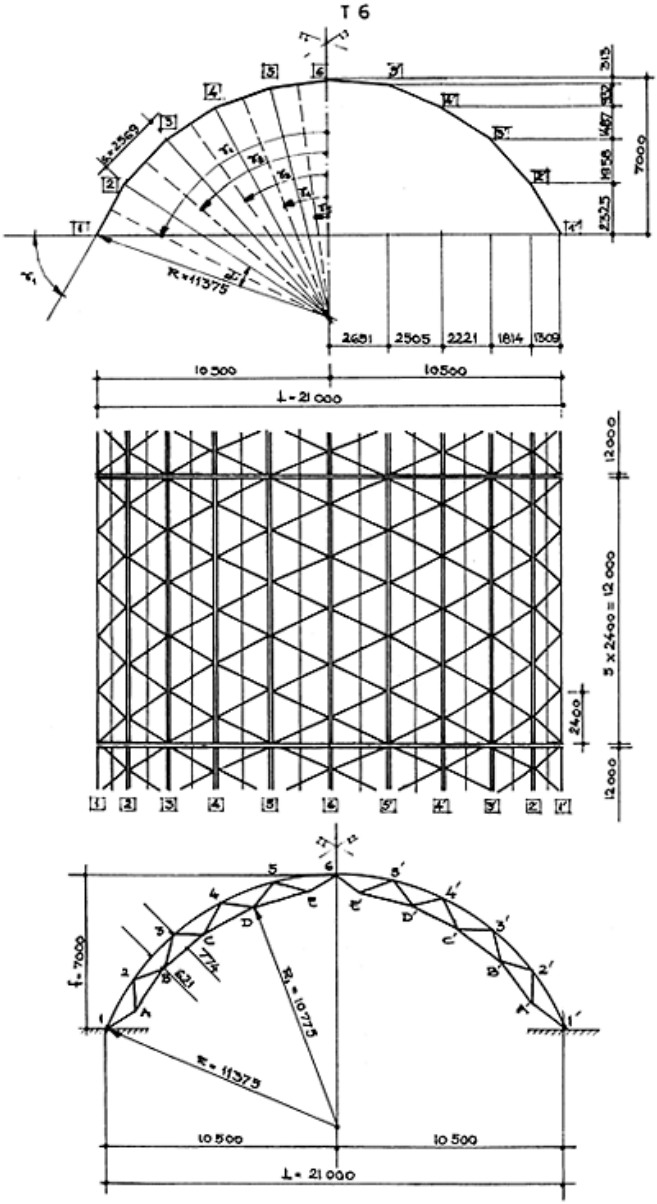

Fig. 22.4.

@Seismicisolation

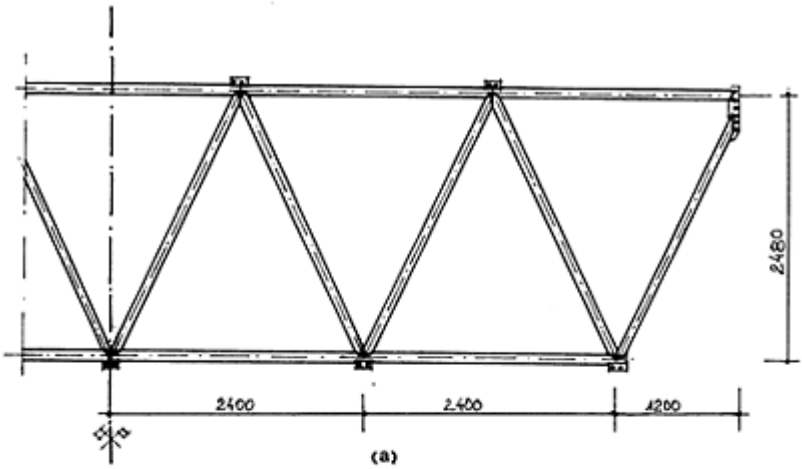

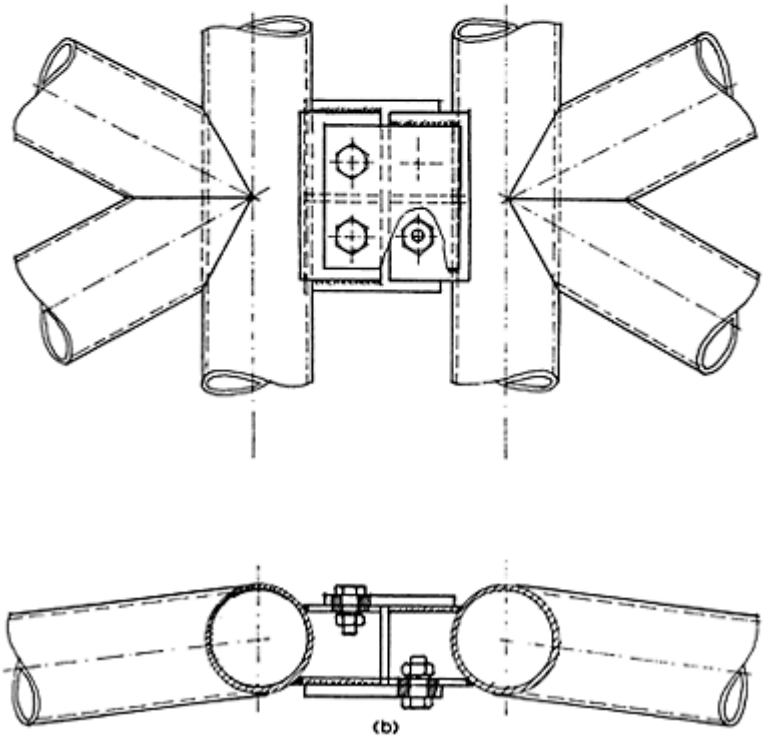

Fig.22.5

@Seismicisolation

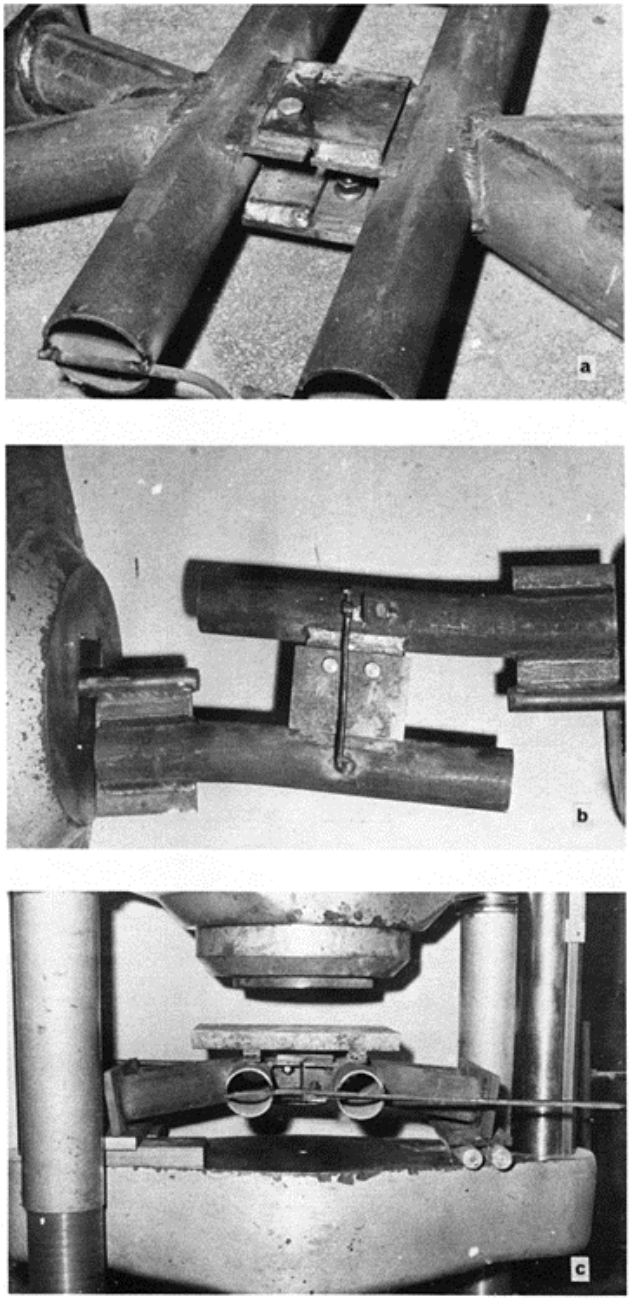

Fig. 22.6.

@Seismicisolation

if a reduced vault span is needed. In each case appropriate stiffening end arches are used. The length of a roof unit is 12.0 m and the possible spans are as follows:

Number of trusses	*Vault span (m)*	*Vault height (m)*
10	21·000	7·000
8	18·382	4·674
6	14·754	2·716

The first two variants could be supported at ground level but the third one needs longitudinal walls or columns for it to be erected on.

All prefabricated units are made of steel tubes (Fig. 22.5(a)) and are connected to each other by precision bolts or site welding (Fig. 22.5(b)). The bolted node behaviour was experimentally checked (Fig. 22.6(a)) under longitudinal shear (Fig. 22.6(b)) and under transverse bending (Fig. 22.6(c)). Longitudinal shear produced insignificant strains. The bending test was necessary for determining the rotational deformations which affect the vault stability.

Using the orthotropic equivalent continuum method the stability analysis resulted in a 38% reduction of the critical load due to node rotational deformations.

The steel consumption is 20·5 kg/m^2 for the 21 m span vault.

3 DESIGN EXAMPLES

3.1 Sports Halls

For five almost identical low capacity (up to 500 seats) sports halls a cylindrical latticed structure was designed (Fig. 22.7). The steel structure has the following component parts (Fig. 22.8):

— two stiffening 32 m span three-hinged trussed arches with triangular cross-section made of steel tubes;
— two end walls made of hot-rolled steel sections;
— the three-bay triangulated barrel vault composed of plane prefabricated trusses with cold-formed channel chords and tubular web members;
— longitudinal edge elements of tubular trusses with triangular cross-section.

The foundations of each arch are connected by a reinforced concrete tie.

The joint between two adjacent vault prefabricated components, i.e. between the two channel chord members, is shown in Fig. 22.9.

The analysis was performed using the computer program NELIN developed by the authors and described in Chapter 9. The resulted deflections of the initial triangulated vault under unsymmetric snow loads were unacceptable and therefore two solutions were studied in order to improve the vault behaviour. The first one consisted of additional tension members as sketched in Fig. 22.10 and the second comprised additional bending-resistant stiffening arches. Comparison between the two corresponding load-deflection curves (see Fig. 22.10) led to the final choice of the latter variant.

@Seismicisolation

Figures 22.11 to 22.15 show some site views during erection. The structural steel consumption is 27 kg/m^2.

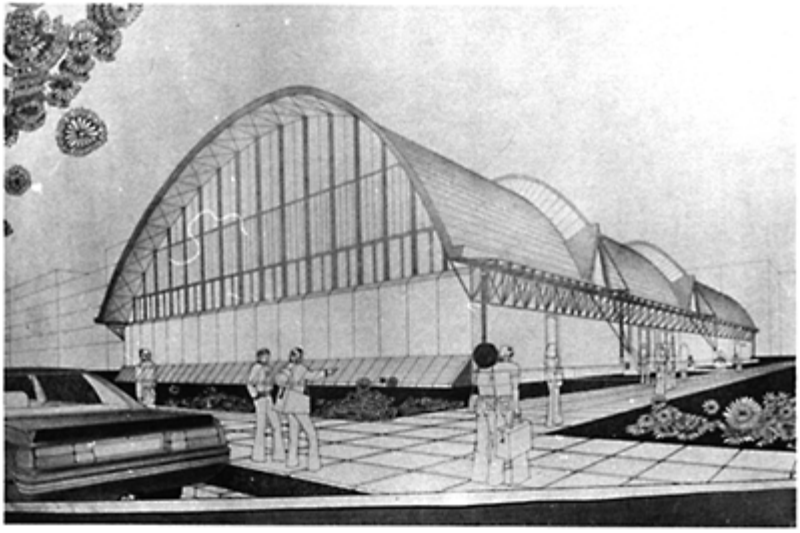

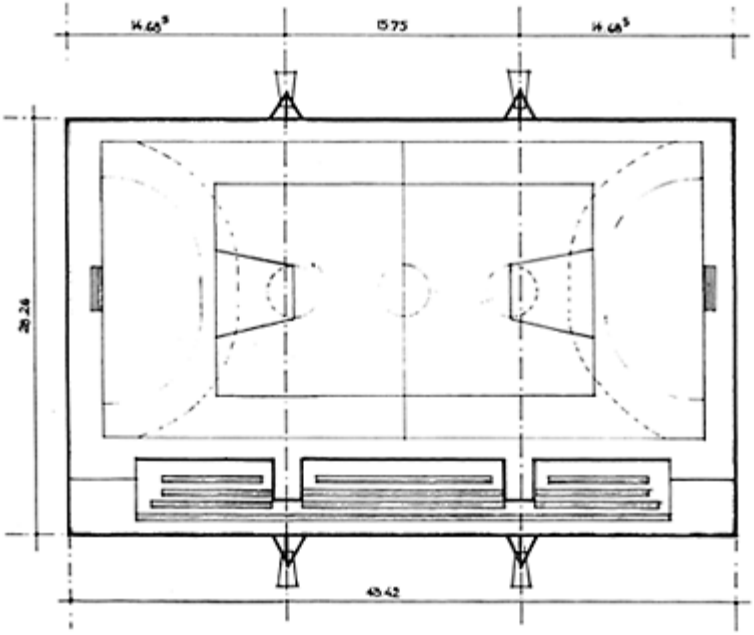

Fig. 22.7.

@Seismicisolation

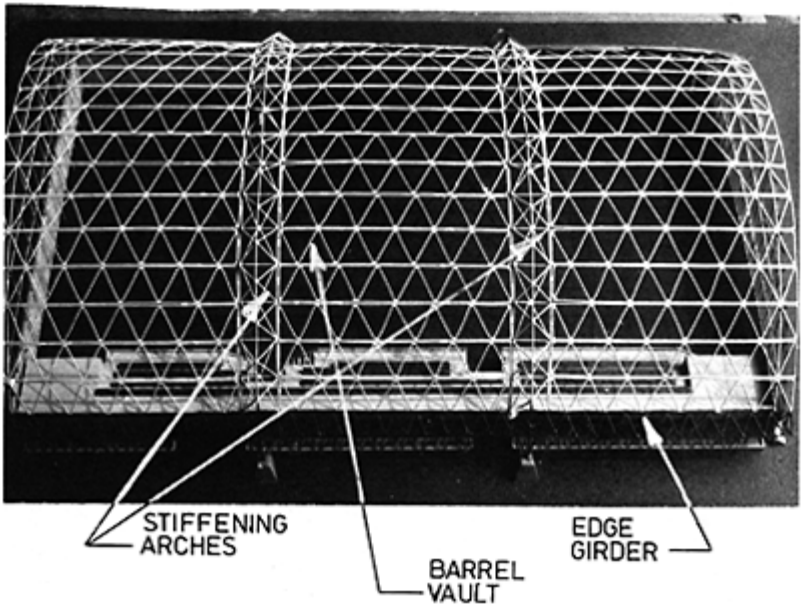

Fig.22.8.

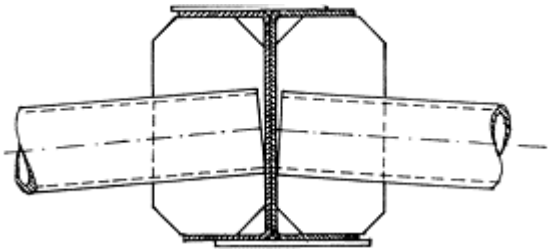

Fig.22.9.

@Seismicisolation

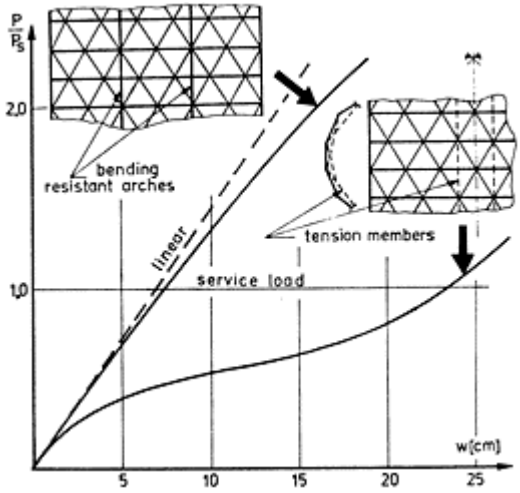

Fig. 22.10.

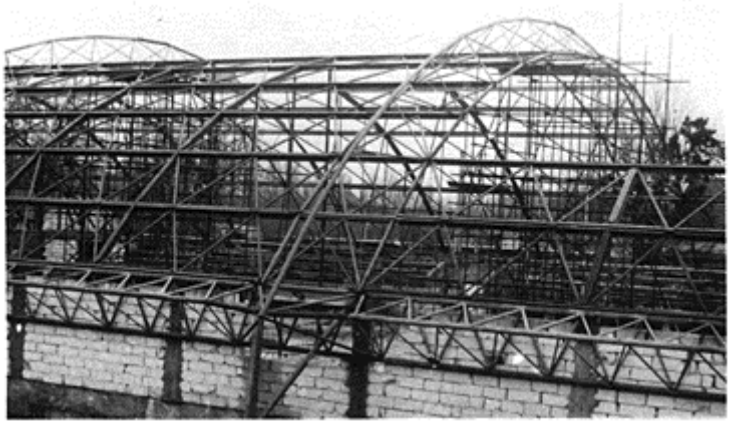

Fig. 22.11.

3.2 Riding House

Many of the prefabricated components of the above described sports hall structures were used for the project of a riding house structure (Fig. 22.16).

In this case the three trussed arches and the end walls support the five bays of the triangulated barrel vault which has a total length of 75 m. The triangular cross-section edge girders were replaced by plane trusses placed in tangent planes to the roof surface.

Both projects, the sports hall and the riding house, were designed at the Building Design Institute IPROTIM and the architect was Nicolae Buşilă.

@Seismicisolation

4 CONCLUSIONS

From the described structures, four sports halls are already in construction. The fabrication and erection processes did not reveal any major difficulties and the acquired erection technique, with a minimum amount of falsework, enables the designers to hope that the interest in this type of structure will result in a marked increase in its use.

Fig. 22.12.

Fig. 22.13.

@Seismicisolation

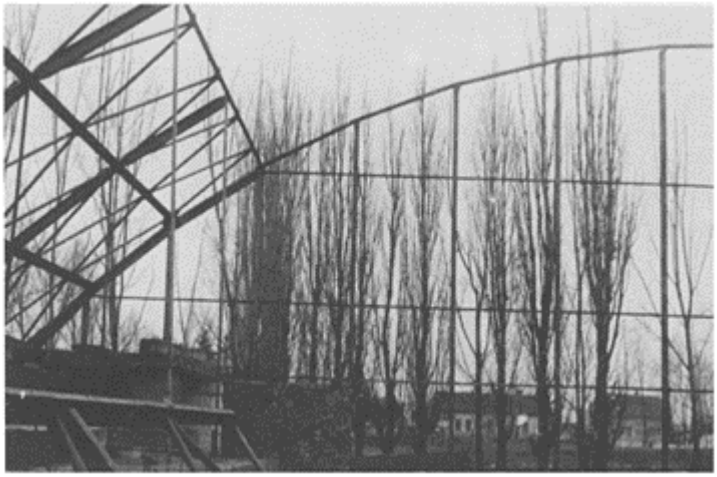

Fig. 22.14.

Fig. 22.15.

@Seismicisolation

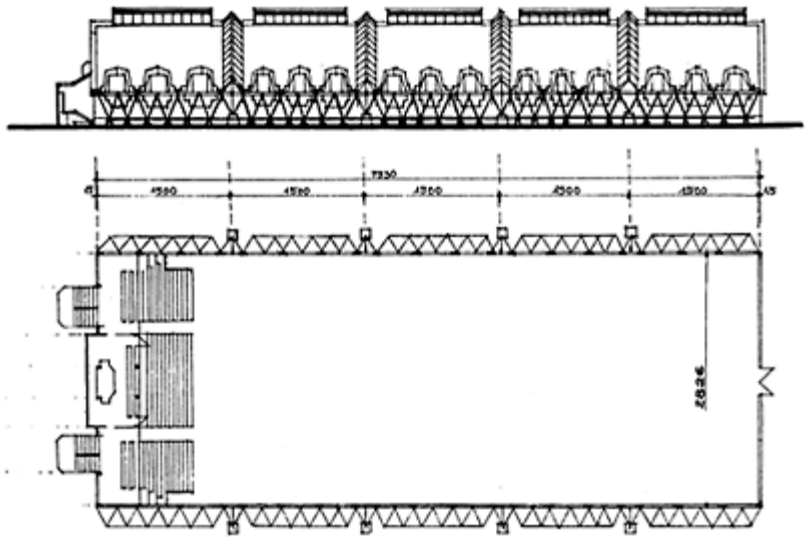

Fig. 22.16.

REFERENCES

1. Gioncu, V. and Ivan, M. *Buckling of Shell Structures*(in Romanian). Editura Academiei RSR, Bucharest, Romania, 1978.
2. Gioncu, V., Băluţ, N., Porumb, D. and Rennon, N. Instability behaviour of triangulated barrel vaults. Short course on the Analysis, Design and Construction of Braced Barrel Vaults, University of Surrey, UK, Sept. 1983.

@Seismicisolation

23
Analysis and Design of a Prefabricated Three-way Trussed Grid Vault

G.J.ZUNZ, R.HOUGH and M.J.BANFI
Ove Arup & Partners, London, UK

1 CLIENT, BRIEF AND SITE

The City of Frankfurt, in seeking a design for its proposed new athletics hall, invited seven architects to enter a limited competition, early in 1981. Among the competitors was the London based practice, Foster Associates, whose submission was awarded first prize. A major feature of the winning scheme was its circular vault roof, and this paper describes the structural analysis and design of the roof, carried out during and since the competition by the Consulting Engineers, Ove Arup & Partners.

Set in a large, flat, forested area on the outskirts of Frankfurt, the 'Waldstadion' sporting complex comprises numerous buildings and arenas, and the site for the new hall was snug between two of these existing facilities, with plenty of open space and trees in the other two directions (Fig. 23.1(b)). Foundation conditions were given as sand and gravel to an indefinite depth.

Based broadly on the recently completed athletics hall at Dortmund, the brief called for enclosure of a 200 m track, two sprint tracks, space for minor events, seating for 3000, and changing rooms and administration areas. Efficient heating and lighting were mentioned in the brief, along with concern for some flanking trees, and the importance of pedestrian movement through the area; the last two factors serving to constrain further the already narrow site.

2 CHOICE OF ROOF SHAPE

2.1 Choice of Prism

Early attempts to cover the required area with circular, elliptical, superelliptical, epicycloidal, or, for that matter, amorphous shapes all conflicted with the narrow site width. Even the narrowest rectangle threatened the trees along one edge, and the free movement of people around the building. In response to these constrictions, a minimum width rectangular arena was sunk into the ground, and roof shapes were examined that would crowd the edge spaces as little as possible. The same width limitations, and also the absence of rock below, worked against cable net or cable stayed solutions.

@Seismicisolation

Other benefits flowed from the depressed floor: easy access to the public viewing level, and the sense of occasion on entering and looking down on the arena (see Fig. 23.1(a)).

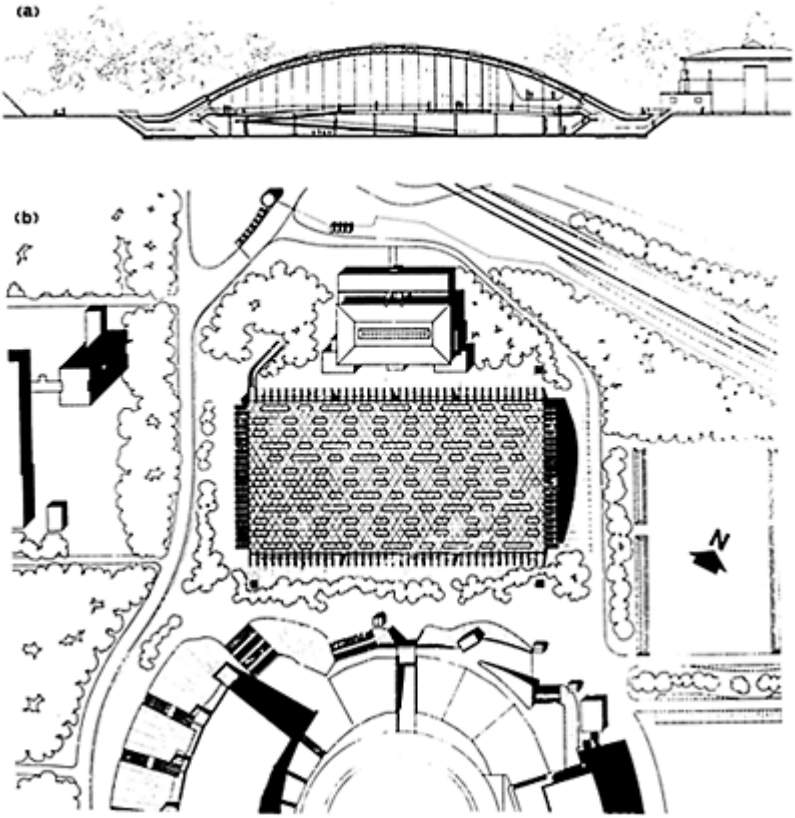

Fig. 23.1. (a) Cross-section through hall and roof, showing mezzanine floor at entry level, and suspended press box. (In plan view, the mezzanine floor comprises a narrow annulus around the arena). (b) Site plan.

Other benefits flowed also from the absorption of the walls into a shaped roof: a low surface/internal volume ratio for efficient heating, opportunities for more generous and more uniform daylighting, and the suggestive power of an arching roof in a sporting context. The fact that the architects had gained notable experience with buildings of simple prismatic shape was obviously relevant as well.

@Seismicisolation

2.2 Choice Among Prisms

The rectangle to be covered by the roof, about 140 m×70 m, offered little opportunity for two-way spanning and this was not pursued. The spectrum of one-way structures that supported trusses on pin-ended wall posts, through fully trussed rectangular portals, were sized and costed ranged from the 'reference' frame comprising horizontal, simply-cranked, rectilinear trussed portals, elliptical and circular trussed arches, and ended with a circular steel plate monocoque with diaphragms separating two stressed surfaces. The cost analysis allowed for the special characteristics of each solution, such as the varying horizontal reactions hence foundation costs, the varying cladding and drainage requirements, and the different fabrication and jointing complexities. The monocoque, not surprisingly, fared badly on the ledger, especially in aluminium, with the rectangular trussed portal the next most expensive, then the simply-supported trusses, the ellipse (with efficient use of internal space but with every joint of different fabrication geometry), then the cranked portals, and lightest and cheapest of all, the circular trussed arch. The sequence bears some witness to the value of 'inverted funicularity', or the minimisation of bending, but it should be mentioned that cladding was expected to be a major part of total cost, and that a severe asymmetrical distribution of snow was, of course, among the load cases. Still, the circular truss was outstandingly efficient, and the early prediction of 35 kg/m^2 structural steel weight (typical areas, including joints) has been realised in the detailed design.

With a radius of 70 m and a span of 69 m between concrete abutments, the vault rises 9 m at its crown to give a maximum floor-to-roof clearance of about 15 m. Structural depth centre-to-centre of chords is 1100 mm. The bonus of the circular shape was, of course, the constant joint geometry and the ease of prefabrication. The challenge to reach across the hall with the least steel was not entirely budgetary: part of it came from the kind of hall that it was to be. Plans for a generous flux of daylight through the roof also depended on achieving very light structural framing.

3 CHOICE OF FRAMING PATTERN

A set of well-spaced, parallel main trusses, spanning the shortest distance and joined with longitudinal purlins, was clearly the simplest choice for the circular vault structure. The reason it was not pursued was the belief, shared by architect and engineer (and no doubt plenty of predecessors) that something more elegant, perhaps even exquisite, but at least more visually interesting, was there to be discovered. Added to that, the bottom chords were carrying at least as much compression as the top ones, so they benefited from a high frequency of longitudinal bracing, and this began to suggest new patterns for the structural grid. The penchant, also shared among the designers, for discrete panel-type cladding and rooflighting units suggested further possibilities for the grid. The simplest pattern that provided legitimate cells was obtained by turning trusses off the short-span direction into a two-way diamond grid. That created the need for frequent longitudinals to contain the grid's spreading tendency, and thus the three-way grid crystallised (Figs. 23.2, 23.9). The choice to offset the longitudinals rather than pass them through the main chord intersection points led to some complications, but it also halved the effective length

@Seismicisolation

of all chords and opened up large hexagonal cells which the architect proceeded to fill with a range of different panel types.

Cell size was determined by the largest panel that could easily be pressed, transported and handled. The hexagons are 3 m across faces, or 1·732 m on a side, giving the structural members attractive slenderness ratios that require only very small permissible stress reductions.

Fixing a space frame chord pattern by no means fixes its web geometry. 'Offset' webbing (visible in plan view) was considered at length but the 'in-line' double Warren webbing had the special attribute of allowing ventilation ducts to pass through it, along offset lines of the same grid. It also provided out-of-roof plane stability to all chord

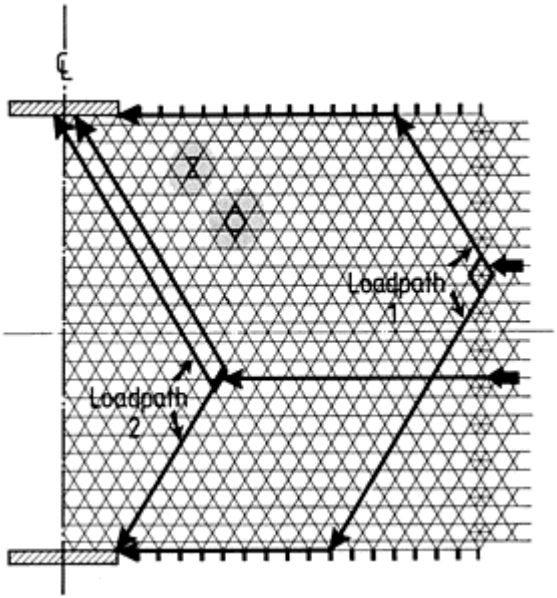

Fig. 23.2. Half roof framing plan.

intersection points, and was fully contained within the proposed prefabricated structural units.

The gable ends were not always straight. At times, advantages seemed to flow from projecting the long sprint track out one end, and from re-shaping the entry area. Structural rules were developed to help guide the choice of random zig-zag gable edges using combinations of grid action, longitudinal cantilevering, and gable post propping, but they all lacked the appealing structural clarity (not to mention analytical simplicity!) of the square end.

@Seismicisolation

4 ANALYSIS OF TRANSVERSE BEHAVIOUR

4.1 The Linear Model

Initially, the vault was viewed as a segmental arch of straight beam-like members, with a small reduction in second moment of area to simulate web member strains, and truss chord and web member forces were deduced by simple analogy with bending and shear in the beam members. Its place was taken by a two-dimensional trussed model, corresponding exactly to the true sectional view of the vault. Members were given equivalent cross-sectional areas, based on the argument represented in Fig. 23.3. The triangular element shown heavily in Fig. 23.3(a) is dimensioned in Fig. 23.3(b), and subjected to arching forces in Fig. 23.3(c), so that its corner node (Z) is displaced to position Z' (relative to reference point X), as shown in Fig. 23.3(d). Figure 23.3(c) will be taken to represent, at different times, the 'chord triangle' and the 'web triangle' of Fig. 23.3(b).

In visualising how Fig. 23.3(c) can be used to represent the action of the general roof pattern (Fig. 23.3(a)), it is probably easiest to imagine that the forces in the longitudinal members arise because of the need to terminate the pattern at the gable edges. At these edges, main chord forces 'turn the corner' into the notional trimming members shown dotted in Fig. 23.3(a), activating entire lengths of longitudinal chords in the process. The

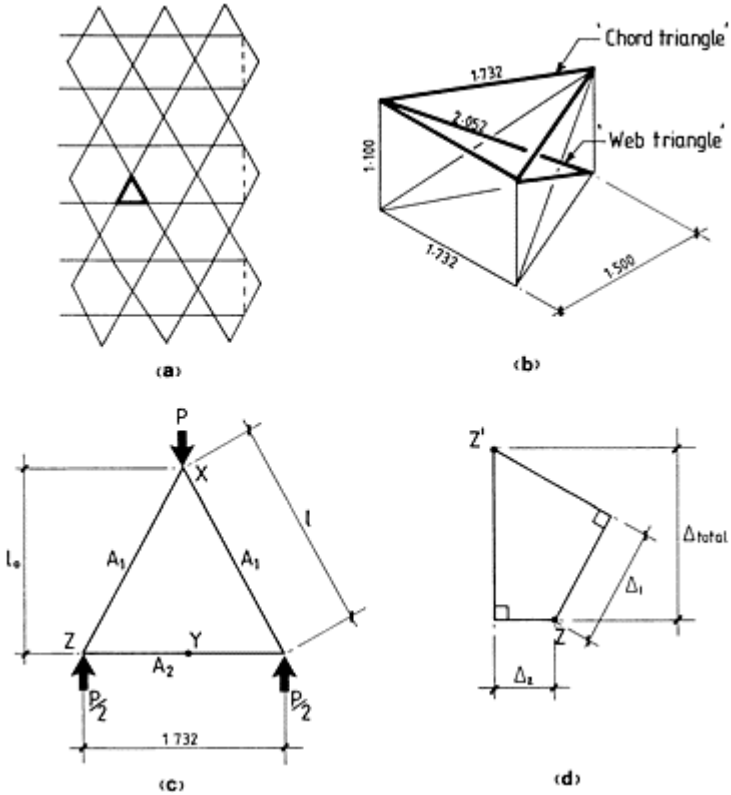

@Seismicisolation

Fig. 23.3. Reduction from 3- to 2-dimensional model for transverse analysis.

function of the dotted members is in fact performed by the more elaborate, fully braced 'spider' prefabricated units of Fig. 23.2.

Referring to Fig. 23.3(c), the compressive shortening of length l of a main chord member (area A_1) is given by

$$\Delta_1 = \frac{Pl^2}{2l_0EA_1}$$

and the tensile lengthening of portion YZ of the longitudinal chord member (area A_2) by

$$\Delta_2 = \frac{3P}{8l_0EA_2}$$

so that from Fig. 23.3(d), the transverse component of the displacement of Z is given by

$$\Delta_{tot} = \frac{P}{E}\left[\frac{0{\cdot}325}{A_2l_0^2} + \frac{0{\cdot}5l^3}{l_0^2A_1}\right]$$

As far as its action in resisting force P is concerned, then, the triangle of members can be replaced by a single transverse arch member of equivalent area:

$$A_0 = \frac{Pl_0}{3{\cdot}464E\,\Delta_{tot}}$$

$$= \frac{A_1l_0}{\dfrac{1{\cdot}732l^3}{l_0^2} + \dfrac{1{\cdot}125}{l_0^2}\cdot\dfrac{A_1}{A_2}}$$

where division by 3·464 m, the spacing of these triangles along the vault, has converted the equivalent area into a value 'per metre of vault'.

Taking dimensions from Fig. 23.3(b) gives for the 'chord triangle'

$$A_0 = \frac{1{\cdot}5A_1}{4 + 0{\cdot}5\dfrac{A_1}{A_2}}$$

and for the 'web triangle',

$$A_0 = \frac{1{\cdot}86A_1}{4{\cdot}324 + 0{\cdot}325\dfrac{A_1}{A_2}}$$

where A_2 has a common value for the two kinds of triangles but A_1 is different. There are, in fact, two, crossed, web triangles for one chord triangle, and their contributions to A_0 are additive.

@Seismicisolation

In this way the three-dimensional vault of Fig. 23.3(a,b) was reduced to an exactly equivalent two-dimensional segmental trussed arch for easier analysis by the PAFEC 75 (level 2.3) program on a DEC 10 computer. Rotational and translational spring stiffnesses were assigned to the arch supports to simulate, respectively, bending in the concrete abutments, and tensile strains across the ground slab that serves to tie the feet of the arch.

This trussed arch model represented only a 1 m strip of roof, so to deduce member forces in the real roof, chord forces from the output were multiplied by

$(1{\cdot}732/\cos 30°)=2{\cdot}0$

and web member forces by

$$(1{\cdot}732 \times 2{\cdot}052/\sqrt{1{\cdot}5^2 + 1{\cdot}1^2}) = 1{\cdot}91$$

4.2 Non-linear Effects

For initial assessment of buckling characteristics, the equivalent trussed arch described above was considered once more as a circular beam, and checked by the methods of Ref. 1. Second moment of area was again decreased slightly to simulate shear flexibility of the truss, using an assumed moment/shear relationship. The radial load required by Ref.1 was given an intensity such that the resulting uniform axial compression in the arch was equal to the peak compression produced by vertical gravity loading under full snow load.

For the case of pinned supports, a safety factor against buckling of 2·6 was indicated, and for fixed supports, 6·0. The former was considered too low, so a decision was made in favour of fixity.

An unfortunate consequence, of course, was the greater peak moment, which now occurred at the supports, under virtually all load cases, but a favourable consequence was the greater stiffness, with peak deflection down around 190 mm, or span/360. Of this, 90 mm was from dead load, 60 mm from snow (uniformly distributed) and 40 mm from thermal contraction.

To assess P–Δ effects and to check the preliminary buckling predictions, a segmental beam arch model was subjected to a series of iterative analyses at progressively larger loads until failure to converge was first detected at a safety factor of 5·0. For this test, loads were of course truly vertical, both symmetrical and asymmetrical snow loads were represented, member property variations were included, and the real rotational and translational spring stiffnesses of the abutments were simulated. At service load levels, final moments at convergence were less than 5% higher than after the first cycle, so subsequent ‘first order’ analyses were considered sufficiently accurate without any attempt to enhance the results for changes in geometry.

4.3 Loads

Structural *self-weight* settled down at 0·34 kN/m^2, allowing 15% for joints, and this figure was used for final analyses.

Cladding comprised about 25% glazed units at 0·77 kN/m^2, and 75% metal units at 0·29 kN/m^2. Disposition of the heavier, glazed units was to be relatively homogeneous so the weighted average of 041 kN/m^2 was applied uniformly across the roof.

@Seismicisolation

Allowance for *services* in the roof (lights, heaters, ventilation ducts and sprinklers) was set at 0·2 kN/m^2, so total dead load became 0·95 kN/m^2.

Snow load, in accordance with DIN 1055 Part 5, was represented by both a uniform 0·75 kN/m^2 and a linearly varying, asymmetric distribution from zero at the roof crown to l·50 kN/m^2 at the abutment.

Temperature variation of ±30 K was taken into account.

Wind loading conformed to DIN 1055 Part 4, and allowed for a peak suction under longitudinal wind that was less than dead load and so was of no consequence for design. For transverse winds, the landscaping arrangement and the shape of the roof itself implied an airflow that would not detach, with a roughly uniform suction across the roof, also less than dead load.

According to DIN 4149 Part 1, the site is in the least onerous of all German *earthquake* zones, for design purposes. Considering the roof s low profile, and the fact that DIN standards allow ultimate strength to be taken into account in assessing response to earthquake, ground acceleration was not included as a load case at this stage.

Rotation of the concrete abutments due to *differential settlement* was discounted when more detailed site information revealed fairly dense sand and gravel with very minor clay seams, and a deep water table. For the spring stiffness of the 150 mm thick ground slab that acts as a tie between abutments, 1% of steel reinforcement was assumed.

4.4 Special Zones

A 5 m wide band of trussing at each gable end was considered to provide support to the cantilevering sunshade louvres. The sunshading construction weighs about 0·25 kN/m^2 and was assumed to collect the usual snow load distributions as well.

Point loads from the suspended press box also affect only a limited band of the arching roof. According to analysis of a beam-element arched grid model of a portion of the roof, there is little spreading of these point loads, and only a narrow zone of trussing needed strengthening.

4.5 Member Forces and Member Design

Chord and web member design forces at quarter-points around the arch are summarised in Fig. 23.4 for the typical zones of the roof. Shear remains small throughout, but bending is often significant. Eccentricity of the thrust line, in terms of truss depth *D*, reaches a peak of −1·12D (negative for negative bending) at the critical abutment under asymmetrical snow loading, putting the top chord into tension. It then turns positive before the crown (+0·35D), negative beyond the crown (−0·24D), and positive at the far abutment (+0·04D). Bottom chord member forces are shown for this case in Fig. 23.5.

Predictably, eccentricities are somewhat smaller for uniform snow load, starting at −0·41D), passing through −0·06D at the quarter-point to +0·22D at the crown.

@Seismicisolation

Load-case	Bottom Chords					max.	Top Chords					max.	Max. Web Force
1	202	114	60	114	202	202	20	90	152	90	20	152	16
2	272	22	66	112	72	272	-104	120	102	40	84	120	34
3	16	3	9	3	16	16	22	4	5	4	22	22	3

Fig. 23.4. Summary of member forces (kN) for major loadcases. Loadcase 1: dead load plus uniform snow load; loadcase 2: dead load plus snow load concentrated towards left; loadcase 3: thermal expansion of 30 K. Compression considered positive in table.

The vulnerable location is clearly the springing point, where the whole load on the roof (and sometimes a bit more!) is effectively carried by the bottom chords in many cases.

Main chord tube sizes needed to receive the design forces over the typical zones vary from 114·3 diameter ×7·1 wall thickness (bottom chord, near supports, dimensions in mm) down to 114·3×3·6 minimum, with web members from 48·3×5·0 to 48·3×2·6. Longitudinal chords are typically 88·9×3·2 with webs at 42·4×3·2.The 'hinged reaction frames' that act as bearings for the roof trussing have chords of 180×100 RHS sections.

In the specially loaded bands, some chord members are increased to 139·7 diameter and some web members to 60·3. All steel is (German) grade ST37·2 to DIN 17100, with a yield strength of 235 N/mm2.

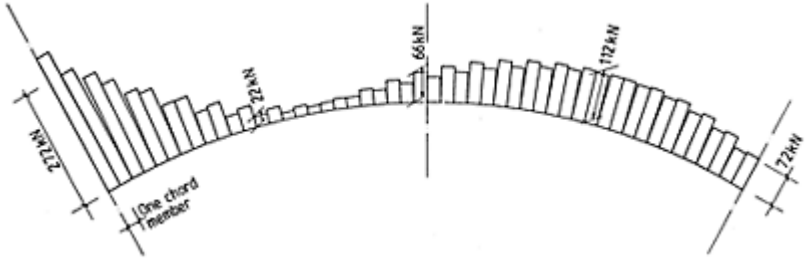

Fig. 23.5. Bottom chord compression for dead load plus asymmetrical snow load.

@Seismicisolation

5 ANALYSIS OF LONGITUDINAL BEHAVIOUR

5.1 The General Problem of Longitudinal Movement

All load conditions produce stresses in the main chords and the main web members, both of which produce, in turn, stress and strain in the longitudinal chord members. These longitudinal strains grow to become significant longitudinal movements near the two gable ends: usually outward because the longitudinal chords are usually, though not always, in tension. This longitudinal tension varies across the arch, just as the main chord compression does, so the subsequent variation in longitudinal strains leads to small 'shear strains' within the overall framing pattern. This effect can be attenuated to an extent by varying the cross-sectional area of longitudinal chord members to reflect the variation in their design forces. Thus, under full design loading, when stresses in the frame are generally high, longitudinal member stresses can be made to approach a common permissible tensile stress, hence a common strain, and hence shear distortions in the frame fortuitously disappear just when they would be most undesirable. This means of reducing the shear was also relevant in choosing the size of the very edgemost longitudinal chord members, as explained in Section 5.3.

These shear distortions could have been ignored, of course, if frame joints had been designed as truly pinned, but their design. by this stage, was progressing steadily towards rigidity. In any event, a derivative effect required investigation. The provision of arches of fully braced or 'spider' prefabricated units across the two gable ends of the frame (see Fig. 23.2) needed for proper termination of main chord forces, also acted to upset the ideal condition of unimpeded shear distortion, by creating an otherwise non-existent shear stiffness in the net. Thus the shear strains led to small changes in the axial forces in the main chord members, which had to be checked.

5.2 A Specific Longitudinal Problem: the Supported Edges

Differential longitudinal strains arising within the body of the roof frame itself, and their resulting secondary stresses, were minor compared to the potential for shear existing between the steel frame and the concrete abutments supporting its edges. With full tension in the longitudinal chords, relative longitudinal movement at the gable ends between roof and abutment was about 40 mm, with a further 20 mm anticipated from differential thermal movement between the thermally protected steel and the thermally exposed concrete.

Two ways of absorbing this shear were considered before deciding to release it explicitly. In the framing plan of Fig. 23.2, the gable 'spider' units tend to join up with the main chord members they serve to trim, to create large corner brackets or 'corbels' within the four corners of the roof, which serve as an alternative and redundant means of containing the tendency of the roof to expand longitudinally. These 'corbels' generate tension in one set of main chords, increasing towards the corner as differential steel/concrete movement increases, and compression in the end row of 'spider' units, also increasing towards the corner. This effect is illustrated by the axial force diagram of Fig. 23.6. This diagram comes from a single surface curved grid model containing simple

@Seismicisolation

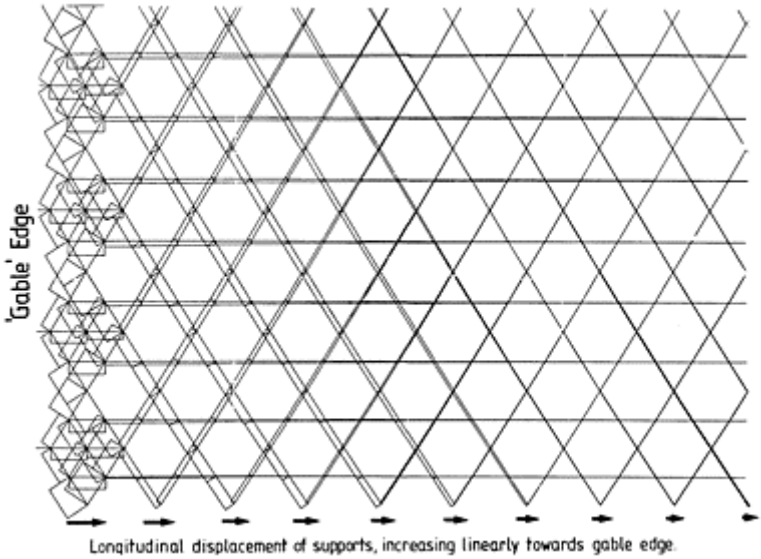

Fig. 23.6. Axial force diagram for linearly varying shear displacement at supported edge.

beam elements, so the fact that simultaneous bending and torsion of the roof modify both main and longitudinal chord forces had to be allowed for by hand calculation in predicting final chord forces arising from an applied longitudinal movement of the supported edges.

Even with this approximate model, final compressions in the main chords of the cornermost units were growing to 3–4 times their previous design values, and this was considered too high a penalty to accept.

The second attempt to absorb the shear effect involved removing some of the bracing within each 'spider' unit (as in Fig. 23.3(a)) so that while they still served their purpose of trimming the main chord forces, they were less effective in helping create those corner 'corbels', and allowed more of the longitudinal expansion tendency actually to occur. Fully braced 'spider' units were then provided at the centre of the roof: they could not be eliminated completely because of their contribution in stabilising the nodes at the intersections of the main chords.

The overall effect now was a reduction in the growth of axial forces in corner chords. While the axial forces came down, though, large moments at the rigid joints took their place, predictably, and the result was still unacceptable.

5.3 Solution of the Edge Problem

The longitudinal movement, then, had to be released, and several rocker/sliding mechanisms were considered. One of them had the roof springing from a row of inclined steel posts. The posts were normal to the roof and leaned back to bear against the

@Seismicisolation

concrete. They extended down to the ground slab to which they were pinned, and near their top ends they could slide longitudinally along the concrete abutments at single rollers transferring compression only. Compression/tension rollers would have been needed had two, separate, top chord/bottom chord sliding joints been proposed for connecting the chords directly to the abutments. The length of the posts gave them a flexibility that eased the peak negative moment in the trussing, but without threatening the stability of the arch itself. Unfortunately, however, the posts could not be worked into the solution for the arrangement of spaces inside the hall.

The solution in fact adopted (Fig. 23.9) features hinged 'reaction frames' rather than sliding joints. As these frames rotate, they generate small longitudinal components of reaction, which are collected by the special longitudinal edge members that link the inward hinges of the reaction frames. Over a short length of each edge, of course, near the mid length of the roof, the reaction frames are fixed against rotation. The very existence of these special longitudinal edge members threatens to recreate a new shear effect within the roof, because they do not undergo load-induced strains compatible with the strains of the adjacent longitudinal chords.

This difficulty, foreshadowed in Section 5.1, was minimised by choosing the cross-sectional area of the special members so that the growth of strain due to the accumulation of the longitudinal reaction components matched, to an extent, the strains in the adjacent chords. No strain mismatch exists among these chords for thermal movements, of course.

A larger, quarter-roof beam-element arched grid model was used to check the effect of any remaining shears. Bending of truss chords in plan view was estimated from this model to be around 1–2 kNm, and additional axial forces were also reassuringly small.

There were difficulties in deducing results from this single surface grid model, as the shearing effect within one surface of members affected their axial forces, hence precipitating bending and torsion in the actual double surface trussing which would in turn have readjusted the forces, and hence modified the initial shearing effect.

Additionally, the role of longitudinal webbing, in preventing differential longitudinal movement of top and bottom surface chords, needed checking. A more thorough three-dimensional analysis of the quarter-roof, probably at a reduced frequency, began to seem inevitable, and is in the planning stage at the time of writing.

5.4 Resistance to Longitudinal Wind

Loadpath 1 on Fig. 23.2 indicates how wind load from the gable wall mullions uses the 'spider' units to pass into the first available main chords. In loadpath 2, wind first enters the longitudinal chords and only passes out into the main chords after first enlisting them in a local bending action. Loadpath 2 is repeated many times, though, which raises its overall stiffness relative to loadpath 1. Both loadpaths also have their respective mirror-image duplicates, that put main chords in tension rather than compression, on the other side of the roof centreline.

A related aspect of the roof's performance is its safety against progressive collapse. Upon the loss of some main chord members, for instance in a local fire, the roof's grid nature allows some redistribution on to adjacent trusses. In the case of longitudinal chord members, given their special offset arrangement, their contribution in containing the roof's tendency to spread relies on their reaching the gable end 'spider' units. Loss of a

@Seismicisolation

longitudinal member then means that some of the latent, redundant, corner 'corbel' action, described in Section 5.2, is called into play in helping contain the spread. The choice of 'fixed' rather than 'pinned' springing points to the arch also provides additional redundancy against overload, in the transverse direction.

6 PREFABRICATION, JOINTING, ERECTION

6.1 Choice of Prefabricated Unit

Decisions about jointing, prefabrication, erection and cladding were inseparable, as in any space frame design, and no one factor dominated.

The frequency of joints in the grid had been determined by the maximum desired cladding panel size, and by the wish to limit the slenderness of individual compression members, as noted in Section 3.1. Brief consideration was given to the possibility of structural units with cladding panels pre-attached, even using composite action between frame and skin. Detracting factors that soon prevailed were the wasteful duplication of structural members at mating edges, the architects' intention that panels should be interchangeable, and the fact that most cladding options favoured their own, separate sub-frame to facilitate waterproofing and drainage.

Of the numerous repeatable units latent in the chosen grid pattern, two were singled out: the 'bowtie' and the 'diamond' (Figs. 23.2 and 23.7). Diamond units had the disadvantage of not assembling to reconstitute the complete roof pattern: alternate sets of longitudinal chord and web members had to be installed separately. The advantages were more persuasive, however:

(i) At 10 kN typical self-weight, it was easily handled by crane, but, being twice as big, required only half as many crane lifts (and field joints) as the bowtie. The latter, however, was still too heavy for hand lifting or hand manipulation during erection once the crane was released.

(ii) The favoured joint ('endplate', rather than 'gusset', see Section 6.2) worked more efficiently on the diamond unit than on the bowtie. On the bowtie, the single bolt experienced high shear in addition to axial force because of its skew orientation in the roof pattern.

@Seismicisolation

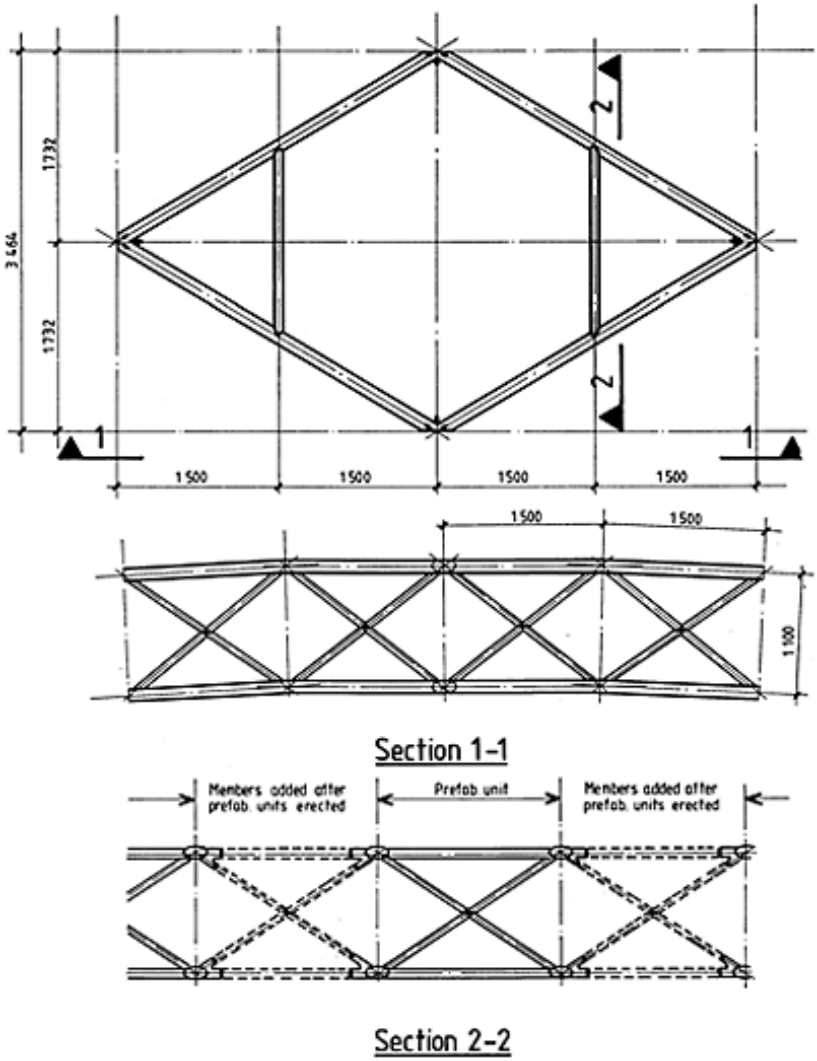

Fig. 23.7. Proposed 'diamond' prefabricated unit.

(iii) The 'fold lines' that give the roof its segmentally curved shape occur at the edges of the hexagonal cells rather than across them, in order to simplify the cladding panels. This meant that, for bowtie units, angle changes in their main chords would have occurred at their field joints rather than at their shop joints, producing, in turn, chord force eccentricity within any of the field joint designs envisaged.

(iv) The fully braced 'spider' units were more easily considered as variations on the diamond unit than on the bowtie unit.

@Seismicisolation

6.2 Choice of Joint Design

The ‘endplate’ joint proposed between the prefabricated units (Fig. 23.8) uses a single M36 HSFG bolt. Except for the small vertical component of web member force passing across it in shear, the joint transfers just symmetrical axial forces. Joints at both the acute and obtuse corners of the units work in a similar way.

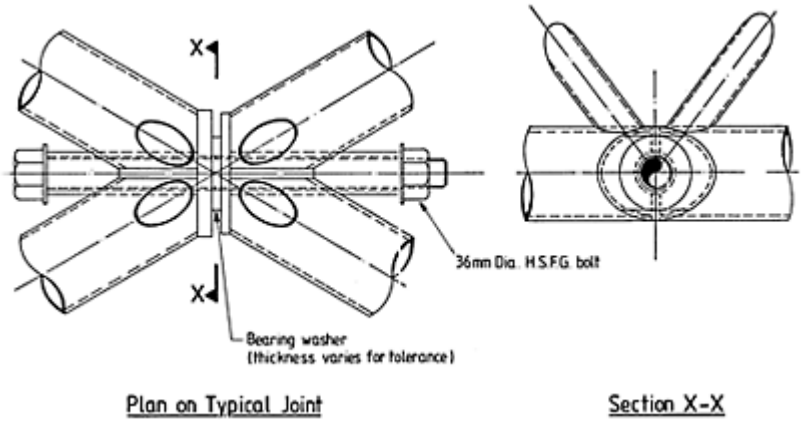

Fig. 23.8. Proposed ‘endplate’ joint between units.

With 4 mm oversize bolt holes in mating end plates, and variable thickness packing washers, tolerance has been provided for all three translational degrees of freedom at each joint. One of the three rotational freedoms has natural tolerance as well. The other two rotational tolerances could have been explicitly accommodated by replacing one of the flat packing washers with a washer spherically ground on one side, fitting against a spherically concave surface in the mating end plate. Careful jigging during unit fabrication should avoid the need for such special washers, however.

@Seismicisolation

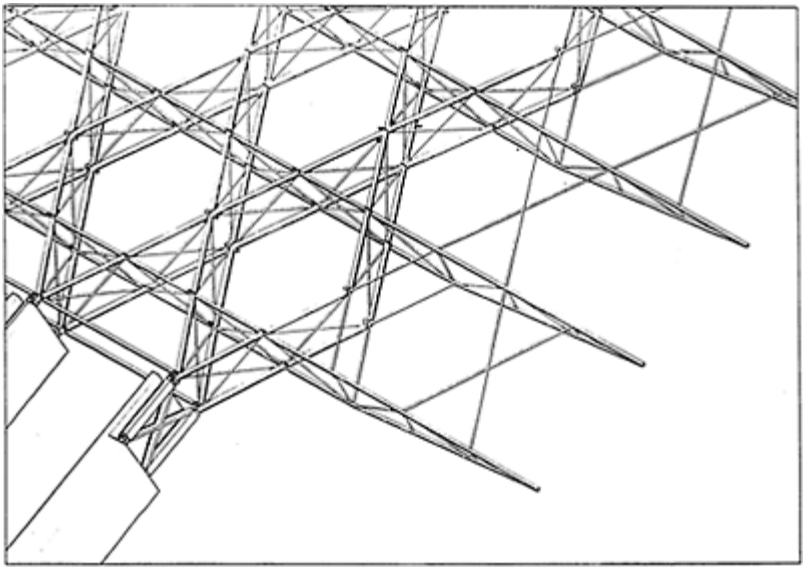

Fig. 23.9. Isometric of truss grid near a corner (bracing to ‘spider’ units omitted for clarity).

An alternative ‘gusset’ type joint was considered at length. It also used a single M36 friction grip bolt, but set normal to the roof surface and loaded in shear rather than axially. Two projecting gussets from one unit meshed with one gusset from the mating unit, providing two faying surfaces once the bolt was installed. Tolerance was provided by generous plate clearances, closed by the bolt, at the expense of a portion of its energy. One disadvantage was that the projecting gussets prevented sub-assemblies of units in the partially erected roof from sliding vertically alongside adjacent assemblies, and this was a requirement of most erection methods envisaged. Another, expressed by the architects, was that the ‘pincer’ action of the bolts in the endplate joint seemed more suggestive of the pattern of forces in the frame than did the shearing action of the flat gussets.

Several patented joint systems were also considered. So far they have been rejected on the grounds of cost and because of difficulties in achieving geometric, stability, or strength requirements at particular nodes in the grid.

In the system proposed the longitudinal chord and web members that are installed after erection of the prefabricated units are bolted to upright gussets that project from the main chord splice joints (Fig. 23.7). The main chords undergo a small angle change at these joints, so the gussets serve also to facilitate the splice.

At the roof springing points, the short, braced ‘reaction frames’, free to rotate against the concrete abutments, are pin-jointed to the first row of units. These frames receive top chord compression and tension, bottom chord compression (tension never occurs there) and vertical shear. Along the gable ends of the roof, the vertical mullions deliver horizontal wind shear to the roof, but receive no axial forces from the roof.

@Seismicisolation

6.3 Erection Methods

Considering, first, methods involving longitudinal progression, there are several ways the roof could be erected, all using a travelling scaffold of circular profile and all involving the addition of successive complete arches of diamond units against an initial gable arch of specially braced units.

Two main requirements of such methods are that they must provide for the introduction of self weight stress into each new completed arch, and that they must provide, at the progressing front, a system of moveable bracing that can account for the temporarily unequilibrated forces in the newly added chord members. Only upon completion of the roof do the longitudinal chords act to contain the spreading effect of the main transverse chords, via the gable 'spider' units. So during erection, a leap-frog system of temporary (but simplified) 'spiders' is needed to provide this containment.

The first provision, for introduction of self weight stress and strain into each new arch, is satisfied either by dropping the new arch from a chocked position on the scaffold, or by jointing the new (unstressed) arch directly to the previous (stressed) arch and then stressing the new arch by turning screw-thread adjustments within the lengths of all the new longitudinal members. The 40 mm maximum discrepancy between stressed and unstressed profiles could be ignored if intermittent propping were provided to the roof as it emerged from behind the travelling scaffold, so that a single, final, depropping operation would stress the whole roof simultaneously.

Probably the simplest erection method, however, would be to progress transversely from opposite abutments simultaneously, propping the full length of the roof twice at each advancing front before reaching the crown. To allow time for completion of the abutments, only a third, or a half, of the full length of the roof need be erected at one time.

All methods assume accurate jig measurement of each unit in the shop so units can be delivered with the necessary packing washers pre-specified.

ACKNOWLEDGEMENTS

The client is presently considering the detailed architectural and engineering design submissions. No date has yet been nominated for further progress on the project, or for its completion.

Architects: Foster Associates

Consulting Engineers: Ove Arup & Partners

Cost Advisers: Davis Belfield & Everest; Monk Dunstone Associates

BIBLIOGRAPHY

Timoshenko, S. *Theory of Elastic Stability*. McGraw-Hill, New York, 1936, p. 225.

@Seismicisolation

24
The Design and Construction of the Liverpool International Garden Festival Exhibition Building

T.RAGGETT
Arup Associates, London, UK

1 EVENT, CLIENT

The Liverpool Garden Festival, using the many examples set by post-war Germany to rejuvenate war devastated areas, was seen by the Government-appointed Merseyside Development Corporation to be a focal point in the attempt to restore Liverpool's former vibrance and arrest its municipal decay.

Early in 1982, MDC invited six architectural practices to submit designs for an exhibition building intended to become the centre piece of the festival. Arup Associates were appointed in mid-1982, and began detailed design in August 1982, with construction commencing in January 1983, for completion by Spring 1984. This paper describes the design and construction of this building with particular emphasis upon the evolution of the structural form.

The festival gardens cover 105 hectares and are sited on a municipal tip, between Toxteth and the river Mersey. Domestic refuse had been deposited over the past 20 years in thicknesses varying from 4 to 10 m.

The building is positioned within an area that was originally a railway marshalling yard serving the nearby docks and wharves. The area had been built up into a platform of hardcore, and partly covered by a mass concrete slab and eventually overlain by about 4 m of domestic refuse. As part of the civil engineering operations (controlled by MDC) the refuse within and around the general building area was removed and reinstated to finished ground level using compacted river dredged sand from the Mersey. The building could therefore be founded on this 4 m layer of sand but the properties (thicknesses, density, compaction, uniformity, etc.) of the underlying hardcore and soils were largely unknown at the time of the competition. Subsequently the hardcore was found to be underlain by a layer of river silt of greatly varying thickness overlying sandstone bedrock.

This, together with the increased surcharge from the sand replacement (the refuse was of low density with voids) suggested that the proposed structure should be reasonably tolerant of differential settlement if expensive foundation solutions were to be avoided.

Measurements of ground movement were recorded during and after sand replacement and were continued throughout the construction period.

@Seismicisolation

These agreed approximately with the predictions made prior to the structural analysis, i.e. a total settlement of 75 mm with a maximum differential of 25 mm.

2 BRIEF

The brief called for a building that could accommodate two quite different uses; initially it would form the focal point of the festival and provide a weathertight enclosure for a variety of events and activities.

Subsequently the building enclosure should be capable of being economically and easily converted into a Sports and Leisure centre. Facilities included divide broadly into three main categories, thus:

(1) a leisure pool,
(2) a multi-purpose sports hall with provision for seating for up to 3000 spectators,
(3) various, smaller scale 'club' activities including squash, gymnasium, projectile hall, etc.

Each of the above have differing spatial, environmental and organisational requirements.

3 EVOLUTION OF ENCLOSURE

The building enclosure was designed with the following principal aims in mind:

(a) To form an enclosure which would both unite and yet define and express the three principal activity areas of pool (dome), hall (vault), and club (dome).
(b) To form a natural relationship to the landscape which would give pleasure within the festival park.
(c) To provide a 7500 m^2 column-free space and so give flexibility for both the festival and sports complex.
(d) To form a minimal external surface requiring little maintenance and being durable and technically efficient in many ways.
(e) To possess an identity reflecting the spirit of the festival and Liverpool's architectural heritage.

4 EVOLUTION OF STRUCTURAL FORM

The structural form is a direct and specific response to the foregoing and comprises two related forms: the dome and the vault.

The dome is halved and rejoined by a linear barrel vault.

The structural efficiency derived from this curvilinear form resulted in low material content and a favourable ratio between surface area, plan area and volume.

The structural configuration was derived principally from the following:

(1) A compatible geometry to unite dome and vault.

@Seismicisolation

(2) The need for dome and vault to have different cladding, suggesting that the domes connect via the lower layer of the double layer vault, thus expressing the transition externally and preserving the clarity of structure within.
(3) A convenient and regular structural grid for the attachment of external and internal cladding.
(4) Evenly distributed building dead and live loads and the ability to absorb differential settlements.
(5) Simplicity and clarity of design, fabrication, construction and perception.

5 PRIMARY STRUCTURE

5.1 Vault

A two-layer barrel vault 78 m long comprises braced arched frames of 3 pin configuration at 3 m centres with upper and lower booms connected by longitudinal members. The lower layer connects through to the domes and supports services and acoustic panels in selected areas plus providing the path for axial forces from the domes. The upper layer supports the external cladding.

Alternate arches are transferred to bipod frames at 6 m centres by means of eaves bracing, and the roof cladding terminates at an eaves gutter which discharges into a rain water pipe above the inclined leg of the bipod.

The building is entered along the sides of the vault.

5.2 Domes

The half domes at each end are of segmental, ribbed, single layer construction with circumferential rings at 3 m centres connected through via the longitudinal members in the lower layer of the vault.

Thus the continuity of the dome rings are maintained and the out-of-plane forces at the junction of dome and vault are resisted by the stiffness of the three end arches combined with their three-dimensional bracing.

Figure 24.1 gives the perspective view of the structure.

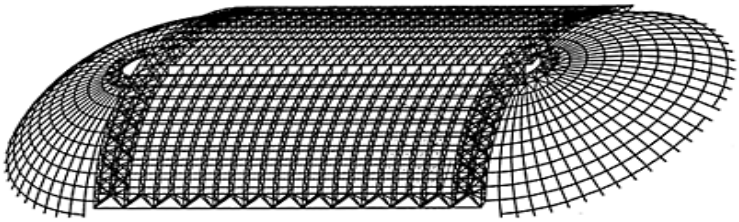

Fig. 24.1. The arrangement of the structural framework for the structure.

@Seismicisolation

6 FOUNDATIONS

Loads on the foundations were relatively small (a typical arch thrust being approximately 450 kN D+L), and the maximum allowable ground bearing pressure was restricted to 150 kN/m2.

The vault foundations were inverted tee reinforced concrete spread footings tied across the vault by 75 mm diameter mild steel bars (pretensioned) to resist the horizontal thrust from the arch.

The dome foundations were concrete ring beams forming two semicircles on plan, connected longitudinally by mild steel pretensioned tie bars.

The diameter of the tie bars was determined by permissible strains (horizontal deflection) rather than stress.

7 MODELLING AND FRAMING CONFIGURATION

It was important that the underside of the vault be a single unbroken line along its length and that the undersides of the connected domes be a continuation of this alignment (like the lane markings of a running track when seen from below).

Studies of the vault frame spacing and configuration considered the ease of fabrication, erection, cladding, module, size and weight of purlins and visual simplicity (Fig. 24.2).

It was concluded that a three pin arch would be the most suitable with all three pins along the axis of the top boom.

The penalty for the choice of three (rather than two) pins was a small increase in the maximum bending moment of 10%, but this was more than compensated for by the ease of fabrication, erection and favourable response to differential settlement.

The location of the pins along the axis of the top boom was not such an obvious choice and was influenced by architectural rather than structural consideration in order to simplify the eaves cladding-gutter detail.

This resulted in an increase in the top boom thrust of 20% above that of the bottom boom and an increase in section size accordingly. The section chosen is of rolled joist section which, when combined with square hollow bracings, combines clarity of line, ease of connection, and the facility to use the lower boom as a runway for an access cradle.

The selected cladding module (3 m×1 m) led to the primary circumferential spacing of

@Seismicisolation

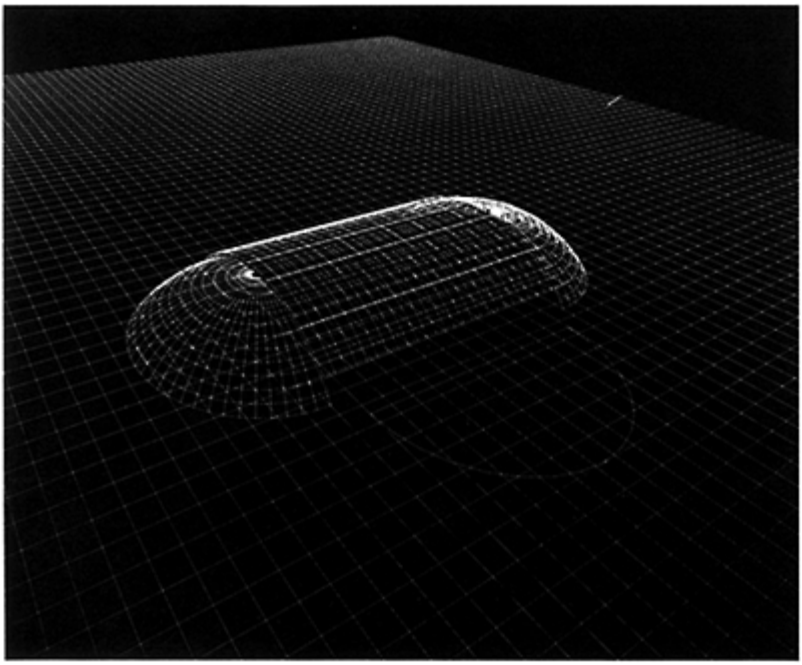

Fig. 24.2. An initial computer drawing of the structure.

the warren truss nodes. This gave eleven equal arc lengths of 3 m measured along the centre line of the upper boom each side of the centre pin. From this came the location of the longitudinal members connecting the arch trusses and dome rings. This can be seen from Fig. 24.3.

Initial studies of the dome discontinuity support showed that stability could not be achieved within the dome structure itself without massive and quite out-of-proportion members. It was therefore decided to make use of one of the dominant architectural features of the building, namely the oculus—the continuation of the ridge ventilator structure.

The principle here was to introduce a semicircular (in plan), triangular (in section) braced girder which would cantilever out from the last three vault frames and pick up the braced in plane ends of the dome ribs. It followed from this that these three end frames be treated as braced bays with in plane and out of plane bracings providing horizontal and vertical reactions respectively to the out of balance forces arising from the dome discontinuity.

The lower longitudinal members run continuously along the length of the building emerging at the dome ends to act as both strut and tie around the circumference of the dome. Due to the increase of dimension of the dome rib above that of the lower boom rib to the trusses this circumferential strut/tie is discontinuous around the dome with a pinned end connection to each dome rib.

@Seismicisolation

Naturally the curved members for both the vault and dome members induce significant

Fig. 24.3. The inside view.

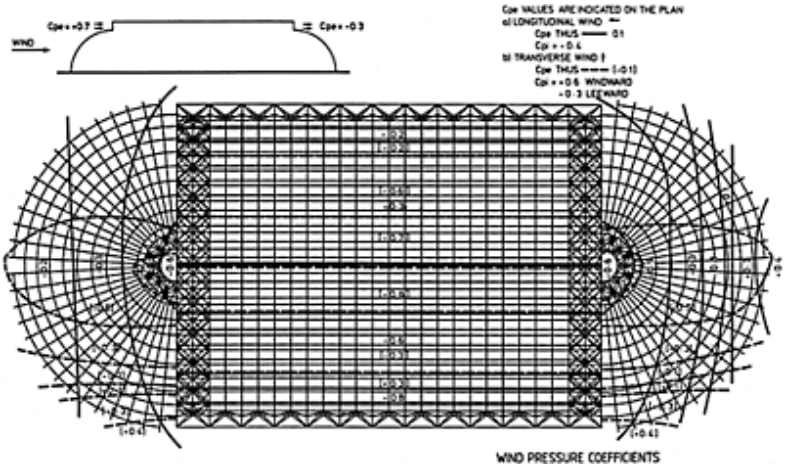

Fig. 24.4. The wind loading pattern.

@Seismicisolation

secondary stresses in the arch and dome ribs and dome purlins. In the case of the dome purlin this tended to reduce flexural stress due to dead and live loads.

8 LOADING

Analytically, the most interesting aspect of a light symmetrical structure concerns its response to asymmetrical loading.

This structure has two principal areas of symmetry and this generated 13 primary load cases involving the analysis of the entire building.

Load case:

1 Comprises the dead load together with a live load of 0·75 kN/m^2 applied to the entire structure.
2/3 Combined dead with asymmetric live load (about both major axes).
4/5 Combined dead load and wind loading.
6/7 Combined load cases 2 to 5 about their appropriate axes.
8 Comprises the dead load with one dome end displaced 25 mm downward at the end of the building relative to its intersection with the vault.
9 Combined the dead load with one of the vault braced bays displaced 25 mm relative to the central vault truss.
10 Combined dead load with a live load applied to one-quarter of one of the domes to simulate an asymmetric load about both axes at this point.
11/12 Combined load cases 1 with 8 and 1 with 9.
13 Investigated the combination of dead load plus a temperature change of 25°C.

Obviously dead load is only taken once when combining load cases.

The wind-loading pattern was assessed using the relevant clauses of CP3 Ch V part 2, combined with recommendations carried in Newbury and Eaton—Wind Loading Handbook.

The wind loading pattern adopted is shown in Fig. 24.4.

9 ANALYSIS

In order to carry out a satisfactory analysis, it was first necessary to understand the structure's behaviour beforehand. A sensible assessment could then be made of the member properties. Small deflections would result from the analysis and thus not conflict with the basic assumptions.

The initial vault arch analyses were calculated by hand, since this is a statically determinate problem. It was initially assumed that most of the longitudinal forces in the vault transferred from the domes would be carried to the foundations in the braced bays. This meant that the preliminary sizing of the vault purlins could be done largely on the basis of the bending moments and deflections induced by the loading applied to the cladding. It was interesting to note that at wider arch centres, it was the heavier purlin section required that made the structure relatively uneconomic, as opposed to the heavier arch sections required.

@Seismicisolation

Other than these preliminary calculations, the analyses required were of highly indeterminate structures. Eventually, because of the importance of the asymmetric loading conditions, it was necessary to form numerical models of the entire structure. These numerical models were analysed by computer.

The program required the structure to be idealised as line elements which intersect at a series of nodes. This naturally meant the preparation of large amounts of input data. Each element was defined as a shear beam; that is, the effects of shear in addition to pure bending were included in the formulation of the element stiffness. The structure was analysed as a pinned structure. This was simulated in the model by incorporating elements of small moment of inertia for the bracings, truss diagonals, ties, purlins and dome circumferential members. The supports were all modelled as pins by releasing the three rotational degrees of freedom.

The behaviour of the dome vault interface is the most interesting. A number of analyses were first performed on one of the dome pieces in isolation. This was to evaluate its behaviour and to determine the mode and degree of support required at the vault. The dome radial members, for architectural and practical reasons, did not run through to the apex, but were stopped at a braced ring beam. The analyses showed that the dome required vertical support at the top of the braced ring beam. This was provided by a triangular braced girder which cantilevered from the braced bay. It was found that by bracing three vault arches in both planes of the vault structure and also perpendicular to these planes, it was sufficient to provide vertical, lateral and torsional stiffness to support the dome. These braced bays were also designed to cater for the horizontal forces on the structure as a whole.

Because of the shape, the structure when fully assembled is very stiff. Theoretically, deflections are of the order of a few millimetres for the symmetrical load-cases and the maximum anywhere on the structure is 25 mm.

The computing facilities available permitted the output of the results for the most heavily loaded members in specified portions of the structure. The results were rigorously inspected for those parts of the structure which were least easy to visualise in terms of structural behaviour, such as the braced bays, stiffened dome rings and dome stiffening girders.

The portion of the structure which works hardest is the braced bay arches, in particular the arch booms. The design conditions for individual members here (as also elsewhere in general) were the load-cases with asymmetric live loading. The RSJ boom sections used elsewhere were in certain cases insufficient in the braced bays. To maintain the uniform appearance in the vault, it was decided to plate the RSJ members, rather than substitute larger members. For architectural reasons, it was desirable that the plating be symmetrically arranged and therefore the extent of plating used was greater than that strictly necessary for structural reasons.

The behaviour of the braced bay was in line with what had been assessed from the preliminary analyses. The one unexpected characteristic of the braced bay assembly which was not immediately obvious from the analysis of the complete structure was that, although it was very stiff vertically and laterally, it had relatively little torsional stiffness in the temporary condition. This manifested itself during erection when the dome was erected against an isolated braced bay which was restrained laterally only. In this condition, the dome radial members acted as arches and the thrust at the upper ends

@Seismicisolation

resulted in some twisting of the braced bay. The movements were not large, but because of the magnifying effects of the three-dimensional circular geometry, they were sufficient to cause problems with fitting the dome circumferential members, as discussed elsewhere.

The design was to BS 449: Part 2. Since deflection of individual members was not generally a design factor, advantage was gained from the use of grade 50 steel. The predominant loading for any member was the axial load. Many of the members were, however, curved and consequently significant secondary moments were induced. The vault purlins and dome ring members also had moments induced from the loading transmitted from the cladding.

The wind load-cases using the increase in permissible stress allowed in BS 449 did not produce more onerous member forces than the asymmetric live loading cases.

The loadcases in which supports were displaced similarly did not induce member loads anywhere in the structure in excess of those resulting from the asymmetric live loading cases.

Because of the flexibility of the structure, it was not anticipated that the effects of expansion would be a problem. The expected movement over the length of the vault would be of the order of the expected bolt slip in that length. The braced bays, however, are a relatively rigid portion of the structure and it was expected that their influence would induce significant member forces in certain places under the temperature loading. This did in fact prove to be so.

Detailed elastic hand analyses were carried out for certain elements—such as the pin details, the joint where the intermediate arch booms split and the stability of the dome radial members.

The ventilator structure at the apex of the vault is supported by the vault and forms no part of the overall framing action.

10 CONSTRUCTION

Quality control and welding procedures were set up, it being essential that all aspects of the work be to the highest standards. Quality control was divided into two areas: one which dealt with the technical performance and appearance of the welded joints and the other with the dimensional accuracy of the completed members and compliance with the corrosion protection specification.

The dimensions of the arch and dome ribs were such that it was not considered practical to transport completed frames and so these were delivered in half frames of approximately 16·5 m length. This meant that full strength site butt welds were required for top and bottom booms for the arch ribs and for the dome ribs.

With overall dimensions of 125 mm and 100 mm for the top and bottom boom members of the arch, highly skilled welding was required. In order to achieve full penetration of the flange butt welds windows were formed in the web to allow sealing runs to be made across the inside of the flanges. Run-on angles were used to give the correct alignment of the flanges and to allow the flange welds to be carried past the end of the flanges, thus avoiding the risk of porosity etc. at their edges. These temporary angles were subsequently cut off and the window plate in the webs welded in.

@Seismicisolation

Problems were experienced particularly at the root of the flanges. These were overcome by slight modifications to the weld preparation of the window plate, which involved carrying the horizontal runs past the corners of the window and overlaying a fillet weld at this junction.

In general the standards set and achieved were as laid down in BS 4870. The methods of testing adopted were magnetic particle and ultrasonic. The X-ray method was not used with the exception of laboratory testing of welder test pieces.

The method of erection adopted by the contractor was to assemble each half arch on the previously erected bipods with the lower pin in position and sitting the free end on a scaffolding tower approximately 3 m high. The upper half frame was then set on the scaffolding tower with the centre pinned end resting on blocks at ground level. The welding jigs were set up and alignment carefully checked with surveying instruments. The welds were then completed and tested (100% of first 6 frame sets). Three arches were assembled at one time with upper and lower longitudinal members in position and starting with the southernmost braced bay. Lifting beams were attached near the top of each 3 frame set of half arches and the two halves lifted by two crawler cranes; the apex pin was then fitted and the arch frames released. Every fourth arch was omitted and then lifted into position, once the three frames either side were erected, from a temporary supporting beam provided at the upper and lower ends of the intermediate arch frame.

The site welding of the dome ribs was carried out in a similar manner to that of the arch frames. The initial method of erection was that the ribs were lifted with a clamped on strongback individually, connecting each via its purlin back to the previously erected and guyed braced bay. The upper ends of the dome ribs were then connected to the upper stiffening girder via upper and lower ring beams.

The stiffening girder and ring beams were assembled in quadrants on the ground and lifted into position on to a scaffold tower at the dome apex. Welds were completed and tested prior to connection of the dome ribs.

It was found that the ribs tended to flatten during the process of erection due to movements in the stiffening girder and braced bay leading to a decrease in the circumferential dimensions and hence to a lack of fit of the curved purlins.

The resolution of this was achieved by the introduction of a supporting ring of scaffolding at approximately the mid-point. This was maintained in position until the whole structure was completed following which the ribs were released gradually on screw jacks and the structure took up its natural form.

11 CLADDING

The envelope is energy efficient and low on maintenance costs.

The dome structures are clad in profiled aluminium sheet with an insulating lining tray providing a high level of heat insulation, acoustic treatment and a vapour barrier to guard against the high humidity levels in the leisure pool.

Figure 24.5 gives the external appearance of the central part of the structure. The aluminium sheets were pressed to the spherical geometry of the dome in tapered sheets of 6 m length (Fig. 24.6). These sheets were connected to circumferential aluminium tubular purlins set at approximately 2·5 m centres up the dome.

@Seismicisolation

The vault cladding was formed from twin wall extruded polycarbonate sheets 20 mm thick having longitudinal ribs approximately 30 mm apart. This type of sheet has been used mainly on the continent although there are a few examples in the UK. It has a very low Young's modulus (2·3 kN/mm^2) and provides excellent resistance to physical damage. It also provides an environment suitable for plant growth.

A fire retardant grade was used achieving flame spread rating Class 1.

The sheets are glazed into aluminium extrusions with neoprene seals giving continuous panels of 3 m×1 m sheets held in place by aluminium capping pieces. The system uses fairly normal glazing details with the exception of a much greater allowance for expansion and of linear expansion typical of the polycarbonate material (approximately 5 times that of steel).

Another aspect of the cladding design was the system of drainage channels formed

Fig. 24.5. The external appearance of the central part.

from the cold-formed inverted channel support to the glazing bars. This was only a fail-safe system to allow for the water seals being bridged or condensation occurring within the sheet.

One of the original ideas which, due to time and financial constraints, was not incorporated was the possibility of using the fluting of the sheet to carry a fluid (coloured or clear) which could be used as a solar collector and, by variation in colour, both as a sun shield and to change the appearance of the building. The initial idea stemmed from a commercially available solar panel using this technique, but the scale of our application demanded considerable research and development of the system.

It remains, however, theoretically possible and worthy of further investigations.

@Seismicisolation

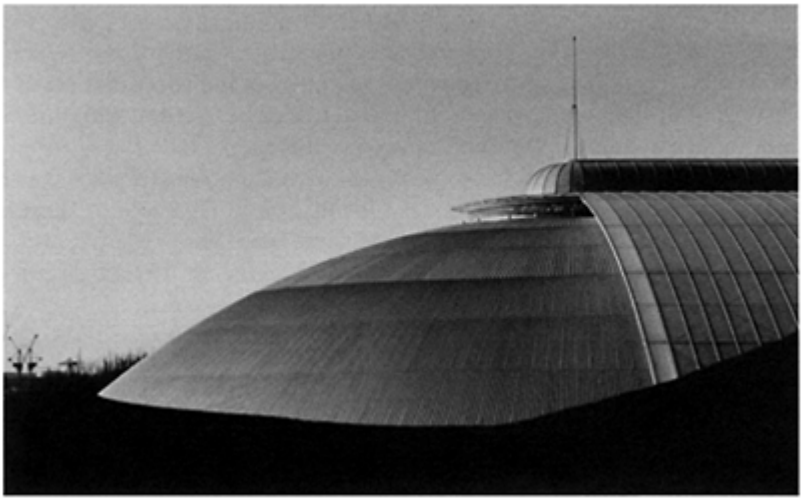

Fig. 24.6. The aluminium cladding panels over the half dome.

12 FACTS AND FIGURES

Enclosed volume	72200 m^3
Enclosed area	7500 m^2
Span of dome	62 m
Span of vault	60 m
Height to u/s of dome	13·8 m
Length of vault	78 mm
Depth of vault truss	1·2 m
Radius of curvature (inner)	41·1 m
Weight of steelwork	300 tonnes

@Seismicisolation

@Seismicisolation

Index

Academy of Montpellier, 227–31
Aerodynamic coefficients, 123
Aeroplane hangars, 7
Airy stress function, 174
Alcan 755T4 extruded aluminium, 254
Aluminium braced barrel vaults, 247–58
Aluminium sheet, 391
Analysis. *See* Structural analysis
Antiprismatic pattern, 68
Approximation index, 310
Arch mode, 36
Architectural aspects, 223–37
Architectural research studies, 236–7
Asbestos concrete models, 306
Asymmetric uniform load condition, 307–13
Axial forces, 96, 99, 102, 104, 106, 107, 110, 113

Beam mode, 36
Bending, 324–7
    moments, 96, 100, 102, 104, 106, 107, 109, 113, 172, 215, 241, 261, 265, 345
    stiffness, 173
    stress, 341, 345
Berlin ice stadium, 269
Berlin Olympic stadium roof, 239–41
Bifurcation
    analysis, 173
    load, 172, 173, 180
Bolted connections, 163
Boundary conditions, 86, 88, 309
Boundary layers
    rough, 126, 129–45
    simulated system, 126
    smooth, 125, 126, 129, 130, 131, 144
    turbulent, 125
Braced barrel vaults
    advantages of, 209
Braced barrel vaults—*contd*.
    American examples, 13–14
    a nalytic procedures. *See* Structural analysis
    construction methods, 201–3, 211–12
    Czechoslovakian examples, 14–15, 30
    disadvantages, 209–11
    early examples, 1–5

@Seismicisolation

early origins, 1
early types, 7
economy, 2
English examples, 24–8
form development, 147–51
French examples, 15–24
German examples, 33
history of development, 1–35
Japanese examples, 14
loading conditions, 151–3
long, 160
main types, 160–1
middle-length, 160
Perspex model, 184–5
possibilities offered by, 208–13
practical applications, 9, 13–28, 225–33
preliminary design, 90–4
recent achievements, 1–35
short, 160
structural arrangement, 197–9
structural behaviour, 90–120
structural system, 260–7
summary of existing work, 115–19
types of bracing, 5–7
see also under specific types
Bracing
configurations, 37
design, 38
types used, 5–7
Buckling
collapse, 161–3
instability, 178, 180
loads, 34, 40, 156–7, 159

Cast iron, 1
Castigliano's theorem, 185
Choleski method, 186
Church Amid Greenery, 351
Cladding, 203, 241, 373, 391–2
Codes of practice, 30
Collapse
loads, 327–30, 338
mechanisms, 161
probability, 338
Comparability index, 321
Composite materials, 183–96
Compression member design, 94
Computer aided design (CAD) methods, 241
Computer drawings, double-elliptic vaults, 70–3
Computer programs, 159
double-elliptic vaults, 69–70

@Seismicisolation

IBM-STRUDL, 315
NELIN, 176, 361
preliminary design, 90
Computer techniques, 159, 207
Concordance index, 320, 323
Continuous barrel vault sluiceway, 257, 258
Continuous braced barrel vaults, 6
Continuous shell elements, 79
Continuum methods, 153
Continuum vaults, 208
Convergent members, 210
Crab shelter, 223
Cross diagonal pattern, general formulae of physical constants of, 84
Cross joints, 262
Crystal Palace, 1–2
Curved members, 210
Cylindrical barrel vaults, 7, 160–1

Damping effects, 301
Dead loads, 199
Deflection(s), 33
check, 93
contours, 98, 111
curves, 322
profiles, 97, 103, 108, 114
Design loads, 199
Diamond lattice system, 149
Diamond-shape chain arches, 215
Diamond Truss system, 214–22
analytical theory, 214–16
automatic design and manufacture, 221
automatic production machines, 218–19
consecutive manufacture, 219
construction method, 217
design techniques, 217
main features, 214
multiformity of structure, 218
Diamond Truss system—*contd.*
production
cost, 220
method, 219–22
techniques, 217–22
productivity, 220
sequence of erection, 217
Discontinuous bending model, 315–17
Discordance values, 320
Discrete field analysis, 38, 153, 175
Discrete members, 210
Displacement
calculation, 85–9
matrix procedure, 153

@Seismicisolation

Double curvature vaults, 329
Double elliptic hemisphere, 66–7
Double-elliptic vaults, 66–75
adaptations, 73–4
basic geometry, 66–7
basic octahedron, 68
computer drawings, 70–3
computer programs, 69–70
polyhedron triangle, 69
possible combinations, 67
possible future developments, 74
subdivision method, 67–8
Double-layer braced barrel vaults, 7, 20, 21, 38, 39, 118, 119, 120, 199, 241
Double-layer lamella barrel vaults, 263, 267, 268, 271–6
Double-layer lamella grids, 265
Doubly curved experimental vaults, 283
Doubly curved members, 210
Drift loads, 153, 200–1

Edwards Air Force Base, 150
Elastic analysis, 34, 183–96
End gable bracing stiffness effect, 117
Equestrian riding ring, 255–7
Equivalent continuous method, 76–89
Equivalent continuum methods, 159, 175
Equivalent depth, 174
Equivalent shell approach, 38, 40
Equivalent Shell Replacement method, 216
Euler force, 178
European Column Curves (ECC), 162, 163 178

Fibre/matrix percentage ratio, 183, 184
Finite element analysis, 40, 151, 184, 208, 342–3
Flexural stiffness, general formulae of, 77–80
Formex formulation, 18, 41–65
Fran stress analysis program, 19
Frankfurt athletics hall, 367–81
buckling characteristics, 372
edge problem, solution of, 376–7
erection methods, 380
framing pattern, choice of, 369–70
joint design, 378–9
linear model, 370–2
loads, 373
longitudinal behaviour, 374–7
supported edges, 375–6
member forces and member design, 373–4
non-linear effects, 372–3
prefabricated unit, choice of, 377–8
prism, choice of, 367–9
resistance to longitudinal wind, 377

@Seismicisolation

roof shape, choice of, 367–9
special zones, 373
transverse behaviour, 370–4
Full scale model tests, 317–19

Gable bracing, 116, 117
General formulae
derivation, 77–81
flexural stiffness, of, 77–80
membrane stiffness, of, 81
physical constants, of, 82–4
General instability, 170–7, 180
Generic formulation, 43
Geodesic pattern, 68
Glass fibre reinforced polyester matrix (GRP), 183–96
Gymnasia
Carpentras, in, 231–3
L. Stockwell Jadwin, 19, 23

Halifax Primary School, 30
Handford Hall School, 30
Height-to-span ratio, 94–6, 104, 105, 107, 119
Hemisymmetric load model, 308–13
Hipped barrel vaults, 5, 74, 266
Hipped ends, 119, 149, 265–7
Homogeneous equations, solutions to, 85–8

IBM-STRUDL computer program, 315
Ice rinks
Czechoslovakian example, 14
Havlíčkův Brod, 264, 265, 273, 275 265, 271
Popovice, 269
Poprad, 271–2
Uherský Brod, 272
Žďár nad Sázavou, 268, 274
Il Palazzetto Dello Sporto, 150
Imperfections, 334–5
Imposed loads, 199–201
Incremental analysis, 333–4
Instability, 159–82, 196, 316
buckling, 178, 180
general, 170–7, 180
interaction between different types, 177–80
line, 167–70, 178
node, 163–7
types, 161
Interconnection patterns, 41, 43, 45–7, 49–51, 54–60, 63, 65
Internal forces, calculation of, 85–9
Iron bars, 1
Iron rods, 2

@Seismicisolation

Isotropic equivalent continuum, 174

Joban Hawaiian Leisure Centre, 15
Jointing details, 261
Joints
    endplate, 378–9
    NODUS system, 205–7, 212
    rhombic lamella structures, 349–51
    rigid, 33, 39
    SDC, 226, 227
    Zollinger lamella roof, 244, 340

Lamella barrel vaults, 116, 259, 260, 263, 264, 280, 354–5
Lamella frame, 199
Large span structures, 259, 279
Lattice
    bars, 215, 216
    members, 197, 210, 271–6
    shell barrel, 27, 28
Latticed structures, 5, 6, 162, 163, 172, 176, 177, 295
Length/width ratio, 6
Lightweight barrel vaults, 30
Lightweight shell construction, 27
Line instability, 167–70, 178
Linear analysis, 34, 40, 185
Liverpool International Garden Festival Exhibition building, 148, 382–93
    analysis, 388–90
    arch booms, 389
    background, 382
    braced bay arches, 389
    brief, 383
    cladding, 391–2
    construction, 390–1
    dome vault interface, 389
    domes, 384
    enclosure, evolution of, 383
    foundations, 384
    loading, 388
    modelling and framing configuration, 385–8
    primary structure, 384
    structural form, evolution of, 383
    vault, 384
Load calculation, 176
Load deflection diagrams, 324
Load factor-axial forces, 193–5
Load factor-displacement relationship, 186, 188–92
Load strain diagrams, 323
Longitudinal panels, 211
Longitudinally spanning vaults
    non-symmetrically loaded, 107–15
    pinned gable end supports, with, 112–15

@Seismicisolation

symmetrically loaded, 105–7, 112–15
L. Stockwell Jadwin Gymnasium, Princeton University, 19, 23

M-shed, West India Docks, 203, 204
Madison Square Garden, 149
Manchester Central Station, 148
Materials economy, 267
Membrane
conditions, 319–24
flexibility, calculation of, 81
forces diagram, 303, 304
stiffness, general formulae of, 81
MERO system, 7, 20, 238–46
applications, 239–46
barrel vault roofing structures in Japan, 245
Berlin Olympic Stadium roof, 239–41
space frame unit preassemblage, 244
Split stadium roof, 241–3
structural analysis aspects, 238–9
Miami Arch, 21, 24
Model analysis, 5
Model tests, 10
Mohr's circle, 307
Moscow (Idaho) stadium, 150
Multi-bay roof, 201
Multi-span braced barrel vault, 203
Münsterland convention hall, 243, 244

National Building Code of Canada, 153
NELIN computer program, 176, 361
Nervi's hangar, 3, 5
Newton-Raphson approach, 241
Niagara Falls Convention Centre, 155–6
Node equilibrium, 175
Node instability, 163–7
NODUS Joint System, 205–7, 212
Non-homogeneous equations, particular solution of 88–9
Non-linear analysis, 40, 173, 185, 241
Non-linear behaviour, 331–3
Non-symmetrically loaded vaults, 101–5, 107–12, 112–15, 119
Normal stresses, 294
Nuclear plant barrel vault, 253–4
Numerical simulation methods, 335–8
Numerically controlled (NC) machines, 218–19

Olympic stadium, 239–41
Ondara barrel vault, 271
Orthogonal cylindrical shells, 85–9
Orthotropic equivalent continuum, 174
Ostrava barrel vault, 270

@Seismicisolation

Paris-Vaugirard tennis court, 255–7
Patent rights, 5
Pearson's X^2 test, 337
Physical constants
determination, 77–81
general formulae, 82–4
Pin-jointed structures, 33, 333
Plastic mechanism approach, 40
Plasticity reduction factor, 178
Poisson's ratio, 216
Post-buckling analysis, 183–96
Potential energy, 176
Precast prefabricated modular reinforced concrete units, 4
Prefabricated barrel vaults, 354–66
Prefabricated steel structures, 2
Prefabricated truss panels, 203–5
Probability
analysis, 331–9
density function, 334–6
Pseudo-random structures, 335–8
Pultrusion technique, 183

Railway stations, 2
Raked supports, 149
Rectangular translation vault, 302
Reinforced concrete barrel vaults, 5
Restraint-compatible deflections, 176
Reticulated barrel vaults, 159, 225
structural behaviour, 299–330
Reticulated models, 298
Reticulated shells, 76–89
Reticulated vaults, 284–6, 354
collapse loads, 328
doubly curved, 283–6
structural analysis, 282–98
structural typology, 315
Reynolds number, 129, 130
Rhombic lamella roof, 340–53
Riding house structure, 364
Riding school in Motěšice, 276
Rigid joints, 33, 39
Rigidity
coefficient, 341
factors, 164
Rigidly jointed shallow vaults, 116
Rigidly jointed space frame members, 92
Rise-to-span ratio, 30
Rise/width ratio, 6

Safety

@Seismicisolation

coefficient, 330
factor, 6
St Mark's Academy, Southboro, Mass., USA, 251–3
St Pancras station, 148
St Venant effect, 36
SAP (Structural Analysis Program), 342
SDC joint, 226, 227
Self-weight, 30–3
Serangoon Country Club, 21, 25
Shear, 324–7
force, 215, 216, 325
stresses, 294, 295
Shell mode, 36–8
Shingu High School gymnasium, 245, 246
Silver Jubilee Girls Secondary School, Bury St Edmunds, 29
Single diagonal patterns, general formulae of physical constants for, 83
Single-layer barrel braced vaults, 5–7, 30, 33, 34, 38, 94, 120, 161, 198
lamella, 262, 263, 267, 268
segmental timber shell, 341
stiffening arches, with, 355–61
three-way, 10, 217
Single-layer slender shell, 265
Slenderness ratio, 30, 178
Sloping beam and rib form, 211
Snap-through buckling, 40
Snow loads, 151, 153, 200–1, 373
Space frame, 38, 315–17
model, 321, 323–7
Space truss approach, 38
Spandrel
joints, 295
members, 291
stresses, 295
Span-to-height ratio, 94
Span-to-rise ratios, 184, 185, 195, 196
Spatial reticulated vaults, collapse load of, 328
Spherobat connector, 237
Sports Centre, Montpellier, 227–31
Sports halls, 361, 364
Swindon, 203
Valencia, 276, 277
Square vault, 303
Stability
boundary concept, 151
considerations, 147–58
Stage shell barrel vault, 247–50
Statistical analysis, 337–8
Steel braced barrel vault roofs, 197–207, 247–81
Romanian examples, 354–66
Steel lamellar vaults, 259
Stiffening arches, 355–61
Stiffness method analysis, 39, 93

@Seismicisolation

computer implementation, 39–40
Strain measurement, 297, 319
Strength/cost ratio, 203
Stress
analysis, 5
determination, 286, 291, 293
distribution, 7–13, 33, 34, 119, 215, 283, 301–7
reversal, 30
state, 315–27
Structural analysis 33–4, 36–40, 153–8, 331
reticulated vaults, 282–330
structural idealisation for, 38–9
Zollinger lamella roof, 340–6
Structural idealisation for analysis, 38–9
Structural response, 36–8
Structural typology of reticulated vaults, 315
Structural weight, 95, 101, 105, 112
Student's *t* test, 337
SUPEREL PUNCH program, 69
SUPERELLIPSOIDS program, 70
Surface
derivation of translation vault, 299–307
pressures, 125
revolution, of, 211
Symmetrically loaded vaults, 94–107, 112–15

Tamagawa Takashimaya gymnasium, 245, 246
Tennis Court SNCF, Paris-Vaugirard, 225–27
TeZet barrel vaults 32, 33
Theatre design proposal, 236
Thin reinforced concrete shells, 5
Three-way braced vaults, 115
grid-type, 12
single-layer, 10, 217
trussed grid, 367–81
Thurleston School, 30
Tied effect, 155
Timber barrel vaults, 28–30
Timber lamella
barrel vaults, 3, 150, 340–53
roof system, 2
structures, 7
Toggle action, 6
Toroidal triangulated shells, 31
Torsional moments, 325
Torsional stress, 341
Translation vaults
collapse load, 327–30
surface derivation, 299–307
Transversely spanning vaults
non-symmetrically loaded, 101–2

@Seismicisolation

pinned horizontal longitudinal boundaries, with non-symmetrically loaded, 103–5
symmetrically loaded, 102–3
symmetrically loaded, 94–105
Triangular grids, general formulae of physical constants for, 82
Triangular skeletal structure, 150
Triangulated barrel values, 159–82, 286–98
Triangulated end diaphragms, 225–7
Triangulated shells, 268
Triodetic system, 7, 247–58
barrel vaults, 31
connectors, 248, 254
tube hub connection, 248
Tubular barrel vault, 236
Twisting, 324–7
moment, 326
Tympana effect, 301–7

Ultimate load curve, 180
Unitruss system, 219, 221

Vaugirard barrel vault, 17
VISIPLOT system, 69

Waldstadion sporting complex, 367
Welded nodes, 163
Wind
direction effects, 129–31
distribution curves, 19
loads, 30, 121–46, 199, 201, 373, 377, 387, 388, 390
pressure, 30, 123, 284
coefficients, 123, 125, 130, 144
distribution, 122, 125–45
tunnel tests, 18, 30, 124
Wrought iron, 1
Wuppermann braced barrel vaults, 33

Yoked columns, 149
Young's modulus, 174, 216

Zollinger lamella roof, 244, 340
analytical results, 343–6
construction principle, 340
deformation behaviour, 343
force magnitudes, 343
horizontal deformation, 346
joint types, 349–51
lamellae and joints used in, 342
large scale experiments, 346–9
structural analysis, 340–6
structure geometry, influence of, 343

@Seismicisolation

variants, 341
vertical deformation, 345

@Seismicisolation